PHYS

Volume 62

THE PHYSICAL REVIEW

A journal [illegible] *published by E. L. Nichols in 1893*

Published by the American [illegible]
for the
AMERICAN PHYSICAL [illegible]

Officers [illegible]

President

E. C. Lawrence
California Institute of [illegible]
Pasadena, California

Vice-President

J. H. Van Vleck
Harvard University
Cambridge, Massachusetts

Secretary

E. U. Condon
Bell Telephone Laboratories
Office:
Columbia University
New York 27, New York

Treasurer

G. B. Pegram
Columbia University
New York 27, New York

Local Secretaries
for the Pacific Coast

J. Kaplan
University of California
Los Angeles
Los Angeles, California

Managing Editor

S. A. Goudsmit
Brookhaven National Laboratory
Upton, Long Island
New York

BOARD OF EDITORS

Editor

S. A. Goudsmit

Associate Editors

J. Bardeen — Harvey Brooks
R. Bozorth — R. F. Christy
J. G. Hoyt — C. L. Critchfield
W. E. Lamb, Jr. — M. Deutsch
A. J. P. Meyer — T. H. Johnson
E. L. Nichols — Bruno Rossi

Manuscripts for publication should be submitted to S. A. Goudsmit, Brookhaven National Laboratory, Upton, Long Island, New York. Authors' institutions are requested to pay a publication charge of $10.00 per page which, if honored, entitles them to 100 free reprints. Reprints will be sent only when paper is published.

Proof and all correspondence concerning papers in the process of publication should be addressed to the Publication Manager, American Institute of Physics, 57 East 55 Street, New York 22, New York.

Subscription Price

United States and Canada [illegible]
Elsewhere [illegible]

Back Numbers

Yearly [illegible] *rates when complete year is available:*
Prior to 1949: $20.00
Thereafter: $27.00

Single issues: $2.50 each, prior to July, 1929;
$1.00 each, July, 1929–December, 1941;
$2.00 each, January, 1942–December, 1946;
$1.00 each, January, 1947–December, 1948;
$1.25 each, thereafter.

General Index, 1893–1920: $4.00.

Subscriptions, renewals, and orders for back numbers should be addressed to the American Institute of Physics, 57 East 55 Street, New York 22, New York.

Change of address in the case of members of the American Physical Society should be addressed to the Treasurer; in the case of other subscribers, to the American Institute of Physics.

[illegible] Professor of Physics, Department, Cornell University, Ithaca, New York

[illegible] published semi-monthly at Prince and Lemon Streets, Lancaster, Pennsylvania

[illegible], 1918, at the Post Office at Lancaster, Pennsylvania, under the Act of [illegible]

[illegible] provided for in paragraph (d-2), section 34.40, P. L. & R. of 1948.

THE
PHYSICAL REVIEW

A journal of experimental and theoretical physics established by E. L. Nichols in 1893

SECOND SERIES, VOL. 82, NO. 5 JUNE 1, 1951

Radiations from Yb^{169}

DON S. MARTIN, JR., ERLING N. JENSEN, FRANCIS J. HUGHES, AND R. T. NICHOLS
*Institute for Atomic Research and Departments of Chemistry and Physics, Iowa State College, Ames, Iowa**
(Received December 18, 1950)

The radiations from Yb^{169} have been examined by means of a thin lens spectrometer and absorption-coincidence techniques. The half-life was found to be 33±1.5 days. The half-life of the metastable state was determined as 0.67μ sec. Yb^{169} decays by electron-capture to Tm^{169}. Eleven gamma-rays were observed in the photoelectron and internal conversion spectra determined with the spectrometer. On the basis of the absorption-coincidence and spectrometer data, two decay schemes are discussed.

I. INTRODUCTION

A STUDY of the radiations of Yb^{169} has been carried out in this laboratory. It has included a determination of the electron and gamma-ray spectra by a thin lens beta-ray spectrometer and coincidence counting-absorption measurements. Although identification of eleven gamma-rays indicated that the decay scheme is complex, considerable information regarding the principal modes of decay has been obtained.

Bothe[1] first reported this activity as the component with the longest half-life (33d) in neutron irradiated ytterbium oxide. Since he identified Tm K x-rays by selective absorption, he proposed an assignment to isotope Yb^{169} with decay by orbital electron capture. On the basis of absorption curves he reported gamma-ray energies of 0.2 and 0.4 Mev. A shorter activity of about 100 hours was shown by Inghram, Hayden, and Hess[2] to belong to Yb^{175}, which decays by emission of β^-. Recently, Cork *et al.*[3] have reported beta-ray spectrometer measurements of the conversion electrons, listing nine lines. McGowan and DeBenedetti[4] in a systematic search for short-lived isomers reported a metastable state in the decay product, Tm^{169}, with a half-life of 1.0 μsec. The metastable state was reported from absorption measurements to be followed by electrons of 0.12 Mev (probably K-electrons from 0.19-Mev γ) and to be preceded by electrons of a 0.4-Mev gamma-transition as well as x-rays.

A one-gram sample of ytterbium oxide was supplied to us by Dr. F. H. Spedding and his co-workers for these and other studies. Effective separation from the light rare earths, including the elements samarium and europium, had been effected in ion exchange columns using Amberlite IR-100 ion exchange resin.[5] The ytterbium had then been further separated from the rare earths other than samarium and europium by repeated sodium amalgam reductions and extractions. Conditions for such extraction have been described extensively by Moeller and Kremers.[6] Lastly, the sample had been precipitated as oxalate, ignited to oxide and irradiated for one month in the Argonne National Laboratory pile. The decay of the radioactivity was followed by means of a hydrogen-filled G-M counter, and each count was compared with that of a uranium oxide counting standard. The decay of the electron fractions showed in addition to the 33-day component short-lived activities consistent with the 4.2-day Yb^{175} and the 7-day Lu^{176} in agreement with the work of Cork *et al.*[3] However, for a sample mounted with 450-mg/cm^2 aluminum before the counter to stop electrons, there was found to be no apparent deviation from a simple decay of 33±1.5 days which was followed over eight half-lives. Even so, some weak gamma-lines were associated with short-lived activity as noted by the spectrometer. Only radiations definitely associated with

* Work performed in the Ames Laboratory of the AEC.
[1] W. Bothe, Z. Naturforsch. **1**, 173 (1946).
[2] Inghram, Hayden, and Hess, Jr., Phys. Rev. **71**, 270 (1947).
[3] Cork, Keller, Rutledge, and Stoddard, Phys. Rev. **78**, 95 (1950).
[4] S. DeBenedetti and F. K. McGowan, Phys. Rev. **74**, 728 (1948).
[5] Spedding, Fulmer, Butler, Gladrow, Gobush, Porter, Powell, and Wright, J. Am. Chem. Soc. **69**, 2812 (1947).
[6] T. Moeller and H. E. Kremers, Ind. Eng. Chem., Anal. Ed. **17**, 798 (1945).

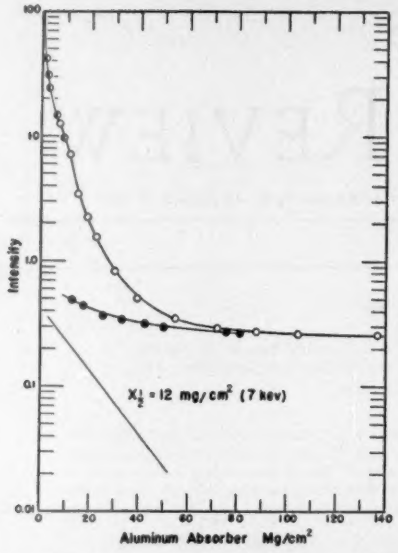

FIG. 1. Aluminum absorption curve for Yb^{169}. ⊙ Mica-window G-M counter. ◑ Windowless counter. ● Electrons removed by magnet.

the long-lived activity have been reported in this paper, and most measurements were performed after decay of the major fraction of the short-lived component.

Following the irradiation, the sample was dissolved in hydrochloric acid and processed through three sodium amalgam extractions. At least 99 percent of the activity was extracted and the absorption curves for the residue indicated that any radiation of significantly different character was certainly less than 0.1 percent of the original.

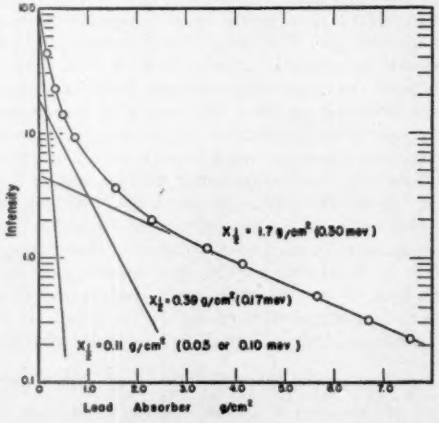

FIG. 2. Lead absorption curve for Yb^{169}.

An aluminum absorption curve of the radiation from Yb^{169} is presented in Fig. 1. A conventional end mica-window G-M counter was used for the high absorber values. The absorption curve from 0 to 9 mg Al/cm² was obtained with a windowless, flowing gas counter produced by the N. Wood Counter Laboratory of Chicago. The curves joined smoothly when an absorber equivalent to the window, air, and Cellophane sample cover was used. The flowing gas counter has proved effective in measuring the conversion electrons from a 25-kev isomeric transition with a half-life of 9 hours in Co^{58m}.[7] It should measure, therefore, the 40-kev Auger electrons that would be expected in about 10–15 percent of the K x-ray transitions. According to the range-energy curve of Glendenin[8] a counter with an air and window thickness of 4.0–4.5 mg/cm² should not detect with appreciable efficiency electrons with an energy of less than 60–80 kev. The absorption curve in Fig. 1 for the windowless counter indicated no exceedingly large group of electrons below that energy. The visual end point of the absorption curve of 80–90 mg Al/cm² would indicate a maximum electron energy of about 0.3 Mev. The absorption of photons in aluminum was also measured with electrons deflected by an Alnico permanent magnet so they could not enter the counter window. Tests with Co^{60} and Ce^{141} activities proved the arrangement effective for electrons of the energies involved. The resulting photon absorption curve is also included in Fig. 1. A soft component, which possessed a half-thickness of 11.8 mg Al/cm², was observed with an intensity about equal to the harder one. Since this corresponds to a photon energy of 7–8 kev, it is presumed to be the Tm L x-ray. Therefore, if the situation is normal in that the intensities of K and L x-ray transitions are not greatly different, the counter detection efficiencies for the 7.2-kev L x-ray and the 50.7-kev K x-ray must be approximately equal.† The main contribution to the electron count appears to fall into two groups, one with a range of about 80–90 mg/cm² and a more intense group with a range of 20–25 mg/cm² corresponding to an energy of 120–140 kev.

The characteristics of the photon component have been determined from the lead absorption curve shown in Fig. 2. An end-window brass counter tube was used. However, an aluminum absorber of 225 mg/cm² was placed immediately before the counter in all measurements. This aluminum would stop all conversion electrons and bring the secondaries into equilibrium with

[7] K. Strauch, Phys. Rev. **79**, 487 (1950).
[8] L. E. Glendenin, Nucleonics **2**, No. 1, 12 (1948).
† *Note added in proof*:—A referee has pointed out that the fluorescence yield for the L x-ray transition is significantly lower than the fluorescence yield of the K transition for which a value of 0.85 has been used. Therefore if the K and L transitions are equally probable, the radiative intensities are proportional to the respective fluorescence yields. Consequently the counter efficiency for the L x-rays is probably somewhat greater than for the K x-rays. This brings the counter efficiencies more in line with the curves of reference 17 but does not change other arguments in this paper.

the primary radiation of interest (30 kev–300 kev). The hardest component, half-thickness of 1.72 g Pb/cm², corresponding to an energy of 0.30 Mev, possessed an intensity of 5 percent. An intermediate component with a half-thickness of 0.39 g Pb/cm² would correspond to an energy of about 0.17 Mev, and it had an intensity of 19 percent. The softest component corresponding to 76 percent cannot be assigned an unambiguous energy value, because it falls in the vicinity of the lead K absorption edge. However, the very high absorption coefficient of most the radiation in Sn, as seen in Fig. 3, indicates that by far the largest fraction of the soft radiation has an energy of about 50–55 kev rather than the 100–110 kev. The soft radiation presumably consisted mostly of the 50-kev Tm K x-radiation and was present in very high counting intensity compared to the gamma-counting rates.

II. THIN LENS SPECTROMETER AND MEASUREMENTS

A. Experimental Arrangement

The radiations from the irradiated ytterbium were examined by means of a thin lens beta-ray spectrometer which has been described previously.[9] The resolution of the spectrometer was 2.1 percent (half-width) except for the inserts shown in Fig. 5, in which case the resolution was somewhat better in order to resolve the lines. Except for curve A of Fig. 6 all the data were obtained with a G-M counter in which the window was a Formvar film having a cutoff at about 15 kev. For curve A of Fig. 6 the window was a much thinner Formvar film supported on a grid. This window had a cutoff at about 5 kev. The spectrometer was calibrated by means of the F conversion line of ThB (1385 $H\rho$) and the annihilation radiation from Zn^{65}. The energies of the gamma-rays have been calculated from the peaks of the lines after applying corrections for the earth's magnetic field, the resolution of the spectrometer, and the surface density of the source.[9]

B. Internal Conversion Spectrum

The internal conversion source, which was grounded, had a surface density of about 7 mg/cm² and was mounted on a polystyrene—Formvar film having a surface density of about 40 micrograms/cm². The internal conversion spectrum is shown in Fig. 4. As can be seen from the figure, there are no beta-particles emitted in the decay of Yb^{169}. The energies of the gamma-rays, as determined from this spectrum, are listed in Table I as conversions in Tm, since the decay is by electron-capture. Conversion lines from eight gamma-rays were observed. In addition, the hump at about 680 gauss-cm, which is labeled $K_a(L)$, is consistent with the energy of Auger electrons from Tm.

[9] Jensen, Laslett, and Pratt, Phys. Rev. 75, 458 (1949).

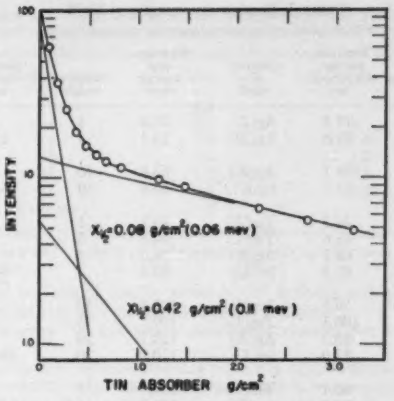

FIG. 3. Tin absorption curve for Yb^{169}.

C. Photoelectron Spectrum

Figure 5 shows the spectrum produced by photoelectrons ejected from a lead foil, having a surface density of 39.3 mg/cm², which was fastened to an aluminum cap covering the source. The lines shown in Fig. 5 can be ascribed to the characteristic x-rays from Tm, due to electron-capture and internal conversion, and six gamma-rays, five of which are also shown in the internal conversion spectrum of Fig. 4. The energies of the gamma-rays and x-rays, as determined from Fig. 5, are listed in Tables I and II respectively as conversions in Pb.

The low energy end of the photoelectron spectrum was also determined by means of a Ag foil having a surface density of 54.0 mg/cm². This photoelectron spectrum is shown by curve B of Fig. 6. In order to determine more definitely the conversion shell of these lines the spectrum was also determined with an In foil having a surface density of 24.3 mg/cm². The data shown by curve A in Fig. 6 were obtained with a more intense source and a G-M counter window having a cutoff at about 5 kev. Figure 6 shows two additional

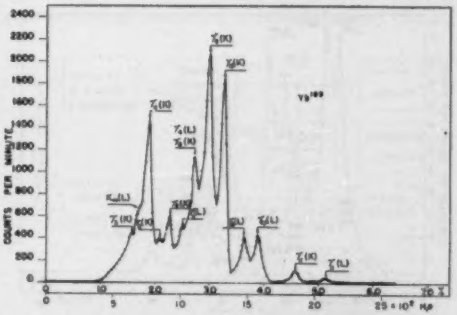
COUNTS PER MIN/TC
2400
2200
2000
1800
1600
1400
1200
1000
800
600
400
200
0
0
5
10
15
20
Yb^{169}
$K_a(L)$
$\gamma_1(K)$
$\gamma_2(K)$
$\gamma_3(K)$
$\gamma_4(K)$
$\gamma_5(K)$
$\gamma_6(K)$
$\gamma_1(L)$
$\gamma_2(L)$
$\gamma_3(L)$
$\gamma_4(L)$
$\gamma_5(L)$
$\gamma_6(L)$
$\gamma_7(L)$
$\gamma_8(L)$
$\gamma_9(L)$
$\gamma_{10}(L)$
$\gamma_{11}(L)$
$\gamma_{12}(L)$
$\gamma_{13}(L)$
$\gamma_{14}(L)$
$\gamma_{15}(L)$
$\gamma_{16}(L)$
$\gamma_{17}(L)$
$\gamma_{18}(L)$
$\gamma_{19}(L)$
$\gamma_{20}(L)$
$\gamma_{21}(L)$
$\gamma_{22}(L)$
$\gamma_{23}(L)$
$\gamma_{24}(L)$
$\gamma_{25}(L)$
$\gamma_{26}(L)$
$\gamma_{27}(L)$
$\gamma_{28}(L)$
$\gamma_{29}(L)$
$\gamma_{30}(L)$
$\gamma_{31}(L)$
$\gamma_{32}(L)$
$\gamma_{33}(L)$
$\gamma_{34}(L)$
$\gamma_{35}(L)$
$\gamma_{36}(L)$
$\gamma_{37}(L)$
$\gamma_{38}(L)$
$\gamma_{39}(L)$
$\gamma_{40}(L)$
$\gamma_{41}(L)$
$\gamma_{42}(L)$
$\gamma_{43}(L)$
$\gamma_{44}(L)$
$\gamma_{45}(L)$
$\gamma_{46}(L)$
$\gamma_{47}(L)$
$\gamma_{48}(L)$
$\gamma_{49}(L)$

TABLE I. Gamma-ray energies of Yb^{169}.

Gamma-ray	Electron energy (corrected) kev	Conversion shell	Gamma-ray energy kev	Relative weight	Average energy kev
1	19.4	Ag(L)	22.6	4	
	22.6	Ag(M)	23.3	2	22.8
2	38.3	Ag(K)	63.8	10	
	35.7	In(K)	63.6	10	63.7
3	34.2	Tm(K)	93.5	3	
	85.6	Tm(L)	94.8	3	
	68.7	Ag(K)	94.2	3	
	67.5	In(K)	95.4	3	94.5
4	50.5	Tm(K)	109.8	10	
	100.5	Tm(L)	109.7	5	
	85.2	Ag(K)	110.7	10	
	83.0	In(K)	110.9	10	110.4
5	60.4	Tm(K)	119.7	5	
	96.2	Ag(K)	121.7	3	120.4
6	71.4	Tm(K)	130.7	10	
	46.4	Pb(K)	134.4	10	
	107.3	Ag(K)	132.8	10	
	104.7	In(K)	132.6	10	132.6
7	54.6	Pb(K)	142.6	3	142.6
8	72.2	Pb(K)	160.2	3	
	100.5	Tm(K)	159.8	5	160.0
9	119.2	Tm(K)	178.5	10	
	168.2	Tm(L)	177.4	5	
	90.1	Pb(K)	178.1	10	
	162.9	Pb(L)	176.6	5	177.9
10	139.5	Tm(K)	198.8	10	
	188.6	Tm(L)	197.8	5	
	110.3	Pb(K)	198.3	10	
	182.8	Pb(L)	196.5	5	
	196.7	Pb(M)	200.5	2.5	198.3
11	248.1	Tm(K)	307.4	10	
	298.9	Tm(L)	308.1	5	
	220.6	Pb(K)	308.6	10	
	294.0	Pb(L)	307.7	5	308.0

gamma-rays that were not observed in either the internal conversion spectrum of Fig. 4 or the photoelectron spectrum of Fig. 5. The gamma-ray and x-ray energies as determined from Fig. 6 and the photoelectron spectrum obtained with the In foil, are listed in Tables I and II, respectively, as conversion in Ag or In as the case may be.

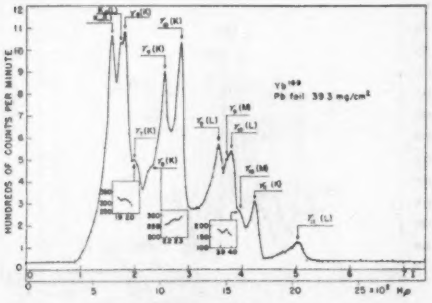

FIG. 5. Spectrum of photoelectrons from a lead foil for Yb^{169}.

In calculating the energies given in Tables I and II the binding energies of the K shells were determined from the critical absorption wavelengths.[10] These values are 88.0, 59.3, 27.9, and 25.5 kev, respectively for Pb, Tm, In, and Ag. The binding energies of the L shells are average experimental values determined from the differences between a number of K and L lines for the respective metal foils. These values are 13.7, 9.2, 3.4, and 3.2 kev, respectively for Pb, Tm, In, and Ag.

The average energies given for the K_α and K_β x-rays in Table II are in good agreement with those given by Compton and Allison,[11] namely, 50.7 kev and 49.8 kev, respectively, for $K_{\alpha 1}$ and $K_{\alpha 2}$, and 57.6 kev for $K_{\beta 1}$. This serves as an excellent check on the calibration of the spectrometer.

Eleven gamma-rays were found for Yb^{169}. Gamma-rays 1, 7, and 8 listed in Table I are in addition to those

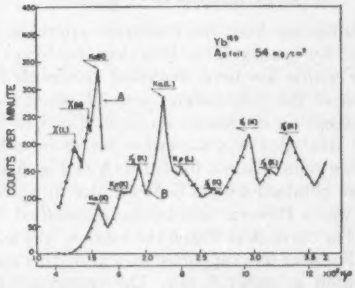

FIG. 6. Spectrum of photoelectrons from a silver foil for Yb^{169}. Curves A and B were obtained with G-M counters with window thicknesses of 0.3 mg/cm² and 0.03 mg/cm², respectively.

given by Cork *et al.*[8] The energy values of the other gamma-rays listed in Table I are in good agreement with those of Cork *et al.* The probable error of the gamma-ray energies given in Table I is estimated to be less than one percent.

D. Intensities of Gamma-Rays and Internal Conversion Electrons

Approximate relative values of the intensities of the gamma-rays and the internal conversion electrons can be obtained from the maximum counting rate of the respective lines. In the case of Figs. 5 and 6 the spread in momentum, owing to the surface densities of the Pb and Ag foils, was greater than the momentum spread which the spectrometer could accept.[9] In this case, *neglecting scattering*, the maximum counting rate for any line is proportional to the number of such quanta

[10] A. H. Compton and S. K. Allison, *X-Rays in Theory and Experiment* (D. Van Nostrand Company, Inc., New York), second edition, p. 791.

[11] Reference 10, p. 784.

emitted by the source, the photoelectric absorption coefficient, the transmission of the counter window and inversely proportional to the spread in momentum produced by the metal foils. The photoelectric absorption coefficients were calculated by means of Gray's[12] empirical formula and the spread in momentum produced by the metal foils by means of a formula given by Heitler.[13] The internal conversion spectrum was treated in a similar manner. Relative intensities have been calculated with respect to gamma-ray 9. Table III gives the approximate relative intensities of the more prominent gamma-rays (q_i/q_9) and internal conversion electrons (e_i/e_9). Where the gamma-ray lines are fairly well separated, these ratios may be in error by a factor of about two.

III. COINCIDENCE MEASUREMENTS

A. Experimental Arrangement

Coincidence counting experiments employing G-M counters with 2.2–2.8-mg/cm² mica windows were performed. The counters had separate high voltage supplies. A block diagram of the electronic arrangement is shown in Fig. 7. As shown in the diagram, the pulses in channel 2 could be applied immediately to the grid of a mixer tube or sent first to a delay circuit which was based on a design by Watts *et al.*[14] This circuit provided a delay of from 2.4 to 20 μsec. By selector switches a choice of gate widths from 0.8 to 1.5 μsec could be obtained for each channel. Pulses were observed on a synchroscope with sweep speeds of 2 or 6 μsec/inch. The sweep was calibrated frequently by an oscillator tuned to the fifth harmonic of a 100 kc crystal, which served as the time scale. The delay time could be read from the scope together with the pulse widths or gates, τ' and τ'' for the separate channels. In the subsequent treatment the following symbols and conventions have been used.

TABLE II. X-ray energies of Tm.

X-ray	Electron energy (corrected) kev	Conversion shell	X-ray energy kev	Relative weight	Average energy kev
K_α	35.3	Pb(L)	49.0	10	
	25.1	Ag(K)	50.6	10	
	47.3	Ag(L)	50.5	10	
	23.0	In(K)	50.9	10	
	47.3	In(L)	50.7	10	50.3
K_β	42.3	Pb(L)	56.0	3	
	32.1	Ag(K)	57.6	5	
	54.5	Ag(L)	57.7	3	
	29.8	In(K)	57.7	5	
	54.5	In(L)	57.9	3	57.4

Superscripts (′) and (″) refer to channel or counter 1 and 2, respectively. Numeral subscripts refer to the transition as indicated in Tables I and II. Subscript "d" indicates a coincidence counting rate with the pulse in channel 2 delayed.

Subscript "c" indicates a coincidence counting rate with no delay.

t_d = time in microseconds that pulse was delayed in channel 2.

$t_\frac{1}{2} = 0.693/\lambda$ = half-life of metastable state in microseconds.

e = an electron component (internal conversion or Auger electrons).

q = a photon component.

α = a gamma-ray conversion coefficient $= e/q$.

n = number of transitions or disintegrations per unit time.

C = a counting rate.

E = a counter efficiency for detecting a radiation particle or photon emitted by the sample.

Preceding radiation = the radiation which precedes the metastable state.

Delayed radiation = radiation which follows the metastable state.

Parallel radiation = radiation from disintegrations which do not pass through the metastable state.

Accidental coincidences are obtained due to the finite gates and would normally be given by:

$$\text{Accidental rate} = (\tau' + \tau'')C'C''. \quad (1)$$

Experimentally determined accidental rates obtained by the use of separated samples for various permutations of the gate widths gave good agreement with values of τ' and τ'' read from the synchroscope. When necessary, the accidentals for delayed counts were computed as indicated by DeBenedetti and McGowan[4] to correct for accidentals missed because of true coincidences. The computed accidental coincidence rate together with the coincidence background, determined for the various counter arrangements employed, were subtracted from each coincidence count also.

TABLE III. Approximate relative intensities of the gamma-rays and internal conversion electrons from Yb^{169}.

Gamma-ray	q_i/q_9	e_i/e_9
2	1.3	
4	2.1	4
6	2.0	0.4
9	1.0	1.0
10	1.7	0.8
11	0.6	0.03
K_α x-ray	9.8*	

* Average from the $K_\alpha(L)$ photoelectrons in silver and in lead.

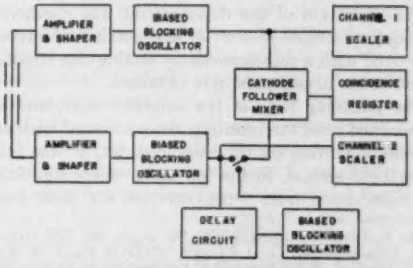

FIG. 7. Block diagram of coincidence circuit.

[12] L. H. Gray, Proc. Cambridge Phil. Soc. **27**, 103 (1931).

[13] W. Heitler, *The Quantum Theory of Radiations* (Oxford University Press, New York, 1944), second edition, p. 219.

[14] R. W. Watts, Manhattan District Report MDDC 741 (unpublished).

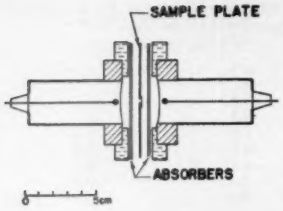

FIG. 8. Coincidence counter arrangement.

The counter arrangement is shown to scale in Fig. 8. Each counter was supported in a Lucite mount so that absorbers could be inserted between the counter and sample in a manner very similar to the conditions under which the absorption curves in Figs. 1–3 were obtained. The sample was prepared by evaporation of a small drop of $YbCl_3$ solution on mica of about 1 to 2 mg/cm² thickness. The mica was supported on a brass plate $\frac{1}{16}$ inch thick, directly in front of a hole with a 3-mm diameter. The bare sample faced counter 1. The brass plate was found necessary to minimize the scattered radiation which passed from one counter to the other. Its effectiveness in preventing this was evidenced by an experiment in which an equilibrium $Sr^{90}-Y^{90}$ sample was counted in this arrangement. Each of these isotopes decays by β^- emission without a gamma.[16] The ratio of coincidences to individual counts obtained was $C_c/C''=1.2\times10^{-3}$. A quantity of this magnitude could be expected to result from coincidence of bremsstrahlung radiation with electrons and is very small compared with the measured $(e-e)_c$ coincidence rates observed with the Yb^{169} samples.

The counter arrangement gave the maximum geometry possible for each counter with a nearly symmetric arrangement and permitted the use of absorbers under the nearly standard conditions of radiochemists for analyzing the radiation counted. Attainment of maximum counting efficiency is of considerable importance since coincidence counting rates are usually low, and long times are required to get results of statistical significance. In general, individual counting rates were maintained less than 7000 counts/min to avoid rapid deterioration of the counter tubes and eliminate excessive losses due to counter dead times which were estimated to be about 250 microseconds.

The operation of the delay circuit was checked by counting a sample of Co^{60} of the maximum intensity employed with a minimum delay setting. No counts in excess of the accidentals were obtained.

The resolving time of the coincidence register was determined from the counting losses incurred with each channel operating on the same counter. It was found to be 0.093 second. In the few cases where significant, the coincidence rates were corrected for these losses. However, intensities were always used so that such corrections were not greater than 5 to 6 percent.

It has been assumed in the treatment that the efficiency of the counters can be separated into factors in the manner:

$$E_i=\omega A_i\epsilon_i, \tag{2}$$

where ϵ is the intrinsic efficiency for counting a particular radiation which penetrates the counter, A is the absorption (and scattering) factor of absorber material placed between the sample and counter, and ω is the effective solid angle or geometry factor. Such a treatment is believed to be valid within the low accuracy of the coincidence measurements resulting from statistical fluctuations. ϵ is very nearly equal to one for an electron penetrating the G-M counter window. ϵ for photons of low energy (<0.5 Mev) is of the order of 10^{-3} to 10^{-2}, but reliable values have not been satisfactorily determined for energies of interest, i.e., 7 to 300 kev. Values of ω' and ω'' were determined with samples of Co^{60} and Au^{198}. For example, ω' was obtained from the coincidence counting rate between electrons and photons measured when the aluminum absorber before counter 2 was sufficient to stop all electrons. A small correction was necessary for the $(q-q)_e$ coincidence rate. Thus, for both the Co^{60} and Au^{198}

$$\omega'=\lim_{A'\to1}(e'-q'')_c/q''=0.115, \tag{3}$$

Since ω' was the largest possible efficiency for the detection of any radiation particles in counter 1, the losses in counting rates caused by two radiation particles from the same disintegration passing through the same counter were small. Similarly, ω'' was found to be 0.135.

With the conventional mica window counters employed, the air-window equivalent for counter 1 amounted to an absorber thickness 3.5 to 4.0 mg/cm². For counter 2 it was 4.5 to 5.5 because of the additional mica sample mount. Of the major peaks shown in Fig. 4 the Auger electrons, e_z, and the conversion electrons e_{4K} and e_{8K}, were certainly not counted, since effective counting efficiencies for these windows would be obtained only for energies greater than 80 kev. Higher energy electrons including the e_{4L} were counted effectively. Apparently, the greatest contribution to the counting rate was the e_{9K} and e_{10K}. This discrimination against the e_{4K} and e_{8K} proved very useful for the interpretation of coincidence data.

B. Decay Period of the Metastable State

The $(e-e)_d$ coincidence rate was measured over the maximum delay time range possible with the equipment. If $(e-e)_{d-obs}$ represents the observed number of delay counts which occurred per unit time with a particular setting of the instrument, the total delay coincidence rate $(e-e)_{d-tot}$ would be defined in the

[16] L. E. Glendenin, NNES-PPR **9B**, Paper No. 7.11.2 (1946); L. E. Glendenin and C. D. Coryell, NNES **9**, Paper 78 (1950). [Reported in G. T. Seaborg and I. Perlman, Revs. Modern Phys. **20**, 585 (1948).]

equation:

$$(e-e)_{d-\omega\omega}=(e-e)_{d-\omega\omega}\lambda\int_{t_d-\tau'}^{t_d+\tau''}e^{-\lambda t}dt$$

$$=(e-e)_{d-\omega\omega}[e^{\lambda\tau'}-e^{-\lambda\tau''}]\exp(-\lambda t_d). \quad (4)$$

Thus for constant gates the observed counting rate decreases exponentially with delay time. The experimental curve is shown in Fig. 9. Individual times could certainly not be measured with an accuracy of better than ± 0.1 μsec. A least squares treatment gives a half-life of 0.67 μsec. The half-life depends upon only the slope of the curve and is therefore independent of the time required to trigger the sweep of the synchroscope. This value does appear to be significantly lower than the 1.0 μsec of DeBenedetti and McGowan.[4] In a recent progress report McGowan[16] has indicated a half-life of 0.75 μsec, presumably determined by means of scintillation counters and delay-line techniques. This revised half-life is certainly in satisfactory agreement with our value.

C. Coincidence Absorption Curves

The coincidence counting rate with no delay was measured with no absorber before counter 1 and various aluminum absorbers before counter 2. Results have been plotted in Fig. 10. With no absorber before either counter the main contribution is due to $(e-e)$ coincidences. With 225 mg Al/cm² before counter 2, the count is due to the $(e'-q'')_e$, of which the largest component is $(e'-q_K'')_e$. For the curve in Fig. 10 giving $(e-e)_e$ it was necessary to subtract the estimated $(e'-q'')_e+(q'-e'')_e$ contributions from the coincidence rate. This component for no absorber was estimated to be four times the $(e'-q'')_e$ rate for the 225-mg Al/cm² absorber, since it contains the $(q_K'-e'')_e$, the $(e'-q''_L)_e$,

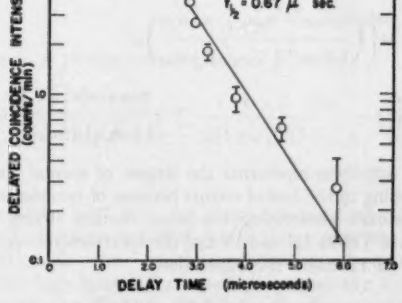

FIG. 9. Decay curve of metastable state in Tm^{169}.

[16] F. K. McGowan, AEC Report ORNL 694, p. 20 (1950), unpublished.

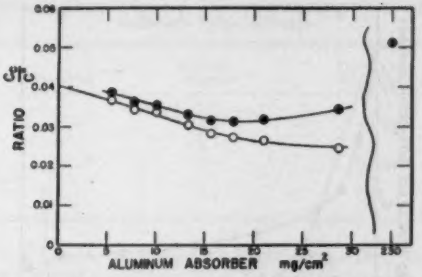

FIG. 10. Aluminum absorption curve for immediate coincidences. ● Total counting rate. ○ Electron component only.

and $(q_L'-e'')_e$, all of about equal magnitude. For intermediate absorbers the $(q_K'-e'')_e$ and $(q_L'-e'')_e$ components were assumed to be proportional to e'' and the $(e'-q_L'')_e$ fraction proportional to the absorption factor for the L x-ray calculated with an 11.8-mg/cm² half-thickness. For the channel gates employed, about one-half of the total delays were counted with the immediate coincidences. It was shown in the subsequent experiment that the contribution of delays to the $(e-e)_e$ coincidence was about 5 percent. However, a large fraction of $(e'-q'')_e$ was actually due to delays between preceding radiation including the original K x-ray accompanying the orbital capture and the conversion electrons following the metastable state.

Coincidence counting rates were also obtained with the pulses on the No. 2 channel fed through the minimum setting of the delay circuit. With the gates used, delays between 0.99 and 3.52 μsec were counted which would mean that on the basis of the 0.67-μsec half-life, 33 percent of the total delays were counted. The absorption curves obtained in these experiments are shown in Fig. 11. Thus, the curve with the absorber before counter 1 represents the absorption characteristics of the delayed radiation, and the curve with the absorber in front of counter 2 represents the absorption characteristics of the preceding radiation.

IV. DECAY SCHEME

Attempts to describe a decay scheme for the principal modes of decay of Yb^{169} which are quantitatively consistent with the intensities from the spectrometer and the coincidence counting rates have been only partially successful. A number of features, however, have been definitely established and are included in the following. Certainly transitions 1, 3, 5, 7, or 8 could not have offered appreciable contributions to the counting rates. The low intensity transition 11 would have been important with thick absorbers, since it was the hardest component. Several qualitative features of the decay scheme are indicated by the coincidence counting rates.

First, the $(e-e)_e/e''$ ratio, illustrated in Fig. 10, is 0.040 when extrapolated to zero window thickness. A comparison with the value of 0.115 for ω' indicates that

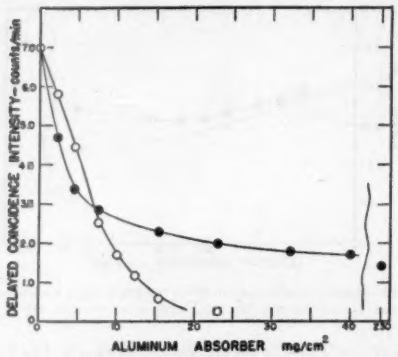

FIG. 11. Aluminum absorption curve for delayed coincidences. ○ Absorber before counter 1-delayed radiation component. ● Absorber before counter 2-immediate radiation component.

most of the electrons counted must be associated with two or possibly more highly internally converted transitions which are in immediate cascade, i.e., which are not separated by the metastable state. Since only L electrons were counted for transitions 4 and 6, it follows that the 9 and 10 electrons must be the ones which are in immediate cascade. The negative slope of the $(\epsilon-e)_c/\epsilon''$ ratio with absorber thickness appears to be real. The very high electron–electron coincidence rate appears to eliminate the decay scheme proposed by Cork *et al.*,[3] in which alternative cascades of 9 and 6, 10 and 4, or 11 can occur, although the energies of each path are within the precision of the spectrometer.

The difference in the absorption curves of the preceding and delayed radiation is also important. Thus, the delayed radiation is essentially an electron component with absorption characteristics similar to those of the total radiation. A thickness of 20 mg Al/cm² sufficed to reduce the delayed radiation nearly to zero. On the other hand, the delayed coincidence rate with 230 mg Al/cm² for the preceding radiation amounted to 20 percent of that for zero absorber, indicating a hard

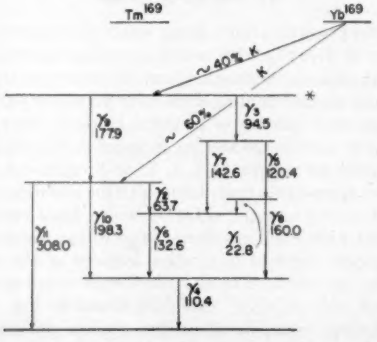

FIG. 12. Decay scheme A. The energies are given in kev.

component. This hard component consists of the gamma-ray photons and K x-rays associated with the orbital capture or the internal conversion process that might precede the metastable state. However, the electron component of the preceding radiation is softer than the total electron. Moreover, $C_{d-\text{tot}}/C''$ was 0.0040, indicating that the delayed cascade of counted conversion electrons was only about 5 percent of the immediate cascade. (With the gates employed, 0.5 of the delays were counted in the experiments of no delay.) A correction was therefore applied to the limiting value of the ratio:

$$\lim_{A''\to 1}(\epsilon-e)_c/\epsilon''=0.040-0.002=0.038.$$

The ratio obtained with 230 mg Al/cm² for $(\epsilon'-q'')_{d-\text{tot}}/q''$ was 0.051. Again this represents a very high value by comparison to ω' and indicates that most of the electrons counted must have followed the metastable state. It also makes the possibility of decay directly to the ground state of Tm^{169} appear very unlikely.

Decay scheme A, which is shown in Fig. 12, is consistent with the gamma-ray energies and intensities obtained from the spectrometer data as listed in Tables I and III. The branching ratios were estimated from the gamma-ray and conversion electron intensities with the aid of the L photoelectrons produced from the lead foil by the Tm K x-rays. Relative intensities per transition and some conversion coefficients based on these branching ratios have been included in Table IV.

This decay scheme agrees qualitatively with the conclusions given previously from the coincidence experiments. A further quantitative test was made by computing some coincidence counting ratios. In all the computations that follow, several terms contributing less than 5 percent to the counting rates have been omitted for simplicity. This is consistent with the accuracy of the coincidence data. Since only the L electrons of γ_4 were counted, the channel 2 electron counting rate extrapolated to zero window is given by

$$\lim_{A''\to 1}\epsilon''=\left[\left(\frac{n_4\alpha_{4L}}{1+\alpha_4}+\frac{n_9\alpha_9}{1+\alpha_9}+\frac{n_{10}\alpha_{10}}{1+\alpha_{10}}\right)\omega''-\frac{n_9\alpha_9\alpha_{10}(\omega'')^2}{(1+\alpha_9)(1+\alpha_{10})}\right]. \quad (5)$$

The last term represents the largest of several corresponding to the loss of counts because of two electrons in cascade penetrating the same counter. Using the data of Tables III and IV and the spectrometer e_{4K}/e_{4L} ratio of 12 makes this expression

$$\lim_{A''\to 1}\epsilon''=n_9\omega''(0.92-0.13\omega''). \quad (6)$$

The expression for the electron–electron coincidences is

given by

$$(\epsilon-\epsilon)_c=n_9\left[\frac{\alpha_9\alpha_{10}(E_9'E_{10}''+E_{10}'E_9'')}{(1+\alpha_9)(1+\alpha_{10})}+\frac{\alpha_9\alpha_{4L}(E_{4L}'E_9''+E_9'E_{4L}'')}{(1+\alpha_9)(1+\alpha_4)}+\frac{n_{10}\alpha_{10}\alpha_{4L}(E_{4L}'E_{10}''+E_{10}'E_{4L}'')}{n_9(1+\alpha_{10})(1+\alpha_4)}\right]. \quad (7)$$

With the counter efficiencies employed, coincidence losses caused by two cascade particles in the same counter can be ignored. Extrapolation to zero window for counter 2 yields:

$$\lim_{A''\to 1}(\epsilon-\epsilon)_c=n_9\omega'\omega''\left[\frac{\alpha_9\alpha_{10}(A_9'+A_{10}')}{(1+\alpha_9)(1+\alpha_{10})}+\frac{\alpha_9\alpha_{4L}(A_9'+A_{4L}')}{(1+\alpha_9)(1+\alpha_4)}+\frac{n_{10}\alpha_{10}\alpha_{4L}(A_{10}'+A_{4L}')}{(1+\alpha_{10})(1+\alpha_4)n_9}\right]. \quad (8)$$

A_{4L}', A_9' and A_{10}' were assumed to be 0.7, 0.75, and 0.75, respectively. With these the computed value of the ratio $(\epsilon-\epsilon)_c/\epsilon''$ is 0.031, which is in approximate agreement with the value 0.038 observed.

The coincidence rate for the preceding photons and delayed radiation $(\epsilon'-q'')_d$ was then computed. For this the counting efficiency for photons was assumed to be independent of energy and has been called E''_q. This assumption should not be too seriously in error, since theoretical calculations indicate that counter photon efficiencies pass through a minimum in the region of interest.[17] Thus,

$$(\epsilon'-q'')_{d-\text{tot}}=\frac{n_9\omega'E_9''}{(1+\alpha_x)}\left[\frac{\alpha_9A_9'}{(1+\alpha_9)}+\frac{0.4n_{10}\alpha_{10}A_{10}'}{(1+\alpha_{10})n_9}+\frac{0.4n_{11}\alpha_{11}A_{11}'}{(1+\alpha_{11})n_9}+\frac{(n_9-0.4n_{11})\alpha_{4L}A_{4L}'}{n_9(1+\alpha_4)}\right]=n_9E_q''0.046. \quad (9)$$

The total photon counting rate is given by:

$$q''=n_9E_q''\left\{\frac{(n_4+n_{11})}{n_9(1+\alpha_x)}+\sum_i\frac{n_i}{n_9(1+\alpha_i)}\left[\frac{\alpha_{iK}}{(1+\alpha_x)}+1\right]\right\}=n_9E_q''9.5. \quad (10)$$

The $(\epsilon'-q'')/q''$ ratio for decay scheme A should be equal, therefore, to 0.0048, which is in serious disagreement with the experimental value of 0.051.

The high intensity assigned to gamma-ray 4 from spectrometer data requires it to be a transition to the ground state. The high experimental value of $(\epsilon'-q'')_{d-\text{tot}}/q''$ is incompatible with such a high intensity for this transition. Since the samples used in the spectrometer must be considered as thick with regard to the low energy electron ranges, large and uncertain corrections were required in order to calculate intensities. Accordingly, decay scheme B shown in Fig. 13 was considered also. In this case, transition 4 was placed before the metastable state and could not have an intensity greater than n_9. Its intensity was assumed to be this maximum value; and, in addition, the intensity of n_9 from a visual comparison of the peaks in Figs. 4 and 5 was taken as 0.5 n_9. The metastable state was chosen as the one at 376 kev following transition 4 and preceding transition 9. It should be noted that these calculations used the spectrometer intensity ratios e_{10}/e_9 and q_{10}/q_9 which were known most accurately, since the transition energies are not greatly different. In addition, the quantities, $(e_i/e_9)(q_9/q_i)$, were used for estimating some of the conversion coefficients. However, in these terms the energy dependence should largely cancel. In this case the electron counting component is taken as

$$\lim_{A''\to 1}\epsilon''=n_9\omega''\left[\frac{\alpha_{10}n_{10}}{(1+\alpha_{10})n_9}+\frac{\alpha_9}{(1+\alpha_9)}+\frac{\alpha_{4L}}{(1+\alpha_4)}+\frac{0.5\alpha_9}{(1+\alpha_9)}\right]\sim 1.9n_9\omega''\alpha_9/(1+\alpha_9). \quad (11)$$

TABLE IV. Decay scheme A. Relative intensities and conversion coefficients for gamma-rays.

Gamma-ray	Relative intensity	Conversion coefficient
	$(e_i+q_i)/(e_9+q_9)$	α_i
4	3.0	1.6
6	1.3	0.2
9	1.0	0.8
10	1.3	0.4
11	0.4	0.04

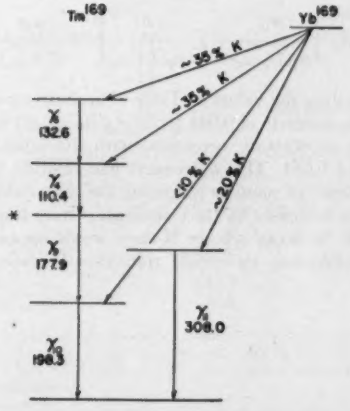

FIG. 13. Decay scheme B. The energies are given in kev.

[17] G. V. Drose, Z. Physik **101**, 474 (1937).

TABLE V. Decay scheme B. Relative intensities and conversion coefficients for gamma-rays.

Gamma-ray	Relative intensity	Conversion coefficient
	$(e_i+q_i)/(e_9+q_9)$	α_i
4	1.0*	3
6	0.5*	0.3
9	1.0	1.6
10	1.1	0.7
11	···	0.08

* Assumed values.

The electron–electron coincidence rate is

$$\lim_{A''\to 1}(e-e)_c=\frac{n_9\omega'\omega''\alpha_9\alpha_{10}(A_9'+A_{10}')}{(1+\alpha_9)(1+\alpha_{10})}. \quad (12)$$

From the experimental value of the ratio of $(e-e)_c/e''=0.038$ and the values of A_9', A_{10}', and ω' used previously, the value of $\alpha_{10}=0.7$ is obtained directly. Other conversion coefficients were computed from the data in Table III by means of the expression

$$\alpha_i=\alpha_{10}(e_i/e_{10})(q_{10}/q_i). \quad (13)$$

The results for decay scheme B are listed in Table V. The rate of the $(e'-q'')_{d-\text{tot}}$ coincidences can be computed from these values by the expression

$$(e'-q'')_{d-\text{tot}}=n_9E_q''\omega'\left[\frac{\alpha_9A_9'}{(1+\alpha_9)}+\frac{\alpha_{10}A_{10}'}{(1+\alpha_{10})}\right]\times\left\{\frac{1}{(1+\alpha_z)}+\frac{n_4}{n_9(1+\alpha_4)}\left[1+\frac{\alpha_{4K}}{1+\alpha_z}\right]+\frac{n_6}{n_9(1+\alpha_6)}\left[1+\frac{\alpha_{6K}}{(1+\alpha_z)}\right]\right\}. \quad (14)$$

The total observed photon count is given by

$$q''=n_9E_q''\left\{\frac{n_{10}}{n_9(1+\alpha_z)}+\sum_i\frac{n_i}{n_9(1+\alpha_i)}\left[1+\frac{\alpha_{iK}}{(1+\alpha_z)}\right]\right. \quad (15)$$

Substituting the values of Table V in these expressions gives an estimate of 0.048 for $(e'-q'')_{d-\text{tot}}/q''$, which is in very satisfactory agreement with the experimental value of 0.051. This agreement has resulted because the number of photons preceding the metastable state has been increased by the contribution from transitions 4 and 6. In decay scheme B there would appear to be no possible way to include transition 11 except as a separate branch for the orbital capture. A number of the other low intensity transitions will not fit into the B level scheme. It should be noted that scheme A employed all of the gamma-rays observed. It would be interesting to have these gamma-ray energies measured with a curved crystal spectrometer of high resolution as described by DuMond.[18] It would seem that contradictions between the results from the spectrometer and the coincidence experiments might be satisfactorily resolved by the use of a double beta-ray spectrometer with coincidence counting of the type described by Feather, Kyles and Pringle.[19]

In decay scheme B the metastable state decays by the emission of only one intense gamma-transition. The evidence indicates that this transition is most likely γ_9; however, the difference in intensities as indicated in Table V does not prevent the possibility of transition 10 preceding 9. The conversion coefficient of 1.6 for gamma 9 indicates that the radiation is probably magnetic 2^1 or 2^2 or electric 2^4.[20] The calculated ratios of e_K/e_L for magnetic 2^1 or 2^2 and electric 2^4 are 8, 7, and 0.3, respectively.[21] Hence, the radiation would not likely be electric 2^4. The calculated half-lives for magnetic dipole and quadrupole radiations with a conversion coefficient of 1.6 are 5.4×10^{-4} and 267 μsec, respectively, compared with our experimental value of 0.7 μsec.[22] This evidence indicates that magnetic quadrupole radiation is the most likely. With the conversion coefficient of α_{10} equal to 0.8, its radiation is probably magnetic dipole. In the reversed case in which gamma 10 precedes gamma 9 and would be the delayed transition, the γ_{10} half-life was calculated to be 174 μsec for magnetic quadrupole and 4.5×10^{-4} μsec for magnetic dipole.

For decay scheme A the metastable state must decay by three alternative transitions and the information for one of these is very incomplete.

The authors wish to express their appreciation to Dr. L. J. Laslett, Dr. W. W. Pratt, and Mr. G. O. Pickens for their assistance in obtaining part of the data, to Mr. E. R. Rathbun, Jr. for construction of the G-M counters used in the spectrometer, and to Mr. J. H. Jonte and Miss D. Christian for some of the chemical operations.

[18] J. W. M. DuMond, Rev. Sci. Instr. **18**, 626 (1947).
[19] Feather, Kyles, and Pringle, Proc. Phys. Soc. (London) **61**, 466 (1948).
[20] Rose, Goertzel, Spinard, Han, and Strong, tables distributed privately.
[21] M. H. Hebb and E. Nelson, Phys. Rev. **58**, 486 (1940).
[22] E. Segrè and A. C. Helmholtz, Revs. Modern Phys. **21**, 271 (1949).

The Scattering of Protons by Tritons

R. S. Claassen, R. J. S. Brown, G. D. Freier, and W. R. Stratton
Department of Physics, University of Minnesota, Minneapolis, Minnesota

(Received February 16, 1951)

The differential cross section for the scattering of protons by tritons has been measured in the angular range of 41.85° to 163° in the laboratory (54.7° to 168.7° in the center-of-mass system) at five energies between 2.54 and 3.50 Mev using protons from the Minnesota electrostatic generator. A small volume (42 cc) scattering chamber with an angular range of 17° to 163° was used for these measurements. Measurements of proton-proton and proton-helium cross sections and a comparison of the results with those obtained previously with a large scattering chamber showed that this small chamber gave results too high (about 3 percent) at the low scattering angles. These measurements determined a correction which was applied in the calculation of the p–T cross sections from the experimental data. The center-of-mass differential cross section varies between a maximum of 0.243×10^{-24} cm² per unit solid angle at 54.7° and 3.5 Mev and a minimum of 0.065×10^{-24} cm² per unit solid angle at 109.5° and 3.5 Mev in the angle and energy range studied. The cross sections considered as a function of angle display a strong minimum, near 100°, in the center-of-mass coordinate system. The cross section for a given angle is a slowly varying function of energy.

I. INTRODUCTION

A GREAT deal of the present theory of nuclear forces is based on quantitative information obtained from experiments in which a detailed study is made of the scattering of protons from light nuclei. The problem reported here is part of a general program of study of the matrix of interactions among all of the light nuclei. Careful work has been done on the measurement of the differential cross section for the scattering of protons by protons,[1–3] protons by deuterons,[4] and protons by helium.[5] While several authors have shown that the p–p data can be fitted by an S-wave phase shift analysis,[6–8] the p–d and p–He data require addition of states of higher angular momentum to account for the scattering from these nuclei of greater spatial extent.[9,10]

Hemmendinger, Jarvis, and Taschek[11,12] have adapted the techniques of scattering measurements to utilize small gas sample targets and have measured the cross section for the scattering of protons by tritons over the energy range available with the 2.5-Mev van de graaff generator at Los Alamos. Although the data obtained by them has not yet been analyzed by the phase shift method, it is apparent from their results that there is a strong nuclear interaction between the proton and triton, and, in particular, an interaction in states of angular momentum greater than zero. It was felt that it would be worthwhile to extend these measurements to the higher energy (3.5 Mev) available with the Minnesota generator and to lower and higher scattering angles, where the effects of the higher angular momentum states would be more pronounced.

II. APPARATUS

Figure 1 shows the essential features of the scattering chamber designed to utilize small gas samples as targets in the study of the angular distribution of the scattered particles and charged reaction products from nuclear collisions. This chamber is similar to the one used by Taschek *et al.*,[13] in that it is a nonplanar chamber; that is, the locus of directions at which scattering can be detected traces out a cone whose vertex is crossed by the incident beam of protons and whose axis is per-

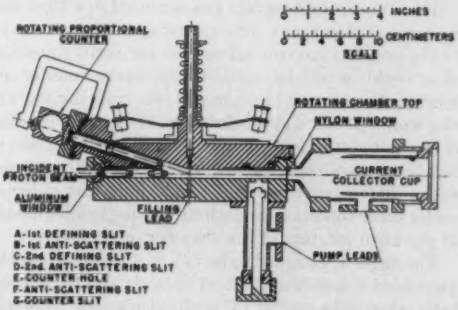

FIG. 1. View of the scattering chamber. The figure is of a plane through the center of the chamber and is drawn with the chamber set for a scattering angle of 163°, the maximum scattering angle for this chamber.

[1] Tuve, Heydenburg, and Hafstad, Phys. Rev. **50**, 806 (1936); Hafstad, Heydenburg, and Tuve, Phys. Rev. **53**, 239 (1938); Heydenburg, Hafstad, and Tuve, Phys. Rev. **56**, 1078 (1939).
[2] Herb, Kerst, Parkinson, and Plain, Phys. Rev. **55**, 998 (1939).
[3] Blair, Freier, Lampi, Sleator, and Williams, Phys. Rev. **74**, 553 (1948).
[4] Sherr, Blair, Kratz, Bailey, and Taschek, Phys. Rev. **72**, 662 (1947).
[5] Freier, Lampi, Sleator, and Williams, Phys. Rev. **75**, 1345 (1949).
[6] Breit, Condon, and Present, Phys. Rev. **50**, 825 (1936); Breit, Thaxton, and Eisenbud, Phys. Rev. **55**, 1018 (1939).
[7] C. L. Critchfield and D. C. Dodder, Phys. Rev. **75**, 419 (1949).
[8] J. D. Jackson and J. M. Blatt, Revs. Modern Phys. **22**, 77 (1950).
[9] C. L. Critchfield, Phys. Rev. **73**, 1 (1948).
[10] C. L. Critchfield and D. C. Dodder, Phys. Rev. **76**, 602 (1949).
[11] Taschek, Jarvis, Hemmendinger, Everhart, and Gittings, Phys. Rev. **75**, 1361 (1949).
[12] Hemmendinger, Jarvis, and Taschek, Phys. Rev. **76**, 1137 (1949).
[13] R. F. Taschek, Rev. Sci. Instr. **19**, 591 (1948).

pendicular to the incident beam. If ϕ denotes the angle of rotation about this axis, α is the angle of the cone, and θ is the desired scattering angle, then

$$\cos\theta = \sin\alpha \cos\phi \tag{1}$$

provided that the zero of ϕ is chosen at the minimum scattering angle.

The solid angle subtended by the counter and the scattering volume are defined by means of a counter slit and counter hole. To maintain good geometry it is necessary to rotate the counter-defining slits about the direction of scattered particles in such a manner that the length of the slit will be perpendicular to the plane formed by the incident and scattered beams. If ω is the angle of rotation of the counter slits, and is taken to be zero at the minimum scattering angle, then

$$\cos\omega = \frac{\cos\alpha \cos\phi}{(1-\sin^2\alpha \cos^2\phi)^{\frac{1}{2}}}. \tag{2}$$

The scattering chamber used in this work was constructed with $\alpha = 73°$. To obtain a given scattering angle θ, the angle ϕ was set to the nearest minute of arc by means of a vernier scale. The true zero for this scale was determined with the aid of mandrils and precision indicators. The angle ω was set to the nearest degree by means of an angular scale mounted on the arm holding the proportional counter.

The chamber was constructed of stainless steel. Figure 1 is a plane view of a section through the center of the chamber, drawn with the counter set at the maximum scattering angle. In order to provide accurate positioning of the upper piece as it was rotated with respect to the main body of the chamber, a circle, seven inches in diameter, of precision ball bearings was provided, running between hardened steel inserts. The side thrust of these bearings accurately centered the top piece as it rotated. The moving vacuum seal was made by a 4½-in. diameter "O" ring shown in solid black.

The counter-defining slit was mounted in a tube and is shown at G in Fig. 1. The mounting tube was coupled to the proportional counter so that the correct position of ω could be set by rotating the entire counter assembly. The moving vacuum seal was made by an "O" ring shown in black in the drawing. The correct position of the counter hole at E was determined by a set of ball bearings outside the "O" ring. The lightly greased rubber "O" rings were tight to a helium leak detector under static conditions and admitted a negligible amount of gas upon rotation of the chamber or counter.

The angle α, designed to be 73°, was measured on the assembled chamber and found to be $73° \pm 40''$, and has been taken to be exactly 73° in all calculations. Mandrils and traveling microscopes were used to make certain that the axis of rotation of the upper chamber passed through the center line of the incident beam hole.

The beam of protons traversing the chamber was defined by slits shown at A and C. The diameter of the hole at A was 0.1079 cm, of that at C, 0.1187 cm. These holes were 5.87 cm apart, allowing a divergence of 1.1° half-angle. The diameter of the defined beam at the exit window was 0.73 cm, and the diameter of the exit window was 0.95 cm. The holes at B (0.1185-cm diam) and at D (0.172-cm diam) prevented the majority of protons scattered from the slit edges from entering the scattering volume.

The counter slit system, which defined the solid angle subtended by the counter and the region from which particles could be scattered into the counter, consisted of a round hole of area A at a distance R from the center of the scattering region and a slit of width $2b$ at a distance $R-h$ from the center. (The hole is at E, the slit at G, in Fig. 1.) The slit width $2b$ was measured on a comparator and found to have an average value of 0.1752 cm, with a ½ percent variation over the length of the slit. The diameter of the hole as measured on the comparator was 0.3570 cm, giving an area of 0.1010 cm². The distances h and R were measured with the aid of mandrils and were found to be 10.038 and 13.670 cm, respectively. The above dimensions, which enter into the calculation of the cross section, are combined into a geometrical constant $G = 2bA/Rh$. The above values give $G = 1.278 \times 10^{-4}$ cm.

The beam of protons from the generator entered the scattering chamber through a 0.15-mil Al window and passed out the opposite side, through a 0.5-mil Nylon window, into a faraday cup. Loss of secondary electron charge from the cup was prevented by electrostatic bias and a transverse magnetic field. The charge collected during a run was stored on a polystyrene condenser. The condenser was discharged through a ballistic galvanometer at the end of a run. The galvanometer was calibrated in place with a L and N standard 0.50 microfarad condenser and a Wolff potentiometer. The calibration was checked periodically during the course of the experiment.

The particles which were scattered through the counter collimating slits and passed through the 0.15-mil Al counter window were detected by a proportional counter filled with an argon-methane mixture. The pulses from the counter were amplified by a preamplifier and amplifier of Los Alamos design[14] (Model 100) equipped with a delay line pulse shaper. The pulses were sorted according to size and counted by a 10-channel differential discriminator, also of Los Alamos design.[15] A slight change in design of the bias circuit made it possible to shift the position of the 5-volt channels in one-volt steps so that the distribution of counts with pulse height could be studied in greater detail. A sliding pulser was used to adjust for equal channel widths to within a few percent.

The presence of hydrogen contamination in the tritium necessiated dealing with a two component target gas system. Since exchange may take place

[14] W. C. Elmore and M. Sands, Electronics, 166 (1949).
[15] Reference 14, p. 241.

between the tritium and the hydrogen absorbed by the walls of the containing vessels, this experiment depended upon an ability to measure the tritium concentration in the chamber. The Los Alamos group has shown that it is possible to measure the hydrogen contamination in the course of the scattering experiment itself.[11,12] A proton suffering an elastic collision loses a fraction of its energy depending upon the angle of scattering and the mass of the scattering center. Since the size of the pulse from a proportional counter varies with the energy of the proton traversing it, it is possible to find an angle and energy at which protons scattered from atoms of different masses will be resolved. In the energy range of 2.5 to 3.5 Mev for the incident protons, scattering angles of 45 to 50 degrees gave good resolution of the two proton groups. Figure 2 shows the pulse distribution owing to protons scattered from tritium and from hydrogen contamination. This graph is a plot of five separate runs. After each run the voltage level of the discriminators was raised one volt, which shifted the center of each channel by one volt. The number of counts in each channel was normalized to unit total pressure and unit charge and was plotted at the voltage at the center of that channel.

Measurements were taken only at angles and energies where the particles passed completely through the counter or were stopped completely in the counter window. This assured a clearly defined pulse distribution. The pulses registered in the lower channels in Fig. 2 are from protons scattered from tritons. The second group of pulses arise from the protons scattered from proton contamination. For angles of 50 degrees or less and energies of 2.5 Mev or greater, the recoil tritons had sufficient energy to penetrate the counter window and pass through the counter. These recoil tritons gave rise to large pulses which were generally registered in the surplus channel of the differential discriminator.

From the number of counts in the proton–proton peak, the known geometry of the chamber, and the known p–p cross section,[2,3] the effective hydrogen pressure can be calculated. The remaining partial pressure is then that of the tritium.

The tritium gas was stored in the form of uranium hydride in a uranium furnace and transferred to the scattering chamber by a handling system of the type designed at Los Alamos.[11] Figure 3 is a schematic diagram of the handling system. The uranium was contained in a quartz envelope, while the rest of the system was constructed of Pyrex glass. A section of ¼-in. stainless steel tubing, maintained at approximately −35°C by a mechanical refrigerator, prevented the mercury vapor from entering the scattering chamber. The Toepler pump arrangement provided for efficient transfer of a small quantity of gas from the storage furnace to the chamber.

About five grams of uranium foil were used in the furnace. A pure deuterium sample stored in and

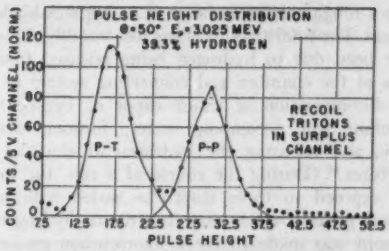

FIG. 2. Pulse-height distribution for protons of 3.03-Mev incident energy scattered at 50° from tritium contaminated with hydrogen. The number of counts per 5 volt channel has been normalized to unit charge and pressure and plotted at the voltage at the center of the channel. The pulses caused by recoil tritons were greater than 55 volts and were recorded in the surplus channel.

evolved from this furnace was analyzed for us on a mass spectrometer by Dr. A. O. C. Nier's group. It had acquired a negligible normal hydrogen impurity. Alternate use of the furnace for hydrogen and deuterium showed no "memory" of the previous gas.

The tritium was obtained from the Radioisotopes Division of the Atomic Energy Commision. Each sample provided sufficient gas to fill the scattering chamber to a pressure of 18 mm of Hg, the normal target pressure used in this experiment. During the course of the experiment, the concentration of hydrogen in the tritium sample rose steadily. This was not due primarily to exchange of tritium with hydrogen in the materials of the chamber, as was found by the Los Alamos group,[11]

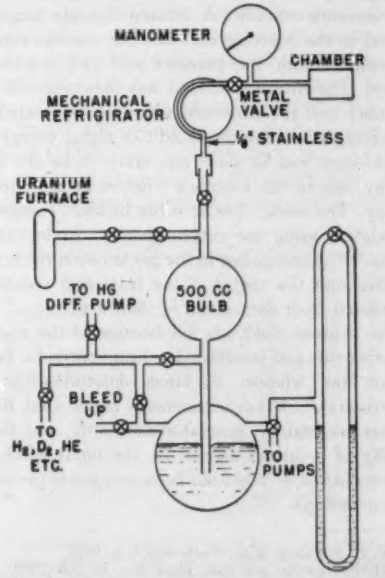

FIG. 3. A schematic diagram of the storage and handling system for the tritium gas.

since a rough calculation showed no appreciable loss of tritium. The total amount of gas rose steadily. This may have been due to hydrogen being released from the walls of the chamber and connecting system or from the decomposition of water vapor or hydrocarbons. Uranium will decompose water, forming uranium oxide, and releasing the hydrogen at elevated temperatures.[16] (During the course of a run, the furnace was exposed to three stopcocks sealed with hydrocarbon grease, which may contribute hydrogen. An attempt was made to use a fluorocarbon grease as a stopcock lubricant, but it proved impractical for vacuum work.)

When a tritium sample became diluted to less than 35 percent tritium, it was removed from the furnace and stored for other work, and a fresh sample was transferred to the furnace.

The pressure of the gas in the chamber was measured by means of a Wallace and Tiernan differential manometer, Model 191. The gauge was calibrated frequently against an oil manometer using Apiezon B oil. After the first weeks of use the calibration settled down and held constant to within 0.02 mm Hg. The gauge was altered for us by the Wallace and Tiernan Company to present only metal surfaces to the gas and was leak tight to a helium leak detector. This gauge proved to be rugged and satisfactory in every respect.

The voltage of the electrostatic generator was controlled and measured by an electrostatic analyzer. The known $Li^7(p,n)$ threshold[17] was used to calibrate the voltage scale and to measure the voltage thickness of the entrance window. A lithium fluoride target was placed in the collector cup and the neutron threshold determined with the entrance and exit windows removed. The entrance window was then replaced in the chamber and the threshold was again measured. The apparent shift of the threshold to a higher energy when the window was in place was taken to be the proton energy loss in the entrance window at the threshold energy. The energy loss at other incident energies was calculated, using the curves given in Livingston and Bethe.[18] The energy lost in the gas between the entrance window and the center of the scattering volume was calculated from data given in their article.[18]

The neutron yield was low because of the small collimating slits and resultant low beam currents. For this reason the window thickness determinations were uncertain by ± 10 kev in the energy region used. Because of this uncertainty, generator instability, and the possibility of a carbon deposit on the input window, an uncertainty of ± 25 kev has been assigned to the incident proton energy.

[16] F. H. Spedding, *et al.*, Nucleonics **4**, 4 (1949).
[17] Herb, Snowdon, and Sala, Phys. Rev. **75**, 246 (1949).
[18] M. S. Livingston and H. A. Bethe, Revs. Modern Phys. **9**, 270 (1937).

III. PROCEDURE

When not in use, the chamber was maintained at a vacuum of 3×10^{-6} mm of Hg or better by means of an oil diffusion pump and liquid air trap. A gas sample evolved from the uranium furnace into the chamber was used for about four hours, after which time it was returned to the uranium for purification.

Immediately after the chamber was filled, the concentration of the gas sample was determined by a run at 45° or 50°. The concentration determination was then used in the calculations for the runs taken with this filling at other angles where the p–p protons could not enter the counter or were not resolved from the p–t protons.

The cross section for scattering at the angle θ is given by

$$\sigma(\theta)=(Y\sin\theta)/(qNnG), \tag{3}$$

where Y is the number of protons counted for charge q, in microcoulombs, of protons which passed through the chamber. N is the number of protons in a microcoulomb, taken to be 6.025×10^{12}; n is the number of nuclei per cm^3 at the target temperature and pressure. (n was calculated by assuming that there are 6.023×10^{23} molecules in 22,412 cm^3 at S.T.P.) The geometry factor has been defined in Sec. II.

In a two-component target system, there will be a yield Y_1 associated with n_1 target nuclei per cm^3 (protons) and a yield Y_2 associated with n_2 target nuclei per cm^3 (tritons). Since $\sigma(\theta)$ is known for the first process, Eq. (3) may be solved for n_1. This, together with a measurement of the total pressure, determined n_2.

The cross section at each angle and energy was measured at least twice, once on each side of the chamber, to reduce any possible asymmetry and reduce the chance of gross errors. Whenever the agreement between measurements was poor, the cross section was remeasured.

IV. TESTING THE CHAMBER

The scattering chamber was checked against the published proton-proton results[2,3] and the proton-helium results.[5] In the process of testing and checking the performance of the chamber, it became apparent that the results were not valid at all angles and energies, the results being high at the lower scattering angles. As explained later, this was attributed to the small volume of the chamber and the resultant close spacing of the walls of the chamber to the incident beam and to the scattering region. Since the error at a given angle and energy was not the same for different nuclear processes, it was necessary to run check measurements over a range of angles and energies with several nuclear scattering processes whose cross sections were known accurately from previous researches.[2,3,5]

The various experimental quantities which enter into the calculation of the cross section, and which might introduce such an error as was found, were rechecked

in the course of this testing. The scattering angle θ was determined from the geometry of the chamber, the measurement of which has been described in Sec. II. Further, to account for the p–He results at 2.5 Mev and 30°, θ would have to be in error by 5° (θ too small), while to account for the p–p results at this angle and energy, θ would have to be in error by 12° (θ too small).

Coulomb scattering from gas impurities could lead to erroneous results at low angles. The helium was shown to have negligible impurity. To eliminate the possibility that Hg vapor from the loading system should contaminate the chamber gas, a liquid air trap was connected directly in front of the exit window. Successive runs with and without cooling of this trap gave the same results within the statistical errors.

At angles above 20°, direct scattering from metal surfaces into the counter contributed a negligible background, as shown by runs taken with the chamber open to the vacuum pumps.

Incorrect energy of the incident protons might give errors which increase with smaller angles and vary with the target gas. The energy of the incident protons was determined by the method described in Sec. II. Furthermore, since both the p–p and p–He cross sections considered as a function of energy have both positive and negative slopes in the energy range under investigation, it was possible to eliminate the possibility that incorrect energy, or an energy spread owing to non-uniform windows, is the sole source of our errors.

Second-order geometry corrections,[7] which account for the finite extent of the incident and scattered beams and the resultant spread in angles, amounted to 1 percent or less for angles of 30° or greater in the energy range investigated.

When the cross section of a single gas in the chamber was measured, the curve of the number of proportional counter pulses per voltage interval *versus* pulse height displayed a sharp peak with a long, low tail (see Fig. 4). It was found that, by extrapolating the sharp peak to the base line, consistent results could be obtained for the yield at a given angle and energy. The discarded tail contained from 4 to 7 percent of the yield in the angular range of 45 to 60 degrees and the energy range of 2 to 3.5 Mev.

The tail of the pulse-height curve (Fig. 4) was attributed to protons which had suffered successive collisions with a gas atom and with the metal of the chamber walls or slits, thereby losing more energy than the correctly scattered protons. At low angles this tail was more pronounced (see Fig. 5), and apparently extended back into the proper proton peak far enough to make the measured yield too high. One might expect that these spurious counts were caused by protons which suffered scattering in the gas at small angles where the cross section is high. Since the low angle cross sections for the scattering of protons from hydrogen and helium are quite different, it is not surprising that the error introduced by these spurious counts was

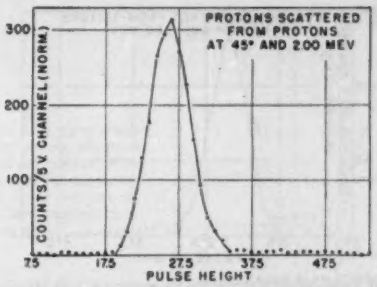

FIG. 4. Pulse-height distribution for protons of 2.00-Mev incident energy scattered at 45° from hydrogen. The number of counts per 5-volt channel has been normalized to unit charge and pressure and plotted at the voltage at the center of the channel.

different for p–p and p–He measurements. In the energy range of 2 to 3.5 Mev and the angular range of 45 to 60 degrees the measured p–p cross sections averaged 3 percent greater than the published values.[2,3] In this same energy and angle range the measured values of the p–He cross sections were 6 percent higher than those published.[6]

Because of the variation of error with target gas, and because the error introduced by this small chamber increased toward lower scattering angles, it was felt that an attempt to correct p–i data for measurements at angles below 40° would be unreliable.

V. CORRECTIONS OF THE DATA

Figure 4 is a plot of the number of pulses per channel *vs* the average pulse height for the protons scattered from protons at 45° and 2 Mev. A tail may be seen extending to the right of the peak. When measurements are made on a two-component gas system at certain angles and energies, the protons scattered from the lighter nuclei will register in the same channels as a portion of the tail from the lower peak. From measurements on pure hydrogen at several appropriate angles and over the energy range of interest here, the con-

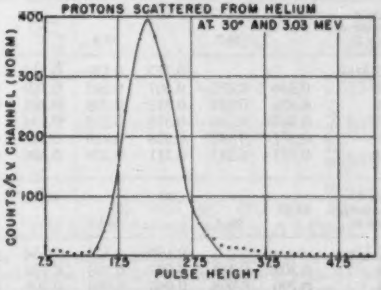

FIG. 5. Pulse-height distribution for protons of 3.03-Mev incident energy scattered at 30° from helium. The number of counts per 5-volt channel has been normalized to unit charge and pressure and plotted at the voltage at the center of the channel.

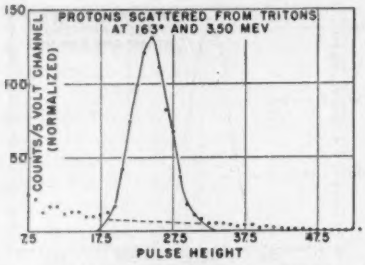

FIG. 6. Pulse-height distribution for protons of 3.50-Mev incident energy scattered at 163° from the tritons in a mixture of tritium and hydrogen. The number of pulses per 5-volt channel has been normalized to unit charge and unit total pressure and plotted at the voltage at the center of the channel.

tribution of the tail of the lower peak to the second peak was determined to be 4.7 percent of the number of counts in the first peak.

As a check on the reliability of the determination of the hydrogen content in a two-component gas target and the reliability of cross-section measurements on the second component using this concentration measurement, a large number of runs were taken on a H_2–He mixture. The majority of measurements were at 2.5 and 3.0 Mev and 50° and 55° scattering angle. For each run a plot was made of the number of counts per channel per unit pressure and charge *vs* the channel voltage. Calculations of the hydrogen content of the gas target and the p–He cross section were made from this graph in the following manner. The sides of the two peaks were extrapolated to zero and the area measured under each peak. Then 4.7 percent of the peak from p–He scattering was subtracted from the peak caused by p–p scattering. For the calculation of hydrogen concentration, 97 percent of the remaining number of counts in the second peak were used. This concentration, with the measured pressure, gave the partial helium pressure, which, with 94 percent of the counts in the first peak, were used to calculate the p–He cross section. The above treatment of the data gave an average value of the hydrogen concentration, which agreed to within 1 percent of the value determined by mass spectrometer means by Dr. Nier's group. For a given angle and energy of the average p–He cross section agreed with the value given by Freier, *et al.*, to well within the probable error quoted by then.[5] On the basis of this satisfactory check on the above method of calculating cross section from the data obtained with this small chamber, it was felt that it would be worthwhile to take observations on the cross section for scattering of protons by a gaseous target of tritium contaminated by hydrogen. The data could then be analyzed by using the methods established by the measurements, corrections, and comparisons described above.

All the data taken on the tritium-hydrogen mixture in the angular range of 40° to 60° were treated as described for the hydrogen-helium mixture, except that 97 percent of the counts in the tritium peak were used. It was felt that the behavior of protons scattered from tritium would follow p–p scattering more closely than p–He because of the similarity of the coulomb scattering in the two isotopes.

At higher angles, above 60°, the background caused by gamma-rays, machine noise, etc., contributed an appreciable amount to the number of pulses counted. Figure 6 is a plot of a typical pulse-height distribution for protons scattered from tritons at 163° and 3.5 Mev, where the background is highest because of the high energy and the close proximity of the counter to the input window, and slit systems, which are a source of gamma-rays. The general background which extends to either side of the peak has been extrapolated across the bottom of the peak, and this background has been subtracted from the number of pulses in the peak. At these higher angles the number of counts was not corrected

TABLE I. Differential scattering cross section for protons on tritium. The values listed under the laboratory angles are laboratory cross section, those under the center-of-mass angles are center-of-mass cross sections. All cross sections are in units of 10^{-24} cm² per unit solid angle.

Lab angle θ	41.85		45		50		60		50		71.5		45	
Recoil angle ϕ														
CM angle Ω		54.7		58.6		64.8		76.8		80		90		90
2.12 Mev			0.270	0.180	0.245	0.170					0.127	0.108		
2.54	0.356	0.232	0.307	0.205	0.269	0.187					0.126	0.107	0.304	0.108
2.74	0.356	0.232	0.312	0.208	0.281	0.195	0.170	0.129	0.296	0.115	0.120	0.102	0.290	0.103
3.03	0.368	0.240	0.318	0.212	0.274	0.190	0.186	0.141	0.318	0.124	0.109	0.093	0.274	0.097
3.25	0.371	0.242	0.328	0.219	0.265	0.184	0.171	0.130	0.296	0.115	0.104	0.089	0.273	0.097
3.50	0.373	0.243	0.311	0.208	0.266	0.184			0.292	0.114	0.103	0.088	0.238	0.084

Lab angle θ	41.85		90		106.6		27.4		120		140		163	
Recoil angle ϕ														
CM angle Ω		96.3		109.5		125		125		136.18		152.4		168.7
2.12 Mev			0.120	0.127	0.134	0.175	0.627	0.177	0.139	0.213				
2.54	0.302	0.101	0.097	0.103	0.106	0.137	0.500	0.141	0.115	0.176	0.127	0.239		
2.74	0.290	0.098	0.088	0.094	0.107	0.159	0.459	0.129	0.114	0.174	0.116	0.218	0.108	0.241
3.03	0.274	0.092	0.080	0.085	0.082	0.107	0.376	0.106	0.091	0.140	0.099	0.186	0.099	0.221
3.25	0.238	0.080	0.071	0.076	0.077	0.099	0.355	0.100	0.088	0.135	0.101	0.190	0.097	0.216
3.50	0.220	0.074	0.061	0.065	0.070	0.091	0.324	0.091	0.078	0.120	0.085	0.160	0.091	0.203

downward by 3 percent as was done at the lower angles. Several measurements made on p–He scattering at high angles, and corrected for background in the manner just described, were in good agreement with the published values.[8]

There are two internal constency checks on these corrections. First, measurements of the p–t cross section at a given angle and energy, using targets with widely varying hydrogen impurity, showed no consistent variation with hydrogen contamination. Second, the center-of-mass cross section for the scattering of protons by tritium could be measured for a range of scattering angles by counting the recoil tritons. In the calculation of cross sections from the recoil data obtained from this small chamber, the full number of recoil counts was

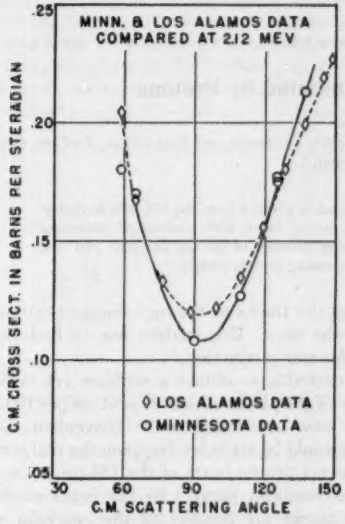

FIG. 7. A comparison of the results obtained at Los Alamos and Minnesota for the center-of-mass cross section at 2.11-Mev incident proton energy.

used. Center-of-mass cross section calculated from observations on the recoil tritons agreed well with those calculated directly from measurements on protons.

VI. EXPERIMENTAL RESULTS

All the data have been treated in the manner described in the section on corrections, and cross sections computed according to the formula in Sec. III. The laboratory cross sections for both the scattered protons and recoil tritons, as well as the center-of-mass cross sections calculated from them, are listed in Table I. The probable error estimated for the measurement of charge was ± 1 percent. The pressure and geometry factor measurements were good to $\pm \frac{1}{2}$ percent. Other contributions to error in the calculated cross section arose from the measurement of the hydrogen contamination, estimated to be good to ± 1 percent, the 3 percent correction for the chamber characteristics, and the correction for background at high scattering angles. For these reasons we have estimated a probable error of ± 5 percent for the results listed.

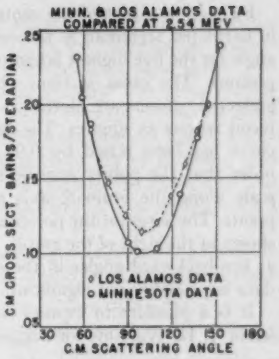

FIG. 8. A comparison of the results obtained at Los Alamos and Minnesota for the center-of-mass cross section at 2.54-Mev incident proton energy.

Figures 7 and 8 are comparisons of the center-of-mass cross sections obtained in this experiment with those obtained by the Los Alamos group[12] at incident proton energies of 2.11 Mev and 2.54 Mev. The center-of-mass cross section in barns per steradian is plotted against the center-of-mass scattering angle. The agreement between the two sets of data is good at both high and low scattering angles. In the region of minimum cross section, at approximately 100° scattering angle, the results of this experiment are approximately 10 percent lower than those of the earlier experiment. This difference is the sum of the estimated probable errors for the two experiments.

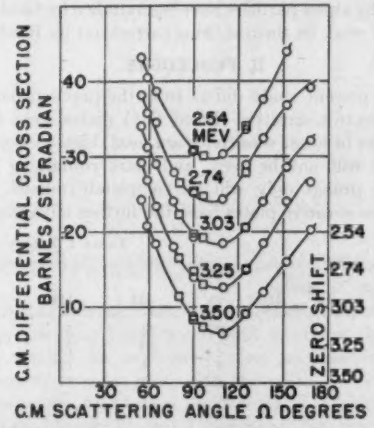

FIG. 9. The center-of-mass cross section in barns per steradian plotted against the center-of-mass scattering angle for the incident proton energies indicated. The cross sections obtained by counting scattered protons are plotted as circles, those from the recoil tritons as squares. The ordinate for each higher curve has been raised by 0.05 barn per steradian. The zeros for the various curves are indicated at the right.

Figure 9 is a plot of the center-of-mass cross section in barns per steradian *vs* the center-of-mass scattering angle for the five highest laboratory energies of incident protons. The cross sections obtained from counting scattered protons are plotted as circles, those from the recoil tritons as squares. The ordinate for each higher curve has been raised by 0.05 barn per steradian in order that the points may be seen more clearly. The scale along the ordinate axis refers to the 3.50-Mev points. The zeros for the points at the lower energies are shown at the right of the graph. The negative curvature at the backward angles in the curve for the 2.74-Mev data is probably not significant.

It is a pleasure to express our appreciation to Professor J. H. Williams for suggesting this problem and for his advice throughout the course of this work. We should also like to thank the other members of the van de graaff group, Dr. G. R. Keepin, Dr. J. M. Blair, and Messrs. M. Fulk, T. F. Stratton, and J. L. Yarnell for their help in taking data. Mr. Rudolph Thorness made significant contributions to the design of the scattering chamber.

This research was done under the partial support of the Office of Naval Research. It was also materially assisted by the University of Minnesota Technical Research Fund subscribed to by General Mills, Inc., Minnespolis Honeywell Regulator Company, Minneapolis Star Journal and Tribune Company, Minnesota Mining and Manufacturing Company, and Northern States Power Company.

PHYSICAL REVIEW VOLUME 82, NUMBER 5 JUNE 1, 1951

Stars in Photographic Emulsions Initiated by Protons

LAWRENCE S. GERMAIN
Radiation Laboratory, Department of Physics, University of California, Berkeley, California, and Reed College, Portland, Oregon
(Received November 24, 1950)

A study has been made of stars in photographic emulsions initiated by protons from the 184-inch Berkeley cyclotron. Ilford G-5 emulsions were exposed to the deflected proton beam with various Al absorbers interposed to obtain protons of various energies. Both the average number of prongs per star and the cross section for star production were found to increase with increasing proton energy.

I. INTRODUCTION

A STUDY has been made of stars in photographic emulsions initiated by protons from the 184-inch Berkeley cyclotron. Stars initiated by deuterons have been studied by Gardner and Peterson,[1] while stars initiated by alpha-particles have been studied by Gardner;[2] further work on them is being carried out by Bowker.

II. PROCEDURE

The present study differs from the previous ones in that electron-sensitive (Ilford G-5) plates were used. If plates of lower sensitivity are used, high energy star prongs will not be seen, and stars containing high energy prongs only will be completely missed. The electron-sensitive plates have the further advantage of recording the tracks of the high energy protons which initiate the stars. This enables one to find the cross section for star production.

It is desirable to obtain a uniform yet fairly light exposure of the plates. About 20 protons per 100-micron field of view was found to be convenient. Such an exposure could be made by dropping the plates through the deflected proton beam of the 184-proton cyclotron with the emulsion parallel to the beam so that the protons tracks are parallel to the emulsion surface. Although the energy of protons in the deflected beam is about 345 Mev, energies as low as 95 Mev were obtained by placing Al absorbers in front of the plates. The proper thicknesses of Al were calculated from the data on the range of protons in Al given by Smith.[3]

TABLE I. Energy distribution of prongs from stars.

Number of prongs \ Energy (Mev)	95	115	135	155	175	195	220	245	295	340
2	18	24	57	43	46	47	55	22	18	34
3	5	20	27	62	43	41	59	29	30	72
4	6	4	21	34	32	32	45	33	25	56
5	2	4	11	18	12	16	28	22	24	50
6	—	1	2	2	4	2	4	2	6	23
7	—	—	—	1	—	—	1	4	4	3
8	—	—	—	—	—	—	—	—	—	2
Total	31	53	118	160	137	138	191	112	107	240
Length of track (m)	50.0	60.4	112.3	179.6	144.7	149.0	169.8	90.6	80.6	175.0

[1] E. Gardner and V. Peterson, Phys. Rev. **75**, 364 (1949).
[2] E. Gardner, Phys. Rev. **75**, 376 (1949).
[3] J. H. Smith, Phys. Rev. **71**, 32 (1947).

The plates were scanned with a magnification of 450 and the position and number of prongs recorded for all stars of two or more prongs. It was felt that one-prong stars could not be unambiguously distinguished from random single track background. The results are summarized in Table I.

A plot of the average number of star prongs as a function of proton energy is given in Fig. 1. The vertical extent of the blocks is the standard error owing to the limited number of events. The horizontal extent of the blocks is an estimate of the energy spread of the protons used. The energy spread is due to three causes: the energy spread of the proton beam, the straggling in energy loss in the Al absorbers, and the energy loss in that part of the plate scanned. Three Mev appears to be a good estimate of the half-width of the energy spread of the deflected proton beam. The straggling of energy loss in the Al absorbers was calculated with the aid of formulas given by Livingston and Bethe[4] and was found to amount to only about 2 Mev for the thickest absorber used. The half-width of energy spread

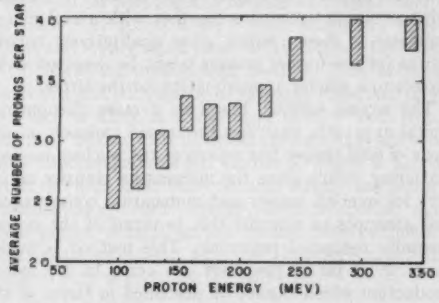

FIG. 1. Plot of average number of star prongs vs proton energy.

because of energy loss in the plate was limited to about 4 Mev. This was accomplished at the expense of scanning smaller areas at the lower energies. From these figures it would appear that 10 Mev is a fair estimate of the energy spread of the protons for all the energies examined.

The number of stars divided by the total length of proton track gives the mean free path for the production of stars of two or more prongs. The total length of proton track was found by counting track sections in a field of view in sample areas. The number of sections multiplied by the diameter of the field of view gives the total length of track in that sample area. About 100 sample areas were examined on each plate. The cross section can be found from the mean free path with the aid of data on the composition of the emulsion given by Ilford. These data are shown in Table II.

The number of atoms per cm³ of emulsion excluding the H was used to calculate the cross section. A proton colliding with a H atom would give proton-proton scattering rather than a star. A few examples of proton-proton scattering were found and were easily distinguished from two-pronged stars. The cross section per atom for the production of stars of two or more prongs is shown as a function of energy in Fig. 2. Scales showing the mean free path in cm of emulsion and g/cm² of emulsion are also given. The horizontal and vertical extent of the blocks have the same significance as they had previously.

These cross sections are in good agreement with those found for alpha-particles by Gardner.[3] Gardner's cross

TABLE II. Composition of Ilford G-5 emulsions.

	Density (g/cm³)	Molal fraction/cm³
Total	3.907	0.1345
Total excluding H	3.851	0.0789

section vs energy curve showed a maximum of nearly 0.3 barn, at an alpha-particle energy of about 150 Mev, and fell off to about 0.2 barn at the maximum energy used, 200 Mev. This decrease of cross section with increase of energy may be due to the fact that Gardner used Eastman NTA emulsions for his study. These plates are less sensitive and would not record stars which had no low energy prongs. Such a star is more likely to be produced at higher energies of the bombarding particle.

At the highest energy studied, the mean free path found in this work is about twice the value of the mean

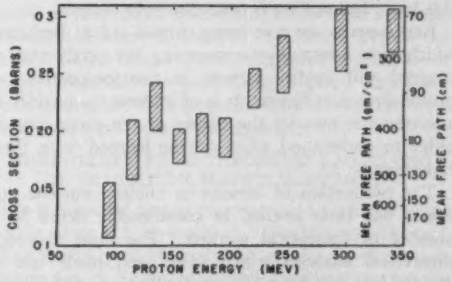

FIG. 2. Plot of cross section per atom for production of stars of 2 or more prongs vs proton energy.

free path of primary cosmic rays, presumably very high energy protons. Thus, one is lead to expect that the cross section for star production will continue to increase at energies above 350 Mev.

The author is indebted to Professor E. O. Lawrence and the Atomic Energy Commission for the use of facilities at the Radiation Laboratory. Many helpful discussions with Dr. Eugene Gardner, Dr. Hugh Bradner, and Dr. W. H. Barkas greatly facilitated the study. The work done at Reed College was assisted by a Cottrell grant from the Research Corporation.

[4] M. S. Livingston and H. A. Bethe, Revs. Modern Phys. 9, 245 (1937).

Production of π-Mesons in Nucleon-Nucleon Collisions

KEITH BRUECKNER*
Radiation Laboratory, University of California, Berkeley, California
(Received October 16, 1950)

The production of π-mesons in nucleon-nucleon collisions as predicted by scalar meson theory, pseudoscalar meson theory with pseudoscalar and pseudovector coupling, and vector theory with vector coupling is compared with the experimental results of the workers at Berkeley. The calculations are made on the basis of third-order perturbation theory using the methods of Feynman and Dyson and also using a phenomenological treatment of the nucleon-nucleon interaction. Account is taken of the fact that the final nucleons are not in plane wave states. It is shown that pseudoscalar theory with pseudovector coupling gives qualitative agreement with experiment.

I. INTRODUCTION

A PROBLEM of considerable interest in meson theory is the production of mesons in nucleon-nucleon collisions. The intimate connection, predicted by meson theory, between this process and ordinary nucleon-nucleon scattering provides an excellent and basic opportunity for testing the fundamental assumptions of meson theory. The meson theory of nuclear forces assumes that π-mesons, found to interact strongly with nuclei, are responsible for the coupling between nucleons. Since this coupling via the meson field implies the existence of virtual mesons in the mutual field of two nucleons, it should be possible, if sufficient energy is available, for virtual mesons to be materialized as free and observable particles. A comparison of the predictions of the theory with the experimental measurements of nucleon-nucleon scattering and of meson production should indicate whether this basic assumption is quantitatively correct.

Experiments are now being carried out at Berkeley[1] which give information concerning the production of charged and neutral mesons in neutron-proton and proton-proton collisions. It is of interest to consider in a systematic manner the theory of the production in order to understand what can be learned from these experiments.

The production of mesons in nucleon–nucleon collisions has been studied in considerable detail by a number of theoretical workers.[2] The most thorough theoretical analyses which have been made can be divided into two types: (1) an application of the meson field theory of nuclear forces to the problem considered as a third-order process, and (2) an attempt to describe phenomenologically the scattering of the nucleons associated with the meson emission, and only the meson emission itself, by meson field theory. The first method suffers from the well-known failure of meson theory to describe nuclear forces in more than a qualitative way and from the more general failure of perturbation theory in the weak coupling approximation applied to problems in which the coupling is not weak. This method can, however, be applied rigorously in the lowest order and with this limitation gives a logically complete description of the process. Also, because of the close relation between high energy nucleon-nucleon scattering (virtual meson exchanges) and meson production (virtual meson exchanges together with a real meson emission), a theory which gives qualitatively correct results for the former process might be expected to be correct to a similar approximation for the latter.

The second method, based on a more phenomenological approach, describes the meson emission on the basis of field theory but separates the nucleon-nucleon scattering, which gives the momentum transfer necessary for over-all energy and momentum conservation, and attempts to describe this in terms of the experimentally measured potentials. This method is inadequate in as far as processes can occur in the meson production which cannot be described in terms of the scattering process preceded or followed by meson emission. Such processes are, for example, the interruption of a virtual meson exchange by a real meson emission. These processes are equivalent to scatterings which take place far off the energy shell, i.e., where energy and momentum are related very differently from the relationship for free particles. Only if such processes give unimportant contributions can the phenomenological approach be approximately correct. However, if this assumption is made, the calculation can be made in a manner much more independent of meson field theory than is the third-order perturbation calculation.

The rigorous treatment of meson production as a third-order process is complicated by mathematical difficulties in the integration of the cross sections over the momenta of the final nucleons to give a result which depends only on the meson momentum. This problem has been partially solved by Morette[3] for pseudoscalar mesons with pseudoscalar coupling; Morette, however, ignored the effects of the Pauli principle and so introduced a rather large error (about 50 percent) in the cross section near threshold. Her expressions for the cross sections also have been averaged over meson and

* Now at Institute for Advanced Study, Princeton, New Jersey.
[1] C. Richman and H. Wilcox, Phys. Rev. **78**, 85(A) (1950). Bjorklund, Crandall, Moyer, and York, Phys. Rev. **77**, 213 (1950). Cartwright, Richman, Whitehead, and Wilcox, Phys. Rev. **78**, 823 (1950). V. Z. Peterson, Ph.D. thesis, U. of Calif., 1950. W. Cartwright and M. Whitehead, private communication.
[2] For references, see Cecile Morette, Phys. Rev. **76**, 1432 (1949).

nucleon charges and, therefore, do not give separately the cross sections for charged and neutral mesons for neutron-proton and proton-proton collisions. Since these separate quantities are those which can be determined experimentally, it is of interest to calculate them. Therefore, we have in Sec. II considered the calculation of the transition matrix elements on the basis of rigorous third-order perturbation theory and obtained the expressions for scalar theory, pseudoscalar theory with pseudoscalar, and pseudovector theory with vector coupling. The calculations are made in the center-of-mass system for energies near threshold, where the velocities of the final particles are small. Corrections of the order of v^2/c^2 for the final nucleons and mesons are neglected, so the results are only applicable for incident nucleon energies of 350 to 400 Mev, corresponding to maximum meson energies in the center-of-mass system of 23 to 44 Mev.

The second method of calculation, treating the nucleon-nucleon interaction phenomenologically, has been carried out by Marshak and Foldy[3] for scalar mesons and for pseudoscalar mesons with pseudovector coupling. They found a zero cross section for scalar mesons and a very small cross section (about 10^{-31} cm^2 at 350 Mev) for pseudoscalar mesons. Both of these results disagree with the experimentally observed[1] large cross section which is of the order of 10^{-26} cm^2. However, their treatment is incorrect because they chose a charge independent nuclear potential which is not in agreement with later data on high energy scattering. Experimentally, high energy neutron-proton and proton-proton scattering are qualitatively different. Approximate agreement with the experimental results at high energy is given by the potentials[4]

$$-g_{NP}^2[(1+P_x)/2][\exp(-\mu r)/4\pi r]$$
for N–P scattering, $g_{NP}^2/4\pi=0.479$, (1)

and

$$+g_{PP}^2(\sigma_1\cdot\nabla/\mu)(\sigma_2\cdot\nabla/\mu)[\exp(-\mu r)/2\pi r]$$
for P–P scattering, $g_{PP}^2/4\pi=0.0209$,

where P_x is the space exchange operator. The choice of the P–P potential is not unique; any potential which predicts a very singular and strong interaction in P states would give approximate agreement with the high energy scattering. This potential is chosen because it corresponds to pseudoscalar theory with pseudovector coupling. Using these potentials, it is of interest to carry out calculations similar to those done by Marshak and Foldy to see whether sufficiently large cross sections can be obtained to explain the experimental results.

This method is applied in Sec. III to the calculation of the transition matrix elements for scalar theory, vector theory with vector coupling, and pseudoscalar theory with pseudovector coupling. For pseudoscalar coupling, it is possible to generalize the P–P potential to its relativistic form, using the equivalence between pseudovector and pseudoscalar coupling pointed out by Nelson.[5] The equivalence theorem gives for the potential the result

$$g_{PP}^2(2M/\mu)^2(\gamma_5)_1(\gamma_5)_2\exp(-\kappa r)/4\pi r. \quad (2)$$

The calculation can then be carried out using this type of interaction. However, it will be shown that for pseudoscalar coupling processes occur in the production of mesons which cannot be described in terms of a potential interaction and which give the largest contribution to the matrix element. A treatment on the basis of a potential model, therefore, is not justified. For such a theory the methods of third-order perturbation theory should give more reliable results. These phenomenological calculations are made in the center-of-mass system and are restricted to energies near threshold, i.e., less than 400 Mev for the incident nucleon in the laboratory system.

An additional important effect, which has been ignored in these calculations, must be considered before comparison with experiment can be made. In the ordinary approach to the problem of meson production, the approximation is made of replacing the wave functions of the initial and final nucleons by plane waves. This approximation is fairly good for the initial nucleons, since it is equivalent to the use of the Born approximation in high energy scattering. However, because of the large amount of energy carried off by the meson in its rest mass, the final nucleons are moving slowly, particularly near thresholds. It was pointed out by Hart and Chew that as a consequence of this it is possible, if the final nucleons are a neutron and a proton, that a deuteron may be formed. In addition, even if the nucleons do not form a deuteron, use of the plane wave approximation for the final nucleons gives very inaccurate results. In the Appendix these effects are considered and are shown to be important.

II. THIRD-ORDER FIELD-THEORETIC CALCULATION OF TRANSITION MATRIX ELEMENTS

The third-order matrix element can be written down directly using the methods of Feynman and Dyson.[6] A Feynman-Dyson diagram for meson production is given in Fig. 1. Seven additional diagrams can be obtained for emission of the meson by the three other nucleons and corresponding diagrams for the cases in which the two initial or final nucleons are interchanged. The matrix element for the diagram of Fig. 1 is

$$f^\lambda(f^\rho)^2\bar{\psi}(3)\left[U_\mu^2\frac{\tau^\lambda 1\tau^\rho}{(p_1-q)_\mu\gamma_\mu-iM}U_\nu^1\right]\psi(1)$$
$$\times\frac{\bar{\psi}(4)U_\nu^1\tau^\rho\psi(2)}{(p_4-p_2)^2+\mu^2}\phi_\mu^\lambda(q), \quad (3)$$

[3] R. Marshak and L. Foldy, Phys. Rev. 75, 1493 (1949).
[4] R. Christian and E. Hart, Phys. Rev. 77, 441 (1950); R. Christian and H. P. Noyes, Phys. Rev. 79, 85 (1950).
[5] E. C. Nelson, Phys. Rev. 60, 830 (1941).
[6] R. P. Feynman, Phys. Rev. 76, 769 (1949). F. J. Dyson, Phys. Rev. 75, 1736 (1949).

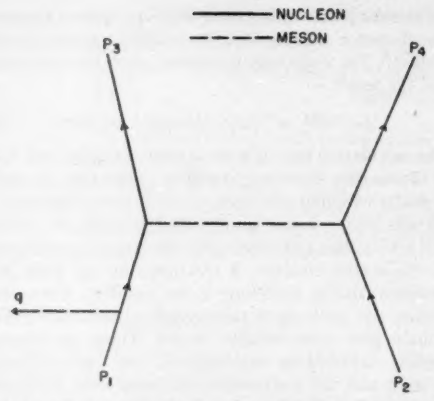

FIG. 1. Feynman-Dyson diagram for meson production by N–N collisions in lowest order. The solid lines represent the nucleons; the dashed lines represent mesons.

where $U_\mu^1=U_\mu^2=\delta_{\mu 0}$ for[7] S(III), and $=\gamma_5\delta_{\mu 0}$ for Ps.Ps(III); $U_\mu^1=(\delta_{\mu 0}\gamma_5/\mu)(P_4-P_2)_\nu\gamma_\nu$, and $U_\mu^2=(\delta_{\mu 0}\gamma_5/\mu)q_\nu\gamma_\nu$ for Ps.Pv(III); $U_\mu^1=U_\mu^2=\gamma_\mu$ for V.V(III); $\phi_\mu{}^\lambda=\phi^\lambda\delta_{\mu 0}$ for S(III), Ps.Ps(III), and Ps.Pv(III); and $\phi_\mu{}^\lambda=\phi_\mu{}^\lambda$ for V.V(III).

We use the symmetrical isotopic spin notation[8]

$$f^\lambda\tau^\lambda=f_1\tau_1+f_2\tau_2+f_3\tau_3+f_4\tau_4.$$

Charge symmetry requires that $f_1=f_2=f/\sqrt{2}$; the use of both f_3 and f_4 corresponds to two choices of sign for the coupling of the neutral mesons to the nucleons, since the expectation value of τ_3 is positive for a neutron and negative for a proton, while the expectation value of τ_4 is positive for both nucleon states.

The seven additional matrix elements can be obtained by various permutations of P_1, P_2, P_3, and P_4, changes of the sign of q_μ, and interchanges of U_μ^2 and U_ν^1, corresponding to an emission of the final meson after the exchange of the virtual meson. In the center-of-mass system these matrix elements are approximately

$$f^\lambda(f^\rho)^2[\psi^*(3)\tau^\lambda\tau^\rho U_1\psi(1)] \times[\psi^*(4)\tau^\rho U_2\psi(2)]/(2M^2\mu^5)^{\frac{1}{2}}, \quad (4)$$

where $U_1=U_2=1$, S(III); $U_1=1$, $U_2=(\boldsymbol{\sigma}\cdot\mathbf{p}_2)\mu/4M^2$, Ps.Ps(III); $U_1=(\boldsymbol{\sigma}\cdot\mathbf{q})(\boldsymbol{\sigma}\cdot\mathbf{p}_1)/\mu^2$, $U_2=(\boldsymbol{\sigma}\cdot\mathbf{p}_2)/\mu$, Ps.Pv-(III); $U_1=|q|/\mu$, $U_2=1$, V.V(III).

The total transition matrix elements given by these expressions, squared and averaged over the spins of the nucleons, are given by the expressions

$$|H_{if}|^2=G_{\rm III}{}^6/2M^2\mu^5, \text{ S(III), Ps.Ps(III),}$$
$$=(G_{\rm III}{}^6/2M^2\mu^5)\cdot(|q|^2/\mu^2), \text{ Ps.Pv(III), V.V(III);} \quad (5)$$

the values of $G_{\rm III}{}^6$ for the various theories and processes are given in Table I. It is apparent that the results are sensitive to the relative choice of sign for the coupling of neutral mesons to neutrons and protons, since the use of f_3, with f_4 set equal to zero, corresponds to the opposite choice of sign for the couplings, while the use of f_4, with f_3 equal to zero, corresponds to the same choice of sign for the couplings. It is interesting to observe that the only theory which predicts the production of neutral mesons in P–P collisions with a cross section comparable with that for charged mesons is Ps.Ps(III). For the other theories, cancellations occur between matrix elements, corresponding to emission of the final meson by the initial or final nucleons, which make the cross section of the order of $(\mu/M)^2$ smaller than for charged meson production.

III. PHENOMENOLOGICAL CALCULATION OF PRODUCTION

In this type of calculation we assume that the process of production can be described by meson emission preceded or followed by the nucleon-nucleon scattering. This, however, is not quite true, since virtual processes occur which cannot be described in terms of such a separation. An analysis of the process, considered as taking place in third order, indicates three basic ways in which a typical process can take place. These are

$$\left.\begin{array}{ll}\text{(a)} & P_1+P'+\omega'\rightarrow P'+P_3\\ \text{(b)}\ P_1+P_2\rightarrow & P_2+P'+\omega'\rightarrow P'+P_3\\ \text{(c)} & P_2+P'+\omega'\rightarrow P_2+P_4+\omega+\omega'\end{array}\right\} \rightarrow P_3+P_4+\omega. \quad (6)$$

It is clear that the virtual meson (ω') exchange in processes (a) and (b) is analogous to that which occurs in scattering; therefore, the exchange can be replaced by the effects of the potential which predicts the scattering. However, in process (c) the real meson (ω) is emitted between the emission and reabsorption of the virtual meson. Such a process cannot occur in the scattering of real nucleons; therefore, its effect cannot be given in terms of the potential model. However, it can be shown easily that such processes will give a rather small contribution, at least for theories in which negative energy states are not important for the virtual nucleons. The energy denominator for these matrix elements is given by

$$1/(E_0-E_1')(E_0-E_2'), \quad (7)$$

where E_0 is the total energy, and E_1' and E_2' are the energies of the two intermediate states. These denominators are (ignoring negative energy states), for processes (a) and (b),

$$1/(\tfrac{1}{2}E_0-E_4-\omega')(E_0-2E_4)=1/(\tfrac{1}{2}\omega-\omega')\omega \quad (8)$$

and, for process (c),

$$1/(\tfrac{1}{2}E_0-W_4-\omega')(\tfrac{1}{2}E_0-\omega-\omega'-E_3) =1(\tfrac{1}{2}\omega-\omega')(-\tfrac{1}{2}\omega-\omega'). \quad (9)$$

Now, since near threshold the energy ω' of the virtual

[7] We shall, in what follows, refer to the third-order computations for scalar, pseudoscalar with pseudoscalar or pseudovector coupling, and vector theory with vector coupling as S(III), Ps.Ps(III), Ps.Pv(III), and V.V(III), respectively.

[8] K. M. Case, Phys. Rev. **76**, 1 (1949).

TABLE I. Values of G_{III}^2 for production of charged mesons and neutral mesons of type 3 (coupled through τ_3) or of type 4 (coupled through τ_4).

		S(III), V.V.(III)	Ps.Ps(III)$\times f_p^2/16M^2$	Ps.Pv(III)$\times(M/\mu)^2$
N–P	π^+, π^-	$f^2(f^2-2f_3^2)^2$	$f^2(f^2+2f_4^2)^2$	$f^2((f^2-2f_4^2)^2\sin^2\theta+(f^2+2f_3^2)^2\cos^2\theta)$
	$\pi^0(3)$	0	$2f_3^2(f_3^2-f_4^2)^2$	$2f_3^2((f_3^2-f_4^2)^2\sin^2\theta+f^4\cos^2\theta)$
	$\pi^0(4)$	0	$2f_4^2((f_3^2-f_4^2)^2+f^4)$	$2f_4^2\sin^2\theta(f^2+f_3^2-f_4^2)^2$
P–P	π^+	$f^2(f^2-2f_3^2)^2$	$f^2(3f^4-4ff_4^2+12f_4^4)$	$f^2((f^2-2f_4^2)^2\sin^2\theta+(f^2+2f_3^2)^2\cos^2\theta)$
	$\pi^0(3)$	0	$64f_3^2(f_3^2+f_4^2)^2$	0
	$\pi^0(4)$	0	$64f_4^2(f_3^2+f_4^2)^2$	0

mesons is much larger than the energy ω of the real meson, these are approximately $-1/\omega\omega'$ for (a) and (b), and $1/\omega'^2$ for (c). Therefore, the contribution from process (c) is smaller than the contribution from processes (a) and (b) in the ratio $\omega/2\omega'$. Since the momentum of the virtual meson is equal to the difference of the momenta of the initial and final nucleons, which at threshold is about $(\mu M)^{\frac{1}{2}}$, the ratio $\omega/2\omega'$ is about $\frac{1}{2}(\mu/M)^{\frac{1}{2}}$ which is about 20 percent. This contribution is negligible only if the ratio of the masses of the meson and nucleon is small; actually, an error of the order of 20 percent in the matrix element can be expected if this term is ignored. A further error arises from the neglect of negative energy states for the virtual nucleons; however, because of the largeness of the energy denominators for such processes, the contribution is negligible for all theories except for pseudoscalar coupling. This case will be discussed in detail below.

We now consider processes leading from the initial state of two nucleons to the final state of two nucleons and a meson. This can take place in two ways, either through a scattering of the two initial nucleons followed by the meson emission, or with the order of these events reversed. We, therefore, have for the matrix element

$$\int drdr'[\psi_F^*(r,r')H(r,r')\psi'(r,r')]$$

$$\times\int\{drdr'[\psi'^*(r,r')S_I(r,r')\psi_I(r,r')]/(E_0-E')\}$$

$$+\int drdr'[\psi_F^*(r,r')S_{II}(r,r')\psi''(r,r')]$$

$$\times\int drdr'[\psi''^*(r,r')H(r,r')\psi_I(r,r')]/E_0-E''. \quad (10)$$

In this expression S_I and S_{II} are the potentials describing the interaction of the initial and final nucleons, H is the operator for meson emission, and E' and E'' are the energies of the two intermediate states. The energy denominators are

$$E_0-E'=(P_1^2/2M)-(P_2^2/2M)-P_1'^2/2M$$
$$=(P_0^2-P'^2)/M, \quad (11)$$
$$E_0-E''=(P_0^2/M)-(P''^2/M)-\omega.$$

(A) Scalar Meson Theory, Vector Meson Theory

We shall now consider the case of two initial protons P_1, P_2 going into a final neutron N_3, proton P_4, and positive meson q. For this case we have the scattering before meson emission in the P–P potential and the scattering after emission in the N–P potential. If we take scalar coupling for the meson, then

$$H=f^\lambda\tau^\lambda\exp(-i\mathbf{q}\cdot\mathbf{r})/(2\omega)^{\frac{1}{2}}. \quad (12)$$

The case of vector coupling can be considered simultaneously, since the coupling is

$$H=f^\lambda\tau^\lambda\gamma_\mu\phi_\mu(r), \quad (13)$$

where γ_μ is the 4-vector formed from the Dirac matrices. This coupling is approximately, for longitudinally polarized mesons,

$$f^\lambda\tau^\lambda|q|/\mu\exp(-i\mathbf{q}\cdot\mathbf{r})/(2\omega)^{\frac{1}{2}} \quad (14)$$

if corrections of the order of v/c for the nucleons are ignored. Therefore, we can obtain this result from that for scalar theory by multiplying the matrix element by $|q|/\mu$.

We find for the matrix element for S(phen)[9]

$$-\sqrt{2}fg_{PP}{}^2M(1-P_{12})$$
$$\times\frac{(\chi_3^*\sigma\cdot(\mathbf{P}_1+\mathbf{P}_4)\chi_1)(\chi_4^*\sigma\cdot(\mathbf{P}_4+\mathbf{P}_1)\chi_2)}{(2\omega)^{\frac{1}{2}}(P_1^2-P_4^2)[\mu^2+(P_1+P_4)^2]}$$
$$+\sqrt{2}fg_{NP}{}^2(1-P_{12})$$
$$\times\frac{(1+P_{34}{}^\sigma)}{2}\frac{(\chi_3^*\chi_1)(\chi_4^*\chi_2)}{(2\omega)^{\frac{1}{2}}\omega[\mu^2+(P_1+P_4)^2]}, \quad (15)$$

where the operator P^σ exchanges the momentum coordinate (corresponding to space exchanges in a coordinate representation), and P exchanges both the momentum and spin coordinates. Near threshold, $P_1\gg P_3$ or P_4. We can also disregard μ^2 relative to P_1^2. We then note that

$$\tfrac{1}{2}(1+P_{34}{}^\sigma)\frac{(\chi_3^*\chi_2)(\chi_4^*\chi_1)}{\mu^2+(P_1+P_4)^2}\cong\frac{(\chi_3^*\chi_2)(\chi_4^*\chi_1)}{P_1^2}.$$

[9] We shall refer to the phenomenological treatment of scalar, vector, and pseudoscalar theories with pseudovector coupling as S(phen), V.V(phen), and Ps.Pv(phen), respectively.

TABLE II. Values of G_{phen}^6 for production of charged mesons and neutral mesons of type 3 and type 4.

Charged		S(phen), V.V(phen) $f^2[(M/\mu\epsilon PP^3)^2+\epsilon NP^2]$	Ps.Pv(phen) $f^2((M/\mu\epsilon PP^3)+\epsilon NP^2)^2$
N–P	$\pi^0(3)$	0	0
	$\pi^0(4)$	0	0
P–P	$\pi^0(3)$	0	0
	$\pi^0(4)$	0	0

The expression finally simplifies to

$$\frac{-(1-P_{12})f}{M\mu^3(\mu)^{\frac{1}{2}}}\left[g_{PP}^2\frac{(\chi_3^*\boldsymbol{\sigma}\cdot\mathbf{P}_1\chi_1)(\chi_4^*\boldsymbol{\sigma}\cdot\mathbf{P}_1\chi_2)}{\mu^2}-g_{NP}^2(\chi_3^*\chi_1)(\chi_4^*\chi_2)\right], \quad (16)$$

where we have set $(P_1^2/2M)-\mu/2$ and $\omega=\mu$, which are their values at threshold.

A similar expression is obtained for an initial neutron and proton going into two final protons and a meson. For processes involving the scattering of two neutrons, the result depends on the choice of the N–N interaction. However, in the absence of any direct information, we shall assume that this is the same as the P–P interaction. The results for these processes are then identical with those given earlier.

For the production of neutral mesons, the analysis is similar to that given here. In this case, however, the nucleon charge is unchanged by the meson emission, and the scattering takes place before and after emission in the same potential. We find that cancellation occurs between the terms representing scattering before or after emission, so that a zero cross section is predicted for neutral mesons in either N–P or P–P collisions.

(B) Pseudoscalar Meson with Pseudovector Coupling

The analysis for pseudovector coupling can be carried out in a similar way. Here we have

$$H=f\tau^\lambda\boldsymbol{\sigma}\cdot\mathbf{q}/\mu\exp(-i\mathbf{q}\cdot\mathbf{r})/(2\omega)^{\frac{1}{2}}. \quad (17)$$

This gives, for the production of charged mesons,

$$-f(1-P_{12})\{g_{PP}^2(\chi_3^*\boldsymbol{\sigma}\cdot\mathbf{q}\boldsymbol{\sigma}\cdot\mathbf{P}_1\chi_1)(\chi_4^*\boldsymbol{\sigma}\cdot\mathbf{P}_1\chi_2)/\mu^2-g_{NP}^2(\chi_3^*\boldsymbol{\sigma}\cdot\mathbf{q}\chi_1)(\chi_4^*\chi_2)\}/M\mu^3(\mu)^{\frac{1}{2}}. \quad (18)$$

For neutral mesons produced in P–P and N–P collisions, we find that, as for scalar mesons, the cross sections are zero (to order $(\mu/M)^2$).

TABLE III. Ratio of third-order to phenomenological matrix elements averaged over angles for production of charged mesons.

Scalar, vector	Pseudovector coupling
$\{(f^2-2f_3^2)/4\pi\}^2$	$\{\frac{1}{3}(f^2-2f_3^2)^2+\frac{2}{3}(f^2+2f_3^2)\}/(4\pi)^2$
$(0.499)^2$	$(0.093)^2$

(C) Pseudoscalar Meson with Pseudoscalar Coupling

For the case of pseudoscalar coupling, we have

$$H=f\tau^\lambda\gamma_5\exp(-iq\cdot r)/(2\omega)^{\frac{1}{2}}. \quad (19)$$

We shall now use the relativistic generalization of the P–P potential, which is

$$g_{PP}^2(2M/\mu)^2(\gamma_5)_1(\gamma_5)_2\exp(-\mu r)/4\pi r. \quad (20)$$

Since negative energy states are important with this form of interaction, we must reconsider the energy denominators in their relativistic form. If the intermediate nucleon is in a negative energy state, its energy is approximately equal to the negative of its rest mass, and we have for the energy denominators for processes (a) and (b), as given in Eq. (6), approximately $1/2M^2$ and for process (c) $-1/2M\omega'$. We also must consider the behavior of the matrix elements describing the emission and reabsorption of the mesons. For transitions between positive energy states, $(\gamma_5)(\gamma_5)\sim(v/c)^2$, where v is the velocity of the nucleus. For transitions to and from negative energy states, $(\gamma_5)(\gamma_5)$ is about 1. Combining these results, we find, for the approximate magnitude of the matrix elements,

Process (a) and (b):

$$2(v/c)^2/\omega\omega'\sim 1/2M\omega'(\mu/M)^{\frac{1}{2}}\cong 0.40/2M\omega'$$

(transitions to positive energy states); (21)

Process (c):

$1/2M\omega'$ (transition to negative energy state).

We see, therefore, that near threshold we cannot neglect the nonpotential-like terms corresponding to process (c) with the virtual nucleon undergoing transitions to negative energy states, since they give the largest contribution to the matrix element. We must refer to the third-order perturbation theory results for a more adequate description of the process of the anomalous case of pseudoscalar coupling.

(D) Summary of Results for Phenomenological Calculation

The squares of the magnitudes of the matrix elements, given by the application of the phenomenological method to the meson production problem, are given by

$$|H_{ij}|^2=G_{\text{phen}}^6/2M^2\mu^5 \quad \text{S(phen)}$$
$$=(G_{\text{phen}}^6/2M^2\mu^5)q^2/\mu^2 \quad \text{Ps.Pv(phen), V.V.(phen).} \quad (22)$$

The values of G_{phen}^6 are listed in Table II. A comparison of these results with those obtained in Sec. II by the third-order calculation for the production of charged mesons is given in Table III. It is apparent that the results obtained by these two methods are approximately equal for not unreasonable choice of the coupling constants. The use of symmetric theory, in which $f=f_3$

TABLE IV. Values of square of magnitude of transition matrix elements, for P–P production of positive mesons, evaluated at zero relative momentum for the final nucleons, leading to singlet and triplet spin state. (All are to be multiplied by $\frac{1}{4}M^2\mu^5$.)

	S(III)	S(phen)	V.V(III)	V.V(phen)	Ps.Ps(III)	Ps.Pv(III)	Ps.Pv(phen)
$\lvert M_{if}(0)(\text{triplet})\rvert^2$	0	0	0	0	$\frac{3}{4}G_{\text{III}}^6$	$G_{\text{III}}^6 2T/\mu$	$G_{\text{phen}}^6 2T/\mu$
$\lvert M_{if}(0)(\text{singlet})\rvert^2$	G_{III}^6	G_{phen}^6	$G_{\text{III}}^6 2T/\mu$	$G_{\text{phen}}^6 2T/\mu$	$\frac{1}{4}G_{\text{III}}^6$	0	0

and f_4 is set equal to zero, however, would predict a zero cross section for[10] S(III) and V.V(III). It is certainly not necessary, however, that such a choice of the coupling constants be made.

IV. CALCULATION OF DIFFERENTIAL CROSS SECTION

We shall consider the specific case of production of positive mesons in P–P collisions. The generalization to other cases can easily be made. To the approximation used in these calculations, the differential cross section in the center-of-mass coordinate system for the production of two nucleons and a meson in a nucleon-nucleon collision is given by the expression

$$d\sigma/d\Omega dT = 2\sqrt{2}M^2\mu[T(T_m-T)]^{\frac{1}{2}}|H_{if}|^2/(4\pi)^3\pi, \quad (23)$$

where T is the meson kinetic energy, T_m is the maximum meson kinetic energy, and H_{if} is the transition matrix element including the effects, discussed in the Appendix, of the interaction of the final nucleons. Using the results of that section, we can write

$$|H_{if}|^2 = |\psi_t(r=0)M_{if}(0)(\text{triplet})|^2 + |\psi_s(r=0)M_{if}(0)(\text{singlet})|^2, \quad (24)$$

where $M_{if}(0)(\text{triplet})$ and $M_{if}(0)$ (singlet) are the matrix elements leading to final triplet and singlet spin states, and $\psi_t(0)$ and $\psi_s(0)$ are the wave functions for the final nucleons in triplet and singlet spin states, respectively, evaluated at $r=0$. Substituting the values for the wave functions, as given in the Appendix, this becomes (setting $E_f=T_m-T$)

$$d\sigma/d\Omega dT = 2(2)^{\frac{1}{2}}M^2\mu[T(T_m-T)]^{\frac{1}{2}} \times\{|M_{if}(0)(\text{triplet})|^2[(V_t+T_m-T)/(\epsilon_t+T_m-T)] + |M_{if}(0)(\text{singlet})|^2(V_s+T_m-T)/(\epsilon_s+T_m-T)\}. \quad (25)$$

The values of $M_{if}(0)(\text{triplet})$ and $M_{if}(0)(\text{singlet})$ are given in Table IV. The relation between the constants G_{III}^6 and G_{phen}^6 and the coupling constants f, f_3, and f_4 is given in Tables I and II.

The total cross section, then, is given approximately by the expressions

$$\frac{4\pi\sqrt{2}M^2\mu T_m^2}{(4\pi)^3}\{|M_{if}(0)(\text{triplet})|^2 \times[\tfrac{1}{4}+(V_t/T_m)(1-2(\epsilon_t/T_m)^{\frac{1}{2}})] + (\text{corresponding term for singlet})\}$$

for S. and Ps.Ps. and

$$\frac{8\pi\sqrt{2}M^2\mu T_m^2}{(4\pi)^3}\left\{\left|\frac{M_{if}(0)(\text{triplet})}{T}\right|^2 \times[\tfrac{1}{16}+(V_t/T_m)(\tfrac{3}{8}+\tfrac{3}{2}(\epsilon_t/T_m)-(\epsilon_t/T_m)^{\frac{1}{2}})] + (\text{corresponding term for singlet})\right\}$$

for V.V and Ps.Pv.

We can now use this cross section, ignoring the possibility of deuteron formation, to estimate the values of the coupling constants. If we assume a cross section at 350 Mev of 2×10^{-28} cm^2 with the corresponding maximum value of the meson kinetic energy in the center-of-mass system of 24.8 Mev, the corresponding values of $G_{\text{III}}^6/(4\pi)^3$ and $G_{\text{phen}}^6/(4\pi)^3$ are given in Table V. The values of the coupling constants f, f_3, and f_4 calculated from these values of $G^6/(4\pi)^3$, by the relation given in Tables I and II, are given in Table VI. For comparison, the values of the coupling constants adjusted to agree with the magnitude of P–P scattering[4] at 350 Mev (about 25 millibarns) are also given. It is apparent that the coupling constants predicted by these two processes, meson production and high energy scattering, are within the same order of magnitude. Conversely, we can conclude that any of the third-order or phenomenological results can correctly predict the order of magnitude of the meson production cross section, for not unreasonable choices of the coupling constants.

Finally, we must consider the additional process which can contribute to meson production, the formation of a deuteron and a meson in a proton–proton collision. The cross section can be calculated easily; we have (see Appendix)

$$d\sigma/d\Omega = |M_{if}(0)(\text{triplet})\psi_D(r=0)|^2 Mq\mu/(8\pi^2P_0) = |M_{if}(0)(\text{triplet})|^2 4(2)^{\frac{1}{2}}(T_m\epsilon_t)^{\frac{1}{2}}V_t M^2\mu/(4\pi)^3. \quad (26)$$

Using the values of the matrix elements given in Table

TABLE V. Values of the constants $G_{\text{III}}^2/4\pi$ and $G_{\text{phen}}^2/4\pi$ giving a total cross section at 350 Mev at 2×10^{-28} cm^2 for production of a positive meson, neutron, and proton in a P–P collision.

	S(III), S(phen)	V.V(III), V.V(phen)	Ps.Ps(III)	Ps.Pv(III) * Ps.Pv(phen)
$G^2/4\pi$	0.268	0.423	0.298	0.513

[10] A similar result was obtained in reference 3.

* Averaged over angles.

TABLE VI. Values of the coupling constants f, f_s, and f_t as given by Tables I, II, and V, and also as predicted by P–P scattering at 350 Mev.

	Meson production	P–P scattering
S(III)	$[f^2(f^2-2f_s^2)^2]^{\frac{1}{2}}/4\pi=0.268$	$(f_s^2+f_t^2)/4\pi=0.142$
S(phen)	$f^2/4\pi=0.0608$	
V.V(III)	$[f^2(f^2-2f_t^2)^2]^{\frac{1}{2}}/4\pi=0.423$	$(f_s^2+f_t^2)/4\pi=0.142$
V.V.(phen)	$f^2/4\pi=0.254$	
Ps.Ps(III)	$[f^2(3f^4-4f^2f_t^2+12f_t^4)^2]^{\frac{1}{2}}/4\pi=3.79$	$(f_s^2+f_t^2)/4\pi=3.73$
Ps.Pv(III)	$f^2[\frac{2}{3}(f^2-2f_t^2)^2+\frac{1}{3}(f^2+2f_s^2)^2]^{\frac{1}{2}}/4\pi=0.145$	$(f_s^2+f_t^2)/4\pi=0.0209$
Ps.Pv(phen)	$f^2/4\pi=0.354$	

IV, the cross sections are

$$d\sigma/d\Omega=(G^2_{\text{III, phen}}/4\pi)^2(T_m/\mu)^{\frac{1}{2}}6.66\times10^{-28}\text{ cm}^2 \quad \text{Ps.Pv(III), Ps.Pv(phen)}$$
$$=G_{\text{III}}{}^2/4\pi)^2(T_m/\mu)^{\frac{1}{2}}2.22\times10^{-26}\text{ cm}^2 \quad \text{Ps.Ps(III).} \quad (27)$$

At 350 Mev, using the values of the constants $G^2/4\pi$ given in Table V, the total cross sections for formation of a deuteron and a meson are

$$\sigma=7.63\times10^{-28}\text{ cm}^2\text{ Ps.Pv(III), Ps.Pv(phen),}$$
$$=2.57\times10^{-28}\text{ cm}^2\text{ Ps.Ps(III).} \quad (28)$$

These cross sections are larger than those in which the final nucleons are not bound (assumed to be 2×10^{-28} cm^2).

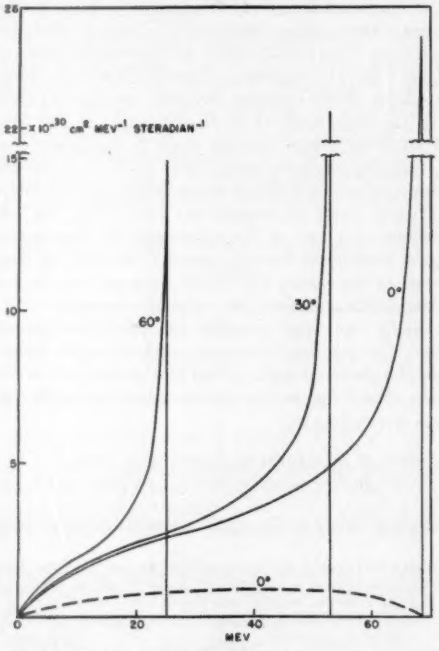

FIG. 2. Differential cross section at 350 Mev in the laboratory system for production of positive scalar mesons in P–P collisions. The solid curve includes the effects of the interactions of the final particles; the dashed curve is the result of the calculations using Born approximation throughout.

The differential cross sections at 350 Mev for proton-proton production of positive mesons are given in Figs. 2 and 3 for scalar theory and for the phenomenological treatment of pseudoscalar theory with pseudovector coupling. For comparison, the cross sections obtained when the Born approximation was made by treating the final nucleon wave functions as plane waves are also given (dashed curves). The very striking effects of the interactions of the final nucleons are obvious. The variation of the total cross sections with energy is given in Table VII, including the contribution to the cross section given when a deuteron is formed. The normalization is again to a total cross section of 2×10^{-28} cm^2 at 350 Mev for the production in which the two final nucleons are unbound.

V. CONCLUSIONS

The experimental results of the Berkeley workers[1] indicate that the cross section per nucleon for proton bombarding carbon is about 2×10^{-28} cm^2 for both charged and neutral mesons. For protons bombarding free protons, the cross section is about the same as for production of charged mesons but appears to be, perhaps, an order magnitude smaller for neutral meson production. It is apparent from the results of Secs. II, III, and IV that the relative size of these cross sections is predicted successfully only by the third-order result for pseudoscalar mesons with pseudovector coupling. The phenomenological result for scalar, vector, and pseudoscalar theory fails in that a zero cross section is predicted for production of neutral mesons in neutron–proton collisions. The third-order result for pseudoscalar theory with pseudoscalar coupling is of the right order of magnitude, except for neutral mesons produced in proton–proton collisions, where a cross section is predicted comparable with that for charged mesons in contradiction to the experimental result. The third-order result for scalar and vector theories is peculiar in that the cross section for neutral mesons vanishes for neutron–proton collisions and also vanishes for charged mesons if $f^2/2$ is taken equal to f_s^2 (Table I), corresponding to the use of symmetrical theory. It is interesting to observe that a small cross section is predicted for neutral meson production in proton-proton col-

lisions by all of the theories except pseudoscalar theory with pseudoscalar coupling. It is somewhat questionable, however, that such cancellations as those which appear in these calculations are to be quantitatively believed, since it is possible that higher order virtual effects would remove the cancellation which appears in lowest order.[11]

The phenomenological calculations are successful in predicting a sufficiently large charged meson cross section for agreement with experiment, because an unsymmetrical choice of the neutron-proton and proton-proton potentials was made. The calculation made by Marshak and Foldy used a symmetrical interaction, and the cancellation which occurred reduced the cross section by 2 or 3 orders of magnitude. It is not necessarily true, however, that all symmetrical theories would give a similar result. A theory which while symmetrical could also predict the high energy nucleon-nucleon scattering would presumably give the same qualitative features as the potential models used in these phenomenological calculations. It is interesting to note that the use of symmetrical theory in the third-order calculation does predict correctly the general magnitudes of the cross sections for pseudovector coupling but gives zero cross sections for scalar and vector theory.

A more detailed prediction of these calculations which is of particular interest in the angular dependence of the cross sections. Only the third-order calculation for pseudoscalar theory with pseudovector coupling gives a non-isotropic angular distribution (in the center of mass system). This is due to the presence of a tensor force in the neutron-proton interaction which couples the orbital motion of the meson to that of the nucleons. This effect is absent in the phenomenological treatment because of the use of a central interaction to describe the neutron-proton interaction.

The experiments on meson production by protons bombarding free protons provide a good opportunity for verifying the detailed predictions of the differential energy spectra. The experimental results of Cartwright *et al.* for meson production in the beam direction are shown in Fig. 4 in comparison with the predictions of pseudoscalar theory with pseudovector coupling. It is apparent that agreement with experiment can be obtained only if the effects of the interactions of the final nucleons are taken into account. The predicted fine structure of the high energy peak resulting from the deuteron formation cannot be resolved with the present experimental data; presumably, an improvement of experimental techniques will make it possible to test this prediction of the theory. Additional data on the angular dependence of the cross sections will also provide a critical test of the theoretical predictions.

The author wishes to thank Professor Robert Serber and Dr. K. M. Watson for many interesting discussions of the theoretical results derived in this paper. He also wishes to thank the experimental workers at Berkeley, particularly Drs. Chaim Richman, Herb York, and Vince Peterson for continuous information about the preliminary results of their work and for their aid in interpreting the experiments. In particular, he wishes to thank William Cartwright and Marian Whitehead for permission to quote the results of their experiment in advance of publication.†

[11] K. A. Brueckner and K. Watson found for neutral meson production by photons that a similar cancellation in pseudoscalar theory was removed in higher orders (Phys. Rev. **79**, 187 (1950)).

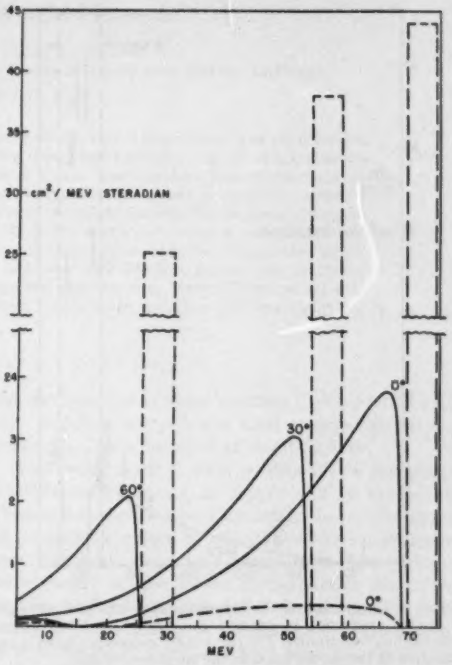

FIG. 3. Differential cross section at 350 Mev in the laboratory system for production of positive pseudoscalar mesons with pseudovector coupling in P–P collisions. The delta-function representing deuteron formation is averaged over a 5-Mev energy interval.

TABLE VII. Variation with energy of total cross section for positive meson production in P–P collisions, in units of 10^{-28} cm². The columns headed "Unbound" are for production leading to a neutron, proton, and meson; those headed "Deuteron" are for production leading to a deuteron and a meson.

	Scalar	Vector	Ps.Ps		Ps.Pv	
(Mev)	Unbound	Unbound	Unbound	Deuteron	Unbound	Deuteron
290	0	0	0	0	0	0
325	1.10	0.64	0.83	2.05	0.53	3.85
350	2.00	2.00	2.00	2.57	2.00	7.63
375	3.08	4.51	3.48	3.07	5.01	13.0

† *Note added in proof:* Recent experimental results of Cartwright, Richman, and Whitehead show that the angular distribution of positive pi-mesons produced in P–P collisions at 343 Mev is almost entirely $\cos^2\theta$ in the center-of-mass system. This is

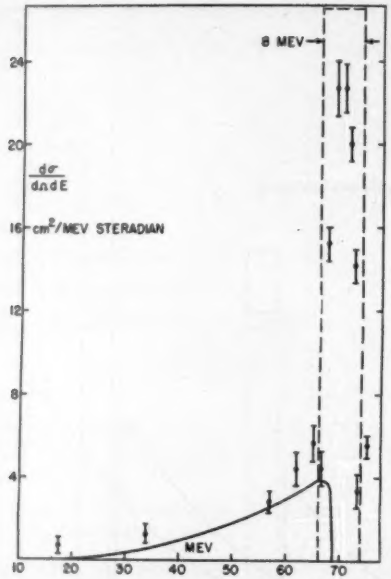

FIG. 4. Comparison of the experimental results of Cartwright *et al.* for production of positive mesons by 340-Mev protons bombarding free protons. The curve is for mesons produced in the direction of the proton beam in the laboratory system.

APPENDIX[12]

Effects of Interaction of Final Nucleons

For simplicity, we restrict ourselves to the case of two initial protons leading to a final neutron, proton, and positive meson. In the calculations described in Secs. II and III, we have made the approximation of representing the wave function of the final nucleons by plane waves. This is equivalent to using the Born approximation to describe the nucleon-nucleon scattering. However, near threshold, where the final nucleons have low energies, the scattering into these final states is poorly represented by the Born approximation applied to the potentials. The calculations can be done in a more satisfactory way if the actual wave function of the final nucleons is used. We can then resolve this into plane waves by the relation

$$\psi_F(\mathbf{r})=\int \alpha_k \exp(i\mathbf{k}\cdot\mathbf{r})d\mathbf{k}, \tag{1}$$

where

$$\alpha_k=[1/(2\pi)^3]\int \psi_F(\mathbf{r})\exp(-i\mathbf{k}\cdot\mathbf{r})d\mathbf{r}. \tag{2}$$

The calculations which we have made can then be considered to represent one of the fourier components of this momentum distribution. We can represent the transition matrix element which leads from the initial state to the final state, in which we have plane outgoing waves of relative momentum k, by $M_{if}(k)$. The transition matrix element to a state $\psi_F(r)$ then will be given by the expression

$$H_{if}=\int d\mathbf{k}\alpha_k M_{if}(k). \tag{3}$$

If we wish further to separate the final state into singlet and triplet spin states, we must consider separately the matrix elements of $M_{if}(k)$ leading to these spin states.

If we insert the definition of α_k, we have

$$H_{if}=[1/(2\pi)^3]\int\int d\mathbf{r}d\mathbf{k}\exp(-i\mathbf{k}\cdot\mathbf{r})\psi_F(r)M_{if}(k). \tag{4}$$

Now if we define

$$[1/(2\pi)^3]\int d\mathbf{k}\exp(-i\mathbf{k}\cdot\mathbf{r})M_{if}(k)=M_{if}'(r), \tag{5}$$

then we have for the matrix element

$$\begin{aligned} H_{if}&=\int\psi_F(r)M_{if}'(r)dr \\ &=\psi_F(r_{hy})\int M_{if}'(r)dr \\ &=\psi_F(r_{hy})M_{if}(0), \end{aligned} \tag{6}$$

where $\psi_F(r_{hy})$ is the value of the final wave function at an average value of r. This separation can be made more acceptable if we note that $M_{if}'(r)$ must be large only for r considerably less than the range of the forces, since the large momentum transfers necessary for meson production lead to a rather singular form for $M_{if}'(r)$. Then, since for low energy nucleons, $\psi_F(r)$ is slowly varying over a region of the size of the meson Compton wavelength, the results will not be sensitive to the particular value of r_{hy}, as long as r_{hy} is considerably less than $\hbar/\mu c$.

This simple result can be applied to the problem of interest. If we wish to calculate the probability that a deuteron is formed, we can take the expectation value of the transition matrix element $M_{if}(0)$ between the initial state of arbitrary spin and the final triplet state, and multiply this by the deuteron wave function evaluated at r_{hy}. Similarly, if we wish to include the effects of the interaction of the slowly moving final nucleons in a singlet or triplet state, we multiply the appropriate values of the matrix elements by the singlet or triplet wave functions evaluated at r_{hy}. We shall use the approximate wave functions for a square well[4] of range 1.53×10^{-13} cm, triplet depth V_t of 52.9 Mev, singlet depth V_s of 41.1 Mev. This gives simple analytic expressions for the wave functions of the deuteron and of the unbound system of neutron and proton of low relative momentum. The use of this nonsingular potential may underestimate the magnitude of the wave functions for small separations; however, the results will not be qualitatively incorrect. The approximate wave functions are

$$\begin{aligned} \psi_D(r)&=\sin[(MV_t)^{\frac{1}{2}}r]/r[(M\epsilon_t)^{\frac{1}{2}}/2\pi]^{\frac{1}{2}}, \\ \psi_{t,s}(r)&=\sin[(M(V_{t,s}-E_f))^{\frac{1}{2}}r]/r[M(\epsilon_{t,s}+E_f)]^{\frac{1}{2}}, \end{aligned} \tag{7}$$

where ϵ_s, ϵ_t are the singlet or triplet binding energy (in magnitude), and E_f is the energy of the final nucleons. The magnitude of these wave functions is quite insensitive to the choice of r_{hy} for r_{hy} less than $\hbar/\mu c$; for simplicity, we shall evaluate them at r_{hy} equal to zero. We then have

$$\begin{aligned} \psi_D(0)&=(MV_t)^{\frac{1}{2}}[(M\epsilon_t)^{\frac{1}{2}}/2\pi]^{\frac{1}{2}}, \\ \psi_{t,s}(0)&=[(V_{t,s}+E_F)/(\epsilon_{t,s}+E_F)]^{\frac{1}{2}}. \end{aligned} \tag{8}$$

It is apparent from these results that the value of the matrix element is considerably increased by the factor $\psi_F(0)$ near threshold, where the final nucleon energy E_f is considerably less than the well depth of about 50 Mev. The factor

$$(V_{s,t}E_f)/(\epsilon_{s,t}+E_f) \tag{9}$$

approaches 1 only for $E_f\gg V$; this condition is not satisfied until the incident nucleon energies are of the order of a Bev. At 350 Mev, where the final nucleon energy varies from 0 to about 25 Mev, this factor varies from about 2 to 25 for the triplet state and from 2 to about 600 for the singlet state. This has the effect of raising the cross section by a factor of about 3 or 4. The effects of the interaction of the final nucleons, therefore, clearly are large and cannot be ignored.

given only by the third-order result for pseudoscalar theory with pseudovector coupling with $f^2=2f_s^2$ (see Table I), supporting the conclusions already reached in this paper.

[12] The material of this Appendix was developed in collaboration with Geoffrey Chew and Edward Hart, to whom the author wishes to express his appreciation.

Fission of Medium Weight Elements*

ROGER E. BATZEL AND GLENN T. SEABORG
Radiation Laboratory and Department of Chemistry, University of California, Berkeley, California
(Received February 19, 1951)

Evidence is presented here which indicates that large fragments (much larger than alpha-particles) are emitted among the competitive products of transmutation throughout the entire range of atomic numbers of the elements. Threshold considerations for the observed nuclear reactions show that the reactions are observed with small cross sections well below the threshold for spallation reactions in which the maximum number of alpha-particles are considered as being emitted from the excited nucleus. The calculated thresholds include the mass difference between the reactants and the products and the excitation energy which the product particles or fragments must have in order to pass over the coulombic barrier. Preliminary experiments on the ranges of recoil fragments from copper irradiated with 340-Mev protons give additional evidence for the emission of heavy fragments. It is suggested that the term "fission" is proper for such reactions, throughout the entire range of atomic numbers, in which the nucleus is split essentially into pieces of comparable weight.

I. INTRODUCTION

THE fission reaction has been observed with high energy accelerator projectiles for elements as light as tantalum,[1] but has not been reported for medium weight elements. Evidence is presented here for occurrence of reactions which are probably most properly described by the term "fission" and which seem to occur, with very small yield, throughout the entire region where this type of reaction is only slightly exoergic or even endoergic with respect to mass balance.

In the course of the detailed investigation of the spallation of copper and the variation of the product yields with energy of the bombarding particle, the threshold for formation of radioactive Cl^{38} (39-minute half-life) from elemental copper was studied. The most energetically economical way in which Cl^{38} might be formed by spallation reactions is by emission from the bombarded copper nucleus of nucleons in groups, such as alpha-particles, instead of single nucleons. The energetic requirement for the spallation reaction $Cu^{63}(p,pn6\alpha)Cl^{38}$, in which the maximum number of alpha-particles is emitted, is roughly 110 Mev. This threshold includes (1) the mass difference between the reactants and the products and (2) the excitation energy which the alpha-particles must have in order to pass over the coulombic barrier.

The production of Cl^{38} was definitely observed at proton bombardment energies beginning at about 60 to 70 Mev with a cross section of some 10^{-32} cm². The cross section increases rapidly to a value of about 10^{-30} cm² at 105 Mev and then increases gradually to a value of about 10^{-28} cm² at 340 Mev. In order to explain the low threshold, it must be assumed that substantially larger particles than alpha-particles are emitted from the excited nucleus, and the reactions are therefore of a type which might more properly be termed fission. As an example, the extreme reaction $Cu^{63}+p\rightarrow Cl^{38}+Al^{25}+n$, which is energetically most economical but still endoergic, has a threshold of about 50 Mev.

This result made it seem worthwhile to investigate another such reaction in copper and to extend the threshold studies to other elements in the middle portion of the periodic system in order to see whether analogous reactions might occur as a general rule. The variation with energy of the yields of radioactive Na^{24} from copper and radioactive $Sc^{42,44}$ from bromine were studied. The formation of radioactive Co^{61} from silver, radioactive Na^{24}, Ga^{66}, and Ga^{72} from tin, and radioactive Ga^{66} and Ga^{72} from barium were also studied. In all cases the observed thresholds were well below the thresholds calculated for the reactions in which the maximum number of alpha-particles are emitted from the nucleus. Additional evidence for fission of the medium weight elements was found from some preliminary experiments on the ranges of recoil fragments from copper irradiated with 340-Mev protons.

II. PROCEDURE

Irradiations with high energy protons were carried out in the circulating beam of the 184-inch frequency modulated cyclotron, and the proton energy was adjusted by varying the radial distance of the target from the origin of the beam. Foil targets 5 to 10 mils thick were used in the cases of copper, silver, and tin. The bromine was bombarded in the form of ammonium bromide powder wrapped in special purity aluminum foil, and the barium was bombarded in the form of barium carbonate wrapped in the special purity aluminum foil. Since the degradation of the energy of the high energy protons is small in traversing the targets used, all targets can be considered thin targets.

The special purity ammonium bromide was synthesized by forming hydrogen bromide from very pure phosphorous tribromide and mixing the gas with very pure gaseous ammonia in a cooled plastic container. The barium carbonate was prepared from special purity

* This work was performed under the auspices of the AEC.
[1] Perlman, Goeckermann, Templeton, and Howland, Phys. Rev. 72, 353 (1947).

barium chloride received from Dr. A. J. Keyes and Dr. A. J. King of Syracuse University.

Determinations of the intensity of the internal, proton beam for the silver bombardments and the tin bombardments, in which the yields of Ga^{66} and Ga^{72} were studied, were made by bombarding aluminum foils in conjunction with the regular target foils. This monitor foil undergoes a nuclear reaction $Al^{27}(p,n2p)Na^{24}$ for which the cross section has been determined as a function of the energy of the bombarding proton.[2] The cross sections for the formation of the Na^{24} and the Cl^{38} from copper were determined by comparing the amounts of the isotopes formed with the amounts of radioactive Cu^{64} formed by the $Cu^{65}(p,pn)Cu^{64}$ reaction in a given bombardment. The cross section for the reaction $Cu^{65}(p,pn)Cu^{64}$ as a function of the energy of the bombarding proton has previously been determined.[3] The cross sections for the formation of the $Sc^{43,44}$ from bromine, the Na^{24} from tin, and the Ga^{66} and Ga^{72} from barium were calculated using an estimated value of $\frac{1}{2}$ microampere for the beam current.

After irradiation, the targets were dissolved, and the elemental fractions for the various nuclides were separated by the chemical procedures to be discussed in detail in Sec. V. Separation procedures were designed to give a radiochemical purification factor of about 10^8 from all other activities formed in the target.

Counting of the activities was done on an end-window, alcohol-quenched, argon-filled, Geiger counter tube with a mica window of ~3-mg/cm² thickness, used in conjunction with a scale of 64 counting circuit. The nuclides were characterized by half-life determinations, absorption measurements, and sign of particulate radiation emitted.

A crude beta-ray spectrometer was used in the determination of the sign of the beta-particles and was especially useful where nuclides with similar half-life, but differing in sign of particle, had to be resolved.

Thresholds for the various reactions include the mass difference between the reactants and products and the excitation energy which the nuclear fragments or alpha-particles must have in order to pass over the potential barrier. Where available, measured mass values for the reactants and products were used in making the mass balance. The masses of radioactive fragments formed, or considered as being formed as products of the nuclear reaction were calculated by adding the mass equivalent of the decay energy of the radioactive nuclide to the mass of the stable daughter nuclide.

The excitation required for the passage over the potential barrier was calculated assuming that the fragments are spherical and tangent at the nuclear radii (taken as 1.48×10^{-13} $A^{\frac{1}{3}}$ cm). Calculations of the coulombic energy requirements for reactions in which a number of alpha-particles are emitted were made on the basis that the alpha-particles come out consecutively. The coulombic requirement for each alpha-particle was calculated on the basis of the alpha-particles being tangent to the daughter nucleus; and, as an example, for the reaction $Cu^{63}(p,pn6\alpha)Cl^{38}$, the first alpha-particle is assumed to be tangent to Co^{59} at the nuclear radius, the second tangent to a Mn^{55} nucleus, etc.

The experiments on the determination of the apparent average ranges of the recoil fragments from copper irradiated with 340-Mev protons were done in the circulating beam of the 184-inch cyclotron. Pieces of Nylon (0.5×2.5 cm) were placed on both sides of the copper foil (0.5×2.5 cm) to catch the recoil fragments. After irradiation, the pieces of copper and Nylon were dissolved, carriers added, and the elemental fractions were separated and measured.

The ranges of the recoil fragments were calculated on the basis of an isotropic distribution and constant range for the recoils. The copper foils were thick relative to the range of the fragments observed. The ratio of the number of atoms of a nuclide appearing in the Nylon catcher foils to the number of atoms in the copper were related to the ranges by the following treatment of the data.

By integration, the expression

$$0.5\int_0^R [(R-x)/R]dx=\tfrac{1}{4}R,$$

where R is the range of the fragments in the copper, and x is the distance from the surface of the copper, shows that $\frac{1}{4}$ of the fragments formed in a thickness R of the surface of the copper will appear in the catcher foils. The relationship $R=(4A_R/A_{tot})T$, where R is the range of the recoil fragment, A_R is the activity collected in the catcher foil, A_{tot} is the activity in the copper foil plus that caught on the Nylon, and T is the thickness of the copper, gives the range R of the recoils in terms of the information determined experimentally.

III. RESULTS

A. Radioactive Products from Copper

Radioactive Cl^{38}

The calculated threshold for the spallation reaction $Cu^{63}(p,pn6\alpha)Cl^{38}$ is about 110 Mev, while the threshold for the extreme reaction $Cu^{63}+p\rightarrow Cl^{38}+Al^{25}+n$ is about 50 Mev.

A plot of the cross section for formation of Cl^{38} from copper is given in Fig. 1. The cross section rises rapidly from 70 Mev to 105 Mev and then increases gradually to a value of 4×10^{-29} cm² at 346 Mev. Below 70 Mev the level of activity formed was so low that identification of the Cl^{38} was not possible; but above 70 Mev the nuclide was identified in all cases through chemical separation, measurement of half-life with a Geiger

[2] R. L. Folger and P. C. Stevenson, unpublished work (1950).
[3] R. E. Batzel and G. T. Seaborg, unpublished work (1950).

counter, and observation of the sign of the beta-particles with a simple beta-ray spectrometer.

With cross sections so low, an immediate question is that of impurities, since a small amount of impurity with a high cross section for formation of Cl^{38} might be a source of the observed activity. Special purity copper foil was used; and a spectrographic analysis submitted with the copper shows less than 0.00007 percent iron, less than 0.0001 percent nickel, less than 0.00005 percent chromium, and less than 0.0001 percent sulfur (the sulfur was chemically analyzed). As an additional check, radioactivation methods were also used to check for all possible impurities which might account for the observed yield of Cl^{38}. The results of the activation experiments are listed in Table I.

Except for the value listed for scandium, the cross sections for the formation of the Cl^{38} listed in column two are experimental results from irradiations of the corresponding elements in column one. The cross-section value for scandium was estimated from the observed cross sections for calcium and titanium. Column three lists the amounts of the different elemental impurities which must be present in the special purity copper to produce the number of atoms of the Cl^{38} observed in the chlorine fraction isolated from the irradiated copper. Column four lists the limits set on the actual amounts of the elemental impurities present in the special purity copper, as determined by spectrographic and radioactivation methods. Column five gives the ratios of the amounts of the Cl^{38} to the amounts of Cl^{34} observed in the chlorine fractions separated from the respective elements after irradiation with 85-Mev protons. The ratios listed may be compared with the ratio of two observed in the chlorine fraction separated from the special purity copper irradiated with 85-Mev protons.

Potassium as a possible impurity in the copper, which might be a source of the observed Cl^{38}, can be eliminated on the basis of the ratio of the number of atoms of Cl^{38} formed compared with the number of atoms of Cl^{34} formed in bombardment of potassium with 85-Mev protons as shown in Table I, aside from the fact that potassium is not a likely impurity in electroplated copper. Calcium impurity was eliminated as a possible source of the activity by considerations shown in the above table: amounts of calcium present, cross section for formation of Cl^{38}, and ratio of Cl^{38} to Cl^{34}. Scandium and titanium were eliminated as possible impurities in the copper by cross-section considerations and results of radioactivation analyses performed by irradiating the copper with 30-Mev protons and determining the amount of radioactive Sc^{44} formed. This separation of Sc^{44} also served as a check on the calcium, since Sc^{44} could be formed by a (p,xn) reaction on calcium. The radioactivation analysis for vanadium was performed by comparing yields of radioactive Cr^{51} formed in 30-Mev proton bombardments of vanadium with the amount of Cr^{51} formed in the copper foil under similar

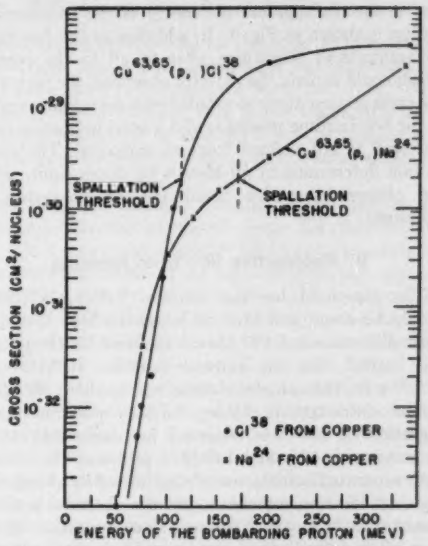

FIG. 1. Cross section for formation of Cl^{38} and Na^{24} from copper as energy of the bombarding proton.

bombardment conditions. The very small cross section for formation of Cl^{38}, as listed in Table I, makes it unlikely for chromium or any of the heavier medium weight elements to be present in amounts which would contribute to the Cl^{38} observed, since their cross sections for formation of Cl^{38} in bombardments with 85-Mev protons would be lower than that obtained for chromium.

Radioactive Na^{24}

The threshold for the reaction $Cu^{63}(p,p3n9\alpha)Na^{24}$ should be about 170 Mev, of which 100 Mev is due to mass difference and 70 Mev to the coulombic requirement. For the extreme reaction $Cu^{63}+p \rightarrow Na^{24}+K^{39}+n$, the calculated threshold is about 50 Mev.

The Na^{24} was characterized by absorption and half-life measurements. A plot of the cross section for forma-

TABLE I. Examination of possible impurity contribution to observed Cl^{38} activity from copper.

Element	Cross section for formation of Cl^{38} at 85 Mev	% Impurity necessary to explain observed activity	% Impurity determined	Ratio of Cl^{38} to Cl^{34} formed in bombardment of element[a]
K	$<10^{-27}$ cm²	>0.001	<0.01 (spect.)	0.06
Ca	$<10^{-27}$	>0.001	<0.0001 (spect.)	0.10
Sc	$<10^{-27}$	>0.001	<0.0001 (rad.)	
Ti	$<10^{-28}$	>0.0016	<0.0001 (rad.)	10.0
V	$<10^{-28}$	>0.01	<0.0001 (rad.)	
Cr	$<10^{-29}$	>0.1	<0.01 (spect.)	

[a] The ratio Cl^{38} to Cl^{34} formed from the copper at 85 Mev is about 2.

tion of the Na^{24} against the energy of the bombarding proton is shown in Fig. 1. In addition to the fact that no amounts of impurities were found in the copper which could explain the activity observed, the fact that the cross section drops so rapidly with decreasing energy of the bombarding proton is also a good indication that the Na^{24} is not formed from an impurity. The cross section determined at 50 Mev is an upper limit, since the observed activity could not be characterized definitely.

B. Radioactive Sc^{44} from Bromine

The threshold for the reaction $Br^{79}(p,p7n7\alpha)Sc^{44}$ should be about 190 Mev, of which 70 Mev is due to mass difference and 120 Mev is required for the potential barrier. For the extreme reaction $Br^{79}+p\rightarrow P^{24}+Sc^{44}+2n$, the calculated threshold is about 80 Mev.

The characteristic 3.9-hr, 1.5-Mev positron disintegration of Sc^{44} was observed in bombardments of bromine with 125- and 140-Mev protons. The chemically separated activity was characterized by absorption and half-life measurements; and the observed activity would include any Sc^{43} formed, since resolution of the two 3.9-hr activities was not possible. An attempt was made to find the characteristic activity of Sc^{44} in bromine bombarded with 100-Mev protons, but the small amount of activity could not be identified definitely. In a bombardment at 70 Mev, the scandium fraction showed only 90 disintegrations per minute of an ~4-hr activity. Comparable bombardments of bromine with 125- and 140-Mev protons yielded about 10,000 and 30,000 disintegrations per minute, respectively, of the 3.9-hr Sc^{44}. The cross section for formation of the Sc^{44} at 125 Mev is on the order of 10^{-32} cm^2 and is in line with the cross section observed for the formation of Cl^{28} from copper.

The fact that the cross section for formation of Sc^{44} falls off so rapidly as the energy of the bombarding proton is lowered from 140 Mev to 70 Mev rules out the possibility that the observed Sc^{44} is formed from small amounts of calcium, scandium, titanium, or vanadium impurities. The cross sections for formation of Sc^{44} from the elements above vanadium would become increasingly smaller in this energy range, so such impurities are not likely. Spectrographic analysis of the ammonium bromide used as target material showed less than 0.001 percent calcium. Scandium, titanium, vanadium, chromium, manganese, iron, cobalt, nickel, copper, zinc, and gallium were not detectable in the spectrographic analysis. The limit set on the amounts of any of these elements present is 0.01 percent. A limit of less than 0.00015 percent iron impurity was set by colorimetric methods.

C. Radioactive Co^{61} from Silver

The production of the nuclide Co^{61} from silver was studied as a function of energy, but the results must be termed borderline owing to a small amount of copper impurity present in the silver. Since the Co^{61} is formed as a spallation product of copper, it was necessary to determine the amount of copper impurity present in the silver, and the radioactivation method was used. Results of the experiments showed 1×10^{-3} percent copper. The variation with energy of the cross section for formation of the Co^{61} from copper was determined, and the contribution of the Co^{61} formed from the copper impurity was subtracted from the total activity of Co^{61} formed during bombardment of the silver. Resolution of the activity showed that about equal amounts were formed from the silver itself and from the 0.001 percent copper impurity in bombardments at 180 Mev. The observed cross section for formation of Co^{61} from silver at this energy is about 10^{-32} cm^2.

For the reaction in which the maximum number of alpha-particles are emitted, $Ag^{107}(p,p6n10\alpha)Co^{61}$, the calculated threshold is about 210 Mev, of which about 90 Mev is brought about by mass difference; and for the reaction $Ag^{107}+p\rightarrow Co^{61}+Sc^{45}+2n$, the calculated threshold is about 60 Mev. Attempts were made to continue the cross section work at energies lower than 180 Mev; but the problem of resolving the Co^{61} activity formed from the small amount of copper impurity and that formed from the silver alone becomes increasingly difficult, since the cross section for formation of Co^{61} from silver becomes smaller as the energy of the bombarding proton is lowered, while the cross section for formation of Co^{61} from the copper impurity is relatively constant in this energy range.

D. Radioactive Products from Tin

Radioactive Na^{24}

The calculated threshold for the reaction in which the maximum number of alpha-particles are emitted is about 425 Mev, of which 230 Mev is due to mass difference. The extrene reaction ${}_{50}Sn^{118}+p\rightarrow Na^{24}+{}_{40}Zr^{94}+n$, which is exoergic by about 8 Mev with respect to mass difference, has a calculated threshold of about 50 Mev.

The plot of the cross section for formation of the Na^{24} *versus* energy is shown in Fig. 2. The cross-section values plotted are good to a factor of two and possibly better, since all the irradiations were carried out under conditions where the beam intensity should have been the same.

The point at 75 Mev represents an upper limit for the yield, since the activity in the sodium fraction was too small to be identified positively as Na^{24}. The shape of the excitation function almost precludes the possibility of impurities just above sodium in the periodic table. The spectroscopic analysis showed the tin to be 99.999 percent pure with no impurities detectable which could explain the observed activities.

Radioactive Ga^{66} and Ga^{72}

The calculated thresholds for the nuclear reactions $Sn^{118}(p,7n10\alpha)Ga^{72}$ and $Sn^{118}(p,13n10\alpha)Ga^{66}$ are about 230 and 280 Mev, respectively; and for the extreme reactions $Sn^{118}+p\rightarrow Ga^{72}+Ca^{48}+2n$ and $Sn^{118}+p\rightarrow Ga^{66}+Ca^{49}+4n$ the thresholds are about 70 and 90 Mev, respectively. The thresholds for formation of Ga^{66} and Ga^{72} from some of the other tin isotopes may be lower by several Mev, but the examples calculated give approximate values on which to base our reasoning.

The purified gallium fraction isolated from the bombarded tin showed the characteristic activities of Ga^{66}(9.5-hr half-life) and Ga^{72}(14.3-hr half-life), and the absorption curve of Fig. 3 shows the presence of the ~3-Mev positron characteristic of Ga^{66}. The gallium activities were identifiable at energies of 150 and 180 Mev with cross sections based on elemental tin of about 10^{-32} cm² and with the value at the higher energy a factor of approximately two times higher than that at the lower energy. Amounts of gallium activity formed in bombardments of tin at 100 Mev were too small to identify definitely, and no gallium activity was observed in the gallium fraction separated from tin bombarded with 80-Mev protons.

The spectrographic analysis presented with the special purity tin showed less than 0.0001 percent arsenic; and no zinc, gallium, or germanium were detectable. The variation of the yield of Ga^{66} with energy of the bombarding particle rules out the probability of the observed activity coming from zinc or gallium, since the cross section for formation of Ga^{66} from zinc or gallium would rise as the energy is lowered from 180 to 80 Mev, while the yield of Ga^{66} from the tin falls off as the energy is lowered.

E. Radioactive Ga^{66} and Ga^{72} from Barium

The calculated threshold for the reaction $Ba^{137}(p,20n13\alpha)Ga^{66}$ is about 370 Mev (200-Mev mass difference and 170-Mev potential barrier). For the extreme reaction $Ba^{137}+p\rightarrow Ga^{66}+Fe^{60}+12n$, the calculated threshold is about 150 Mev. The threshold for formation of Ga^{72} by a similar extreme reaction is some 40 Mev lower.

The gallium fraction isolated from barium irradiated with 335-Mev protons showed the characteristic activities of Ga^{66} and Ga^{72}. The cross sections for formation of these nuclides are about equal and are around 10^{-31} cm². The special purity barium contained no spectroscopically detectable impurities, with the exception of a trace of iron. Only the single irradiation was performed, because of the lack of sufficient special purity barium; but the observed cross section is in line with the others reported and seems to indicate that the gallium isotopes are probably formed by a fission reaction.

F. Evidence from Recoil Experiments

Some recent experiments on the range of recoil fragments from copper bombarded with 340-Mev protons have been done in conjunction with this work. Preliminary results indicate that larger fragments than alpha-particles must be emitted from the bombarded nucleus in order to explain the observed energies of the recoils.

Assuming an isotropic distribution for the recoil fragments from the irradiated copper (as discussed in Sec. II), it was found that Cr^{49} nuclei have an average apparent range of about 0.3 mg/cm² of copper against the direction from which the incident protons approach the target, and a range of about 2.5 mg/cm² of copper with the direction of the beam. Using the formulas for stopping power developed by Knipp and Teller[4] for calculating the energy losses brought about by electronic and nuclear interactions, the energy of the recoils against the beam was found to be about 1 Mev and with the beam, about 13 Mev.

There is a distortion of the recoil distribution, owing to the momentum imparted to the nucleus by the impinging proton, causing more recoil nuclei to appear with the beam and fewer against the beam. Since the ranges were calculated on the basis of an isotropic distribution for the recoils, the calculated range with the beam is larger and that against the beam is smaller than the actual range. The range distribution was corrected, assuming 5 Mev as the kinetic energy that the Cr^{49} fragment received when the excited copper nucleus split, and assuming that the excited nucleus has had momentum transferred to it by the impinging proton equivalent to 1 Mev of kinetic energy for the excited nucleus. The corrected ranges were about 0.6 mg/cm² of copper against the beam and about 2.2 mg/cm² of copper with the beam, and they are equivalent to energies of about 2.0 Mev and 10 Mev, respectively. These energies correspond to 5.2 Mev of kinetic energy imparted to the Cr^{49} fragment when the excited nucleus breaks up and correspond to a momentum transfer to the copper nucleus equivalent to about 1 Mev of kinetic energy.

A reaction which seems to explain the observed recoil energies is $Cu^{63}+p\rightarrow Cr^{49}+C^{12}+3n$. The C^{12} would leave the excited nucleus with a kinetic energy of about 20 Mev, which is just equivalent to the height of the potential barrier, and would give a recoil energy of about 5 Mev to the Cr^{49}. Explanation of the observed results in terms of the emission of smaller fragments, such as neutrons, protons, or alpha-particles would require a great deal of asymmetry in both the energy and distribution of the particles in the process of the break down of the excited nucleus. The observed transfer of momentum to the copper nucleus corresponds to an excitation of the nucleus which would be consistent with the reaction written. In line with the

[4] J. Knipp and E. Teller, Phys. Rev. **59**, 659 (1941).

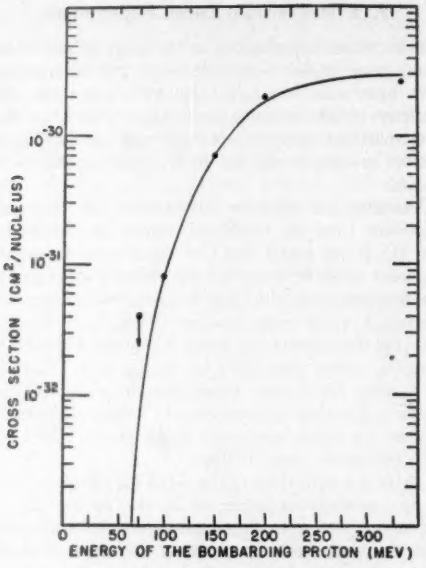

FIG. 2. Cross section for formation of Na^{24} from tin as energy of the bombarding proton.

results of the previous sections, it seems reasonable to assume that a reaction of the type written for the formation of Cr^{49} is correct.

IV. DISCUSSION

The coulombic energy requirement for the emission of the charged particles in the above reactions gives rise to a large contribution to the calculated threshold, and the possibility of the alpha-particles being emitted at energies well below the top of the coulombic barrier should be considered, since in some cases the observed thresholds exceed the values of the mass requirements alone. Calculations of the transmission coefficient[5] for the coulombic barrier show that the time required for a succession of alpha-particles to be emitted with excitation energies well below the top of the barrier is too long to allow this type of nuclear reaction to compete with other reactions in which neutrons and protons (coming out over the barrier) are emitted. It is possible, however, that the coulombic requirement is lowered somewhat because of the effective lowering of the potential barrier at high excitation energies.[6] The only observed thresholds which are borderline are those of the Co^{61} from silver and Ga^{66} and Ga^{72} from barium. The other thresholds are well below the values which could be explained by penetration or an effective lowering of the barrier at the high excitation energies.

The shapes of the excitation curves for the formation of Na^{24} and Cl^{38} from copper are quite similar in the low energy region. This similarity could be attributed to the fact that they are formed by reactions which require about the same amount of excitation energy. The extreme fission reactions have about the same threshold, and the Na^{24} fragment corresponds to a very reasonable complementary fragment corresponding to Cl^{38}. The excitation curves for the formation of Na^{24} and Cl^{38} from copper probably represent sums of several reactions contributing to the total observed cross section. In the low energy range, the main contribution is probably that of the pure fission reaction, while, as the energy is raised, reactions in which smaller fragments are given off begin to contribute to the total reaction. At the high energy end, spallation reactions probably begin to contribute markedly. The difference in the two curves at the higher energies is probably due to the larger contribution of the direct formation of Cl^{38} by spallation reactions.

It is interesting to note that the emission of nuclear fragments a little larger than alpha-particles has been observed in high energy nuclear reactions on medium weight elements. The "hammer tracks" of Li^8 are very well known in reactions induced by cosmic radiation and have also been identified as a reaction product of 340-Mev proton and 190-Mev deuteron bombardments of some of the medium weight elements.[7] Evidence has also been found for the existence of lithium isotopes as a reaction product of 50- to 340-Mev proton and helium

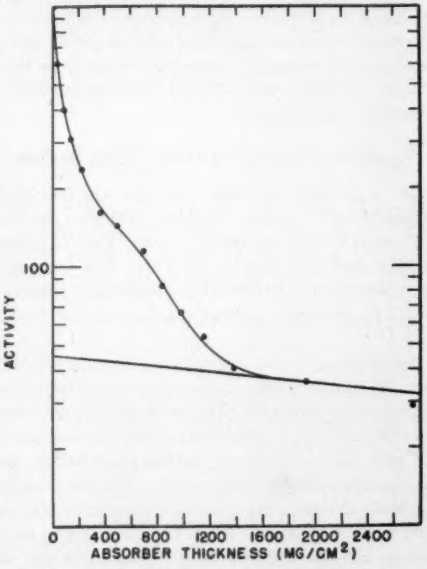

FIG. 3. Aluminum absorption curve for gallium fraction from tin bombarded with 180-Mev protons.

[5] G. Gamow, Z. Physik **51**, 204 (1928).
[6] K. J. Le Couteur, Proc. Phys. Soc. (London) **A63**, 259 (1950).
[7] S. Wright, Phys. Rev. **77**, 742 (1950).

ion bombardments of tin.[8] Radioactive Be^7 has also been identified as a product of 340-Mev proton bombardments of some of the medium weight elements.[8] Heavy fragments have also been observed in reactions induced by cosmic radiations.[9–11]

Apparently, when the energy threshold requirements are met, large fragments are emitted among the competitive products of nuclear reactions throughout the entire range of atomic numbers of the elements. This is certainly not surprising, and the measured yields reported here seem to be quite reasonable. It seems certain that the size of the fragments varies continuously from those (neutrons, protons, and alpha-particles) which accompany what are conveniently called spallation reactions, through intermediate sizes (for example, Li^8, etc.), on up to sizes such that the nucleus is split essentially into several pieces of comparable weight. Apparently, a number of reactions in which there occurs the latter type of nuclear splitting have been observed in the present investigation, and perhaps the term "fission" is as proper a name as any to apply to the process. As a result of this work it seems that fission reactions occur in all nuclei if the necessary excitation energy is available.

V. EXPERIMENTAL DETAILS

A. 184-Inch Cyclotron Bombardments

All targets were bombarded in the internal beam of the 184-inch cyclotron. Foils were used as target materials in the cases of the copper, silver, and tin; for the bromine bombardments, very pure ammonium bromide powder wrapped in special purity aluminum foil was used; and for the barium bombardments, very pure barium carbonate wrapped in the special purity aluminum foil was used. These targets were mounted on the end of a movable probe, and the energy of the bombarding proton was selected by an accurate adjustment of the radial distance from the origin of the beam to the leading edge of the target.

The maximum energy of the bombarding proton is a function of the radial distance from the origin of the beam to the leading edge of the target; and since the variation of the energy with radius is known precisely, the precision with which the bombarding energy can be selected depends on the measurement of the distance from the leading edge of the target to the origin of the beam. The measurements are probably good to within 5 Mev at energies of 100 Mev. The spread in energies of the particles for a given radial setting varies from about 3 percent at 348 Mev to 15 to 20 percent at energies around 60 to 70 Mev. This spread in the energy of the particles does not affect the maximum energy of the particles for a given radial setting, since the spread is due to the fact that some of the paths of the particles, though circular, have centers which oscillate about the origin of the beam, and the fixed circular path gives the maximum energy to the particle for a given radial setting of the target.

B. Chemical Separation Procedures

The chemical separation procedures must meet severe requirements, since the amount of interfering radioactivities must be reduced to such a degree that the nuclides of interest can be accurately measured by their characteristic radiations. The cross sections for formation of the nuclides produced in the targets bombarded in this series of studies vary from about 10^{-24} cm^2 down to the observed cross sections of about 10^{-32} cm^2. Since the number of atoms of the radio-nuclides which were studied here were extremely small compared with the number of atoms of the interfering radionuclides, it was necessary that the chemical separation procedures give a radioactive decontamination of at least 10^8 from all other radioactivities formed in the targets.

Sodium from Copper

The copper target was dissolved in concentrated hydrochloric acid and hydrogen peroxide, and 5 mg of sodium chloride was added as carrier. Carriers for the elements zinc through potassium were added, the solution adjusted to 1.5*N* in hydrochloric acid, and the copper precipitated as the sulfide. The solution was boiled to dryness to remove the excess acid, the residue dissolved, and then the solution made alkaline with ammonium hydroxide. Hydrogen sulfide was added, and the sulfides and hydroxides were precipitated. Additional 3-mg portions of carriers zinc through scandium were added and precipitated. This scavenging process was repeated twice. Excess hydrochloric acid was added to the alkaline sulfide solution, the acidified solution boiled to dryness, and the ammonium chloride driven off. The residue was dissolved in water, the solution checked to make sure it was neutral, and the sodium precipitated as the sodium zinc uranyl acetate. Two 5-ml portions of zinc uranyl acetate were used to wash the precipitate, and the precipitate was then dissolved in absolute ethyl alcohol saturated with hydrogen chloride gas. The resulting solution was cooled in an ice bath and the sodium chloride separated by centrifugation. The sodium chloride precipitate was washed with a 5-ml portion of the alcohol-hydrogen chloride solution. The sodium chloride was dissolved in water and the solution neutralized with potassium hydroxide. The sodium was again precipitated as sodium zinc uranyl acetate, and the precipitate was then washed with additional zinc uranyl acetate and dissolved in absolute alcohol saturated with hydrogen chloride. An additional portion of the alcohol-hydrogen chloride solution was added to wash the precipitate, and then the precipitate was transferred to a plate for counting.

[8] L. Marques and I. Perlman, Phys. Rev. **81**, 953 (1951).
[9] Harding, Lattimore, and Perkins, Proc. Roy. Soc. (London) **A196**, 325 (1949).
[10] D. H. Perkins, Proc. Roy. Soc. (London) **A203**, 399 (1950).
[11] M. M. Addario and S. Tamburino, Phys. Rev. **80**, 749 (1950).

Chlorine from Copper

The copper target was dissolved in concentrated nitric acid and 5 mg of chlorine as sodium chloride added to the solution. The chlorine was distilled and trapped in a solution made up of 3 to 4 ml of water containing 2 to 3 drops of concentrated nitric acid and sufficient silver nitrate to precipitate the 5 mg of chlorine as silver chloride. The resulting solution was heated almost to boiling to coagulate the precipitate. The precipitate was separated and washed with dilute nitric acid. The silver chloride was dissolved in ammonium hydroxide and carriers for zinc, copper, nickel, cobalt, and iron added. The ferric hydroxide precipitate was removed by centrifugation and a slight excess of iodine added as sodium iodide. The silver iodide precipitate was removed, the solution made 0.5*N* in nitric acid, 5 to 10 mg of bromine added as sodium bromide, the bromide and iodide oxidized with persulfate, and the bromine and iodine distilled. Silver nitrate was added to the solution and silver chloride was precipitated again. The precipitate was washed with dilute nitric acid and redissolved in dilute ammonium hydroxide. Carriers for zinc, copper, nickel, cobalt, and iron were again added and the ferric hydroxide precipitate removed. The solution was acidified with nitric acid and the silver chloride reprecipitated. The steps for separation of bromine should not be necessary, but were used in order to provide for the eventuality of a very small amount of selenium impurity in the copper which might form some interfering bromine radioactivities during the bombardment of the copper.

Scandium from Bromine

The ammonium bromide powder was dissolved in water, 5 mg of scandium carrier added, the solution adjusted to a *p*H of 3.0, and then transferred to a separatory funnel (consisting of a 40-ml calibrated centrifuge cone with a stopcock sealed to the bottom). Ten ml of 0.5*N* thenoyltrifluoroacetone in benzene was added and the mixture stirred for 5 minutes to extract the chelate compound which scandium forms with the thenoyltrifluoroacetone. The organic layer containing the scandium was washed 3 times with 10-ml portions of water, and then the scandium was extracted from the organic phase with 10 ml of 1*N* hydrochloric acid. Five mg each of arsenic, selenium, and germanium carriers were added. The solution was made alkaline with ammonium hydroxide; and hydrogen sulfide was added to form the polysulfides of selenium, arsenic, and germanium. The scandium precipitates as the hydroxide from this alkaline solution. The precipitate was washed with ammonium sulfide and the scandium dissolved in 6*N* hydrochloric acid. Iron and gallium carriers were added and extracted from the acid solution with ethyl acetate. Approximately 5 mg of arsenic carrier was added and arsenic sulfide precipitated. Another 5 mg of arsenic carrier was added and the arsenic again precipitated as the sulfide. The solution was made alkaline with ammonium hydroxide to precipitate the scandium as the hydroxide. The precipitate was dissolved in hydrochloric acid and the solution adjusted to a *p*H of 3.0. The scandium was extracted with 10 ml of 0.5*M* thenoyltrifluoroacetone, the organic layer washed with water, and the scandium extracted from the organic layer with 1*N* hydrochloric acid. The solution containing the scandium was adjusted to 0.5*N* in hydrochloric acid, and 0.2 ml of 27*N* hydrofluoric acid was added to precipitate scandium fluoride. The precipitate was washed with 5 ml of 0.5*N* hydrochloric acid containing 2 drops of 27*N* hydrofluoric acid. The scandium fluoride precipitate was dissolved in sulfuric acid, the hydrofluoric acid distilled, and the scandium precipitated as the hydroxide.

Cobalt from Silver

The silver target was dissolved in nitric acid, 5 mg of cobalt added, and the silver precipitated as silver chloride. Approximately 5 mg of iron carrier was added and the solution made alkaline with ammonium hydroxide. The ferric hydroxide precipitate was washed with hot ammonium chloride and the wash added to the supernatant solution. Approximately 5 mg of strontium carrier was added and strontium carbonate precipitated by adding sodium carbonate. The strontium carbonate precipitation was repeated and the supernatant solution adjusted to 0.3*N* in hydrochloric acid. Five-mg portions of cadmium, palladium, and copper carrier were added to the solution and the sulfide precipitated with hydrogen sulfide. The supernatant solution was made alkaline with ammonium hydroxide and the cobalt precipitated as cobalt sulfide. The precipitate was washed with water to remove the ammonium sulfide and then dissolved in nitric acid. Silver carrier was added to the solution and silver chloride precipitated to remove any silver which might not have been removed. The solution was made alkaline with potassium hydroxide, and the cobalt hydroxide precipitate was removed. The cobalt hydroxide was dissolved in acetic acid and potassium cobaltinitrite precipitated by adding an equal volume of a hot saturated solution of potassium nitrite. The precipitate was washed and then dissolved in concentrated hydrochloric acid. The solution was adjusted to 0.1*N* in hydrochloric acid, and 3 g of sodium thiocyanate was added. The thiocyanate complex ion of cobalt was extracted into a one to one mixture of amyl alcohol and diethyl ether. The cobalt was extracted from the alcohol-ether layer with 6*N* aqueous ammonium hydroxide and the cobalt precipitated as the sulfide. The sulfide precipitate was dissolved in concentrated nitric acid, the solution neutralized with potassium hydroxide and then acidified with acetic acid. The cobalt was precipitated in the final form as potassium cobaltinitrite.

Sodium from Tin

The separation of the sodium from the tin is almost the same as that for the separation from copper. Dif-

ferent carriers, ruthenium, palladium, molybdenum, silver, strontium, rubidium, lanthanum, iron, and calcium were added and then precipitated several times to remove the interfering activities. The subsequent sodium precipitations were carried out in the manner given in the section on sodium from copper.

Gallium from Tin

The tin target was dissolved in concentrated hydrochloric acid with just sufficient concentrated nitric acid added dropwise to speed the dissolving of the tin. Five mg of gallium carrier and "hold-back" carriers for iron, antimony, ruthenium, and molybdenum were added to the solution. The solution was adjusted to 7.75*N* in hydrochloric acid and the gallium extracted with isopropyl ether. The ether layer was washed six times with 10 ml portions of 7.75*N* hydrochloric acid. The gallium was extracted from the ether layer with water. The water layer was adjusted to 1*N* in hydrochloric acid and the sulfides precipitated with hydrogen sulfide. Milligram amounts of molybdenum, antimony, and palladium were added to the supernatant solution and the sulfides precipitated. Molybdenum, antimony, and palladium carriers were again added and the sulfides precipitated. Three mg of antimony carrier was added to the supernatant solution and antimony sulfide precipitated. The antimony sulfide precipitation was repeated three more times. The supernatant solution was boiled to remove the hydrogen sulfide and then adjusted to 1*N* in sodium hydroxide. The ferric ion, which follows the gallium through the chemical separations, precipitates here as the hydroxide. Three mg of strontium was added and the strontium precipitated as the carbonate. Five mg of iron carrier was added and the hydroxide precipitated. The solution was adjusted to 7.75*N* in hydrochloric acid and the gallium extracted with isopropyl ether. The ether layer was washed three times with 10-ml portions of 7.75*N* hydrochloric acid, and the gallium was extracted from the ether layer with water. Five mg of ruthenium carrier and 5 ml of concentrated perchloric acid were added and the resulting solution evaporated to dryness. Five ml of concentrated perchloric acid was again added and the solution again evaporated to dryness. The residue was taken up in 1*N* hydrochloric acid, 2 mg of antimony carrier added, and the antimony precipitated as the sulfide. Two mg of antimony was again added to the solution and the sulfide precipitated. The solution was boiled to remove the hydrogen sulfide and adjusted to a *p*H of 5.5 with sodium hydroxide to precipitate gallium hydroxide. The hydroxide precipitate was dissolved and adjusted to 7.75*N* with hydrochloric acid. The gallium was extracted with isopropyl ether and the ether layer washed twice with 10-ml portions of 7.75*N* hydrochloric acid. The gallium was extracted from the organic layer with water and the water layer adjusted to a *p*H of 5.5 with sodium hydroxide to precipitate the gallium hydroxide.

Gallium from Barium

The procedure used for the chemical separation of gallium from the irradiated barium was essentially the same as that described in the section "sodium from tin."

Chromium from Copper

The irradiated copper or the Nylon catcher foils were dissolved in concentrated nitric acid and the nitrate converted to the chloride by boiling with hydrochloric acid. Carriers for the elements calcium through zinc were added, the solution adjusted to 2*N* in hydrochloric acid, and the copper precipitated as the sulfide. The supernatant solution was made alkaline with ammonium hydroxide and the alkaline sulfides precipitated. The precipitate was dissolved in concentrated nitric acid and manganese dioxide precipitated by adding potassium chlorate. The supernatant solution was adjusted to about 0.1*N* in nitric acid, and cooled in an ice bath. Hydrogen peroxide was added to form the blue peroxychromic acid, which was extracted into diethyl ether. The ether layer was washed four times with 5-ml portions of water acidified with two drops of concentrated nitric acid. Five ml of water made alkaline with sodium hydroxide was added to extract the chromium from the ether layer. The ether was removed by evaporation and the chromium oxidized completely with hydrogen peroxide in the alkaline solution. After boiling to remove the excess peroxide, the solution was made slightly acid, and the chromium precipitated in the final form as barium chromate.

We wish to thank Mr. James T. Vale and the group operating the 184-inch cyclotron for the irradiations performed in the course of these studies.

The Absolute Absorption Coefficient of Germanium and the Fine Structure in the *K* Edge of Some of its Compounds*

H. GLASER†
Rowland Physical Laboratory, Johns Hopkins University, Baltimore, Maryland
(Received December 7, 1950)

The fine structure of the *K* absorption limit of Ge in GeH_4, Ge_2H_6, $GeCl_4$, and $GeBr_4$ has been obtained with absolute values under conditions of high resolution with a double crystal x-ray spectrometer. Results are compared with existent theory and previous measurements and discrepancies are pointed out. The question of the location of an absorption edge is considered along with the Kossel structure appearing in the germanium hydrides.

I. INTRODUCTION

UNDER high resolution the absorption edges of particular elements frequently exhibit a fine structure which depends not only on the element in question, but also on the compound of which the element may be a part, and on the physical state of the material.

Monatomic gases possess a Kossel structure[1] arising in transitions from inner levels to optical levels. Depending on the width of the inner level, the separation of the appropriate valence levels, and the resolving power of the spectrometer, a pronounced structure extending over a few volts may appear as in the case of argon,[2] or no structure whatever may be resolved as in the case of krypton.[3]

The Kossel structure may equally well exist in gaseous molecules, but the optical levels for the atom in question would be considerably modified by the molecular field. Moreover, such structure may be obscured by a more prominent type of structure of a different origin (see below).

When the absorbing element occurs in the solid state or is part of a solid compound, structure may extend over a few hundred volts. A theoretical explanation has been given by Kronig in terms of the Bragg reflection at the lattice planes.[4]

Interference effects may occur with gaseous molecules also to give rise to a fine structure to which we shall refer as "Kronig" structure. (The structure in crystals referred to above has generally been designated as Kronig structure.) Structure of this type has been studied in the diatomic molecules, bromine,[3,5-7] and chlorine,[7,8] and in the polyatomic molecules, arsenic trichloride[9,10] and germanium tetrachloride.[9-12] Bromine and chlorine display a single pronounced peak inasmuch as successive ones expected are too small to distinguish from experimental error. A number of maxima and minima occur in the polyatomic molecules $AsCl_3$, $GeCl_4$, $GeBr_4$, and similar compounds where the structure remains quite detectable even beyond the seventh peak. A theoretical calculation of the fine structure to be expected in a gaseous molecule has been carried out most completely[13] for $GeCl_4$. The electron wave originating in the photoelectric absorption process will be scattered by the other atoms in the molecule giving rise to a reflected wave superimposed on the outgoing wave. The probability of transition between the bound *K* state of the electron and the free state where it has kinetic energy, w, is proportional to $|P|^2$ where $P=\int \varphi_K \varepsilon r \varphi_w d\tau$.

In the case of an isolated atom this probability (as a function of energy) would decrease smoothly from some maximum value, but in a molecule it may oscillate. The wave function, φ_w, is the sum of the wave function of an escaping free electron with energy, w, and the scattered waves which cause the value of φ_w and of the integral to oscillate as the various waves interfere constructively or destructively. The absorption coefficient will therefore show an oscillation with frequency. Roughly speaking, this picture is the basis for the Kronig structure in a gaseous molecule.

While it is difficult to develop a quantitative theory for the Kronig structure in crystals, it has been possible to obtain an explicit expression for the ratio, χ, of the absorption coefficient of an atom, A, bound in a diatomic molecule, AB, to that of the isolated atom as a function of the energy of the ejected electron.[14] Moreover, if the absorbing atom, A, is contained in a polyatomic molecule, $AB_1\cdots B_i$, it can be shown[15] that the ratio, χ, is given to a good approximation by

$$\chi-1=\sum_i(\chi_i-1), \qquad (1)$$

* Part of a thesis submitted to the Faculty of Philosophy in conformity with the requirements for the degree of Doctor of Philosophy.
† Now at Texas Technological College, Lubbock, Texas.
[1] W. Kossel, Z. Physik **1**, 119 (1920).
[2] Lyman G. Parratt, Phys. Rev. **56**, 295 (1939).
[3] C. H. Shaw, Phys. Rev. **57**, 877 (1940).
[4] R. de L. Kronig, Z. Physik **70**, 317 (1931); **75**, 191 (1932).
[5] Bernard Cioffari, Phys. Rev. **51**, 630 (1937).
[6] S. T. Stephenson, Phys. Rev. **50**, 790 (1936).
[7] T. M. Snyder and C. H. Shaw, Phys. Rev. **57**, 882 (1940).
[8] A. E. Lindh, Compt. rend. **172**, 1175 (1921); dissertation, Lund (1923).
[9] D. Coster and G. H. Klamer, Physica **1**, 889 (1934).
[10] S. T. Stephenson, Phys. Rev. **71**, 84 (1947).
[11] T. D. Drynski and R. Smoluchowski, Physica **6**, 929 (1939).
[12] C. H. Shaw, Phys. Rev. **70**, 643 (1946).
[13] Hartree, Kronig, and Petersen, Physica **1**, 889 (1934).
[14] R. de L. Kronig, Z. Physik **75**, 468 (1932).
[15] H. Petersen, dissertation, Groningen; Arch. Néerland. sci. **14**, 165 (1933).

where χ_i is the value of χ to which the atom, B, would give rise if it formed a diatomic molecule with A. The fine structures are therefore additive.

The theory[14] has been applied to $GeCl_4$ because of several favorable circumstances: the scattering atoms are sufficiently massive to scatter the photoelectrons strongly; the absorption edge of the Ge atom falls in a spectral region of sufficient resolution to delineate the fine structure; the molecule is symmetrical, all four Cl atoms contributing equally; the interatomic distance of Ge—Cl is known[15] from electron diffraction experiments to be 2.10A; the atomic field of the chlorine atom has been solved; an adequate vapor density can be obtained at low enough temperatures; the gas is stable.

If one chooses the K absorption edge and restricts himself to the nonvacuum region and to regions of dispersion greater than about 3 seconds of arc per volt, the elements available are Cr ($Z=24$) to Sr ($Z=38$). Cr, Mn, Fe, Co, Ni, Cu, Zn, Rb, and Sr compounds are not easily vaporized. Kr does not ordinarily form compounds. Ga, Ge, As, Se, and Br remain to be considered. Kronig structure has been reported for $GeCl_4$, $AsCl_3$, and Br_2; gallium halides are convenient for this type of study, but the selenium compounds tend to decompose at temperatures required for suitable vapor pressures. The compounds of Ga, Ge, and As are not equally desirable. Ge compounds are preferred because they yield the most pronounced structure with four scatterers instead of three; its halides have lower boiling points; it is less dangerous to handle than arsenic; Ga seems to form no gaseous compound with hydrogen comparable to AsH_3 or GeH_4. The existence of such a gaseous hydrogen compound is required to answer the question which originally suggested this investigation.

If for $GeCl_4$ one averages the absorption coefficient through the structure on the high frequency side of the K edge one would expect intuitively that the average mass absorption coefficient would be the same as that of isolated germanium. The ideal solution to this question would involve the use of an absorption cell of monatomic germanium vapor. An evaporated film of germanium would be inadmissible because it would exhibit its own Kronig structure peculiar to its crystalline state. A close approximation to the idealized case of a monatomic vapor of germanium is germane, GeH_4, since the H atoms would not be expected to scatter by a measurable amount. One would anticipate, therefore, a structureless absorption edge with which the structure-rich germanium halides could be compared. The present work obtains the ratio of the average absolute absorption coefficient of Ge in the germanium halides to that of Ge in germane, which, as far as Kronig structure is concerned, behaves like an isolated Ge atom. The theory gives for this ratio a value between 1.1 and 1.15 on the basis of certain convenient assumptions and the omission of certain terms difficult to evaluate but which are estimated to be small in their effect. Physically, one expects this ratio to be unity and so these simplifications may need to be re-examined. The existent theoretical predictions with regard to both position and number of the maxima and minima are also compared with experiment, and the question of an absorption edge position and width considered.

[14] R. Wierl, Ann. Physik 8, 521 (1931).

II. EXPERIMENTAL

The spectrometer used was a Societé Génevoise double crystal instrument.[17] Many sets of calcites were rejected before a set giving satisfactory rocking curve and line widths was found. In each case the crystals were aligned in both the $(1, -1)$ and $(1, +1)$ positions by visual observation of the copper K_α lines on a fluorescent screen, the criterion for adjustment being the sharp appearance and disappearance of the copper lines as the second crystal was rotated. Measurements were then made on the rocking curve and CuK_{α_1} line widths. The set of crystals finally selected gave rocking curve widths of 10.5″ and 8.7″ at 1.54 and 1.11A, respectively, and a $(1, +1)$ CuK_{α_1} width of 41″, values which are within a second of the best reported values.[18]

The high voltage and x-ray tube current were electronically regulated to within 0.01 and 0.1 percent, respectively, over 4-minute intervals.[19] At a power of 22 kv and 30 ma as used, the direct intensity was about 5000 counts per two-minute interval from the continuous radiation of the tungsten target, and higher in the neighborhood of some weak tungsten emission lines. The voltage was purposely kept as low as 22 kv in order not to excite second-order radiation of 0.557A.

X-ray intensities were measured with a 30-cm chlorine-quenched argon counter (with scale of 64 and mechanical counter) over two minute intervals timed by a synchronous, motor-driven switch.

The absorption cells were of the in-blown glass window type, of soft glass, and generally with 10-cm absorption path lengths. The latter were measured accurately by means of a traveling microscope. Two fingerlike extensions were provided, the upper for attaching to a glass system for the purpose of filling the cell and the lower for freezing out the material with liquid N_2 during the sealing-off process. A mercury manometer as part of the glass system was used to read pressures for all the absorption cells except $GeBr_4$, whose vapor pressure was too low at room temperature. The purified $GeBr_4$ was added to its cell by means of an eye dropper. In all cases air was removed from the cells before sealing off. The cells were all filled at known room

[17] We are greatly indebted to the University of Chicago for making this instrument available to us for this work. The assistance of Professor Zachariasen in making the loan possible is highly appreciated.

[18] J. A. Bearden and C. H. Shaw, Phys. Rev. 48, 18 (1935).

[19] The planning and construction of the high voltage power supply were done largely by Mr. Earl H. Byerly.

temperatures to relatively low pressures:[20] GeH_4, 128.9 mm and 145.2 mm; $GeCl_4$, 99.14 mm; Ge_2H_6, 79.73 mm; Cl_2, 298.2 mm; HBr, 550.0 and 403.8 mm. (A knowledge of the mass absorption coefficients of chlorine and bromine was required in the calculations on the germanium halides.) The $GeBr_4$ cell was used at 156 mm at a temperature of approximately 145°C. The actual masses of material are in the range of 10 to 60 mg, and except for $GeBr_4$, densities were always calculated by means of the van der waals equation.

The densities represented by these conditions of temperature and pressure were so selected that all of the absorption cells except that of $GeBr_4$ would give rise to satisfactory counting rates while used at room temperature. Such low densities are preferred in maintaining counting rates far above background and in eliminating the necessity of temperature controlled ovens which other investigators have used.[9–12] For $GeBr_4$, however, with a vapor pressure of only 4 mm at room temperature, an oven had to be provided. The $GeBr_4$ cell was covered with thin asbestos paper, wound

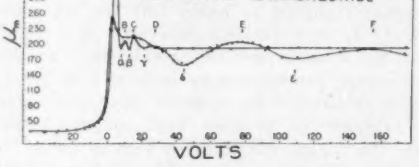

FIG. 1. Superposed graphs of the absolute absorption coefficient of Ge in GeH_4 and $GeCl_4$ as a function of energy separation from the K edge.

with nichrome wire and heat-insulated with glass cloth. The temperature was maintained at an estimated 20° above that required for complete evaporation of the $GeBr_4$ liquid so that temperature control was not critical. In fact, by the proper choice of the density of material in each cell no liquid phase existed, and hence there was no temperature control problem.

To insure that the cell was accurately returnable to its absorbing position in the x-ray beam, a cell holder was mounted on a platform which could translate on a track with V-shaped runways. A stop was provided and the whole structure was attached rigidly to the spectrometer posts. The cell holder had a number of degrees of freedom sufficient for optimum adjustment of the cell in the x-ray beam.

The background correction was determined by measuring the intensity while the second crystal was rotated beyond the position at which it passed diffracted radiation at both the longer and shorter wavelengths. As the second crystal was rotated beyond this position (at 1 to 1.5 Bragg angle degrees away from the Ge absorption edge setting), the background was found to be fairly constant. This extrapolated average count was taken as the background and determined similarly for I and I_0.

The determination of the absolute absorption coefficient necessarily involved a correction for the absorption of the glass windows, for the change in air path by approximately 10 cm as the cell was placed in the beam and for absorption by other atoms in the molecule. The calculation for $GeCl_4$, for example, yielded for the absolute absorption coefficient of Ge

$$\mu_{Ge}=[1/(\rho x)_{Ge}][\log(I_0/I)+\log f]-(\mu\rho x)_{Cl}/(\rho x)_{Ge},$$

where ρ denotes density, x the absorption path length, I_0 the intensity recorded by the Geiger counter without absorption cell in position, I the intensity with the cell in position, and

$$f=\exp(10\mu\rho)_{air}/\exp(\mu\rho x)_{glass}=I_1/I_0.$$

I_1 denotes the value of I with $GeCl_4$ frozen out. The ratio $(\rho x)_{Cl}/(\rho x)_{Ge}=\rho_{Cl}/\rho_{Ge}$ is determinable from the atomic weights, while the absorption coefficient of Cl (or of Br) was separately determined.

The procedure used in taking data was to measure for two minutes at each point the direct intensity, I_0, and then the intensity, I, after absorption through the cell, and to repeat a number of times until the desired accuracy could be obtained. Ten to twenty thousand counts were registered for each point on the high frequency side of the edge, and twenty-five to fifty thousand on the low frequency side. For the direct intensity forty to sixty thousand counts were recorded. Points were taken at 2″ intervals on the high peaks, and at 3″, 5″, 10″, or larger intervals elsewhere. The counts were corrected for scattered radiation, the absorption of the glass windows and of Cl, Br, or H atoms was determined, and the absorption coefficient of Ge was calculated as above. The probable error in μ arising from statistical fluctuation in counts is less than 2 percent. The relative values of μ are thus considered to be accurate to 2 percent. The absolute values, which depend on measured pressures, lengths of cells, background, absorption of glass and of other atoms in the compounds are considered to be accurate to within 3 percent.

III. RESULTS AND DISCUSSION

In Figs. 1, 2, and 3 the absolute absorption coefficient of Ge at its K edge is plotted as a function of energy for the gaseous molecules GeH_4, $GeCl_4$ (superposed with GeH_4 in order to facilitate a comparison of the magnitudes of the absorption coefficient), Ge_2H_6, and $GeBr_4$. The original data for these germanium compounds extend to about 45 v on the low frequency side and 175 v on the high frequency side of the edge. For digermane, only the significant region near the edge

[20] Dr. Gordon K. Teal of the Bell Telephone Laboratories very kindly supplied the GeH_4 and the Ge_2H_6 needed for this investigation.

has been plotted, inasmuch as the absorption coefficient levels off to a constant value on either side.

Consider first the question of the location of an absorption edge and the determination of its width. Definite conclusions concerning the position and width of an absorption edge can be drawn, in some cases, for monatomic gases. An absorption edge of a monatomic gas is customarily established at the energy position at which transitions to the optical continuum begin. The location of this point on the energy scale requires an analysis of the absorption edge whether structure be apparent or not, the structure being designated as Kossel structure. The K edge of argon, for example, exhibits a pronounced absorption peak followed by some smaller maxima and minima. Paratt[2] resolved the structure into its components using the optical p-terms of potassium, for when a $1s$ electron is ejected into the optical levels it will find itself in a field approximating that of the element $Z+1$. Hence, all of the energy intervals between the resonance absorption lines $1s \rightarrow np$, $n>3$, are known. These absorption lines are characterized by the same width, which, since the widths of the optical levels are negligible, is also the width of the inner K state according to the theory of line widths.[21] From the main resonance line that width is 0.58 ev. In view of the definition of the edge position, that of argon is 2.71 ev (the ionization limit of potassium minus the energy interval between the terms $4s$ and $4p$) from the peak of the main resonance line and to shorter wavelengths. Since the width of the main edge is essentially that of the K state, its width is 0.58 ev. The shape of the main edge is, moreover, an arctangent curve.[22] With position, shape, and width known, the main edge can be drawn in readily, and as a result of the resolution it is found to be located at 3.5 to 4 X.U. less than was assumed previously. (The edge was usually placed at the center of the main rise.)

Krypton does not allow such fortunate and definite conclusions. The width of its K state is about 2.1 ev, the optical levels of rubidium are more closely spaced, and the physical resolving power about 78 percent less. The K edge of krypton therefore appears as structureless. Shaw[3] made a "reasonable" resolution into components presumably from a knowledge of the optical levels and ionization potential of rubidium, with the aid of which he was able to place the main edge of krypton to perhaps within half a volt. It is important to bear in mind that the optical energy scheme of ionized krypton was fairly well known from the terms of element $Z+1$.

Another favorable circumstance sometimes occurs in the case of metals where bands of energy replace simple optical levels. If certain assumptions are approximately satisfied, one can obtain both the position and the width of the edge from the experimental absorption

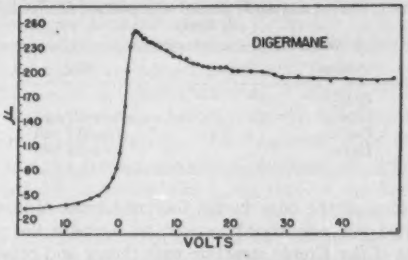

FIG. 2. The absolute absorption coefficient of Ge in Ge_2H_6 as a function of energy separation from the K edge.

curve with the help of the theory of Richtmyer, Barnes, and Ramberg.[22]

In contrast to the examples above the germanium compounds here studied present a different picture, for in none of these cases does the electronic energy scheme appear to be known and each molecule becomes an individual problem. Nor can the theory of Richtmyer, Barnes, and Ramberg be applied. As a result no definitive statement can be made concerning the position of the Ge edge or its width, nor can a quantitative interpretation be given of the associated Kossel structure. The picture is complicated further by the presence of both Kossel and Kronig structure in some of the compounds.

In a personal communication, Professor Kronig compares the molecule GeH_4 with the krypton atom by thinking of GeH_4 as Ge^{IV-} ion in the electron shell of which four hydrogen nuclei are embedded. The absorption maximum could then be associated with the transition of the K electron to the $5p$-orbit of the krypton-like system. The peak thus represents Kossel structure.

Physically, the Kossel structure exists for the four molecules of germanium studied; but, since the molecular field varies from compound to compound, it is difficult to state whether or not the spectrometer would resolve Kossel structure for all four, even in the absence of Kronig structure. The prominent Kronig structure in the halides in any case has obscured any Kossel structure that would otherwise have manifested itself. For the reasons cited above, a comparison of the

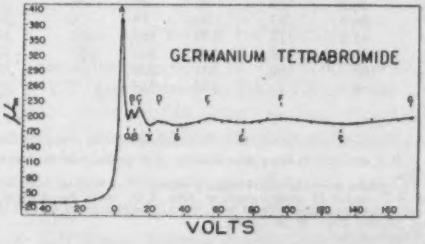

FIG. 3. The absolute absorption coefficient of Ge in $GeBr_4$ as a function of energy separation from the K edge.

[2] V. Weisskopf and E. Wigner, Z. Physik 63, 54 (1930).
[3] Richtmyer, Barnes, and Ramberg, Phys. Rev. 46, 843 (1934).

TABLE I. Shift of arbitrarily defined edge position relative to that of GeH_4.

Substance	Shift
GeH_4	0
Ge_2H_6	0.5±0.2 volt
$GeCl_4$	0.8±0.2 volt
$GeBr_4$	0.9±0.2 volt

position of the edge in the four molecules cannot be carried out properly. However, to compare the positions of the Kronig structure with theory and previous experiment some scheme had to be adopted. It was decided for the sake of convenience to select the point representing the average absorption coefficient between the mean on the high frequency side and on the low. This point is roughly at $\mu=110$ for all the germanium compounds (and would be the point of the edge if the theory of Richtmyer, Barnes, and Ramberg applied). While this choice is arbitrary, it should be pointed out that the methods previously used to locate the edge were equally arbitrary.[9-12] Table I lists the shift to shorter wavelengths of the particular point selected using that of GeH_4 as reference.

Judging from the positions of the fine structure of the $GeCl_4$, serious discrepancies appear to exist between theory and experiment (both of which exist for this halide only). These disagreements are demonstrated under the high resolution of the double crystal x-ray spectrometer, but they escaped notice in the early experiments performed under relatively poor resolution. Table II compares the positions of the structure predicted by the theory, the present measurements, and the tabulated results of other investigators.

From Table II it is clear why it was believed earlier that experiment supported theory. Above 50 volts, experiment and theory appeared to agree quite well, but the serious disagreements occur near the edge for the most part. (Uncertainty in edge position would be a maximum of 3 volts.) If one of the first few peaks and valleys of the present work were eliminated, the same sort of agreement would arise, i.e., if peak *E* were placed in the row for peak *D*, etc. Then agreement would exist at energies in excess of 50 v (as previously found[9-11]) but still not at smaller energies. The early single crystal photographic work simply could not resolve narrow structure (the peaks *A*, *B*, *C*, and *D* extending through about 27 v tended to coalesce into a single peak), while in the double crystal work[10] several factors operated against proper detection of structure: (1) a rocking curve width of as much as 13″ (the predominant factor), (2) probable temperature fluctuations due to the use of a Variac-controlled oven, (3) moving the absorption position of the cell slightly between runs. The rocking curve width should be in the neighborhood of 8″ for best results, an oven need not be used, and the cell is best not disturbed during runs.

Shaw[12] has also obtained the curve for $GeCl_4$ and with very fine resolution, but not with the absolute absorption coefficient. As did Stephenson, Shaw used for the jump of the absorption coefficient at the edge a value interpolated from adjacent atomic numbers, but that value (7.95) now appears to be in error (see below). He did not tabulate the positions of the structure, but from inspection his maxima and minima agree fairly well in position with those reported here for $GeCl_4$.

TABLE II. Comparison with theory and previous experiments of energy positions in volts of the fine structure maxima and minima for $GeCl_4$; and present values for $GeBr_4$.

Structure[a]	Present work[b]	Theory[c]	Ref.[d]	Ref.[e]	Ref.[f]	$GeBr_4$ present work
A	3.85	2.8			3.4	3.26
α	7.41	10.5			8.5	6.82
B	9.48	19		16	18	8.75
β	11.8	27				10.6
C	14.4	40				13.2
γ	20.8	59	50	48	46	19.3
D	26.9	85	86	79	74	24.6
δ	43.8	117	120	110	117	35.6
E	77.3	155	160	160	157	53.0
ϵ	108	196	203	208		73.7
F	154		257	258		95.8
ζ						131
G						172

[a] *A*, *B*, *C*, etc. refer to absorption maxima; α, β, γ, etc., refer to absorption minima.
[b] The values were calculated using a dispersion of 6.95 seconds/volt at 1114 X.U. and 6.72 seconds/volt at 1096 X.U., being based upon the newest physical constants listed by J. W. M. DuMond and E. R. Cohen, Revs. Modern Phys. 20, 82 (1948).
[c] Reference 13.
[d] Reference 9.
[e] Reference 11.
[f] Reference 10.

TABLE III. Experimental values of mass absorption coefficients at Ge *K* edge.

Substance	Value
Ge, low frequency side	30.5±3%
Ge, high frequency side	191.0±3%
Chlorine	42.6±1%
Rate of change approximately	0.23% per 8.6 volts
Bromine	36.1±1%
Rate of change approximately	0.21% per 8.6 volts

The discrepancy between theory and experiment goes beyond the positions of the maxima and minima and their numbers, for as stated earlier the average χ has a theoretical value of 1.1 to 1.15. As one averages out the structure over a sufficient energy interval, one expects physically a value of unity for χ and Fig. 1 shows the average value of χ to be unity within experimental error. The same conclusion holds in comparing $GeBr_4$ with GeH_4 or Ge_2H_6 with GeH_4. The magnitudes found for the mass absorption coefficients of Ge, Cl, and Br at the wave length of the Ge *K* edge (1114 X.U.) are shown in Table III. The mass absorption coefficient of Ge at its *K* edge jumps by a factor of 6.3 instead of 8 as previously assumed.

Among the factors contributing to the disagreement between theory and experiment, probably the most

serious is the assumption that the ejected electron finds itself in the field of a purely neutral chlorine atom, or in reality, of four such atoms. Another potential source of error may occur in the approximation leading to the additive result in Eq. (1). It was estimated by Petersen[16] that a double summation, quite laborious to evaluate, which takes account of molecular configuration, could be neglected, leading to this additive result.

Digermane represents an interesting case in that one would expect to see results similar to the Kossel structure peak of GeH_4 and at the same time at least a single Kronig structure peak as found for Cl_2 or Br_2. The experimental curve shows a peak at the same energy position as found for GeH_4, but it is of greater width with two "steps" suggesting a washed out structure. Any Kronig structure contribution can only be a small, wide maximum.

Structure for the two germanium halides presents similar features; but the positions of the structure are closer together for the tetrabromide (Table II), and the amplitudes for the latter are in general smaller. While it is true that the more massive bromine atoms ought to scatter more effectively, the increase in internuclear distance leads to the reverse effect. Until the correct fields of the bromine atoms in $GeBr_4$ are known, the fine structure cannot be calculated and so the experimental results are not compared with theory.

In view of the results obtained, it appears that the theory needs revision before it can be relied upon for quantitative predictions. The theoretical value of the ratio of the average absorption coefficient of Ge in the polyatomic molecule, $GeCl_4$, to that of the isolated atom is too high; the number and positions of the theoretically predicted maxima and minima are not in agreement with experiment. In addition the correct location of the position of the Ge edge and the determination of its width require first a resolution and analysis of the experimental curve.

The author wishes to express his gratitude to Professor J. A. Bearden, under whose direction this work was carried out. It is a pleasure to acknowledge helpful discussions with Professor R. de L. Kronig, Dr. G. L. Rogosa, and Dr. G. Schwarz. Thanks are also due to Dr. T. H. Berlin for valuable suggestions regarding the manuscript.

PHYSICAL REVIEW VOLUME 82, NUMBER 5 JUNE 1, 1951

Particle Spin and Rotation

NATHAN ROSEN
University of North Carolina, Chapel Hill, North Carolina

(Received September 21, 1950)

It is proposed to treat the spin of a particle phenomenologically by considering the particle as a small rotating sphere, the rotation of which is described by euler parameters. If the rotation is quantized in the space of the euler parameters, one obtains both integral and half-integral values for the spin. In this way one arrives at a formalism in which the spin components can be represented as differential operators in the Schroedinger representation.

FROM the standpoint of group theory, the spin of an electron is connected with the two-valued representations of the rotation group in three dimensions. In the present paper an attempt is made to investigate some properties of a model in which this connection is used.

1. ROTATION PARAMETERS

Let us consider a free particle with spin as a small rotating rigid sphere. Let us take two cartesian coordinate systems with origins at the center of the sphere, one, XYZ, with axes having fixed directions in space, the other, $X'Y'Z'$, rigidly attached to the sphere. To describe the rotation of the sphere one can make use of the euler angles θ, φ, ψ, where θ is the angle between the Z and Z' axes, φ is the angle between the Y axis and the intersection of the XY and $X'Y'$ planes, and ψ is the angle between the latter and the Y' axis. However, for the present purpose we shall introduce instead the euler parameters[1] defined by the relations

$$\begin{aligned}\xi&=\sin\tfrac{1}{2}\theta\sin\tfrac{1}{2}(\psi-\varphi),\\ \eta&=\sin\tfrac{1}{2}\theta\cos\tfrac{1}{2}(\psi-\varphi),\\ \zeta&=\cos\tfrac{1}{2}\theta\sin\tfrac{1}{2}(\psi+\varphi),\\ \chi&=\cos\tfrac{1}{2}\theta\cos\tfrac{1}{2}(\psi+\varphi),\end{aligned}\tag{1}$$

so that

$$\xi^2+\eta^2+\zeta^2+\chi^2=1.\tag{2}$$

In terms of these parameters, the direction cosines of the $X'Y'Z'$ axes relative to the XYZ axes are homogeneous quadratic functions,[1] so that changing the signs of all the parameters leaves the orientation of the sphere unchanged.

For the sake of greater generality and convenience, let us now take four new parameters ξ_k $(k=1, 2, 3, 4)$

[1] E. T. Whittaker, *Analytical Dynamics* (Cambridge University Press, London, 1937, or New York, 1944), pp. 8–16.

defined by

$$\xi=\xi_1/\rho, \quad \eta=\xi_2/\rho, \quad \zeta=\xi_3/\rho, \quad \chi=\xi_4/\rho, \tag{3}$$

where

$$\rho=(\sum \xi_k^2)^{\frac{1}{2}}. \tag{4}$$

Summations, unless otherwise indicated, are to be taken over the values 1 to 4. The space spanned by these parameters will be referred to as ξ-space.

From the properties of the euler angles and parameters[1] it is found that the components of angular velocity of the sphere with respect to XYZ are given by

$$\omega_i=2(\xi_4\dot{\xi}_i-\xi_i\dot{\xi}_4+\xi_k\dot{\xi}_l-\xi_l\dot{\xi}_k)/\rho^2, \quad (ikl)=(123), \tag{5}$$

where the relation $(ikl)=(123)$ means that (i, k, l) form a cyclic permutation of $(1, 2, 3)$ and a dot denotes differentiation with respect to the time. Similarly, the components of angular velocity with respect to $X'Y'Z'$ are given by

$$\omega_i'=2(\xi_4\dot{\xi}_i-\xi_i\dot{\xi}_4-\xi_k\dot{\xi}_l+\xi_l\dot{\xi}_k)/\rho^2, \quad (ikl)=(123). \tag{6}$$

The square of the angular velocity is then given by

$$\begin{aligned}\omega^2&=4\sum_{i<k}(\xi_i\dot{\xi}_k-\xi_k\dot{\xi}_i)^2/\rho^2\\&=4(\sum \xi_i^2\sum \dot{\rho}^2)/\rho^2.\end{aligned} \tag{7}$$

If the sphere representing the particle is assumed to have a moment of inertia I about any axis through its center, then its kinetic energy is given by

$$T=\tfrac{1}{2}I\omega^2=2I(\sum \xi_i^2\sum \dot{\rho}^2)/\rho^2. \tag{8}$$

The generalized momentum components are given by

$$\pi_i=\partial T/\partial\dot{\xi}_i=4I(\rho\dot{\xi}_i-\xi_i\dot{\rho})/\rho^3, \tag{9}$$

whence

$$\sum \pi_i^2=4I^2\omega^2/\rho^2. \tag{10}$$

The angular moment components of the sphere relative to XYZ and $X'Y'Z'$, respectively, are

$$M_i=I\omega_i, \quad M_i'=I\omega_i' \quad (i=1, 2, 3), \tag{11}$$

so that the square of the angular momentum is given by

$$M^2=I^2\omega^2=\tfrac{1}{4}\rho^2\sum \pi_i^2. \tag{12}$$

On the other hand, one can define in the ξ-space generalized angular momentum components

$$\mu_{ij}=\xi_i\pi_j-\xi_j\pi_j=4I(\xi_i\dot{\xi}_j-\xi_j\dot{\xi}_i)/\rho^2, \tag{13}$$

so that Eqs. (5) and (6) can be written

$$\begin{aligned}\omega_i&=(\mu_{4i}+\mu_{kl})/2I,\\ \omega_i'&=(\mu_{4i}-\mu_{kl})/2I, \quad (ikl)=(123).\end{aligned} \tag{5a}$$

It follows then that

$$\begin{aligned}M_i&=\tfrac{1}{2}(\mu_{4i}+\mu_{kl}),\\ M_i'&=\tfrac{1}{2}(\mu_{4i}-\mu_{kl}), \quad (ikl)=(123),\end{aligned} \tag{14}$$

and

$$M^2=\tfrac{1}{4}\sum_{i<j}\mu_{ij}^2. \tag{15}$$

To quantize the system in the ξ-space, one introduces commutation relations

$$\xi_k\pi_l-\pi_l\xi_k=i\hbar\delta_{kl}. \tag{16}$$

It follows from this that the μ_{ij} obey the usual commutation relations for angular momentum

$$\mu_{jk}\mu_{lm}-\mu_{lm}\mu_{jk}=i\hbar(\mu_{jl}\delta_{km}+\mu_{km}\delta_{jl}-\mu_{jm}\delta_{kl}-\mu_{kl}\delta_{jm}). \tag{17}$$

From Eqs. (14) and (17) it follows that the components M_j satisfy the usual commutation relations

$$M_jM_k-M_kM_j=i\hbar M_l, \quad (jkl)=(123). \tag{18}$$

On the other hand, for the components M_j' one obtains commutation relations of the form[2]

$$M_j'M_k'-M_k'M_j'=-i\hbar M_l', \quad (jkl)=(123). \tag{19}$$

The components M_j and M_k' commute, for all values of j and k.

2. POLAR COORDINATES

To investigate the quantization of the rotation in ξ-space it is desirable to introduce polar coordinates. Several different polar coordinate systems suggest themselves, but perhaps one of the most convenient is given by the relations:

$$\begin{aligned}\xi_1&=\rho\sin\alpha\cos\beta,\\ \xi_2&=\rho\sin\alpha\sin\beta,\\ \xi_3&=\rho\cos\alpha\sin\gamma,\\ \xi_4&=\rho\cos\alpha\cos\gamma,\end{aligned} \tag{20}$$

where $0\leqq\alpha\leqq\pi/2$, $0\leqq\beta<2\pi$, $0\leqq\gamma<2\pi$. Comparing this set of equations with Eq. (1), we see that

$$\alpha=\theta/2, \quad \beta=\tfrac{1}{2}(\varphi-\psi+\pi), \quad \gamma=\tfrac{1}{2}(\varphi+\psi). \tag{21}$$

The substitution of (20) into (8) gives for the classical kinetic energy

$$T=2I(\dot{\alpha}^2+\dot{\beta}^2\sin^2\alpha+\dot{\gamma}^2\cos^2\alpha). \tag{22}$$

From this, by the usual procedure for the case of curvilinear coordinates, one obtains as the Schroedinger equation

$$\nabla^2\Psi=-K^2\Psi, \tag{23}$$

where

$$K^2=8IT_e/\hbar^2=4(M^2)_e/\hbar^2, \tag{24}$$

the subscript e indicating the eigenvalue of the quantity in question, and

$$\begin{aligned}\nabla^2\Psi=\frac{1}{\sin\alpha\cos\alpha}\Big[\frac{\partial}{\partial\alpha}\Big(\sin\alpha\cos\alpha\frac{\partial\Psi}{\partial\alpha}\Big)\\ +\operatorname{ctn}\alpha\frac{\partial^2\Psi}{\partial\beta^2}+\tan\alpha\frac{\partial^2\Psi}{\partial\gamma^2}\Big].\end{aligned} \tag{25}$$

Separating variables and imposing on Ψ the conditions of finiteness, continuity, and single-valuedness

[1] O. Klein, Z. Physik 58, 730 (1929).

in the ξ-space, one gets as a solution

$$\Psi = G(\alpha)\sin^{|m|}\alpha\cos^{|n|}\alpha e^{i(m\beta+n\gamma)}, \tag{26}$$

where $m, n = 0, \pm 1, \pm 2, \cdots$, and

$$G(\alpha) = F(a, b; c; \sin^2\alpha), \tag{27}$$

where F is the hypergeometric function,

$$\begin{aligned} a &= \tfrac{1}{2}[|m|+|n|+1+(K^2+1)^{\frac{1}{2}}], \\ b &= \tfrac{1}{2}[|m|+|n|+1-(K^2+1)^{\frac{1}{2}}], \\ c &= |m|+1, \end{aligned} \tag{28}$$

and where, to make Ψ well-behaved, one must have

$$b = -p \quad (p = 0, 1, 2, \cdots), \tag{29}$$

or, setting $L = |m|+|n|+2p$,

$$K^2 = L(L+2). \tag{30}$$

Writing $L = 2S$ and using (24), we get

$$(M^2)_s = \hbar^2 S(S+1), \tag{31}$$

where $S = 0, \frac{1}{2}, 1, \frac{3}{2}, \cdots$. If the value of S is given, then m and n must satisfy the condition

$$S - \tfrac{1}{2}(|m|+|n|) = p. \tag{32}$$

Representing the μ_{jk} by operators, we have

$$\mu_{12}\Psi = -i\hbar\partial\Psi/\partial\beta = m\hbar\Psi, \tag{33}$$

$$\mu_{43}\Psi = -i\hbar\partial\Psi/\partial\gamma = n\hbar\Psi,$$

so that, by (14),

$$M_s\Psi = \tfrac{1}{2}\hbar(m+n)\Psi. \tag{34}$$

If, for $(M_s)_s$, the eigenvalue of M_z, we write $M_s\hbar$, then it follows that

$$M_s = \tfrac{1}{2}(m+n). \tag{35}$$

Similarly, if for $(M_s')_s$ we write $M_s'\hbar$, then

$$M_s' = \tfrac{1}{2}(n-m), \tag{36}$$

so that

$$m = M_s - M_s', \quad n = M_s + M_s'. \tag{37}$$

From (32) it follows that for a given value of S

$$M_s, M_s' = S, S-1, \cdots, -S+1, -S. \tag{38}$$

There are $2S+1$ different values of M_s, and for each such value there are $2S+1$ different states characterized by different values of M_s', giving a total of $(2S+1)^2$ states.

If one changes the signs of all four ξ-coordinates, the orientation of $X'Y'Z'$ relative to XYZ is left unchanged. Such a change of signs is brought about in the polar coordinate system by changing β to $\beta+\pi$, γ to $\gamma+\pi$. Now, if S is zero or an integer, m and n are both odd or both even, and Ψ remains unchanged; if S is a half-odd-integer, either m or n only is odd, and Ψ changes sign. Hence Ψ, as a function of ordinary space, is single-valued in the first case and double-valued in the second. In the first case the wave functions and eigenvalues are essentially the same as those obtained in the "symmetrical top" calculations[3] for the sphere.

The fact that, for S a half-odd-integer, the wave functions are double-valued functions in ordinary space does not appear to cause any difficulty.[4] It can be readily shown that if one operates on a wave function characterized by L, M_s, M_s' with a component M_j one obtains a linear combination of wave functions with the same L and M_s', but various values of M_s. Hence the criterion of acceptability proposed by Pauli is fulfilled.

3. CASE $S = \frac{1}{2}$

As a simple example, consider the case (say that of the electron) $S = \frac{1}{2}$, for which $M_s, M_s' = \pm\frac{1}{2}$. One readily obtains for this case the following four wave functions:

$$\begin{aligned} M_s = +\tfrac{1}{2}, M_s' = +\tfrac{1}{2}: &\quad \Psi_1 = \cos\alpha e^{i\gamma}/\pi, \\ = -\tfrac{1}{2} \quad = +\tfrac{1}{2}: &\quad \Psi_2 = i\sin\alpha e^{-i\beta}/\pi, \\ = +\tfrac{1}{2}, \quad = -\tfrac{1}{2}: &\quad \Psi_3 = i\sin\alpha e^{i\beta}/\pi, \\ = -\tfrac{1}{2}, \quad = -\tfrac{1}{2}: &\quad \Psi_4 = \cos\alpha e^{-i\gamma}/\pi, \end{aligned} \tag{39}$$

where the functions have been normalized and the phases chosen so that the matrices of the angular momentum components are given by

$$2M_j/\hbar = \sigma_j = -i\alpha k\alpha_l, \quad (jkl) = (123), \tag{40}$$

the σ's being the doubled Pauli spin matrices and the α's the Dirac matrices. With these functions one finds that the matrices of the M_s' are given by

$$\begin{aligned} 2M_z'/\hbar &= -i\alpha_1\alpha_2\alpha_3, \quad 2M_y'/\hbar = -\alpha_1\alpha_2\alpha_3\alpha_4, \\ 2M_x'/\hbar &= \alpha_4. \end{aligned} \tag{41}$$

If one is concerned only with the components M_i, then one can take a set of states associated with a single eigenvalue M_s'. For instance, one can take only Ψ_1 and Ψ_2 and thus obtain the two-rowed Pauli spin matrices. On the other hand, if one takes all four Ψ's, then one can form the above six four-rowed matrices which, together with their products, formally give the full set of Dirac matrices.

4. EXTERNAL FIELD AND PARTICLE MOTION

Let us assume that the particle has a magnetic moment associated with its spin, so that the magnetic moment is given by $\lambda\mathbf{M}$. If it is situated in a uniform magnetic field $\mathfrak{H}$, then the hamiltonian describing the rotation of the sphere in this field will be

$$H = T - \lambda\mathbf{M}\cdot\mathfrak{H}, \tag{42}$$

or, if one takes the Z axis in the direction of $\mathfrak{H}$,

$$H = T - \lambda\mathfrak{H}M_s. \tag{43}$$

It is evident that, if one sets up a Schroedinger equation

[3] F. Reiche and H. Rademacher, Z. Physik **39**, 444 (1926).
[4] E. Schroedinger, Ann. Physik **32**, 49 (1938); W. Pauli, Helv. Phys. Acta **12**, 147 (1939).

for this case, the solution for Ψ will be the same as was obtained above in the absence of a field and the change in the energy due to the field will be given by $-\lambda\hbar\mathfrak{H}M_z$.

Thus far we have considered the sphere as rotating about a fixed center, i.e., the particle as being at rest. To take account of the motion of the particle, one sets up a Schroedinger equation with a hamiltonian that includes both translational and rotational kinetic and potential energy, associated with the position and momentum of the particle as well as its spin. The difference between the present procedure and the usual one (Pauli) lies in the fact that spin components are here represented by differential operators instead of matrices. Substituting $\pi_k=-i\hbar\partial/\partial\xi_k$ in (14), one obtains the spin components in the operator form. Alternatively, in terms of the polar variables α, β, γ one finds

$$
\begin{aligned}
(M_x+iM_y)\Psi&=\frac{-ih}{2}e^{i(\beta+\gamma)}\\
&\quad\times\left(\frac{\partial\Psi}{\partial\alpha}+i\operatorname{ctn}\alpha\frac{\partial\Psi}{\partial\beta}-i\tan\alpha\frac{\partial\Psi}{\partial\gamma}\right),\\
(M_x-iM_y)\Psi&=\frac{-ih}{2}e^{-i(\beta+\gamma)}\\
&\quad\times\left(\frac{\partial\Psi}{\partial\alpha}-i\operatorname{ctn}\alpha\frac{\partial\Psi}{\partial\beta}+i\tan\alpha\frac{\partial\Psi}{\partial\gamma}\right),\\
M_z\Psi&=\frac{-ih}{2}\left(\frac{\partial\Psi}{\partial\beta}+\frac{\partial\Psi}{\partial\gamma}\right),\\
(M_x'+iM_y')\Psi&=\frac{-ih}{2}e^{i(\beta-\gamma)}\\
&\quad\times\left(\frac{\partial\Psi}{\partial\alpha}+i\operatorname{ctn}\alpha\frac{\partial\Psi}{\partial\beta}+i\tan\alpha\frac{\partial\Psi}{\partial\gamma}\right),\\
(M_x'-iM_y')\Psi&=\frac{-ih}{2}e^{i(\gamma-\beta)}\\
&\quad\times\left(\frac{\partial\Psi}{\partial\alpha}-i\operatorname{ctn}\alpha\frac{\partial\Psi}{\partial\beta}-i\tan\alpha\frac{\partial\Psi}{\partial\gamma}\right),\\
M_z'\Psi&=\frac{-ih}{2}\left(\frac{\partial\Psi}{\partial\gamma}-\frac{\partial\Psi}{\partial\beta}\right).
\end{aligned}
\tag{44}
$$

The wave function for a given state will consist of a single component which, however, will depend on the ξ's, in addition to the position coordinates.

5. DISCUSSION

In discussing the rotating sphere model of the electron, mention might be made of the work of M. H. Payne,[5] in which the electron spin is treated by means of bipolar coordinates, the electron being regarded as a point mass moving on the surface of a sphere. However, not only the model, but also the point of view there are quite different from those of the present work.

The chief purpose of considering the spin as a rotation described by variables in the ξ-space is to enable one to represent the spin components by operators (in the Schroedinger representation) as well as by matrices. From the formal standpoint this appears desirable, since it permits one to treat all physical variables in a uniform manner. On the other hand, it is well known[6] that in the case of an electron the rotating sphere model leads to serious difficulties if the sphere is taken to have the classical electron radius. These difficulties may be associated with the necessity for changes in some of our physical concepts when we are dealing with very small dimensions. It is possible that, after such changes, the rotating sphere model may nevertheless retain an approximate validity. For the present, at any rate, the spin description considered here has to be regarded as a phenomenological one.

In conclusion, the author wishes to express his indebtedness to Professor E. L. Hill for helpful advice.

APPENDIX

If one takes a polar coordinate system defined by

$$
\begin{aligned}
\xi_1&=\rho\sin u\sin v\cos w,\\
\xi_2&=\rho\sin u\sin v\sin w,\\
\xi_3&=\rho\sin u\cos v,\\
\xi_4&=\rho\cos u,
\end{aligned}
$$

where $0\leqslant u\leqslant\pi$, $0\leqslant v\leqslant\pi$, $0\leqslant w<2\pi$, then in Eq. (23) one has

$$
\nabla^2\Psi=\frac{1}{\sin^3 u}\frac{\partial}{\partial u}\left(\sin^3 u\frac{\partial\Psi}{\partial u}\right)+\frac{1}{\sin^2 u\sin v}\frac{\partial}{\partial v}\left(\sin v\frac{\partial\Psi}{\partial v}\right)+\frac{1}{\sin^2 u\sin^2 v}\frac{\partial^2\Psi}{\partial w^2}.
$$

In this case the well-behaved solutions of the equation are found to be

$$
\Psi=R(u)P_l(\cos v)e^{im w},
$$

where $l=0, 1, 2, \cdots$, $|m|=l, l-1, \cdots$, and

$$
R(u)=(\sin u)^{-\frac{1}{2}}P_{L+\frac{1}{2}}^{l+\frac{1}{2}}(\cos u)
$$

in terms of an associated Legendre function with $L=l, l+1, \cdots$. This can also be written $\sin^l u Q(\cos u)$, where Q is a polynomial of degree $L-l$. In terms of L, K is again given by (30), and the total number of states for a given value of L is readily counted up to be $(L+1)^2=(2S+1)^2$.

---

[5] M. H. Payne, Phys. Rev. **65**, 39 (1944).

[6] G. E. Uhlenbeck and S. Goudsmit, Naturwiss. **13**, 953 (1925).

A Collective Description of Electron Interactions. I. Magnetic Interactions*

DAVID BOHM AND DAVID PINES†
Palmer Physical Laboratory, Princeton University, Princeton, New Jersey
(Received December 4, 1950)

A new approach to the treatment of the interactions in a collection of electrons is developed, which we call the collective description. The collective description is based on the organized behavior produced by the interactions in an electron gas of high density; this organized behavior results in oscillations of the system as a whole, the so-called "plasma oscillations." The collective description, in contrast to the usual individual particle description, describes in a natural way the long-range correlations in electron positions brought about by their mutual interaction. In this paper we confine our attention to the magnetic interactions between the electrons; the coulomb interactions will be discussed in a subsequent paper.

The transition from the usual single-particle description to the collective description of the electron motion in terms of organized oscillations is obtained by a suitable canonical transformation. The complete hamiltonian for a collection of charges interacting with the transverse electromagnetic field is re-expressed as a sum of three terms. One involves the collective field coordinates and expresses the degree of excitation of organized oscillations. The others represent the kinetic energy of the electrons and the residual particle interaction, which is not describable in terms of the organized oscillations, and corresponds to a screened interparticle force of short range.

Both a classical and a quantum-mechanical treatment are given, and the criteria for the validity of the collective description are discussed.

I. INTRODUCTION

BECAUSE of the long range of the coulomb force, the interactions in a collection of electrons involve many particles simultaneously. However, the usual description of these electron interactions is based on a free-particle approximation. In a metal, for instance, the motion of a given electron is assumed to be independent of the motion of all the other electrons in first approximation. The effect of the other electrons on this electron is then represented by a smeared-out potential, which can be determined by using the self-consistent field methods of Hartree and Fock. This means that the effects of the correlations in the positions of the electrons brought about by the long range of the coulomb force are almost entirely neglected; we can therefore expect that in any problem in which the electron-electron interactions are important, as, for example, the calculation of the cohesive energy or the electronic contribution to the specific heats at low temperatures, the free-particle model may not be adequate. In order to obtain a better mathematical treatment of this problem, we have adopted a new approach based on a collective description of the motion. This collective description is most appropriate for systems of high particle density.

It is well known that an electron gas of high density[1] can undergo organized oscillations resembling sound waves.[2,3] These oscillations, the so-called "plasma oscillations," represent the effects of the long-range correlation of electron positions brought about by coulomb interactions. A description in terms of these organized oscillations therefore provides a natural way of treating the long-range electron interactions, and leads to greater insight into the dynamical behavior of the electron gas than is afforded by the free-particle approximation. Thus, it may be expected that such a collective description will make possible a better understanding of the interactions between the electrons in a metal.

In a treatment of these organized oscillations,[3] one considers a particular fourier component of the average field, proportional to

$$\exp[i(\mathbf{k}\cdot\mathbf{x}-\omega t)].$$

For small amplitudes (which are of interest to us here), the linear approximation is valid, and an arbitrary field can therefore be expanded as a sum of such trigonometric terms. In response to this oscillating field, each electron undergoes a small corresponding trigonometric change in its velocity and in its contribution to the mean charge density. Owing to the long range of the coulomb force, the mean field at each point can become quite large as a result of the cumulative effects of small contributions arising from each particle. The condition for sustained oscillations is that the field arising from the response of the particles must be consistent with the field producing this response. This requirement leads to a dispersion relation connecting ω and k. For longitudinal waves the approximate dispersion relation, good for long wavelengths, is[3]

$$\omega^2=(4\pi n_0e^2/m)+3k^2\kappa T/m, \qquad (1)$$

where n_0 is the electron density, T the temperature, and κ is Boltzmann's constant. For infinite wavelength,

* Submitted in part by David Pines to Princeton University in partial fulfillment of the requirements for the degree of Doctor of Philosophy.

† Now at Randal Morgan Laboratory of Physics, University of Pennsylvania, Philadelphia, Pennsylvania.

[1] The electron gas must be neutralized by an approximately equal density of positive charge. In practice the positive charge can usually be regarded as immobile relative to the electrons, and for the most applications can also be regarded as smeared out uniformly throughout the system.

[2] L. Tonks and I. Langmuir, Phys. Rev. 33, 195 (1929).

[3] D. Bohm and E. P. Gross, Phys. Rev. 75, 1851 and 1864 (1949); Paper A discusses the origin of mediumlike behavior; Paper B deals with the excitation and damping of oscillations.

this reduces to the well-known plasma frequency,

$$\omega_p^2 = 4\pi n_0 e^2/m.$$

There are, however, certain limitations on the collective description of the electron gas in terms of organized longitudinal oscillations which arise from the fact that these oscillations cannot be sustained for wavelengths shorter than a critical distance known as the Debye length,

$$\lambda_D = (\kappa T/4\pi n_0 e^2)^{\frac{1}{2}} \cong \bar{V}/\omega_p. \tag{2}$$

This length is of the order of the distance traveled during the period of an oscillation by a particle moving with the mean thermal speed, $\bar{V}$, and thus might reasonably be expected to constitute a limitation on organized oscillation. It may be shown, furthermore, that whenever there is a static field in the electron gas, either externally imposed or arising from a lack of charge neutrality, the electrons redistribute themselves in such a way as to screen out the field within a distance of the order of a Debye length.[4]

Screening and organized oscillation are different but related manifestations of the collective behavior of the electron gas, brought about by cumulative responses of the particles to the average force; and the Debye length determines the smallest distance for which this collective behavior is significant. Thus, one effectively obtains a separation between the long-range part of the force, which is best described collectively, and the short-range part, which is best described in terms of the coordinates of the individual particles. The higher the density, the shorter the distances at which the collective description applies, and the more useful this description becomes. For a metal, the Debye length is of the order of 10^{-8} cm; and therefore, the collective description is applicable practically down to interparticle distances.

Organized transverse oscillations of an electron gas are also possible. These oscillations are electromagnetic waves strongly modified by the fields arising from the collective particle response. Such oscillations are obtained in the transmission of radio waves through a highly ionized medium, such as the heaviside layer. The organized transverse oscillations can be given a treatment similar to that of the longitudinal oscillations.[2,5] The dispersion relation for these waves is

$$\omega^2 \cong \omega_p^2 + c^2k^2.$$

The minimum wavelength for which the collective behavior is important is, in this case,

$$\lambda_C \cong c/\omega_p.$$

This distance is clearly much longer than the Debye length.

In order to obtain a collective description of the electrons in a metal we must use a quantum-mechanical treatment, since the electron gas is highly degenerate. Previous treatments of the organized oscillations of an electron gas have been comparatively unsystematic in that hamiltonian methods were not employed, so that the results were not extensible to quantum theory. In our treatment of the collective description hamiltonian methods will be employed throughout.

Let us consider the hamiltonian for a collection of charges interacting with the electromagnetic field, the particles and the field being described by appropriate canonical coordinates. This hamiltonian may be represented schematically as

$$H_0 = H_{\text{part}} + H_{\text{inter}} + H_{\text{field}} \tag{3}$$

where H_{part} represents the kinetic energy of the electrons, H_{inter} represents the interaction between the electrons and the electromagnetic field, and H_{field} represents the energy contained in the electromagnetic field.

Our program is to find a canonical transformation to a new set of variables which will provide a collective description of the system leading to results classically equivalent to those obtained in the noncanonical treatment. Thus, we shall require that the new field variables oscillate independently of the new particle variables with the characteristic frequency of organized oscillation. When we do this we find that the hamiltonian in the collective description can be represented schematically as

$$H^{(1)} = H^{(1)}{}_{\text{part}} + H_{\text{osc}} + H_{\text{part int}}, \tag{4}$$

where $H^{(1)}{}_{\text{part}}$ corresponds to the kinetic energy in these new coordinates and H_{osc} is a sum of harmonic oscillator terms with frequencies given by the dispersion relation for organized oscillations. $H_{\text{part int}}$ then corresponds to a screened force between particles, which is large only for distances shorter than the appropriate minimum distance associated with organized oscillations. Thus, we obtain explicitly in hamiltonian form the effective separation between long range collective interactions, described here in terms of organized oscillations, and the short-range interactions between individual particles.[6]

In our treatment, certain approximations must be made, which are discussed in detail in Sec. II, in connection with the collective approximation. These approximations reflect the fact that while the effect of the average field on an individual particle is small, these cumulative small contributions from each particle

[4] P. Debye and E. Huckel, Physik Z. 24, 185 (1923). This phenomenon was first studied in connection with highly ionized electrolytes.

[5] For a treatment along the lines of Bohm and Gross, reference 3, see D. Pines, PhD. thesis, Princeton University (1950).

[6] In the case of longitudinal oscillations, this model for electron interactions provides a physical basis for the hitherto empirical use of a screened coulomb force to represent correlation effects. Furthermore, it predicts a screening radius which produces agreement with the experimental results for both the electronic contribution to the specific heat of a metal, and the width of the tail of the soft x-ray emission curve for sodium. D. Bohm and D. Pines, Phys. Rev. 80, 903 (1950).

to the average field may produce a large change in these fields relative to what they would be in a medium of low charge density. Thus, perturbation theory is applied to the solution for the motion of each particle in the average field of all the others, but cannot be applied in similar fashion for the solution of the field equations of motion. On the other hand, because of the high density of particles, we may assume that only the response of a particle which is in phase with the field producing it will be important and that other responses which depend on the position of the particle can be neglected.

We confine our attention in this paper to the collective description of the interactions between electrons brought about through the medium of the transverse electromagnetic field. These magnetic interactions are weaker than the corresponding coulomb interactions by a factor of approximately v^2/c^2 and, consequently, are not usually of great physical interest. However, the canonical treatment of the transverse field is more straightforward mathematically than that of the longitudinal field; and since we would like to illustrate clearly the techniques and approximations involved in our methods, we therefore investigate first the role of the organized transverse oscillations in a description of electron interactions. In Sec. II, we give a classical treatment and discuss in detail the collective approximation and the effective residual interparticle force. In Sec. III we give the analogous quantum-mechanical treatment of the collective description. The longitudinal oscillations will be treated in a subsequent paper.

II. THE CLASSICAL CANONICAL TRANSFORMATION TO THE COLLECTIVE DESCRIPTION

(A) Generating Function for the Transformation

The hamiltonian for a collection of charges interacting with a transverse electromagnetic field may be written

$$H=\sum_i[\mathbf{p}_i+e\mathbf{A}(\mathbf{x}_i)/c]^2/2m + \int([E^2(\mathbf{x})+H^2(\mathbf{x})]/8\pi)d\mathbf{x}. \quad (5)$$

We expand $\mathbf{A}(\mathbf{x})$ in a fourier series in a cube of volume L^3, and impose periodic boundary conditions. Thus,

$$\mathbf{A}(\mathbf{x})=\sum_{k\mu}(4\pi c^2/L^3)^{\frac{1}{2}}q_{k\mu}\boldsymbol{\varepsilon}_{k\mu}\exp(i\mathbf{k}\cdot\mathbf{x}), \quad (6)$$

where $\boldsymbol{\varepsilon}_{k\mu}$ is a unit polarization vector, and for this transverse field, μ takes on values 1 and 2, representing the two possible values of polarization perpendicular to the direction of propagation. The wave number vector $\mathbf{k}$ is assumed to take on both plus and minus values, i.e., $k_s=2\pi n_s/L$, where $n_s=-\infty\cdots+\infty$, etc. To ensure that $\mathbf{A}(\mathbf{x})$ is real, we take

$$\boldsymbol{\varepsilon}_{k\mu}=\boldsymbol{\varepsilon}_{-k\mu}, \quad q_{k\mu}=(q_{-k\mu})^*. \quad (7)$$

Then, following the usual treatments,[7] it can be shown that our hamiltonian (5) becomes:

$$H=\sum_i(p_i^2/2m)+\sum_{ik\mu}(4\pi e^2/L^3)^{\frac{1}{2}}[(\mathbf{p}_i\cdot\boldsymbol{\varepsilon}_{k\mu})/m]q_{k\mu}\exp(i\mathbf{k}\cdot\mathbf{x}_i) + \sum_{ikl\mu\nu}(2\pi e^2/mL^3)q_{k\mu}q_{l\nu}\boldsymbol{\varepsilon}_{k\mu}\cdot\boldsymbol{\varepsilon}_{l\nu}\exp[i(\mathbf{k}+\mathbf{l})\cdot\mathbf{x}_i] + \tfrac{1}{2}\sum_{k\mu}(p_{k\mu}p_{-k\mu}+c^2k^2q_{k\mu}q_{-k\mu}). \quad (8)$$

Here $p_{k\mu}$ is the canonical conjugate to $q_{k\mu}$, and we also have

$$p_{k\mu}=(p_{-k\mu})^*. \quad (9)$$

We find it convenient, for reasons which will become clear later, to split up the term

$$(2\pi e^2/mL^3)\sum_{ikl\mu\nu}{}' q_{k\mu}q_{l\nu}\boldsymbol{\varepsilon}_{k\mu}\cdot\boldsymbol{\varepsilon}_{l\nu}\exp[i(\mathbf{k}+\mathbf{l})\cdot\mathbf{x}_i]$$

in those terms for which $\mathbf{l}=-\mathbf{k}$ and $\mathbf{l}\neq-\mathbf{k}$. When this is done, our hamiltonian corresponds to the schematic hamiltonian of the previous section, with

$$H_{\text{par}}=\sum_i p_i^2/2m, \quad (10a)$$

$$H_{\text{inter}}=\sum_{ik\mu}(4\pi e^2/m^2L^3)^{\frac{1}{2}}(\mathbf{p}_i\cdot\boldsymbol{\varepsilon}_{k\mu})q_{k\mu}\exp(i\mathbf{k}\cdot\mathbf{x}_i) + (2\pi e^2/mL^3)\sum_{\substack{kil\mu\nu\\ l\neq-k}}q_{k\mu}q_{l\nu}\boldsymbol{\varepsilon}_{k\mu}\cdot\boldsymbol{\varepsilon}_{l\nu} \times\exp[i(\mathbf{k}+\mathbf{l})\cdot\mathbf{x}_i], \quad (10b)$$

$$H_{\text{field}}=\tfrac{1}{2}\sum_{k\mu}[p_{k\mu}p_{-k\mu}+(c^2k^2+\omega_p^2)q_{k\mu}q_{-k\mu}]. \quad (10c)$$

We will now show that a canonical transformation to the new coordinates $(X_i, P_i; Q_k, \Pi_k)$, which is generated by $S(x_i, P_i; q_k, \Pi_k)$ as given below, constitutes the desired transformation to the collective description. This generating function is

$$S(x_i, P_i; q_k, \Pi_k)=\sum_i\mathbf{x}_i\cdot\mathbf{P}_i+\sum_{k\mu}q_{k\mu}\Pi_{k\mu} + F(x_i, P_i; q_k, \Pi_k), \quad (11)$$

where

$$F(x_i, P_i; q_k, \Pi_k)=\sum_{k\mu}\xi_{k\mu}(\mathbf{P}_i)q_{k\mu}\Pi_{k\mu}-(4\pi e^2/m^2L^3)^{\frac{1}{2}}i \times\sum_{l\nu j}(\mathbf{P}_j\cdot\boldsymbol{\varepsilon}_{l\nu})\frac{[(\mathbf{l}\cdot\mathbf{P}_j/m)q_{l\nu}+i\Pi_{-l\nu}]}{\omega^2-(\mathbf{l}\cdot\mathbf{P}_j)^2/m^2}\exp i\mathbf{l}\cdot\mathbf{x}_j. \quad (12)$$

$\xi_{k\mu}(\mathbf{P}_i)$ depends only on the particle momenta and is of the order v^2/c^2; it will be determined in the course of working out the consequences of this transformation (see Eq. (25)); ω represents the frequency of the organized transverse field oscillations.[8] With this gener-

[7] See, for instance, G. Wentzel, *The Quantum Theory of Fields* (Interscience Publishers, Inc., New York, 1949), Chapter IV.

[8] It will be seen that ω depends on the momentum P_i. However, this dependence is of the second order (in v/c), and the corresponding changes in the transformation equations may be neglected.

ating function we obtain the following equations relating the old and new coordinates:

$$p_{i\lambda}=\frac{\partial S}{\partial x_{i\lambda}}=P_{i\lambda}+\left(\frac{4\pi e^2}{m^2L^3}\right)^{\frac{1}{2}}\sum_{l\nu}\left\{\frac{\mathbf{P}_i\cdot\boldsymbol{\epsilon}_{l\nu}}{\omega^2-(\mathbf{l}\cdot\mathbf{P}_i)^2/m^2}\right.$$
$$\left.\times\{(\mathbf{l}\cdot\mathbf{P}_i/m)q_{l\nu}+i\Pi_{l\nu}\}l_\lambda\exp(i\mathbf{l}\cdot\mathbf{x}_i)\right\}, \quad (13)$$

$$X_{i\lambda}=\partial S/\partial P_{i\lambda}=x_{i\lambda}+(4\pi e^2/m^2L^3)^{\frac{1}{2}}$$
$$\times\sum_{l\nu}\{[i(\epsilon_{l\nu})_\lambda/[\omega^2-(\mathbf{l}\cdot\mathbf{P}_i)^2/m^2]]$$
$$\times[[(\mathbf{l}\cdot\mathbf{P}_i)/m]q_{l\nu}+i\Pi_{-l\nu}]$$
$$+[(\mathbf{P}_i\cdot\boldsymbol{\epsilon}_{l\nu})l_\lambda/[\omega^2-(\mathbf{l}\cdot\mathbf{P}_i)^2/m^2]]$$
$$\times[[\omega^2+(\mathbf{l}\cdot\mathbf{P}_i/m)^2]q_{l\nu}+2i(\mathbf{l}\cdot\mathbf{P}_i/m)\Pi_{-l\nu}]\}$$
$$\times\exp(i\mathbf{l}\cdot\mathbf{x}_i)+\sum_{k\mu}\Pi_{k\mu}q_{k\mu}(\partial\xi_{k\mu}/\partial P_{i\lambda}), \quad (14)$$

$$p_{k\mu}=\partial S/\partial q_{k\mu}=\Pi_{k\mu}(1+\xi_{k\mu})$$
$$-(4\pi e^2/m^2L^3)^{\frac{1}{2}}i\sum_j\{(\mathbf{P}_j\cdot\boldsymbol{\epsilon}_{k\mu})(\mathbf{k}\cdot\mathbf{P}_j)/$$
$$m[\omega^2-(\mathbf{k}\cdot\mathbf{P}_j/m)^2]\}\exp(i\mathbf{k}\cdot\mathbf{x}_j), \quad (15)$$

$$Q_{-k\mu}=\partial S/\partial\Pi_{-k\mu}=q_{-k\mu}(1+\xi_{k\mu})-(4\pi e^2/m^2L^3)^{\frac{1}{2}}$$
$$\times\sum_j\{(\mathbf{P}_j\cdot\boldsymbol{\epsilon}_{k\mu})/[\omega^2-(\mathbf{k}\cdot\mathbf{P}_j/m)^2]\}\exp(i\mathbf{k}\cdot\mathbf{x}_j). \quad (16)$$

We see that there is a rather complicated interrelationship between the old and the new coordinates defined by these equations. We will not be able to solve these equations *exactly* to obtain the old coordinates in terms of the new coordinates or vice versa. We could obtain approximate expressions for the old coordinates in terms of the new, and then determine what form the hamiltonian will take in terms of the new variables. However, we feel that the nature of the collective approximation will be revealed more clearly by a somewhat different procedure. We will substitute the "mixed" expressions for p_i, $p_{k\mu}$, and $q_{k\mu}$ [(13), (15), and (16)], into our old hamiltonian and thus obtain a hamiltonian in terms of both old and new coordinates. However, this hamiltonian can be simplified considerably with the aid of the collective approximation, and after achieving this simplification, we then express the hamiltonian entirely in terms of the new variables.

B. Nature of the Collective Approximation

The approximations we find it necessary to make, in order to apply the collective description to the electron gas, have been grouped by us under the general heading of the collective approximation. The collective approximation involves the following requirements:

(1) The short-range electron-ion and electron-electron collisions are neglected. This assumes that we are dealing with an electron gas in which the mean free time for such collisions is considerably longer than the period of an organized oscillation. Actually, such collisions tend to disrupt the organized oscillation of the system as a whole; but if they are not too frequent, they lead only to a small damping of the oscillations.[9] The long free path needed for the validity of this approximation actually occurs because of the screening of the long-range part of the force, which leaves only the short-range interactions to be accounted for in terms of collisions.

(2) The organized oscillations are assumed to be of sufficiently small amplitude that each particle suffers only a small perturbation in its straight line motion due to the combined fields of all the other particles. Thus, we will neglect quadratic field terms in the electron or field equations of motion and apply perturbation theory to the particle motions. This is the customary linear approximation, appropriate for small oscillations.

(3) We distinguish between two kinds of response of the electrons to a wave. One of these is in phase with the wave, so that the phase difference between the particle response and the wave producing it is independent of the position of the particle. This is the response which contributes to the organized behavior of the system. The other response has a phase difference with the wave producing it which depends on the position of the particle. Because of the general random location of the particles, this second response tends to average out to zero when we consider a large number of electrons, and we shall neglect the contributions arising from this. This procedure we call the "random phase approximation."

(4) We shall assume the smallness of $(\mathbf{k}\cdot\mathbf{v})/\omega$. In our case, $\omega/k\gtrsim c$, so that the smallness of $(\mathbf{k}\cdot\mathbf{v})/\omega$ follows from the smallness of v/c. For longitudinal oscillations, however, we can have small $(\mathbf{k}\cdot\mathbf{v})/\omega$ only for wavelengths appreciably longer than the Debye length, λ_D. This follows because λ_D is essentially $\bar{v}/\omega$, where $\bar{v}$ is a suitable mean speed. Thus, the collective description is applicable only for long enough wavelengths. This result agrees with the general conclusion cited previously that both statically and dynamically a dense ion gas exhibits organized behavior only for wavelengths longer than λ_D or λ_C.

The collective approximation is similar to a complete perturbation theory treatment in that perturbation theory is applied to the particle motion. The difference between the two approaches lies in the assumptions made regarding the fields produced by the particles. For instance, in Eqs. (15), and (16) we see that the old and new field coordinates and momenta differ by a series of terms summed over all particle coordinates. A complete perturbation theoretical treatment would require that this sum be small, but we do not make this assumption here. Instead we note that the small modifications of the net field arising from each particle may add up to a large change of the average field.

The principal advantage of the collective approximation is that it does not require a small cumulative response to the fields. Thus, in this approximation we shall retain terms in the hamiltonian proportional to the square of the vector potential, whereas in a perturbation treatment these would be discarded, since they are formally of second order in the perturbing potential. As we shall see, in the case of high particle density, these can bring about a significant modification in the behavior of the electromagnetic field.

[9] This damping is discussed in detail in Bohm and Gross, reference 3.

C. Results of the Transformation; the Hamiltonian for the Collective Description

Let us now see what effect the transformation has on the various terms in our hamiltonian. Using Eq. (13) we have

$$H_{\text{part}}=\sum_i P_i^2/2m+(4\pi e^2/m^2L^3)^{\frac{1}{2}}\sum_{il\nu}[(\mathbf{l}\cdot\mathbf{P}_i)/m]$$
$$\times[\mathbf{P}_i\cdot\boldsymbol{\varepsilon}_{l\nu}]\frac{\{[(\mathbf{l}\cdot\mathbf{P}_i)/m]q_{l\nu}+i\Pi_{-l\nu}\}}{\omega^2-[(\mathbf{l}\cdot\mathbf{P}_i)/m]^2}\exp(i\mathbf{l}\cdot\mathbf{x}_i)$$
$$+\frac{2\pi e^2}{mL^3}\sum_{kl\mu\nu i}\frac{(\mathbf{P}_i\cdot\boldsymbol{\varepsilon}_{l\nu})(\mathbf{P}_i\cdot\boldsymbol{\varepsilon}_{k\mu})(\mathbf{k}\cdot\mathbf{l})/m}{[\omega^2-(\mathbf{l}\cdot\mathbf{P}_i/m)^2][\omega^2-(\mathbf{k}\cdot\mathbf{P}_i/m)^2]}$$
$$\times\{(\mathbf{l}\cdot\mathbf{P}_i/m)q_{l\nu}+i\Pi_{-l\nu}\}\{((\mathbf{k}\cdot\mathbf{P}_i)/m)q_{k\mu}+i\Pi_{-k\mu}\}$$
$$\times\exp[i(\mathbf{k}+\mathbf{l})\cdot\mathbf{x}_i]. \quad (17)$$

We consider the terms for which $\mathbf{l}=-\mathbf{k}$, and $\mathbf{l}\neq-\mathbf{k}$, separately in the quadratic field terms in (17). When $\mathbf{l}=-\mathbf{k}$, this quadratic term reduces to

$$\frac{2\pi e^2}{mL^3}\sum_{k\mu\nu i}\frac{(\mathbf{P}_i\cdot\boldsymbol{\varepsilon}_{k\mu})^2k^2}{m[\omega^2-(\mathbf{k}\cdot\mathbf{P}_i/m)^2]}$$
$$\{(\mathbf{k}\cdot\mathbf{P}_i/m)^2q_{k\mu}q_{-k\mu}+\Pi_{k\mu}\Pi_{-k\mu}\} \quad (18)$$

provided we assume an isotropic distribution of the $\mathbf{P}_i$. Using Eq. (13) we may write the terms arising from H_{inter} as

$$H_{\text{inter}}=(4\pi e^2/m^2L^3)^{\frac{1}{2}}\sum_{ik\mu}q_{k\mu}(\mathbf{P}_i\cdot\boldsymbol{\varepsilon}_{k\mu})\exp(i\mathbf{k}\cdot\mathbf{x}_i)$$
$$+\frac{4\pi e^2}{m^2L^3}\sum_{\substack{ikl\mu\nu\\ l\neq-k}}\left\{\frac{(\mathbf{l}\cdot\boldsymbol{\varepsilon}_{k\mu})(\mathbf{P}_j\cdot\boldsymbol{\varepsilon}_{k\mu})}{\omega^2-(\mathbf{l}\cdot\mathbf{P}_i/m)^2}\right.$$
$$\times[(\mathbf{l}\cdot\mathbf{P}_i/m)q_{l\nu}q_{-k\mu}+i\Pi_{-l\nu}q_{k\mu}]$$
$$\left.+\tfrac{1}{2}(\boldsymbol{\varepsilon}_{k\mu}\cdot\boldsymbol{\varepsilon}_{l\nu})q_{k\mu}q_{l\nu}\right\}\exp[i(\mathbf{k}+\mathbf{l})\cdot\mathbf{x}_i], \quad (19)$$

where we have split up the terms for which $\mathbf{l}=-\mathbf{k}$, and $\mathbf{l}\neq-\mathbf{k}$, and applied the transversality condition $\sum_\alpha \mathbf{k}\cdot\boldsymbol{\varepsilon}_{k\mu}=0$. It is convenient to group the terms arising from the application of (15) and (16) to H_{field} as follows:

$$H_{\text{field}}=\sum_{k\mu}\{(\Pi_{k\mu}+\partial F/\partial q_{k\mu})(\Pi_{-k\mu}+\partial F/\partial q_{-k\mu})$$
$$+\omega^2[Q_{k\mu}Q_{-k\mu}-2q_{k\mu}(\partial F/\partial\Pi_{-k\mu})$$
$$-(\partial F/\partial\Pi_{k\mu})(\partial F/\partial\Pi_{-k\mu})]\}$$
$$+\tfrac{1}{2}\sum_{k\mu}(c^2k^2+\omega_p^2-\omega^2)q_{k\mu}q_{-k\mu}. \quad (20)$$

This particular combination is taken because F is a function of q_k. We then obtain

$$H_{\text{field}}=\tfrac{1}{2}\sum_{k\mu}\{\Pi_{k\mu}\Pi_{-k\mu}(1+2\xi_{k\mu})$$
$$+\omega^2(Q_{k\mu}Q_{-k\mu}-2\xi_{k\mu}q_{k\mu}q_{-k\mu})+(\omega_p^2+c^2k^2-\omega^2)q_{k\mu}q_{-k\mu}\}$$
$$-\left(\frac{4\pi e^2}{m^2L^3}\right)^{\frac{1}{2}}\sum_{j\xi\mu}\frac{\mathbf{P}_j\cdot\boldsymbol{\varepsilon}_{k\mu}(1+\xi_{k\mu})}{\omega^2-(\mathbf{k}\cdot\mathbf{P}_j/m)^2}$$
$$\times\{-i(\mathbf{k}\cdot\mathbf{P}_j/m)\Pi_{-k\mu}+\omega^2q_{k\mu}\}\exp(i\mathbf{k}\cdot\mathbf{x}_j)-(2\pi e^2/m^2L^3)$$
$$\times\sum_{ijk\mu}\frac{\{(\mathbf{P}_i\cdot\boldsymbol{\varepsilon}_{k\mu})(\mathbf{P}_j\cdot\boldsymbol{\varepsilon}_{k\mu})[\omega^2-(\mathbf{k}\cdot\mathbf{P}_i/m)(\mathbf{k}\cdot\mathbf{P}_j/m)]\}}{[\omega^2-(\mathbf{k}\cdot\mathbf{P}_i/m)^2][\omega^2-(\mathbf{k}\cdot\mathbf{P}_j/m)^2]}$$
$$\times\exp[i\mathbf{k}\cdot(\mathbf{x}_i-\mathbf{x}_j)]. \quad (21)$$

In (21) we have neglected terms involving $\xi_{k\mu}^2$, since these are of order v^4/c^4, and for the particles with which we will be concerned $v^2/c^2\ll1$.

The sum of the expressions (17), (19), and (21) will give us our hamiltonian (8) expressed in terms of a mixture of the old and new coordinates. When we add these expressions, we find that those terms which are linear in the field coordinates are reduced to

$$-(4\pi e^2/m^2L^3)^{\frac{1}{2}}\sum_{jk\mu}\xi_{k\mu}(\mathbf{P}_j\cdot\boldsymbol{\varepsilon}_{k\mu})$$
$$\times\frac{\{\omega^2q_{k\mu}+i(\mathbf{k}\cdot\mathbf{P}_j/m)\Pi_{-k\mu}\}}{\omega^2-(\mathbf{k}\cdot\mathbf{P}_j/m)^2}\exp(i\mathbf{k}\cdot\mathbf{x}_j). \quad (22)$$

But this term is of order v^2/c^2 smaller than our original H_{inter}, Eq. (10b). We could devise a further canonical transformation which would eliminate terms of this order too, but this would only introduce corrections of order v^4/c^4 in the interparticle force. Since we will confine ourselves to the terms of lowest order (v^2/c^2) in the interaction between particles, we can neglect this small term (22) entirely.

Let us now investigate the quadratic field terms resulting from the sum of (17), (19), and (21). These fall into two categories, which are given in (23) and (24) below:

$$\frac{2\pi e^2}{mL^3}\sum_{\substack{ikl\mu\nu\\ k\neq-l}}\left\{\frac{(\mathbf{P}_i\cdot\boldsymbol{\varepsilon}_{l\nu})(\mathbf{P}_i\cdot\boldsymbol{\varepsilon}_{k\mu})\mathbf{l}\cdot\mathbf{k}[(\mathbf{l}\cdot\mathbf{P}_i/m)(\mathbf{k}\cdot\mathbf{P}_i/m)q_{l\nu}q_{k\mu}-\Pi_{k\mu}\Pi_{l\nu}+2i(\mathbf{k}\cdot\mathbf{P}_i/m)q_{k\mu}\Pi_{-l\nu}]}{m^2[\omega^2-(\mathbf{k}\cdot\mathbf{P}_i/m)^2][\omega^2-(\mathbf{l}\cdot\mathbf{P}_i/m)^2]}\right.$$
$$\left.+\frac{2(\mathbf{l}\cdot\boldsymbol{\varepsilon}_{k\mu})(\mathbf{P}_i\cdot\boldsymbol{\varepsilon}_{l\nu})}{m[\omega^2-(\mathbf{l}\cdot\mathbf{P}_i/m)^2]}\left[\left(\frac{\mathbf{l}\cdot\mathbf{P}_i}{m}\right)q_{l\nu}q_{-k\mu}+i\Pi_{-l\nu}q_{k\mu}\right]+q_{k\mu}q_{l\nu}(\boldsymbol{\varepsilon}_{k\mu}\cdot\boldsymbol{\varepsilon}_{l\nu})\right\}\exp[i(\mathbf{k}+\mathbf{l})\cdot\mathbf{x}_i], \quad (23)$$

$$\frac{2\pi e^2}{mL^3}\sum_{k\mu i}\frac{(\mathbf{P}_i\cdot\boldsymbol{\varepsilon}_{k\mu})^2k^2}{m^2[\omega^2-(\mathbf{k}\cdot\mathbf{P}_i/m)^2]}\left\{\left(\frac{\mathbf{k}\cdot\mathbf{P}_i}{m}\right)^2 q_{k\mu}q_{-k\mu}+\Pi_{k\mu}\Pi_{-k\mu}\right\}$$

$$+\tfrac{1}{2}\sum_{k\mu}\{(c^2k^2+\omega_p{}^2-\omega^2)q_{k\mu}q_{-k\mu}+2\xi_{k\mu}(\Pi_{k\mu}\Pi_{-k\mu}-\omega^2q_{k\mu}q_{-k\mu})\}+\tfrac{1}{2}\sum_{k\mu}(\Pi_{k\mu}\Pi_{-k\mu}+\omega^2Q_{k\mu}Q_{-k\mu}). \quad (24)$$

The terms in (23) are all quadratic in the field variables, and in addition have a phase factor $\exp[i(\mathbf{k}+\mathbf{l})\cdot\mathbf{x}_i]$, the argument of which never vanishes. In order to discuss these terms, we transform from the old coordinates x_i to the new coordinates X_i, according to Eq. (14). We will then have two types of terms; those in which x_i is replaced by X_i, and those which arise from the difference between x_i and X_i. Now the X_i, because $H_{\text{part int}}$ is a screened short-range interaction, behave to a good degree of approximation like the coordinates of a free particle. We may then assume that these are distributed at random, as in a perfect gas. Since we have a very large number of particles, the nonvanishing argument of the phase factor, $\exp[i(\mathbf{k}+\mathbf{l})\cdot\mathbf{X}_i]$, will cause the contribution of those terms in which it is present to average out to zero. This is essentially the random-phase approximation.

The effects of the correlations in the x_i are represented in the difference between x_i and X_i. However, the terms arising from this difference multiply quadratic field terms; and it may be shown that the resultant products either make nonlinear contributions to the equations of motion, which we neglect in the linear approximation, or average out to zero because they contain a phase factor with nonvanishing argument.[9] Thus, in general, terms which are quadratic in the field variables and contain a phase factor with nonvanishing argument may be neglected in the collective approximation.

When we consider the terms in (24), we see that if we take

$$\xi_{k\mu}=-(2\pi e^2/mL^3)\sum_i k^2(\mathbf{P}_i\cdot\boldsymbol{\varepsilon}_{k\mu}/m)^2/[\omega^2-(\mathbf{k}\cdot\mathbf{P}_i/m)^2], \quad (25)$$

then the quadratic terms in $\Pi_{k\mu}\Pi_{-k\mu}$, reduce to $\frac{1}{2}\sum_{k\mu}\Pi_{k\mu}\Pi_{-k\mu}$. We similarly see that with this choice of $\xi_{k\mu}$, the quadratic terms in $q_{k\mu}q_{-k\mu}$ become

$$\tfrac{1}{2}\sum_{k\mu}q_{k\mu}q_{-k\mu}\left\{c^2k^2+\omega_p{}^2+(4\pi e^2/mL^3)\times\sum_i\frac{\{k^2(\mathbf{P}_i\cdot\boldsymbol{\varepsilon}_{k\mu}/m)^2[\omega^2+(\mathbf{k}\cdot\mathbf{P}_i/m)^2]\}}{[\omega^2-(\mathbf{k}\cdot\mathbf{P}_i/m)^2]^2}-\omega^2\right\}; \quad (26)$$

but, if we take

$$\omega^2=c^2k^2+\omega_p{}^2+(4\pi e^2/mL^3)\times\sum_i\frac{\{(\mathbf{P}_i\cdot\boldsymbol{\varepsilon}_{k\mu}/m)^2k^2[\omega^2+(\mathbf{k}\cdot\mathbf{P}_i/m)^2]\}}{[\omega^2-(\mathbf{k}\cdot\mathbf{P}_i/m)^2]^2}, \quad (27)$$

then this term vanishes. This choice of ω^2 is just the dispersion relation for transverse plasma oscillations.[2,10] Thus we see that we have reduced the field terms represented in (24) to

$$\tfrac{1}{2}\sum_{k\mu}(\Pi_{k\mu}\Pi_{-k\mu}+\omega^2Q_{k\mu}Q_{-k\mu}). \quad (28)$$

The remaining terms are given by

$$-\frac{2\pi e^2}{m^2L^3}\sum_{ij\neq k\mu}\frac{(\mathbf{P}_i\cdot\boldsymbol{\varepsilon}_{k\mu})(\mathbf{P}_j\cdot\boldsymbol{\varepsilon}_{k\mu})[\omega^2-(\mathbf{k}\cdot\mathbf{P}_i/m)(\mathbf{k}\cdot\mathbf{P}_j/m)]}{[\omega^2-(\mathbf{k}\cdot\mathbf{P}_i/m)^2][\omega^2-(\mathbf{k}\cdot\mathbf{P}_j/m)^2]}\times\exp[i\mathbf{k}\cdot(\mathbf{x}_i-\mathbf{x}_j)]. \quad (29)$$

We now wish to express this term entirely in terms of our new coordinates. One can show, using the linear approximation and the random-phase approximation, that the lowest order (in v/c) field term resulting from substituting our expression for x_i, (14) into (29), is

$$-\left(\frac{4\pi e^2}{m^2L^3}\right)^{\frac{1}{2}}\sum_{ik\mu}\frac{\xi_{k\mu}\omega^2(\mathbf{P}_i\cdot\boldsymbol{\varepsilon}_{k\mu})q_{k\mu}}{\omega^2-(\mathbf{k}\cdot\mathbf{P}_i/m)^2}\exp(i\mathbf{k}\cdot\mathbf{X}_i). \quad (30)$$

This term, which is of the same sort as (22), may be neglected for the same reason—that its inclusion will lead to fourth-order terms in v/c in $H_{\text{part int}}$.[11] Thus, we obtain, to this order of approximation, only the above term (29) with x_i replaced by X_i.

Our transformed hamiltonian, expressed entirely in terms of the new coordinates, the "collective" variables, thus takes the form:

$$H^{(1)}=\sum_i(P_i^2/2m)+\tfrac{1}{2}\sum_{k\mu}\Pi_{k\mu}\Pi_{-k\mu}+\omega^2Q_{k\mu}Q_{-k\mu}-(2\pi e^2/m^2L^3)\times\sum_{ij\mu}\frac{\{(\mathbf{P}_i\cdot\boldsymbol{\varepsilon}_{k\mu})(\mathbf{P}_j\cdot\boldsymbol{\varepsilon}_{k\mu})[\omega^2-(\mathbf{k}\cdot\mathbf{P}_i/m)(\mathbf{k}\cdot\mathbf{P}_j/m)]\}}{[\omega^2-(\mathbf{k}\cdot\mathbf{P}_i/m)^2][\omega^2-(\mathbf{k}\cdot\mathbf{P}_j/m)^2]}\times\exp[i\cdot\mathbf{k}(\mathbf{X}_i-\mathbf{X}_j)]. \quad (31)$$

This is just the hamiltonian we sought, as discussed in Sec. I, with

$$H^{(1)}{}_{\text{part}}=\sum_i P_i^2/2m, \quad (32a)$$

[10] This differs from the dispersion relation quoted by Langmuir in the terms of order v^2/c^2 which he neglected. It may be shown, using methods similar to those of Langmuir, that the above dispersion relation is obtained when these terms are not neglected—see D. Pines, reference 5.

[11] The term in Eq. (14) involving $\partial\xi/\partial P_i$ leads to quadratic field terms multiplied by phase factors which do not vanish. According to the general properties of the collective approximation this term can be neglected.

$$H_{\text{osc}}=\tfrac{1}{2}\sum_{k\mu}\Pi_{k\mu}\Pi_{-k\mu}+\omega^2 Q_{k\mu}Q_{-k\mu}, \quad (32b)$$

$$H_{\text{part int}}=-(2\pi e^2/m^2L^3)$$
$$\times\sum_{ij\mu}\frac{(\mathbf{P}_i\cdot\boldsymbol{\varepsilon}_{k\mu})(\mathbf{P}_j\cdot\boldsymbol{\varepsilon}_{k\mu})[\omega^2-(\mathbf{k}\cdot\mathbf{P}_i/m)(\mathbf{k}\cdot\mathbf{P}_j/m)]}{[\omega^2-(\mathbf{k}\cdot\mathbf{P}_i/m)^2][\omega^2-(\mathbf{k}\cdot\mathbf{P}_j/m)^2]}$$
$$\times\exp[i\mathbf{k}\cdot(\mathbf{X}_i-\mathbf{X}_j)]. \quad (32c)$$

We see that the new field and particle variables no longer interact. The new field coordinates carry out oscillations of frequency ω given by the transverse field dispersion relation, Eq. (27), and thus correctly describe the organized transverse oscillations. The new particle coordinates act like those of a free particle, to the extent that we are able to neglect $H_{\text{part int}}$, which represents an effective residual particle interaction.

D. Effective Residual Particle Interaction

Let us now investigate $H_{\text{part int}}$ in some detail. It effectively corresponds to that part of the magnetic interaction between electrons which is not describable in terms of the organized transverse oscillations. Since $\omega^2\gtrsim c^2k^2$, we see that this term will be at least of order v^2/c^2 smaller in magnitude than the corresponding coulomb interaction between the electrons, which is given by

$$(2\pi e^2/L^3)\sum_{ijk}(1/k^2)\exp[i\mathbf{k}\cdot(\mathbf{x}_i-\mathbf{x}_j)].$$

Hence, we shall consider only the lowest order (in v/c) terms represented in (32c), neglecting those terms of order v^4/c^4 as compared with the coulomb term. The lowest order terms may be written:

$$H_{\text{part int}}\cong-(2\pi e^2/m^2L^3)$$
$$\times\sum_{ijk\mu}\frac{(\mathbf{P}_i\cdot\boldsymbol{\varepsilon}_{k\mu})(\mathbf{P}_j\cdot\boldsymbol{\varepsilon}_{k\mu})}{\omega^2-(\mathbf{k}\cdot\mathbf{P}_i/m)^2}\exp[i\mathbf{k}\cdot(\mathbf{X}_i-\mathbf{X}_j)]. \quad (33)$$

Now to this order of approximation, we may write $\omega^2=c^2k^2+\omega_p^2$, so that we have

$$H_{\text{part int}}=-\frac{2\pi e^2}{m^2L^3}\sum_{ijk\mu}\left\{\frac{(\mathbf{P}_i\cdot\boldsymbol{\varepsilon}_{k\mu})(\mathbf{P}_j\cdot\boldsymbol{\varepsilon}_{k\mu})}{c^2k^2+\omega_p^2-(\mathbf{k}\cdot\mathbf{P}_i/m)^2}\right\}$$
$$\times\exp[i\mathbf{k}\cdot(\mathbf{X}_i-\mathbf{X}_j)]. \quad (34)$$

We now compare the above expression with the analogous term in the hamiltonian from which may be derived the Biot-Savart law for the magnetic interaction between particles. This may be shown to be

$$H_{\text{magn int}}=-(2\pi e^2/m^2L^3)$$
$$\times\sum_{ijk\mu}\frac{(\mathbf{P}_i\cdot\boldsymbol{\varepsilon}_{k\mu})(\mathbf{P}_j\cdot\boldsymbol{\varepsilon}_{k\mu})}{c^2k^2-(\mathbf{k}\cdot\mathbf{P}_i/m)^2}\exp[i\mathbf{k}\cdot(\mathbf{X}_i-\mathbf{X}_j)]. \quad (35)$$

Because of the presence of ω_p^2 in the denominator in Eq. (34), we see that when the ion density is large, the interaction is greatly reduced for small values of k, or to put it another way, screened out for sufficiently large interparticle distances. To see this in more detail, let us evaluate $H_{\text{part int}}$ in terms of the interparticle distances. First, we carry out the sum over polarization directions, obtaining

$$H_{\text{part int}}=-\frac{2\pi e^2}{m^2L^3}\sum_{ijk}\frac{\{P_i\cdot P_j-(\mathbf{k}\cdot\mathbf{P}_i)(\mathbf{k}\cdot\mathbf{P}_j)/k^2\}}{c^2k^2+\omega_p^2-(\mathbf{k}\cdot\mathbf{P}_i/m)^2}$$
$$\times\exp[i\mathbf{k}\cdot(\mathbf{X}_i-\mathbf{X}_j)]. \quad (36)$$

For simplicity we consider only the first term in $H_{\text{part int}}$ and we neglect $(\mathbf{k}\cdot\mathbf{P}_i/m)^2$ in the denominator, since it will always be order v^2/c^2 smaller than c^2k^2. We replace the sum over k by an integral, multiplying by the density in k space, $(L/2\pi)^3$. We thus have:

$$H^{(1)}{}_{\text{part int}}=-[2\pi e^2/m^2(2\pi)^3]\sum_{ij}\mathbf{P}_i\cdot\mathbf{P}_j\int dk$$
$$\times\{[1/\omega_p^2+c^2k^2]\exp[i\mathbf{k}\cdot(\mathbf{X}_i-\mathbf{X}_j)]\}. \quad (37)$$

The integral over k yields just

$$2\pi^2[\exp\{-[\omega_p/c]|\mathbf{X}_i-\mathbf{X}_j|\}]/|\mathbf{X}_i-\mathbf{X}_j|,$$

so we have

$$H^{(1)}{}_{\text{part int}}=-(e^2/2)\sum_{ij}(\mathbf{P}_i\cdot\mathbf{P}_j/m^2)$$
$$\times[\exp\{-(\omega_p/c)|\mathbf{X}_i-\mathbf{X}_j|\}]/|\mathbf{X}_i-\mathbf{X}_j|. \quad (38)$$

This leads to a screened Biot-Savart law of interaction between the particles, with the interaction being screened out at distances $\sim c/\omega_p$. For a metal, where $n_0\sim10^{22}$, this screening distance is $\sim3\times10^{-5}$ cm.

III. QUANTUM-MECHANICAL TRANSFORMATION TO THE COLLECTIVE DESCRIPTION

A. Generating Function for the Transformation

We now carry out a quantum-mechanical treatment of the preceding classical material. We shall see that the quantum-mechanical calculation yields essentially the same results as the classical treatment in the preceding section.

We find it convenient to work in the following representation. We expand in terms of the creation and annihilation operators for the transverse field, $a_{k\mu}$ and $(a_{k\mu})^*$,

$$\mathbf{A}(\mathbf{x})=\sum_{k\mu}(2\pi\hbar c^2/\omega L^3)^{\frac{1}{2}}[a_{k\mu}\exp(i\mathbf{k}\cdot\mathbf{x})$$
$$+a_{k\mu}{}^*\exp(-i\mathbf{k}\cdot\mathbf{x})]\boldsymbol{\varepsilon}_{k\mu}. \quad (39)$$

These are connected with $p_{k\mu}$ and $q_{k\mu}$ by the following relations:

$$\begin{aligned}a_{k\mu}&=(\omega/2\hbar)^{\frac{1}{2}}[q_{k\mu}+i(p_{-k\mu}/\omega)],\\ a_{k\mu}{}^*&=(\omega/2\hbar)^{\frac{1}{2}}[q_{k\mu}-i(p_{-k\mu}/\omega)],\\ q_{k\mu}&=(\hbar/2\omega)^{\frac{1}{2}}[a_{k\mu}+a_{-k\mu}{}^*],\\ p_{k\mu}&=-i(\hbar\omega/2)^{\frac{1}{2}}[a_{k\mu}-a_{-k\mu}{}^*].\end{aligned} \quad (40)$$

Using these, one can show that the classical hamiltonian (8), which is equally valid in the quantum-mechanical case, leads to the following hamiltonian[12] in this representation:

$$H=\sum_i(p_i^2/2m)+(e/m)\sum_{k\mu i}(2\pi\hbar/\omega L^3)^{\frac{1}{2}}(\mathbf{p}_i\cdot\boldsymbol{\varepsilon}_{k\mu})$$
$$\times(a_{k\mu}+a_{-k\mu}^*)\exp(i\mathbf{k}\cdot\mathbf{x}_i)+(2\pi e^2/mL^3)$$
$$\times\sum_{\substack{kl\mu\nu i\\ l\neq -k}}(\hbar/\omega)(\boldsymbol{\varepsilon}_{k\mu}\cdot\boldsymbol{\varepsilon}_{l\nu})(a_{k\mu}+a_{-k\mu}^*)(a_{l\nu}+a_{-l\nu}^*)$$
$$\times\exp[i(\mathbf{k}+\mathbf{l})\cdot\mathbf{x}_i]+\tfrac{1}{2}\sum_{k\mu}\hbar\omega(a_{k\mu}a_{k\mu}^*+a_{k\mu}^*a_{k\mu})$$
$$+\tfrac{1}{4}\sum_{k\mu}[\hbar(\omega_p^2+c^2k^2-\omega^2)/\omega][a_{k\mu}a_{k\mu}^*+a_{k\mu}^*a_{k\mu}$$
$$+a_{-k\mu}a_{k\mu}+a_{-k\mu}^*a_{k\mu}^*]. \quad (41)$$

We may adopt the schematic notation of Sec. I, with

$$H_{\text{part}}=\sum_i(p_i^2/2m), \quad (42a)$$

$$H_{\text{inter}}=(e/m)\sum_{k\mu}(2\pi\hbar/\omega L^3)^{\frac{1}{2}}(a_{k\mu}+a_{-k\mu}^*)(\mathbf{p}_i\cdot\boldsymbol{\varepsilon}_{k\mu})$$
$$\times\exp(i\mathbf{k}\cdot\mathbf{x}_i)+(4\pi e^2/mL^3)\sum_{\substack{kl\mu\nu i\\ l\neq -k}}(\hbar/2\omega)(\boldsymbol{\varepsilon}_{k\mu}\cdot\boldsymbol{\varepsilon}_{l\nu})$$
$$\times(a_{k\mu}+a_{-k\mu}^*)(a_{l\nu}+a_{-l\nu}^*)\exp[i(\mathbf{k}+\mathbf{l})\cdot\mathbf{x}_i], \quad (42b)$$

$$H_{\text{field}}=\tfrac{1}{2}\sum_{k\mu}\hbar\omega(a_{k\mu}a_{k\mu}^*+a_{k\mu}^*a_{k\mu})$$
$$+\tfrac{1}{4}\sum_{k\mu}[\hbar(\omega_p^2+c^2k^2-\omega^2)/\omega][a_{k\mu}a_{k\mu}^*+a_{k\mu}^*a_{k\mu}$$
$$+a_{-k\mu}a_{k\mu}+a_{k\mu}^*a_{-k\mu}^*]. \quad (42c)$$

The order of factors in (42b) is not essential because, due to the transversality condition, $\mathbf{p}_i\cdot\boldsymbol{\varepsilon}_{k\mu}$ commutes with $\exp(i\mathbf{k}\cdot\mathbf{x}_i)$. We are working in the Heisenberg representation and our operators satisfy the usual commutation rules:

$$\begin{aligned}[a_{k\mu}^*, a_{l\nu}]&=\delta_{kl}\delta_{\mu\nu},\\ [a_{k\mu}^*, a_{l\nu}^*]&=[a_{k\mu}, a_{l\nu}]=0,\\ [p_{i\lambda}, x_{j\mu}]&=(\hbar/i)\delta_{ij}\delta_{\lambda\mu},\\ [p_{i\lambda}, p_{j\mu}]&=[x_{i\lambda}, x_{j\mu}]=0.\end{aligned} \quad (43)$$

Just as we did in the classical case, we now seek to find a canonical transformation to the collective description, in which the field coordinates describe the organized transverse oscillations. The transformation theory most suited to our purpose is briefly as follows.[13] We define new operators $(\mathbf{X}_i, \mathbf{P}_i)$ which possess the same eigenvalues, and satisfy the same commutation rules as the $(\mathbf{x}_i, \mathbf{p}_i)$ by

$$\begin{aligned}\mathbf{x}_i&=\{\exp(-iS/\hbar)\}\,\mathbf{X}_i\{\exp(iS/\hbar)\},\\ \mathbf{p}_i&=\{\exp(-iS/\hbar)\}\,\mathbf{P}_i\{\exp(iS/\hbar)\},\end{aligned} \quad (44a)$$

and similarly

$$a_{k\mu}=\{\exp(-iS/\hbar)\}A_{k\mu}\{\exp(iS/\hbar)\}. \quad (44b)$$

We may consider (44a) and (44b) as operator equations, and take S to be a function of the new operators $(\mathbf{X}_i, \mathbf{P}_i, A_{k\mu}, A_{k\mu}^*)$ only. S will be the quantum-mechanical analog of our classical generating function. The relationship between the old and the new hamiltonians may similarly be viewed as an operator equation:

$$H=\{\exp(-iS/\hbar)\}\mathcal{H}\{\exp(iS/\hbar)\} \quad (44c)$$

where $\mathcal{H}$ represents the hamiltonian expressed in the new coordinates.

The desired canonical transformation to the "collective" representation is then defined by the following generating function

$$S=-(ei/m)\sum_{il\nu}(2\pi\hbar/\omega L^3)^{\frac{1}{2}}$$
$$\times\{[(\mathbf{P}_i\cdot\boldsymbol{\varepsilon}_{l\nu})A_{l\nu}/(\omega-(\mathbf{l}\cdot\mathbf{P}_i/m)+\hbar l^2/2m)]\exp(i\mathbf{l}\cdot\mathbf{X}_i)$$
$$-[\exp(-i\mathbf{l}\cdot\mathbf{X}_i)][A_{l\nu}^*\mathbf{P}_i\cdot\boldsymbol{\varepsilon}_{l\nu}]/$$
$$(\omega-(\mathbf{l}\cdot\mathbf{P}_i/m)+\hbar l^2/2m)\}. \quad (45)$$

B. Consequences of the Transformation

In working out the consequences of this transformation, we shall expand the exponentials, $\exp(\pm iS/\hbar)$, so that (44c) may be written:

$$H=\mathcal{H}-(i/\hbar)[S,\mathcal{H}]-(1/2\hbar^2)[S,[S,\mathcal{H}]]$$
$$+(i/6\hbar^3)[S,[S,[S,\mathcal{H}]]]+\cdots. \quad (46)$$

We will classify terms according to the power of S they contain—i.e., $[S,\mathcal{H}]$ is the first-order commutator of S and $\mathcal{H}$. We shall see that the terms arising from $[S,[S,[S,\mathcal{H}]]]$, and higher order commutators can be neglected if we restrict our attention to the lowest order terms in v/c.

The following relationships are useful in applying (46):

$$p_{i\lambda}=P_{i\lambda}-(i/\hbar)[S,P_{i\lambda}]+\cdots$$
$$=P_{i\lambda}+(e/m)\sum_{l\nu}(2\pi\hbar/\omega L^3)^{\frac{1}{2}}l_\lambda$$
$$\times\{[(\mathbf{P}_i\cdot\boldsymbol{\varepsilon}_{l\nu})A_{l\nu}/(\omega-(\mathbf{l}\cdot\mathbf{P}_i/m)+\hbar l^2/2m)]$$
$$\times[\exp(i\mathbf{l}\cdot\mathbf{X}_i)]+[\exp(-i\mathbf{l}\cdot\mathbf{X}_i)]$$
$$[A_{l\nu}^*\mathbf{P}_i\cdot\boldsymbol{\varepsilon}_{l\nu}/(\omega-(\mathbf{l}\cdot\mathbf{P}_i/m)+\hbar l^2/2m)]\}, \quad (47)$$

[12] This hamiltonian differs from the customary one, because we have expanded in terms of an arbitrary oscillation frequency ω, rather than taking $\omega=ck$.

[13] Quantum-mechanical transformation theory is developed in, for instance, P. A. M. Dirac, *Principles of Quantum Mechanics* (Oxford University Press, London, 1935), second edition.

$$\exp(i\mathbf{k}\cdot\mathbf{x}_i)=\exp(i\mathbf{k}\cdot\mathbf{X}_i)-(i/\hbar)[S,\exp(i\mathbf{k}\cdot\mathbf{X}_i)]+\cdots$$
$$=\exp(i\mathbf{k}\cdot\mathbf{X}_i)-(e/mc\hbar)\sum_{l\nu}(2\pi\hbar/\omega L^3)^{\frac{1}{2}}$$
$$\times\{\mathbf{P}_i\cdot\boldsymbol{\varepsilon}_{l\nu}A_{l\nu}[1/(\omega-(\mathbf{l}\cdot\mathbf{P}_i/m)+\hbar l^2/2m)$$
$$-1/(\omega-(\mathbf{l}\cdot\mathbf{P}_i/m)+(\hbar l^2/2m)-\hbar\mathbf{l}\cdot\mathbf{k}/m)]$$
$$\times\exp[i(\mathbf{k}+\mathbf{l})\cdot\mathbf{X}_i]+[\exp[i(\mathbf{k}-\mathbf{l})\cdot\mathbf{X}_i]]$$
$$\times\mathbf{P}_i\cdot\boldsymbol{\varepsilon}_{l\nu}A_{l\nu}^*[1/(\omega-(\mathbf{l}\cdot\mathbf{P}_i/m)+(\hbar l^2/2m)$$
$$-\hbar\mathbf{l}\cdot\mathbf{k}/m)-1/(\omega-(\mathbf{l}\cdot\mathbf{P}_i/m)+\hbar l^2/2m)]$$
$$+\hbar\mathbf{k}\cdot\boldsymbol{\varepsilon}_{l\nu}[(\exp(i\mathbf{k}\cdot\mathbf{X}_i))(A_{l\nu}/(\omega-(\mathbf{l}\cdot\mathbf{P}_i/m)$$
$$+\hbar l^2/2m))\exp(i\mathbf{l}\cdot\mathbf{X}_i))-(\exp(-i\mathbf{l}\cdot\mathbf{X}_i))$$
$$\times(A_{l\nu}^*/(\omega-(\mathbf{l}\cdot\mathbf{P}_i/m)+\hbar l^2/2m))$$
$$\times(\exp(-i\mathbf{k}\cdot\mathbf{X}_i))]\},\quad(48)$$

$$a_{k\mu}=A_{k\mu}-(i/\hbar)[S,A_{k\mu}]+\cdots$$
$$=A_{k\mu}-(e/mc\hbar)\sum_i(2\pi\hbar/\omega L^3)^{\frac{1}{2}}[\exp(-i\mathbf{k}\cdot\mathbf{X}_i)]$$
$$\times[(\mathbf{P}_i\cdot\boldsymbol{\varepsilon}_{k\mu})/(\omega-(\mathbf{k}\cdot\mathbf{P}_i/m)+\hbar k^2/2m)].\quad(49)$$

The calculation of the commutators for (47) and (49) is trivial. In obtaining (48) one encounters commutators like

$$[\{1/(\omega-(\mathbf{l}\cdot\mathbf{P}_i/m)+\hbar l^2/2m)\},\{\exp(i\mathbf{k}\cdot\mathbf{X}_i)\}].$$

Such a commutator may be easily calculated, provided one notices that:

$$\{1/[\omega-\mathbf{l}\cdot\mathbf{P}_j/m+\hbar l^2/2m]\}\exp(i\mathbf{k}\cdot\mathbf{X}_i)$$
$$=\exp(i\mathbf{k}\cdot\mathbf{X}_i)\{1/[\omega-\mathbf{l}\cdot\mathbf{P}_j/m+\hbar l^2/2m-\hbar\mathbf{l}\cdot\mathbf{k}\delta_{ij}/m]\}.\quad(50)$$

That (50) is true, may be seen by multiplying both sides by $(\omega-\mathbf{l}\cdot\mathbf{P}_j/m+\hbar l^2/2m)$ and commuting this with $\exp(i\mathbf{k}\cdot\mathbf{X}_i)$ on the right-hand side. Using (50), we see that:

$$[\{1/(\omega-(\mathbf{l}\cdot\mathbf{P}_j/m)+\hbar l^2/2m)\},\exp(i\mathbf{k}\cdot\mathbf{X}_i)]$$
$$=\{\exp(i\mathbf{k}\cdot\mathbf{X}_i)\}\{1/(\omega-(\mathbf{l}\cdot\mathbf{P}_j/m)+(\hbar l^2/2m)$$
$$-\hbar\delta_{ij}\mathbf{l}\cdot\mathbf{k}/m)-1/(\omega-(\mathbf{l}\cdot\mathbf{P}_j/m)+\hbar l^2/2m)\}.\quad(51)$$

We now consider the first-order terms arising from H_{part} and $\frac{1}{2}\sum_{k\mu}\hbar\omega(a_{k\mu}a_{k\mu}^*+a_{k\mu}^*a_{k\mu})$. These are given by

$$-(i/\hbar)[S,\{\sum_i(P_i^2/2m)+\tfrac{1}{2}\sum_{k\mu}\hbar\omega(A_{k\mu}A_{k\mu}^*+A_{k\mu}^*A_{k\mu})\}]$$
$$=-(e/m)\sum_{k\mu}(2\pi\hbar/\omega L^3)^{\frac{1}{2}}\{(A_{k\mu}+A_{-k\mu}^*)$$
$$\times(\mathbf{P}_i\cdot\boldsymbol{\varepsilon}_{k\mu})\exp(i\mathbf{k}\cdot\mathbf{X}_i)\},\quad(52)$$

as may be verified using the commutation rules analogous (43) for the new coordinates. But these terms thus cancel one of the zero-order terms arising from H_{inter}, which we denote by

$$\mathcal{H}^I{}_{\text{inter}}=(e/m)\sum_{k\mu}(2\pi\hbar/\omega L^3)^{\frac{1}{2}}(A_{k\mu}+A_{-k\mu}^*)$$
$$\times(\mathbf{P}_i\cdot\boldsymbol{\varepsilon}_{k\mu})\exp(i\mathbf{k}\cdot\mathbf{X}_i).\quad(53)$$

Thus, there are no interaction terms of this order (in v/c) in the new hamiltonian. The vanishing of the linear field terms in this order is one of the desired properties of the hamiltonian appropriate for the collective description.

When we consider the terms arising from the second-order commutators in H_{part} and $\frac{1}{2}\sum_{k\mu}\hbar\omega(a_{k\mu}a_{k\mu}^*+a_{k\mu}^*a_{k\mu})$, we see that they will yield just minus one-half the terms given by the first-order commutator arising from $\mathcal{H}^I{}_{\text{inter}}$, and that all of the terms arising from the higher order commutators in these two terms will bear a similar simple arithmetical relationship to the terms in the next-lower order commutator in $\mathcal{H}^I{}_{\text{inter}}$. The first-order commutator of S and $\mathcal{H}^I{}_{\text{inter}}$ is:

$$-(i/\hbar)[S,\mathcal{H}^I{}_{\text{inter}}]=-(ei/mc\hbar)\sum_{k\mu i}(2\pi\hbar/\omega L^3)^{\frac{1}{2}}$$
$$\times\{[S,(\mathbf{P}_i\cdot\boldsymbol{\varepsilon}_{k\mu})](A_{k\mu}+A_{-k\mu}^*)(\exp(i\mathbf{k}\cdot\mathbf{X}_i))$$
$$+(\mathbf{P}_i\cdot\boldsymbol{\varepsilon}_{k\mu})[S,(A_{k\mu}+A_{-k\mu}^*)](\exp(i\mathbf{k}\cdot\mathbf{X}_i))$$
$$+(\mathbf{P}_i\cdot\boldsymbol{\varepsilon}_{k\mu})(A_{k\mu}+A_{-k\mu}^*)[S,(\exp(i\mathbf{k}\cdot\mathbf{X}_i))]\}.\quad(54)$$

It is quite straightforward, but tedious to show that this reduces to

$$-(4\pi e^2/m^2L^3)\sum_{k\mu ij}\{(\mathbf{P}_i\cdot\boldsymbol{\varepsilon}_{k\mu})(\mathbf{P}_j\cdot\boldsymbol{\varepsilon}_{k\mu})/$$
$$[\omega^2-((\mathbf{k}\cdot\mathbf{P}_j/m)+\hbar k^2/2m)^2]\}\exp[i\mathbf{k}\cdot(\mathbf{X}_i-\mathbf{X}_j)],\quad(55a)$$
$$+\frac{4\pi e^2}{m^3L^3}\sum_{ik\mu}\frac{(\hbar k^2/2\omega)(\mathbf{P}_i\cdot\boldsymbol{\varepsilon}_{k\mu})^2}{[\omega-(\mathbf{k}\cdot\mathbf{P}_i/m)]^2-\hbar^2k^4/4m^2}$$
$$\times\{A_{k\mu}A_{k\mu}^*+A_{k\mu}^*A_{k\mu}+A_{k\mu}A_{-k\mu}+A_{k\mu}^*A_{-k\mu}^*\}.\quad(55b)$$

In reducing (54) to (55a) and (55b) we have neglected a number of terms which are quadratic in field variables and are multiplied by a phase factor with nonvanishing argument, $\exp[i(\mathbf{k}+\mathbf{l})\cdot\mathbf{X}_i]$. This is the same approximation we made in the classical case, when we neglected the corresponding terms (23). The justification used for the classical approximation may be directly applied to this case. Since, as we have noted, the second-order commutators arising from H_{part} and $\frac{1}{2}\sum_{k\mu}\hbar\omega(a_{k\mu}a_{k\mu}^*+a_{k\mu}^*a_{k\mu})$ yield just $-\frac{1}{2}\{-(i/\hbar)[S,\mathcal{H}^I{}_{\text{inter}}]\}$, then the combined contribution of these terms and the first-order commutator with $\mathcal{H}^I{}_{\text{inter}}$ to our hamiltonian will be $-(i/2\hbar)[S,\mathcal{H}_{\text{inter}}]$ or one-half the sum of (55a) and (55b).

In addition to the unconsidered higher order commutators in the terms we have already discussed, there are two terms we have not yet investigated. One is a

quadratic term in the field variables in H_{inter},

$$(4\pi e^2/mL^3)\sum_{\substack{kl\mu\nu\\ l\neq -k}}(\hbar/2\omega)(\boldsymbol{\varepsilon}_{k\mu}\cdot\boldsymbol{\varepsilon}_{l\nu})(a_{k\mu}+a_{-k\mu}^*)\times(a_{l\nu}+a_{-l\nu}^*)\exp[i(\mathbf{k}+\mathbf{l})\cdot\mathbf{x}_i].$$

This term may be neglected because it is quadratic in the field variables and contains a phase factor $\exp[i(\mathbf{k}+\mathbf{l})\cdot\mathbf{x}_i]$ with nonvanishing argument. The other term is from H_{field}, and is, to first order,

$$\tfrac{1}{4}\sum_{k\mu}(\omega_p^2+c^2k^2-\omega^2)(\hbar/\omega)\{A_{k\mu}A_{k\mu}^*+A_{k\mu}^*A_{k\mu}+A_{k\mu}A_{-k\mu}+A_{k\mu}^*A_{-k\mu}^*-(i/\hbar)[S,(A_{k\mu}A_{k\mu}^*+A_{k\mu}^*A_{k\mu}+A_{k\mu}A_{-k\mu}+A_{k\mu}^*A_{-k\mu}^*)]\}. \quad (56)$$

On comparing the zero-order terms in (56) with the quadratic field terms resulting from $-(i/2\hbar)[S,3\mathcal{C}^I{}_{\text{inter}}]$ obtained from (55), we see that the sum of these will vanish if we take:

$$\omega^2=\omega_p^2+c^2k^2+(4\pi e^2/mL^3)\sum_{ik\mu}(k^2/\mathbf{P}_i\cdot\boldsymbol{\varepsilon}_{k\mu})^2/m^2\}\times\{1/(\omega-\mathbf{k}\cdot\mathbf{P}_i/m)^2-\hbar^2k^4/4m^2\}. \quad (57)$$

This is our quantum-mechanical dispersion relation for the organized transverse oscillations. It is almost identical with the analogous classical dispersion relation (27), and reduces to the latter as $\hbar\to 0$.

When we combine all of the terms we have considered thus far, and assume that the frequency of the organized oscillations is specified by (57), we obtain

$$3\mathcal{C}=\sum_i(P_i^2/2m)+\tfrac{1}{2}\sum_{k\mu}\hbar\omega(A_{k\mu}A_{k\mu}^*+A_{k\mu}^*A_{k\mu})-\frac{2\pi e^2}{m^2L^3}\sum_{ij\mu}\left\{\frac{(\mathbf{P}_i\cdot\boldsymbol{\varepsilon}_{k\mu})(\mathbf{P}_j\cdot\boldsymbol{\varepsilon}_{k\mu})}{\omega^2-[(\mathbf{k}\cdot\mathbf{P}_j/m)+\hbar k^2/2m]^2}\right\}\times\exp[i\mathbf{k}\cdot(\mathbf{X}_i-\mathbf{X}_j)], \quad (58)$$

where we have used Eqs. (55a), (55b), (56), and (57), and taken one-half of the sum of the terms in (55a) and (55b). This is just our desired hamiltonian for the collective description. It reduces to the classical hamiltonian (31) as $\hbar\to 0$. $H_{\text{part int}}$ is here given by

$$H_{\text{part int}}=-\frac{2\pi e^2}{m^2L^3}\sum_{ij\mu}\frac{(\mathbf{P}_i\cdot\boldsymbol{\varepsilon}_{k\mu})(\mathbf{P}_j\cdot\boldsymbol{\varepsilon}_{k\mu})}{\omega^2-[(\mathbf{k}\cdot\mathbf{P}_j/m)+\hbar k^2/2m]^2}\times\exp[i(\mathbf{k}\cdot(\mathbf{X}_i-\mathbf{X}_j)]. \quad (59)$$

It is essentially the same as our classical result (32c) since the $\hbar k^2/2m$ term is unimportant for most cases of interest.

We may neglect the terms arising from the higher order commutators we have not yet considered, for the higher order commutators in that part of H_{field} given in (56) are of the same character as those resulting from (55b). Thus, we see all of the higher order commutators will be arithmetical fractions of those resulting from $[S,[S,3\mathcal{C}^I{}_{\text{inter}}]]$. But as may be seen from (55a) and (55b) the lowest order term arising from $[S,[S,3\mathcal{C}^I{}_{\text{inter}}]]$ will be a factor of v^2/c^2 smaller than H_{inter}, and may be neglected, just as (22) was in the classical case, since its inclusion would lead to a fourth or higher power of v/c in $H_{\text{part int}}$.

Thus, in all respects the quantum-mechanical results are essentially the same as those obtained with our classical treatment of the previous sections. We find that we must carry out the same approximations for this case, and the analysis of $H_{\text{part int}}$ will yield results similar to those of Sec. II.

IV. CONCLUSION

In conclusion, we should like to point out that we have verified, both classically and quantum-mechanically, our qualitative picture of the role of organized transverse oscillations in electron interactions. We have seen that, by a suitable canonical transformation to the collective variables, we can show that the effects of magnetic interaction are divided naturally into the two components discussed earlier:

(1) The long-range part, ($\lambda>c/\omega_p$). This is responsible for the long-range organized behavior of the electrons, leading to modified transverse field oscillations. We may interpret these interactions as being redescribed in terms of the coordinates of the modified transverse oscillations.

(2) The short-range part, ($\lambda<c/\omega_p$), given by $H_{\text{part int}}$, which does not contribute to the organized behavior, and represents the residual particle-interaction after the organized behavior of the system has been taken into account.

Furthermore, in those regions in which organized behavior is unimportant (i.e., $\lambda<c/\omega_p$), the new hamiltonian reduces to the appropriate particle hamiltonian, in which the electrons interact according to the Biot-Savart law, and the transverse fields oscillate with frequency $\omega=ck$. For, as we have seen, $H_{\text{part int}}$ describes the Biot-Savart law for short wavelengths, and in this limit our dispersion relation becomes $\omega^2=c^2k^2$.

The Twice-Forbidden Transition of Cs^{137} and the Law of Beta-Decay*

L. M. LANGER AND R. J. D. MOFFAT
Department of Physics, Indiana University, Bloomington, Indiana
(Received February 19, 1951)

The shape of the beta-spectrum of the direct 1.17 Mev, 8 percent abundant transition between the $g_{7/2}$ ground state of Cs^{137} and the $d_{3/2}$ ground level of Ba^{137} has been studied in detail in a magnetic spectrometer. The shape of the spectrum can be adequately described by a twice-forbidden factor, C_{2T}, resulting from the tensor form of interaction. Neither the axial vector form nor the combination S–A–P are capable of accounting for the data.

I. INTRODUCTION

THE shape of the beta-spectrum of the weak, twice-forbidden transition of Cs^{137} has been studied in detail in order to determine which of the possible forms of the Fermi theory[1] is the correct one. The general validity of the Fermi theory, as applied to allowed transitions, now appears to be well established.[2–6] The details of the theory[7] can, however, be formulated in different ways, depending essentially on the transformation properties of the product of the wave functions associated with the emitted electron and neutrino. Five invariant forms are possible: scalar, vector, tensor, axial vector, or pseudoscalar.

It happens that the choice of a single one of the interaction forms has no influence on the shape of the spectrum of an allowed transition. Therefore, measurements of such "allowed spectra" offer no means of determining which of the particular forms of the theory is correct.

Certain linear combinations of the interaction forms are also possible. In particular, the combination S–A–P proposed by Wigner and Critchfield[8] is of interest, since it implies a symmetry in the wave functions of the initial and final nuclei as well as those of the electron and neutrino. It has been shown[9] that the combinations S–A–P and V–T are the only ones which need be considered, largely because of an interference effect, an additional energy-dependent term to the distribution formula for the allowed beta-transition. This term is of the form $(1\pm a/W)$, where W is the electron energy and a is a constant. Since the allowed spectrum is already adequately described without this additional term, it is inferred that all other possible combinations may be disregarded.

For the forbidden transitions, the shape of the beta-spectrum may depend upon the form of the interaction. In general, a beta-spectrum is given by the distribution formula

$$Nd\eta \sim C(W_0, W, Z)F(Z, W)\eta^2(W_0-W)^2d\eta.$$

$Nd\eta$ is the number of electrons in the momentum interval $d\eta$. W_0 is the maximum energy (including rest energy) of the electron. W_0-W is c times the momentum of the neutrino, if that particle has zero rest mass.[10] $F(Z, W)$ is the "coulomb factor" and represents the effect of the electrostatic field on the emitted electron. The factor $C(W_0, W, Z)$ arises from the matrix elements measuring the overlapping of the initial and final nuclear states. For allowed transitions this factor is independent of the energy for all of the interaction forms. In the case of such allowed spectra, the distribution is determined mainly by the "statistical factor" $\eta^2(W_0-W)^2d\eta$, which would be characteristic of any momentum distribution resulting from the sharing of a given energy release, W_0, between a pair of particles.

It is also to be expected that for some forbidden transitions the spectra will have the allowed shape. This arises from the dominance of certain energy independent terms in the expression for C.[11,12] This is particularly so for once-forbidden transitions involving a change of parity and a spin change of 0 or 1 unit. However, for once-forbidden transitions involving a change of 2 units of angular momentum, all matrix elements but one vanish, and the expression for C yields a unique energy dependence. A spectrum of this type was first reported[13] in the decay of Y^{91}. The shape of the spectrum of this transition can be satisfactorily explained by setting C proportional to $a\sim[W^2-1+(W_0-W)^2]$. This energy dependence is provided by either the axial vector or the tensor forms of interaction. It could, obviously, also result from S–A–P with negligible contributions from S and P. This same characteristic spectrum shape has since been identified in at least a dozen other beta-disintegrations.[14] Whereas these

* This work was assisted by a grant from the Frederick Gardner Cottrell Fund for the Research Corporation and by the joint program of the ONR and AEC.

[1] E. Fermi, Z. Physik **88**, 161 (1934).
[2] J. Lawson and J. Cork, Phys. Rev. **57**, 982 (1940).
[3] C. S. Wu and R. D. Albert, Phys. Rev. **75**, 315 (1949).
[4] Langer, Moffat, and Price, Phys. Rev. **76**, 1725 (1949).
[5] G. E. Owen and C. S. Cook, Phys. Rev. **76**, 1726 (1949).
[6] Price, Motz, and Langer, Phys. Rev. **77**, 798 (1950).
[7] E. J. Konopinski, Revs. Modern Phys. **15**, 209 (1943).
[8] C. Critchfield and E. P. Wigner, Phys. Rev. **60**, 412 (1941).
[9] M. Fierz, Z. Physik **104**, 553 (1937); S. R. DeGroot and H. A. Tolhoek, Physica **16**, 456 (1950).
[10] Cook, Langer and Price, Phys. Rev. **74**, 548 (1948).
[11] L. M. Langer and H. C. Price, Jr., Phys. Rev. **76**, 641 (1949).
[12] L. M. Langer, Phys. Rev. **77**, 50 (1950).
[13] L. M. Langer and H. C. Price, Jr., Phys. Rev. **75**, 1109 (1949).
[14] A partial list of references to the work on some of these decays appears in the excellent review article by C. S. Wu, Revs. Modern Phys. **22**, 386 (1950). The transition of Br^{84} is listed in this article

once-forbidden shapes have been useful in interpreting the predictions of the nuclear shell model[15] and in confirming the validity of Gamow-Teller selection rules[16] by reducing the form of the interaction to either tensor or axial vector, they alone are not capable of yielding a decision as to which of these two interaction forms is correct.

In addition to the once-forbidden shape, a unique energy dependence is also predicted for the twice-forbidden transition involving no change of parity and a change of 3 units of angular momentum. In this case, the forbidden factor, C, is proportional to $c\sim 3(W^2-1)^2+3(W_0-W)^4+10(W-1)(W_0-W)^2$ and again results from either the tensor or the axial vector interaction. Spectra of this shape have been observed[17,18] for Cl^{36}, and Be^{10}.

The spectrum to be discussed in the present paper is of particular interest because it offers a means of choosing between the tensor and the axial vector interactions. The decay in question is the direct transition from the ground state of Cs^{137} to the ground level of Ba^{137}. An attractive feature of this transition is that the spin of the radioactive parent as well as that of the stable daughter have been measured experimentally.[19,20] The $g_{7/2}$ ground level of Cs^{137} decays in either of two ways with a total half-life of 37 years. In over 90 percent of the time, the decay is to a metastable state of Ba^{137} by a negatron emission with a maximum energy of 0.51 Mev. The metastable level of 2.6 minutes half-life then proceeds to the $d_{3/2}$ ground level of Ba^{137} by the emission of a gamma-ray of 0.661 Mev.[21] The alternative mode of decay is the direct beta-transition to the ground level of Ba^{137}

The low energy beta-transition has been studied by various investigators.[11,22–24] Its shape has been generally interpreted as that of the once-forbidden, $\Delta I=2$, class discussed above, although the exact determination of the shape has always been complicated by the necessity of correcting for the small but finite contribution from the high energy group.

The weak beta-group, with a maximum energy of 1.17 Mev, results then from a twice-forbidden transition involving a spin change of 2 and no change of parity. Because of the nonvanishing of matrix elements, whose evaluation is somewhat arbitrary, the energy dependence of the factor $C(W_0, W, Z)$ is, in this case, not unique. However, it will be shown below that it is not possible to fit the experimental data with the axial vector interaction for any values of the adjustable parameters. Furthermore, the combination S–A–P is also ruled out. On the other hand, the tensor form of interaction can be made to give a very good fit.

Another advantage to be found in working with this 1.17-Mev group of Cs^{137} arises from the fact that, since the transition is only slightly twice-forbidden ($ft\approx 10^{12}$), a source can be obtained of sufficiently high specific activity so as to permit a reliable measurement of the spectrum shape.

II. EXPERIMENTAL METHOD

The measurements of the spectra of the high energy Cs^{137} group were made in the 40-cm radius of curvature, 180 degree focusing, shaped magnetic field spectrometer.[25] This instrument is particularly well suited for measuring the shape of the weak 1.17-Mev spectrum in the presence of the much more intense 0.51-Mev group. The large clearances provide adequate space for effective antiscattering baffles. The large distance and thick absorbing core between the source and the detector results in no background interference from the gamma-radiation even with the relatively intense sources employed in this investigation.

Preliminary measurements indicated that there was some slight amount of scattering of low energy electrons off the edge of the main defining baffle (located midway between source and detector). This baffle, which was 0.625 inch thick, had originally been designed for the universal use of the spectrometer with electrons of much higher energy. Some electrons from the intense low energy group were bouncing off the edge of this baffle and getting to the detector. When the thickness of this baffle was reduced to 0.125-inch Al (sufficient for stopping all electrons from Cs^{137}), the number of scattered electrons became completely negligible. As a check, the spectrum was measured for several different openings of the defining baffle. No further change in the spectrum was introduced by the change in geometry. Also, the addition of an extra antiscattering baffle, installed in a plane 18 degrees up from that of the detecting slit, did not change the measured distribution.

Measurements were made with both single- and double-bead 3-mg/cm^2 mica end-window counters. The use of the double-bead counter and a pulse height selector has the advantage that, in addition to lowering the background, it also discriminates against any scattered electrons which might pass through the detecting slit but whose trajectories would not have the proper curvature for traversal of both sections of the counter.

Some caution must be applied in using a double-bead counter for the measurement of a momentum distribution. In general, such a counter will have a detec-

as being of the once-forbidden $\Delta I=2$ type. This apparently is not correct; see R. B. Duffield and L. M. Langer, Phys. Rev. **81**, 203 (1951). In addition, the decay of Rb^{88} has also been found to exhibit this characteristic "a" shape; see Bunker, Langer, and Moffat, Phys. Rev. **81**, 30 (1951).

[15] M. G. Mayer, Phys. Rev. **78**, 16 (1950).
[16] G. Gamow and E. Teller, Phys. Rev. **49**, 895 (1936).
[17] C. S. Wu and L. Feldman, Phys. Rev. **76**, 693 (1949).
[18] L. Feldman and C. S. Wu, Phys. Rev. **76**, 697 (1949).
[19] Davis, Nagle, and Zacharias, Phys. Rev. **76**, 1068 (1949).
[20] O. H. Arroe, Phys. Rev. **77**, 645 (1949).
[21] L. M. Langer and R. D. Moffat, Phys. Rev. **77**, 74 (1950).
[22] C. L. Peacock and A. C. G. Mitchell, Phys. Rev. **75**, 1272 (1949).
[23] J. S. Osaba, Phys. Rev. **76**, 345 (1949).
[24] H. M. Agnew, Phys. Rev. **77**, 655 (1950).
[25] L. M. Langer and C. S. Cook, Rev. Sci. Instr. **19**, 257 (1948).

tion efficiency which is a function of the energy of the incident particles. This arises from the fact that, at low energies, there is more large angle scattering of the electrons passing through the mica window. Some of these will not traverse both sections of the counter. Also, at very high energies, the probability of an incident electron producing an ion pair in both sections of the counter will become less with increasing energy if the length of path in each counter section is small. A correction for these effects can be made by determining the ratio of double-size to single-size pulses as a function of energy, with a strong beta-source. It turns out, conveniently, that in our case, the double-bead counter sensitivity is esentially constant over the relatively narrow energy band explored in this investigation.

For the present experiment, both the source and the detector slit had widths of 0.6 cm, so that the resolution of the instrument was about 0.75 percent.

Two different sources were prepared from two different fission product samples obtained from Oak Ridge. The first source contained about 3 mC and had an average surface density of 0.4 mg/cm². The second source was about 3 times as intense and had an average density of 1.7 mg/cm². Both sources were spread quite uniformly with the aid of insulin[26] over a 0.6-cm by 2.5-cm rectangle. The backing for the sources was 0.0002-inch aluminum covered with a 3-μg/cm² layer of zapon. The source was covered by a 1.5-μg/cm² layer of zapon. Although the thickness of the sources and of the backings is more than might be esthetically desirable, it is felt that no measurable distortion resulted over the energy range of particular interest, *viz.*, from 0.7 Mev to 1.17 Mev. The agreement of the data obtained from both sources is indicative of this, as is the very small amount of energy degeneration evident on the low energy side of the internal conversion line. On the other hand, the aluminum backing provides a mechanically strong, electrically grounded support for the extremely intense, long-lived sources. Repeated runs, taken over a period of weeks, showed that there was no apparent decay of the source because of sublimation or any other causes.

The strength of the sources were such that counting rates in the region of the twice-forbidden spectrum, at energies just above the conversion lines of the 0.661-Mev gamma-ray, were from several hundred per minute to about 2500 per minute, depending on the size of the opening in the defining slit. The background with the double-bead counter was 11 counts per minute. All the data were taken with statistical accuracies of from 1 to 3 percent.

The magnetic field measurements were made by means of a continuously rotating coil arrangement.[27] The instrument is calibrated in terms of the internal conversion line from the 0.4112-Mev gamma-ray of Au^{198}. The K line from the 0.661-Mev[29] gamma-ray of Cs^{137} served as a useful monitor in the present investigation.

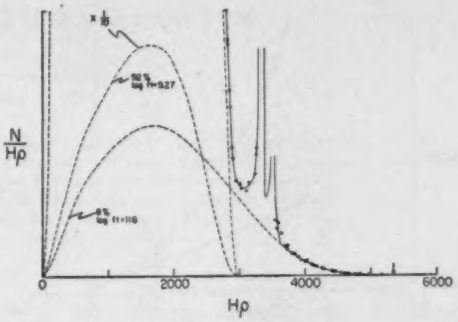

FIG. 1. Beta-spectra of Cs^{137}.

III. RESULTS

Figure 1 is a momentum distribution plot of some typical data obtained in this investigation. The resolution of the spectrum into two groups is done on the basis of the forbidden spectra analysis described below. The extrapolation of the high energy group results from the fit of the tensor "forbidden factor," C_{2T} appropriate for a twice-forbidden transition involving no change of parity and a spin change of 2. After the 1.17-Mev group was properly subtracted, the 0.51-Mev group was extrapolated to lower energies as a once-forbidden spectrum resulting from a transition involving a spin change of 2 and a change of parity. The spectrum shapes of the two groups are obviously quite different from each other and also from an "allowed shape." The relative intensities of the two groups are 92 percent for the 0.51-Mev group and 8 percent for the 1.17-Mev group. This abundance of the high energy group is somewhat greater than earlier estimates of less than 5 percent, based upon less exact analyses.[22,23] The "comparative half-lives," on the basis of the present data are given by $\log ft = 9.2$ for the 0.51-Mev group and $\log ft = 11.6$ for the 1.17-Mev group.

Figure 2 shows the ordinary allowed ($C=1$) and also the appropriate twice-forbidden ($C=C_{2T}$) Fermi plot of the data. The straight line plot obtained with the tensor "forbidden factor," C_{2T}, extrapolates to an end point of 1.17 Mev. This is consistent with the value of $W_0 = 3.29$ mc² assumed for the calculation of C_{2T}, and is also in agreement with the sum of the energy of 0.51 Mev obtained for the inner group plus the gamma-ray energy of 0.661 Mev.

The value of C_{2T} was calculated from the very good approximations appearing in Konopinski's review article.[7] To obtain a good fit with C_{2T}, it was only necessary to use the dominant terms containing the matrix elements A_{ij} and T_{ij}. The ratio of A_{ij}/T_{ij}, chosen to obtain the best fit to the data, is 7.43. The fit is not very sensitive to the choice of a value for the

[26] L. M. Langer, Rev. Sci. Instr. **20**, 216 (1949).
[27] L. M. Langer and F. R. Scott, Rev. Sci. Instr. **21**, 522 (1950).

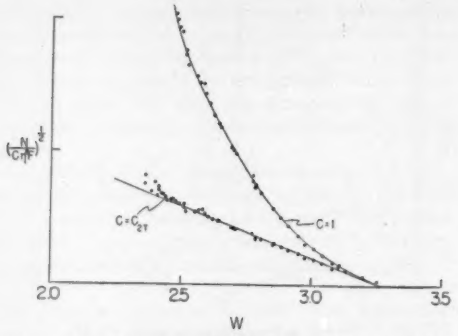

FIG. 2. Ordinary ($C=1$) Fermi plot and tensor forbidden ($C=C_{2T}$) Fermi plot of the 1.17-Mev beta-group of Cs^{137}.

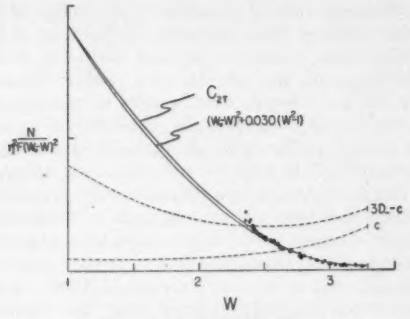

FIG. 3. Energy dependence of "forbidden factors" for the twice-forbidden Cs^{137} beta-group.

nuclear radius (*viz.*, the distance at which the wave functions are evaluated). A very good approximation for the energy dependence of C_{2T} is given by $(W_0-W)^2+k(W^2-1)$. For the present case, $k=0.030$ gives a good fit. Figure 3 shows how the experimental and theoretical "forbidden factors" depend on the energy W. Such a plot is a more sensitive test of the fit than the Fermi plot. The good agreement provided by the tensor interaction is apparent.

The broken line curves in Fig. 3 illustrate the energy dependence of the two terms which, when multiplied by positive coefficients, can combine to make up the axial vector "forbidden factor," C_{2A}.[7] It is quite obvious that there is no way of adding these curves so as to obtain the energy dependence demanded by the data.

Furthermore, since the linear combination $S-A-P$ can only add more D_- energy dependence, it appears that this combination also cannot fit the experimental data.

It is perhaps interesting to note that the curvature of the ordinary allowed Fermi plot of the data of the high energy Cs^{137} group is similar to that observed for the spectrum of RaE.[28-30]

[28] G. J. Neary, Proc. Roy. Soc. (London) **A175**, 71 (1940).
[29] L. M. Langer, Phys. Rev. **75**, 328 (1949).
[30] R. Morrissey and C. S. Wu, Phys. Rev. **75**, 1288 (1949).

IV. CONCLUSION

The shapes of the beta-spectra of allowed transitions can be described by any one of the five possible invariant forms of the Fermi theory, *viz.* scalar, vector, tensor, axial vector, or pseudoscalar. Also, the linear combinations $S-A-P$ and $V-T$ should be considered.

The shapes of beta-spectra resulting from transitions involving a spin change of one unit greater than the degree of forbiddenness (e.g., once-forbidden $\Delta I=2$, twice-forbidden $\Delta I=3$) can be described by *either* the axial vector *or* the tensor interactions, but not by the scalar, vector, or pseudoscalar forms alone.

The high energy transition between the $g_{7/2}$ ground state of Cs^{137} and the $d_{3/2}$ ground level of Ba^{137} results in a beta-spectrum whose measured shape can be explained by the "forbidden factor," C_{2T}, arising from the tensor form of interaction. Furthermore, neither the axial vector form of interaction or the linear combination $S-A-P$ are capable of accounting for the experimental data. The linear combination $V-T$ remains as a possibility. However, the addition of the vector term does not help explain anything which is not already adequately described by the tensor form alone.

It is concluded, therefore, that the law of beta-decay is such that when subject to a Lorentz transformation the product of the electron and neutrino wave functions, $\psi_e\psi_\nu$, behaves like a tensor.

The Coupling of a Dirac Field to a Kemmer Field

ABRAHAM KLEIN*
Harvard University, Cambridge, Massachusetts
(Received November 20, 1950)

A method is given whereby a Dirac field can be so coupled to a Kemmer field as to reproduce any of the invariant coupling terms "permitted" in the usual wave formulation of meson theory. This is done independently of any statement of connection of the Kemmer wave function with the wave functions of the wave formulation. A special reducible representation of the Kemmer matrices is employed which permits the theory to be developed along lines closely analogous to the Dirac theory. As a single illustration of the utility of the theory, the nuclear forces are calculated to lowest nonvanishing order.

I. INTRODUCTION

EVEN in the early days of meson theory it was pointed out, by Duffin,[1] that a synthesis of the meson theories for particles of spin zero and spin one was possible in which the fundamental field equation was a linear equation of the Dirac type. The special properties of the fields involved were expressed by the properties of the matrices, which obey an algebra more complicated than that of the Dirac matrices.

The formal apparatus of the theory was developed in detail by Kemmer[2] and in another form by Belinfante.[3] The Kemmer formalism was then applied to the treatment of problems involving the interaction of the meson field with the electromagnetic field by Booth and Wilson[4] and extended to problems involving the specific nuclear interactions by Wilson.[5]

In the work of the English school,[2,4,5] a distinction was made between what is called the "particle" aspect of meson theory on the one hand and the "wave" aspect on the other. For example, the scattering of photons by mesons exhibits the particle aspect, whereas the exchange of virtual mesons envisaged as the mechanism of nuclear forces exhibits the wave aspect. On the basis of the applications made of the Kemmer formalism, it was concluded that this formalism is particularly suitable for the treatment of problems in which the particle aspect of mesons predominates; for such problems one can devise projection operator techniques similar to those employed in treating the collisions problems of quantum electrodynamics. For the treatment of problems such as the nuclear forces, however, it was concluded that the better-known wave formulation is preferable.

In the work of Wilson,[5] a detailed *a priori* correspondence was set up between the components of the Kemmer wave function and the tensors of the spin-one theory. More recently, Harish-Chandra[6] has shown that the connection between the two formulations can be established by the requirement that certain linear combinations of the components of the Kemmer wave function transform as the components of a vector. The appropriate linear combination can be characterized independently of any special representation. This leads to an elegant deduction of the wave formulation from the Kemmer formulation and statement of meson–nucleon coupling terms. There remains, however, a certain dichotomy in the algebraic treatment of the spin-zero and spin-one theories.

The object of the present investigation is to present an alternative approach to the problem of coupling a nucleon (Dirac) field to a Kemmer field in a manner general enough to free completely the theory of any dependence on the usual wave formulation. This can be done by the use of little more than the algebra of the Dirac matrices. By employing a representation of the Kemmer matrices which contains each irreducible representation just once, we are enabled to treat spin-zero and spin-one theories uniformly through a large portion of any problem; it is only in the evaluation of the final answer that it is necessary to specify in detail the particular transformation property of the meson field of interest.

We shall restrict ourselves to an explanation of the method of coupling the two fields and to an application of the resultant formalism to the calculation of the nuclear forces to lowest nonvanishing order. This will suffice to indicate the utility of the formulation for practical applications to problems involving the "wave" aspects of the meson and to show that the physical content of the theory parallels that of the more usual wave formulation. These ends can be achieved within the framework of the lagrangian formulation of the c-number theory, to which we shall confine ourselves.

II. THE FREE KEMMER FIELD

To describe the Kemmer field, we employ a sixteen-component wave function $\phi_{\alpha\beta}$, $(\alpha, \beta = 1, 2, 3, 4)$, which transforms under Lorentz transformations as the direct product of two Dirac one-particle wave functions and

* Based, in part, on the last section of a thesis presented in partial fulfillment of the requirements for the degree of Doctor of Philosophy at Harvard University, June, 1950.

[1] R. J. Duffin, Phys. Rev. **54**, 114 (1938).

[2] N. Kemmer, Proc. Roy. Soc. (London) **A173**, 91 (1939).

[3] F. J. Belinfante, Physica **6**, 849 (1939). Belinfante achieves some of the results of the present paper by use of a special representation of the Dirac matrices.

[4] F. Booth and A. H. Wilson, Proc. Roy. Soc. (London) **A175**, 483 (1940).

[5] A. H. Wilson, Proc. Cambridge Phil. Soc. **36**, 363 (1940).

[6] Harish-Chandra, Proc. Roy. Soc. (London) **A186**, 502 (1946).

which satisfies the equation

$$(\beta_\mu p_\mu+\kappa_m)\phi(x)=0 \tag{1}$$

in the absence of coupling with any other field. Here[7] $p_\mu=-i\partial/\partial x_\mu$ ($\mu=1, 2, 3, 4$), κ_m is the inverse Compton wavelength for the field under consideration, and the β_μ are 16×16 matrices which satisfy the commutation relations

$$\beta_\mu\beta_\nu\beta_\lambda+\beta_\lambda\beta_\nu\beta_\mu=-\delta_{\mu\nu}\beta_\lambda-\delta_{\lambda\nu}\beta_\mu. \tag{2}$$

For the β_μ, we employ a special reducible representation already noted by Duffin:[1]

$$\beta_\mu=\tfrac{1}{2}(\gamma_\mu^{(1)}I^{(2)}+I^{(1)}\gamma_\mu^{(2)}), \tag{3}$$

where $\gamma_\mu^{(i)}$ is a Dirac four-by-four matrix, and $I^{(i)}$ is the 4×4 unit matrix. The superscript indicates the index of $\phi_{\alpha\beta}(x)$ on which the matrices operate. We shall work with matrices which are skew-hermitian, and which satisfy the commutation relations

$$\gamma_\mu\gamma_\nu+\gamma_\nu\gamma_\mu=-2\delta_{\mu\nu}. \tag{4}$$

We can then show that (2) follows from (3) and (4). We shall also have use for the hermitian matrices

$$\gamma_0=-i\gamma_4, \quad \beta_0=-i\beta_4. \tag{5}$$

From (2) or (3) and (4), it follows that the β_μ, which are themselves skew-hermitian, have the eigenvalues 0, $\pm i$.

The 16×16 matrices of Eq. (3), together with all linearly independent matrices which can be formed from them, 126 in all, constitute a representation of the algebra (2), which is reducible to one 10×10, one 5×5, and one 1×1 representation; the three representations cited are the irreducible representations of the algebra. As stated by Pauli,[8] Géhéniau[9] has carried out explicitly the decomposition into irreducible representations and found that the symmetrical part of ϕ, consisting of 10 independent components, embraces a 4-vector and an antisymmetric tensor; the antisymmetric part of ϕ, consisting of the remaining 6 components, splits into a scalar which is associated with the trivial (identically vanishing) one-rowed representation and a psueodscalar and pseudovector associated with the 5-rowed representation. Thus, by means of Eqs. (1), (2), and (3), we are enabled to treat simultaneously the pseudoscalar and vector meson theories. It will, in fact, emerge quite clearly from the treatment to follow that the dual theories are just as simply extracted from the 16-component representation by the usual distinction in reflection properties.

In addition to ϕ, we define the Pauli-adjoint wave function, $\bar{\phi}(x)$, by

$$\bar{\phi}(x)=\phi^*(x)\gamma_0^{(1)}\gamma_0^{(2)}, \tag{6}$$

from which we can show that $\bar{\phi}$ satisfies

$$(\beta_\mu^T p_\mu-\kappa_m)\bar{\phi}(x)=0, \tag{7}$$

where the superscript T indicates the transposed matrix. The definition (6) is equivalent to the more usual one,[2]

$$\bar{\phi}(x)=\phi^*(x)(2\beta_0^2-1), \tag{8}$$

as one easily verifies from (3).

In the presence of an electromagnetic field, $A_\mu(x)$, by the introduction of the gauge-covariant derivative, Eq. (1) is enlarged to

$$[\beta(p-eA)+\kappa_m]\phi(x)=0, \tag{9}$$

using scalar product notation, from which one derives

$$[-\beta^T(p+eA)+\kappa_m]\bar{\phi}(x)=0. \tag{10}$$

Since the β_μ^T satisfy the commutation relations (Eq. (2)) if the β_μ do, there must exist a matrix C_K such that

$$\beta_\mu^T=-C_K^{-1}\beta_\mu C_K. \tag{11}$$

It follows that

$$[\beta(p+eA)+\kappa_m]\phi'(x)=0, \tag{12}$$

where

$$\phi'(x)=C_K\bar{\phi}(x) \tag{13}$$

is the charge-conjugate solution to $\phi(x)$. C_K can be given explicitly in terms of the charge-conjugating matrix, C, of the Dirac field, which is defined by

$$\gamma_\mu^T=-C^{-1}\gamma_\mu C. \tag{14}$$

For (14) implies that

$$(\gamma_\mu^{(1)})^T+(\gamma_\mu^{(2)})^T = -(C^{(2)})^{-1}(C^{(1)})^{-1}[\gamma_\mu^{(1)}+\gamma_\mu^{(2)}]C^{(1)}C^{(2)}, \tag{15}$$

in virtue of the fact that matrices with different superscripts commute. C_K is then given by

$$C_K=C^{(1)}C^{(2)}. \tag{16}$$

Since $C^T=-C$,

$$C_K^T=C_K. \tag{17}$$

The sign change compared to the spin-a-half case is an essential one and may be made the basis of a proof that we are dealing with a field of bosons.

Finally, the equations of motion (1) and (7) can be derived from the lagrangian density

$$\mathfrak{L}(x)=-\bar{\phi}(x)(\beta p+\kappa_m)\phi(x). \tag{18}$$

III. COUPLING OF A DIRAC FIELD TO A CHARGED KEMMER FIELD

We seek a method, independent of any special representation of the 16-component Kemmer wave function, of so coupling the Kemmer field to a Dirac field as to reproduce the transformation properties of the various couplings employed in the more usual wave formulation of the meson theories.

The essential observation is as follows: We know that

[7] We employ natural units, $\hbar=c=1$.
[8] W. Pauli, Revs. Modern Phys. 13, 203 (1941).
[9] F. Géhéniau, *L'Electron et Photon* (Paris, 1938).

the quantity $\bar{\psi}_\alpha\psi_\alpha$, is a scalar, where ψ is a four-component Dirac spinor and $\bar{\psi}$ its adjoint. Since $\phi_{\alpha\beta}$ is assumed to transform as $\psi_\alpha\psi_\beta$, we seek a matrix A such that $\psi_\alpha A_{\alpha\beta}\psi_\beta$ will be a scalar. Such a matrix is well known.[10] It is the charge-conjugating matrix, C, of the Dirac theory, or, more precisely, its inverse. Thus, it follows that

$$(C^{-1}\psi)\psi=\bar{\psi}'\psi=\text{scalar}. \tag{19}$$

$C^{-1}\phi$ is then a linear combination of the components of ϕ with the transformation peoperties of a scalar. This assumes that the charge-conjugate wave function ψ' transforms under space reflections as does ψ. We have the freedom of choosing that ψ' transform as the negative of ψ, and it is just this freedom which will permit the dual theories to be subsumed by the present treatment. We may consider $C^{-1}\phi$ either as the trace of the product of two four-by-four matrices,

$$C^{-1}\phi=\textstyle\sum_{\alpha,\beta} C_{\alpha\beta}{}^{-1}\phi_{\beta\alpha}, \tag{20}$$

or more conveniently, for the purposes of deriving equations of motion from a lagrangian, as a scalar product of two 16-component vectors,

$$C^{-1}\phi=C_{\alpha\beta}{}^{-1}\phi_{\alpha\beta}, \tag{21}$$

which is the definition we adopt. Because of the antisymmetry of C^{-1}, (20) and (21) are negatives of one another. In virtue of the antisymmetry, too, of C^{-1}, it is easily seen that the linear combination (21) of the components of ϕ contains only the antisymmetric part of ϕ, which is just what we would expect on the basis of the remarks of Sec. II.

For the charged theory under consideration, the scalar coupling of a scalar meson field to the nucleon field is then given by

$$f\bar{\psi}\tau_+\psi C^{-1}\phi+\text{c.c. (complex conjugate)}. \tag{22}$$

Here f is a real coupling constant, $\tau_+=\frac{1}{2}(\tau_1+i\tau_2)$, where $\boldsymbol{\tau}=(\tau_1,\tau_2,\tau_3)$ is the isotopic-spin matrix. With $\tau_-=\frac{1}{2}(\tau_1-i\tau_2)$, we compute the complex conjugate term by noting first that

$$(\bar{\psi}\tau_+\psi)^*=\bar{\psi}\tau_-\psi, \tag{23}$$

and then that

$$(C^{-1}\phi)^*=-\phi_{\alpha\beta}{}^*C_{\alpha\beta}, \tag{24}$$

since $(C^{-1})^*=-C$. From Eq. (14), we obtain the relation

$$-C_{\alpha\beta}=(\gamma_0)_{\alpha\delta}C_{\delta\lambda}(\gamma_0)_{\beta\lambda}. \tag{25}$$

Inserted in (24), (25) leads to

$$(C^{-1}\phi)^*=\bar{\phi}C. \tag{26}$$

The invariant coupling term made up of scalars is then

$$f\bar{\psi}\tau_+\psi C^{-1}\phi+f\bar{\psi}\tau_-\psi\bar{\phi}C. \tag{27}$$

To describe the other types of coupling in which we are interested, it turns out that the properties of the set of sixteen linearly independent Dirac matrices, γ_A, with respect to the charge-conjugating matrix C^{-1}, prove to be just what we need. We choose the set

$$\gamma_A=(I,\ \gamma_\mu,\ \sigma_{\mu\nu}=\tfrac{1}{2}i(\gamma_\mu\gamma_\nu-\gamma_\nu\gamma_\mu),\ \gamma_5\gamma_\mu,\ \gamma_5=\gamma_1\gamma_2\gamma_3\gamma_4).$$

As is well known, γ_AC^{-1} is either symmetric or antisymmetric, being symmetric for γ_A, either a vector or a tensor, and antisymmetric for all other cases. By employing the matrices[11] $\gamma_A{}^TC^{-1}$, we can form covariant sets of quantities involving the meson field ϕ, to be coupled with quantities of like transformation property involving the nucleon field ψ.

The general invariant coupling term is then[12]

$$f\bar{\psi}\gamma_A\tau_+\psi\gamma_A{}^TC^{-1}\phi+\text{c.c.} \tag{28}$$

The c.c. term immediately assumes the form

$$-f\bar{\psi}\gamma_0\gamma_A{}^\dagger\gamma_0\tau_-\psi\phi^*\gamma_A{}^\dagger C = -f\bar{\psi}\gamma_0\gamma_A\gamma_0\tau_-\psi\phi^*\gamma_AC, \tag{29}$$

since the hermitian conjugate matrix $\gamma_A{}^\dagger=\pm\gamma_A$. The Kemmer part of (29) is

$$-\phi_{\alpha\beta}{}^*(\gamma_A)_{\alpha\delta}C_{\delta\beta}. \tag{30}$$

Using Eq. (25) and the equation

$$\gamma_0\gamma_A\gamma_0=\pm\gamma_A, \tag{31}$$

it becomes

$$\pm\phi_{\alpha\beta}{}^*(\gamma_0)_{\alpha\epsilon}(\gamma_A)_{\epsilon\lambda}(\gamma_0)_{\lambda\delta}(\gamma_0)_{\beta\sigma}C_{\sigma\rho}(\gamma_0)_{\rho\beta} = \pm\bar{\phi}_{\epsilon\rho}(\gamma_A)_{\epsilon\rho}C_{\sigma\rho}=\pm\bar{\phi}\gamma_AC. \tag{32}$$

The use of (31), now in the nucleon part of (28), together with (32), restores the plus sign; and (28) can thus be written as

$$f\bar{\psi}\gamma_A\tau_+\psi\bar{\eta}_A\phi+f\bar{\psi}\gamma_A\tau_-\psi\bar{\phi}\eta_A, \tag{33}$$

where we have introduced the symbols,

$$\gamma_A{}^TC^{-1}=\bar{\eta}_A,\quad \gamma_AC=\eta_A. \tag{34}$$

η_A and $\bar{\eta}_A$ are actually complex conjugates to within a minus sign. The sign difference, where present, can be removed by the introduction of a factor of i in the appropriate γ_A; but this is hardly essential for our purposes.

We can see now that in order to maintain the plus sign in both terms of (33), it is necessary to use $\gamma_A{}^T$ in *one* of the $\bar{\eta}_A$, η_A. It is thus a matter of convention.

We may look upon (15) as representative of any particular type of coupling, or as a linear combination of several couplings, if we permit the coupling "constant" f to change values in the course of a summation over A.

IV. CHARGE-SYMMETRICAL COUPLING

The coupling terms of the previous section can be extended to charge-symmetrical form. To do this, we

[10] W. Pauli, Ann. inst. Henri Poincaré 6, 109 (1936).

[11] See below for the reason for preferring $\gamma_A{}^T$ to γ_A.

[12] There should be no ambiguity if we make f stand for the coupling constant of the particular theory under discussion. Summation over the indices represented by A is assumed.

introduce a decomposition of the Kemmer ϕ into self-charge-conjugate functions,[8] which is the immediate generalization of the decomposition of a complex scalar or vector field into two real fields. We tentatively define

$$\phi_1=\phi+\phi', \quad \phi_2=i(\phi-\phi'), \tag{35}$$

where ϕ' is the charge conjugate of ϕ. The inverse of (35) is

$$\phi=\tfrac{1}{2}(\phi_1-i\phi_2), \quad \phi'=\tfrac{1}{2}(\phi_1+i\phi_2). \tag{36}$$

From either (35) or (36), it is apparent that ϕ_1 and ϕ_2 are self-charge-conjugate functions. The possibility of this decomposition proceeds from the fact that, in the absence of an electromagnetic field, ϕ and ϕ' satisfy the same equation.

To introduce (36) into (33), we must first rewrite

$$\begin{aligned}\bar{\phi}\gamma_A C&=\bar{\phi}_{\alpha\beta}(\gamma_A)_{\alpha\delta}C_{\delta\beta}\\&=(C^{(1)})_{\alpha\lambda}{}^{-1}(C^{(2)})_{\beta\rho}{}^{-1}\phi_{\lambda\rho}'(\gamma_A)_{\alpha\delta}C_{\delta\beta}\\&=C_{\alpha\lambda}{}^{-1}\phi_{\lambda\rho}'(\gamma_A)_{\alpha\rho}\\&=(\gamma_A{}^T)_{\rho\alpha}C_{\alpha\lambda}{}^{-1}\phi_{\lambda\rho}'\\&=+\gamma_A{}^TC^{-1}\phi' \text{ if } \gamma_A{}^TC^{-1} \text{ is symmetric,}\\&=-\gamma_A{}^TC^{-1}\phi' \text{ if } \gamma_A{}^TC^{-1} \text{ is antisymmetric.}\end{aligned} \tag{37}$$

We must thus distinguish (temporarily) two cases. If the plus sign holds in (37), we can rewrite (33) as

$$f\bar{\psi}\gamma_A\tau_1\psi\gamma_A{}^TC^{-1}(\phi+\phi')+if\bar{\psi}\gamma_A\tau_2\psi\gamma_A{}^TC^{-1}(\phi-\phi'); \tag{38s}$$

but if the minus sign holds, it takes the form

$$f\bar{\psi}\gamma_A\tau_1\psi\gamma_A{}^TC^{-1}(\phi-\phi')+if\bar{\psi}\gamma_A\tau_2\psi\gamma_A{}^TC^{-1}(\phi+\phi'). \tag{38a}$$

It is now possible to introduce (36) into (38s) immediately and thereby find that the latter becomes

$$f\bar{\psi}\gamma_A\tau_1\psi\gamma_A{}^TC^{-1}\phi_1+f\bar{\psi}\gamma_A\tau_2\psi\gamma_A{}^TC^{-1}\phi_2. \tag{39s}$$

We may then define a third self-charge-conjugate function ϕ_3, which satisfies the same equation in the absence of an electromagnetic field as do ϕ_1 and ϕ_2, and which is to be associated with a neutral meson and, therefore, in the usual manner of the symmetrical meson theory, with the third axis of isotopic spin space and with τ_3. By the addition of the appropriate term to (39s), we may write it in the form of a scalar product in isotopic-spin space:

$$f\bar{\psi}\gamma_{+A}\tau\psi\bar{\eta}_A\phi. \tag{40s}$$

From its construction, (40s) is real.

As it stands, (38a) is not amenable to the same treatment as is (38s); but it can be made to be if we impose further restrictions on the decomposition (35), (36) in a manner consistent with the equation of motion for ϕ. We have already pointed out that if we decompose ϕ into a sum of a symmetric and an antisymmetric part,

$$\phi=\phi^{(s)}+\phi^{(a)}, \tag{41}$$

then each part separately satisfies Eq. (1). Instead, then, of imposing the condition that ϕ_1 and ϕ_2 each be self-charge-conjugate functions, we now require, consistently, that each be written in the form ($i=1, 2$)

$$\phi_i=\phi_i{}^{(s)}+i\phi_i{}^{(a)}, \tag{42}$$

where $\phi_i{}^{(s)}$ and $\phi_i{}^{(a)}$ are each self-charge-conjugate. If we substitute (42) into (36) and then separately equate the symmetric and antisymmetric parts, we find

$$\begin{aligned}\phi^{(s)}&=\tfrac{1}{2}(\phi_1{}^{(s)}-i\phi_2{}^{(s)}), \quad \phi^{(a)}=\tfrac{1}{2}i(\phi_1{}^{(a)}-i\phi_2{}^{(a)}),\\ \phi'^{(s)}&=\tfrac{1}{2}(\phi_1{}^{(s)}+i\phi_2{}^{(s)}), \quad \phi'^{(a)}=-\tfrac{1}{2}i(\phi_1{}^{(a)}+i\phi_2{}^{(a)});\end{aligned} \tag{43}$$

the inverse of (43) is

$$\begin{aligned}\phi_1{}^{(s)}&=(\phi^{(s)}+\phi'^{(s)}), \quad \phi_2{}^{(s)}=i(\phi^{(s)}-\phi'^{(s)}),\\ \phi_1{}^{(a)}&=-i(\phi^{(a)}-\phi'^{(a)}), \quad \phi_2{}^{(a)}=(\phi^{(a)}+\phi'^{(a)}).\end{aligned} \tag{44}$$

By comparison of (43) and (44) with 35) and (36), it can be seen that the steps leading to (40s) are still correct, since any contributions from the antisymmetric part of ϕ vanish identically. Moreover, (38a) can now be written as

$$\begin{aligned}&if\bar{\psi}\gamma_A\tau_1\psi\bar{\eta}_A\phi_1{}^{(a)}+if\bar{\psi}\gamma_A\tau_2\psi\bar{\eta}_A\phi_2{}^{(a)}\\&\qquad=f\bar{\psi}\gamma_A\tau_1\psi\bar{\eta}_A\phi_1+f\bar{\psi}\gamma_A\tau_2\psi\bar{\eta}_A\phi_2,\end{aligned} \tag{39a}$$

since here the symmetric contributions vanish. The introduction, now, of a third wave function ϕ_3, defined by

$$\phi_3=\phi_3{}^{(s)}+i\phi_3{}^{(a)}, \tag{45}$$

allows us to enlarge (39a) to

$$f\bar{\psi}\gamma_A\tau\psi\bar{\eta}_A\phi. \tag{40a}$$

We have thus succeeded in including both cases in the simple coupling terms (40s) or (40a).

It should be noted that an alternative form of writing (40) is available, namely,

$$f\bar{\psi}\gamma_A\tau\psi\bar{\phi}\eta_A, \tag{46}$$

since (46) is the complex conjugate of a coupling term that is real.

Finally, the lagrangian density of the coupled system can be written as

$$\mathfrak{L}(x)=-\bar{\psi}(\gamma p+\kappa_N)\psi-\bar{\phi}(\beta p+\kappa_m)\phi+f\bar{\psi}\gamma_A\tau\psi\bar{\eta}_A\phi. \tag{47}$$

V. DUAL THEORIES

As will be seen below, the useful interactions, of those specified in the preceding sections, are those pertinent to the pseudoscalar and vector meson theories. In order to be able to treat the dual theories, we make use of the possibility mentioned after Eq. (19). We specify that $C^{-1}\phi$ is to be regarded as a pseudoscalar, so that, for example, one form of invariant interaction is

$$f\bar{\psi}\gamma_5\tau_+\psi C^{-1}\phi+\text{c.c.} \tag{48}$$

The general form of the invariant interaction term is

$$f\bar{\psi}\gamma_5\gamma_A\tau_+\psi\gamma_A{}^TC^{-1}\phi+\text{c.c.} \tag{49}$$

The procedure of Sec. III for determining the complex conjugate (c.c.) term in (49) is still valid with but slight modification. Having chosen γ_5 to be hermitian, f will

now be either pure real or pure imaginary according to whether γ_5 anticommutes or commutes with γ_A. With this specification, the considerations of Secs. III and IV can be carried through as before. For the charged theory, the coupling term is of the form

$$f\bar{\psi}\gamma_5\gamma_A\tau_+\psi\bar{\eta}_A\phi+f\bar{\psi}\gamma_5\gamma_A\tau_-\psi\bar{\phi}\eta_A, \tag{50}$$

which in the symmetrical theory becomes

$$f\bar{\psi}\gamma_5\gamma_A\tau\psi\bar{\eta}_A\phi. \tag{51}$$

VI. DEDUCTION OF SPIN-ZERO AND SPIN-ONE THEORIES

The previous considerations suggest that it should be possible to deduce the spin-zero and spin-one field equations directly from the Kemmer equation. It will perhaps suffice to demonstrate the procedure for the case of free fields.

If we write the Kemmer equation, in the form we are employing, in all its detail,

$$\tfrac{1}{2}[((\gamma_\mu)_{\alpha_1\alpha_2}\delta_{\beta_1\beta_2}+\delta_{\alpha_1\alpha_2}(\gamma_\mu)_{\beta_1\beta_2})p_\mu + \kappa_m\delta_{\alpha_1\alpha_2}\delta_{\beta_1\beta_2}]\phi_{\alpha_2\beta_2}=0, \tag{52}$$

multiply by $(\gamma_A{}^TC^{-1})_{\alpha_1\beta_1}$ and sum over repeated indices, we can, by use of (14), easily derive the equation

$$\tfrac{1}{2}(\gamma_\mu{}^T\gamma_A{}^T-\gamma_A{}^T\gamma_\mu{}^T)C^{-1}p_\mu\phi+\kappa_m\gamma_A{}^TC^{-1}\phi=0. \tag{53}$$

We now permit A to run the gamut of allowed values. If, for example, we take $\gamma_A{}^T=I$, we deduce

$$\kappa_mC^{-1}\phi=0. \tag{54}$$

Thus, if $\kappa_m\neq0$, as we suppose, $C^{-1}\phi$, a scalar (or a pseudoscalar), vanishes.

To deduce the spin-zero equations, we first put $\gamma_A{}^T=\gamma_5{}^T$, from which results

$$(\gamma_5\gamma_\mu)^TC^{-1}p_\mu\phi+\kappa_m\gamma_5{}^TC^{-1}\phi=0; \tag{55}$$

or if we define

$$\gamma_5{}^TC^{-1}\phi=U, \tag{56}$$

$$i(\gamma_5\gamma_\mu)^TC^{-1}\phi=U_\mu, \tag{57}$$

$$(\partial U_\mu/\partial x_\mu)-\kappa_mU=0. \tag{58}$$

To find the relationship between U and U_μ, we set $\gamma_A{}^T=(\gamma_5\gamma_\nu)^T$ in (53) and easily deduce

$$U_\nu=(1/\kappa_m)\partial U/\partial x_\nu. \tag{59}$$

Equations (58) and (59) are the correct spin-zero equations.

For the spin-one case, we first set $\gamma_A{}^T=\gamma_\nu{}^TC^{-1}$, which leads us to the equation

$$\sigma_{\mu\nu}{}^TC^{-1}(\partial\phi/\partial x_\mu)+\kappa_m\gamma_\nu{}^TC^{-1}\phi, \tag{60}$$

or

$$(\partial G_{\mu\nu}/\partial x_\mu)-\kappa_mV_\nu=0, \tag{61}$$

if we set

$$\sigma_{\mu\nu}{}^TC^{-1}\phi=G_{\nu\mu}=-G_{\mu\nu}, \tag{62}$$

and

$$\gamma_\mu{}^TC^{-1}\phi=V_\mu. \tag{63}$$

Finally, if we take $\gamma_A{}^T=\sigma_{\lambda\nu}{}^TC^{-1}$, we establish the identification

$$G_{\lambda\nu}=(1/\kappa_m)[(\partial V_\nu/\partial x_\lambda)-(\partial V_\lambda/\partial x_\nu)]. \tag{64}$$

Equations (61) and (64) are the correct spin-one equations.

VII. CALCULATION OF THE NUCLEAR FORCES

As a single illustration of the utility of the formulation given above, we will calculate the nuclear forces to lowest nonvanishing order. This is most simply done within the framework of the c-number theory by means of a semiclassical derivation. We have merely to insert into the interaction energy,[13]

$$H=-f\int d^3x j_A(x)\bar{\eta}_A\phi(x), \tag{65}$$

where we have set $j_A(x)=\bar{\psi}\gamma_A\tau\psi(x)$, and d^3x equals the three-dimensional volume element, the source-dependent part of $\phi(x)$, and divide the result by two by the usual argument that we are counting each interaction between source points twice.

To find an appropriate expression for $\phi(x)$, we solve the field equation

$$(\beta p+\kappa_m)\phi(x)=fj_A(x)\eta_A, \tag{66}$$

derivable from the lagrangian density (47). The solution of (66) is

$$\phi(x)=\phi^{(0)}(x)+f\int K(x-x')\eta_Aj_A(x')d^4x', \tag{67}$$

($d^4x=d^3xdx_0$), where $\phi^{(0)}(x)$ is a solution of the homogeneous equation and $K(x-x')$ is an appropriate Green's function satisfying the inhomogeneous equation for a point source, $\delta(x-x')$, in four dimensions,

$$(\beta p+\kappa_m)K(x-x')=\delta(x-x'). \tag{68}$$

For our present purposes, it is not essential to specify *which* Green's function accompanies *which* solution of the homogeneous equation, since we make no use of $\phi^{(0)}(x)$ and since all Green's functions differ by a solution of the homogeneous equation. The latter, when inserted into the interaction energy gives a vanishing contribution in virtue of the absence of real first-order effects. $\bar{\psi}(x)$, $\psi(x)$ are to lowest order solutions of the Dirac equation for free particles.

For convenience, we will consider the time integral of the interaction energy, which we denote by V. By

[13] What we have termed the interaction energy is, strictly speaking, the negative of the coupling term in the lagrangian. What is usually termed the interaction energy can then be found by carrying out the transformation to hamiltonian form. This is done in the appendix.

(65), subsequent remarks, and (67), V is given by

$$V=-\tfrac{1}{2}f^2\int d^4x d^4x' j_A(x)\bar{\eta}_A K(x-x')\eta_B j_B(x'). \quad (69)$$

Equation (69) is the result in symbolic form for any of the couplings we have considered.

To proceed further we need, first of all, a representation of $K(x-x')$. The solution of (68) is

$$K(x)=\frac{1}{(2\pi)^4}\int d^4p\,\exp(ipx)\frac{1}{\beta p+\kappa_m}, \quad (70)$$

where $px=\mathbf{p}\cdot\mathbf{r}-p_0x_0$. It differs from the Green's function for the Dirac field in the rationalization of the denominator. We note that in the identity

$$1/(\beta p+\kappa_m)=\kappa_m^{-1}[1-\beta p(\beta p-\kappa_m)\{(\beta p)^2-\kappa_m^2\}^{-1}], \quad (71)$$

the second term vanishes for $\beta p=0$. For $\beta p\neq 0$, we may multiply numerator and denominator by βp and use the commutation relations Eq. (2) to prove that the denominator becomes $\beta p(-p^2-\kappa_m^2)$. We may thus write

$$\begin{aligned}1/(\beta p+\kappa_m)&=\kappa_m^{-1}[1-\beta p(\beta p-\kappa_m)(p^2+\kappa_m^2)^{-1}]\\&=1/(p^2+\kappa_m^2)[\kappa_m-\beta p+\kappa_m^{-1}(p^2+(\beta p)^2)],\end{aligned} \quad (72)$$

and consequently

$$K(x)=[(\beta p-\kappa_m)-\kappa_m^{-1}(p^2+(\beta p)^2)]G(x), \quad (73)$$

with

$$G(x)=-\frac{1}{(2\pi)^4}\int d^4p\,\exp(ipx)\frac{1}{p^2+\kappa_m^2}. \quad (74)$$

Our problem has now been reduced to the evaluation of

$$\bar{\eta}_A[(\beta p-\kappa_m)-\kappa_m^{-1}(p^2+(\beta p)^2)]\eta_B \quad (75)$$

for the various possibilities for the η_A. In what follows we employ the definition (3) for the β_μ-matrices. In terms of these, (75) is a sum of the contributions

$$T_1=\tfrac{1}{2}(\bar{\eta}_A)_{\alpha\beta}p_\sigma[(\gamma_\sigma)_{\alpha\rho}\delta_{\beta\epsilon}+(\gamma_\sigma)_{\beta\epsilon}\delta_{\alpha\rho}](\eta_B)_{\rho\beta}, \quad (76)$$

$$T_2=(\bar{\eta}_A)_{\alpha\beta}(-\kappa_m)\delta_{\alpha\rho}\delta_{\beta\epsilon}(\eta_B)_{\rho\beta}, \quad (77)$$

$$T_3=(\bar{\eta}_A)_{\alpha\beta}(-p^2/\kappa_m)\delta_{\alpha\rho}\delta_{\beta\epsilon}(\eta_B)_{\rho\beta}, \quad (78)$$

and

$$\begin{aligned}T_4=(\bar{\eta}_A)_{\alpha\beta}(-p_\sigma p_\tau/4\kappa_m)&[(\gamma_\sigma)_{\alpha\rho}\delta_{\beta\epsilon}+(\gamma_\sigma)_{\beta\epsilon}\delta_{\alpha\rho}]\\&\times[(\gamma_\tau)_{\rho\eta}\delta_{\epsilon\xi}+(\gamma_\tau)_{\epsilon\xi}\delta_{\rho\eta}](\eta_B)_{\eta\xi}.\end{aligned} \quad (79)$$

We may note immediately that T_1 will vanish in all cases, since it will involve the trace of an odd number of γ_μ matrices, whereas T_2 and T_3 have the same matrix dependence.

We consider several cases of interest.

A. Pseudoscalar Theory. Pseudoscalar Coupling

Here

$$\bar{\eta}_A=\gamma_5{}^TC^{-1}, \quad \eta_B=\gamma_5 C. \quad (80)$$

Noting that $\gamma_5{}^TC^{-1}=C^{-1}\gamma_5$, we see that

$$\begin{aligned}T_2&=(\gamma_5C^{-1})_{\alpha\beta}(-\kappa_m)\delta_{\alpha\rho}\delta_{\beta\epsilon}(\gamma_5C)_{\rho\beta}\\&=-\kappa_m(C^{-1}\gamma_5)_{\alpha\beta}(\gamma_5C)_{\alpha\beta}=\text{trace}\kappa_m=4\kappa_m,\end{aligned} \quad (81)$$

since $(\gamma_5C)_{\alpha\beta}=-(\gamma_5C)_{\beta\alpha}$, and $(\gamma_5C)^2=1$. Similarly, we have

$$T_3=4p^2/\kappa_m. \quad (82)$$

For T_4, we merely evaluate one of the terms. Consider

$$\begin{aligned}-p_\sigma p_\tau/4\kappa_m&(C^{-1}\gamma_5)_{\alpha\beta}(\gamma_\sigma)_{\alpha\rho}\delta_{\beta\epsilon}(\gamma_\tau)_{\rho\eta}\delta_{\epsilon\xi}(\gamma_5C)_{\eta\xi}\\&=(p_\sigma p_\tau/4\kappa_m)\ \text{tr}C^{-1}\gamma_5\gamma_\sigma\gamma_\tau\gamma_5C=-p^2/\kappa_m.\end{aligned} \quad (83)$$

The other three terms each yield the same value, so that

$$T_4=-4p^2/\kappa_m, \quad (84)$$

which cancels T_3.

From (69), (75), (81), (82), and (84), we therefore find

$$V=-2f^2\kappa_m\int d^4x d^4x' j_5(x)G(x-x')j_5(x'). \quad (85)$$

This is the usual *form* of the interaction energy (time integral thereof) for the pseudoscalar-pseudoscalar theory, if we look upon V as a second-quantized operator.[14] From (85) we may extract the static nuclear potential energy or the Møller interaction of two nucleons.

B. Scalar Coupling

Here

$$\bar{\eta}_A=C^{-1}, \quad \eta_B=C. \quad (86)$$

In accordance with the remarks of Sec. I, we must expect the result to be that which would be found by setting $\beta_\mu=0$. We easily derive

$$T_2=4\kappa_m, \quad T_3=4p^2/\kappa_m, \quad (87)$$

and $T_4=0$.

We therefore find

$$\begin{aligned}V&=-\frac{2f^2}{\kappa_m}\int d^4x d^4x' j(x)(p^2+\kappa_m^2)G(x-x')j(x')\\&=\frac{2f^2}{\kappa_m}\int d^4x[j(x)]^2,\end{aligned} \quad (88)$$

since $G(x)$ satisfies the equation

$$(p^2+\kappa_m^2)G(x)=-\delta(x). \quad (89)$$

Equation (88) is a contact interaction. T_2 and T_3 are, indeed, the contributions of the terms of Eq. (75) which do not contain β_μ.

It may at first sight appear strange that a particle which cannot exist in the free state (Sec. VI), leads to a nonvanishing lagrangian when interaction is taken

[14] P. T. Matthews, Phys. Rev. **76**, 684 (1949). Strictly speaking, we must subtract the one-particle and vacuum expectation values of (85).

into account. In the appendix it is shown that, in fact, such particles also have zero interaction energy.

C. Pseudoscalar Theory. Pseudovector Coupling

$$\bar{\eta}_A=(\gamma_5\gamma_\mu)^TC^{-1}=-C^{-1}\gamma_\mu\gamma_5, \quad \eta_B=\gamma_5\gamma_\nu C. \quad (90)$$

In a perfectly straightforward way, we then find

$$T_2=4\kappa_m\delta_{\mu\nu}, \quad T_3=(4p^2/\kappa_m)\delta_{\mu\nu}. \quad (91)$$

On the other hand, the terms of T_4 are not all equal. If we consider, for example, the contribution of the first term in each of the brackets of Eq. (79), we find

$$\tfrac{1}{4}(p_\sigma p_\tau/\kappa_m)(C^{-1}\gamma_\mu\gamma_5)_{\alpha\beta}(\gamma_\sigma)_{\alpha\rho}\delta_{\beta\nu}(\gamma_\tau)_{\rho\eta}\delta_{\alpha\xi}(\gamma_5\gamma_\nu C)_{\eta\xi}$$
$$=-\tfrac{1}{4}(p_\sigma p_\tau/\kappa_m)\ \mathrm{tr}\gamma_\mu\gamma_\sigma\gamma_\tau\gamma_\nu=(-p^2/\kappa_m)\delta_{\mu\nu}. \quad (92)$$

If we consider the contribution, say, of the first term of the first bracket and the second term of the second bracket, this may easily be brought into the form

$$\tfrac{1}{4}(p_\sigma p_\tau/\kappa_m)(C^{-1}\gamma_\mu\gamma_5\gamma_\tau)_{\alpha\xi}(\gamma_\sigma\gamma_5\gamma_\nu C)_{\alpha\xi}$$
$$=(\tfrac{1}{4}p_\sigma p_\tau/\kappa_m)(C^{-1}\gamma_\mu\gamma_\tau\gamma_5)_{\alpha\xi}(\gamma_5\gamma_\sigma\gamma_\nu C)_{\alpha\xi}$$
$$=(\tfrac{1}{4}p_\sigma p_\tau/\kappa_m)\{\delta_{\mu\tau}\delta_{\sigma\nu}(C^{-1}\gamma_5)_{\alpha\xi}(\gamma_5 C)_{\alpha\xi}$$
$$+i\delta_{\mu\tau}(C^{-1}\gamma_5)_{\alpha\xi}(\gamma_5\sigma_{\sigma\nu}C)_{\alpha\xi}$$
$$+i\delta_{\sigma\nu}(C^{-1}\sigma_{\mu\tau}\gamma_5)_{\alpha\xi}(\gamma_5 C)_{\alpha\xi}$$
$$-(C^{-1}\sigma_{\mu\tau}\gamma_5)_{\alpha\xi}(\gamma_5\sigma_{\sigma\nu}C)_{\alpha\xi}\}, \quad (93)$$

where we have used

$$\gamma_\mu\gamma_\nu=-\delta_{\mu\nu}-i\sigma_{\mu\nu}. \quad (94)$$

The second and third terms of (93) vanish. The first and fourth terms are readily evaluated and equal

$$(-2p_\sigma p_\tau/\kappa_m)\delta_{\mu\tau}\delta_{\sigma\nu}+(p^2/\kappa_m)\delta_{\mu\nu}. \quad (95)$$

The remaining terms of T_4 are equal to (92) and (95), respectively. Therefore,

$$T_4=(-4p_\sigma p_\tau/\kappa_m)\delta_{\mu\tau}\delta_{\sigma\nu}. \quad (96)$$

Collecting results, we find

$$V=-\frac{2f^2}{\kappa_m}\int d^4xd^4x'j_{5\mu}(x)(p^2+\kappa_m^2)G(x-x')j_{5\mu}(x')$$
$$+\frac{2f^2}{\kappa_m}\int d^4xd^4x'j_{5\mu}(x)p_\mu p_\nu G(x-x')j_{5\nu}(x')$$
$$=\frac{2f^2}{\kappa_m}\int d^4x[j_{5\mu}(x)]^2$$
$$-\frac{8f^2\kappa_N{}^2}{\kappa_m}\int d^4xd^4x'j_5(x)G(x-x')j_5(x'). \quad (97)$$

The first term of (97) results from the use of (89); the second term was obtained by an integration by parts and application of Dirac's equation for a free particle. It is the expected term and, if present alone, would give equivalence of coupling to the lowest order. But in addition there is an invariant contact interaction. This is again seen to be the contribution which one would get if $\beta\phi$ was set equal to zero and is thus, in a sense, the contribution from the dynamically dependent part of the field. In the appendix it is shown that it is effectively absent in the interaction hamiltonian.

D. Vector Theory

By the methods already illustrated, we find, for the case of vector coupling, that

$$V=2f^2\kappa_m\int d^4xd^4x'j_\mu(x)G(x-x')j_\mu(x'), \quad (98)$$

the desired result; but in the case of tensor coupling, the result is analogous to the result for derivative coupling in the pseudoscalar theory, namely,

$$V=\frac{4f^2}{\kappa_m}\int d^4x[j_{\mu\nu}(x)]^2+\frac{8f^2}{\kappa_m}\int d^4xd^4x'(\partial/\partial x_\nu)$$
$$\times j_{\mu\nu}(x)G(x-x')(\partial/\partial x_\lambda')j_{\mu\lambda}(x'), \quad (99)$$

which contains, in addition to the desired result, an invariant contact interaction. Finally, the results for the dual theories follow almost directly from the above. One has only to take into account the altered properties of the nucleon densities.

ACKNOWLEDGMENT

It is a pleasure to thank Professor J. Schwinger for suggesting the present approach and for essential advice and encouragement during the course of the investigation. Most of the work was done while the author was under an AEC predoctoral fellowship.

APPENDIX

We compute the hamiltonian in the usual way in order to demonstrate that the interaction part thereof can be cast into a form which makes it abundantly clear that the conjectures of the previous section about the cancellation of contact interactions were justified. We start from the lagrangian density (47) and note a fact of which we have already made use, namely, that the interaction term may be written in one of two alternative forms, either as $fj_A\bar{\eta}_A\phi$, or as $fj_A\bar{\phi}\eta_A$, since the two are complex conjugates and each is real (symmetrical coupling).

Noting that the canonical momenta for nucleon and meson are

$$\pi^N=i\bar{\psi}\gamma_0, \quad (A1)$$
$$\pi^m=i\bar{\phi}\beta_0, \quad (A2)$$

respectively, we find immediately, for the hamiltonian density,

$$\mathcal{H}=\bar{\psi}(\boldsymbol{\gamma}\cdot\mathbf{p}+\kappa_N)\psi+\bar{\phi}(\boldsymbol{\beta}\cdot\mathbf{p}+\kappa_m)\phi-fj_A\bar{\phi}\eta_A, \quad (A3)$$

where, for example.,

$$\boldsymbol{\gamma}\cdot\mathbf{p}=\sum_{i=1}^{3}\gamma_ip_i.$$

From (A3), we must eliminate the dependent components $(1-\beta_0{}^2)\phi$ by use of the initial condition

$$\boldsymbol{\beta}\cdot\mathbf{p}\beta_0{}^2\phi+\kappa_m(1-\beta_0{}^2)\phi=(1-\beta_0{}^2)\eta_Aj_A, \quad (A4)$$

which is derived directly from the Kemmer equation, Eq. (66), by multiplication from the left by $1-\beta_0{}^2$. One application of

(A4) to (A3) yields

$$\mathcal{H}=\bar{\psi}(\gamma\cdot\mathbf{p}+\kappa_N)\psi+\kappa_m\bar{\phi}\beta_0{}^2\phi+\bar{\phi}\boldsymbol{\beta}\cdot\mathbf{p}(1-\beta_0{}^2)\phi-fj_A\bar{\phi}\beta_0{}^2\eta_A$$
$$=\mathcal{H}_0{}^N+\kappa_m\bar{\phi}\beta_0{}^3-(\mathbf{p}\bar{\phi}\boldsymbol{\beta})(1-\beta_0{}^2)\phi-fj_A\bar{\phi}\beta_0{}^2\eta_A, \quad \text{(A5)}$$

where, in the second form of (A5), we have integrated by parts, assuming, in fact, that we are computing the total hamiltonian. Another application of (A4) now yields, after some rearrangement and use of the fact that $\beta_0\beta_k\beta_0=0$,

$$\mathcal{H}=\mathcal{H}_0{}^N+\mathcal{H}_0{}^m+\mathcal{H}^{Nm}, \quad \text{(A6)}$$

where

$$\mathcal{H}_0{}^m=\kappa_m\bar{\phi}\beta_0{}^2\phi+\kappa_m{}^{-1}p_k\bar{\phi}\beta_0{}^2\beta_k\beta_l\beta_0{}^2p_l\phi \quad \text{(A7)}$$

is the hamiltonian for the free Kemmer field, and

$$\mathcal{H}^{Nm}=-fj_A\bar{\phi}\beta_0{}^3\eta_A-f\kappa_m{}^{-1}p_k\bar{\phi}[\beta_k-\beta_k\beta_0{}^3]\eta_Aj_A \quad \text{(A8)}$$

is the interaction hamiltonian.

Equation (A8) may be put into a form more perspicuous for our purposes by noting that the summation over k in the second term may be extended to a summation over the fourth index. We then apply

$$p_\mu\bar{\phi}\beta_\mu=\kappa_m\bar{\phi}-f\bar{\eta}_Aj_A. \quad \text{(A9)}$$

The result is

$$\mathcal{H}^{Nm}=-fj_A\bar{\phi}\eta_A+(f^2/\kappa_m)j_B\bar{\eta}_B(1-\beta_0{}^3)\eta_Aj_A$$
$$=-fj_A\bar{\eta}_A\phi+(f^2/\kappa_m)j_B\bar{\eta}_B(1-\beta_0{}^3)\eta_Aj_A. \quad \text{(A10)}$$

In this form it is seen that the interaction hamiltonian consists of the negative of the coupling term in the lagrangian plus a contact interaction. The latter contributes only when β_0 has the eigenvalue zero. Using the methods of Sec. VI, it may be shown that (A10) leads to an interaction energy which contains no contact interactions. In particular, in the case in which $\gamma_A=I$, the interaction energy vanishes identically.

PHYSICAL REVIEW VOLUME 82, NUMBER 5 JUNE 1, 1951

Disintegration Scheme of Re^{186}

FRANZ R. METZGER AND R. D. HILL
Physics Department, University of Illinois, Urbana, Illinois*

(Received February 8, 1951)

The radiations from Re^{186} have been studied by means of beta-ray spectrometers and scintillation counting techniques. It has been found that Re^{186} decays both by beta-emission and by K-capture. Three partial beta-ray spectra of 1.07-, 0.93-, and 0.3-Mev maximum energies have abundances of 76, 19, and 0.4 percent, respectively, and lead to the ground state and 137- and 627-kev excited states of Os^{186}. Two K-capture branches of 3 and 2 percent abundances lead to the ground state and a 123-kev excited state of W^{186}. Transitions between these states give rise to electric quadrupole gamma-rays of 137 and 123 kev and other relatively weak magnetic dipole gamma-rays of 764- and 627-kev energy. A decay scheme in which spins and parities are assigned to all the levels is proposed.

I. INTRODUCTION

THE 90-hour activity of Re^{186} which is strongly induced in rhenium by slow neutron capture is known[1-3] to emit both beta and gamma-rays. It seems well established[4] that the maximum beta-ray energy is 1.07 Mev, but there is some doubt[3] that the spectrum is simple. A number of gamma-rays have been reported and, while the 137-kev line was observed by most workers, the evidence for the existence of other lines was conflicting.

In the work presented in this paper, it will be shown that the disintegration of Re^{186} proceeds by both beta-ray emission and K-capture. Both decays are found to be complex and associated with the emission of gamma-rays and conversion electrons. Although the experiments using different techniques are strongly correlated, they will be described in separate sections; one dealing with spectrometer measurements, the other with coincidence absorption experiments.

* This work was supported in part by the joint program of ONR and AEC.

[1] Cork, Shreffler, and Fowler, Phys. Rev. **74**, 1657 (1948).
[2] Beach, Peacock, and Wilkinson, Phys. Rev. **76**, 1585 (1949).
[3] P. J. Grant and R. Richmond, Proc. Phys. Soc. (London) **A62**, 573 (1949).
[4] L. M. Langer and H. C. Price, Phys. Rev. **76**, 641 (1949).

II. SPECTROSCOPIC MEASUREMENTS

The sources used were pile-irradiated Re metal powder obtained from Oak Ridge. Experiments on these sources were performed about a week after irradiation, thus allowing the 19-hour Re^{188} activity to decay to less than one percent of the total activity.

The pulse-height distribution from a scintillation counter irradiated with the Re gamma-rays was followed for a period of three months. After Re^{186} had decayed to less than one-thousandth of its initial activity, a 1-Mev gamma-ray was found to be present in the remaining source. Both the energy and decay of this gamma-ray are consistent with the assumption that the 50d-Re^{184} had been produced in the irradiation but was, at the time of our experiments, contributing less than 0.01 percent of the total activity.

A. Conversion Electron Spectrum

The spectrum observed with a photographic 180° spectrograph showed the existence of conversion lines from a 137-kev gamma-ray converted in osmium, and also of lines from a 123-kev gamma-ray converted in wolfram. Three gamma-rays have been observed by Cork, Shreffler, and Fowler[1] in this energy region, but

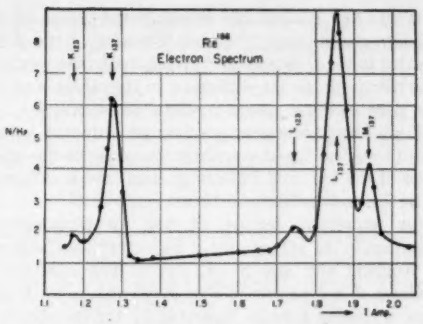

FIG. 1. Electron spectrum of Re^{186} in the energy region between 50 and 150 kev.

there is no indication in our spectrum of a third gamma-ray as suggested by these workers.

The relative intensities of the conversion lines were derived from the spectrum shown in Fig. 1, which was obtained using a lens spectrometer in conjunction with a thin source (~0.1 mg/cm²). We estimate that the conversion lines of the 137-kev transition are approximately ten times more intense than the corresponding lines of the 123-kev gamma-ray. The K/L ratio of the 137-kev transition is 0.6±0.1 and the L/M ratio is 4.4.

Combining the values obtained by different observers, we consider 0.057 as the best value for the ratio of the number of 137-L electrons to the total number of beta-rays. (This value is corrected for the contribution of 123-L electrons which were not resolved by other workers from the 137-L conversion line.)

From the higher resolution spectrum of the 180° instrument it is observed that the 137-L_I line is approximately as intense as the 137-L_{III} conversion line.

B. Beta-Ray Spectrum

The beta-ray spectrum of Re^{186} was measured using a lens spectrometer, and considerable care was taken to obtain accurate determinations of the points at the upper end of the spectrum. The Fermi plot of this

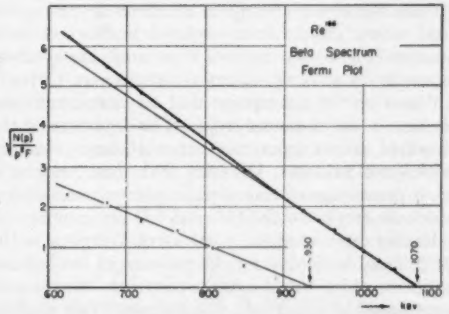

FIG. 2. Fermi plot of the beta-ray spectrum of Re^{186}.

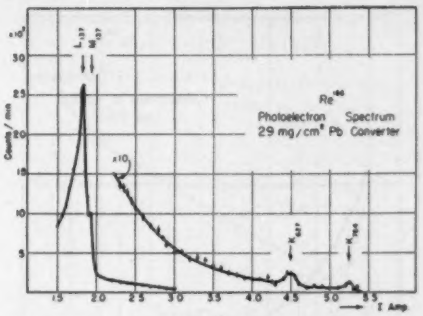

FIG. 3. Photoelectron spectrum of Re^{186} using a lead converter.

spectrum, which is given in Fig. 2, exhibits a small change of slope in the region of 900 kev. Analysis of the plot, assuming allowed shape spectra, indicates an 83 percent component of upper end point 1.07 Mev and a remaining 17 percent component of upper end point 0.93±0.05 Mev. The presence of a partial spectrum of this lower energy agrees qualitatively with the results of Grant and Richmond.[3]

C. Photoelectron Spectrum

A number of photoelectron spectra were taken in the lens spectrometer using different atomic number converters. Curves for lead and tin are given in Figs. 3 and 4. They confirm the existence of gamma-rays of 137 and 123 kev and, in the case of lead, point to the presence of two equally intense gamma-rays of 627 and 764 kev. These gamma-rays can be identified with the hard component reported on the basis of absorption experiments by Cork, Shreffler, and Fowler,[1] and also by Grant and Richmond.[3] No indication of either a 212-[3] or a 275-kev[3] gamma-ray was obtained. The number of quanta of these energies is certainly less than one percent of the number of 137-kev quanta. The K-photoelectron line of a 275-kev gamma-ray, and the L-lines of 275- and 212-kev gamma-rays, would appear in the spectrum of Fig. 3 between 2.2 and 2.8 amp. The

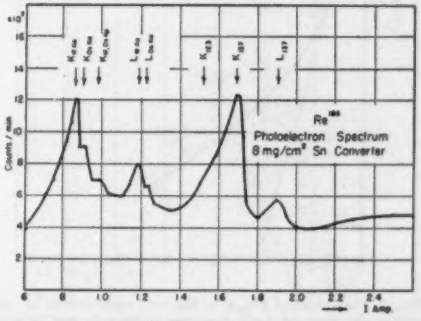

FIG. 4. Photoelectron spectrum of Re^{186} using a tin converter.

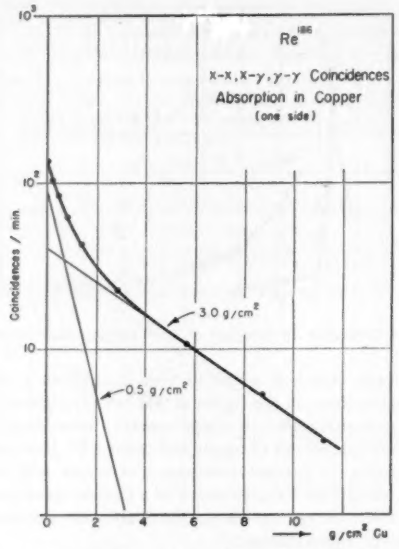

FIG. 5. Absorption of x–x, x–γ, and γ–γ coincidences by copper absorbers in front of one counter.

K-line of a 212-kev gamma-ray would also appear in the spectrum of Fig. 4 at a current of 2.31 amp. The strong line in the Pb photoelectron spectrum interpreted by Beach, Peacock, and Wilkinson[2] as the K-line of a 212-kev gamma-ray is really the L-line of the 137-kev gamma-ray. The high intensity of the L-line relative to the K-line in their Pb photoelectron spectrum is attributable to the difference in degradation of the two photoelectron groups in the thick converter.

From the photoelectron spectrum obtained with a thin (5 mg/cm²) gold converter, the ratio of the intensities of the 137- and 123-kev gamma-rays is estimated to be 9 ± 2.

An important feature of the tin photoelectron spectrum is the appearance of partly resolved lines due to wolfram and osmium K x-rays. The existence of wolfram K x-rays proves that Re^{186} decays by K-capture, a process already suggested by the conversion of the 123-kev gamma-ray in wolfram. From the photoelectron spectrum we estimate the wolfram K x-rays to be approximately 1.5 times more intense than the osmium K x-rays.

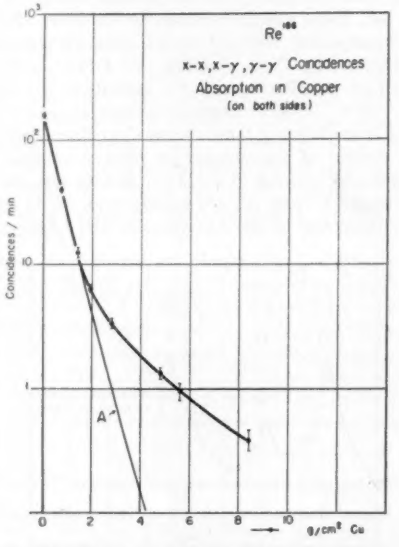

FIG. 6. Absorption of x–x, x–γ, and γ–γ coincidences by copper absorbers in front of both counters. Curve A was calculated assuming the absence of γ–γ coincidences.

III. COINCIDENCE ABSORPTION EXPERIMENTS

Sodium iodide scintillation counters were used in these experiments. Crystal thicknesses varied from 0.5 to 30 mm, depending on the radiation being investigated. Counting efficiencies for different energy radiations were estimated from total gamma-ray absorption cross sections, assuming complete detection of secondary electrons. The resolving time of the coincidence circuit was 1.2×10^{-7} second.

A. Gamma-Gamma-Coincidences

After absorbing all electrons from the source in beryllium, the coincidence rate between electromagnetic radiations was measured as a function of the thickness of copper absorber. The curves of Figs. 5 and 6 were obtained with absorbers in front of one counter and in front of both counters, respectively. The curve of Fig. 5 can be decomposed into two parts with half-value thicknesses of 0.5 and 3.0 g/cm² copper, values which are consistent with the absorption of x-rays (~60 kev) and gamma-rays (130 ± 20 kev). In the experiment using absorbers on one side, the large intensity of the x-ray component at zero absorber thickness indicates a large contribution of x–x coincidences.

From the strong absorption exhibited in the experiment where absorbers were placed in front of both counters (Fig. 6), we conclude that x-rays are involved in practically all of the observed coincidences. Curve A is drawn on the assumption that all coincidences are of the x–x and x-gamma types. The departure of the measured points from this curve at large absorber thicknesses indicates, however, that there remains a small percentage of true gamma-gamma-coincidences, which we ascribe to the 137- and 627-kev groups.

Having established the existence of K-capture in the Re^{186} decay we looked for the presence of annihilation radiation which would indicate positrons. The counters were biased to detect only gamma-rays above approximately 200 kev, and the gamma-gamma-coincidence

rates were determined with the counters at 180° and 90° to each other. With approximately one millicurie of Re^{186}, the 180° and 90° coincidence rates did not differ by more than 0.5 coincidences per minute. From the strength of the source and the over-all detection efficiency it is estimated that there is less than one positron, if any, in 10^7 disintegrations.

B. Beta-Gamma-Coincidences

With all absorbers removed from one counter, the coincidence rate as a function of the thickness of copper absorber in front of the other counter was determined. After the subtraction of x–x and x–gamma coincidence rates, the curve shown in Fig. 7 was obtained. This curve indicates that some of the beta-rays are coincident with a gamma-ray of 130±20 kev (3.4 g/cm²) and an x-ray of ~60 kev (0.5 g/cm²). The number of beta-gamma-coincidences per beta-ray is approximately four times less than the rate to be expected if all beta-rays are followed by a gamma-ray of 137 kev. Since McGowan[5] has shown that the 137-kev excited state has a life-time of less than 2×10^{-9} second, the low beta-gamma-coincidence rate cannot be ascribed to a lifetime which is longer than the coincidence resolving time (1.2×10^{-7} second), and must be attributed to a branching of the beta-decay.

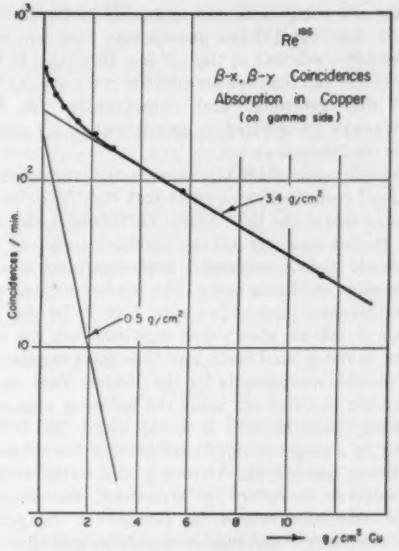

FIG. 7. Absorption of β–x and β–γ coincidences by copper absorbers in front of the γ-ray counter.

IV. DISCUSSION

The foregoing experiments lead immediately to the main features of the decay scheme shown in Fig. 8. Further details of this scheme will now be discussed.

A. Multipolarity of Gamma-Rays

The value of 0.03 for the K-conversion coefficient of the 137-kev gamma-ray, which was reported by Beach, Peacock, and Wilkinson,[2] is approximately five times less than the minimum theoretical value for the conversion of a gamma-ray of this energy.[6] According to the present suggested decay scheme, the number of K-conversion electrons has to be compared, not with the total beta-ray spectrum, but with the 17 percent branch, and this leads to a value of the order 0.5 for the K-conversion coefficient of the 137-kev gamma-ray.

Owing to the uncertainties with which the abundance of the partial beta-ray spectrum and the K/L ratio of the 137-kev gamma-ray are known, the K-conversion coefficient obtained from spectroscopic data is rather inaccurate. A more precise value can be obtained from the beta-gamma-coincidence absorption data of Fig. 7. The magnitudes of the 137-kev and the osmium K x-ray components at zero absorber thickness, corrected for fluorescent yield and counter efficiencies, give directly a value of 0.35±0.1 for the K conversion coefficient of the 137-kev gamma-ray. Comparing this value with the extrapolated theoretical conversion coefficients of Rose,[6] agreement is only possible for electric quadrupole for which the theoretical value is 0.43.

Since the ratios of the numbers of conversion electrons as well as the numbers of gamma-rays of the 137- and 123-kev transitions are identical to within the experimental error, it is inferred that the two gamma-rays, which are of much the same energy, are of the same multipole order.

As mentioned above, the 137- and 123-kev transitions are electric quadrupoles; and, therefore, if it is assumed, that the ground states of the even–even nuclei, Os^{186} and W^{186}, have spin 0, the 137- and 123-kev levels must have spin 2 and the same parity as the ground states.

From a single absorption experiment the hard

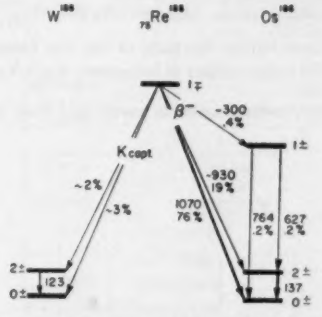

FIG. 8. Proposed disintegration scheme of Re^{186}. Transition energies are given in kev.

[5] F. K. McGowan, Phys. Rev. 79, 404 (1950).
[6] M. E. Rose and others, "Tables of K-conversion coefficients" (unpublished).

gamma-ray component was estimated to be 25 times weaker than the 137-kev gamma-ray. Since the total conversion coefficient of the 137-kev transition is 1.06, the 137-kev gamma-rays are emitted in 9 percent of the Re^{186} disintegrations, and consequently the hard gamma-rays are emitted in approximately 0.4 percent of the disintegrations.

The difference of 137 kev between the energies of the two hard gamma-rays suggests that they occur on the beta-ray side of the Re^{186} decay. Furthermore, since the two gamma-rays are of comparable intensities and differ only slightly in energies, both transitions must be of the same multipole order. The 764-kev excited state must therefore have either spin 1 or 2. In the next section it will be shown that this level has the same parity as the ground state, and thus there remain only two possible assignments for the 764-kev level, one of which can be ruled out using the following argument. An assignment of spin 2 would make the 627-kev transition a magnetic dipole and the 764-kev transition an electric quadrupole. According to a recent analysis of multipole radiation by Weisskopf[7] the magnetic dipole transition would be favored in comparison with the electric quadrupole transition and this is in contradiction with experiment. The most probable spin value of the 764-kev state is therefore 1, thus characterizing the two hard gamma-rays as magnetic dipole radiations.

B. Beta-Ray Transitions

On the basis of spectroscopic measurement it was shown that there is a 17 percent lower energy branch of the beta-ray spectrum. As this analysis assumed allowed shapes of the beta-spectra, it was important to substantiate the branching ratio by an independent measurement. A value of the branching ratio can be obtained from a combination of the following data:

(1) The ratio of the number of K-conversion electrons of the 137-kev gamma-ray to the total number of beta-rays:

$$N_K/(N_{\beta_1}+N_{\beta_2})=0.034.$$

(2) The K-conversion coefficient determined from the beta-gamma-coincidence data: $N_K/N_\gamma=0.35$.

(3) The total conversion coefficient: $N_K+N_L+N_M/N_\gamma=1.06$.

From these values the ratio of the low energy beta-group to the total number of beta-rays, $N_{\beta_1}/(N_{\beta_1}+N_{\beta_2})$, is found to be 0.20. The good agreement of this value with that derived from the Fermi plot probably indicates that both partial spectra have allowed shapes.

Using the observed intensities of the partial beta-ray spectra, the following ft-values[8] have been obtained: $(ft)_{0.3\ \mathrm{Mev}}=1.6\times10^8$; $(ft)_{0.93\ \mathrm{Mev}}=1.3\times10^8$; $(ft)_{1.07\ \mathrm{Mev}}=0.5\times10^8$. All three beta-disintegrations are therefore of the same degree of forbiddenness and might be classified as first forbidden. In these circumstances the Re^{186} ground state possesses a parity opposite to that of the three osmium levels reached by beta-disintegrations.

If it is assumed that both partial spectra have allowed shapes, one can tentatively assign spin 1 to the ground state of Re^{186}, since both spin 0 and 2 would lead to either one of the spectra having an α-type shape.[9]

C. K-Capture

Re^{186} decays to some extent by K-capture. The branch leading to the 123-kev level of wolfram comprises approximately two percent of all disintegrations, and there is also a K-capture branch leading to the ground state of W^{186}.

It has been found from the photoelectron experiments that wolfram K x-rays are 1.5 times more abundant than osmium K x-rays. From the intensity of the 137-kev gamma-ray and its K-conversion coefficient it is calculated from osmium K x-rays occur in approximately 3.5 percent of the Re^{186} disintegrations, and wolfram K x-rays in 5 percent of the disintegrations. Thus, K-capture transitions to the ground state of W^{186} occur in 3 percent of the Re^{186} disintegrations.

The observation of an appreciable amount of K-capture leading to the 123-kev level may be taken as indicating that the Re^{186}—W^{186} mass difference must be larger than 200 kev. On the other hand, an upper limit of 1.2 Mev for this mass difference can be deduced from the fact that there is less than one positron in 10^7 Re^{186} disintegrations. For a 2 percent K-capture branch from Re^{186}, the ft-values corresponding to the above energy limits are 7×10^6 and 2.5×10^5, respectively. This implies that the transitions on the K-capture side of Re^{186} are of the same degree of forbiddenness as the beta-ray transitions. Acceptance of this conclusion leads to the assignment of parities for the W^{186} levels as shown in Fig. 8.

[7] Privately circulated notes, to appear as a book on nuclear physics.

[8] E. J. Konopinski, Revs. Modern Phys. **15**, 209 (1943).

[9] C. S. Wu, Revs. Modern Phys. **22**, 386 (1950).

Nuclear Gyromagnetic Ratios. III

ROBERT E. SHERIFF* AND DUDLEY WILLIAMS
Mendenhall Laboratory of Physics, Ohio State University, Columbus, Ohio
(Received January 26, 1951)

The super-regenerative oscillator techniques described in earlier reports have been modified by introduction of a tuned narrow band amplifier with chart recorder and by improvements in magnetic-field regulation. Magnetic resonance frequencies of various nuclei have been compared with the resonance frequencies of H^1, D^2, Li^7, and Sc^{45}, which have been used as "standards." Ratios of the observed resonance frequencies to the proton resonance frequency in the same magnetic field are given for the following nuclear species: Be^9, B^{11}, F^{19}, Na^{23}, Al^{27}, P^{31}, V^{51}, Mn^{55}, Cu^{63}, Cu^{65}, Br^{79}, Br^{81}, Rb^{87}, Nb^{93}, I^{127}, Cs^{133}, La^{139}, Tl^{205}, and Tl^{203}. The nuclear magnetic moments of these species have been determined in terms of the proton moment from the known spins and the observed frequency ratios after making diamagnetic corrections; values for the nuclear magnetic moments are listed.

In earlier reports from this laboratory[1,2] super-regenerative oscillator techniques for observing nuclear magnetic resonance phenomena have been described. The present paper gives a brief description of certain modifications of the earlier techniques and gives a tabulation of the results obtained for various nuclei by means of the improved techniques.

EXPERIMENTAL METHODS

In Fig. 1 is shown a block diagram of the apparatus employed. The coil of the tank circuit of a super-regenerative oscillator is located between the poles of a large electromagnet. In searching for a magnetic resonance, a sample containing the nuclei of interest is placed in the coil and the magnetic field is varied slowly by means of a clockdrive operating a potentiometer in the control circuit of the magnet-current regulator; the regulator circuit employs electronic regulation of the current supplied through hard tubes to the high resistance magnet windings. At resonance

$$h\nu = g\mu_n H \tag{1}$$

the amplitude of oscillation of the super-regenerative circuit decreases. This amplitude change is observed by means of a narrow-band amplifier tuned to the 45-cycles/sec frequency of the magnetic-field modulator shown in the figure. The output of this narrow-band amplifier is applied to a recorder and to an oscilloscope, which is employed as a monitoring device.

After the resonance corresponding to the central frequency of the oscillator spectrum has been located, the magnetic field is held constant by means of the regulator while the oscillator frequency is carefully measured by means of the heterodyne frequency meter shown in Fig. 1. With the magnetic field unchanged, the frequency of the oscillator is changed until a resonance is observed for one of the nuclear species employed as "standards." The nuclear g-factor g_x of the nucleus being studied can then be determined in terms of the standard g_s by the relation

$$g_x = g_s(\nu_x/\nu_s), \tag{2}$$

where ν_x and ν_s are resonance frequencies for the two nuclear species in the same magnetic field.

Tests have shown that the regulator is capable of maintaining the magnet *currents* constant to 1 part in 30,000 for several hours. Operational experience indicates that the magnetic field itself can be held constant to at least 1 part in 20,000; this conclusion is based on observations of signal constancy obtained when the magnetic field is adjusted for a narrow resonance peak and for a position on the sharply rising shoulder of a resonance line. It is probable that improvement in regulation could be obtained by using the proton resonance to control the field, but this has not yet been done.

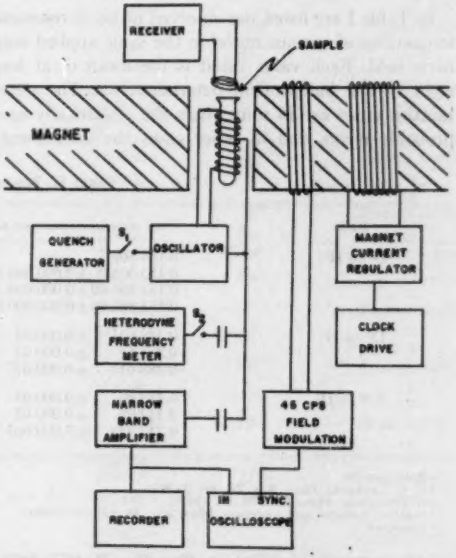

FIG. 1. Block diagram of apparatus.

* AEC Fellow. Present address: California Research Corporation, LaHabra, California.
[1] J. R. Zimmerman and D. Williams, Phys. Rev. **76**, 350 (1949).
[2] W. H. Chambers and D. Williams, Phys. Rev. **76**, 638 (1949).

TABLE I. Resonance frequency ratios.

Nuclei compared	Resonance frequency ratio	Sample
Be^9 to D^2	0.915 475±0.000 07	$BeCl_2$, D_2O+$NiCl_2$
B^{11} to Li^7	0.825 615±0.000 04	$Na_2B_2O_4$, $LiC_2H_3O_2$+$Mn(C_2H_3O_2)_2$
F^{19} to H^1	0.940 86±0.000 05	HF
Na^{23} to Sc^{45}	1.088 83±0.000 05	$Na_2B_2O_4$, $ScCl_3$
	1.088 72±0.000 06	NaBr, $ScCl_3$
Al^{27} to Sc^{45}	1.072 61±0.000 05	$AlCl_3$, $ScCl_3$
P^{31} to Li^7	1.041 82±0.000 05	H_3PO_4+$CuCl_2$, $LiC_2H_3O_2$+$Mn(C_2H_3O_2)_2$
V^{51} to Sc^{45}	1.081 56±0.000 05	powdered V_2O_5, $ScCl_3$
Mn^{55} to Sc^{45}	1.020 28±0.000 05	$Ca(MnO_4)_2$, $ScCl_3$
Cu^{63} to Sc^{45}	1.091 25±0.000 06	powedered Cu_2Cl_2, $ScCl_3$
Cu^{65} to Sc^{45}	1.169 51±0.000 06	powdered Cu_2Cl_2, $ScCl_3$
Cu^{65} to Cu^{63}	1.071 78±0.000 05	powdered Cu_2Cl_2
Br^{79} to Sc^{45}	1.031 45±0.000 05	NaBr, $ScCl_3$
Br^{81} to Sc^{45}	1.111 65±0.000 06	NaBr, $ScCl_3$
Br^{81} to Br^{79}	1.077 75±0.000 05	NaBr
Rb^{87} to Al^{27}	1.255 29±0.000 06	Rb_2CO_3+$CuCl_2$, $AlCl_3$
Nb^{93} to Sc^{45}	1.006 13±0.000 05	Nb_2O_5+HF, $ScCl_3$
I^{127} to D^2	1.303 17±0.000 06	KI, D_2O+$NiCl_2$
Cs^{133} to D^2	0.854 49±0.000 04	CsCl+$CuCl_2$, D_2O+$NiCl_2$
La^{139} to D^2	0.920 25±0.000 06	$LaCl_3$+$CuCl_2$, D_2O+$NiCl_2$
Tl^{205} to Tl^{203}	1.009 83±0.000 05	$TlC_2H_3O_2$+$Mn(C_2H_3O_2)_2$
Tl^{203} to H^1	0.577 02±0.000 03	$TlC_2H_3O_2$+$Mn(C_2H_3O_2)_2$, H_2O+$FeCl_2$

The radiofrequencies employed in the present work were in the 5 to 10 mc/sec range, and the quench frequency was usually in the range 5 to 15 kc/sec. The theory of the super-regenerative oscillator and a more detailed description of the circuits are being published elsewhere.

DISCUSSION OF RESULTS

In Table I are listed the observed ratios of resonance frequencies of various nuclei in the same applied magnetic field. Each value listed is the mean of at least eight careful independent determinations. The uncertainties given are in some cases the statistically most probable errors and in other cases the instrumental uncertainty of 1 part in 20,000 imposed by the limitations of the magnet current regulator. In each case the larger of these uncertainties is listed. The samples used are also listed in Table I; all samples were aqueous solutions except the ones used for V and Cu. In samples containing magnetic catalysts, the concentration of the catalyst was kept as low as possible and was of the order of 0.03 molar.

Since the recent precise measurements[3] of the absolute value of the proton moment, it has become conventional to use the proton moment as a "primary standard" in work on nuclear resonance absorption and to express the results of measurements in terms of ratios of resonance frequencies of various nuclei to the resonance frequency of the proton in the same magnetic field. In the present work, it was convenient in making frequency measurements to use the deuteron D^2, Li^7, and Sc^{45} as "secondary standards." The ratios of the resonance frequencies of these nuclei to the resonance frequency of the proton are listed in Table II. The results obtained by various investigators are given in the second column of this table and the values used as "standard" are given in the last column.

Through the use of the secondary frequency standards listed in Table II, it is possible to express the observed resonance frequencies for the nuclei listed in Table I in terms of the proton resonance frequency. This has been done; and the results are presented in Table III along with corresponding ratios obtained by other methods, which are included for purposes of comparison.

A few brief comments concerning the results obtained for the various nuclear species are given below:

Be^9: Considereable difficulty was encountered in matching the beryllium signal with that of the deuteron, since there appeared to be a significant difference in line shape. The result obtained is considerably higher than that given in our earlier work[2] but is in excellent agreement with the work of Dickinson.[4]

TABLE II. Resonances used as standards.

Ratio	Value resonance frequency ratio	Reference	Value used as standard
D^2 to H^1	0.153 507 5	a	
	0.153 505 9 ±0.000 000 8	b	
	0.153 506 69±0.000 000 25	c	
	0.153 506 06±0.000 000 05	d	0.153 506
Li^7 to H^1	0.388 625 ±0.000 04	e	
	0.388 62 ±0.000 02	f	
	0.388 611 ±0.000 017	g	0.388 617±0.000 017
Sc^{45} to H^1	0.242 90 ±0.000 03	h	
	0.242 95 ±0.000 02	i	
	0.242 939 ±0.000 003	j	0.242 939±0.000 003

[a] Reference 20.
[b] E. C. Levinthal, Phys. Rev. **78**, 204 (1950).
[c] G. Lindstrom, Phys. Rev. **78**, 817 (1950).
[d] Smaller, Yasaitis, and Anderson, Phys. Rev. **80**, 137 (A) (1950).
[e] Reference 5.
[f] Reference 1.
[g] Reference 8.
[h] W. G. Proctor and F. C. Yu, Phys. Rev. **78**, 471 (1950).
[i] R. E. Sheriff and D. Williams, Phys. Rev. **79**, 175 (1950).
[j] D. M. Hunten, Phys. Rev. **78**, 806 (1950).

[3] Hipple, Sommer, and Thomas, Phys. Rev. **76**, 1877 (1949).
[4] W. C. Dickinson and T. F. Wimett, Phys. Rev. **75**, 1769 (1949).

TABLE III. Frequency ratios to the proton frequency.

Nucleus	Sample	Value	Uncertainty (%)	Intermediate standard	Reference
Be^{9}	BeF_2	0.140 5187±0.000 0020	(0.002)		4
	$BeCl_2$	0.140 34 ±0.000 07	(0.050)		2
	$BeCl_2$	0.140 531 ±0.000 011	(0.008)	D^2	Present study
B^{11}	BCl_3(?)	0.320 85 ±0.000 06	(0.019)		5
	$Na_2B_2O_4$	0.320 76 ±0.000 09	(0.028)		1
	$K_2B_2O_4$	0.320 827 ±0.000 004	(0.001)		6
	$Na_2B_2O_4$	0.320 848 ±0.000 021	(0.007)	Li^7	Present study
F^{19}	$C_2F_3Cl_3$	0.940 934			
	HF*	0.940 816	±0.000 015	(0.002)	8
	HF	0.940 77 ±0.000 10	(0.011)		9
	SbF_3	0.940 86			
	HF*	0.940 75	±0.000 17	(0.018)	1
	HF	0.940 86 ±0.000 05	(0.005)		Present study
Na^{23}	NaI or NaCl	0.264 50 ±0.000 03	(0.011)		5
	$NaAsO_2$	0.264 54 ±0.000 07	(0.026)		1
	$Na_2B_2O_4$	0.264 518 ±0.000 014	(0.005)	Sc^{45}	Present study
	NaBr	0.264 492 ±0.000 015	(0.006)	Sc^{45}	Present study
Al^{27}	$AlCl_3$	0.260 56 ±0.000 03	(0.011)		5
	$AlCl_3$	0.260 62 ±0.000 11	(0.042)		1
	$AlCl_3$	0.260 579 ±0.000 013	(0.005)	Sc^{45}	Present study
P^{31}	P_2O_5 or P	0.404 96 ±0.000 09	(0.022)	Na^{23}	10
	P_2O_5(?)	0.404 81 ±0.000 04	(0.010)		5
	H_3PO_4+cat	0.404 98 ±0.000 11	(0.027)		2
	H_3PO_4+cat	0.404 869 ±0.000 026	(0.006)	Li^7	Present study
V^{51}	V_2O_5, HCl	0.262 91 ±0.000 02	(0.008)	Na^{23}	12
	pwd V_2O_5	0.262 67 ±0.000 06	(0.023)	B^{11}	11
	pwd V_2O_5	0.262 753 ±0.000 012	(0.005)	Sc^{45}	Present study
Mn^{55}	$LiMnO_4$	0.247 90 ±0.000 03	(0.012)	Na^{23}	13
	$Ca(MnO_4)_2$	0.247 86 ±0.000 12	(0.048)	Na^{23}	11
	$Ca(MnO_4)_2$	0.247 866 ±0.000 012	(0.005)	Sc^{45}	Present study
Cu^{63}	pwd Cu_2Cl_2	0.265 09 ±0.000 06	(0.023)	Na^{23}	14
	Cu_2Cl_2	0.265 056 ±0.000 050	(0.019)		5
	Cu_2Cl_2+cat	0.265 15 ±0.000 05	(0.019)		1
	pwd Cu_2Cl_2	0.265 107 ±0.000 015	(0.006)	Sc^{45}	Present study
Cu^{65}	pwd Cu_2Cl_2	0.283 95 ±0.000 06	(0.021)	Cu^{63}	14
	Cu_2Cl_2	0.283 91 ±0.000 06	(0.021)		5
	Cu_2Cl_2+cat	0.284 04 ±0.000 09	(0.032)		1
	pwd Cu_2Cl_2	0.284 120 ±0.000 015	(0.005)	Sc^{45}	Present study
Br^{79}	NaBr	0.250 57 ±0.000 08	(0.032)	Br^{81}	15
	NaBr	0.250 59 ±0.000 05	(0.020)		1
	NaBr	0.250 579 ±0.000 012	(0.005)	Sc^{45}	Present study
Br^{81}	NaBr	0.270 04 ±0.000 08	(0.030)	Na^{23}	15
	LiBr	0.270 03 ±0.000 08	(0.030)		5
	NaBr	0.270 14 ±0.000 05	(0.019)		1
	NaBr	0.270 063 ±0.000 015	(0.006)	Sc^{45}	Present study
Rb^{87}	RbCl	0.327 18 ±0.000 07	(0.022)		5
	Rb_2CO_3+cat	0.327 18 ±0.000 16	(0.049)		1
	Rb_2CO_3+cat	0.327 101 ±0.000 023	(0.007)	Al^{27}	Present study
Nb^{93}	Nb_2O_5+HF	0.244 43 ±0.000 13	(0.053)	B^{11}	16
	Nb_2O_5+HF	0.244 428 ±0.000 012	(0.005)	Sc^{45}	Present study
I^{127}	pwd NaI	0.200 14 ±0.000 06	(0.030)	Na^{23}	10
	KI	0.200 03 ±0.000 07	(0.035)		1
	KI	0.200 044 ±0.000 010	(0.005)	D^2	Present study
Cs^{133}	CsCl	0.131 13 ±0.000 04	(0.031)	Li^7	5
	CsCl+cat	0.130 93 ±0.000 14	(0.107)		2
	CsCl+cat	0.131 169 ±0.000 006	(0.005)	D^2	Present study
La^{139}	$LaCl_3$+cat	0.141 16 ±0.000 14	(0.100)		2
	$LaCl_3$	0.141 251 ±0.000 014	(0.010)		17
	$LaCl_3$+cat	0.141 264 ±0.000 009	(0.006)	D^2	Present study
Tl^{203}	$TlC_2H_3O_2$	0.571 4 ±0.000 1	(0.017)		18
	$TlC_2H_3O_2$	0.571 499 ±0.000 050	(0.009)		9
	$TlC_2H_3O_2$+cat	0.571 40 ±0.000 04	(0.007)	Tl^{205}	Present study
Tl^{205}	$TlC_2H_3O_2$	0.577 0 ±0.000 01	(0.017)		18
	$TlC_2H_3O_2$	0.577 135 ±0.000 050	(0.009)		9
	$TlC_2H_3O_2$+cat	0.577 02 ±0.000 03	(0.005)		Present study

* Equivalent value for HF, according to Dickinson (reference 7).

TABLE IV. Nuclear g-values and nuclear magnetic moments.

Nucleus	Diamagnetic correction	Nuclear g-value	Spin	Nuclear magnetic moment (nuclear magnetons)
H^{1*}	1.000 03	5.585 10±0.000 00	1/2	2.792 55±0.000 00
D^{2*}	1.000 03	0.857 37±0.000 00	1	0.857 37±0.000 14
Li^{7*}	1.000 08	2.170 64±0.000 10	3/2	3.255 96±0.000 14
Be^{9}	1.000 12	0.784 98±0.000 06	3/2	1.177 46±0.000 09
B^{11}	1.000 17	1.792 27±0.000 12	3/2	2.688 40±0.000 18
F^{19}	1.000 39	5.256 84±0.000 28	1/2	2.628 42±0.000 14
Na^{23}	1.000 54	1.478 09±0.000 08	3/2	2.217 14±0.000 12
Al^{27}	1.000 72	1.456 41±0.000 07	5/2	3.641 01±0.000 17
P^{31}	1.000 91	2.263 30±0.000 14	1/2	1.131 65±0.000 07
Sc^{45*}	1.001 51	1.358 89±0.000 02	7/2	4.756 11±0.000 06
V^{51}	1.001 71	1.470 01±0.000 07	7/2	5.145 03±0.000 23
Mn^{55}	1.001 92	1.387 01±0.000 07	5/2	3.467 53±0.000 17
Cu^{63}	1.002 39	1.484 19±0.000 08	3/2	2.226 28±0.000 13
Cu^{65}	1.002 39	1.590 63±0.000 08	3/2	2.385 94±0.000 13
Br^{79}	1.003 08	1.403 83±0.000 07	3/2	2.105 74±0.000 10
Br^{81}	1.003 08	1.512 98±0.000 08	3/2	2.269 47±0.000 13
Rb^{87}	1.003 33	1.832 91±0.000 13	3/2	2.749 37±0.000 19
Nb^{93}	1.003 83	1.370 38±0.000 07	9/2	6.166 70±0.000 30
I^{127}	1.005 45	1.123 35±0.000 05	5/2	2.808 38±0.000 13
Cs^{133}	1.005 73	0.736 79±0.000 03	7/2	2.578 77±0.000 12
La^{139}	1.006 02	0.793 72±0.000 05	7/2	2.778 02±0.000 18
Tl^{203}	1.009 83	3.222 72±0.000 22	1/2	1.611 36±0.000 11
Tl^{205}	1.009 83	3.254 66±0.000 17	1/2	1.627 33±0.000 08

* Value used as a standard.

B^{11}: Agreement with previous work[1,5,6] is excellent.

F^{19}: Dickinson[7] has found that the fluorine resonance in different chemical compounds occurs at slightly different frequencies. If a Dickinson correction is applied to the data of Siegbahn and Lindstrom[8] and the data of Zimmerman[1] in order to obtain a value for the resonance in HF, agreement of their values with the present result and with the result of Poss[9] is satisfactory.

Na^{23}: The results obtained in the present work seem to indicate that the Na^{23} resonance frequency is slightly higher in $Na_2B_2O_4$ than in NaBr. However, both frequencies fall within the limits obtained by Bitter[5] and Zimmerman[1] in earlier studies.

Al^{27}: The present value is in excellent agreement with earlier results.[1,5]

P^{31}: Considerable difficulty was encountered in matching the phosphorus peak pattern with the Li^{7} pattern, but the final result falls within the limits established by earlier investigations.[2,5,10]

V^{51}: Although the vanadium resonance is quite weak, the resonance-frequency value obtained confirms the value given in our preliminary report[11] but disagrees with the result obtained by Knight and Cohen.[12]

Mn^{55}: Agreement with the nuclear-induction results of Proctor and Yu[13] is excellent.

Cu^{63} and Cu^{65}: The present value for Cu^{63} is in good agreement with earlier values.[1,5,14] A somewhat asymmetrical line shape was obtained for Cu^{65}, and the resulting value of the resonance frequency is somewhat higher than that obtained by other investigators.

Br^{79}, Br^{81}, Rb^{87}: Present values fall well within the limits established in earlier work.[1,5,15]

Nb^{93}: The present result confirms the preliminary value obtained in this laboratory.[16]

I^{127}: The value obtained is within the limits established by earlier work of Zimmerman[1] but is significantly lower than the value obtained by Pound.[10]

Cs^{133}: Unambiguous matching of the caesium and deuteron signals was difficult to achieve. The value given in the table is in agreement with Bitter's results,[5] but a different matching procedure might well have yielded a result in agreement with Chambers' value.[2] The complex resonance pattern given by the superregenerative oscillator proved a serious hindrance in the case of Cs^{133}; further work on this resonance by another method might be desirable.

La^{139}: The present value falls within the limits established by Chambers[2] and Dickinson.[17]

Tl^{203} and Tl^{205}: The present values are in excellent agreement with those obtained by Proctor[18] but are lower than those reported by Poss.[9]

NUCLEAR g-FACTORS AND MAGNETIC MOMENTS

The values of nuclear g-factors cannot be determined by direct substitution of observed frequency ratios ν_x/ν_s in Eq. (2), since, owing to the diamagnetic effects of atomic electrons, the local fields at the nuclei being compared may be slightly different even though the externally applied fields may be the same. However, by applying the diamagnetic correction developed by Lamb,[19] one can obtain nuclear g-factors in terms of the g-factor for the proton; in cases for which nuclear spins are known, nuclear magnetic moments can also be calculated. In obtaining the g-factors and magnetic moments listed in Table IV, the frequency ratios obtained in the present study were used in connection with the recent Bureau of Standards value[3] for the proton moment,

$$\mu_{\text{proton}} = 2.79255 \pm 0.00010 \text{ nuclear magnetons,}$$

and the nuclear spins listed in Mack's survey paper.[20] The Lamb diamagnetic corrections in the second column of Table IV are the factors applied to the observed frequency ratios in obtaining the listed values of the g-factors and nuclear moments.

The authors take pleasure in expressing their appre-

[5] F. Bitter, Phys. Rev. **75**, 1326 (1949).
[6] D. A. Anderson, Phys. Rev. **76**, 434 (1949).
[7] W. C. Dickinson, Phys. Rev. **77**, 736 (1950).
[8] K. Siegbahn and G. Lindstrom, Arkiv. Fyz. **1**, 193 (1949).
[9] H. L. Poss, Phys. Rev. **75**, 600 (1949).
[10] R. V. Pound, Phys. Rev. **73**, 1112 (1948).
[11] Chambers, Sheriff, and Williams, Phys. Rev. **78**, 640 (1950).
[12] W. D. Knight and V. W. Cohen, Phys. Rev. **76**, 1421 (1949).
[13] W. G. Proctor and F. C. Yu, Phys. Rev. **77**, 716 (1950).
[14] R. V. Pound, Phys. Rev. **73**, 523 (1948).
[15] R. V. Pound, Phys. Rev. **72**, 1273 (1947).
[16] Sheriff, Chambers, and Williams, Phys. Rev. **78**, 476 (1950).
[17] W. C. Dickinson, Phys. Rev. **76**, 1414 (1949).
[18] W. G. Proctor, Phys. Rev. **75**, 522 (1949).
[19] W. E. Lamb, Phys. Rev. **60**, 817 (1941).
[20] J. E. Mack, Revs. Modern Phys. **22** 64 (1950).

ciation to Dr. W. H. Chambers and Mr. Yu Ting for their assistance in certain phases of the experimental work. Grateful acknowledgment is also made to the Graduate School, Research Foundation, and University Development Fund of Ohio State University for research grants and to the Atomic Energy Commission for a research fellowship granted (to R.E.S.) for this work.

PHYSICAL REVIEW VOLUME 82, NUMBER 5 JUNE 1, 1951

The $Mn^{55}(p,n)Fe^{55}$ Neutron Spectrum*

P. H. Stelson and W. M. Preston
Laboratory for Nuclear Science and Engineering, Massachusetts Institute of Technology, Cambridge, Massachusetts

(Received February 19, 1951)

A thin (20-kev) target of manganese on a tantalum backing was bombarded by monoenergetic protons of 2.97, 3.42, and 3.77 Mev from the Rockefeller electrostatic generator. Nuclear emulsion plates (Eastman NTB, 200 microns thickness) were mounted 15 cm from the target at 0° and 90° with respect to the incident proton beam. The resulting neutron spectra, obtained from the analysis of 2400 proton recoil tracks, show well-defined groups which correspond to excited states in Fe^{55} at 0.42, 0.94, 1.36, and 2.08 Mev. The group corresponding to the level at 1.36 Mev has an unusually large width indicating that this level is complex. The Q-value for the ground-state reaction was measured to be -1.05 ± 0.05 Mev, giving the threshold for neutron production as 1.07 ± 0.05 Mev. Levels in Fe^{55} at 0.935 and 1.41 Mev have been found by Deutsch and Hedgran from a study of the decay scheme of Co^{55}. These levels correspond closely to two of the levels reported here.

I. INTRODUCTION

THE investigation of the Co^{55} decay scheme by Deutsch and Hedgran[1] indicates the existence of excited states in the Fe^{55} nucleus at 0.935 and 1.41 Mev. From a study of the neutron spectrum produced by the $Mn^{55}(p,n)Fe^{55}$ reaction at proton-bombarding energies well above the threshold (1.18 Mev;[2] 1.02 Mev[3]), information can be obtained concerning the positions of excited levels in the residual nucleus, Fe^{55}, and the relative transition probabilities from the compound nucleus to these levels. Since the selection rules for $\beta-\gamma$ decay are more stringent than those for the (p,n) process, one would expect the (p,n) investigation to confirm the levels obtained from the $\beta-\gamma$ decay and to disclose, possibly, the existence of additional levels not excited in the $\beta-\gamma$ decay. We have performed an experiment in which the neutron spectra produced by bombarding a thin manganese target with monoenergetic protons from the Rockefeller electrostatic generator were measured by means of proton recoils in photographic emulsions.

II. EXPERIMENTAL METHOD

A 20-kev manganese metal[3a] target on a tantalum backing was bombarded by 2.97-, 3.42-, and 3.77-Mev protons. Proton energies were measured by a generating voltmeter calibrated by the $Li^7(p,n)$ threshold at 1.882 Mev. Eastman NTB plates of 200 microns thickness were placed a mean distance of 15 cm from the target at 0° and 90° with respect to the incident proton beam. The processed emulsions were systematically scanned at 950× magnification (oil immersion) and proton recoil tracks within 10 degrees of the neutron direction were accepted for measurement. The range-energy relation used to convert proton recoil track lengths to neutron energy E_n was obtained by measuring the $Li^7(p,n)$ spectrum at several bombarding energies and the d–d spectrum at a single deuteron-bombarding energy.

Three corrections were applied to the data to obtain plots of relative neutron intensity *vs* neutron energy: (1) the correction for the variation of the (n,p) collision cross section with energy, (2) the correction for the different probability of leaving the emulsion for tracks of different length, and (3) the correction for the variation with neutron energy of the spacing of the experimental points. The second correction is quite small for the present investigation. The third correction was applied to make the area under a given peak represent the relative intensity of the peak.

III. DISCUSSION

The corrected data, based on about 2400 measured tracks, are given in Figs. 1 and 2 as plots of relative neutron intensity *vs* neutron energy. Figure 1 shows the neutron spectrum at 0° and 90° with respect to the incident proton beam when a bombarding energy of 3.42 Mev was employed. Figure 2 shows the spectrum at 0° with proton-bombarding energies of 2.97 and 3.77 Mev. An indication of the statistical accuracy of the data is given by the conventional symbols placed

* This work was supported by the ONR and BuShips.
[1] M. Deutsch and A. Hedgran, Phys. Rev. **75**, 1443 (1949).
[2] Richards, Smith, and Browne, Phys. Rev. **80**, 524 (1950).
[3] J. J. G. McCue and W. M. Preston, private communication.
[3a] The manganese metal with a purity of 99.5 percent was obtained from the Fairmount Chemical Company.

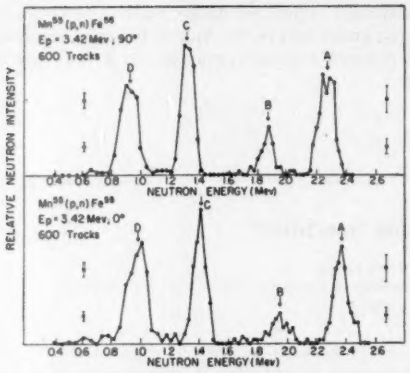

FIG. 1. Neutron spectra resulting from the bombardment of a thin manganese target with 3.42-Mev protons. The photographic plates were placed at 0° and 90° with respect to the incident proton beam.

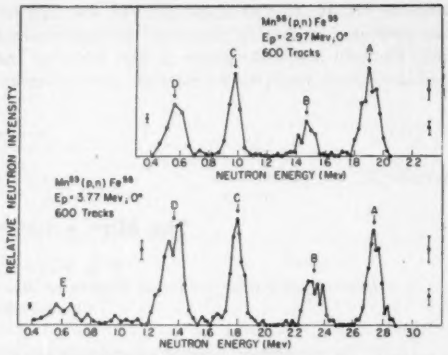

FIG. 2. Neutron spectra resulting from the bombardment of a thin manganese target with 2.97- and 3.77-Mev protons. The photographic plates were placed at 0° with respect to the incident proton beam.

in the figures. The corrections which must be applied to the data to obtain relative neutron intensity cause the statistical accuracy to decrease with increasing neutron energy.

Four groups *A*, *B*, *C*, and *D* are evident in all the spectra, while at the highest bombarding energy a fifth group *E* appears. The measured *Q*-values of these groups are given in Table I. The peaks designated by *A* give a *Q*-value for the ground-state transition of -1.05 ± 0.05 Mev and hence a threshold for the $Mn^{55}(p,n)Fe^{55}$ reaction of 1.07 ± 0.05 Mev. Richards, Smith, and Browne[2] studied the neutron yield from a thick manganese target as a function of proton bombarding energy and obtained a threshold of 1.18 ± 0.01 Mev, a value which is not in good agreement with that obtained by the method reported here. However, McCue and Preston[3] have performed an experiment similar to that of Richards, *et al.*, and find a lower value of 1.02 ± 0.02 Mev for the threshold.

The shift in energy of the neutron groups *A*, *B*, *C* and *D* at $E_p=3.42$ Mev with emergent angle ($0°\rightarrow90°$) is consistent with a target nucleus of $A\sim55$. A spectrum of 200 tracks (not shown) was measured at the highest proton-bombarding energy at 90° to the proton beam to establish the fact that group *E* also exhibited a shift in energy consistent with $A\sim55$. The observations at 0° and 90°, therefore, permit the elimination of the possibility of any of the neutron groups originating from target surface contamination by much lighter elements with larger (p,n) cross sections. However, the possibility that such contamination could produce neutron groups with sufficient intensity to be observable is unlikely. Carbon and oxygen are the two most likely contaminators and only the C^{13} and O^{18} isotopes, which have small relative abundances in the natural elements, have low enough (p,n) thresholds to produce neutrons at the proton energies employed.

The resolution of the photographic plate, proton recoil method of measuring neutron spectra increases with increasing neutron energy and therefore the half-widths of the neutron groups increase with decreasing energy. However, group *D* appears to have an unusually large half-width. Group *C* at $E_p=2.97$ and 3.42 Mev falls approximately at the same neutron energies as group *D* at $E_p=3.42$ and 3.77 Mev; and, hence, an effective comparison of the half-widths can be made. This indicates that group *D* has approximately 60 kev more width than *C*, suggesting that group *D* is complex; a level separation of 60 kev results if it is assumed that this peak is due to two levels equally strongly excited.

An energy level diagram presenting the results of the present investigation and those of Deutsch and Hedgran on the decay of Co^{55} is given in Fig. 3. It is seen that there is good correspondence between their level at 0.935 Mev and the level at 0.94 Mev. The cor-

TABLE I. Measured *Q*-values for the neutron groups shown in Figs. 1 and 2. The last column gives the average excitation energy above the ground state (group *A*) and therefore indicates the location of levels in the residual nucleus Fe^{55}.

Neutron group	*Q*-value (Mev) $E_p=2.97$; 0°	$E_p=3.42$; 90°	$E_p=3.42$; 0°	$E_p=3.77$; 0°	Average	Neutron group	Average excitation energy (ΔQ in Mev)
A	−1.06	−1.05	−1.05	−1.03	-1.05 ± 0.05	*A*	
B	−1.49	−1.45	−1.47	−1.45	-1.47 ± 0.05	*B*	0.42
C	−1.99	−2.01	−2.00	−1.96	-1.99 ± 0.05	*C*	0.94
D	−2.38	−2.42	−2.43	−2.41	-2.41 ± 0.05	*D*	1.36
E				−3.13	-3.13 ± 0.07	*E*	2.08

TABLE II. Relative transition probabilities, t, of the neutron groups shown in Figs. 1 and 2. The relative transition probability divided by the square root of the neutron energy and normalized to unity, $t/E_n^{\frac{1}{2}}$, is also given. The indicated errors are those due to statistics only; no attempt has been made to include other possible errors such as the inability to apply the selection criteria equally well to the long and short tracks.

Neutron group	Relative transition probability [t] $E_p=2.97$; 0°	$E_p=3.42$; 90°	$E_p=3.42$; 0°	$E_p=3.77$; 0°
A	0.37±0.03	0.28±0.03	0.26±0.03	0.22±0.02
B	0.12±0.02	0.09±0.02	0.09±0.02	0.13±0.02
C	0.26±0.02	0.31±0.02	0.30±0.02	0.21±0.01
D	0.25±0.02	0.32±0.02	0.35±0.02	0.35±0.03
E				0.09±0.01
	Relative transition probability (normalized to unity) [$t/(E_n)^{\frac{1}{2}}$] (neutron energy)$^{\frac{1}{2}}$			
A	0.28±0.02	0.22±0.02	0.21±0.02	0.17±0.02
B	0.11±0.02	0.08±0.02	0.08±0.02	0.10±0.01
C	0.27±0.02	0.32±0.02	0.30±0.02	0.20±0.02
D	0.34±0.02	0.39±0.02	0.42±0.02	0.38±0.03
E				0.15±0.02

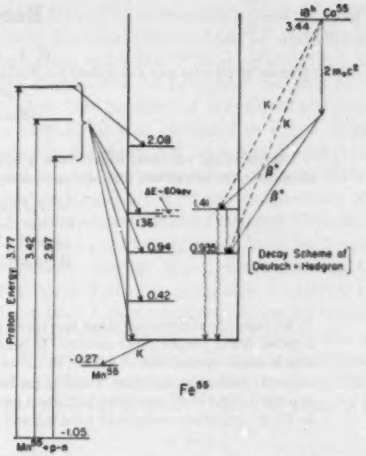

FIG. 3. Energy level diagram for the Fe^{55} nucleus.

respondence between their level at 1.41 Mev and our doublet level at 1.36 Mev is somewhat less satisfactory but is within the accuracy of the measurements involved in the two experiments.

The relative transition probabilities, t, of the different groups at the three proton-bombarding energies are listed in Table II. The quantity $t/E_n^{\frac{1}{2}}$ (normalized to unity) is also given, since, according to theory,[4] this quantity should be a measure of the "matrix element," i.e., the energy dependence of the emitted neutron has been removed. The quantities $t/E_n^{\frac{1}{2}}$ should depend on the relation of the angular momentum, I, of the target nucleus, $Mn^{55}(I=5/2)$, to the angular momenta, I', of the levels of the residual Fe^{55} nucleus. A given excited state of the residual nucleus can, in general, be reached in a number of ways, i.e., by different vectorial combinations of the angular momenta of the target nucleus, incident proton and emerging neutron. Using the theory developed by Tyson[5] for calculating the effect of the coulomb plus angular momentum barrier on the incident protons, one obtains for 3.5-Mev protons incident on manganese cross sections for the s, p, d, f, and g waves of 0.030, 0.054, 0.024, 0.005, and 0.0005 barn, respectively. The theory indicates, therefore, that there is a relatively good chance of the proton carrying in 0, 1, 2, or even 3 units of orbital angular momentum, and when this, together with the intrinsic spin of the proton, is added vectorially to the 5/2 value of the target nucleus, a large range of possible values for the angular momentum of the highly excited states of the compound nucleus is obtained. At the high excitation energy of the compound nucleus (~10–12 Mev) one would expect a small level spacing and hence many levels are available for excitation in the energy increment of 30 kev, determined largely by the target thickness. These compound states then decay to levels of Fe^{55} by the emission of a neutron which is also capable of carrying several units of angular momentum. The ratios of the cross sections for the emission of s, p, d, f, and g wave neutrons of 2.0 Mev from the Fe^{55} nucleus are calculated to be 1.0:2.5:2.1:0.6:0.1 using the formulas given by Blatt and Weisskopf.[6]

These considerations suggest that the study of the neutron spectrum of $Mn^{55}(p,n)Fe^{55}$ induced by protons of several Mev energy should disclose the existence of levels in Fe^{55} with angular momentum values of 1/2 up to a fairly large value of perhaps 13/2 or 15/2. Levels with I' values not too different from the 5/2 value of the target nucleus should have approximately the same value of $t/E_n^{\frac{1}{2}}$. One would also expect the $t/E_n^{\frac{1}{2}}$ values to become more uniform at higher proton energies since the restrictions on the angular momenta of the incident and emerging nucleons become less severe. It is interesting to note at the highest proton bombarding energy the groups A, C, and E have about the same $t/E_n^{\frac{1}{2}}$ values and if group D is taken to be a doublet, the value of $t/E_n^{\frac{1}{2}}$ is approximately the same as for A, C, and E. However, the intensity of group B is definitely low, which suggests that the I' value for this level is quite different from 5/2 and is therefore probably quite large. This is concordant with the fact that this level is not excited in the $\beta-\gamma$ decay of Co^{55}, where more stringent selection rules are operative.

[4] Feshbach, Peaslee, and Weisskopf, Phys. Rev. **71**, 145 (1947).
[5] J. K. Tyson, Ph.D. thesis, MIT (1948).
[6] J. M. Blatt and V. F. Weisskopf, MIT Technical Report No. 42 (May, 1950).

Energy Levels in Li^7

H. E. Gove and J. A. Harvey
Department of Physics and Laboratory for Nuclear Science and Engineering, Massachusetts Institute of Technology, Cambridge, Massachusetts*

(Received January 25, 1951)

The following reactions which show a new level in Li^7 at the listed excitation energy have been studied using protons, deuterons, and alphas of energies 7.9, 14, and 31 Mev, respectively, from the MIT cyclotron:

$Li^7(p,p')Li^{7*}$	$E_x=4.67\pm0.08$ Mev
$Li^7(\alpha,\alpha')Li^{7*}$	$E_x=4.79\pm0.22$ Mev
$Li^7(d,d')Li^{7*}$	$E_x=4.86\pm0.15$ Mev
$Be^9(d,\alpha)Li^{7*}$	$E_x=4.76\pm0.15$ Mev
Mean	$E_x=4.77\pm0.10$ Mev.

In all cases the differential range spectra of the emitted groups were measured in aluminum absorbers using a gated triple proportional counter. In addition, a low energy group was found in the $Be^9(d,\alpha)$ reaction which would correspond to a level in Li^7 at 7.50 ± 0.17 Mev. No corresponding group was observed in the inelastic scattering reactions. Possible explanations of this are given. Preliminary results on the $Li^7(d,t)Li^{6*}$ and the $Li^6(p,p')Li^{6*}$ reactions indicate a level in Li^6 at 2.15 ± 0.2 Mev. There is also evidence for two levels in Li^8 at excitation energies of 1.0 ± 0.2 and 2.3 ± 0.2 Mev from the $Li^7(d,p)Li^{8*}$ reaction.

I. INTRODUCTION

CONSIDERABLE theoretical attention has been devoted to the properties of the Li^7 nucleus because it is one of the "simplest of the complex nuclei." The discovery of a 480-kev level[1] led to the prediction that the ground state and this excited level form a ^2P doublet.[2] The presence of a level at 7.48 Mev[3] has been reported but no other levels have been found to date. Considerable evidence[4,5] favors an assignment of $\frac{1}{2}$ to the angular momentum of the first excited state; however other evidence[6-9] indicates a higher value of angular momentum suggesting that this excited level forms a ^2F doublet with the ground state. The presence of any other excited levels between the 480 kev and the 7.48-Mev levels would be of some interest.[10,11]

Many investigators have searched for additional levels in Li^7 and have found none. The level at 480 kev has been found from the γ-radiation following the Be^7 decay[12] and the alpha-groups[6] from the thermal neutron capture of B^{10}. However both of these reactions are limited energetically to low excitation levels. A gamma-ray corresponding to the 480-kev level has been measured from inelastic scattering of low energy alphas[13] and protons.[14] In some recent work[15] the reaction $Li^6(d,p)Li^7$ has been employed for an accurate measurement of the excitation energy of the 480-kev level. In addition, a search was made for other levels up to an excitation energy of about 3 Mev, and none were found. Inglis[16] and Buechner and Strait,[17] using low energy deuterons to study the reaction $Be^9(d,\alpha)Li^7$, $Q_0=7.15$ Mev, have searched carefully the region from the ground state to an excitation energy of 3.5 Mev. In both cases, no evidence was found for any excited levels in Li^7 except for the level at 480 kev. The measurements by Inglis[16] show a rising background of alpha-particles starting at an excitation energy of about 3 Mev, which is attributed to the reaction $Be^9(d,2\alpha)T$. The threshold for this reaction is expected to occur at an excitation energy in Li^7 of 2.5 Mev. Measurements on the yield of alpha-particles from neutron bombardment of lithium show a resonance at a neutron energy of 270 kev.[3] This was attributed to a level in Li^7 at 7.48 Mev. Recent measurements[18] on the total neutron cross section of lithium also show a resonance at 270 kev, which is assigned to a level in Li^8 at 2.27 Mev. The close agreement between the energy of the resonances found in the two experiments leaves some doubt whether they arise from different processes.

From this discussion it can be seen that the region of excitation energies between 3.5 and 7.25 Mev has not been covered by any of the methods employed to date.

* This work has been supported in part by the joint program of the ONR and AEC.

[1] L. H. Rumbaugh and L. R. Hafstad, Phys. Rev. **50**, 681 (1936).
[2] D. R. Inglis, Phys. Rev. **50**, 783 (1936).
[3] J. M. Blair, quoted by Goldsmith, Ibser, and Feld, Revs. Modern Phys. **19**, 259 (1947).
[4] B. Rose and A. R. W. Wilson, Phys. Rev. **78**, 68 (1950). B. T. Feld, Phys. Rev. **75**, 1618 (1949). S. Devons, Proc. Phys. Soc. (London) **62A**, 580 (1949).
[5] Littauer, Proc. Phys. Soc. (London) **63**, 294 (1950).
[6] J. K. Bøggild, Kgl. Danske Vid. Sels. Math.-fys. Medd. **23**, 4, 26 (1945).
[7] D. R. Inglis, Phys. Rev. **74**, 1876 L (1950).
[8] S. S. Hanna and D. R. Inglis, Phys. Rev. **75**, 1767 (1949).
[9] R. Avery and C. H. Blanchard, Phys. Rev. **78**, 704 (1950).
[10] D. R. Inglis, Phys. Rev. **77**, 724 L (1950).
[11] A. M. Feingold and E. P. Wigner, Phys. Rev. **79**, 221 A (1950).
[12] N. P. Heydenburg and G. L. Locher, Phys. Rev. **53**, 1016 (1938).
[13] K. Siegbahn and H. Slatis, Arkiv Mat. Astron. Fysik **34A**, No. 15 (1946).
[14] Fowler, Lauritsen, and Rubin, Phys. Rev. **75**, 1471A (1949).
[15] Buechner, Strait, Stergiopoulos, and Sperduto, Phys. Rev. **74**, 1569 (1948) and private communication.
[16] D. R. Inglis, Phys. Rev. **78**, 104 (1950).
[17] W. W. Buechner and E. N. Strait, Phys. Rev. **76**, 1547 (1949).
[18] R. K. Adair, Phys. Rev. **79**, 1018 L (1950).

Since there is available from the MIT cyclotron an emergent beam of either protons, deuterons, or alpha-particles of energies 8 Mev, 16 Mev, and 32 Mev, respectively, it was suggested by D. R. Inglis that an attempt be made to investigate Li^7 and in particular the unexplored region. Preliminary measurements on the $Li^7(d,d')Li^{7*}$ reaction made in this laboratory[19] indicated the presence of a level in this region.

The possible reactions which could be employed using targets of normal isotopic abundance were $Be^9(d,\alpha)Li^7$, $Li^7(d,d')Li^{7*}$, $Li^7(\alpha,\alpha')Li^{7*}$, and $Li^7(p,p')Li^{7*}$. This paper presents the results from the study of these four reactions.

II. APPARATUS

The apparatus and the general techniques of measurement have been described in a series of recent papers.[20–22]

In brief, the apparatus employs a gated triple proportional counter which responds to charged particles terminating in its third section after passing through variable aluminum absorber foils. In this way charged particles resulting from deuteron, alpha, or proton bombardment of thin targets can be identified and the differential range spectrum can be measured. The detector can be rotated to measure the variation in energy and intensity with angle.

The Q-values of excited levels are measured relative to a reference value which is usually the Q-value of the ground-state group. The approximate energy of this group is obtained from the measured range in the aluminum absorber foils to which is added the range of half the target thickness and the triple counter depth. Substituting this energy and the known Q-value into the Q-equation, we obtain the bombarding energy. Using this bombarding energy and the energies of the excited groups, their Q-values can be obtained.

III. THE REACTION $Li^7(p,p')Li^{7*}$

The lithium targets were prepared by rolling lithium metal of natural isotopic abundance between two thin aluminum foils. Chemical reactions with air were minimized by the use of mineral oil. The targets were kept under oil until ready to use and then washed in a solvent and quickly inserted into the target chamber. They retained their metallic appearance, indicating that very little surface impurities had been formed.

To study the $Li^7(p,p')Li^{7*}$ reaction a 1 mg/cm^2-lithium target was bombarded with 7.9-Mev protons.

Figure 1 shows the spectrum obtained at 50°. In addition to the elastically scattered protons from Li^7 three lower energy proton groups are observed. Two of these groups are assigned to inelastically scattered protons from Li^7 and correspond to Q-values of -0.49 and -4.68 Mev. The intermediate peak is assigned to inelastically scattered protons from Li^6 and corresponds to an excitation of 2.2 Mev.[23] This agrees with a level at 2.15 Mev found from the $Li^7(d,t)Li^6$ reaction to be discussed later. The position of the elastically scattered protons from Li^6 is also indicated in Fig. 1. The 4.68-Mev group is superimposed on a broad background at all angles, which probably arises from a three-body disintegration. If any other groups due to elastic protons from Li^7 were present to about 5 percent of the intensity of the 4.68-Mev group, they would have been detected.

The inelastic proton group corresponding to the 4.68-Mev level and the elastically scattered proton group have been measured at several angles from 25° to 70°. The elastically scattered proton group was measured at 30° before and after each run to compensate for any drifts. Table I summarizes the results normalized, in energy, to the elastic peak at 30°. The mean of the Q-values at the different angles is -4.67 Mev. The accuracy is estimated to be 80 kev because of an uncertainty of 2 mg/cm^2 in range (equivalent to 100 kev uncertainty in bombarding energy). The resultant errors due to the uncertainty in angle and the estimation of the positions of the peaks are small, and the effects are random. The value of the excitation energy of this level in Li^7 from this reaction is 4.67 ± 0.08 Mev.

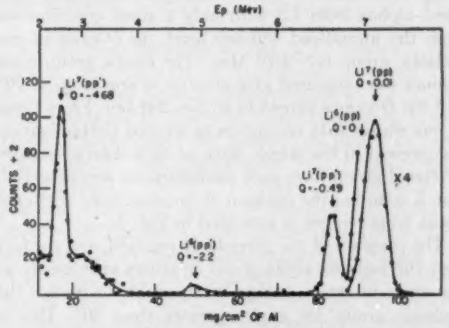

FIG. 1. A proton spectrum at 50° from a 1 mg/cm^2-lithium target bombarded with 7.9-Mev protons. The three main peaks are caused by the elastic and inelastic scattering from Li^7. An inelastic peak from Li^6 also is evident. The position of the elastic peak from Li^6 is indicated. It is obscured by the elastic scattering from Li^7.

IV. THE REACTION $Li^7(\alpha,\alpha')Li^{7*}$

To study this reaction a 2-mg/cm^2 lithium target was bombarded with 31-Mev alpha-particles and the range spectrum of the alphas was measured. Figure 2 shows the spectrum taken at 20°. It consists of elastically and

[19] MIT Laboratory for Nuclear Science and Engineering Progress Report, July 1, 1950 (unpublished).
[20] Boyer, Gove, Harvey, Deutsch, and Livingston, Rev. Sci. Instr. 22, 311 (1951).
[21] J. A. Harvey, Phys. Rev. 81, 353 (1951).
[22] H. E. Gove, Phys. Rev. 81, 364 (1951).
[23] Some preliminary work performed independently at about the same time as that reported here by W. M. Harris at the University of Rochester indicates a level at an excitation energy of about 2.2 Mev in Li^6. An enriched Li^6 target was bombarded with 6-Mev protons, and a low intensity inelastic proton group corresponding to this level was observed.

TABLE I. Q-values for the elastic and inelastic proton groups and their differences at a series of angles for the $Li^7(p,p')Li^{7*}$ reaction assuming $Q=0$ for the elastic group at 30°.

Laboratory angle (θ) (degrees)	Q_{el} (Mev)	Q_{inel} (Mev)	$Q_{inel}-Q_{el}$ (Mev)
25	0.00	−4.67	−4.67
30	0.00	−4.65	−4.65
35	+0.01	−4.67	−4.68
40	+0.05	−4.63	−4.68
45	−0.02	−4.68	−4.66
50	+0.07	−4.60	−4.67
55	−0.01	−4.67	−4.66
60	−0.01	−4.70	−4.69
65	−0.04	−4.70	−4.66
70	−0.03	−4.70	−4.67
Mean	0.00	−4.67	−4.67

inelastically scattered alphas, and alphas from the three-body disintegration $Li^7(\alpha,2\alpha)T$. If the long-range group is assumed to consist mainly of elastically scattered alphas from Li^7 with only a small contribution from the unresolved 480-kev level, the Q-value of the inelastic group is −4.79 Mev. The elastic group from lithium was measured at a number of angles up to 70° and the Q-values agreed to within 200 kev. From these it was shown that no carbon or oxygen contamination was present in the target, since no sign of an elastically scattered group from such contaminants was observed. For illustration the position of the elastically scattered group from oxygen is indicated in Fig. 2.

The presence of the three-body reaction, and the fact that the inelastic alpha-group decreases in intensity as the angle increases, makes it impossible to resolve the inelastic group for angles greater than 30°. This is illustrated in Fig. 3 which shows the spectrum at 50°. Therefore, the shift of this peak with angle cannot be used to eliminate the possibilities of contaminants. These are eliminated, however, by the absence of the corresponding elastic peaks.

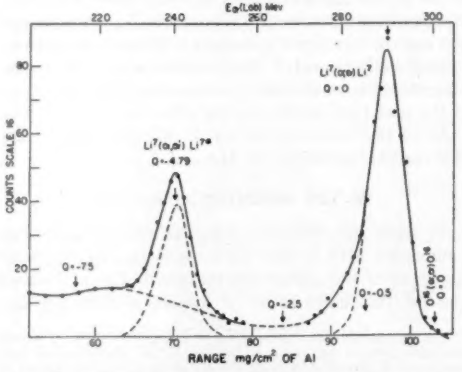

FIG. 2. An alpha-spectrum at 20° from a 2-mg/cm² lithium target bombarded with 31-Mev alphas. If an elastically scattered peak from oxygen were present, it would appear at the range indicated.

A probable error of 200 kev is ascribed to the value of 4.79 Mev for the excitation energy of the inelastic group. This rather large uncertainty results from the aforementioned inability to observe the group at a number of angles and arises from uncertainties in angle, bombarding energy, and difference in range.

The comparison between the elastically scattered alphas from aluminum ($Q=0$) and the long-range group from lithium results in a Q-value for this lithium group of $+0.2\pm0.2$ Mev. Part of the probable error in this case results from uncertainties in target thickness, since peaks from two different targets are being compared. The fact that the above Q-value is positive by 200 kev makes it rather likely that the 480-kev level is of low intensity. On the basis of this assumption, the excitation energy of the new level in Li^7 is 4.8 ± 0.2 Mev.

There is no sign of a level at 7.5 Mev. The expected position of this peak is indicated in Fig. 2.

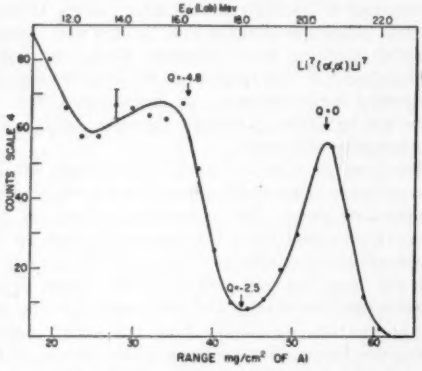

FIG. 3. An alpha-spectrum at 50° from the same lithium target as in Fig. 2 bombarded with 31-Mev alphas. The inelastic alpha-group is not resolved at the wider angles.

V. THE REACTION $Li^7(d,d')Li^{7*}$

A thin lithium target, about 4 mg/cm², was bombarded with 14-Mev deuterons, and the resulting proton, deuteron, and triton spectra were studied. Figure 4 shows the spectrum taken at 30° with discriminator settings maximized for deuterons. The longest range group of deuterons at this angle comprises mainly the elastically scattered deuterons with only a small contribution from the 480-kev level. Again a group of inelastic deuterons is found corresponding to a level in Li^7 at 4.87 Mev. This is superimposed on a rising background which can be ascribed to a three-body reaction. The expected position of a level at 7.5 Mev is shown.

The inelastic deuteron peak at 4.87 Mev has been observed at several angles up to 70°. The shift with angle agrees with that computed for deuterons from lithium rather than protons or tritons, which also occur in this energy region. Figure 5 shows the deuteron

spectrum taken at 60° showing the elastic and inelastic peaks. A comparison between the ranges of the elastically scattered deuterons from a 4-mg/cm² carbon (polyethylene) target ($Q=0$) and the lithium target demonstrates that the long-range deuteron group from lithium at 30° is principally the elastic group ($Q=-0.04 \pm 0.08$ Mev). However, at 60° both the elastic group and the unresolved 480-kev level appear to be present to about equal intensity ($Q=-0.27 \pm 0.10$ Mev). In both cases, however, the Q-values of the inelastic peak are the same.

Figure 6 shows the spectrum at 30° resulting from deuteron bombardment of lithium when the discriminator settings are maximized for tritons. Two triton groups of equal intensity are observed corresponding to the ground state and an excited level at about 2.15 Mev in Li^6. This agrees with the preliminary observations on $Li^7(d,t)Li^6$ made in this laboratory of a level at about

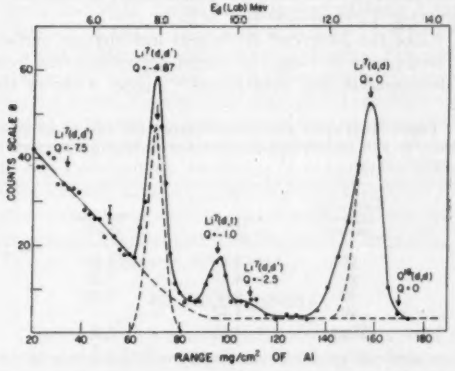

FIG. 4. A spectrum of deuterons and tritons at 30° from a 4-mg/cm² lithium target bombarded with 14-Mev deuterons. The discriminator settings are optimized for deuterons. There is a small triton contribution to the inelastic deuteron peak, equivalent in intensity to the triton group shown, as indicated in Fig. 6.

2.1 Mev.[19] This is to be compared with the deuteron spectrum of Fig. 4. The excited triton group coincides with the inelastic deuteron group at this angle; but since Fig. 6 demonstrates that this excited triton group is at most equal in intensity to the ground-state triton group and since the latter is shown with low intensity in Fig. 4, one must conclude that the peak in Fig. 4 is correctly assigned to deuterons. By a similar argument, using the fact that the elastic deuteron group appears in both spectra, one can conclude that the lowest energy group consists principally of tritons.

Several arguments can be used to eliminate the possibility of contaminants contributing to any of the groups observed. The most convincing proofs are the absence of the elastically scattered deuteron group corresponding to a contaminant and the correct shift of the inelastic deuteron peak with angle.

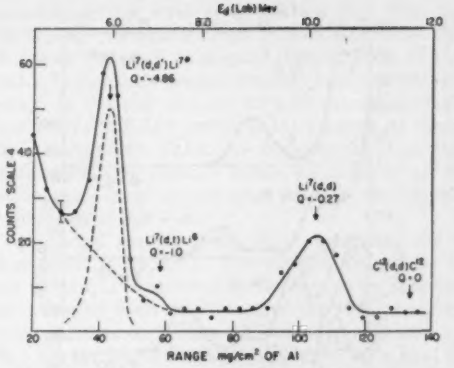

FIG. 5. A deuteron spectrum at 60° from the lithium target used in Fig. 4 bombarded with 14-Mev deuterons. If an inelastically scattered peak from carbon were present it would occur at the range indicated.

Earlier measurements of the (d,p) spectrum from lithium demonstrated that protons were not contributing to the inelastic deuteron peak of Fig. 4. This (d,p) spectrum also showed three reasonably intense proton groups beyond the range of the elastic deuteron peak. One of these corresponded to the ground-state group from $Li^7(d,p)Li^8$. The other two indicated the possible existence of excited levels at about 1.0 and 2.3 Mev in Li^8. The spectrum at greater ranges showed low intensity proton groups from carbon and oxygen contamination. These excited levels in Li^8 were not investigated in any detail and they may be due to contaminations. Greater care was exercised in preparing the subsequent lithium targets from which the inelastic scattering data were obtained.

A low intensity long-range group of protons was also observed corresponding to the unresolved ground state and 480-kev level from $Li^6(d,p)Li^7$. A search was made

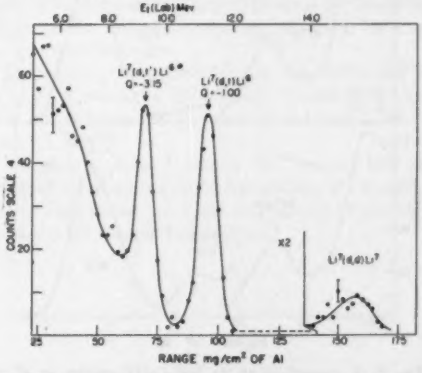

FIG. 6. A spectrum of tritons and deuterons at 30° from the lithium target used in Fig. 4 bombarded with 14-Mev deuterons. The discriminator settings are optimized for tritons.

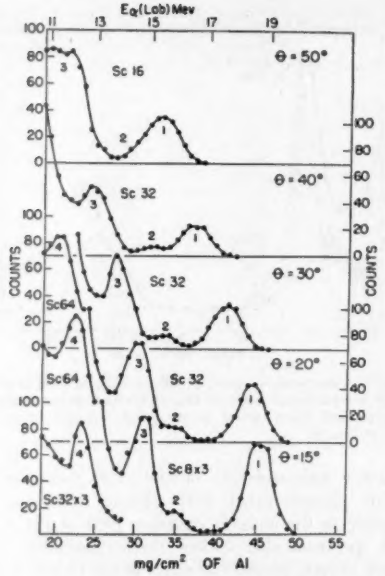

FIG. 7. $Be^9(d,\alpha)Li^7$ spectra at several angles, from a 2-mg/cm² Be-target bombarded with 14-Mev deuterons. The range, in mg/cm² of Al, includes the counter depth and half-target thickness. The alpha-energies in the laboratory system are also indicated. Peak 2 arises from an an oxygen contamination, while the remaining three are from Be. The ordinate represents the number of counts on the designated scaling factors.

for a group corresponding to the 4.8-Mev level in Li^7 which would occur about 400 kev higher than the ground-state peak from the $Li^7(d,p)Li^8$ reaction at the forward angles. However, because of the low abundance of Li^6 in the target (about 7 percent) and the fact that it is so close to the intense ground-state peak from $Li^7(d,p)Li^8$, it could not be detected.

The results obtained from deuteron bombardment of lithium show a level in Li^7 at 4.86±0.15 Mev, a level in Li^6 at 2.15±0.2 Mev, and possibly two levels in Li^8 at 1.0±0.2 Mev and 2.3±0.2 Mev. The probable errors in each case result from effects previously discussed. Again, no group corresponding to a level at 7.5 Mev in Li^7 was observed.

VI. THE REACTION $Be^9(d,\alpha)Li^7$

The spectrum of alpha-particles arising from the bombardment of Be^9 with 14-Mev deuterons is shown in Fig. 7 at a series of angles from 15° to 50°. The target employed was a 2-mg/cm² foil of Be^9. The longest range group comprises both the ground-state group and the 480-kev level. The third and fourth peaks correspond to levels at 4.76 and 7.50 Mev in Li^7.

Since the 2-mg/cm² Be targets had obvious surface discoloration, a 1-mg/cm² target apparently free from contaminants was substituted.[24] Figure 8 shows the comparison between the alpha-spectra at 30° from both targets. Except for the second peak whose Q-value agrees with that from the reaction $O^{16}(d,\alpha)N^{14}$ $Q=3.1$ Mev the spectra are identical. Further confirmation that oxygen contamination was present in the 2-mg/cm² target was obtained by investigating the $Be^9(d,p)Be^{10}$ spectra. Again, a peak due to $O^{16}(d,p)O^{17}$ was found in the proton spectrum from the 2-mg/cm² target but not from the 1-mg/cm² target.

TABLE II. Q-value differences between the long-range group and the two excited groups from the $Be^9(d,\alpha)Li^7$ reaction at several angles.

Laboratory angle (θ) (degrees)	Q_1-Q_2 (Mev)	Q_1-Q_4 (Mev)
15	4.51	7.23
20	4.47	7.28
30	4.69	7.28
40	4.40	
Mean	4.52	7.26

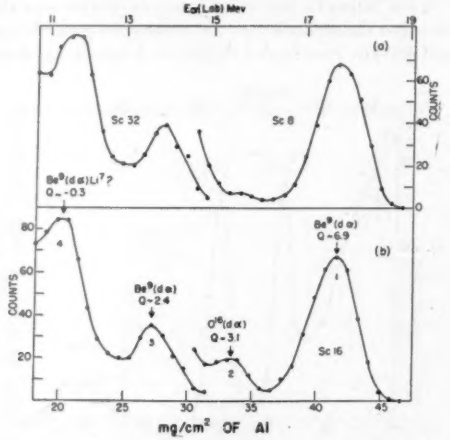

FIG. 8. A comparison of the $Be^9(d,\alpha)Li^7$-spectra at 30° with 14-Mev deuterons using 2 different target thicknesses: (a) a 1 mg/cm² and (b) a 2-mg/cm² Be target. Peak 2, arising from oxygen contamination, is observed to change in intensity.

The spectra at various angles shown in Fig. 8 were compared with the long-range group taken at 30° before and after each run. The mean value of the position of this peak was then employed to correct the range coordinates of the spectra to compensate for any changes in deuteron energy or discriminator drift. Table II lists the difference in Q-values between the third and fourth peaks and the long range peak at each angle. These values have been calculated after subtracting the rising background of alpha-particles on which the two short range groups are superimposed. This background can

[24] We wish to thank Dr. Hugh Bradner for kindly supplying us with the beryllium targets.

be attributed[16] to the three-body process $Be^9(d,2\alpha)T$ which can be expected to have a threshold at an excitation energy of 2.5 Mev.

In order to assign the measured Q-value differences of 4.52 and 7.26 Mev to energy levels in Li^7 one must decide how great a contribution the unresolved 480-kev level is making to the long-range group. Measurements made at lower bombarding energies[16] show the intensity of the excited group to be substantially the same as that of the ground state. Comparing the Q-value of this long range group with that of the oxygen group at 30° gives a value 0.25±0.10 Mev lower than the known value of 7.15 Mev for the $Be^9(d,\alpha)$ reaction. Hence, it is reasonable to assume that the two groups are of about equal intensity. Since the Q-values of the long range group agree to within 30 kev at the various angles, the relative intensities are constant.

If one makes this assumption, it is necessary to add half the separation of 480 kev to the values computed above to obtain the excitation energy of these higher levels. This results in values of 4.76±0.15 Mev and 7.50±0.17 Mev for the excitation energies. The probable errors listed result from uncertainties in angle, counter depth, bombarding energy, and range difference, as well as the relative intensities of the two peaks in the long range group. The level at 7.5 Mev was not observed in either the inelastic scattering of deuterons or alphas from Li^7, and since it occurs in the virtual region of Li^7, there exists the possibility that it may arise from some nuclear mechanism other than the reaction $Be^9(d,\alpha)Li^{7*}$. This will be discussed subsequently.

VII. CONCLUSIONS

Charged particle groups corresponding to a level in Li^7 at about 4.8 Mev have been found by the four reactions studied. Averaging the four values gives 4.77±0.10 Mev for the excitation energy. It is also clear from the data that no additional levels appear in Li^7 between the one at 480 kev and the one at 4.8 Mev despite the use of high bombarding energies.

The angular distribution of the inelastic proton group corresponding to the 4.8 level from the $Li^7(p,p')Li^{7*}$ reaction shows no significant variation in intensity between 32° and 84° in the center-of-mass system (half the points lie within ±10 percent of the mean). It is impossible to estimate intensities to better than ten percent because of the presence of a background arising from the three-body disintegration. It is possible to measure only the intensity of the alpha-group corresponding to the level in Li^7 at 4.8 Mev from the $Be^9(d,\alpha)Li^7$ reaction between 15° and 40°. While this is clearly too small an angular interval to be of any value, the intensity is approximately constant over this range. In this case and also for both the $Li^7(\alpha,\alpha')Li^{7*}$ and the $Li^7(d,d')Li^{7*}$ reactions the presence of three-body backgrounds makes any measurement of angular distribution very difficult. Hence, no estimate can be made from these experimental data of the angular momentum of this level.

A charged particle group which would indicate a level in Li^7 at 7.50±0.17 Mev has been found only in the $Be^9(d,\alpha)Li^7$ reaction. This level agrees with the observations of Blair, who measured the yield of alphas from neutrons on lithium and found a resonance at $E_n=270$ kev which has been interpreted[3] as a level in Li^7 at 7.48 Mev. However, recent measurements of Adair[18] show a resonance in the total neutron cross section of lithium at 270 kev which he attributes to a level in Li^8 at 2.27 Mev. He also points out that some of the alphas contributing to the resonance found by Blair might be due to the reaction $Li^7(n,\gamma)Li^8$, where Li^8 decays to Be^{8*} which immediately breaks up into two alphas. Preliminary measurements reported here on the reaction $Li^7(d,p)Li^8$, $Q=-0.19$ Mev, indicate levels in Li^8 at about 1.0 and 2.3 Mev which confirms Adair's interpretation. It does seem unusual that both an excited level in Li^7 and one in Li^8 should be virtual against neutron emission by the same value of 230 kev.

In view of this it is possible that the low energy alpha-group found when Be^9 is bombarded with deuterons should not be assigned to a level of 7.5 Mev in Li^7. We propose as a plausible nuclear process the $Be^9(d,t)Be^8$ reaction in which tritons are emitted with low energies and the Be^8 nuclei, left in highly excited states, recoil within a small cone of angles in the forward direction. This recoiling Be^8 nucleus immediately breaks up into two alpha-particles. These high energy alphas may then correspond to the group we observe. On the other hand, it is also possible that this level is not observed in either of the inelastic scattering processes because of nuclear selection rules.

Preliminary measurements on the $Li^7(d,t)Li^8$ and $Li^7(d,p)Li^8$ reactions show a level in Li^8 at 2.15±0.2 Mev and possibly two levels in Li^8 at 1.0±0.2 Mev and 2.3±0.2 Mev.

We wish to thank Professors M. Deutsch and M. S. Livingston for many helpful discussions. We should also like to express our gratitude to the crew of the M.I.T. cyclotron for their able assistance.

On Gauge Invariance and Vacuum Polarization

JULIAN SCHWINGER
Harvard University, Cambridge, Massachusetts
(Received December 22, 1950)

This paper is based on the elementary remark that the extraction of gauge invariant results from a formally gauge invariant theory is ensured if one employs methods of solution that involve only gauge covariant quantities. We illustrate this statement in connection with the problem of vacuum polarization by a prescribed electromagnetic field. The vacuum current of a charged Dirac field, which can be expressed in terms of the Green's function of that field, implies an addition to the action integral of the electromagnetic field. Now these quantities can be related to the dynamical properties of a "particle" with space-time coordinates that depend upon a proper-time parameter. The proper-time equations of motion involve only electromagnetic field strengths, and provide a suitable gauge invariant basis for treating problems. Rigorous solutions of the equations of motion can be obtained for a constant field, and for a plane wave field. A renormalization of field strength and charge, applied to the modified lagrange function for constant fields, yields a finite, gauge invariant result which implies nonlinear properties for the electromagnetic field in the vacuum. The contribution of a zero spin charged field is also stated. After the same field strength renormalization, the modified physical quantities describing a plane wave in the vacuum reduce to just those of the maxwell field; there are no nonlinear phenomena for a single plane wave, of arbitrary strength and spectral composition. The results obtained for constant (that is, slowly varying fields), are then applied to treat the two-photon disintegration of a spin zero neutral meson arising from the polarization of the proton vacuum. We obtain approximate, gauge invariant expressions for the effective interaction between the meson and the electromagnetic field, in which the nuclear coupling may be scalar, pseudoscalar, or pseudovector in nature. The direct verification of equivalence between the pseudoscalar and pseudovector interactions only requires a proper statement of the limiting processes involved. For arbitrarily varying fields, perturbation methods can be applied to the equations of motion, as discussed in Appendix A, or one can employ an expansion in powers of the potential vector. The latter automatically yields gauge invariant results, provided only that the proper-time integration is reserved to the last. This indicates that the significant aspect of the proper-time method is its isolation of divergences in integrals with respect to the proper-time parameter, which is independent of the coordinate system and of the gauge. The connection between the proper-time method and the technique of "invariant regularization" is discussed. Incidentally, the probability of actual pair creation is obtained from the imaginary part of the electromagnetic field action integral. Finally, as an application of the Green's function for a constant field, we construct the mass operator of an electron in a weak, homogeneous external field, and derive the additional spin magnetic moment of $\alpha/2\pi$ magnetons by means of a perturbation calculation in which proper-mass plays the customary role of energy.

I. INTRODUCTION

QUANTUM electrodynamics is characterized by several formal invariance properties, notably relativistic and gauge invariance. Yet specific calculations by conventional methods may yield results that violate these requirements, in consequence of the divergences inherent in present field theories. Such difficulties concerning relativistic invariance have been avoided by employing formulations of the theory that are explicitly invariant under coordinate transformations, and by maintaining this generality through the course of calculations. The preservation of gauge invariance has apparently been considered to be a more formidable task. It should be evident, however, that the two problems are quite analogous, and that gauge invariance difficulties naturally disappear when methods of solution are adopted that involve only gauge invariant quantities.

We shall illustrate this assertion by applying such a gauge invariant method to treat several aspects of the problem of vacuum polarization by a prescribed electromagnetic field. The calculation of the current associated with the vacuum of a charged particle field involves the construction of the Green's function for the particle field in the prescribed electromagnetic field. This vacuum current can be exhibited as the variation of an action integral with respect to the potential vector, which action effectively adds to that of the maxwell field in describing the behavior of electromagnetic fields in the vacuum. We shall relate these problems to the solution of particle equations of motion with a proper-time parameter. The equations of motion, which involve only electromagnetic field strengths, provide the desired gauge invariant basis for our discussion.

Explicit solutions can be obtained in the two situations of constant fields, and fields propagated with the speed of light in the form of a plane wave.[1] For constant (that is, slowly varying) fields, a renormalization of field strength and charge yields a modified lagrange function differing from that of the maxwell field by terms that imply a nonlinear behavior for the electromagnetic field. The result agrees precisely with one obtained some time ago by other methods and a somewhat different viewpoint.[2] The modified physical quantities characterizing the plane wave in the vacuum revert to those of the maxwell field after the same field strength renormalization. For weak arbitrarily varying fields, perturbation methods can be applied to the equations of motion. This will be discussed in Appendix A.

The consequences thus obtained are useful in connection with a class of problems in which gauge invari-

[1] That the Dirac equation can be solved exactly, in the field of a plane wave, was recognized by D. M. Volkow, Z. Physik **94**, 25 (1935).

[2] W. Heisenberg and H. Euler, Z. Physik **98**, 714 (1936). V. Weisskopf, Kgl. Danske Videnskab. Selskabs. Mat.-fys. Medd. **14**, No. 6 (1936).

ance difficulties have been encountered[3]—the multiple photon disintegration of a neutral meson. Without further extensive calculation, we shall obtain approximate gauge invariant expressions for the interaction of a zero-spin, neutral meson with two photons, where the intermediate nuclear interaction may be scalar, or the equivalent pseudoscalar and pseudovector couplings.

The utility of the proper-time technique to be exploited in this paper, apart from its value in obtaining rigorous solutions in a few special cases, lies in its isolation of the divergent aspects of a calculation in integrals with respect to the proper-time, a parameter that makes no reference to the coordinate system or the gauge. Indeed, we shall show that the customary perturbation procedure of expansion in powers of the potential vector does yield gauge invariant results, provided only that the proper-time integration is reserved to the last. The technique of "invariant regularization"[4] represents a partial realization of this proper-time method through the use of specially weighted integrals over the conjugate quantity, the square of the proper mass.

Finally, in Appendix B we shall employ the Green's function of an electron in a weak, homogeneous, external field to calculate the second-order electromagnetic mass, thereby providing a simple derivation of the second-order correction to the electron magnetic moment.

II. GENERAL THEORY

The field equations, commutation relations, and current vector of the Dirac field are given by[5]

$$\begin{aligned}&\gamma_\mu(-i\partial_\mu-eA_\mu(x))\psi(x)+m\psi(x)=0,\\&(i\partial_\mu-eA_\mu(x))\bar\psi(x)\gamma_\mu+m\bar\psi(x)=0,\end{aligned}\tag{2.1}$$

$$\{\psi(\mathbf{x},x_0),\bar\psi(\mathbf{x}',x_0)\}=\gamma_0\delta(\mathbf{x}-\mathbf{x}'),\tag{2.2}$$

$$j_\mu(x)=\tfrac{1}{2}e[\bar\psi(x),\gamma_\mu\psi(x)],\tag{2.3}$$

where

$$\tfrac{1}{2}\{\gamma_\mu,\gamma_\nu\}=-\delta_{\mu\nu}\tag{2.4}$$

and

$$\gamma_0=-i\gamma_4,\quad \gamma_0^2=1.\tag{2.5}$$

The structure of the current operator,

$$j_\mu(x)=-e(\gamma_\mu)_{\beta\alpha}\tfrac{1}{2}[\psi_\alpha(x),\bar\psi_\beta(x)],\tag{2.6}$$

which arises from an explicit charge symmetrization, can be related to a time symmetrization by introducing chronologically ordered operators. Thus, with the notation

$$(A(x_0)B(x_0'))_+=\begin{cases}A(x_0)B(x_0'), & x_0>x_0'\\ B(x_0')A(x_0), & x_0<x_0',\end{cases}\tag{2.7}$$

and

$$\epsilon(x-x')=\begin{cases}1, & x_0>x_0'\\ -1, & x_0<x_0',\end{cases}\tag{2.8}$$

we have

$$(\psi_\alpha(x)\bar\psi_\beta(x'))_+\epsilon(x-x')=\begin{cases}\psi_\alpha(x)\bar\psi_\beta(x'), & x_0>x_0'\\ -\bar\psi_\beta(x')\psi_\alpha(x), & x_0<x_0'.\end{cases}\tag{2.9}$$

Therefore

$$\tfrac{1}{2}[\psi_\alpha(x),\bar\psi_\beta(x)]=(\psi_\alpha(x)\bar\psi_\beta(x'))_+\epsilon(x-x')]_{x'\to x},\tag{2.10}$$

provided one takes the average of the forms obtained by letting x' approach x from the future, and from the past. The quantity of actual interest here is the expectation value of $j_\mu(x)$ in the vacuum of the Dirac field,

$$\langle j_\mu(x)\rangle=ie\,\mathrm{tr}\gamma_\mu G(x,x')]_{x'\to x},\tag{2.11}$$

where

$$G(x,x')=i\langle(\psi(x)\bar\psi(x'))_+\rangle\epsilon(x-x'),\tag{2.12}$$

and tr indicates the diagonal sum with respect to the spinor indices.

The function $G(x,x')$ satisfies an inhomogeneous differential equation which is obtained by noting that

$$\begin{aligned}&[\gamma(-i\partial-eA(x))+m]G(x\,x')\\&\quad=\langle\gamma_0\{\psi(x),\bar\psi(x')\}\rangle\delta(x_0-x_0'),\end{aligned}\tag{2.13}$$

where the right side expresses the discontinuous change in form of $G(x,x')$ as x_0 is altered from $x_0'-0$ to $x_0'+0$. According to Eq. (2.2), therefore, we have

$$[\gamma(-i\partial-eA(x))+m]G(x,x')=\delta(x-x');\tag{2.14}$$

that is, $G(x,x')$ is a Green's function for the Dirac field. We shall not discuss which particular Green's function this is, as specified by the associated boundary conditions, since no ambiguity enters if actual pair creation in the vacuum does not occur, which we shall expressly assume.

It is useful to regard $G(x,x')$ as the matrix element of an operator G, in which states are labeled by space-time coordinates as well as by the suppressed spinor indices:

$$G(x,x')=(x|G|x').\tag{2.15}$$

The defining differential equations for the Green's function is then considered to be a matrix element of the operator equation

$$(\gamma\Pi+m)G=1,\tag{2.16}$$

where

$$\Pi_\mu=p_\mu-eA_\mu\tag{2.17}$$

is characterized by the operator properties

$$[x_\mu,\Pi_\nu]=i\delta_{\mu\nu},\quad[\Pi_\mu,\Pi_\nu]=ieF_{\mu\nu},\tag{2.18}$$

and

$$F_{\mu\nu}=\partial_\mu A_\nu-\partial_\nu A_\mu\tag{2.19}$$

is the antisymmetrical field strength tensor.

With this symbolism, it is easy to show that the

[3] H. Fukuda and Y. Miyamoto, Prog. Theor. Phys. 4, 347 (1949).

[4] W. Pauli and F. Villars, Revs. Modern Phys. 21, 434 (1949).

[5] We employ units in which $\hbar=c=1$. Note that also $\bar\psi=\psi^\dagger\gamma_0$, since $\gamma_0\gamma_\mu$, $\mu=0,1,2,3$ form hermitian matrices.

vacuum current vector,

$$\langle j_\mu(x)\rangle = ie\,\mathrm{tr}\gamma_\mu(x|G|x), \tag{2.20}$$

is obtained from an action integral by variation of $A_\mu(x)$. This is accomplished by exhibiting

$$\delta W^{(1)} = \int (dx)\delta A_\mu(x)\langle j_\mu(x)\rangle = ie\,\mathrm{Tr}\gamma\delta A G \tag{2.21}$$

as a total differential, subject to $\delta A_\mu(x)$ vanishing at infinity. In the second version of $\delta W^{(1)}$, δA_μ denotes the operator with the matrix elements

$$(x|\,\delta A_\mu|\,x') = \delta(x-x')\delta A_\mu(x), \tag{2.22}$$

and Tr indicates the complete diagonal symmation, including spinor indices and the continuous space-time coordinates. Now

$$-e\gamma\delta A = \delta(\gamma\Pi+m), \tag{2.23}$$

and

$$G = \frac{1}{\gamma\Pi+m} = i\int_0^\infty ds\,\exp\{-i(\gamma\Pi+m)s\}, \tag{2.24}$$

so that

$ie\,\mathrm{Tr}\gamma\delta A G$

$$= \delta\left[i\int_0^\infty dss^{-1}\,\mathrm{Tr}\exp\{-i(\gamma\Pi+m)s\}\right], \tag{2.25}$$

in virtue of the fundamental property of the trace,

$$\mathrm{Tr}AB = \mathrm{Tr}BA. \tag{2.26}$$

Thus, to within an additive constant,

$$W^{(1)} = i\int_0^\infty dss^{-1}e^{-ims}\,\mathrm{Tr}\exp\{-i\gamma\Pi s\} = \int (dx)\mathfrak{L}^{(1)}(x), \tag{2.27}$$

where the lagrange function $\mathfrak{L}^{(1)}(x)$ is given by

$$\mathfrak{L}^{(1)}(x) = i\int_0^\infty dss^{-1}e^{-ims}\,\mathrm{tr}(x|\exp\{-i\gamma\Pi s\}|x). \tag{2.28}$$

An alternative representation, and the one we shall actually employ for calculations, is obtained by writing

$$G = (-\gamma\Pi+m)[m^2-(\gamma\Pi)^2]^{-1} = [m^2-(\gamma\Pi)^2]^{-1}(-\gamma\Pi+m) \tag{2.29}$$

or

$$G = (-\gamma\Pi+m)i\int_0^\infty ds\,\exp[-i(m^2-(\gamma\Pi)^2)s]$$

$$= i\int_0^\infty ds\,\exp[-i(m^2-(\gamma\Pi)^2)s](-\gamma\Pi+m). \tag{2.30}$$

In virtue of the vanishing trace of an odd number of γ-factors, we have

$ie\,\mathrm{Tr}\gamma\delta A G$

$$= -\mathrm{Tr}\delta(\gamma\Pi)\gamma\Pi\int_0^\infty ds\,\exp[-i(m^2-(\gamma\Pi)^2)s] \tag{2.31}$$

$$= \delta\left[\tfrac{1}{2}i\int_0^\infty dss^{-1}\exp[-i(m^2-(\gamma\Pi)^2)s]\right],$$

which again involves the fundamental trace property (2.26). Thus,

$$\mathfrak{L}^{(1)}(x) = \tfrac{1}{2}i\int_0^\infty dss^{-1}\exp(-im^2s)\,\mathrm{tr}(x|\,U(s)\,|x), \tag{2.32}$$

$$U(s) = \exp(-i\mathfrak{K}s),$$

where

$$\mathfrak{K} = -(\gamma\Pi)^2 = \Pi_\mu{}^2 - \tfrac{1}{2}e\sigma_{\mu\nu}F_{\mu\nu}, \tag{2.33}$$

and

$$\sigma_{\mu\nu} = \tfrac{1}{2}i[\gamma_\mu, \gamma_\nu]. \tag{2.34}$$

We now see that the construction of $G(x, x')$ and $\mathfrak{L}^{(1)}(x)$ devolves upon the evaluation of

$$(x'|\,U(s)\,|x'') = (x(s)'|\,x(0)'')\,. \tag{2.35}$$

The latter notation emphasizes that $U(s)$ may be regarded as the operator describing the development of a system governed by the "hamiltonian," $\mathfrak{K}$, in the "time" s, the matrix element of $U(s)$ being the transformation function from a state in which $x_\mu(s=0)$ has the value $x_\mu{}''$ to a state in which $x_\mu(s)$ has the value $x_\mu{}'$. Thus, we are led to an associated dynamical problem in which the space-time coordinates of a "particle" depend upon a proper time parameter, in a manner determined by the equations of motion

$$\begin{aligned} dx_\mu/ds &= -i[x_\mu, \mathfrak{K}] = 2\Pi_\mu, \\ d\Pi_\mu/ds &= -i[\Pi_\mu, \mathfrak{K}] = e(F_{\mu\nu}\Pi_\nu + \Pi_\nu F_{\mu\nu}) \\ &\quad + \tfrac{1}{2}e\sigma_{\lambda\nu}(\partial F_{\lambda\nu}/\partial x_\mu) = 2eF_{\mu\nu}\Pi_\nu \\ &\quad - ie(\partial F_{\mu\nu}/\partial x_\nu) + \tfrac{1}{2}e\sigma_{\lambda\nu}(\partial F_{\lambda\nu}/\partial x_\mu). \end{aligned} \tag{2.36}$$

The transformation function is characterized by the differential equations,[6]

$$i\partial_s(x(s)'|\,x(0)'') = (x(s)'|\,\mathfrak{K}\,|x(0)''), \tag{2.37}$$

$$(-i\partial_\mu' - eA_\mu(x'))(x(s)'|\,x(0)'') = (x(s)'|\,\Pi_\mu(s)\,|x(0)''), \tag{2.38}$$

$$(i\partial_\mu'' - eA_\mu(x''))(x(s)'|\,x(0)'') = (x(s)'|\,\Pi_\mu(0)\,|x(0)''), \tag{2.39}$$

and the boundary condition

$$(x(s)'|\,x(0)'')]_{s\to 0} = \delta(x'-x''). \tag{2.40}$$

[6] A proper time wave equation, in conjunction with the second-order Dirac operator, has been discussed by V. Fock, Physik. Z. Sowjetunion 12, 404 (1937). See also Y. Nambu, Prog. Theor. Phys. 5, 82 (1950).

We shall now illustrate, for the elementary situation $F_{\mu\nu}=0$, the procedure which will be employed in the following sections for constructing the transformation function.

The equations of motion read

$$d\Pi_\mu/ds=0, \quad dx_\mu/ds=2\Pi_\mu, \tag{2.41}$$

whence

$$\Pi_\mu(s)=\Pi_\mu(0), \tag{2.42}$$

and

$$(x_\mu(s)-x_\mu(0))/s=2\Pi_\mu(0). \tag{2.43}$$

Therefore

$$\begin{aligned}\mathfrak{K}=\Pi^2&=\tfrac{1}{4}s^{-2}(x(s)-x(0))^2=\tfrac{1}{4}s^{-2}[x^2(s)\\&\quad-2x(s)x(0)+x^2(0)]+\tfrac{1}{4}s^{-2}[x(s),x(0)]\\&=\tfrac{1}{4}s^{-2}[x^2(s)-2x(s)x(0)+x^2(0)]-2is^{-1},\end{aligned} \tag{2.44}$$

since

$$[x_\mu(s),x_\nu(0)]=[x_\mu(0)+2s\Pi_\mu(0),x_\nu(0)]=-2is\delta_{\mu\nu}, \tag{2.45}$$

Having ordered the coordinate operators so that $x(s)$ everywhere stands to the left of $x(0)$, we can immediately evaluate the matrix element of $\mathfrak{K}$ in Eq. (2.37), thus obtaining

$$\begin{aligned}&i\partial_s(x(s)'|x(0)'')\\&\quad=[\tfrac{1}{4}s^{-2}(x'-x'')^2-2is^{-1}](x(s)'|x(0)''),\end{aligned} \tag{2.46}$$

the solution of which is

$$(x(s)'|x(0)'')=C(x',x'')s^{-2}\exp[i\tfrac{1}{4}(x'-x'')^2/s]. \tag{2.47}$$

To determine the function $C(x',x'')$, we note that

$$\begin{aligned}(x(s)'|\Pi_\mu(s)|x(0)'')&=(x(s)'|\Pi_\mu(0)|x(0)'')\\&=((x_\mu'-x_\mu'')/2s)(x(s)'|x(0)''),\end{aligned} \tag{2.48}$$

which, in conjunction with Eqs. (2.38) and (2.39), implies that

$$\begin{aligned}&(-i\partial_\mu'-eA_\mu(x'))C(x',x'')\\&\quad=(i\partial_\mu''-eA_\mu(x''))C(x',x'')=0,\end{aligned} \tag{2.49}$$

or

$$\begin{aligned}&C(x',x'')=C\Phi(x',x''),\\&\Phi(x',x'')=\exp\left[ie\int_{x''}^{x'}dx_\mu A_\mu(x)\right].\end{aligned} \tag{2.50}$$

The line integral in Eq. (2.50) is independent of the integration path, since $F_{\mu\nu}=0$. Finally, the constant C is fixed by the boundary condition (2.40). It is evident that Eq. (2.47) does have the character of a delta-function as s approaches zero, provided

$$Cs^{-2}\int(dx)\exp(i\tfrac{1}{4}x^2/s)=1; \tag{2.51}$$

that is,

$$C=-i(4\pi)^{-2}. \tag{2.52}$$

Therefore,

$$\begin{aligned}(x(s)'|x(0)'')=-i(4\pi)^{-2}&\Phi(x',x'')s^{-2}\\&\times\exp[i\tfrac{1}{4}(x'-x'')^2/s],\end{aligned} \tag{2.53}$$

and the Green's function is obtained as

$$\begin{aligned}G(x',x'')&=i\int_0^\infty ds\exp(-im^2s)\\&\quad\times(x(s)'|(-\gamma\Pi+m)|x(0)'')\\&=(4\pi)^{-2}\Phi(x',x'')\int_0^\infty dss^{-2}\exp(-im^2s)\\&\quad\times\left(-\gamma\frac{(x'-x'')}{2s}+m\right)\exp\left[i\tfrac{1}{4}\frac{(x'-x'')^2}{s}\right].\end{aligned} \tag{2.54}$$

An equivalent, and more familiar procedure, is to employ the representation labeled by the eigenvalues of Π_μ. Now

$$\begin{aligned}(\Pi(s)'|\Pi(0)'')&=(\Pi(0)'|U(s)|\Pi(0)'')\\&=\delta(\Pi'-\Pi'')\exp(-i\Pi'^2s),\end{aligned} \tag{2.55}$$

while $(x(s)'|\Pi(s)')$ is determined by

$$\begin{aligned}&(-i\partial_\mu'-eA_\mu(x'))(x(s)'|\Pi(s)')\\&\quad=\Pi_\mu'(x(s)'|\Pi(s)'),\end{aligned} \tag{2.56}$$

and the normalization condition

$$\int(\Pi(s)'|x(s)')(dx')(x(s)'|\Pi(s)'')=\delta(\Pi'-\Pi''), \tag{2.57}$$

to be

$$\begin{aligned}&(x(s)'|\Pi(s)')\\&\quad=(2\pi)^{-2}\exp\left[ie\int_0^{x'}dxA\right]\exp(ix'\Pi').\end{aligned} \tag{2.58}$$

Therefore,

$$\begin{aligned}&(x(s)'|x(0)'')\\&\quad=\int(x(s)'|\Pi(s)')(d\Pi')(\Pi(s)'|\Pi(0)'')\\&\qquad\times(d\Pi'')(\Pi(0)''|x(0)'')\\&\quad=(2\pi)^{-4}\Phi(x',x'')\int(d\Pi')\\&\qquad\times\exp[i(x'-x'')\Pi'-i\Pi'^2s],\end{aligned} \tag{2.59}$$

and

$$\begin{aligned}G(x',x'')&=i(2\pi)^{-4}\Phi(x',x'')\\&\quad\times\int_0^\infty ds\int(d\Pi')\exp[i(x'-x'')\Pi']\\&\quad\times(-\gamma\Pi'+m)\exp[-i(\Pi'^2+m^2)s],\end{aligned} \tag{2.60}$$

which reduce to Eqs. (2.53) and (2.54) on performance of the Π' integration.

III. CONSTANT FIELDS

The equations of motion (2.36) here simplify to

$$dx_\mu/ds=2\Pi_\mu, \quad d\Pi_\mu/ds=2eF_{\mu\nu}\Pi_\nu, \tag{3.1}$$

or, in matrix notation,

$$dx/ds=2\Pi, \quad d\Pi/ds=2eF\Pi. \tag{3.2}$$

The symbolic solution of these equations is

$$\begin{aligned}\Pi(s)&=e^{2eFs}\Pi(0),\\ x(s)-x(0)&=[(e^{2eFs}-1)/eF]\Pi(0),\end{aligned} \tag{3.3}$$

whence

$$\begin{aligned}\Pi(0)&=eF(e^{2eFs}-1)^{-1}(x(s)-x(0))\\ &=\tfrac{1}{2}eFe^{-eFs}\sinh^{-1}(eFs)(x(s)-x(0)),\end{aligned} \tag{3.4}$$

and

$$\begin{aligned}\Pi(s)&=\tfrac{1}{2}eFe^{eFs}\sinh^{-1}(eFs)(x(s)-x(0))\\ &=(x(s)-x(0))\tfrac{1}{2}eFe^{-eFs}\sinh^{-1}(eFs).\end{aligned} \tag{3.5}$$

The latter form involves the fact that

$$\tilde{F}=-F, \quad (F_{\mu\nu}=-F_{\nu\mu}). \tag{3.6}$$

We now consider

$$\begin{aligned}\mathcal{K}+\tfrac{1}{2}e\sigma F=\Pi^2(s)&=(x(s)-x(0))K(x(s)-x(0)),\\ K&=\tfrac{1}{4}e^2F^2\sinh^{-2}(eFs).\end{aligned} \tag{3.7}$$

In rearranging the order of these operators, the following commutator is required:

$$\begin{aligned}[x(s),x(0)]&=[x(0)+(eF)^{-1}(e^{2eFs}-1)\Pi(0),x(0)]\\ &=i(eF)^{-1}(e^{2eFs}-1).\end{aligned} \tag{3.8}$$

Thus

$$\begin{aligned}\mathcal{K}+\tfrac{1}{2}e\sigma F=x(s)Kx(s)&-2x(s)Kx(0)+x(0)Kx(0)\\ &-\tfrac{1}{2}i\,\mathrm{tr}eF\coth(eFs),\end{aligned} \tag{3.9}$$

where tr again denotes a diagonal summation, and we have employed the fact that

$$\mathrm{tr}(F)=0, \tag{3.10}$$

which follows from Eq. (3.6). The resulting differential equation (2.37)

$$\begin{aligned}i\partial_s(x(s)'|x(0)'')=[&-\tfrac{1}{2}e\sigma F+(x'-x'')K(x'-x'')\\ &-\tfrac{1}{2}i\,\mathrm{tr}eF\coth(eFs)](x(s)'|x(0)''),\end{aligned} \tag{3.11}$$

has the solution

$$\begin{aligned}(x(s)'|x(0)'')=C(x',x'')&e^{-L(s)}s^{-2}\\ \times\exp[&\tfrac{1}{4}i(x'-x'')eF\coth(eFs)(x'-x'')]\\ &\cdot\exp(i\tfrac{1}{2}e\sigma Fs),\end{aligned} \tag{3.12}$$

$$L(s)=\tfrac{1}{2}\,\mathrm{tr}\ln[(eFs)^{-1}\sinh(eFs)].$$

To determine $C(x',x'')$, we employ

$$\begin{aligned}(x(s)'|\Pi(s)|x(0)'')=&\tfrac{1}{2}[eF\coth(eFs)+eF]\\ &\times(x'-x'')(x(s)'|x(0)''),\end{aligned} \tag{3.13}$$

and

$$\begin{aligned}(x(s)'|\Pi(0)|x(0)'')=&\tfrac{1}{2}[eF\coth(eFs)-eF]\\ &\times(x'-x'')(x(s)'|x(0)''),\end{aligned} \tag{3.14}$$

in conjunction with Eq. (3.12), to obtain the differential equations

$$[-i\partial_\mu'-eA_\mu(x')-\tfrac{1}{2}eF_{\mu\nu}(x'-x'')_\nu]C(x',x'')=0, \tag{3.15}$$

$$[i\partial_\mu''-eA_\mu(x'')-\tfrac{1}{2}eF_{\mu\nu}(x'-x'')_\nu]C(x',x'')=0. \tag{3.16}$$

The solution of Eq. (3.15) has the form

$$\begin{aligned}C(x',x'')&\\ =C(x'')\exp&\left[ie\int_{x''}^{x'}dx(A(x)+\tfrac{1}{2}F(x-x''))\right],\end{aligned} \tag{3.17}$$

in which the integral is independent of the integration path, since $A_\mu(x)+\frac{1}{2}F_{\mu\nu}(x-x'')_\nu$ has a vanishing curl. However, by restricting the integration path to be a straight line connecting x' and x'', we may, in virtue of Eq. (3.6), simply write

$$\begin{aligned}C(x',x'')&=C\Phi(x',x''),\\ \Phi(x',x'')&=\exp\left[ie\int_{x''}^{x'}dxA(x)\right],\end{aligned} \tag{3.18}$$

and, with C a constant, attain the solution of (3.15) and (3.16). The constant C has the value

$$C=-i(4\pi)^{-2} \tag{3.19}$$

since the limiting form of $(x(s)'|x(0)'')$ as $s\to 0$ is independent of the external field.

Finally, then

$$\begin{aligned}(x(s)'|x(0)'')=-i(4\pi)^{-2}&\Phi(x',x'')e^{-L(s)}s^{-2}\\ \times\exp[&i\tfrac{1}{4}(x'-x'')eF\coth(eFs)(x'-x'')]\\ &\cdot\exp[i\tfrac{1}{2}e\sigma Fs],\end{aligned} \tag{3.20}$$

and the Green's function $G(x',x'')$ is obtained from (2.30) in the two equivalent forms,

$$\begin{aligned}G(x',x'')&=i\int_0^\infty ds\exp(-im^2s)\\ &\quad\times[-\gamma_\mu(x(s)'|\Pi_\mu(s)|x(0)'')\\ &\qquad+m(x(s)'|x(0)'')]\\ &=i\int_0^\infty ds\exp(-im^2s)\\ &\quad\times[-(x(s)'|\Pi_\mu(0)|x(0)'')\gamma_\mu\\ &\qquad+m(x(s)'|x(0)'')],\end{aligned} \tag{3.21}$$

which will be given explicitly on substituting Eqs. (3.13), (3.14), and (3.20).

The lagrange function $\mathfrak{L}^{(1)}(x)$ is now computed as

$$\begin{aligned}\mathfrak{L}^{(1)}(x)&=\tfrac{1}{2}i\int_0^\infty dss^{-1}\exp(-im^2s)\\ &\qquad\times\mathrm{tr}(x(s)'|x(0)'')]_{x',x''\to x}\\ &=(1/32\pi^2)\int_0^\infty dss^{-3}\exp(-im^2s)\\ &\qquad\times e^{-L(s)}\,\mathrm{tr}\exp(i\tfrac{1}{2}e\sigma Fs).\end{aligned} \tag{3.22}$$

We may exhibit this more explicitly as a real quantity by a deformation of the integration path, which is

effectively the substitution $s\rightarrow -is$:

$$\mathfrak{L}^{(1)}(x)=-(1/32\pi^2)\int_0^\infty dss^{-3}\exp(-m^2s)\times e^{-l(s)}\operatorname{tr}\exp(\tfrac{1}{2}e\sigma Fs),$$
$$l(s)=\tfrac{1}{2}\operatorname{tr}\ln[(eFs)^{-1}\sin(eFs)]. \tag{3.23}$$

Indeed, we could have initially employed the integral representation

$$[m^2-(\gamma\Pi)^2]^{-1}=\int_0^\infty ds\exp[-(m^2-(\gamma\Pi)^2)s], \tag{3.24}$$

which exists in consequence of the restriction on real pair creation. This, however, would have obscured the proper time interpretation.

To evaluate the Dirac matrix trace, we employ the following spin matrix property:

$$\tfrac{1}{2}\{\sigma_{\mu\nu},\sigma_{\lambda\kappa}\}=\delta_{\mu\lambda}\delta_{\nu\kappa}-\delta_{\mu\kappa}\delta_{\nu\lambda}+i\epsilon_{\mu\nu\lambda\kappa}\gamma_5, \tag{3.25}$$

where

$$\gamma_5=i\gamma_1\gamma_2\gamma_3\gamma_4,\quad \gamma_5{}^2=-1, \tag{3.26}$$

and $\epsilon_{\mu\nu\lambda\kappa}$ is 1, or -1, if $(\mu\nu\lambda\kappa)$ forms an even, or odd permutation of (1234), and is zero otherwise. In terms of the dual field strength tensor,

$$F_{\mu\nu}{}^*=\tfrac{1}{2}i\epsilon_{\mu\nu\lambda\kappa}F_{\lambda\kappa}, \tag{3.27}$$

we have

$$(\tfrac{1}{2}\sigma_{\mu\nu}F_{\mu\nu})^2=\tfrac{1}{2}F_{\mu\nu}{}^2+\tfrac{1}{2}\gamma_5F_{\mu\nu}F_{\mu\nu}{}^*, \tag{3.28}$$

thus introducing the fundamental scalar

$$\mathfrak{F}=\tfrac{1}{4}F_{\mu\nu}{}^2=\tfrac{1}{2}(\mathbf{H}^2-\mathbf{E}^2), \tag{3.29}$$

and pseudoscalar

$$\mathfrak{G}=\tfrac{1}{4}F_{\mu\nu}F_{\mu\nu}{}^*=\mathbf{E}\cdot\mathbf{H} \tag{3.30}$$

constructed from the field strengths. Since

$$(\tfrac{1}{2}\sigma F)^2=2(\mathfrak{F}+\gamma_5\mathfrak{G}), \tag{3.31}$$

and $\gamma_5{}^2=-1$, it follows that $\frac{1}{2}\sigma F$ has the four eigenvalues

$$(\tfrac{1}{2}\sigma F)'=\pm(2(\mathfrak{F}\pm i\mathfrak{G}))^{\frac{1}{2}}. \tag{3.32}$$

Therefore,

$$\operatorname{tr}\exp(\tfrac{1}{2}e\sigma Fs)=4\operatorname{Re}\cosh es(2(\mathfrak{F}+i\mathfrak{G}))^{\frac{1}{2}}\equiv 4\operatorname{Re}\cosh esX, \tag{3.33}$$

where Re denotes the real part of the subsequent expression. Note, incidentally, that

$$X^2=(\mathbf{H}+i\mathbf{E})^2. \tag{3.34}$$

The eigenvalues of the matrix $F=(F_{\mu\nu})$ are required for the construction of $\exp(-l(s))$. They can be obtained with the aid of the easily verifiable relations,

$$F_{\mu\lambda}F_{\lambda\nu}{}^*=-\delta_{\mu\nu}\mathfrak{G}, \tag{3.35}$$

and

$$F_{\mu\lambda}{}^*F_{\lambda\nu}{}^*-F_{\mu\lambda}F_{\lambda\nu}=2\delta_{\mu\nu}\mathfrak{F}. \tag{3.36}$$

From the eigenvalue equation

$$F_{\mu\nu}\psi_\nu=F'\psi_\mu, \tag{3.37}$$

and its equivalent according to Eq. (3.35),

$$F_{\mu\nu}{}^*\psi_\nu=-(1/F')\mathfrak{G}\psi_\mu, \tag{3.38}$$

we obtain by iteration:

$$F_{\mu\lambda}F_{\lambda\nu}\psi_\nu=(F')^2\psi_\mu,\quad F_{\mu\lambda}{}^*F_{\lambda\nu}{}^*\psi_\nu=(1/(F')^2)\mathfrak{G}^2\psi_\mu. \tag{3.39}$$

The identity (3.36) then yields the eigenvalue equation

$$(F')^4+2\mathfrak{F}(F')^2-\mathfrak{G}^2=0, \tag{3.40}$$

which has the solutions $\pm F^{(1)}$, $\pm F^{(2)}$, with

$$F^{(1)}=(i/\sqrt{2})[(\mathfrak{F}+i\mathfrak{G})^{\frac{1}{2}}+(\mathfrak{F}-i\mathfrak{G})^{\frac{1}{2}}],$$
$$F^{(2)}=(i/\sqrt{2})[(\mathfrak{F}+i\mathfrak{G})^{\frac{1}{2}}-(\mathfrak{F}-i\mathfrak{G})^{\frac{1}{2}}]. \tag{3.41}$$

Expressed in terms of these eigenvalues,

$$e^{-l(s)}=(es)^2F^{(1)}F^{(2)}/\sin(eF^{(1)}s)\sin(eF^{(2)}s)=\frac{2(es)^2F^{(1)}F^{(2)}}{\cos es(F^{(1)}-F^{(2)})-\cos es(F^{(1)}+F^{(2)})}, \tag{3.42}$$

or

$$e^{-l(s)}=(es)^2\mathfrak{G}/\operatorname{Im}\cosh esX, \tag{3.43}$$

where Im designates the imaginary part of the following expression.

The final result for $\mathfrak{L}^{(1)}$ is

$$\mathfrak{L}^{(1)}=-\frac{1}{8\pi^2}\int_0^\infty dss^{-3}\exp(-m^2s)\times\left[(es)^2\mathfrak{G}\frac{\operatorname{Re}\cosh esX}{\operatorname{Im}\cosh esX}-1\right], \tag{3.44}$$

in which we have supplied the additive constant necessary to make $\mathfrak{L}^{(1)}$ vanish in the absence of a field. The first term in the expansion of $\mathfrak{L}^{(1)}$ for weak fields is

$$\mathfrak{L}^{(1)}\simeq-\frac{e^2}{12\pi^2}\int_0^\infty dss^{-1}\exp(-m^2s)\mathfrak{F}. \tag{3.45}$$

On separating this explicitly, and adding the lagrange function of the maxwell field,

$$\mathfrak{L}^{(0)}=-\mathfrak{F}=\tfrac{1}{2}(\mathbf{E}^2-\mathbf{H}^2), \tag{3.46}$$

we obtain the total lagrange function

$$\mathfrak{L}=-\left[1+\frac{e^2}{12\pi^2}\int_0^\infty dss^{-1}\exp(-m^2s)\right]\mathfrak{F}-\frac{1}{8\pi}\int_0^\infty dss^{-3}\exp(-m^2s)\times\left[(es)^2\frac{\operatorname{Re}\cosh esX}{\operatorname{Im}\cosh esX}-1-\tfrac{2}{3}(es)^2\mathfrak{F}\right]. \tag{3.47}$$

The logarithmically divergent factor that multiplies the maxwell lagrange function may be absorbed by a change of scale for all fields, and a corresponding scale change, or renormalization, of charge. If we identify the quantities thus far employed by a zero subscript, and introduce new units of field strength and charge according to

$$\begin{gathered}\mathfrak{F}+i\mathfrak{G}=(1+Ce_0^2)(\mathfrak{F}_0+i\mathfrak{G}_0),\\ e^2=e_0^2/(1+Ce_0^2),\\ C=\frac{1}{12\pi^2}\int_0^\infty ds\, s^{-1}\exp(-m^2s),\end{gathered}\tag{3.48}$$

we obtain the finite, gauge invariant result

$$\begin{aligned}\mathfrak{L}=&-\mathfrak{F}-\frac{1}{8\pi^2}\int_0^\infty dss^{-3}\exp(-m^2s)\\ &\times\left[(es)^2\mathfrak{G}\frac{\operatorname{Re}\cosh esX}{\operatorname{Im}\cosh esX}-1-\tfrac{2}{3}(es)^2\mathfrak{F}\right]\\ =&\tfrac{1}{2}(\mathbf{E}^2-\mathbf{H}^2)+\frac{2\alpha^2}{45}\frac{(\hbar/mc)^3}{mc^2}\\ &\times[(\mathbf{E}^2-\mathbf{H}^2)^2+7(\mathbf{E}\cdot\mathbf{H})^2]+\cdots.\end{aligned}\tag{3.49}$$

In the latter expansion, the conventional rationalized units have been reinstated, and $\alpha=e^2/4\pi\hbar c$.

Incidentally, the addition to the lagrange function produced by a spin zero charged field is obtained from Eq. (3.23) by omitting the Dirac trace, and multiplying by (-2). Thus,

$$\begin{aligned}\mathfrak{L}_{\text{spin }0}{}^{(1)}=&\frac{1}{16\pi^2}\int_0^\infty dss^{-3}\exp(-\mu^2s)\\ &\times\left[\frac{(es)^2\mathfrak{G}}{\operatorname{Im}\cosh esX}-1\right],\end{aligned}\tag{3.50}$$

in which μ designates the mass of the spinless particle, and an additive constant has been supplied as in Eq. (3.44). The first term in the expansion for weak fields is separated explicitly by writing

$$\begin{aligned}\mathfrak{L}_0{}^{(1)}=&-\frac{e^2}{48\pi^2}\int_0^\infty dss^{-1}\exp(-\mu^2s)\mathfrak{F}\\ &+\frac{1}{16\pi^2}\int_0^\infty dss^{-3}\exp(-\mu^2s)\\ &\times\left[\frac{(es)^2\mathfrak{G}}{\operatorname{Im}\cosh esX}-1+\tfrac{1}{3}(es)^2\mathfrak{F}\right].\end{aligned}\tag{3.51}$$

If we take into account the existence of both spin 0 and spin $\frac{1}{2}$ charged fields,

$$\mathfrak{L}=\mathfrak{L}^{(0)}+\mathfrak{L}_0{}^{(1)}+\mathfrak{L}_{\frac{1}{2}}{}^{(1)},\tag{3.52}$$

and a renormalization of the form (3.48), with

$$\begin{aligned}C=&C_0+C_{\frac{1}{2}}\\ =&\frac{1}{48\pi^2}\int_0^\infty dss^{-1}\exp(-\mu^2s)\\ &+\frac{1}{12\pi^2}\int_0^\infty dss^{-1}\exp(-m^2s),\end{aligned}\tag{3.53}$$

yields

$$\begin{aligned}\mathfrak{L}=&-\mathfrak{F}-\frac{1}{8\pi^2}\int_0^\infty dss^{-3}\exp(-m^2s)\\ &\times[(es)^2\mathfrak{G}(\operatorname{Re}/\operatorname{Im})-1-\tfrac{2}{3}(es)^2\mathfrak{F}]\\ &+\frac{1}{16\pi^2}\int_0^\infty dss^{-3}\exp(-\mu^2s)\\ &\times[(es)^2\mathfrak{G}(1/\operatorname{Im})-1+\tfrac{1}{3}(es)^2\mathfrak{F}]\\ =&\tfrac{1}{2}(\mathbf{E}^2-\mathbf{H}^2)+\frac{2\alpha^2}{45}\frac{(\hbar/mc)^3}{mc^2}[(\mathbf{E}^2-\mathbf{H}^2)^2+7(\mathbf{E}\cdot\mathbf{H})^2]\\ &+\frac{\alpha^2}{90}\frac{(\hbar/\mu c)^3}{\mu c^2}\left[\frac{7}{4}(\mathbf{E}^2-\mathbf{H}^2)^2+(\mathbf{E}\cdot\mathbf{H})^2\right]+\cdots.\end{aligned}\tag{3.54}$$

The physical quantities characterizing the field are comprised in the energy momentum tensor

$$\begin{aligned}T_{\mu\nu}=&\delta_{\mu\nu}\mathfrak{L}-(\partial\mathfrak{L}/\partial F_{\rho\lambda})F_{\nu\lambda}\\ =&-(F_{\mu\lambda}F_{\nu\lambda}-\delta_{\mu\nu}\tfrac{1}{4}F_{\lambda\kappa}{}^2)(\partial\mathfrak{L}/\partial\mathfrak{F})\\ &+\delta_{\mu\nu}(\mathfrak{L}-\mathfrak{F}(\partial\mathfrak{L}/\partial\mathfrak{F})-\mathfrak{G}\partial\mathfrak{L}/\partial\mathfrak{G}).\end{aligned}\tag{3.55}$$

The maxwell tensor

$$T_{\mu\nu}{}^{(M)}=F_{\mu\rho}F_{\rho\lambda}-\delta_{\mu\nu}\tfrac{1}{4}F_{\lambda\kappa}{}^2\tag{3.56}$$

is obtained from $\mathfrak{L}=-\mathfrak{F}$, the weak field approximation of Eq. (3.49). The next terms in the expansion of $\mathfrak{L}$ yield

$$\begin{aligned}T_{\mu\nu}=&T_{\mu\nu}{}^M\left(1-\frac{16}{45}\alpha^2\frac{(\hbar/mc)^3}{mc^2}\mathfrak{F}\right)\\ &-\delta_{\mu\nu}\frac{2}{45}\alpha^2\frac{(\hbar/mc)^3}{mc^2}(4\mathfrak{F}^2+7\mathfrak{G}^2)+\cdots.\end{aligned}\tag{3.57}$$

IV. PLANE WAVE FIELDS

A plane wave, traveling with the speed of light, is characterized by the field strength tensor

$$F_{\mu\nu}=f_{\mu\nu}F(\xi),\quad \xi=n_\mu x_\mu,\tag{4.1}$$

where n_μ is a null vector,

$$n_\mu{}^2=0,\tag{4.2}$$

and $F(\xi)$ is an arbitrary function. The constant tensor $f_{\mu\nu}$, and its dual $f_{\mu\nu}{}^*$, are restricted by the conditions

$$n_\mu f_{\mu\nu}=0,\quad n_\mu f_{\mu\nu}{}^*=0,\tag{4.3}$$

from which are derived

$$f_{\mu\lambda}f_{\lambda\nu}^{*}=0,\quad f_{\mu\lambda}f_{\lambda\nu}=f_{\mu\lambda}^{*}f_{\lambda\nu}^{*}=-n_{\mu}n_{\nu}. \tag{4.4}$$

The latter statement also includes a convention concerning the scale of $f_{\mu\nu}$.

The proper time equations of motion in this external field,

$$\begin{aligned} dx_{\mu}/ds&=2\Pi_{\mu},\\ d\Pi_{\mu}/ds&=2eF(\xi)f_{\mu\nu}\Pi_{\nu}+n_{\mu}eF'(\xi)\tfrac{1}{2}\sigma_{\lambda\nu}f_{\mu\nu}, \end{aligned} \tag{4.5}$$

admit several first integrals. Thus

$$d(n_{\mu}\Pi_{\mu}(s))/ds=0, \tag{4.6}$$

and

$$d(f_{\mu\nu}^{*}\Pi_{\nu}(s))/ds=0. \tag{4.7}$$

In addition,

$$d(f_{\mu\nu}\Pi_{\nu}(s))/ds=-n_{\mu}eF(\xi)d\xi/ds, \tag{4.8}$$

since

$$d\xi/ds=2n\Pi; \tag{4.9}$$

and therefore

$$d(f_{\mu\nu}\Pi_{\nu}+n_{\mu}eA(\xi))/ds=0, \tag{4.10}$$

where

$$dA(\xi)/d\xi=F(\xi). \tag{4.11}$$

In arriving at Eq. (4.10), it is necessary to recognize that $d\xi/ds$ commutes with ξ, in virtue of

$$[\xi, n\Pi]=[n_{\mu}x_{\mu}, n_{\nu}\Pi_{\nu}]=in_{\mu}^{2}=0. \tag{4.12}$$

Since $n\Pi$ is a constant of the motion, Eq. (4.9) can be integrated to yield

$$(\xi(s)-\xi(0))/s=2n\Pi, \tag{4.13}$$

from which we infer that

$$[\xi(s), \xi(0)]=2s[n\Pi, \xi(0)]=0. \tag{4.14}$$

The constant vector encountered on integration of Eq. (4.10),

$$f_{\mu\nu}\Pi_{\nu}+n_{\mu}eA(\xi)=C_{\mu}, \tag{4.15}$$

has the following evident properties:

$$\begin{aligned} &n_{\mu}C_{\mu}=0,\quad f_{\mu\nu}^{*}C_{\nu}=0,\quad f_{\mu\nu}C_{\nu}=-n_{\mu}n\Pi,\\ &C_{\mu}^{2}=(n\Pi)^{2}. \end{aligned} \tag{4.16}$$

The elimination of $f_{\mu\nu}\Pi_{\nu}$ from the equation of motion, with the aid of Eq. (4.15), gives

$$\begin{aligned} d\Pi_{\mu}/ds=(d/d\xi)[&2C_{\mu}eA(\xi)-n_{\mu}e^{2}A^{2}(\xi)\\ &+n_{\mu}eF(\xi)\tfrac{1}{2}\sigma f], \end{aligned} \tag{4.17}$$

whence

$$\begin{aligned} \Pi_{\mu}=\tfrac{1}{2}dx_{\mu}/ds=(1/2n\Pi)[&2C_{\mu}eA(\xi)-n_{\mu}e^{2}A^{2}(\xi)\\ &+n_{\mu}eF(\xi)\tfrac{1}{2}\sigma f]+D_{\mu}, \end{aligned} \tag{4.18}$$

where D_{μ} is an integration constant. Note, incidentally, that

$$f_{\mu\nu}^{*}\Pi_{\nu}=f_{\mu\nu}^{*}D_{\nu}, \tag{4.19}$$

which is independent of s, in agreement with Eq. (4.7).

On integrating Eq. (4.18) with respect to s, we find that

$$\begin{aligned} x_{\mu}(s)-x_{\mu}(0)=-\frac{1}{2(n\Pi)^{2}}\int_{\xi(0)}^{\xi(s)}d\xi[&2C_{\mu}eA(\xi)-n_{\mu}e^{2}A^{2}(\xi)\\ &+n_{\mu}eF(\xi)\tfrac{1}{2}\sigma f]+2D_{\mu}s. \end{aligned} \tag{4.20}$$

With the constant D_{μ} determined by Eq. (4.20), Eq. (4.18) states that

$$\begin{aligned} \Pi_{\mu}(s)=&\frac{(x_{\mu}(s)-x_{\mu}(0))}{2s}+\frac{s}{(\xi(s)-\xi(0))}\\ &\times[2C_{\mu}eA(\xi(s))-n_{\mu}e^{2}A^{2}(\xi(s))+n_{\mu}eF(\xi(s))\tfrac{1}{2}\sigma f]\\ &-\frac{s}{(\xi(s)-\xi(0))^{2}}\int_{\xi(0)}^{\xi(s)}d\xi[2C_{\mu}eA(\xi)\\ &-n_{\mu}e^{2}A^{2}(\xi)+n_{\mu}eF(\xi)\tfrac{1}{2}\sigma f]. \end{aligned} \tag{4.21}$$

We can finally evaluate C_{μ} as

$$\begin{aligned} C_{\mu}&=f_{\mu\nu}\Pi_{\nu}+n_{\mu}eA\\ &=\frac{f_{\mu\nu}(x_{\nu}(s)-x_{\nu}(0))}{2s}+\frac{n_{\mu}}{\xi(s)-\xi(0)}\int_{\xi(0)}^{\xi(s)}d\xi eA(\xi). \end{aligned} \tag{4.22}$$

The commutation properties of these operators are involved in the construction of the transformation function. As is already indicated in the commutativity of $\xi(s)$ and $\xi(0)$, these commutation relations are greatly simplified by the special nature of the external field. Thus to evaluate $[x_{\mu}(0), x_{\mu}(s)]$, we employ Eq. (4.21) to express $x_{\mu}(0)$ in terms of $x_{\mu}(s)$, $\Pi_{\mu}(s)$, $\xi(s)$, and $\xi(0)$. Now

$$[\xi(0), x_{\mu}(s)]=[\xi(s)-2sn\Pi, x_{\mu}(s)]=2isn_{\mu}, \tag{4.23}$$

and, in virtue of $n_{\mu}C_{\mu}=n_{\mu}^{2}=0$, we have simply

$$[x_{\mu}(s), x_{\mu}(0)]=[-2s\Pi_{\mu}(s), x_{\mu}(s)]=8is. \tag{4.24}$$

No other nonvanishing commutator intervenes in bringing $\mathfrak{K}$ to the form

$$\begin{aligned} \mathfrak{K}=&\tfrac{1}{4}s^{-2}(x_{\mu}^{2}(s)-2x_{\mu}(s)x_{\mu}(0)+x_{\mu}^{2}(0))-2is^{-1}\\ &+\frac{1}{\xi(s)-\xi(0)}\int_{\xi(0)}^{\xi(s)}d\xi[e^{2}A^{2}(\xi)-eF(\xi)\tfrac{1}{2}\sigma f]\\ &-\frac{1}{(\xi(s)-\xi(0))^{2}}\left[\int_{\xi(0)}^{\xi(s)}d\xi eA(\xi)\right]^{2}, \end{aligned} \tag{4.25}$$

in which a constant added to $A(\xi)$ is without effect, as required by the corresponding ambiguity of Eq. (4.11).

The solution of the differential equation (2.37) is

$$\begin{aligned} (x(s)'\,|\,x(0)'')=&C(x', x'')s^{-2}\exp[i\tfrac{1}{4}(x'-x'')^{2}/s]\\ &\times\exp\left[-is/(\xi'-\xi'')\int_{\xi''}^{\xi'}d\xi[e^{2}A^{2}-eF\tfrac{1}{2}\sigma f]\right]\\ &\times\exp\left[is\left(1/(\xi'-\xi'')\int_{\xi''}^{\xi'}d\xi eA\right)^{2}\right], \end{aligned} \tag{4.26}$$

where

$$\xi'=n_\mu x_\mu', \quad \xi''=n_\mu x_\mu''. \tag{4.27}$$

The function $C(x', x'')$ is determined by the differential equations (2.38) and (2.39), in conjunction with Eq. (4.26). Thus,

$$\left[-i\partial_\mu'-eA_\mu(x')-f_{\mu\nu}(x'-x'')_\nu\frac{1}{\xi'-\xi''}\left(eA(\xi')\right.\right.$$
$$\left.\left.-\frac{1}{\xi'-\xi''}\int_{\xi''}^{\xi'}d\xi eA(\xi)\right)\right]C(x', x'')=0. \tag{4.28}$$

The solution of this equation will be obtained in terms of a line integral which is independent of the integration path. Again choosing the path to be a straight line, we find simply

$$C(x', x'')=C\exp\left[ie\int_{x''}^{x'}dx_\mu A_\mu(x)\right]=C\Phi(x', x''), \tag{4.29}$$

in view of the antisymmetry of $f_{\mu\nu}$. It is evident that

$$C=-i(4\pi)^{-2}. \tag{4.30}$$

Only the behavior of the transformation function for $x_\mu'\simeq x_\mu''$ is of actual interest in applications to vacuum polarization phenomena. Now for $\xi'\simeq\xi''$,

$$\frac{1}{\xi'-\xi''}\int_{\xi''}^{\xi'}d\xi A^2(\xi)-\left[\frac{1}{\xi'-\xi''}\int_{\xi''}^{\xi'}d\xi A(\xi)\right]^2$$
$$\simeq\tfrac{1}{12}(\xi'-\xi'')^2F^2[\tfrac{1}{2}(\xi'+\xi'')], \tag{4.31}$$

and

$$(\xi'-\xi'')^2F^2=(x'-x'')_\mu n_\mu F^2 n_\nu(x'-x'')_\nu$$
$$=-(x'-x'')_\mu F_{\mu\lambda}F_{\lambda\nu}(x'-x'')_\nu, \tag{4.32}$$

according to Eqs. (4.1) and (4.4). Therefore, for $x_\mu'\simeq x_\mu''$

$$(x(s)'|x(0)'')\simeq-i(4\pi)^{-2}\Phi(x', x'')s^{-2}$$
$$\times\exp[i\tfrac{1}{2}s^{-1}(x'-x'')_\mu(\delta_{\mu\nu}+\tfrac{1}{3}(es)^2F_{\mu\lambda}F_{\lambda\nu})(x'-x'')_\nu]$$
$$\times\exp(\tfrac{1}{2}ie\sigma_{\mu\nu}F_{\mu\nu}s), \tag{4.33}$$

which is identical with the transformation function for a constant field, as simplified by the special characteristics of the field now under consideration; namely,

$$\mathfrak{F}=0, \quad \mathfrak{G}=0. \tag{4.34}$$

We can conclude, without further calculation, that the physical quantities characterizing the plane wave field, the components of the energy-momentum tensor $T_{\mu\nu}$, will be identical in form with those of a constant field that obeys Eq. (4.34). On referring to Eq. (3.57), we see that $T_{\mu\nu}$ for a plane wave is just that of the maxwell field, which may be simplified further to

$$T_{\mu\nu}=F_{\mu\lambda}F_{\nu\lambda}=n_\mu n_\nu F^2(\xi). \tag{4.35}$$

Thus, there are no nonlinear vacuum phenomena for a single plane wave, of arbitrary strength and spectral composition.

V. γ-DECAY OF NEUTRAL MESONS

In this section we shall apply the results of our proper-time method to compute the effective coupling between a zero spin neutral meson and the electromagnetic field, as produced by the polarization of the proton vacuum. This interaction manifests itself in a spontaneous decay of the neutral meson into two photons.

The lagrange function for a spinless neutral meson field, in scalar interaction with the proton-antiproton field, is given by

$$\mathfrak{L}=-\tfrac{1}{2}[(\partial_\nu\phi)^2+\mu^2\phi^2]-g\phi\tfrac{1}{2}[\bar\psi, \psi]. \tag{5.1}$$

To find an approximate expression for the resultant coupling between the neutral meson field and the electromagnetic field, we replace $\frac{1}{2}[\bar\psi, \psi]$ by its vacuum expectation value, calculated in the presence of a homogeneous electromagnetic field. The use of the latter to represent the photons emitted in the spontaneous neutral meson decay introduces a small error, which is measured by the square of the meson-proton mass ratio, $(\mu/M)^2\simeq 1/40$. On the other hand, by ignoring the effect of the meson field on the proton vacuum, we obtain only the initial approximation of a perturbation treatment. Now

$$\langle\tfrac{1}{2}[\bar\psi(x), \psi(x)]\rangle=i\,\mathrm{tr}G(x, x)$$
$$=-M\int_0^\infty ds\exp(-iM^2s)\,\mathrm{tr}(x|\,U(s)\,|x)$$
$$=-\partial\mathfrak{L}^{(1)}(x)/\partial M, \tag{5.2}$$

according to Eqs. (2.30) and (2.31). Thus, the effective lagrange function coupling term between the neutral meson and the electromagnetic field is given by

$$\mathfrak{L}'(x)=g\phi(x)\partial\mathfrak{L}^{(1)}(x)/\partial M, \tag{5.3}$$

which clearly also follows directly from the proton field equation of motion,

$$[\gamma(-i\partial-eA)+M+g\phi]\psi=0, \tag{5.4}$$

in the approximation which treats $\phi(x)$ as a weak, slowly varying, prescribed field. If we retain only the leading term in the expansion of $\mathfrak{L}^{(1)}$ for weak fields, Eq. (3.45), we have

$$\partial\mathfrak{L}^{(1)}/\partial M\simeq(e^2/6\pi^2)M\int_0^\infty ds\exp(-M^2s)\mathfrak{F}$$
$$=(2\alpha/3\pi)(1/M)\mathfrak{F}. \tag{5.5}$$

Therefore the effective coupling term is

$$\mathfrak{L}'=(\alpha/3\pi)(g/M)\phi(\mathbf{H}^2-\mathbf{E}^2), \tag{5.6}$$

which describes the decay of a stationary meson, into two parallel polarized photons, at the rate

$$1/\tau=(\alpha^2/144\pi^2)(g^2/\hbar c)(\mu/M)^2(\mu c^2/\hbar). \tag{5.7}$$

A pseudoscalar interaction between the spinless neutral meson field and the proton field is described by the term

$$g\phi(x)\tfrac{1}{2}[\bar{\psi}(x),\gamma_5\psi(x)] \tag{5.8}$$

in the lagrange function. For our purposes, this is replaced by

$$\begin{aligned}\mathfrak{L}'(x)&=g\phi(x)\langle\tfrac{1}{2}[\bar{\psi}(x),\gamma_5\psi(x)]\rangle\\&=ig\phi(x)\,\mathrm{tr}\gamma_5 G(x,x)\\&=-g\phi(x)M\int_0^\infty ds\exp(-iM^2s)\\&\qquad\times\mathrm{tr}\gamma_5\langle x|U(s)|x\rangle.\end{aligned}\tag{5.9}$$

The transformation function (3.20), with $-is$ substituted for s, yields

$$\mathfrak{L}'=-g\phi M(4\pi)^{-2}\int_0^\infty ds s^{-2}\exp(-M^2s)\epsilon^{-1(s)}\times\mathrm{tr}\gamma_5\exp(\tfrac{1}{2}e\sigma Fs). \tag{5.10}$$

Now, the eigenvalues of $\frac{1}{2}\sigma F$, as related to those of γ_5 by Eq. (3.31), give

$$\mathrm{tr}\gamma_5\exp(\tfrac{1}{2}e\sigma Fs)=-4\,\mathrm{Im}\cosh esX. \tag{5.11}$$

In view of Eq. (3.43), we obtain, without further approximation, simply

$$\begin{aligned}\mathfrak{L}'&=g\phi(e^2/4\pi^2)M\int_0^\infty ds\exp(-M^2s)\mathcal{G}\\&=(\alpha/\pi)(g/M)\phi\mathbf{E}\cdot\mathbf{H}.\end{aligned}\tag{5.12}$$

This effective coupling term implies the decay of a stationary neutral meson, into two perpendicularly polarized photons, at the rate

$$1/\tau=(\alpha^2/64\pi^3)(g^2/\hbar c)(\mu/M)^2(\mu c^2/\hbar). \tag{5.13}$$

The pseudovector interaction term,

$$(g/2M)\partial_\mu\phi(x)(1/2i)[\bar{\psi}(x),\gamma_5\gamma_\mu\psi(x)], \tag{5.14}$$

is formally equivalent to (5.8) for the problem under discussion, in the approximation to which it is being treated. This is demonstrated by a partial integration, combined with the use of the Dirac equation (2.1). Yet it has been found difficult[3,7] to verify the equivalence in the actual results of calculation. Such discrepancies between formal and explicit calculations may be produced by insufficient attention to the limiting processes implicit in the formalism. We shall demonstrate that, with appropriate care, the proper equivalence between the pseudoscalar and pseudovector couplings is indeed exhibited.

The effective pseudovector interaction between the meson and electromagnetic field is given by

$$\begin{aligned}\mathfrak{L}'(x)&=(g/2M)\partial_\mu\phi(x)\langle(1/2i)[\bar{\psi}(x),\gamma_5\gamma_\mu\psi(x)]\rangle\\&=(g/2M)\partial_\mu\phi(x)\,\mathrm{tr}\gamma_5\gamma_\mu G(x,x)\\&\qquad\rightarrow-(g/2M)\phi(x)\partial_\mu[\mathrm{tr}\gamma_5\gamma_\mu G(x,x)],\end{aligned}\tag{5.15}$$

where the last version represents the results of integrating by parts. We now remark that this derivative has the following meaning:

$$\begin{aligned}\partial_\mu[\mathrm{tr}\gamma_5\gamma_\mu G(x,x)]=\lim_{x',x''\to x}&[(\partial_\mu'-ieA_\mu(x'))\\&+(\partial_\mu''+ieA_\mu(x''))]\,\mathrm{tr}\gamma_5\gamma_\mu G(x',x''),\end{aligned}\tag{5.16}$$

in which the structure of the right side is dictated by the requirement that only gauge covariant quantities be employed. We shall verify that the straightforward evaluation of Eq. (5.16) yields the pseudoscalar coupling (5.12), without further difficulty.

According to Eq. (3.21)

$$\begin{aligned}&\mathrm{tr}\gamma_5\gamma_\mu G(x',x'')\\&=-i\,\mathrm{tr}\gamma_5\gamma_\mu\gamma_\nu\int_0^\infty ds\exp(-iM^2s)\\&\qquad\times\langle x(s)'|\Pi_\nu(s)|x(0)''\rangle\\&=-i\,\mathrm{tr}\gamma_\nu\gamma_5\gamma_\mu\int_0^\infty ds\exp(-iM^2s)\\&\qquad\times\langle x(s)'|\Pi_\nu(0)|x(0)''\rangle.\end{aligned}\tag{5.17}$$

The result of averaging these two equivalent expressions is

$$\begin{aligned}&\mathrm{tr}\gamma_5\gamma_\mu G(x',x'')\\&=i\,\mathrm{tr}\gamma_5\int_0^\infty ds\exp(-iM^2s)\\&\qquad\times\langle x(s)'|\tfrac{1}{2}(\Pi_\nu(s)-\Pi_\nu(0))|x(0)''\rangle\\&\qquad-\mathrm{tr}\gamma_5\sigma_{\mu\nu}\int_0^\infty ds\exp(-iM^2s)\\&\qquad\times\langle x(s)'|\tfrac{1}{2}(\Pi_\nu(s)+\Pi_\nu(0))|x(0)''\rangle.\end{aligned}\tag{5.18}$$

We shall be content to evaluate Eq. (5.18) in the approximation of weak fields. On referring to Eqs. (3.4), (3.5), and (3.20), it is apparent that the leading term in this approximation is

$$\begin{aligned}&\mathrm{tr}\gamma_5\gamma_\mu G(x',x'')\\&=-(e/64\pi^2)\,\mathrm{tr}\gamma_5\sigma_{\mu\nu}\sigma_{\lambda\kappa}(x'-x'')_\nu F_{\lambda\kappa}\Phi(x',x'')\\&\qquad\times\int_0^\infty ds s^{-2}\exp(-iM^2s)\exp[i\tfrac{1}{4}(x'-x'')^2/s]\\&=(e/8\pi^2)F_{\mu\nu}^*(x'-x'')_\nu\Phi(x',x'')\\&\qquad\times\int_0^\infty ds s^{-2}\exp(-iM^2s)\exp[i\tfrac{1}{4}(x'-x'')^2/s],\end{aligned}\tag{5.19}$$

[7] J. Steinberger, Phys. Rev. **76**, 1180 (1949).

with the aid of Eqs. (3.25) and (3.27). Since we are concerned with the behavior of this quantity only for $x' \simeq x''$, we may evaluate the proper time integral by an appropriate simplification. For $x' \simeq x''$,

$$\int_0^\infty ds s^{-2} \exp(-iM^2 s) \exp[i\tfrac{1}{4}(x'-x'')^2/s]$$

$$\simeq \int_0^\infty ds s^{-2} \exp[i\tfrac{1}{4}(x'-x'')^2/s]$$

$$= \int_0^\infty d(s^{-1}) \exp[i\tfrac{1}{4}(x'-x'')^2 s^{-1}]$$

$$= 4i/(x'-x'')^2. \tag{5.20}$$

Therefore,

$$\mathrm{tr}\gamma_k \gamma_\mu G(x', x'') \simeq (ie/2\pi^2)\Phi(x', x'') F_{\mu\nu}^*(x'-x'')_\nu (x'-x'')^{-2}. \tag{5.21}$$

To obtain the quantity of actual interest, Eq. (5.16), we observe that

$$[(\partial_\mu' - ieA_\mu(x')) + (\partial_\mu'' + ieA_\mu(x''))]\Phi(x', x'') \times F_{\mu\nu}^*(x'-x'')_\nu (x'-x'')^{-2} = ie\Phi(x', x'') F_{\mu\nu}^*(x'-x'')_\nu F_{\mu\lambda}(x'-x'')_\lambda (x'-x'')^{-2}, \tag{5.22}$$

according to Eqs. (3.15) and (3.16). But, in view of Eq. (3.35),

$$F_{\mu\nu}^*(x'-x'')_\nu F_{\mu\lambda}(x'-x'')_\lambda = \mathcal{G}(x'-x'')^2, \tag{5.23}$$

and

$$\partial_\mu[\mathrm{tr}\gamma_k \gamma_\mu G(x, x)] = -(e^2/2\pi^2)\mathcal{G} \lim_{x' \to x''} \Phi(x', x'') = -(2\alpha/\pi)\mathcal{G}. \tag{5.24}$$

Thus, Eq. (5.15) yields

$$\mathfrak{L}' = (\alpha/\pi)(g/M)\phi \mathbf{E} \cdot \mathbf{H}, \tag{5.25}$$

in complete agreement with Eq. (5.12).

VI. PERTURBATION THEORY

We shall now discuss the approximate evaluation of

$$W^{(1)} = i\tfrac{1}{2} \int_0^\infty ds s^{-1} \exp(-im^2 s) \mathrm{Tr} U(s), \tag{6.1}$$

by an expansion in powers of eA_μ and $eF_{\mu\nu}$. For this purpose, we write

$$\mathcal{H} = \mathcal{H}_0 + \mathcal{H}_1, \tag{6.2}$$

where

$$\mathcal{H}_0 = p^2 \tag{6.3}$$

and

$$\mathcal{H}_1 = -e(pA + Ap) - \tfrac{1}{2}e\sigma F + e^2 A^2. \tag{6.4}$$

To obtain the expansion of $\mathrm{Tr}U(s)$ in powers of $\mathcal{H}_1$, we observe that $U(s)$ obeys the differential equation

$$i\partial_s U(s) = (\mathcal{H}_0 + \mathcal{H}_1) U(s). \tag{6.5}$$

The related operator

$$V(s) = U_0^{-1}(s) U(s), \tag{6.6}$$

where

$$U_0(s) = \exp(-i\mathcal{H}_0 s), \tag{6.7}$$

is determined by

$$i\partial_s V(s) = U_0^{-1}(s)\mathcal{H}_1 U_0(s) V(s) \tag{6.8}$$

and

$$V(0) = 1. \tag{6.9}$$

One can combine Eqs. (6.8) and (6.9) in the integral equation

$$V(s) = 1 - i\int_0^s ds' U_0^{-1}(s')\mathcal{H}_1 U_0(s') V(s'), \tag{6.10}$$

and construct the solution by iteration:

$$V(s) = 1 - i\int_0^s ds' U_0^{-1}(s')\mathcal{H}_1 U_0(s') + (-i)^2 \int_0^s ds' U_0^{-1}(s')\mathcal{H}_1 U_0(s') \times \int_0^{s'} ds'' U_0^{-1}(s'')\mathcal{H}_1 U_0(s'') + \cdots. \tag{6.11}$$

On introducing new variables of integration, $u_1, u_2, \cdots$, according to

$$s' = su_1, \quad s'' = s'u_2, \cdots, \tag{6.12}$$

we obtain the expansion

$$U(s) = \exp(-i\mathcal{H}s) = U_0(s) + (-is)\int_0^1 du_1 U_0((1-u_1)s)\mathcal{H}_1 U_0(u_1 s) + \cdots + (-is)^n \int_0^1 u_1^{n-1} du_1 \cdots \int_0^1 du_n \times U_0((1-u_1)s)\mathcal{H}_1 U_0(u_1(1-u_1)s)\cdots \times U_0(u_1 \cdots u_{n-1}(1-u_n)s) \times \mathcal{H}_1 U_0(u_1 \cdots u_n s) + \cdots. \tag{6.13}$$

Instead of taking the trace of this expression directly, which would involve further simplification, we remark that

$$\mathrm{Tr}U(s) - \mathrm{Tr}U_0(s) = -is\int_0^1 d\lambda \,\mathrm{Tr}[\mathcal{H}_1 \exp(-i(\mathcal{H}_0 + \lambda\mathcal{H}_1)s)] \tag{6.14}$$

and insert the expansion (6.13) for $\exp[-i(\mathcal{H}_0 + \lambda\mathcal{H}_1)s]$.

Thus,

$$\mathrm{Tr}U(s)=\mathrm{Tr}U_0(s)+(-is)\,\mathrm{Tr}[\mathfrak{C}_1U_0(s)]$$

$$+\tfrac{1}{2}(-is)^2\int_0^1 du_1\,\mathrm{Tr}[\mathfrak{C}_1U_0((1-u_1)s)\mathfrak{C}_1U_0(u_1s)]+\cdots$$

$$+\frac{(-is)^{n+1}}{n+1}\int_0^1 u_1^{n-1}du_1\cdots\int_0^1 du_n$$

$$\times\mathrm{Tr}[\mathfrak{C}_1U_0((1-u_1)s)\mathfrak{C}_1\cdots$$

$$\times\mathfrak{C}_1U_0(u_1\cdots u_ns)]+\cdots. \quad (6.15)$$

We shall retain only the first nonvanishing field dependent terms in this expansion:

$$W^{(1)}=\tfrac{1}{2}ie^2\int_0^\infty dss^{-1}\exp(-im^2s)$$

$$\times\Big\{-is\,\mathrm{Tr}[A^2\exp(-ip^2s)]$$

$$+\tfrac{1}{2}(-is)^2\int_{-1}^1\tfrac{1}{2}dv\,\mathrm{Tr}[(pA+Ap)\exp(-ip^2\tfrac{1}{2}(1-v)s)$$

$$\times(pA+Ap)\exp(-ip^2\tfrac{1}{2}(1+v)s)]$$

$$+\tfrac{1}{2}(-is)^2\int_{-1}^1\tfrac{1}{2}dv\,\mathrm{Tr}[\tfrac{1}{2}\sigma F\exp(-ip^2\tfrac{1}{2}(1-v)s)$$

$$\times\tfrac{1}{2}\sigma F\exp(-ip^2\tfrac{1}{2}(1+v)s)]\Big\}. \quad (6.16)$$

For convenience, the variable u_1 has been replaced by $\frac{1}{2}(1+v)$. The evaluation of these traces is naturally performed in a momentum representation. The matrix elements of the coordinate dependent field quantities depend only on momentum differences,

$$(p+\tfrac{1}{2}k|A_\mu|p-\tfrac{1}{2}k)=(2\pi)^{-4}\int(dx)e^{-ikx}A_\mu(x)$$

$$\equiv(2\pi)^{-3}A_\mu(k), \quad (6.17)$$

and

$$(p|A_\mu{}^2|p)=(2\pi)^{-4}\int(dx)A_\mu{}^2(x)$$

$$=(2\pi)^{-4}\int(dk)A_\mu(-k)A_\mu(k). \quad (6.18)$$

Therefore

$$W^{(1)}=\frac{2ie^2}{(2\pi)^4}\int_0^\infty dss^{-1}\exp(-im^2s)\Big\{-is\int(dk)$$

$$\times A_\mu(-k)A_\mu(k)\int(dp)\exp(-ip^2s)$$

$$+\tfrac{1}{2}(-is)^2\int_{-1}^1\tfrac{1}{2}dv\int(dk)\int(dp)2p_\mu A_\mu(-k)$$

$$\times\exp(-i(p+\tfrac{1}{2}k)^2\tfrac{1}{2}(1-v)s]$$

$$\times2p_\nu A_\nu(k)\exp[-i(p-\tfrac{1}{2}k)^2\tfrac{1}{2}(1+v)s]$$

$$+\tfrac{1}{2}(-is)^2\int_{-1}^1\tfrac{1}{2}dv\int(dk)\int(dp)\,\tfrac{1}{4}\,\mathrm{tr}\tfrac{1}{2}\sigma F(-k)$$

$$\times\exp[-i(p+\tfrac{1}{2}k)^2\tfrac{1}{2}(1-v)s]\tfrac{1}{2}\sigma F(k)$$

$$\times\exp[-i(p-\tfrac{1}{2}k)^2\tfrac{1}{2}(1+v)s]\Big\}. \quad (6.19)$$

We thus encounter the elementary integrals

$$\int(dp\exp(-ip^2s)=-i\pi^2s^{-2}, \quad (6.20)$$

$$\int(dp)\exp[-i(p^2+(k^2/4))s+ipkvs]$$

$$=-i\pi^2s^{-2}\exp[-i(k^2/4)(1-v^2)s], \quad (6.21)$$

and

$$\int(dp)p_\mu p_\nu\exp[-i(p^2+(k^2/4))s+ipkvs]$$

$$=-\exp(-i\tfrac{1}{4}k^2s)(vs)^{-2}(\partial/\partial k_\mu)(\partial/\partial k_\nu)$$

$$\times\int(dp)\exp(-ip^2s+ipkvs)$$

$$=-i\pi^2s^{-2}(-i\tfrac{1}{2}s^{-1}\delta_{\mu\nu}+\tfrac{1}{4}v^2k_\mu k_\nu)$$

$$\times\exp[-i\tfrac{1}{4}k^2(1-v^2)s]. \quad (6.22)$$

It is convenient to replace the $\delta_{\mu\nu}$ term of the last integral by an expression which is equivalent to it in virtue of the integration with respect to v. Now

$$\int_{-1}^1\tfrac{1}{2}dv\exp[-i\tfrac{1}{4}k^2(1-v^2)s]$$

$$=1-is\tfrac{1}{2}k^2\int_{-1}^1\tfrac{1}{2}dvv^2\exp[-i\tfrac{1}{4}k^2(1-v^2)s], \quad (6.23)$$

so that, effectively

$$\int (dp)p_\mu p_\nu \exp[-i(p^2+\tfrac{1}{4}k^2)s+ipkvs]$$
$$=-\tfrac{1}{2}\pi^2 s^{-3}\delta_{\mu\nu}-i\pi^2 s^{-2}\tfrac{1}{4}v^2(k_\mu k_\nu-\delta_{\mu\nu}k^2)$$
$$\times\exp[-i\tfrac{1}{4}k^2(1-v^2)s]. \quad (6.24)$$

On inserting the values of the various integrals, and noticing that

$$(k_\mu k_\nu-\delta_{\mu\nu}k^2)A_\mu(-k)A_\nu(k)=-\tfrac{1}{2}F_{\mu\nu}(-k)F_{\mu\nu}(k), \quad (6.25)$$

we obtain immediately the gauge invariant form (with $s\rightarrow -is$)

$$W^{(1)}=-\frac{e^2}{4\pi^2}\int(dk)\tfrac{1}{2}F_{\mu\nu}(-k)F_{\mu\nu}(k)\int_0^1 dv(1-v^2)$$
$$\times\int_0^\infty ds s^{-1}\exp\{-[m^2+\tfrac{1}{4}k^2(1-v^2)]s\}. \quad (6.26)$$

This has been achieved without any special device, other than that of reserving the proper-time integration to the last.

A significant separation of terms is produced by a partial integration with respect to v, according to

$$\int_0^1 dv(1-v^2)\int_0^\infty ds s^{-1}\exp\{-[m^2+\tfrac{1}{4}k^2(1-v^2)]s\}$$
$$=\tfrac{2}{3}\int_0^\infty ds s^{-1}\exp(-m^2s)-\tfrac{1}{2}k^2\int_0^1 dv(v^2-\tfrac{1}{3}v^4)$$
$$\times\int_0^\infty ds\exp\{-[m^2+\tfrac{1}{4}k^2(1-v^2)]s\}. \quad (6.27)$$

Adding the action integral of the maxwell field, which is expressed in momentum space by

$$W^{(0)}=-\int(dk)\tfrac{1}{4}F_{\mu\nu}(-k)F_{\mu\nu}(k), \quad (6.28)$$

we obtain the modified action integral,

$$W=-\left[1+\frac{e^2}{12\pi^2}\int_0^\infty ds s^{-1}\exp(-m^2s)\right]$$
$$\times\int(dk)\tfrac{1}{4}F_{\mu\nu}(-k)F_{\mu\nu}(k)$$
$$+\frac{e^2}{4\pi^2}\int(dk)\tfrac{1}{4}F_{\mu\nu}(-k)F_{\mu\nu}(k)k^2$$
$$\times\int_0^1 dv\frac{v^2(1-\frac{1}{3}v^2)}{m^2+\frac{1}{4}k^2(1-v^2)}. \quad (6.29)$$

The field strength and charge renormalization contained in Eq. (3.48) then produces the finite gauge invariant result,[8]

$$W=-\int(dk)\tfrac{1}{4}F_{\mu\nu}(-k)F_{\mu\nu}(k)$$
$$\times\left[1-\frac{\alpha}{4\pi}\frac{k^2}{m^2}\int_0^1 dv\frac{v^2(1-\frac{1}{3}v^2)}{1+(k^2/4m^2)(1-v^2)}\right]. \quad (6.30)$$

The restriction which we have thus far imposed, that no actual pair creation occurs, corresponds to the requirement that $1+(k^2/4m^2)(1-v^2)$ never vanishes. This will be true if $-k^2<4m^2$, for all k_μ contained in the fourier representation of the field. Indeed, it is evident from energy and momentum considerations that to produce a pair by the absorption of a single quantum the momentum vector of the latter must be time-like and must have a magnitude exceeding $2m$. We shall now simply remark that, to extend our results to pair-producing fields, it is merely necessary to add an infinitesimal negative imaginary constant to the denominator of Eq. (6.30) and interpret the positive imaginary contribution to W thus obtained with the statement that

$$|e^{iW}|^2=e^{-2\,\mathrm{Im}W} \quad (6.31)$$

represents the probability that no actual pair creation occurs during the history of the field. The infinitesimal imaginary constant, as employed in

$$\lim_{\epsilon\rightarrow+0}\frac{1}{x-i\epsilon}=P\frac{1}{x}+\pi i\delta(x), \quad (6.32)$$

represents a familiar device for dealing with real processes. We obtain from Eq. (6.30) that

$$2\,\mathrm{Im}W=\tfrac{1}{2}\alpha\int(dk)\tfrac{1}{4}F_{\mu\nu}(-k)F_{\mu\nu}(k)\frac{k^2}{m^2}\int_0^1 dvv^2$$
$$\times\left(1-\frac{v^2}{3}\right)\delta\left[1+\frac{k^2}{4m^2}(1-v^2)\right]$$
$$=\alpha\int_{-k^2>4m^2}(dk)(-\tfrac{1}{4})F_{\mu\nu}(-k)F_{\mu\nu}(k)$$
$$\times\left(1-\frac{4m^2}{(-k^2)}\right)^{\frac{1}{2}}\frac{1}{3}\left(2+\frac{4m^2}{(-k^2)}\right). \quad (6.33)$$

For the weak fields that are being considered, Eq. (6.33) is just the probability that a pair is created by the field. It should be noticed, incidentally, that

$$-\tfrac{1}{4}F_{\mu\nu}(-k)F_{\mu\nu}(k)=\tfrac{1}{2}[|\mathbf{E}(k)|^2-|\mathbf{H}(k)|^2] \quad (6.34)$$

[8] The corresponding result for a spin zero charged field is obtained by omitting the spin term of Eq. (6.19), and multiplying the remainder with $(-\frac{1}{2})$. This effectively substitutes $\frac{1}{6}v^4$ for $(v^2-\frac{1}{3}v^4)$, in Eq. (6.30).

is actually positive for a pair-generating field. This follows, for example, from the vanishing of the magnetic field in the special coordinate system where k_μ has only a temporal component.

An alternative version of Eq. (6.33) is obtained by replacing the field with the current required to generate this field, according to the maxwell equations

$$\begin{aligned} ik_\mu F_{\mu\nu}(k) &= -J_\nu(k), \\ k_\mu F_{\nu\lambda}(k)+k_\nu F_{\lambda\mu}(k)+k_\lambda F_{\mu\nu}(k) &= 0. \end{aligned} \tag{6.35}$$

Now

$$\begin{aligned} k_\lambda{}^2 F_{\mu\nu}(-k)F_{\mu\nu}(k) &= 2k_\nu F_{\nu\mu}(-k)k_\lambda F_{\lambda\mu}(k) \\ &= 2J_\mu(-k)J_\mu(k), \end{aligned} \tag{6.36}$$

so that[9]

$$2\,\mathrm{Im}W=(\alpha/8m^2)\int_{-k^2>4m^2}(dk)J_\mu(-k)J_\mu(k) \times(1-\gamma)^{\frac{1}{2}}\gamma^{\frac{1}{2}}(2+\gamma), \tag{6.37}$$

where

$$\gamma=4m^2/(-k^2). \tag{6.38}$$

It is now appropriate to notice that the integral (3.49), representing the lagrange function for a uniform field, has singularities, unless $\mathcal{G}=0$, $\mathcal{F}>0$, corresponding to a pure magnetic field in an appropriate coordinate system. This is the analytic expression of the fact that pairs are created by a uniform electric field. In particular, for $\mathcal{G}=0$, $-2\mathcal{F}=\mathcal{E}^2>0$, which invariantly characterizes a pure electric field, the lagrange function proper time integral,

$$\mathfrak{L}=\tfrac{1}{2}\mathcal{E}^2-(1/8\pi^2)\int_0^\infty ds s^{-3}\exp(-m^2 s) \times[e\mathcal{E}s\cot(e\mathcal{E}s)-1+\tfrac{1}{3}(e\mathcal{E}s)^2], \tag{6.39}$$

has singularities at

$$s=s_n=n\pi/e\mathcal{E}, \quad n=1, 2, \cdots. \tag{6.40}$$

If the integration path is considered to lie above the real axis, which is an alternative version of the device embodied in Eq. (6.32), we obtain a positive imaginary contribution to $\mathfrak{L}$,

$$2\,\mathrm{Im}\mathfrak{L}=\frac{1}{4\pi}\sum_{n=1}^{\infty}s_n{}^{-2}\exp(-m^2 s_n) =\frac{\alpha^2}{\pi^2}\mathcal{E}^2\sum_{n=1}^{\infty}n^{-2}\exp\left(\frac{-n\pi m^2}{e\mathcal{E}}\right). \tag{6.41}$$

This is the probability, per unit time and per unit volume, that a pair is created by the constant electric field.

We must now consider, in the framework of this special problem, the connection between the proper time method and that of "invariant regularization." The vacuum polarization addition to the action integral has the general structure

$$W^{(1)}=\int(dk)A_\mu(-k)K_{\mu\nu}(k, m^2)A_\nu(k). \tag{6.42}$$

The proper-time technique yields the coefficient $K_{\mu\nu}(k, m^2)$ in the form

$$K_{\mu\nu}(k, m^2)]_p=\int_0^\infty ds\exp(-im^2 s)K_{\mu\nu}(k, s), \tag{6.43}$$

where $K_{\mu\nu}(k, s)$ is a finite, gauge invariant quantity; infinities appear only in the final stage of integrating s to the origin. In effect, this method substitutes a lower limit, s_0, in the proper time integral and reserves the limit, $s_0\to 0$, to the end of the calculation. If, on the contrary, the proper-time technique is not explicitly introduced, $K_{\mu\nu}(k, m^2)$ will be represented by divergent integrals which lead, in general, to non-gauge invariant results. The regulator technique avoids the difficulty by introducing a suitable weighted integration with respect to the square of the proper mass, thus substituting for $K_{\mu\nu}(k, m^2)$, the quantity

$$K_{\mu\nu}(k, m^2)]_R=\int_{-\infty}^{\infty}d\kappa\rho(\kappa)K_{\mu\nu}(k, \kappa). \tag{6.44}$$

The "regulator" $\rho(\kappa)$ must reduce to $\delta(\kappa-m^2)$, in an appropriate limit, and will produce gauge invariant results in this problem if the following integral conditions are satisfied:

$$\int_{-\infty}^{\infty}d\kappa\rho(\kappa)=0, \quad \int_{-\infty}^{\infty}d\kappa\kappa\rho(\kappa)=0. \tag{6.45}$$

Expressed in terms of the fourier transformed quantities,

$$\begin{aligned} R(s)&=\int_{-\infty}^{\infty}d\kappa e^{-i\kappa s}\rho(\kappa), \\ K_{\mu\nu}(k, s)&=(1/2\pi)\int_{-\infty}^{\infty}d\kappa e^{i\kappa s}K_{\mu\nu}(k, \kappa), \end{aligned} \tag{6.46}$$

we have

$$K_{\mu\nu}(k, m^2)]_R=\int_{-\infty}^{\infty}dsR(s)K_{\mu\nu}(k, s), \tag{6.47}$$

while the conditions on $\rho(\kappa)$ appear as

$$R(0)=0, \quad R'(0)=0, \quad R(s)\to\exp(-im^2 s). \tag{6.48}$$

Now observe that the proper time method yields $K_{\mu\nu}(k, m^2)$ in the form (6.47), with

$$K_{\mu\nu}(k, s)=0, \quad s<0, \tag{6.49}$$

and

$$\begin{aligned} R(s)&=\exp(-im^2 s), && s>s_0 \\ &=0, && s<s_0. \end{aligned} \tag{6.50}$$

[9] A simple example, to which this formula may be applied, is the creation of a pair in a nuclear $j=0\to 0$ transition. J. R. Oppenheimer and J. Schwinger, Phys. Rev. 56, 1066 (1939).

This $R(s)$, and all its derivatives, vanishes at the origin, thus satisfying the regulator conditions as $s_0 \to 0$. It appears, then, that regularization is a procedure for inserting, into a calculation that does not employ it, enough of the structure provided by the proper time representation to ensure gauge invariant results.

APPENDIX A

It is our purpose here to use the proper time equations of motion (2.36) for the computation of the current induced in the vacuum by a weak, arbitrarily varying field:

$$F_{\mu\nu}(x) = [1/(2\pi)^2]\int (dk) e^{ikx} F_{\mu\nu}(k). \tag{A.1}$$

In the absence of a field, the equations of motions are solved by

$$\Pi_\mu(s) = \Pi_\mu(0), \quad x_\mu(s) = x_\mu(0) + 2\Pi_\mu(0)s. \tag{A.2}$$

As a first approximation for weak fields, we accordingly write

$$d\Pi_\mu(s)/ds = [e/(2\pi)^2]\int (dk) F_{\mu\nu}(k) \{e^{ik(x(0)+2\Pi(0)s)}, \Pi_\nu(0)\}$$
$$+ e/(2\pi)^2 \int (dk) ik_\mu \tfrac{1}{2}\sigma_{\lambda\nu} F_{\lambda\nu}(k) e^{ik(x(0)+2\Pi(0)s)}. \tag{A.3}$$

On integrating with respect to s, one obtains

$$\Pi_\mu(s) - \Pi_\mu(0) = [e/(2\pi)^2]\int (dk) F_{\mu\nu}(k)$$
$$\times \int_0^s ds' \{e^{ik(x(0)+2\Pi(0)s')}, \Pi_\nu(0)\}$$
$$+ e/(2\pi)^2 \int (dk) ik_\mu \tfrac{1}{2}\sigma_{\lambda\nu} F_{\lambda\nu}(k)$$
$$\times \int_0^s ds' e^{ik(x(0)+2\Pi(0)s')}. \tag{A.4}$$

A second integration yields

$$\frac{x_\mu(s) - x_\mu(0)}{2s} = \Pi_\mu(0) + e/(2\pi)^2 \int (dk) F_{\mu\nu}(k)$$
$$\times \int_0^s ds'(1 - s'/s) \{e^{ik(x(0)+2\Pi(0)s')}, \Pi_\nu(0)\}$$
$$+ \frac{e}{(2\pi)^2}\int (dk) ik_\mu \tfrac{1}{2}\sigma F(k)$$
$$\times \int_0^s \left(ds' \left(1 - \frac{s'}{s}\right) e^{ik(x(0)+2\Pi(0)s')}\right), \tag{A.5}$$

and therefore

$$\tfrac{1}{2}(\Pi_\mu(s) + \Pi_\mu(0))$$
$$= \frac{x_\mu(s) - x_\mu(0)}{2s} + \frac{e}{(2\pi)^2}\int (dk) F_{\mu\nu}(k)$$
$$\times \int_0^s ds' \left(\frac{s'}{s} - \tfrac{1}{2}\right) \{e^{ik(x(0)+2\Pi(0)s')}, \Pi_\nu(0)\}$$
$$+ \frac{e}{(2\pi)^2}\int (dk) ik_\mu \tfrac{1}{2}\sigma F(k)$$
$$\times \int_0^s ds' \left(\frac{s'}{s} - \tfrac{1}{2}\right) e^{ik(x(0)+2\Pi(0)s')}. \tag{A.6}$$

The induced current is equivalently expressed by

$$\langle j_\mu(x)\rangle = e\ \mathrm{tr}\gamma_\mu \left(x|(\gamma\Pi - m)\int_0^\infty ds \exp(-im^2 s) U(s)|x\right)$$
$$= e\int_0^\infty ds \exp(-im^2 s)\ \mathrm{tr}\gamma_\mu\gamma_\nu (x(s')'|\Pi_\nu(s)|x(0'')]_{s',s''\to s}, \tag{A.7}$$

and

$$\langle j_\mu(x)\rangle = e\ \mathrm{tr}\gamma_\mu \left(x\left|\int_0^\infty ds \exp(-im^2 s) U(s)(\gamma\Pi - m)\right|x\right)$$
$$= e\int_0^\infty ds \exp(-im^2 s)\ \mathrm{tr}\gamma_\nu\gamma_\mu (x(s')'|\Pi_\nu(0)|x(0'')]_{s',s''\to s}. \tag{A.8}$$

On averaging the two forms, we find that

$$\langle j_\mu(x)\rangle = -e\int_0^\infty ds \exp(-im^2 s)$$
$$\times \mathrm{tr}(x(s)'|\tfrac{1}{2}(\Pi_\mu(s) + \Pi_\mu(0))|x(0'')]_{s',s''\to s}$$
$$- ie\int_0^\infty ds \exp(-im^2 s)$$
$$\times \mathrm{tr}\sigma_{\mu\nu}(x(s)'|\tfrac{1}{2}(\Pi_\nu(s) - \Pi_\nu(0))|x(0'')]_{s',s''\to s}. \tag{A.9}$$

It may be noted here that no current exists in the absence of a field, since

$$\lim_{s'-s''\to \pm 0} (x(s')'|x_\mu(s) - x_\mu(0)|x(0'')) = 0, \tag{A.10}$$

and, therefore, only the transformation function in the absence of a field is required for the first-order evaluation of Eq. (A.9). Now

$$\mathrm{tr}\sigma_{\mu\nu}(x(s')'|\tfrac{1}{2}(\Pi_\nu(s) - \Pi_\nu(0))|x(0'')$$
$$= [2e/(2\pi)^2]\int (dk)(\partial F_{\mu\nu}/\partial x_\nu)(k) s\int_{-1}^1 \tfrac{1}{2}dv$$
$$\times (x(s)'|\exp[i(kx(s)\tfrac{1}{2}(1+v) + kx(0)\tfrac{1}{2}(1-v)]|x(0'')], \tag{A.11}$$

in which the variable s' has been replaced by v, according to

$$s' = s(1+v)/2. \tag{A.12}$$

The operators $kx(s)$ and $kx(0)$ do not commute:

$$[kx(s), kx(0)] = 2s[k\Pi(0), kx(0)] = -2isk^2. \tag{A.13}$$

We may, however, employ the easily established theorem,

$$e^{A+B} = e^A e^B e^{-\frac{1}{2}[A,B]}, \tag{A.14}$$

for operators A and B that commute with their commutator $[A, B]$. Thus,

$$\exp[i(kx(s)\tfrac{1}{2}(1+v) + kx(0)\tfrac{1}{2}(1-v))]$$
$$= \exp[ikx(s)\tfrac{1}{2}(1+v)]\exp[ikx(0)\tfrac{1}{2}(1-v)]$$
$$\times \exp[-ik^2\tfrac{1}{4}(1-v^2)s], \tag{A.15}$$

and

$$\mathrm{tr}\sigma_{\mu\nu}(x(s)'|\tfrac{1}{2}(\Pi_\nu(s) - \Pi_\nu(0))|x(0'')]_{s',s''\to s}$$
$$= [2e/(2\pi)^2]\int (dk) e^{ikx}(\partial F_{\mu\nu}/\partial x_\nu)(k) s\int_{-1}^1 \tfrac{1}{2}dv$$
$$\times \exp[-ik^2\tfrac{1}{4}(1-v^2)s](-i)/(4\pi)^2 s^2. \tag{A.16}$$

A similar treatment applies to

$$\mathrm{tr}(x(s)'|\tfrac{1}{2}(\Pi_\nu(s) + \Pi_\nu(0))|x(0'')]_{s',s''\to s}$$
$$= \frac{2e}{(2\pi)^2}\int (dk) F_{\mu\nu}(k) s\int_{-1}^1 \tfrac{1}{2}dv\, v(x(s')'|\{\exp[i(kx(s)\tfrac{1}{2}(1+v)$$
$$+ kx(0)\tfrac{1}{2}(1-v))], (x_\nu(s) - x_\nu(0))/2s\}|x'(0))]_{s',s''\to s}. \tag{A.17}$$

With the aid of the commutation relations,

$$[e^{ikx(0)\frac{1}{2}(1-v)}, x_\nu(s)] = -k_\nu(1-v)se^{ikx(0)\frac{1}{2}(1-v)},$$
$$[e^{ikx(s)\frac{1}{2}(1+v)}, x_\nu(0)] = k_\nu(1+v)se^{ikx(s)\frac{1}{2}(1+v)}, \tag{A.18}$$

this reduces to

$$\mathrm{tr}(x(s)'|\tfrac{1}{2}(\Pi_\mu(s) + \Pi_\mu(0))|x(0'')]_{s',s''\to s}$$
$$= -[2ie/(2\pi)^2]\int (dk) e^{ikx}(\partial F_{\mu\nu}/\partial x_\nu)(k) s\int_{-1}^1 \tfrac{1}{2}dv v^2$$
$$\times \exp[-ik^2\tfrac{1}{4}(1-v^2)s](-i)/(4\pi)^2 s^2. \tag{A.19}$$

We have thus obtained

$$\langle j_\mu(x)\rangle = -(\alpha/2\pi)(2\pi)^{-2}\int (dk) e^{ikx}(\partial F_{\mu\nu}/\partial x_\nu)(k)\int_0^1 dv(1-v^2)$$
$$\times \int_0^\infty ds s^{-1} \exp\{-[m^2 + \tfrac{1}{4}k^2(1-v^2)]s\}, \tag{A.20}$$

in which the substitution $s \to -is$ has again been introduced. This is precisely the current derived from the action integral $W^{(1)}$ of Eq. (6.26), and further discussion proceeds as in Sec. VI.

APPENDIX B

An electron in interaction with its proper radiation field, and an external field, is described by the modified Dirac equation,[10]

$$\gamma_\mu(-i\partial_\mu-eA_\mu(x))\psi(x)+\int(dx')M(x,x')\psi(x')=0. \quad \text{(B.1)}$$

To the second order in e, the mass operator, $M(x,x')$, is given by

$$M(x,x')=m_0\delta(x-x')+ie^2\gamma_\mu G(x,x')\gamma_\mu D_+(x-x'). \quad \text{(B.2)}$$

Here $G(x,x')$ is the Green's function of the Dirac equation in the external field, and $D_+(x-x')$ is a photon Green's function, expressed by

$$D_+(x-x')=(4\pi)^{-2}\int_0^\infty dtt^{-2}\exp[i\tfrac{1}{4}(x-x')^2/t]. \quad \text{(B.3)}$$

We shall suppose the external field to be weak and uniform. Under these conditions, the transformation function $(x(s)|x(0)')$, involved in the construction of $G(x,x')$, may be approximated by

$$(x(s)|x(0)')\simeq-i(4\pi)^{-2}\Phi(x,x')s^{-2}\times\exp[i\tfrac{1}{4}(x-x')^2/s]\exp(i\tfrac{1}{2}e\sigma F); \quad \text{(B.4)}$$

that is, terms linear in the field strengths enter only through the Dirac spin magnetic moment. The corresponding simplification of the Green's function, obtain by averaging the two equivalent forms in Eq. (3.21), is

$$G(x,x')\simeq(4\pi)^{-2}\Phi(x,x')\int_0^\infty dss^{-2}\exp(-im^2s)\times\exp[i\tfrac{1}{4}(x-x')^2/s]\tfrac{1}{2}\left\{\frac{-\gamma(x-x')}{2s}+m,\exp(i\tfrac{1}{2}e\sigma F)\right\}. \quad \text{(B.5)}$$

The mass operator is thus approximately represented by

$$M(x,x')=m_0\delta(x-x')+[ie^2/(4\pi)^4]\Phi(x,x')\int_0^\infty dss^{-2}\int_0^\infty dtt^{-2}\times\exp(-im^2s)\exp\left[i\tfrac{1}{4}(x-x')^2\left(\frac{1}{s}+\frac{1}{t}\right)\right]\times\gamma_\lambda\tfrac{1}{2}\left\{\frac{-\gamma(x-x')}{2s}+m,\exp(i\tfrac{1}{2}e\sigma F)\right\}\gamma_\lambda, \quad \text{(B.6)}$$

or

$$M(x,x')=m_0\delta(x-x')+[ie^2/(4\pi)^4]\Phi(x,x')\times\int_0^\infty dss^{-2}\exp(-im^2s)\int_0^s dww^{-2}\exp[i\tfrac{1}{4}(x-x')^2/w]\times[-4m-s^{-1}\gamma(x-x')+\tfrac{1}{2}i\{\gamma(x-x'),\tfrac{1}{2}e\sigma F\}], \quad \text{(B.7)}$$

in which we have replaced t by the variable w,

$$w^{-1}=s^{-1}+t^{-1}, \quad \text{(B.8)}$$

and employed properties of the Dirac matrices, notably

$$\gamma_\lambda\sigma_{\mu\nu}\gamma_\lambda=0. \quad \text{(B.9)}$$

We shall also write

$$\begin{aligned}(x-x')_\mu\Phi(x,x')\exp[i\tfrac{1}{4}(x-x')^2/w]&=2w(-i\partial_\mu-eA_\mu(x)-\tfrac{1}{2}eF_{\mu\nu}(x-x')_\nu)\Phi(x,x')\exp[i\tfrac{1}{4}(x-x')^2/w]\\&\simeq[2w(-i\partial_\mu-eA_\mu(x))-2w^2eF_{\mu\nu}(-i\partial_\nu-eA_\nu(x))]\times\Phi(x,x')\exp[i\tfrac{1}{4}(x-x')^2/w],\end{aligned} \quad \text{(B.10)}$$

which gives

$$\begin{aligned}M(x,x')=m_0\delta(x-x')+[e^2/(4\pi)^2]\int_0^\infty dss^{-2}\exp(-im^2s)&\times\int_0^s dw[2m(2-w/s)+(2w/s)(\gamma(-i\partial-eA)+m)\\&-2mw(1-w/s)i\tfrac{1}{2}e\sigma F-iw(1+w/s)\\&\times[\gamma(-i\partial-eA)+m,\tfrac{1}{2}e\sigma F]](x(w)|x(0)'),\end{aligned} \quad \text{(B.11)}$$

in virtue of the relation

$$[\gamma(-i\partial-eA),\tfrac{1}{2}e\sigma F]=2ie\gamma F(-i\partial-eA). \quad \text{(B.12)}$$

We now introduce a perturbation procedure in which the mass operator assumes the role customarily played by the energy. To evaluate $\int(dx')M(x,x')\psi(x')$, we replace $\psi(x')$ by the unperturbed wave function, a solution of the Dirac equation associated with the mass m (we need not distinguish, to this approximation, between the actual mass m and the mechanical mass m_0). The x' integration can be effected immediately,

$$\begin{aligned}\int(x(w)|x(0)')(dx')\psi(x')&=\int(x|U(w)|x')(dx')\psi(x')\\&=\exp(im^2w)\psi(x),\end{aligned} \quad \text{(B.13)}$$

since $\psi(x)$ is an eigenfunction of $\mathcal{H}$, with the eigenvalue $-m^2$. Therefore, on discarding all terms containing the operator of the Dirac equation, which will not contribute to

$$\int(dx)(dx')\psi(x)M(x,x')\psi(x'),$$

we obtain

$$[\gamma(-i\partial-eA)+m-\mu'\tfrac{1}{2}\sigma F]\psi=0, \quad \text{(B.14)}$$

where

$$m=m_0+(\alpha/2\pi)m\int_0^\infty dss^{-1}\int_0^s dws^{-1}(2-w/s)\times\exp[-im^2(s-w)] \quad \text{(B.15)}$$

represents the mass of a free electron, and

$$\mu'=(\alpha/2\pi)em i\int_0^\infty ds\int_0^s(dw/s)(w/s)(1-w/s)\times\exp[-im^2(s-w)] \quad \text{(B.16)}$$

describes an additional spin magnetic moment. Both integrals are conveniently evaluated by introducing

$$u=1-w/s, \quad \text{(B.17)}$$

and making the replacement $s\to-is$, which yields

$$\begin{aligned}m=m_0+(\alpha/2\pi)m\int_0^\infty dss^{-1}\int_0^1 du(1+u)\exp(-m^2us)\\=m_0+(3\alpha/4\pi)m\left[\int_0^\infty dss^{-1}\exp(-m^2s)+\infty\right],\end{aligned} \quad \text{(B.18)}$$

and

$$\begin{aligned}\mu'=(\alpha/2\pi)em\int_0^\infty ds\int_0^1 duu(1-u)\exp(-m^2us)\\=(\alpha/2\pi)(e/m)\int_0^1 du(1-u)=(\alpha/2\pi)(e\hbar/2mc).\end{aligned} \quad \text{(B.19)}$$

We thus derive the spin magnetic moment of $\alpha/2\pi$ magnetons produced by second-order electromagnetic mass effects.

[10] The concepts employed here will be discussed at length in later publications.

The Spin Relaxation Time of Chromium Alum

EIICHI ISHIGURO
Physics Department, Faculty of Science, Ochanomizu University, Tokyo, Japan

KENJIRO KAMBE
University of Electro-Communications, Tokyo, Japan

AND

TUNEMARU USUI
Physics Department, Faculty of General Culture, University of Tokyo, Tokyo, Japan

(Received January 8, 1951)

The theoretical expression for the spin relaxation time of Cr−K-alum is derived when the static magnetic field is not present. In this derivation we have made use of the method of moments and assumed that the absorption line has a gaussian shape. In calculating the second moment, we have taken into account, straightforwardly, the small crystalline splitting of the lowest orbital state of the Cr ion. The result is compared with the expression derived by Broer and with the experimental value. We have concluded that a small contribution of exchange interaction must be present. Our estimation shows that the exchange constant $\bar{A}$ is about 4.9×10^{-15} erg.

I. INTRODUCTION

WHEN a paramagnetic crystal is placed in an oscillating magnetic field, the spin system of the crystal absorbs energy from the oscillating field. This phenomenon is called spin absorption. The shape of the absorption curve can be determined in principle by the so-called method of moments developed by several authors.[1–4] Broer,[1] Van Vleck,[2] and Wright[3] applied this method to the case of no crystalline splitting and obtained rather good agreement with experiments.

In the case when there are crystalline splittings, scarcely any work has been done except the simple argument of Broer[1] and the formal treatment of Pryce and Stevens.[4] Recently, we calculated rigorously the second moment of the Larmor line of the spin absorption in a nickel fluosilicate crystal, and we investigated the magnitude of the exchange interaction between nickel ions in this crystal.[5] In the case of an aperiodic line, however, the effect of crystalline splitting has received only an approximate treatment by Broer.[1] He proposed, for the spin relaxation time ρ', the following expression:

$$\rho'=(\pi/2)^{\frac{1}{2}}\nu_0^{-1}[1-\sum\sum_{(n,d)}|M_{nn'}|^2/\sum_n\sum_{n'}|M_{nn'}|^2]. \quad (1)$$

Here ν_0 is the root-mean-square frequency calculated by assuming no crystalline splittings. The factor in the bracket was introduced by Broer to incorporate the effect of the crystalline splitting. The subscript (n, d) denotes a summation over nondiagonal matrix elements. However, both the second moment and the area of the distribution function may be modified by the presence of crystalline splitting. Hence it is of interest to make an accurate calculation of the second moment inclusive of the effect of the crystalline splitting. The spin relaxation time in the absence of a constant magnetic field can then be obtained if the gaussian hypothesis concerning line shape is utilized. The purpose of the present paper is to present a calculation of this character for the aperiodic line of Cr−K-alum, one of the substances which has been well studied by paramagnetic relaxation experiments.[6]

The lattice of Cr ions in this crystal is face-centered cubic and the unit cell contains four Cr ions.[7] The crystalline field acting on a Cr ion has trigonal symmetry, the axis of which coincides with one of the four body-diagonals of the unit cube. The direction of this axis is different for each of the four ions in a unit cell. Because of this fact, the calculation of the second moment is rather complicated.

II. DERIVATION OF THE SPIN RELAXATION TIME

The hamiltonian of the spin system of Cr-alum can be written in the form:

$$H=\sum_i W_i+\sum\sum_{i>j}T_{ij} \quad (2)$$

with

$$W_i=-\tfrac{1}{2}\delta S_{\zeta i}^2 \quad (3)$$

and

$$T_{ij}=(\bar{A}_{ij}+g^2\beta^2r_{ij}^{-3})(\mathbf{S}_i\cdot\mathbf{S}_j) -3g^2\beta^2r_{ij}^{-5}(\mathbf{S}_i\cdot\mathbf{r}_{ij})(\mathbf{S}_j\cdot\mathbf{r}_{ij}). \quad (4)$$

Here W_i denotes the one-ion energy of the ith Cr^{+++} ion, δ is the splitting of the lowest spin quartet, and $S_{\zeta i}$ is the ζ_i component of the spin vector of the ion when the ζ_i axis is along the axis of the trigonal field acting on the ith ion. It must be noted, in this connection, that directions of each ζ_i axis are staggered from one

[1] L. J. F. Broer, Physica **10**, 80 (1943).
[2] J. H. Van Vleck, Phys. Rev. **74**, 1168 (1948).
[3] A. Wright, Phys. Rev. **76**, 1826 (1949).
[4] M. H. L. Pryce and K. W. H. Stevens, Proc. Phys. Soc. (London) **A63**, 36 (1950).
[5] Ishiguro, Kambe, and Usui, to be published.
[6] C. J. Gorter, *Paramagnetic Relaxation* (Elsevier Publishing Company, Inc., New York, 1947).
[7] H. Lipson and C. A. Beevers, Proc. Roy. Soc. (London) **A148**, 664 (1935).

ion to another in a unit cell. The other notation in the expression (4) is the same as that of Van Vleck.[2]

The component of the total spin operator in the direction of oscillating field, which we take as the x direction, may be written as

$$S_x=\sum_i S_{xi}=\sum_i (l_{x\xi_i}S_{\xi_i}+l_{x\eta_i}S_{\eta_i}+l_{x\zeta_i}S_{\zeta_i}), \quad (5)$$

where ξ_i, η_i axes are taken such that they form a set of coordinate axes in combination with the ζ_i axis defined above, and $l_{x\xi_i}$, $l_{x\eta_i}$ and $l_{x\zeta_i}$ are the direction cosines connecting the x axis with the ξ_i, η_i, ζ_i axes referred to the ith ion.

In calculating the moments of the distribution function $f(\nu)$, defined as usual,[3] we must select the so-called semidiagonal part of the hamiltonian $\mathcal{H}$, i.e., the part which commutes with the one-ion energy term, $\sum_i W_i$. We must also select the semidiagonal part of the spin component S_x, in order to calculate the distribution function of the aperiodic line. We shall use, in the following, the convention that the bar on any operator means its semidiagonal part. It is to be noted that the semidiagonal part of a product of some operators is not, in general, equal to the product of the semidiagonal parts of its component operators.

If we use the projection operators A_i and B_i, which correspond to the doubly degenerate states $M_{si}'=\pm\frac{1}{2}$ and $M_{si}'=\pm\frac{3}{2}$ of the ith ion, respectively, we can write

$$\bar{S}_x=\sum_i \bar{S}_{xi}=\sum_i (l_{x\xi_i}A_iS_{\xi_i}A_i+l_{x\eta_i}A_iS_{\eta_i}A_i+l_{x\zeta_i}S_{\zeta_i}), \quad (6)$$

and

$$\bar{T}_{ij}=A_iA_jT_{ij}A_iA_j+B_iB_jT_{ij}B_iB_j+A_iB_jT_{ij}A_iB_j +A_iB_jT_{ij}B_iA_j+B_iA_jT_{ij}B_iA_j+B_iA_jT_{ij}A_iB_j. \quad (7)$$

Substituting the expression (4) for T_{ij} in the foregoing equation, we get

$$\bar{T}_{ij}=\sum_{\alpha_i}\sum_{\beta_j} C_{\alpha_i\beta_j}(\overline{S_{\alpha_i}S_{\beta_j}}), \quad (8)$$

with

$$C_{\alpha_i\beta_j}=(A_{ij}+g^2\beta^2r_{ij}^{-3})l_{\alpha_i\beta_j}-3g^2\beta^2r_{ij}^{-3}n_{\alpha_i}{}^in_{\beta_j}{}^i, \quad (9)$$

where the summations $\sum_{\alpha_i}$ and $\sum_{\beta_j}$ are taken over ξ_i, η_i, ζ_i and ξ_j, η_j, ζ_j, respectively, and

$$l_{\alpha_i\beta_j}=\cos(\alpha_i,\beta_j), \quad n_{\alpha_i}{}^i=\cos(\alpha_i,r_{ij}) \quad n_{\beta_j}{}^i=\cos(\beta_j,r_{ij})$$

where r_{ij} is a vector drawn from the ith ion to the jth ion.

The area (the zero-th moment) and the second moment of $f(\nu)$ can be determined by the following formulas

$$\text{area} \quad \int_0^\infty f(\nu)d\nu=g^2\beta^2\,\mathrm{Sp}\bar{S}_x{}^2, \quad (10)$$

$$\text{second moment} \quad \int_0^\infty \nu^2 f(\nu)d\nu=-\hbar^{-2}g^2\beta^2\,\mathrm{Sp}[\bar{H},\bar{S}_x]^2, \quad (11)$$

with $[\bar{H},\bar{S}_x]=\bar{H}\bar{S}_x-\bar{S}_x\bar{H}$.

The commutator of $\bar{H}$ and $\bar{S}_x$ can be written as

$$[\bar{H},\bar{S}_x]=[\sum\sum_{i>j}\bar{T}_{ij},\bar{S}_x]=\sum\sum_{i\neq j}[\bar{T}_{ij},\bar{S}_{xi}] =\sum\sum_{i\neq j}\sum_{\alpha_i}\sum_{\beta_j}\sum_{\lambda_i} C_{\alpha_i\beta_j}l_{x\lambda_i} \times[(\overline{S_{\alpha_i}S_{\beta_j}}),\bar{S}_{\lambda_i}], \quad (12)$$

where $\sum_{\lambda_i}$ is taken over ξ_i, η_i, ζ_i. Then we obtain

$$[\bar{H},\bar{S}_x]^2=\sum_{i\neq j,\,k\neq l,\,\alpha_i,\beta_j,\,\gamma_k,\delta_l,\lambda_i,\mu_k} l_{x\lambda_i}l_{x\mu_k}C_{\alpha_i\beta_j}C_{\gamma_k\delta_l}[(\overline{S_{\alpha_i}S_{\beta_j}}),\bar{S}_{\lambda_i}][(\overline{S_{\gamma_k}S_{\delta_l}}),\bar{S}_{\mu_k}]. \quad (13)$$

For a powder sample, we can average the expression (13) over all directions of the x axis; $\langle[\bar{H},\bar{S}_x]^2\rangle_{\text{Av}}$. If we take the spur, we find

$$\mathrm{Sp}\langle[\bar{H},\bar{S}_x]^2\rangle_{\text{Av}}=\tfrac{1}{3}\sum_{i\neq j,\,\alpha_i,\beta_j,\gamma_k,\delta_l,\lambda_i,\mu_k} l_{\lambda_i\mu_k}C_{\alpha_i\beta_j}C_{\gamma_k\delta_l}\,\mathrm{Sp}\{[(\overline{S_{\alpha_i}S_{\beta_j}}),\bar{S}_{\lambda_i}][(\overline{S_{\gamma_k}S_{\delta_l}}),\bar{S}_{\mu_k}]\}$$

$$=\tfrac{1}{3}\{\sum_{i\neq j,\,\alpha_i,\beta_j,\gamma_i,\delta_j,\lambda_i}C_{\alpha_i\beta_j}C_{\gamma_i\delta_j}\,\mathrm{Sp}([(\overline{S_{\alpha_i}S_{\beta_j}}),\bar{S}_{\lambda_i}][(\overline{S_{\gamma_i}S_{\delta_j}}),\bar{S}_{\lambda_i}])$$

$$+\sum_{i\neq j,\,\alpha_i,\beta_j,\gamma_i,\delta_j,\lambda_i\neq j} l_{\lambda_i\neq_j}C_{\alpha_i\beta_j}C_{\gamma_i\beta_j}\,\mathrm{Sp}([(\overline{S_{\alpha_i}S_{\beta_j}}),\bar{S}_{\lambda_i}][(\overline{S_{\gamma_i}S_{\delta_j}}),\bar{S}_{\neq_j}]). \quad (14)$$

After some tedious manipulation we finally obtain

$$\mathrm{Sp}\langle[\bar{H},\bar{S}_x]^2\rangle_{\text{Av}}=-\tfrac{1}{3}(2S+1)^N\sum_{i\neq j}\{(67/48)(C_{\xi\xi}{}^2+C_{\eta\eta}{}^2)+\tfrac{8}{9}C_{\xi\xi}{}^2+(27/24)(C_{\eta\xi}{}^2+C_{\xi\eta}{}^2+C_{\xi\xi}{}^2+C_{\xi\xi}{}^2)$$

$$-(17/24)l_{\xi\xi}(C_{\xi\xi}C_{\eta\eta}-C_{\xi\eta}C_{\eta\xi})-\tfrac{1}{2}(l_{\eta\eta}C_{\xi\xi}C_{\xi\xi}-l_{\eta\xi}C_{\xi\xi}C_{\xi\eta}+l_{\xi\xi}C_{\xi\xi}C_{\eta\eta}-l_{\xi\eta}C_{\xi\xi}C_{\eta\xi}+l_{\xi\eta}C_{\eta\xi}C_{\xi\xi}$$

$$-l_{\xi\xi}C_{\eta\xi}C_{\xi\eta}+l_{\eta\xi}C_{\xi\xi}C_{\xi\eta}-l_{\xi\xi}C_{\xi\xi}C_{\eta\eta}+l_{\xi\xi}C_{\eta\xi}C_{\xi\eta}-l_{\xi\eta}C_{\eta\xi}C_{\xi\xi}+l_{\eta\xi}C_{\xi\xi}C_{\xi\eta}$$

$$-l_{\eta\xi}C_{\xi\eta}C_{\xi\xi}+l_{\xi\eta}C_{\xi\xi}C_{\eta\xi}-l_{\xi\xi}C_{\xi\xi}C_{\eta\eta})\}, \quad (15)$$

where we have omitted i and j in subscripts for reasons of simplicity, e.g., $l_{\xi\eta}$ stands for $l_{\xi_i\eta_j}$, $C_{\xi\eta}$ for $C_{\xi_i\eta_j}$. We can simplify this expression by averaging over all directions of ξ_i, η_i, ξ_j, and η_j axes, fixing the directions of ζ_i and ζ_j axes. This process may be justified since these axes may take arbitrary directions in the planes per-

[3] See, for instance, Gorter, reference 6, Chapter IV.

pendicular to ζ_i and ζ_j axes. After some elementary calculations we find

$$-\mathrm{Sp}\langle[\bar{H},\bar{S}_z]^2\rangle_{\mathrm{Av}}=((2S+1)^N/96)\sum_{j(\neq i)}'\{(135-27l_{\zeta i}l_{\zeta j})^2\bar{A}_{ij}^2+[36-108(n_{\zeta i}{}^i)^2]\bar{A}_{ij}g^2\beta^2r_{ij}^{-3}$$
$$+[432+27l_{\zeta i}l_{\zeta j}-54(n_{\zeta i}{}^i)^2-81(n_{\zeta i}{}^in_{\zeta j}{}^j)^2]g^4\beta^4r_{ij}^{-6}\}. \quad (16)$$

If we take account of the exchange interaction only between nearest neighbors, the above equation reduces to

$$-\mathrm{Sp}\langle[\bar{H},\bar{S}_z]^2\rangle_{\mathrm{Av}}=\tfrac{1}{4}N(2S+1)^N\{33\bar{A}^2+(145/16)g^4\beta^4\sum_{j(\neq i)}'r_{ij}^{-6}+\tfrac{1}{2}g^4\beta^4\sum_{j(\neq i)}^{(\mathrm{s.c.})}r_{ij}^{-6}-(9/8)g^4\beta^4\sum_{j(\neq i)}'(n_{\zeta i}{}^i)^2r_{ij}^{-6}$$
$$-(27/16)g^4\beta^4\sum_{j(\neq i)}'(n_{\zeta i}{}^in_{\zeta j}{}^j)^2r_{ij}^{-6}\}. \quad (17)$$

The values of the requisite lattice sums are as follows; for f.c.c. lattice with lattice constant d,

$$\sum_{j(\neq i)}'r_{ij}^{-6}=115.2d^{-6},\quad \sum_{(j\neq i)}'(n_{\zeta i}{}^i)^2r_{ij}^{-6}=59.8d^{-6},$$
$$\sum_{j(\neq i)}'(n_{\zeta i}{}^in_{\zeta j}{}^j)^2r_{ij}^{-6}=8.59d^{-6}.$$

for s.c. lattice with lattice constant d,

$$\sum_{j(\neq i)}^{(\mathrm{s.c.})}r_{ij}^{-6}=8.40d^{-6}.$$

Using these values for the sums in Eq. (17), we finally obtain

$$-g^2\beta^2\,\mathrm{Sp}\langle[\bar{H},\bar{S}_z]^2\rangle_{\mathrm{Av}}$$
$$=g^2\beta^2(2S+1)^NN\{(33/2)\bar{A}^2+483g^4\beta^4d^{-6}\}. \quad (18)$$

The area of $f(\nu)$, Eq. (10), can be easily obtained; the result is

$$g^2\beta^2\,\mathrm{Sp}\langle\bar{S}_z^2\rangle_{\mathrm{Av}}=\tfrac{3}{4}g^2\beta^2(2S+1)^NN. \quad (19)$$

If it were not for the crystalline splitting, the expressions corresponding to Eqs. (18) and (19) would be

$$-g^2\beta^2\,\mathrm{Sp}[H,S_z]^2=g^2\beta^2(2S+1)^NN(1080g^4\beta^4d^{-6}), \quad (18')$$
$$g^2\beta^2\,\mathrm{Sp}S_z{}^2=(5/4)g^2\beta^2(2S+1)^NN. \quad (19')$$

If we assume the gaussian curve as the shape of $f(\nu)$, the spin relaxation time ρ' can be calculated by the following formulas:

$$\rho'=(\pi/2\nu_m{}^2)^{\frac{1}{2}}, \quad (20)$$

where $\nu_m{}^2$ denotes the mean square frequency defined as the quotient of (11) by (10). For Cr-alum, from Eqs. (10), (11), (18), (19), and (20), we obtain, as our final result, the following expression for ρ':

$$\rho'=(\pi/2)^{\frac{1}{2}}h(644g^4\beta^4d^{-6}+22\bar{A}^2)^{-\frac{1}{2}}. \quad (21)$$

If we assume $\delta=0$, we must make use of Eqs. (18′) and (19′) instead of Eqs. (18) and (19), and we will get the following expression as the spin relaxation time:

$$\rho_0'=(\pi/2)^{\frac{1}{2}}h(864g^4\beta^4d^{-6})^{-\frac{1}{2}}. \quad (21')$$

III. COMPARISON WITH EXPERIMENT AND DISCUSSION

The experimental value of ρ' is given by Volger.[9] He measured the spin absorption at 78 Mc/sec and obtained $\rho'=1.6\times10^{-9}$ sec for Cr−K-alum.

According to Broer's formula (1), ρ' is always smaller than ρ_0'. The reduction factor is the bracketed expression in Eq. (1), which equals $\frac{3}{5}$ in the case of Cr−K-alum, in agreement with the ratio of (19) to (19′). Then $\rho'=3\rho_0'/5=0.9\times10^{-9}$ sec, if we use the following values of constants: $h=6.624\times10^{-27}$ erg sec,[10] $\beta=0.9273\times10^{-20}$ erg/gauss,[10] $g=1.99$,[11] $d=12.2$A.[7] This value is too small compared with the experimental value.

When we use the expression (21), we can explain the experimental value by taking into account the exchange interaction. If we assume $\bar{A}=0$ in the Eq. (21), we get $\rho'=1.76\times10^{-9}$ sec. Therefore, we may conclude that a small contribution of exchange interaction is present. Owing to the inaccuracy of the experimental value and possible error involved in using the gaussian hypothesis, we can estimate only the order of magnitude of $\bar{A}$. When we substitute ρ' in Eq. (21) with the above mentioned experimental value, we can estimate the absolute magnitude of $\bar{A}$. This procedure gives $|\bar{A}|=4.9\times10^{-19}$ erg.

If the whole shape of the distribution function $f(\nu)$ were determined experimentally, we could compare the theoretically derived expression for the second moment directly with the experimental value of the second moment. The measurements have been performed, however, only up to 78 Mc/sec, while the peak of $\nu^2f(\nu)$ must be near 10^3 Mc/sec. So it is possible to determine experimentally only the value of $f(0)$, which is usually expressed in terms of the spin relaxation time ρ'.

In the case of no crystalline splittings and no static magnetic field, Wright has calculated the fourth moment of $f(\nu)$. In this case, the exchange interaction

[9] J. Volger, thesis, Leyden (1946).
[10] R. T. Birge, Revs. Modern Phys. **13**, 233 (1941).
[11] Whitmer, Weidner, and Weiss, Phys. Rev. **73**, 1468 (1948).

does not contribute to the second moment, and the calculation must be carried to at least the fourth moment in order to take into account the exchange interaction. In our case, however, the exchange interaction already contributes to the second moment. Hence the contributions from the fourth and still higher moments to the spin relaxation time will be relatively unimportant. In fact, even the calculation of the second moment is quite laborious, and it will be practically impossible to calculate the fourth moment.

In conclusion, we should like to express our sincere thanks to Professor Masao Kotani for his encouragement and guidance. We also appreciate the helpful discussions of Mr. K. Tomita and Mr. S. Koide. For the publication of this paper, we are very much indebted to Professor Van Vleck for his interest and good offices.

PHYSICAL REVIEW VOLUME 82, NUMBER 5 JUNE 1, 1951

Spin-Spin Interaction*

R. E. Trees
University of Pennsylvania, Philadelphia, Pennsylvania
(Received February 7, 1951)

Araki has suggested that spin-spin and spin-other-orbit interactions have an appreciable effect on the intervals of multiplets in spectra of heavy elements. He has shown that for a large number of elements the three intervals of a quartet (or the four of a quintet, etc.) can be calculated from a relation involving two arbitrary constants. We have calculated the matrix elements of spin-spin interaction for d^n configurations, so that comparison can be made between different multiplets. The results are applied to 8 multiplets of Fe III, taking account of nondiagonal spin-orbit elements with second-order perturbation theory. The agreement obtained seems to warrant the conclusion that spin-spin effects are appreciable. An analysis of the electrostatic interaction in the d^5 configuration of Fe III has also been made.

I. INTRODUCTION

IT has been suggested that spin-spin and spin-other-orbit interactions are important in explaining the intervals of multiplets in atomic spectra even when the nuclear charge is large.[1] The demonstration offered consists in showing that for many elements the three intervals of a quartet (or the four of a quintet, etc.) can be calculated from a relation involving two arbitrary constants, one of which arises from spin-orbit and spin-other-orbit diagonal matrix elements and has a Landé dependence on J, and the other originating in spin-spin diagonal matrix elements with J entering in a more complex fashion (see relation (11) below). It has been pointed out[2] that the neglect of nondiagonal elements of spin-orbit interaction and the use of two parameters to explain each set of multiplet levels make this demonstration inconclusive. By calculating spin-spin and spin-other-orbit matrix elements completely, the different pairs of constants for each of the multiplets of a given configuration are expressible in terms of a much smaller number of radial parameters, and the intervals of triplets can also be analyzed. In the case of d^n configurations, spin-spin interaction and spin-other-orbit interaction are expressible in terms of two radial parameters;[3] and if the parameter for spin-orbit interaction is included, the number of parameters is thus reduced to three. In the present paper, only the matrix elements of spin-spin interaction for d^n configurations have been calculated.

II. THEORY

The calculation is simplified by the use of Racah's methods.[4] The spin-spin interaction will be indicated by H_m^{II} as defined in Marvin.[5] With a few minor redefinitions, Araki's results[1] show that this is a scalar product of the type considered in II (32′); i.e.,

$$H_m^{II}=\sum_{i>j} T_{ij}^{(2)}\cdot U_{ij}^{(2)}. \tag{1}$$

It follows from II (38) that

$$(l^n\alpha SLJM|H_m^{II}|l^n\alpha'S'L'JM)$$
$$=(-)^{S+L'-J}W(SLS'L';J2)$$
$$\times(l^n\alpha SL\|T^{(22)}\|l^n\alpha'S'L'), \tag{2}$$

where $T^{(22)}$ is by definition the double tensor whose scalar part is given by (1) (see II §5). The function W is defined in II (36), and for diagonal elements has the

* Part of a dissertation presented to the faculty of The Graduate School of the University of Pennsylvania in candidacy for the degree of Doctor of Philosophy.

[1] G. Araki, Prog. Theor. Phys. **3**, 152 (1948); **3**, 262 (1948). Relation (1) has been given by L. Eisenbud and E. Wigner, Proc. Natl. Acad. Sci. U.S. **27**, 281 (1941).

[2] G. Reach, private communication.

[3] This follows by extension of the arguments given by Aller, Ufford, and Van Vleck, Astrophys. J. **109**, 42 (1949).

[4] G. Racah, Phys. Rev. **61**, 186 (1942); **62**, 438 (1942); **63**, 367 (1943); **76**, 1352 (1949). These will be referred to as I, II, III, and IV, respectively.

[5] H. H. Marvin, Phys. Rev. **71**, 102 (1947). The radial parameters used in this paper are the ones defined by Marvin for d^5.

TABLE I. $(d^n SL\|T^{(22)}\|d^n S'L')$.

n	SL	$S'L'$	$(d^n SL\|T^{(22)}\|d^n S'L')$
2	^3P	^3P	$-84(M_0+12M_2)$
2	^1P	^1F	$24(14)^{\frac{1}{2}}(M_0-13M_2)$
2	^3F	^3F	$12(14)^{\frac{1}{2}}(M_0-38M_2)$
3	^2P	^4P	$-4(42)^{\frac{1}{2}}(M_0-18M_2)$
3	^2P	^4F	$-2(3)^{\frac{1}{2}}(22M_0+104M_2)$
3	^4P	^4P	$56(6)^{\frac{1}{2}}(M_0-18M_2)$
3	^4P	^2D	$-8(105)^{\frac{1}{2}}(M_0+2M_2)$
3	^4P	^2F	$8(42)^{\frac{1}{2}}(M_0+32M_2)$
3	^4P	^4F	$-16(21)^{\frac{1}{2}}(2M_0-11M_2)$
3	^2D	^4F	$24(5)^{\frac{1}{2}}(M_0-48M_2)$
3	^2F	^4F	$-(42)^{\frac{1}{2}}(14M_0-52M_2)$
3	^4F	^4F	$-16(21)^{\frac{1}{2}}(M_0+7M_2)$
3	^4F	^2G	$-6(30)^{\frac{1}{2}}(3M_0-74M_2)$
3	^4F	^2H	$4(330)^{\frac{1}{2}}(M_0-8M_2)$
4	^1S	^5D	$-240(35)^{\frac{1}{2}}M_2$
4	^3P	^3P	$24(M_0-78M_2)$
4	^3P	^3D	$-6(10)^{\frac{1}{2}}(M_0+2M_2)$
4	^3P	^5D	$-18(70)^{\frac{1}{2}}(M_0+2M_2)$
4	^3P	^3F	$48(M_0-28M_2)$
4	^1D	^5D	$1800M_2$
4	^3D	^3D	$-30(21)^{\frac{1}{2}}/7(M_0-128M_2)$
4	^3D	^5D	$30(3)^{\frac{1}{2}}(3M_0-44M_2)$
4	^3D	^3F	$12(15)^{\frac{1}{2}}(3M_0-19M_2)$
4	^3D	^3G	$60(7)^{\frac{1}{2}}/7(M_0-93M_2)$
4	^5D	^5D	$-210(M_0-8M_2)$
4	^5D	^1F	$-300(14)^{\frac{1}{2}}M_2$
4	^5D	^3F	$12(105)^{\frac{1}{2}}(M_0-23M_2)$
4	^5D	^1G	$180(110)^{\frac{1}{2}}M_2$
4	^5D	^3G	$180(M_0-3M_2)$
4	^3F	^3F	$-12(14)^{\frac{1}{2}}(M_0+22M_2)$
4	^3F	^3G	$-24(10)^{\frac{1}{2}}(M_0-18M_2)$
4	^3F	^3H	$12(110)^{\frac{1}{2}}(M_0+7M_2)$
4	^3G	^3G	$-12(462)^{\frac{1}{2}}/7(M_0-58M_2)$
4	^3G	^3H	$12(22)^{\frac{1}{2}}(M_0-33M_2)$
4	^3H	^3H	$-12(143)^{\frac{1}{2}}(M_0-8M_2)$
5	^2S	^4D	$-6(10)^{\frac{1}{2}}(3M_0-104M_2)$
5	^6S	^5D	$240(105)^{\frac{1}{2}}M_2$
5	^6S	^4D	$42(30)^{\frac{1}{2}}(M_0-8M_2)$
5	^2D	^4D	$180(14)^{\frac{1}{2}}/7(M_0-18M_2)$
5	^2D	^4G	$-60(70)^{\frac{1}{2}}/7(M_0+24M_2)$
5	^4D	^4D	$120(14)^{\frac{1}{2}}/7(M_0+22M_2)$
5	^4D	^2F	$2400M_2$
5	^4D	^2G	$48(385)^{\frac{1}{2}}/7(M_0-18M_2)$
5	^4D	^4G	$-48(70)^{\frac{1}{2}}/7(2M_0+9M_2)$
5	^2F	^4G	$6(10)^{\frac{1}{2}}(7M_0-66M_2)$
5	^2G	^4G	$-30(14)^{\frac{1}{2}}/7(M_0+122M_2)$
5	^4G	^4G	$-240(77)^{\frac{1}{2}}/7(M_0-13M_2)$
5	^4G	^2I	$-12(65)^{\frac{1}{2}}(M_0+12M_2)$

form

$$W(SLSL;J2)=(-)^{S+L-J}2\left\{\frac{(2S-2)!(2L-2)!}{(2S+3)!(2L+3)!}\right\}^{\frac{1}{2}}\times[3K(K+1)-4L(L+1)S(S+1)], \quad (3)$$

where

$$K=J(J+1)-L(L+1)-S(S+1),$$

which agrees with the J dependence given by Araki. Relation (2) need not be restricted to l^n configurations.

The calculation of the last factor on the right of (2) can be carried out by use of a formula suggested by IV(1). The tensor $T^{(22)}$ is of the form

$$T_n^{(pq)}=\sum_{i>j} t_{ij}^{(pq)}, \quad (4)$$

where the subscript "n" indicates a summation over all pairs for n equivalent electrons. Because of the equivalence of the electrons, all terms in the sum contribute the same quantity to the total matrix element. If terms involving the nth electron are removed, the number of terms is reduced in the ratio $(n-2)/n$ so that

$$(l^n\alpha SL\|T_n^{(pq)}\|l^n\alpha'S'L')=[n/(n-2)](l^n\alpha SL\|T_{n-1}^{(pq)}\|l^n\alpha'S'L'). \quad (5)$$

(If the tensor were of the form II(61), i.e.,

$$T_n^{(pq)}=\sum_i t_i^{(pq)}, \quad (6)$$

then the factor $n/(n-2)$ would be replaced by $n/(n-1)$ in this and subsequent relations.) Because vector coupling formulas do not apply to configurations with more than two equivalent electrons, linear combinations of vector coupled eigenfunctions must be used if the explicit dependence of the state on the nth electron is to be indicated. Using eigenfunctions of the form III(8), it follows from (5) that

$$\begin{aligned}(l^n\alpha SL\|T_n^{(pq)}\|l^n\alpha'S'L')&=[n/(n-2)]\sum_{\substack{\alpha_1S_1L_1\\ \alpha_2S_2L_2}}(l^n\alpha SL[l^{n-1}(\alpha_1S_1L_1)lSL)\\&\times(l^{n-1}(\alpha_1S_1L_1)l_nSL\|T_{n-1}^{(pq)}\|l^{n-1}(\alpha_2S_2L_2)l_nS'L')\\&\times(l^{n-1}(\alpha_2S_2L_2)lS'L']l^n\alpha'S'L'). \quad (7)\end{aligned}$$

A generalization of II(44a) can be made to get the relation

$$\begin{aligned}(\alpha s_1l_1s_2l_2SL\|T^{(pq)}\|\alpha's_1'l_1's_2l_2S'L')&=(-)^{s_2+l_2-s_1'-l_1'-S-L+p+q}[(2S+1)(2L+1)\\&\times(2S'+1)(2L'+1)]^{\frac{1}{2}}(\alpha s_1l_1\|T^{(pq)}\|\alpha's_1'l_1')\\&\times W(s_1Ss_1';s_2p)W(l_1Ll_1'L';l_2q). \quad (8)\end{aligned}$$

Relation (8) can be derived from the commutator relation II(23) using the SLM_SM_L scheme in the same way as II(44a) was derived. Using (8) in (7) gives the desired relation:

$$\begin{aligned}(l^n\alpha SL\|T^{(pq)}\|l^n\alpha'S'L')&=(-)^{L+S-l-1+p+q}[n/(n-2)]\\&\times[(2S+1)(2L+1)(2S'+1)(2L'+1)]^{\frac{1}{2}}\\&\times\sum_{\substack{\alpha_1S_1L_1\\ \alpha_2S_2L_2}}(-1)^{L_2+S_2}(l^n\alpha SL[l^{n-1}(\alpha_1S_1L_1)lSL)\\&\times(l^{n-1}\alpha_1S_1L_1\|T^{(pq)}\|l^{n-1}\alpha_2S_2L_2)\\&\times(l^{n-1}(\alpha_2S_2L_2)lS'L']l^n\alpha'S'L')\\&\times W(S_1SS_2S';\tfrac{1}{2}p)W(L_1LL_2L';lq). \quad (9)\end{aligned}$$

The matrix elements of spin-spin interaction for all two-electron configurations involving s, p, and d elec-

trons have been calculated by Marvin.[5] The one element for p^3 has been calculated by Aller, Ufford, and Van Vleck.[3] To calculate the elements for d^n configurations, Marvin's elements for d^2 are compared with (2) to obtain $(d^2 2SL\|T^{(22)}\|d^2 2S'L')$. Relation (9) is then used with $p=q=2$ and α replaced by the seniority number "v" (defined in III §6) to calculate $(d^n vSL\|T^{(22)}\|d^n v'S'L')$. This procedure is repeated to obtain the elements for d^4 and d^6 configurations.

According to the results of this calculation, nonvanishing matrix elements exist only between states with the same seniority number, and the values of the elements in (5) are fully defined if vSL are given; i.e.,

$$(d^n vSL\|T^{(22)}\|d^n v'S'L') = \delta_{vv'}(d^v vSL\|T^{(22)}\|d^v vS'L'). \quad (10)$$

The 48 quantities listed in Table I are therefore sufficient to calculate all of the spin-spin matrix elements for d^n configurations (there are 210 nonvanishing elements for the ten possible configurations). As an example, the diagonal element for the $J=4$ level of the $d^6\ {}^5D$ term ($v=4$) is, according to (2) and (10),

$$(d^6\ {}^5D_4M\,|H_m^{II}|\,d^6\ {}^5D_4M) = W(2222;42)(d^4\ {}^5D\|T^{(22)}\|d^4\ {}^5D).$$

Substituting from (3) and Table I, we see this to be

$$(d^6\ {}^5D_4M\,|H_m^{II}|\,d^6\ {}^5D_4M) = -12(M_0-8M_2).$$

Similarly, for the $J=3$ level it can be shown that the matrix element has the value 24 (M_0-8M_2), so that the interval between these two levels is altered by the amount $36(M_0-8M_2)$.

III. COMPARISON WITH EXPERIMENT

The d^6 configuration of the spectrum of Fe III was chosen for analysis,[6] as the energy levels (with the exception of two high singlets) are all known and are so low that configuration interaction should be small. Moreover, d^6 and d^4 configurations have the largest number of multiplets with nonvanishing diagonal spin-spin elements to make comparison with.

To obtain the eigenfunctions for the five pairs of terms of the same kind that occur in the d^6 configuration, an analysis of the electrostatic interaction energy must first be made. The formulas for this energy have been taken in the same form as II(85), with "$6A$" replaced by a new constant, here indicated by "A." The data has been fitted by the method of least squares, and the results are given in Table II. The mean deviation is 876 cm^{-1}.

An analysis was first made considering only diagonal spin-orbit, diagonal spin-other-orbit, and diagonal spin-spin interactions. The procedure is the same as used by Araki,[1] and in his approximation the interval between the level "J" and "$J-1$" is of the form

$$\Gamma_J = E_J - E_{J-1} = C_1 J + C_2 J[2J^2 - 2L(L+1) - 2S(S+1) + 1]. \quad (11)$$

There are two constants in this expression which are determined from the two intervals for the triplets of d^6. The four intervals of the ^5D of d^6 can be combined in pairs to give three independent evaluations of these constants, thus giving an additional check on the consistency. The first five columns of Table III give the results of this analysis for 8 multiplets of the d^6 configuration of Fe III. The three independent determinations of the constants C_1 and C_2 furnished by the ^5D are defined by the pairs of intervals Γ_4 and Γ_3, Γ_3 and Γ_2, and Γ_2 and Γ_1, reading down in Table III. The sixth and seventh columns of Table III give the magnitudes of the two terms on the right side of Eq. (11), and have been called the spin-orbit part (it has C_1 as factor) and the spin-spin part (it has C_2 as factor) for brevity.

By assuming that the constant C_1 is determined chiefly by the spin-orbit interaction, one gets approximate values of the parameter ζ_d of spin-orbit interaction. The calculation is made using the relation III(25), and the resulting values of ζ_d are given in the final column of Table III. Partly owing to neglect of nondiagonal spin-orbit elements, the results are not very consistent and are particularly bad for the two ^3F terms. If these two terms are omitted, the remaining six terms lead to a value $\zeta_d = 413 \pm 21$.

The effect of nondiagonal spin-orbit elements has been estimated by second-order perturbation theory, the experimental values being adjusted to the positions they would occupy if the effects of nondiagonal elements were absent. These revised energy levels are

TABLE II. Term values of the $3d^6$ configuration of Fe III (cm^{-1}).

Term	Obs.	Calc.	Diff.
^5D	422	688	266
^3P	20032	21642	1610
^3H	20251	19321	−930
^3F	21635	22115	480
^3G	24837	24003	−834
^1I	30355	28637	−1718
^3D	30783	30558	−225
^1G	30886	30320	−566
^1S	34812	35152	340
^1D	35803	37253	1450
^1F	42896	42684	−212
$^3F'$	50260	50166	−94
$^3P'$	49992	50640	648
$^1G'$	57221	56848	−373
$^1D'$		76137	
$^1S'$		98720	

$A = 15F_0 - 14F_2 - 420F_4 = 20354.2$
$B = F_2 - 5F_4 = 936.49$
$C = 35F_4 = 3721.66$
Mean deviation = ±876 cm^{-1}

[6] B. Edlen and P. Swings, Astrophys. J. 95, 532 (1942).

TABLE III. Analysis of intervals of multiplets of d^6 configuration of Fe III (no correction for nondiagonal spin-orbit elements).

Level	Energy	Interval	C_1	C_2	Sp. orb. part	Sp. sp. part	ζ_d
^5D, $J=4$	−0.8	−436.2	−103.8	−0.58	−415.3	−20.9	415.2
3	435.4	−302.7	−103.0	−0.42	−309.0	6.3	412.0
2	738.1	−193.5	−101.4	−0.31	−202.8	9.3	405.6
1	931.6	−94.9			−101.4	6.5	
0	1026.5						
^3P, $J=2$	19404.0	−1283.6	−621.5	−20.28	−1243.0	−40.6	421
1	20687.6	−520.1			−621.5	101.4	
0	21207.7						
^3H, $J=6$	20050.3	−249.7	−39.4	−0.24	−236.4	−13.3	394
5	20300.0	−181.1			−197.0	15.9	
4	20481.1						
^3F, $J=4$	21461.4	−237.7	−56.9	−0.5	−227.6	−10.0	566
3	21699.1	−157.3			−170.7	13.4	
2	21856.4						
^3G, $J=5$	24558.0	−382.1	−66.3	−1.45	−331.5	−50.6	442
4	24940.1	−201.5			−265.2	63.7	
3	25141.6						
^1D, $J=3$	30857.0	141.6	31.6	5.2	94.8	46.8	379
2	30715.4	−9.6			63.2	−72.8	
1	30725.0						
$^1F'$, $J=4$	50275.3	−19.1	10.1	−2.98	40.4	−59.5	590
3	50294.4	110.3			30.3	80.0	
2	50184.1						
$^1P'$, $J=2$	50411.5	835.4	419.6	−1.95	839.2	−3.8	429
1	49576.1	429.1			419.6	9.5	
0	49147.0						

defined by the relation

$$E^a(SLJ)=E^0(SLJ)+\sum_{S'L'}\frac{|(d^5SLJ|\sum \mathbf{L}_i\cdot\mathbf{S}_i|d^5S'L'J)|^2\zeta_d^2}{E^0(S'L'J)-E^0(SLJ)}, \quad (12)$$

where $E^0(SLJ)$ are the energy levels given by experiment, and the sum is over all terms of the d^6 configuration of Fe III except the term that is to be adjusted. The value $\zeta_d=425$ was assumed, since this was found by trial to be more consistent than 413 with the value of ζ_d obtained from the corrected calculation. The values of the revised energy levels are given in the second column of Table IV. Except for the calculated values of C_2 and the calculated spin-spin parts, the other columns of Table IV are calculated from the revised energy levels in the same way as the corresponding columns of Table III were calculated from the original experimental data.

To calculate C_2 it is assumed that the spin-spin part is due solely to spin-spin interaction, which was the assumption made in the original derivation of Eq. (11). By use of Eqs. (2), (3), and (10), it may then be shown that the constant C_2 should theoretically have the value

$$C_2=12\left\{\frac{(2L-2)!(2S-2)!}{(2L+3)!(2S+3)!}\right\}^{\frac{1}{2}}(d^5vSL\|T^{(22)}\|d^5vSL) \quad (13)$$

for the terms occuring only once in d^6; thus, for the ^5D we have

$$C_2=-(M_0-8M_2).$$

For the other terms of d^6, linear combinations of these values must be taken appropriate to the eigenfunction considered. The two parameters M_0 and M_2 were determined by least squares with the spin-spin parts of Table IV as the experimental data and were found to be $M_0=0.304$ and $M_2=0.018$. With these values of the parameters, the calculated values of C_2 are determined from (13), and the calculated spin-spin part is the value of the second term on the right-hand side of (11).

Again omitting both ^3F terms, the value of the spin-orbit parameter obtained from the values in column 8 of Table IV is $\zeta_d=429\pm16$, which is reasonably consistent with the assumed value of 425. The mean square value of the experimentally defined spin-spin parts in column 7 of Table IV is 9 cm^{-1}, while the mean deviation between the calculated and experimental values of the spin-spin parts is 4 cm^{-1}.

IV. DISCUSSION OF ERRORS

The major sources of error in the calculation occur in the correction for the nondiagonal elements of spin-orbit interaction. Most important is the uncertainty in the value of the radial parameter ζ_d which might possibly be in error by 4 percent. The average error in the spin-spin part would be about 3 cm^{-1} from the full error in ζ_d. The matrix elements also may be in error owing to errors in the choice of eigenfunctions. The agreement obtained between two calculations with widely different values of the parameters of electrostatic interaction indicates that the error will be less than 2 cm^{-1} for any reasonable values of the radial parameters. A third source of inaccuracy is the use of perturbation theory instead of solving for the eigenvalues of the matrices.

TABLE IV. Analysis of intervals of multiplets of d^6 configuration of Fe III (energy corrected for nondiagonal spin-orbit elements).

Level	Energy	Interval	C_1	C_2	Sp. orb. part	Sp. sp. part	ζ_d	C_2 (calc.)	Sp. sp. part (calc.)
^5D, $J=4$	30.9	−422.1	−104.7	−0.10	−418.8	−3.3	419	−0.160	−5.8
3	453.0	−312.6	−104.4	−0.04	−313.2	0.6	418		2.4
2	765.6	−207.7	−103.0	0.06	−206.0	−1.7	412		4.8
1	973.3	−104.2			−103.0	−1.2			3.4
0	1077.5								
^3P, $J=2$	19416.8	−1248.7	−620.8	−3.56	−1241.6	−7.1	421	−3.258	−6.5
1	20665.5	−603.0			−620.8	17.8			16.3
0	21268.5								
^3H, $J=6$	20076.6	−284.5	−45.9	−0.17	−275.4	−9.1	459	−0.064	−3.5
5	20361.1	−218.4			−229.5	11.1			4.2
4	20579.5								
^3F, $J=4$	21581.7	−177.4	−44.6	0.05	−178.4	1.0	444	−0.253	−5.1
3	21759.1	−135.0			−133.8	−1.2			6.8
2	21894.1								
^3G, $J=5$	24496.9	−327.9	−65.8	0.03	−328.9	1.0	438	0.127	4.4
4	24824.8	−264.2			−253.0	−1.2			−5.6
3	25089.0								
^3D, $J=3$	30876.4	109.9	33.6	1.02	100.8	9.1	403	0.857	7.7
2	30766.5	52.9			67.2	−14.3			−12.0
1	30713.6								
$^3F'$, $J=4$	50280.0	56.8	15.9	−0.34	63.6	−6.8	933	−0.175	−3.5
3	50223.2	56.5			47.4	9.1			4.7
2	50166.7								
$^3P'$, $J=2$	50389.6	821.7	414.5	−3.64	829.0	−7.3	425	−3.698	−7.4
1	49567.9	432.7			414.5	18.2			18.5
0	49135.2								

This would lead to only a small error, as the nondiagonal elements are of the order of a tenth the distance between levels at the largest. Further sources of error, such as configuration interaction, might also affect the results. An experimental check may be made by computing the spin-spin parts for the ^5D using the two extreme values of C_2 (i.e., −0.10 and 0.06); the mean square difference between the two sets of spin-spin parts is 4 cm^{-1}. It seems safe to conclude that the mean square error of the spin-spin parts in column 7 of Table IV lies within the limits 2–6 cm^{-1}.

The very large value of ζ_d for the $^3F'$ level in Table IV seems to be caused by the smallness of C_1. It was noted that the calculation of ζ_d depends strongly on the values chosen for the parameters of the electrostatic interaction; this is also true to some extent for the ^3F level.

V. CONCLUSION

The preceding analysis of the d^6 configuration of Fe III is an effort to explain 18 deviations from the Landé rule. Although a spin-spin interaction was assume in making the calculations, this is not essential as C_1 can be determined by least squares, and the part of the interval not following the Landé rule would be very nearly equal to the spin-spin parts of Tables III and IV.

Nondiagonal spin-orbit interaction is important in explaining deviations from the Landé rule. The mean square value of the spin-spin parts of Table III is 47 cm^{-1}, and this is reduced to 9 cm^{-1} when nondiagonal spin-orbit interactions are allowed for. Part of this remaining deviation is, no doubt, due to the approximate methods used, but it seems unlikely that all the error is due to this.

By correcting for spin-spin interaction, the remaining deviation can be reduced from 9 cm^{-1} to 4 cm^{-1}. Half of the spin-spin parts of Table IV are greater than 7 cm^{-1}; and in the case of the $^3F'$ and ^3D they are more than 10 percent of the interval, so that the deviations to be explained are appreciable compared with known sources of error. Only two parameters were used to explain 18 deviations. There is an agreement in sign in all cases except the ^3F and the ^5D, and the latter would also agree if C_2 were taken as the lowest experimental value, −0.10 (the magnitudes of the spin-spin parts of the ^5D would then agree much better also). The agreement in magnitude is only fair, however, as the difference is more than 50 percent of the experimental value for 4 of the 8 multiplets. The fact that the radial parameters are found to be positive and that $M_2 < M_0/7$ is in accord with the restrictions placed on these parameters by their definition in terms of radial integrals.[6,7]

One can avoid the difficulty of separating a spin-spin part by calculating the matrix elements of spin-other-orbit interaction in a manner similar to that used for spin-spin interaction, so that the entire interval is then defined in terms of three parameters. Since the same

[7] The estimate of C_2 for the d^2 ^3D of Fe III (−0.16) is much smaller than the value −0.475 ($\rho=0.95\pm0.1$) obtained by M. H. L. Pryce [Phys. Rev. **80**, 1107 (1950)], neglecting spin-orbit nondiagonal elements. Equation (13) agrees with his Eq. (3) for the ^5D of d^5 and d^6, the ^3F of d^2 and d^6, and the ^4F of d^3 and d^7.

radial parameters are involved in spin-other-orbit interaction and spin-spin interaction, they will probably have effects of the same order of magnitude on the interval. It should then be possible to get more consistent values of ζ_d when C_1 is corrected for spin-other-orbit interaction, and this would be a check on the preceding analysis.

I wish to thank Dr. C. W. Ufford for suggesting this problem and for many helpful discussions during the course of the work.

PHYSICAL REVIEW VOLUME 82, NUMBER 5 JUNE 1, 1951

Half-Life of I^{129} and the Age of the Elements*

S. KATCOFF, O. A. SCHAEFFER, AND J. M. HASTINGS
Chemistry Department, Brookhaven National Laboratory, Upton, Long Island, New York
(Received February 15, 1951)

The specific activities of several samples of methyl iodide containing I^{129} were measured with proportional counters, and the ratios of I^{129} to I^{127} were determined with a 60° sector type mass spectrometer. The half-life of I^{129} was found to be $(1.72\pm0.09)\times10^7$ years. The time interval between the formation of the elements and the formation of the earth calculated from this value is 2.7×10^9 years. It was assumed that most of the Xe^{129} present on the earth at present originated from decay of I^{129} after the formation of the earth and that the original cosmic abundance of I^{129} was about equal to that of the stable I^{127}.

I. HALF-LIFE DETERMINATION

THE half-life of I^{129} was found by measuring the absolute disintegration rates, isotopic compositions, and total iodine contents of several samples obtained from fission product iodine that was separated from a uranium slug which had received a 4-year irradiation in the Oak Ridge pile and had cooled for 21 months.

For the chemical separation the uranium was dissolved in concentrated hydrochloric acid to which a few mg of iodine carrier had been added. After oxidation with hydrogen peroxide the elementary iodine was removed by counter-current extraction into carbon tetrachloride. It was purified by six or eight (see below) chemical cycles consisting of reduction to iodide, extraction into water, re-oxidation to iodine, and re-extraction into carbon tetrachloride. The iodine was finally precipitated as PdI_2, which was washed and dried. Then it was decomposed by heating to 350° in an evacuated glass system; the evolved iodine vapor was collected in a tube containing methanol and red phosphorus. This mixture was heated at 110° for one hour to make methyl iodide, which was then passed over anhydrous calcium chloride to separate it from excess methanol. The methyl iodide was used for the activity measurements and the isotope ratio determinations.

The counters[1] were 2 cm in diameter and 30 cm long with silver cathodes and 2-mil wolfram center wires. They were operated in the proportional region with a 5000-volt power supply, a non-overloading pulse amplifier, and an Atomic Instrument Company scaler, model 101A. The counter gas was methane at one atmosphere. Preliminary experiments were performed to study the effect of adding small amounts of methyl iodide to the methane. It was found that the counter plateau disappeared and that the counting rate of a Co^{60} γ-ray standard started to decrease as the partial pressure of methyl iodide was increased above 50 microns. Therefore, the measurements were made with the radioactive methyl iodide samples at partial pressures between 17 and 38 microns and with the counters operating at 3800 volts on both voltage and gain plateaus. Each sample was counted at least twice for periods of 20 to 150 minutes for total recorded counts $>10^4$. Then the counter was cooled to $-195°$ for one hour and the methane pumped off leaving the methyl iodide behind. This was then distilled, by warming the counter to room temperature, into a small tube containing a 30-mg piece of sodium and cooled with liquid nitrogen. This tube was set aside for the quantitative iodine determination. The counter was refilled with methane and the background counting rate determined. This was usually found to be somewhat higher than what it had been before the active methyl iodide had been in the counter. Apparently, anywhere, from 0 to 12 percent (average of 5 percent) of the methyl iodide remained in the counters. The backgrounds used in the calculations were those measured after the methyl iodide was distilled out. The operation of the counters was always checked by means of the Co^{60} standard. Its counting rate, corrected for I^{129} activity and background, remained the same within one percent, independent of the counter used and the amount of active methyl iodide therein. The total volumes and cathode volumes of the counters were measured at the conclusion of the experiments by adding water to them from a buret. It was shown by Bernstein and Ballentine[1] that the cathode volume is equal to the sensitive volume and that the observed counting rate is very nearly equal

* Research carried out under the auspices of the AEC.
[1] W. Bernstein and R. Ballentine, Rev. Sci. Instr. **21**, 158 (1950).

TABLE I. Data for determination of half-life.

No. of sample	No. of counter	Cathode vol. / Total vol.	Moles of CH_3I in counter	Counter bkd. (c/m)	Activity of I^{129} (c/m) (corr. for bkd.)	Half-life (years)
1a	7	0.859	1.698×10^{-7}	127	467	1.62×10^{7}
1b	8	0.867	1.468×10^{-7}	117	376	1.75×10^{7}
1c	7	0.859	1.838×10^{-7}	183	470	1.74×10^{7}
1d	8	0.867	1.995×10^{-7}	137	506	1.77×10^{7}
2a	6	0.864	0.970×10^{-7}	169	250	1.71×10^{7}
2b	7	0.859	0.925×10^{-7}	148	238	1.71×10^{7}
2c	8	0.867	1.434×10^{-7}	119	370	1.72×10^{7}
2d	10	0.864	1.810×10^{-7}	95	462	1.73×10^{7}
2e	8	0.867	1.688×10^{-7}	131	427	1.75×10^{7}

to the actual disintegration rate within this volume for C^{14}. In the present work it was assumed that these conditions apply also.

The small tube containing the methyl iodide transferred from the counter was heated with the sodium to 250° for 20 minutes in order to form NaI. Then water vapor diluted with helium was passed in to react with the excess sodium. The mixture in the tube was dissolved in 3 ml of water and its iodine content determined quantitatively by a potentiometric titration with 1.01×10^{-4} molar silver nitrate solution against a calomel electrode. This analytical method was tested first by titrating eight 22-μg samples of iodide from a stock solution. The mean deviation from the average was less than 2 percent, and the agreement with a gravimetric analysis of the stock solution in which two 13.5-mg samples of silver iodide were precipitated was better than 4 percent. The analytical method was also tested by filling counters with amounts of inactive methyl iodide measured with a manometer and expanded by a known amount, adding an atmosphere of methane, and then proceeding as in the final experiments. In five samples with methyl iodide pressures between 16 and 142 microns the average agreement was 7 percent, but the methyl iodide pressure determinations were not very accurate and no correction was made for the methyl iodide which remained behind in the counter. In one run when no methyl iodide was added a zero blank was obtained.

Two different isotopic analyses were performed. The first, (No. 1), was done with the CH_3I which was prepared from the iodine that had been through six purification cycles and from which samples 1a–1d were taken. Isotopic analysis No. 2 and samples 2a–2e were taken from the iodine that had undergone eight purification cycles. The single collector 60° sector type mass spectrometer[2] that was used had 70-volt ionizing electrons, a 4000-volt ion accelerating potential, and magnetic scanning. Several preliminary runs were made with ordinary CH_3I (only I^{127}). For analysis No. 1, the ratios of the ion current at mass 129 to that at mass 127 (I^+ peaks) in six successive runs were: 0.0707, 0.0703, 0.0701, 0.0701, 0.0713, and 0.0702. The average was 0.0704. In analysis No. 2, the ratios in four runs were: 0.0714, 0.0691, 0.0685, 0.0682; average: 0.0694. Since a compensating hairpin-type leak was used, a correction for fractionation had to be made: The ratios were multiplied by (mass of CH_3I^{127}/mass of CH_3I^{129})[1]. Thus, the corrected ratios for analyses No. 1 and No. 2, respectively, are: 0.0699 and 0.0689; or 6.53 and 6.45 atomic percent I^{129}. For some of the runs the complete spectrum was computed using these ratios and the pattern for ordinary CH_3I. The maximum deviation was less than 2 percent for any mass. The isotopic ratios found are probably accurate to ±2 percent even considering the possible systematic errors.

Table I gives the data and results for each sample. The average of the nine values for the half-life of I^{129} is 1.72×10^{7} years with an over-all estimated probable error of 5 percent. A half-life of $(3\pm1)\times10^{7}$ years based on experiments in which the activity of solid samples of AgI containing I^{129} was measured has been reported by Parker, *et al.*[3] They also report a maximum β-ray energy of 100–135 kev in good agreement with the value of 130 kev found in this work by observing that the range of the β-rays in aluminum is about 22 mg/cm^2.

II. AGE OF THE ELEMENTS

It was first pointed out by Suess[4] that a lower limit for the time interval, t, between the formation of the elements and the formation of the earth's atmosphere could be calculated if the half-life of I^{129} were known. Any I^{129} still in existence when the earth was first able to retain its atmosphere must have decayed to Xe^{129} and therefore increased the abundance of this isotope over its primeval value. By making the plausible assumption that the original abundance of I^{129} was approximately equal[4–6] to that of I^{127}, it is only necessary to compare the present abundance in the earth's crust of I^{127} with that of Xe^{129}. Suess used values of 1 g/cm^2 and 10^{-4} g/cm^2 for these abundances, respec-

[2] O. A. Schaeffer and J. M. Hastings, J. Chem. Phys. **18**, 1048 (1950).

[3] Parker, Creek, Herbert, Lantz, and Martin, Oak Ridge National Laboratory Report No. 286, p. 53, 1949 (unpublished).

[4] H. E. Suess, Z. Physik **125**, 386 (1948).

[5] H. E. Suess, Z. Naturforsch. **2a**, 311 (1947).

[6] J. Mattauch and S. Flügge, *Nuclear Science Tables* (Interscience Publishers, Inc., New York), p. 104.

tively, and calculated a lower limit for t of 10 I^{129} half-lives. From the systematics of nuclear abundance data, he thought that Xe^{129} did not have an abnormally high abundance compared to the other Xe isotopes.

Aten,[7] however, has pointed out that in all cases, where an odd isotope occurs between two even ones, the odd one is always less abundant than the sum of the abundances of the other two. The only exception is Xe^{129} whose abundance is 26.23 percent while Xe^{128} and Xe^{130} have abundances of 1.90 percent and 4.07 percent, respectively. Therefore, most of the Xe^{129} present in the atmosphere today originated by decay of I^{129} after the formation of the earth just as most of the A^{40} originated from decay of K^{40}.

It was suggested by Dr. M. Goldhaber of this Laboratory that t probably could be calculated more accurately by comparing the I^{127}/K^{40} abundance ratio with the Xe^{129}/A^{40} abundance ratio. In this way the terrestrial abundance data given by Goldschmidt[8] can be applied directly; and as a first approximation it can be assumed that the atmosphere contains the same fraction of the earth's Xe^{129} that it does of the earth's A^{40}. The following equation was used:

$$(I^{127}e^{-\lambda t}/K^{40})_T=(Xe^{129}/A^{40}).$$

I^{127} refers to an abundance[8] of 0.24 atom per 10^6 atoms of silicon; λ is the disintegration constant of I^{129}; K^{40} refers to the number of atoms (per 10^6 atoms of Si) which have decayed to A^{40} in time T, the age of the earth, 3.35×10^9 years.[9] Its present abundance was taken as 0.0119 percent of the total potassium abundance of 44,200 atoms[8] per 10^6 Si atoms; its half-life -1.27×10^9 years[10] with 12 percent decaying to A^{40}. The A^{40} in the equation refers to its abundance in the atmosphere by volume, 0.93 percent; and Xe^{129} refers to the radiogenic Xe^{129} which is assumed to be *20 percent* of the total Xe abundance in the atmosphere, 8×10^{-6} percent Xe by volume.[11] This leaves 6.23 percent Xe^{129} which is not radiogenic. Thus, the rule of Aten is approximately satisfied, and the rule which states that two odd isotopes of an element have roughly the same abundance[5,6] is not seriously violated either (abundance of Xe^{131} is 21.2 percent).

Solving the equation for t gives 15.4 half-lives of I^{129} or 2.7×10^8 years for the time between the formation of the elements and the formation of the earth. Thus, the age of the elements $(T+t)$ is 3.6×10^9 years. This calculation of t is very insensitive to the accuracy of the assumptions and approximations that were used. For example, if the amount taken for radiogenic Xe^{129} is wrong by a factor of 10 the error in t is only 22 percent.

[7] A. H. W. Aten, Jr., Phys. Rev. **73**, 1206 (1948).
[8] V. M. Goldschmidt, Geochem. Verteilungsgesetze IX, Videnskapsakademien, Oslo (1937).
[9] A. Holmes, Nature **159**, 127 (1947).
[10] G. A. Sawyer and M. L. Wiedenbeck, Phys. Rev. **79**, 480 (1950).
[11] G. Damköhler, Z. Elektrochem. **41**, 74 (1935).

PHYSICAL REVIEW VOLUME 82, NUMBER 5 JUNE 1, 1951

Conservation of Angular Momentum in the Statistical Theory of Nuclear Reactions

L. WOLFENSTEIN
Carnegie Institute of Technology, Pittsburgh, Pennsylvania
(Received January 27, 1951)

The conservation of total angular momentum J, z-component of angular momentum m, and parity p are considered in connection with the statistical theory of nuclear reactions. Results are obtained for the angular distribution of a single group of outgoing particles and for the cross section as a function of the spin of the residual nucleus. The energy and angular distributions are also considered for the case in which many groups are observed simultaneously. The density of nuclear states as a function of spin affects results appreciably.

INTRODUCTION

WHEN a particle of energy less than 50 Mev strikes a nucleus it is usually pictured as forming a compound nucleus.[1] In this process the incident energy is distributed among the many particles of the nucleus with the result that the incident particle can no longer be distinguished from the others. The outgoing product particles of the collision are the products of the decay of the compound nucleus. The state of the compound nucleus and, consequently, its decay products are often said to be independent of the way in which the compound nucleus is produced. This statement must be qualified, however, by the condition that any compound nuclear state must have the same total angular momentum J, z-component of total angular momentum m, and parity p as the initial state.[2] The conservation of J and p, as has been noted a number of times,[3] results in selection rules which forbid transitions between certain compound nuclear states and particular initial or final states. Little mention, however, has been made of the conservation of m, which may be said to have as its

[1] N. Bohr, Nature **137**, 344 (1936).
[2] It is assumed here and throughout that the initial state is resolved into a sum of products of spin and orbital functions which in turn can be expressed as a sum of states with particular values of J, m, and p.
[3] For example, H. A. Bethe, Revs. Modern Phys. **9**, 108 (1937).

consequence that the compound nucleus "remembers" the axis of incidence of the initial particles. In the present paper these conservation principles are applied to nuclear reactions in which the compound nucleus has so large a density of levels that it may be treated by the statistical, or continuum theory.[4,5] In particular, the angular distribution of such reactions is discussed.

GENERAL FORMULATION

A collision is considered of particle a with spin s and particle α with spin i in which both spins are unpolarized. The general procedure is to resolve the initial state into states characterized by the set of quantum numbers $(ljJmp)$, where l is the orbital angular momentum, and j is the vector sum of i and s. The parity p is actually not an independent quantum number but is determined by the value of l. It is noted separately, however, since it is conserved and l is not. If only a single compound nuclear state is involved, a fairly simple equation can be written for the angular distribution of the product particles. Even for this case, however, the equation contains a number of constants about which theory tells us very little. These constants describe the spin-orbit coupling of the compound state relative to the initial particle states and to the final particle states. Several attempts have been made to determine the constants in this equation (or in the corresponding equation for two or three compound states) for particular reactions.[6]

In the statistical theory it is assumed that the transition from the initial state of particles a and α to the compound state, and the decay of the compound state to particles b and β can be treated as independent processes. This may be interpreted as meaning that if a large number of compound levels are considered, the phase relations between the matrix elements of the transition to the compound state, and those from the compound state, are random.[3,4] Consequently, one may define $\sigma(Jmp, a\alpha ljm_j\theta)$ = cross section for capture of a by α forming a compound nucleus with quantum numbers (Jmp) starting with a plane wave making an angle θ with the z-axis, in a spin state characterized by the quantum numbers (jm_j), and considering only contributions from orbital angular momentum l. This may be written[7]

$$\sigma(Jmp, a\alpha ljm_j\theta) = |A(lm-m_jm_j\theta)|^2 \times (ljJm|ljm-m_jm_j)^2\sigma_{al}\xi(Jp, a\alpha lj). \quad (1)$$

The first factor in Eq. (1) is proportional to the square of a coefficient in the expansion of the incident plane wave function $\psi_\theta(\Theta)$ in terms of spherical harmonics $Y_l^{m_l}(\Theta)$,[8] where $m_l = m - m_j$. Since angles measured relative to the axis of incidence are given by $(\Theta-\theta)$,

$$\psi_\theta(\Theta) = \text{const} P_l^0(\Theta-\theta).$$

By the addition theorem for legendre polynomials, it follows that

$$|A(lm_l\theta)| \equiv |\text{const}\int \psi_\theta(\Theta) Y_l^{m_l}(\Theta)\, d\Omega| = \text{const} P_l^{m_l}(\theta). \quad (1a)$$

Equation (1) has been written so that this first factor equals unity (times δ_{m_l0}) for the usual choice of θ equals zero. This will follow from Eq. (1a) if the proportionality constant is set equal to unity.

The second factor in Eq. (1) represents the usual coefficients for combining angular momenta.[9] The third factor,

$$\sigma_{al} = (2l+1)\pi\lambda_a^2 P_{al}, \quad (1b)$$

is the product of the "target area" for particles of angular momentum l and the penetration factor P_{al} for the combined angular momentum and coulomb barriers. The last factor plays the role of a "sticking probability," which will be assumed later to be independent of the various quantum numbers.

Similarly,[10] $\Gamma(Jmp, b\beta\mathbf{ljm}_j\theta)d\Omega/4\pi$ = width (averaged over a large number of compound levels all at essentially the same energy) for decay of a compound nucleus with quantum numbers (Jmp) to form particles b and β moving along a line making an angle $\boldsymbol{\theta}$ with the z-axis, within a solid angle $d\boldsymbol{\Omega}$, and in a spin state characterized by the quantum numbers $(\mathbf{jm}_j)$, considering only orbital angular momentum $\mathbf{l}$.

Applying the law of detailed balancing,

$$\Gamma(Jmp, b\beta\mathbf{ljm}_j\theta) = D^{Jp}\frac{\sigma(Jmp, b\beta\mathbf{ljm}_j\theta)}{2\pi^2\lambda_b^2} = \frac{D^{Jp}}{2\pi}(\mathbf{lj}Jm|\mathbf{lj}m-\mathbf{m}_j\mathbf{m}_j)^2(2l+1) \times P_{bl}\xi(Jp, b\beta\mathbf{lj})|A(\mathbf{l}m-\mathbf{m}_j\theta)|^2, \quad (2)$$

[4] This theory as used here is described by V. F. Weisskopf, Lecture Series in Nuclear Physics (U. S. Govt. Printing Office, December, 1947), p. 80.

[5] J. M. Blatt and V. F. Weisskopf, "Theory of nuclear reactions," Technical Report No. 42 (Massachusetts Institute of Technology, 1950) (unpublished).

[6] $Li^7(p,\alpha)\alpha$: C. Critchfield and E. Teller, Phys. Rev. **60**, 10 (1941); D. R. Inglis, Phys. Rev. **74**, 21 (1948); $Li^6(d,\alpha)\alpha$: R. Resnick and D. R. Inglis, Phys. Rev. **76**, 1318 (1949); $Li^7(p,n)$: G. Breit and I. Bloch, Phys. Rev. **74**, 397 (1948); $F^{19}(p,\alpha)$: E. Gerjuoy, Phys. Rev. **58**, 503 (1940); C. Y. Chao, Phys. Rev. **80**, 1035 (1950).

[7] A rigorous derivation may be given following the method of reference 5. The only assumption is that there is no *elastic* scattering with a change of orbital angular momentum. This assumption follows from the statistical, or continuum theory in which the only appreciable elastic nuclear scattering is due to the surface of the nucleus. Equation (10.16) of reference 5 may be seen to be a sum over l of Eq. (1) above for the case $\theta=0°$ by replacing $\eta_{ll'}$ by $(1-\xi P_{al})^{\frac{1}{2}}\delta_{ll'}$. Incidentally, this derivation shows that, with the assumption mentioned, it is possible to isolate contributions to the cross section from different l values.

[8] The argument Θ here stands for both polar and azimuthal angles. On the other hand φ is simply a polar angle since the results are independent of φ as long as polarization of spins is not considered. The functions $P_l^{m_l}(\theta)$ then are associated legendre polynomials normalized to $2/(2l+1)$.

[9] Condon and Shortley, *Theory of Atomic Spectra* (The Macmillan Company, New York, 1935), p. 73. The tables given there have been extended by Dr. David Falkoff, who kindly sent me a copy of this work.

[10] Values after collision are indicated by bold-face type, except in subscripts where they can be distinguished by the fact that they are not in italic type.

where D^{Jp} is the average spacing of compound nuclear levels with quantum numbers (Jp). This differs from the usual formulation[11] only in the designation of the direction $\boldsymbol{\theta}$ and the quantum numbers m and $\mathbf{m}_j$. To obtain the usual form, one may define

$$\Gamma_b=\int \sum_{m\mathbf{m}_j} \Gamma(Jmp, b\beta\mathbf{lj}\mathbf{m}_j\boldsymbol{\theta})d\Omega/4\pi,$$
$$\sigma_b=\sum_{m\mathbf{m}_j} \sigma(Jmp, b\beta\mathbf{lj}\mathbf{m}_j 0). \tag{2a}$$

It then follows from Eq. (2) that

$$\Gamma_b=(D^{Jp}\sigma_b/2\pi^2\lambda_b^2). \tag{2b}$$

However, Γ_b and σ_b are of doubtful significance because they are summed over m independently, whereas m is actually conserved throughout the reaction. If one omits the summation over m in Eq. (2a), thus defining $\Gamma_b(m)$ and $\sigma_b(m)$, one finds a relation less simple than Eq. (2b):

$$\Gamma_b(m)=\frac{D^{Jp}\sigma_b(m)}{2\pi^2\lambda_b^2(2\mathbf{l}+1)(\mathbf{lj}Jm|\mathbf{lj}0m)^2}.$$

The differential cross section of the reaction is given by

$$\sigma(a\alpha, b\beta\boldsymbol{\theta})=\sum_{\mathbf{j}}\sum_{\mathbf{m}_j=-\mathbf{j}}^{\mathbf{j}}\sum_{l=J-\mathbf{j}}^{J+\mathbf{j}}{}'\sum_{l=0}^{\infty}\sum_{j=|i-s|}^{i+s}\sum_{m=-j}^{j}\sum_{J=|l-j|}^{l+j}\frac{\sigma(Jmp, a\alpha ljm0)}{(2i+1)(2s+1)}\times\frac{\Gamma(Jmp, b\beta\mathbf{lj}\mathbf{m}_j\boldsymbol{\theta})}{\int\sum_{c\gamma\mathbf{l}'\mathbf{j}'\mathbf{m}_{j'}}\Gamma(Jmp, c\gamma\mathbf{l}'\mathbf{j}'\mathbf{m}_{j'}\boldsymbol{\theta}')d\Omega'/4\pi}. \tag{3}$$

Here the first factor represents the formation of the compound nucleus (the incident θ equals zero) and the second represents the width for outgoing particles b and β at angle $\boldsymbol{\theta}$ divided by the total width for all possible decay products. The sums over m and j represent an average over the initial polarization of the spins[12] which averaging also requires the division by $(2i+1)(2s+1)$. The sum over initial orbital angular momenta l automatically gives the sum over parity. The sum over $\mathbf{l}$ is restricted to even or odd values, depending on the parity p and the intrinsic parities of b and β; this restriction is indicated by the prime on the summation sign. The sum over $(\mathbf{jm}_j)$ represents an integration over the outgoing spin space, which is required since the final polarization is not measured. If a single residual state is assumed, $\mathbf{j}$ ranges from $|\mathbf{i}-\mathbf{s}|$ to $(\mathbf{i}+\mathbf{s})$.

A fundamental assumption involved in the derivation of Eq. (3) is the possibility of neglecting interference terms between outgoing waves differing as to the quantum numbers $(Jmp\mathbf{lj}\mathbf{m}_j)$. This is justified as follows:

(1) There cannot possibly be any interference from terms corresponding to different values of m because the incident spins are unpolarized and $m=m_j$. Similarly, in summing over the outgoing spins, any interference terms between states having different values of $\mathbf{j}$ or $\mathbf{m}_j$ would drop out.

(2) The neglect of interference terms between outgoing waves arising from compound states, with different values of J or p, follows from the assumption that the reaction can be divided into two independent parts, the formation and the decay of the compound nucleus. One way of stating this is to say that these interference terms cancel out when averaging over many compound states for each value of J and p because the outgoing waves have random phases.

(3) Interference terms between different outgoing orbital angular momenta $\mathbf{l}$ arising from the same compound state do not enter σ (see reference 7), and consequently, by the law of detailed balancing, will not enter Γ.

The main concern here is in the distribution of outgoing particles as to energy, angle, etc. Thus the denominator of the second term in Eq. (3) is of interest only insofar as it depends on the quantum numbers (Jmp). Substituting from Eqs. (1a) and (2) into this denominator and making use of the identity

$$\sum_{\mathbf{m}_{j'}}(\mathbf{l}'\mathbf{j}'Jm|\mathbf{l}'\mathbf{j}'m-\mathbf{m}_{j'}\mathbf{m}_{j'})^2=1, \tag{4}$$

the denominator is equal to

$$\frac{D^{Jp}}{2\pi}\sum_{c\gamma}\sum_{\mathbf{l}'}{}'\sum_{\mathbf{j}'=|J-\mathbf{l}'|}^{J+\mathbf{l}'}P_{c\mathbf{l}'}\xi(Jp, c\gamma\mathbf{l}'\mathbf{j}')=(D_{Jp}/2\pi)\langle\xi(Jp, c\gamma)\rangle F(J), \tag{5}$$

where

$$F(J)\equiv\sum_{c\gamma}\sum_{\mathbf{l}'}{}'\sum_{\mathbf{j}'=J-\mathbf{l}'}^{J+\mathbf{l}'}P_{c\mathbf{l}'}.$$

It is assumed that ξ is independent of $\mathbf{l}'$ and $\mathbf{j}'$, and some kind of average over c and γ is factored out of the summation. The function $F(J)$ (times D) represents the dependence on J of the yield of the final product of interest plus all competing possibilities.

The summation over outgoing particles c in Eq. (5) may usually be limited to neutrons, because the penetration factor for outgoing neutrons is much greater than for charged particles. The sum over residual nuclei γ requires a knowledge of the density of residual nuclear states as a function of energy, spin, and parity. Here it is assumed that the density is independent of parity and that the dependence on spin and energy may be separated, giving

$$\rho(E_c, \mathbf{i})dE_c=\rho_c(\mathbf{i})W(E_c)dE_c \tag{6}$$

[11] Reference 4, p. 87.
[12] G. Breit and B. T. Darling, Phys. Rev. 71, 402 (1947).

= number of residual nuclear states corresponding to an outgoing neutron energy between E_c and E_c+dE_c and residual nuclear spin $\mathbf{i}$. (The $(2i+1)$ degenerate states corresponding to different m_i values are counted as one state.) The number of final states with a total spin $\mathbf{j}$ may be expressed by a similar equation by introducing

$$\rho_c(\mathbf{j})=\tfrac{1}{2}\{\rho_c(\mathbf{i}=\mathbf{j}+\tfrac{1}{2})+\rho_c(\mathbf{i}=\mathbf{j}-\tfrac{1}{2})\}. \quad (6a)$$

The function $F(J)$ then becomes

$$F(J)=\int \sum_{l'} \sum_{j'=|J-l'|}^{J+l'} \rho_c(\mathbf{j}')P_{cl'}(E_c)W(E_c)dE_c. \quad (7)$$

The main contribution to Eq. (7) becomes from low values of $\mathbf{l}'$ corresponding to low energies E_c for which the density $W(E_c)$ is large; as a consequence, only values of $\mathbf{j}'$ close to $\mathbf{j}'=J$ contribute to the sum over $\mathbf{j}'$. Approximating $\rho(\mathbf{j}')$ as a linear function of $\mathbf{j}'$ over this interval

$$F(J)=\int [\sum_{l'=0}^{J} \rho_c(J)P_{cl'}(E_c)(2l'+1) + \sum_{l'=J+1}^{\infty} \rho_c(\mathbf{l}')P_{cl'}(E_c)(2J+1)]W(E_c)dE_c. \quad (7a)$$

The first term in the brackets is the more important, except for J less than 2 or 3. If it is assumed that[13]

$$\rho_c(J)=\text{const}(2J+1), \quad (8)$$

at least for the values of J for which the second term in Eq. (7a) is important, the two terms become identical in form and

$$F(J)\sim\rho_c(J).$$

Making use of Eqs. (1) through (3) and (5), one finds for the outgoing distribution

$$\sigma(a\alpha, b\beta\boldsymbol{\theta})=\frac{\pi\lambda_a^2}{(2i+1)(2s+1)} \times\sum_{l=0}^{\infty}\sum_{j=|i-s|}^{i+s}\sum_{m=-j}^{j}\sum_{J=|l-j|}^{l+j}(ljJm|lj0m)^2(2l+1) \times P_{al}\xi(Jp, a\alpha)\sum_{j=|i-s|}^{i+s}\sum_{l=|J-j|}^{J+j}{}'\sum_{m_j=-j}^{j}\frac{\xi(Jp, b\beta)}{\langle\xi(Jp, c\gamma)\rangle} \times(2l+1)(\mathbf{lj}Jm|\mathbf{lj}m-\mathbf{m}_j\mathbf{m}_j)^2\frac{P_{bl}}{F(J)}|P_l^{m-m_j}(\boldsymbol{\theta})|^2. \quad (9)$$

ANGULAR DISTRIBUTION

Equation (9) gives the angular distribution of a single outgoing group of particles b resulting from the collision of particles a and α, assuming statistical theory can be applied to the compound nucleus. Of course, statistical theory is not being applied to the residual nucleus, since only a single residual nuclear state β is considered. A very simple case is one in which the spins (i, s, $\mathbf{i}$, and $\mathbf{s}$) are zero, giving for the angular distribution

$$\sigma(a\alpha, b\beta\boldsymbol{\theta})\sim\sum_{l=0}^{\infty}\frac{(2l+1)^2}{F(l)}P_{al}P_{bl}|P_l^0(\boldsymbol{\theta})|^2, \quad (10)$$

assuming that the ξ factors are independent of l. The amount of anisotropy is determined by the maximum value of l effective in the sum which depends on the ability of the incident and outgoing particles to overcome the angular momentum barrier. It should be emphasized that only the factor $\{(2l+1)^2/F(l)\}$ in Eq. (10) is dependent on the detailed assumptions of the present formulation; the general features of the equation, including the anisotropy, follow directly from conservation of orbital angular momentum. If there is only one possible final state so that the sum over c and γ in Eq. (3) does not appear, the angular distribution is for the case of no spins

$$\sigma(a\alpha, b\beta\boldsymbol{\theta})\sim\sum_{l=0}^{\infty}(2l+1)^2P_{al}|P_l^0(\boldsymbol{\theta})|^2. \quad (10a)$$

The main features of the angular distribution (Eq. (9)) are (a) symmetry about 90° and usually (b) peaks in the forward and backwards directions. The former follows from the fact that interference terms between outgoing waves of different parity are assumed to cancel out. The latter is expected because the initial zero value for m_l should show itself in a large intensity for the outgoing wave with $\mathbf{m}_l$ equal to zero, which wave is peaked in the forward direction. While this is certainly the case when no spins are present (Eq. (10)), it is not always true when large nuclear spins are involved.

To get a measure of the anisotropy it is convenient to obtain, from Eq. (9), expressions proportional to the average cross section

$$\sigma_{bt}\equiv(1/4\pi)\int\sigma d\Omega,$$

and the cross section for $\boldsymbol{\theta}=0°$. Once again ignoring the dependence of the ξ factors on J

$$\sigma_{bt}(a\alpha, b\beta)\sim\sum_{l=0}^{\infty}\sum_{j=|i-s|}^{i+s}\sum_{J=|l-j|}^{l+j}\frac{P_{al}(2J+1)}{F(J)} \times\sum_{j=|i-s|}^{i+s}\sum_{l=|J-j|}^{J+j}{}'P_{bl}, \quad (11a)$$

$$\sigma(a\alpha, b\beta 0)\sim\sum_{l=0}^{\infty}\sum_{j=|i-s|}^{i+s}\sum_{m=-j}^{j}\sum_{J=|l-j|}^{l+j}\frac{P_{al}(2l+1)}{F(J)} \times(ljJm|lj0m)^2\sum_{j=|i-s|}^{i+s}\sum_{l=|J-j|}^{J+j}{}' \times(\mathbf{lj}Jm|\mathbf{lj}0m)^2(2l+1)P_{bl}. \quad (11b)$$

[13] This assumption is not unreasonable (see Appendix B).

TABLE I. Ratio of forward yield $\sigma(0)$ to average cross section σ_{Av} as a function of residual nuclear spin $\mathbf{i}$ and maximum effective outgoing orbital angular momentum $\mathbf{l}_{max}$. Initial spins are zero.

i	$\mathbf{l}_{max}$	Case A (Yes or No)	Case B (No)	Case B (Yes)
1/2	0	1	1	1
	1	1.33	1.37	1.50
	2	1.80	2.00	2.10
	3	2.28	2.66	2.74
	4	2.78	3.32	3.38
	5	3.27	3.98	4.04
3/2	0	1	1	1
	1	1	1.18	1
	2	1.12	1.37	1.20
	3	1.33	1.62	1.47
	4	1.56	1.90	1.78
	5	1.80	2.20	2.09

The anisotropy will be particularly sensitive to l_{max} and $\mathbf{l}_{max}$, the maximum values of l and $\mathbf{l}$, respectively, effective in the sums; in fact, the lower of these sets an absolute bound on the degree of anisotropy of any reaction.[14] It will also be sensitive to the values of $\mathbf{i}$ and $\mathbf{s}$, since the larger these are the less directly the conservation of m is reflected in the outgoing orbital functions.

Calculations have been made of this anisotropy under the following assumptions:

(1) i and s are equal to zero.

(2) $\mathbf{s}=\frac{1}{2}$.

(3) As an approximation the penetration factors P_{al} and P_{bl} are assumed equal to unity for $l\leqslant l_{max}$, and $\mathbf{l}\leqslant\mathbf{l}_{max}$, respectively, and equal to zero otherwise.

(4) The incident energy is sufficiently large that $l_{max}\geqslant\mathbf{l}_{max}+\mathbf{i}+\mathbf{s}$.

(5) Two forms of $F(J)$ are considered:

Case A. $F(J)$ is proportional to $2J+1$, which corresponds to Eq. (8).

Case B. $F(J)$ is constant for all values of J greater than zero; $F(0)$ equals $\frac{1}{2}F(1)$. An analysis of Eq. (7) indicates that this corresponds approximately to $\rho_c(\mathbf{j})$ constant for reasonable choices of $W(E_c)$.

Results are given in Table I for various values of $\mathbf{i}$ and $\mathbf{l}_{max}$. "No" or "Yes" indicates that the product of the intrinsic parities of the final particles is the same as, or different from that of the initial particles. For Case A the results are independent of parity change and can be expressed analytically (Appendix A).

$$\sigma_{Av}(a\alpha, b\beta)\sim\tfrac{1}{2}(2\mathbf{i}+1)(2\mathbf{l}_{max}-\mathbf{i}+\tfrac{3}{2}) \quad \text{for } \mathbf{l}_{max}\geqslant\mathbf{i}-\tfrac{1}{2}, \tag{12a}$$

$$\sigma_{Av}(a\alpha, b\beta)\sim(\mathbf{l}_{max}+1)^2 \quad \text{for } \mathbf{l}_{max}\leqslant\mathbf{i}-\tfrac{1}{2}, \qquad \sigma(a\alpha, b\beta 0)\sim(\mathbf{l}_{max}+1)^2. \tag{12b}$$

The distribution is isotropic for $\mathbf{i}$ greater than $\mathbf{l}_{max}$, while for $\mathbf{l}_{max}$ considerably greater than $\mathbf{i}$, the anisotropy is approximately

$$\frac{\sigma(0)}{\sigma_{Av}}=\frac{\mathbf{l}_{max}+1}{2\mathbf{i}+1}+\frac{1}{4}. \tag{13}$$

The results are not so simple if the limiting value l_{max} of the entering orbital angular momentum must be considered; that is, assumption (4) is not valid. It is then possible that for some values of the residual nuclear spin the forward yield is less than the average. A particular example is shown in Table II; the results labeled $l_{max}>9$ correspond to Eqs. (12). Except for (4), the assumptions listed above (Case A) have been used.

TABLE II. Ratio of forward yield $\sigma(0)$ to average cross section σ_{Av} for $\mathbf{l}_{max}=3$ as a function of $\mathbf{i}$ and under two assumptions for l_{max}. Initial spins are zero.

i	$l_{max}=4$ (No)	$l_{max}=4$ (Yes)	$l_{max}>9$ (Yes or No)
1/2	2.28	2.28	2.28
3/2	1.15	1.33	1.33
5/2	0.98	0.82	1.07
7/2	0.70	0.88	1
9/2	0.96	0.70	1
11/2	0.80	1.13	1
13/2	1.60	0.86	1

Commonly, a single outgoing group of particles is not observed but rather all outgoing groups within a certain energy range. Equation (9) should then be modified by including a factor $\rho_b(\mathbf{j})W(E_b)dE_b$ (see Eq. (6a)), extending the summation over $\mathbf{j}$ to all values, and integrating over the energy range. It is not clear whether any anisotropy will remain after this summation; the results depend upon the details of the assumptions, particularly, the form of $\rho_b(\mathbf{j})$. Three possibilities have been considered:

Case α. The density $\rho_b(\mathbf{j})$ of residual nuclear states corresponding to the outgoing particles b of interest is proportional to $(2\mathbf{j}+1)$[13] for all values of $\mathbf{j}$ that are possible. This is clearly inconsistent with assumption (4) previously used. Using the others of the previous assumptions (Case A), it is shown in Appendix A that the angular distribution is essentially isotropic. This result is clearly independent of $\mathbf{s}$, l_{max}, and $\mathbf{l}_{max}$, and therefore of assumptions (2) and (3).

Case β. The density $\rho_b(\mathbf{j})$ is constant as a function of $\mathbf{j}$. Using a constant for $\rho_c(\mathbf{j})$ in Eq. (7) gives Case B for $F(J)$ to a good approximation. Using the previous assumptions (except assumption 4), calculations have been made for the case $l_{max}=4$; the resulting values of the anisotropy as measured by $\sigma(0)/\sigma_{Av}$ are 1.14 for $\mathbf{l}_{max}=2$, and 1.23 for $\mathbf{l}_{max}=3$.

Case γ. The density $\rho_b(\mathbf{j})$ is limited to a maximum value j_0, being given by

$$\rho_0(\mathbf{j})=\text{const}(2\mathbf{j}+1) \quad \mathbf{j}\leqslant j_0, \qquad \rho_b(\mathbf{j})=0 \quad \mathbf{j}>j_0. \tag{14}$$

Assumption (4) is now applicable provided $l_{max}\geqslant\mathbf{l}_{max}+j_0$. Using all the previous assumptions (once again Case A), one finds the anisotropy given in Table III.

[14] E. Eisner and R. G. Sachs, Phys. Rev. **72**, 680 (1947); L. Wolfenstein and R. G. Sachs, Phys. Rev. **73**, 528 (1948); C. N. Yang, Phys. Rev. **74**, 764 (1948).

It should be noted that the assumptions used for this case are not completely consistent, since if Eq. (14) were used for $\rho_c(\mathbf{j})$ the resulting $F(J)$ would not be that assumed (Case A). However, it should be noted that the residual nuclei α, corresponding to the outgoing low-energy neutrons c, may have a considerably greater excitation energy than the residual nuclei β corresponding to outgoing particles b, particularly if high-energy particles b are being selected. Thus, it may not be unreasonable to assume a cut-off in $\rho_b(\mathbf{j})$ but not in $\rho_c(\mathbf{j})$.

OTHER RESULTS

Equation (11a) may also be considered as giving the energy distribution of the outgoing particles if the summation over $\mathbf{j}$ is replaced by a sum over residual nuclear states with a density given by Eqs. (6) and (6a).

$$\sigma_{kb}\sim\sum_{l=0}^{\infty}\sum_{j=|i-s|}^{i+s}\sum_{J=|l-j|}^{l+j}\frac{P_{al}(2J+1)}{F(J)}\times\sum_{l=0}^{\infty}\sum_{j=|J-l|}^{J+l}P_{bl}\rho_b(\mathbf{j})W(E_b)dE_b.$$

To simplify this result one may approximate $\rho_b(\mathbf{j})$ as a linear function of $\mathbf{j}$, as was done in deriving Eq. (7a).

$$\sigma_{kb}\sim\sum_{l=0}^{\infty}\sum_{j=|i-s|}^{i+s}\sum_{J=|l-j|}^{l+j}P_{al}\frac{2J+\bar{1}}{F(J)}\times\{\rho_b(J)\sum_{l=0}^{J}P_{bl}(E_b)(2l+1)W_b(E_b)+(2J+1)\sum_{l>J}P_{bl}(E_b)\rho_b(l)W_b(E_b)\}dE_b. \quad (15)$$

The first term in the brackets has the form usually given for the energy distribution, but the second term shows a dependence of the energy distribution on the density as a function of spin. Indeed, the usual form for the distribution is obtained only if (Eq. (8)) is assumed for $\rho_b(l)$. It should be noted also that the $(2l+1)$ factor enters from quite different considerations than usual in the present derivation. An alternative simplification follows from assuming no initial spins, initial l_{max} very large, and $F(J)$ proportional to $2J+1$;

$$\sigma_{kb}\sim\sum_{l=0}^{\infty}\{\sum_{j=0}^{l}\rho_b(\mathbf{j})(2\mathbf{j}+1)+\sum_{j>l}\rho_b(\mathbf{j})(2l+1)\}P_{bl}(E_b)W_b(E_b)dE_b.$$

The equations obtained may also be used to determine the dependence of the cross section for a single outgoing group on the spin of the residual nucleus, other things being equal. The cross section tends to be larger for larger residual nuclear spins because the larger spin provides a greater number of modes of decay for the compound nucleus, unless these are forbidden by the angular-momentum barrier. This is clearly seen in Eq. (12a). Thus, for $\mathbf{l}_{max}=4$, the cross section increases by a factor of almost 3 from $\mathbf{i}=\frac{1}{2}$ to $\mathbf{i}\geqslant 9/2$. On the other hand, the forward yield (Eq. (12b)) is independent of $\mathbf{i}$.

COMPARISON WITH EXPERIMENT

Results of several types of experiments are affected by these considerations:

(1) The angular distribution of a single outgoing group of particles. Such measurements might help to identify the spin of the residual nuclear state; however, it is experimentally difficult to find an isolated group of product particles when the incident energy is large enough to allow the use of statistical theory for the compound nucleus. Of the data available, that of Wyly[15] on the $N^{14}(d, p)N^{15}$ is particularly suggestive. Although only 2- to 3-Mev deuterons were used, the compound nucleus had an excitation of 22 Mev, and the angular distribution varied little with bombarding energy. Two proton groups were observed. One showed forward and backward peaks, approximate symmetry about 90°, and was known to correspond to $\mathbf{i}=\frac{1}{2}$; the second was essentially isotropic and had a much larger yield. This suggested that the second corresponded to a larger value of $\mathbf{i}$. Unfortunately, quantitative calculations are in complete disagreement. The observed anisotropy is much larger than the calculated; furthermore, since the second group has a lower energy, it would not be expected to have a larger yield than the first, even if it corresponded to a larger value of $\mathbf{i}$.

TABLE III. Ratio of forward yield $\sigma(0)$ to average cross section σ_{kb}, averaged over many residual nuclear states with a spin distribution given by Eq. (14).

	l_{max}			
j_b	2	3	4	5
4	1.05	1.11	1.19	1.30
6	1.03	1.05	1.09	1.19
8	1.02	1.03	1.05	1.08

(2) The angular distribution of all outgoing particles in a certain energy interval. Here the results of the theory are more ambiguous. Cohen has analyzed data on the angular distribution of (α, n) reactions studied with threshold detectors by Allen and others.[16] He finds, for practically all nuclei, a distribution symmetric about 90°, with peaks in the forward and backward directions. The present analysis indicates that this small anisotropy is not at all inconsistent with the statistical theory of nuclear reactions. The results are in qualitative agreement with the assumption of a constant density of residual states as a function of spin (Case β) or a cutoff in the density (Case γ), but are not consistent with a density proportional to $(2i+1)$ with no cutoff. On the other hand, the large anisotropy, unsymmetrical about

[15] L. D. Wyly, Phys. Rev. **76**, 104 (1949).
[16] B. L. Cohen, Ph.D. Thesis (Carnegie Institute of Technology, 1950); Allen, Nechaj, Sun, and Jennings, Phys. Rev. **76**, 188 (1949).

90°, observed in (d, n) and (d, p) reactions,[17] is completely inconsistent with statistical theory and definitely requires a different mechanism.

(3) The relative yield of different outgoing particle groups. This might give some information as to the relative spins of different residual nuclear states; however, this effect may be smaller than expected fluctuations.

(4) The energy distribution of outgoing particles. The usual equations are modified significantly only for fairly high outgoing energies.

APPENDIX A

Derivation of Eqs. (12a) and (12b)

Starting with Eq. (11a) and setting the initial spins equal to zero, so that $J=l$, one finds for a single value of j

$$\sigma_{kl}\sim\sum_{J=0}^{\infty} P_{0J}\frac{2J+1}{F(J)}\sum_{l=|J-j|}^{J+j}{}' P_{bl}.$$

The prime on the summation indicates that

$$(-1)^l(-1)^J(-1)^\delta=1,$$

where δ is zero, if the final intrinsic parity (that is, the product of the intrinsic parities of the final particles) is the same as the initial, and one otherwise. Making assumptions (3), (4), and (5) (Case A), and changing the order of summation,

$$\sigma_{kl}\sim\sum_{l=0}^{l_{\max}}\sum_{J=l-j}^{l+j}{}' (1). \tag{16}$$

For a fixed value of $\mathbf{l}$, the sum over J gives

$$\begin{array}{lll}\mathbf{j}+1 & \text{if} & \mathbf{j}\leq\mathbf{l}\quad (-1)^{j+\delta}=1,\\ \mathbf{j} & \text{if} & \mathbf{j}\leq\mathbf{l}\quad (-1)^{j+\delta}=-1,\\ \mathbf{l}+1 & \text{if} & \mathbf{j}\geq\mathbf{l}\quad (-1)^{j+\delta}=1,\\ \mathbf{l} & \text{if} & \mathbf{j}\geq\mathbf{l}\quad (-1)^{j+\delta}=-1.\end{array}$$

If these are now summed over $\mathbf{j}$ equal to $\mathbf{i}-\frac{1}{2}$ and $\mathbf{i}+\frac{1}{2}$, the results are clearly independent of δ, and Eq. (16) becomes, for $\mathbf{l}_{\max}\geq(\mathbf{i}+\frac{1}{2})$,

$$\sigma_{kl}\sim\sum_{l=i+\frac{1}{2}}^{l_{\max}}(2i+1)+\sum_{l=0}^{i-\frac{1}{2}}(2l+1)=\tfrac{1}{2}(2i+1)(2l_{\max}-i+\tfrac{3}{2}).$$

If $\mathbf{l}_{\max}\leqslant(\mathbf{i}-\frac{1}{2})$,

$$\sigma_{kl}\sim\sum_{l=0}^{l_{\max}}(2l+1)=(l_{\max}+1)^2.$$

Similarly, from Eq. (11b), one finds for a single value of $\mathbf{j}$

$$\begin{aligned}\sigma(0)&=\sum_{l=0}^{l_{\max}}\sum_{J=|l-j|}^{l+j}{}'(\mathbf{l}j J0|\mathbf{l}j00)^2(2l+1)\\ &=(l_{\max}+1)^2\quad\text{for}\quad(-1)^{\delta+j}=1\\ &=0\qquad\text{for}\quad(-1)^{\delta+j}=-1.\end{aligned}$$

Here use has been made of the normalization condition

$$\sum_{J=|l-j|}^{l+j}(\mathbf{l}jJ0|\mathbf{l}j00)^2=1$$

plus the fact that this combination coefficient vanishes if $(\mathbf{l}+\mathbf{j}+J)$ is odd. For the case of $\mathbf{s}=\frac{1}{2}$ and given $\mathbf{i}$, there is always one even and one odd possibility for $\mathbf{j}$ so that summing over $\mathbf{j}$ gives Eq. (12b) independent of $\mathbf{i}$ or of δ.

It is worth noting in passing the important effect of parity change for the case $\mathbf{s}=0$; that is, the inelastic scattering of fast alpha-particles from a target of spin zero. In this case the forward scattering is zero if $\delta+\mathbf{i}$ is odd, whereas there will be a pronounced forward peak if $\delta+\mathbf{i}$ is even.

Sum Over Residual Nuclear States (Case α)

Now it is desired to introduce a limit $l_{\max}$ on the J summation and to sum over $\mathbf{j}$, using a weighting factor $\rho(\mathbf{j})\sim(2\mathbf{j}+1)$. This gives, from Eq. (16), changing the order of summation,

$$\sigma_{kl}\sim\sum_{J=0}^{l_{\max}}\sum_{l=0}^{l_{\max}}\sum_{j=|J-l|}^{J+l}(2j+1)=\sum_{J=0}^{l_{\max}}\sum_{l=0}^{l_{\max}}(2J+1)(2l+1).$$

Similarly,

$$\sigma(0)\sim\sum_{J=0}^{l_{\max}}\sum_{l=0}^{l_{\max}}\sum_{j=|J-l|}^{J+l}(2j+1)(\mathbf{l}jJ0|\mathbf{l}j00)^2(2l+1)$$

$$=\sum_{J=0}^{l_{\max}}\sum_{l=0}^{l_{\max}}(2J+1)(2l+1)=\sigma_{kl},$$

where the relationship

$$\sum_{j=|J-l|}^{J+l}(2j+1)(\mathbf{l}jJ0|\mathbf{l}j00)^2=2J+1$$

has been used.

APPENDIX B

Level Density as a Function of Spin

A very rough discussion will be given here as to the forms to be expected for the function $\rho(\mathbf{i})$, which represents the density of residual nuclear levels as a function of spin $\mathbf{i}$. Suppose a single nucleon carries all the excitation; then it is to be expected that all values of angular momentum up to a fairly large value are approximately equally probable since the energy separating different angular momentum levels is small compared to the excitation energy. The result is quite different if the excitation energy is shared equally by two nucleons. For each nucleon it might be assumed that all values of angular momentum are equally probable, but if the interaction energy between the two nucleons is assumed to be small, the probability of a resultant angular momentum $\mathbf{i}$ is proportional to $(2\mathbf{i}+1)$. The reason for this is simply that the larger the total angular momentum, the more combinations of two angular momenta one can find having this as a possible resultant. This result can be generalized somewhat. If (a) the different values of angular momentum for the individual nucleons have a probability which may be approximated as a linear function of angular momentum over every interval of length $2I$, and if (b) the probability of an individual nucleon angular momentum greater than I is much larger than that for less than I, then it follows that the probability of a resultant angular momentum $\mathbf{i}$ is proportional to $(2\mathbf{i}+1)$ for $\mathbf{i}$ less than or equal to I. The results hold for more than two nucleons sharing the excitation; however, if many nucleons share the excitation, it is unlikely that the hypotheses are applicable.

For outgoing particles of spin $\frac{1}{2}$ it is convenient to use $\rho(\mathbf{j})$ defined by Eq. (6a) rather than $\rho(\mathbf{i})$. It is immediately evident that if $\rho(\mathbf{i})$ is a linear function of $\mathbf{i}$, such as $(2\mathbf{i}+1)$, then $\rho(\mathbf{j})$ is exactly the same function of $\mathbf{j}$.

[17] See reference 13, also Falk, Creutz, and Seitz, Phys. Rev. **76**, 322 (1949); C. E. Falk, Ph.D. Thesis (Carnegie Institute of Technology, 1950); P. Ammiraju, Phys. Rev. **76**, 1421 (1949); H. Gove, Phys. Rev. **78**, 345 (1950).

The Measurement of e/M by Cyclotron Resonance

H. Sommer, H. A. Thomas, and J. A. Hipple
National Bureau of Standards, Washington, D. C.

(Received January 8, 1951)

The cyclotron resonance frequency of the proton has been measured using a new method. By measuring the spin precessional frequency of the proton in the same magnetic field, the proton magnetic moment in nuclear magnetons has been determined as $\mu_p=2.79276\pm0.00006$. In combination with other data this result can be used directly to determine the charge-to-mass ratio of the proton $e/M_p=9579.4_2\pm0.3$ emu/g, the faraday $F=9652.0_3\pm0.3$ emu/g (physical scale), and the ratio of the proton mass to the electron mass $M_p/m_e=1836.12\pm0.05$. A preliminary value for the H_2-D doublet is given.

INTRODUCTION

THE cyclotron resonance phenomenon has appeared to be an attractive method of measuring the charge-to-mass ratio of ions ever since the development of the cyclotron. In contrast to the usual mass spectroscopic method, stringent geometrical conditions other than the uniformity of the magnetic field are not required. For relative measurements, such as the determination of packing fractions, it is only necessary to measure frequency.

Until recently this application of cyclotron resonance had not been successfully exploited, but activity in this field during the last year or so has resulted in important advances.[1-7] A major portion of this paper describes a method of measuring the ratio of the spin precessional frequency of the proton $\omega_s=\gamma_p B$ to the cyclotron frequency of the proton $\omega_c=eB/M$ in the same magnetic field by a device which we have called the omegatron. From this ratio one can obtain* the proton moment in nuclear magnetons,[6] the faraday,[5] and, in combination with the result of Gardner and Purcell,[4] the ratio of the mass of the proton to the mass of the electron. This paper also describes the measurement of the mass difference of the (H_2-D) doublet.

In the note describing the omegatron,[5] a preliminary value for the faraday was given as an illustration of the potentialities of the method. Subsequent studies revealed shifts in the resonance frequency due to the presence of weak electric fields. One section of this paper describes the success that has been attained in measuring the magnitude of the shifts attributable to this cause.

[1] S. A. Goudsmit, Phys. Rev. **74**, 622 (1948).
[2] J. A. Hipple and H. A. Thomas, Phys. Rev. **75**, 1616 (1949).
[3] Richards, Hays, and Goudsmit, Phys. Rev. **76**, 180(A) (1949).
[4] J. H. Gardner and E. M. Purcell, Phys. Rev. **76**, 1262 (1949).
[5] Hipple, Sommer, and Thomas, Phys. Rev. **76**, 1877 (1949).
[6] F. Bloch, Phys. Rev. **79**, 234(T) (1950).
[7] L. G. Smith, Phys. Rev. **81**, 295 (1951).
* *Note added in proof:* The authors combined the result of this experiment with several selected atomic constants recently determined in related experiments to illustrate the relationship of this new measurement with previous values. Since this manuscript was submitted, this relationship has been described more completely in the reports of J. A. Bearden and H. M. Watts [Phys. Rev. **81**, 73 (1951)] and J. W. M. DuMond and E. R. Cohen [A least-squares adjustment of the atomic constants as of December, 1950 (privately distributed)].
[8] L. W. Alvarez and F. Bloch, Phys. Rev. **57**, 111 (1940).

PART I. THE OMEGATRON

Principle of Method

It is not surprising that the cyclotron has been considered as an instrument for precise mass measurement. However, significant measurements have not been made with conventional cyclotrons because of the difficulty of attaining adequate resolution. In order to get high resolution, it is necessary for the ions to make a large number of revolutions. This requires that the applied rf voltage and the resulting radial increment per cycle be small. Since the ordinary cyclotron depends upon rf focusing, as well as magnetic focusing, the rf voltage cannot be reduced sufficiently to obtain the required resolution. The omegatron effectively overcomes this limitation.

As shown in Figs. 1 and 2, the ions are produced within the analyzer region of the omegatron by an axial electron beam (in the direction of the magnetic field). A positive trapping voltage applied to the guard rings produces an electric field which retards the loss of ions in the axial direction so that the rf field can act

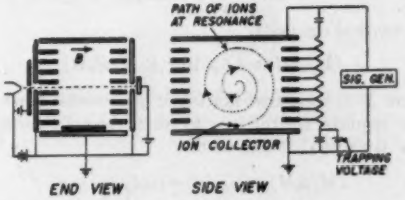

FIG. 1. Simplified diagram of the omegatron showing method of applying rf and dc voltages.

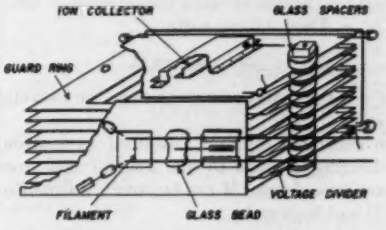

FIG. 2. Cut-away view of the omegatron used in measuring ν_a/ν_c.

on the ions over a greater number of cycles. The rf voltage is applied to two parallel electrodes and also to the guard rings through a bleeder to establish a uniform rf field, although a uniform field is not necessary except for the purpose of checking the theoretical equations. If the frequency of the applied voltage is the same as the cyclotron frequency, the ions will be accelerated in orbits of increasing size (Archimedes' spiral) and eventually strike the collector, thus producing an indication of resonance.

An analysis of the motion of a charged particle having a charge-to-mass ratio e/M, starting from rest under the influence of an rf electric field $E=E_0 \sin\omega t$ which is applied at right angles to a steady magnetic field B, shows that the particle will describe a spiral path with an angular velocity of $(\omega+\omega_c)/2$ and with a radius given by

$$r=(E_0/B\epsilon)\sin(\epsilon t/2), \tag{1}$$

where $\epsilon=|\omega-\omega_c|\ll\omega_c$ and $\omega_c=eB/M$. Thus, for $\epsilon\neq 0$, the radius r will "beat"—i.e., it will go through successive maxima and minima at an angular frequency of $|(\omega-\omega_c)/2|$. At resonance, $\epsilon=0$, and Eq. (1) becomes

$$r=E_0t/2B. \tag{2}$$

If a collector is placed at some fixed distance R_0 from the origin, the charged particles or ions will never reach the collector if $(E_0/B\epsilon)<R_0$. Thus, for any fixed value of E_0/B, there is a critical value $\epsilon'=E_0/R_0B$ for which the ions will just reach the collector. If the resolution $M/\Delta M$ is defined as $(M/\Delta M)=(\omega_c/2\epsilon')=(\nu_c/\Delta\nu)$, where $\Delta\nu$ is measured at the base of the resonance peaks, then it follows that

$$\frac{M}{\Delta M}=\frac{\omega_cR_0B}{2E_0}=\frac{R_0B^2e}{2E_0M}. \tag{3}$$

In practical cgs units,

$$(M/\Delta M)=4.8\times10^{-5}(R_0B^2/E_0M), \tag{4}$$

where M is measured in atomic mass units. Since the time required for the ions to reach the collector when $\epsilon=\epsilon'$ is $t'=\pi/\epsilon'$, it follows that

$$(M/\Delta M)=(\omega_c/2\epsilon')=(\omega_ct'/2\pi)=n', \tag{5}$$

where n' is the number of revolutions the ions make before reaching the collector when $\epsilon=\epsilon'$. The time required for the ions to reach the collector at resonance is $t=2t'/\pi$. Thus, we can write

$$M/\Delta M=\pi n/2, \tag{6}$$

where n is the number of revolutions the ions make at resonance.

The maximum radius r_m attained by nonresonant ions differing in mass by the amount ΔM from the resonant ions of mass M can be obtained from Eqs. (1) and (2) and is given by

$$r_m=2MR_0/(n\pi\Delta M).$$

For a fractional mass separation of only 1/1100 and for $n=7000$ revolutions, $r_m=R_0/10$. Thus, the non-resonant ions remain very near the center.

The total length of path L of the resonant ions can be determined by resolving the rf field into two rotating components each of which has half the applied amplitude. Since the ions obtain their final energy V from that component which always acts in the direction of motion, it follows that $L=V/(\frac{1}{2}E_0)$. From this equation, it can be shown that

$$L=n\pi R_0.$$

Although the rf voltage applied to the omegatron is only a fraction of a volt, the final energy of the ions is relatively large. For example, the H^+ ion attains a final energy of about 1000 ev in a magnetic field of 4700 gauss for $R_0=1$ cm. For a resolution of 10,000 the rf field as calculated from Eq. (4) is $E_0=0.1$ volt/cm. At resonance, the time required for the ions to reach the collector as obtained from Eq. (2) is one millisecond; and since the frequency $\omega_c/2\pi$ is about 7 Mc, the ions make about 7000 revolutions before reaching the collector with a total path length of 220 meters. Since the radius increases linearly with the number of revolutions, the increment per cycle is R_0/n or approximately 1.4 microns. The optimum trapping voltage has been found to be of the order of 0.1 volt.

Equation (4) indicates that for constant B the resolution varies inversely with the mass; but if E_0 is decreased as the mass is increased in such a manner that the number of revolutions remains the same, then the resolution will be constant. This, however, requires that the ions of higher mass be trapped longer, and the maximum length of time that the ions can be trapped imposes a limit on the attainable resolution.

Experimental Arrangement

The original omegatron shown in Fig. 2 consists of two 3×5 cm parallel plates (rf plates), two centimeters apart, with eight parallel guard rings of the same outer dimensions equally spaced between the plates. A tungsten filament 0.007 cm in diameter produces the electrons which are collimated by the 0.05-cm aperture in the draw-out electrode. The accelerated electron beam passes midway between the rf plates and falls on an electron collector which is used to monitor the beam current. An ion collector, inserted through a slot in one of the rf plates, is used to measure the resonant ion current. The whole assembly, including the voltage divider for the guard rings, is enclosed in a glass tube 4.7 cm in diameter.

The omegatron and the entire vacuum system as well as the electrometer tube are mounted so that they can be easily removed from the magnet gap. Thus, the magnetic field in the space normally occupied by the omegatron can be readily measured by inserting a nuclear resonance probe. The magnet, nuclear resonance regulator, and nuclear resonance probe used with the

omegatron have already been described[9] in connection with the measurement of the gyromagnetic ratio of the proton.

The resonance peak can be scanned by varying the frequency or the magnetic field. For high resolution operation, it is convenient to use a crystal controlled oscillator and to scan by varying the magnetic field. In order to scan magnetically, a small pair of Helmholtz coils is mounted on either side of the regulator probe. A small current through these coils tends to change the field at the sample, but the regulator action changes the main field to keep the net field at the sample constant. Thus, the field can be shifted very smoothly and precisely over a range of $\pm 1/5000$.

Performance

There are relatively few adjustments to make in operating the omegatron. The electron accelerating voltage is normally held fixed at 67.5 volts. The electron beam current is controlled by a simple regulator circuit similar to the one described by Winn and Nier.[10] In general, the trapping voltage and electron current are adjusted for maximum peak height as the rf voltage is decreased in magnitude while operating at fixed pressure. Highest available resolution is attained when minimum convenient peak height is reached. Figure 3 shows the variation of resolution with rf voltage. A normal working peak usually corresponds to an ion current of about 3×10^{-14} amp whereas electrometer fluctuations are about 4×10^{-16} amp. A high resolution peak is shown in Fig. 4.

The operating pressure as indicated on the ionization gauge located on the pumping arm was usually of the order of 10^{-7} to 10^{-6} mm Hg; however, several measurements of H^+ and H_2O^+ were made at an indicated background pressure of 3×10^{-8} mm Hg, the best attainable vacuum. The omegatron is extremely sensitive; and, by sacrificing resolution, virtually all the resonant ions produced can be collected. This is indicated by the fact that the ion current does not increase indefinitely as the rf voltage is increased and flat-topped peaks are obtained.

Although nearly all measurements with the omegatron up to the present time have been made with the very light masses, the spectrum up to mass 100 has been roughly scanned on several occasions. In particular, measurements at higher masses have been restricted to a few checks at mass 28, where a maximum resolution of 5000 was obtained.

PART II. APPLICATION TO THE MEASUREMENT OF ATOMIC CONSTANTS

The accurate measurement of the cyclotron resonant frequency of the proton has importance in the field of atomic constants as summarized briefly in the introduction. One of the major problems involved in this application of the omegatron is the displacement of resonance from the true cyclotron frequency.

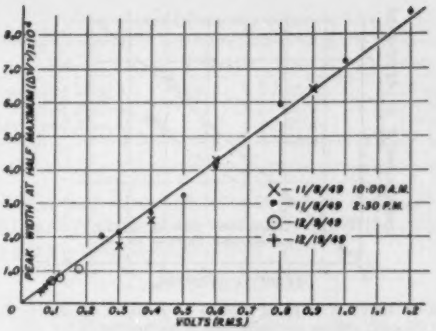

FIG. 3. Variation of resolution with rf voltage.

Frequency Shifts

The observed cyclotron resonance in the omegatron differs from the simple relation, $\omega_c = eB/M$, because of radial electrostatic fields within the tube. These radial fields originate from at least two sources, not altogether independent—from the applied trapping voltage, and from any space charge within the omegatron. Particularly, for the measurement of e/M in absolute units, it is necessary to determine the magnitude of this shift in the resonant frequency.

If a radial electric field $E(r)$ is superimposed on an axial magnetic field, then the equation of motion is

$$M\omega^2 r + eE(r) = \omega reB.$$

Thus, we can write

$$\omega \doteq \omega_c\left[1-\frac{E(r)M}{reB^2}\right]. \tag{7}$$

An approximate analysis of the electric field in the omegatron due to the trapping voltage shows that this field increases linearly with r. It follows from Eq. (7)

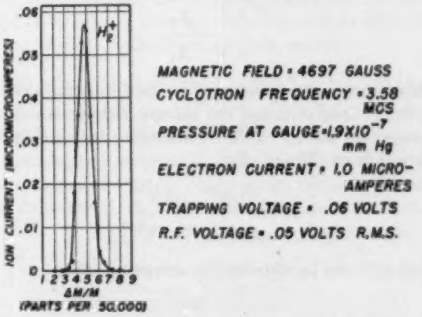
ION CURRENT (MICROMICROAMPERES)
ΔM/M
(PARTS PER 50,000)
MAGNETIC FIELD = 4697 GAUSS
CYCLOTRON FREQUENCY = 3.58 MCS
PRESSURE AT GAUGE = 1.9X10⁻⁷ mm Hg
ELECTRON CURRENT = 1.0 MICRO-AMPERES
TRAPPING VOLTAGE = .06 VOLTS
R.F. VOLTAGE = .05 VOLTS R.M.S.

FIG. 4. The H_3^+ peak with a resolution of approximately 1 in 35,000 at half-maximum.

[9] Thomas, Driscoll, and Hipple, J. Research Natl. Bur. Standards 44, 569 (1950), RP 2104.

[10] E. B. Winn and A. O. Nier, Rev. Sci. Instr. 20, 773 (1949).

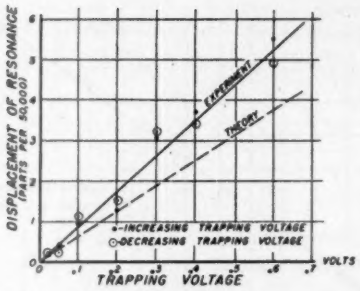

FIG. 5. Effect of trapping voltage on resonant frequency. The trapping voltage normally used is approximately 0.1 volt.

that the shift in resonance is independent of r. This shift has a theoretical magnitude of 1/80,000 per 0.1 volt of trapping voltage. As Fig. 5 shows, experimental investigation shows this effect to be 1/50,000, the additional shift presumably being due to space charge.

Although the shift in resonance could be calculated from the trapping voltage using a constant of proportionality as determined from the slope in Fig. 5, this constant would be a function of space charge condition, and furthermore there would be the difficulty of determining when actual zero trapping voltage exists. A more satisfactory technique has been developed for determining the frequency shift for each measurement.

As Eq. (7) shows, the frequency shift is proportional to the mass. Thus, if resonance is observed at frequency $\nu^{(1)}$ for the proton whose isotopic weight is A_1, and in quick succession under the same operating conditions, resonance is observed at frequency $\nu^{(m)}$ for an ion whose isotopic weight is A_m, then it follows that

$$\nu^{(1)}=\nu_c^{(1)}-A_1K\nu_c^{(1)}, \tag{8}$$

$$\nu^{(m)}=\nu_c^{(m)}-A_mK\nu_c^{(m)}, \tag{9}$$

where ν_c is the true cyclotron resonant frequency and K is the shift factor determined by the particular operating conditions. A third equation is obtained from the ratios of the true cyclotron frequencies

$$\frac{\nu_c^{(1)}}{\nu_c^{(m)}}=\frac{A_m}{A_1}. \tag{10}$$

These three equations can be used to determine $\nu_c^{(1)}$ given $\nu^{(1)}$ and $\nu^{(m)}$ and the isotopic weights which are known accurately. The correction factor K can be derived from (8) and (9):

$$K=\frac{A_m\nu^{(m)}-A_1\nu^{(1)}}{A_1A_m\left[\nu^{(m)}-\nu^{(1)}\right]}. \tag{11}$$

Then $\nu_c^{(1)}$ can be obtained by rewriting (8) as

$$\nu_c^{(1)}=\frac{\nu^{(1)}}{1-A_1K}. \tag{12}$$

This method of correction has been used with measurements made on the three pairs H^+ and H_2^+, H^+ and D_2^+, and H^+ and H_2O^+. As shown in Fig. 6, the correction factors as calculated from either H^+ and H_2^+ or from H^+ and D_2^+ result in values of the ratio of the spin precessional frequency of the proton ν_n to its cyclotron resonant frequency ν_c that agree well within the average deviation of either. The agreement of the correction factors determined from additional measurements made on the trio of masses H^+, H_2^+, and D_2^+ gave added confidence in this method of determining the frequency correction. The effect of space charge on the correction factor was clearly demonstrated in one particular case when a negative pulse was applied to the trapping voltage to sweep out the positive space charge. Under these conditions the sign of the correction factor was reversed, apparently the result of negative space charge. Nevertheless, the corrected value of ν_n/ν_c agreed with the average of the other values.

Measurement of ν_n/ν_c

Because of the frequency shift, each measurement of the ratio ν_n/ν_c for the proton requires the determination of the cyclotron frequency for ions of two different masses. The frequencies of the corresponding crystal oscillators were adjusted so that both cyclotron resonance peaks occurred at about the same magnetic field. The position of each peak was then determined by plotting peak height *versus* Helmholtz coil current, or by recording the coil current corresponding to 85 percent of maximum peak height on each side of the peak. Several sets of readings were usually made. The omegatron was then removed from the gap and replaced by a nuclear resonance probe using a water sample with adjusted relaxation time. (This water sample was subsequently checked against the standard oil sample

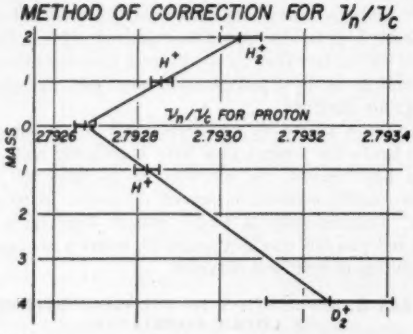

FIG. 6. Determination of the true value of ν_n/ν_c from H^+ and H_2^+ (top portion of figure) and from H^+ and D_2^+ (lower portion of figure). The uncorrected values of ν_n/ν_c for the proton as calculated from measurements on H^+, H_2^+, and D_2^+ are shown as well as the resultant value of ν_n/ν_c when pairs of measurements are combined to determine the correction factor. It is evident that measurements made with H^+ and H_2^+ or with H^+ and D_2^+ converge to the same corrected value of ν_n/ν_c.

used in determining the gyromagnetic ratio.) The coil current necessary to produce nuclear resonance at a frequency ν_n was recorded. The observed cyclotron oscillator frequencies were then reduced to the value corresponding to this coil current. These frequencies $\nu^{(1)}$ and $\nu^{(m)}$ were then substituted into Eqs. (11) and (12) to obtain K and $\nu_c^{(1)}$. The calibration of the Helmholtz coils was not critical, since the oscillator frequencies were initially adjusted to produce resonance near the magnetic field corresponding to ν_n.

The frequencies of the crystal oscillators were measured by using a signal calibrator which was standardized against the standard frequency transmissions of station WWV. This signal calibrator produced reference frequencies throughout the frequency spectrum. The crystal oscillators were usually adjusted so that the beat produced with one of the reference frequencies was some harmonic of the 440 cps or 600 cps modulation of WWV so that direct comparison could be made on an oscilloscope.

The results of measurements made in July and August 1950 are tabulated in Table I. These measurements were made under considerably varied operating conditions and with resolutions between 5000 and 10,000 (resolution measured at approximately 5 percent of maximum peak height). All measurements were made with the guard rings grounded for rf. The value of K was usually of the order of 6 parts per 100,000. If some measurements extending back to February, 1950, are included, there is no appreciable change in the value of ν_n/ν_c although these earlier runs were made at lower resolution and with less favorable techniques.

Suspected sources of systematic errors were checked whenever possible. The magnetic effect of the filament current was determined by reversing the current between several of the measurements. The net result indicated that the error from this source is less than 5 parts per million. The magnetic shielding effect due to the electrodes (55 Cu–45 Ni) was checked at the conclusion of this series of runs by carefully removing the rf electrode and replacing it after a proton resonance sample was placed within the omegatron. It was found that the field within the omegatron was the same as the field in the magnet gap with the omegatron removed to within 2 parts in a million. There remains a slight asymmetry in the cyclotron resonance peak whose meaning is still undetermined. However, we feel that the ratio of ν_n/ν_c lies within the range

$$\nu_n/\nu_c = 2.79268_5 \pm 0.00006,$$

where ν_n is the observed nuclear resonance frequency in the standard oil sample. The assigned error is several times the estimated probable error.

Proton Moment

The experimentally determined ratio ν_n/ν_c is the uncorrected value of the proton moment in nuclear magnetons.[8] Since the total diamagnetic correction for our standard oil sample as reported by Thomas[11] is 28.1 parts per million, the resultant value of the proton moment in nuclear magnetons is

$$\mu_p = 2.79276 \pm 0.00006.$$

Thomas used the magnetic shielding constant for H_2 calculated by Ramsey[12] in obtaining the above diamagnetic correction. If the more recent value reported by Newell[13] is used, the value of the proton moment as reported is unchanged. Using the value given by Hylleraas and Skavlem,[14] the proton moment becomes $\mu_p = 2.79277 \pm 0.00006$. Bloch and Jeffries[15] have recently reported a value of the proton moment using an inverted cyclotron. If we apply a diamagnetic correction of 28.1 parts per million, their value becomes

$$\mu_p = 2.79252 \pm 0.0002.$$

TABLE I. Summary of data.

Basis	No. of values	ν_n/ν_c	Av. dev.
Mass 1 and Mass 2	20	2.792684	$\pm 27\times10^{-6}$
Mass 1 and Mass 4	18	2.792682	$\pm 22\times10^{-6}$
Mass 1 and Mass 18	7	2.792701	$\pm 9\times10^{-6}$
Average	45	2.792685	$\pm 25\times10^{-6}$

Specific Charge of the Proton

The charge-to-mass ratio of the proton is given by the relation,

$$e/M_p = \gamma_p(\nu_c/\nu_n).$$

Taking into consideration the errors associated with ν_n/ν_c and with γ_p, the gyromagnetic ratio without diamagnetic correction,[12] the result is

$$e/M_p = 9579.4_2 \pm 0.3 \text{ emu/g}.$$

Faraday

The faraday can be calculated from e/M_p and the isotopic weight of the proton A_1 using the formula

$$F = A_1(e/M_p) = A_1\gamma_p(\nu_c/\nu_n),$$
$$F = 9652.0_2 \pm 0.3 \text{ emu/g (physical scale)}.$$

Craig and Hoffman[16] have recently reported the value $F = 9651.93$ with an average deviation of 0.26 using the electrochemical method with sodium oxalate.

Ratio of the Proton Mass to the Electron Mass

If the value of ν_n/ν_c for the proton is multiplied by the ratio of the cyclotron frequency of the electron to the precessional frequency of the proton as measured by Gardner and Purcell[4] (both ratios without diamagnetic correction), M_p/m_e can be calculated.

$$M_p/m_e = 1836.12 \pm 0.05.$$

[11] H. A. Thomas, Phys. Rev. **80**, 901 (1950).
[12] N. F. Ramsey, Phys. Rev. **78**, 699 (1950).
[13] G. F. Newell, Phys. Rev. **80**, 476 (1950).
[14] E. Hylleraas and S. Skavlem, Phys. Rev. **79**, 117 (1950).
[15] F. Bloch and C. D. Jeffries, Phys. Rev. **80**, 305 (1950).
[16] D. N. Craig and J. I. Hoffman, Phys. Rev. **80**, 487 (1950).

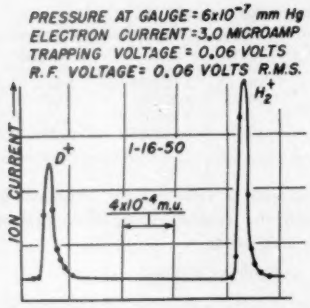

FIG. 7. H_2-D doublet.

PART III. APPLICATIONS IN MASS SPECTROSCOPY

Mass Measurement

One of the most important applications of the omegatron should be in the field of precise mass measurement. Even at this early stage in the development, the omegatron has sufficient resolution for precise measurements at the low masses, and it should be possible to construct an omegatron capable of significant measurements at higher masses. In addition, the omegatron has the advantage of high sensitivity and the measurements can be made in terms of frequency. The shift in resonance due to the trapping field should be relatively unimportant in doublet mass spectroscopy, although space charge conditions may produce some difficulties.

Preliminary measurements of the (H_2-D) doublet have been made. A typical doublet is shown in Fig. 7. Measurements over a period of several days have shown a deviation of less than 1 part per million, although on occasion shifts of several times this amount have been observed. The resultant tentative value is $(15.45\pm0.08)\times10^{-4}$ amu Roberts and Nier[17] have recently reported 15.49×10^{-4} with a somewhat smaller error.

Analytical Applications

Although no effort has been made in this laboratory to develop the omegatron as an analytical instrument, its simplicity and high sensitivity indicate considerable promise in this field. The absence of slits defining the ion beam and the wide choice of travel time suggest the desirability of using the omegatron in studying several aspects of ionization and dissociation of molecules by electron impact.

Although the mass spectrum can be scanned by changing either the frequency or the magnetic field, the latter method seems most advantageous. It can be shown from Eq. (4) that by scanning magnetically ΔM remains constant. This is a definite advantage when a recorder is used, since the width of the recorded peaks remains constant. Thus, the instrument can be set for maximum scanning rate over the entire mass range, and a linear mass scale will be recorded if the magnetic field is made to vary linearly with time.

Variations

Modifications in the original omegatron would undoubtedly improve the performance and eliminate some of the shortcomings reported in this paper. For certain low resolution applications, the design could probably be simplified. Detection by magnetic resonance absorption[18] eliminates the ion collector and associated electrometer.

In order to increase resolution, it is necessary either to increase the number of revolutions or to determine more critically a change in phase of the circulating ions. The number of revolutions corresponding to a minimum detectable ion current may be increased by increasing the magnetic field, by increasing the sensitivity of the detector, or by increasing the trapping efficiency.

In the omegatron with uniform field, the resolution is determined by the number of revolutions required for the ions to get 90° out of phase with the applied voltage. If sensitivity to this phase difference could be increased, the resolution would be improved for the same number cycles. This principle was first applied by Bloch[6] to an "inverted" cyclotron in which harmonics of the resonant frequency are used. The same effect has been obtained in this laboratory with a small cyclotron, using either harmonics or pulses. The idea might be adapted to the omegatron by applying to closely spaced electrodes a sharp pulse which affects only the outer orbits. Although this has been attempted, no significant success has been attained.

Several methods of reducing space charge have been tried and are being considered further. The most direct approach is to pulse periodically the trapping voltage in such a manner that the positive space charge is swept out. However, this results in a decrease in the collected resonant ion current. A more elaborate technique employs a dc bias between the rf plates. This voltage should cause the nonresonant ions to "walk" or drift out of the analyzer region continuously, while the resonant ions attain sufficient radius to strike a displaced collector before drifting out of the analyzer region.

Other variations have been suggested but not critically examined as yet. However, it is probable that the omegatron or some of its variations will find applications in various fields.

Acknowledgment

The authors are indebted to Dr. E. U. Condon for the analysis of the frequency shift due to a radial electric field, to Dr. F. P. Phelps and his associates for the preparation of quartz crystals, to the members of the Bureau Tube Laboratory for the construction of a modified omegatron, and to Dr. R. D. Huntoon for his helpful suggestions.

[17] T. R. Roberts and A. O. Nier Phys. Rev. **77**, 746 (1950).

[18] H. Sommer and H. A. Thomas, Phys. Rev. **78**, 806 (1950).

Direct Photodisintegration Processes in Nuclei*

ERNEST D. COURANT†
Brookhaven National Laboratory, Upton, New York
(Received September 5, 1950)

The unexpectedly large (γ,p) cross sections found in many moderately heavy nuclei are interpreted in terms of a direct photodisintegration process. The gamma-ray quantum is supposed to be absorbed by one proton in the nucleus, which is then emitted without the formation of an intermediate compound nucleus. The cross section for this process is small compared with that for the formation of a compound nucleus (which would almost always lead to the eventual emission of a neutron), but it has to be only a few millibarns to account for the experimental results. It is shown in this paper that if the nucleus is represented by a square well potential, the calculated cross sections turn out to be smaller than the experimental ones, but much larger than those obtained from the statistical theory.

The angular distribution of the emitted protons should be of the form $A+B\sin^2\theta$, where θ is the angle between the incoming photon and the proton, and the ratio B/A depends on the angular momentum of the proton in the nucleus. This is confirmed by experimental results; from the experimental values of B/A it appears that protons with $l=0$ in the nucleus contribute considerably to the effect in Rh and Ag. Feenberg's "wine bottle" potential can account for this more easily than the square well.

The theory is applicable to fast photoneutron emission as well, and recent experiments by Poss show that fast photoneutrons are indeed emitted anisotropically.

It is suggested that similar direct interaction mechanisms may account for the deviations of (n,p) cross sections from those predicted by the theory, as found recently by Wäffler.

I. INTRODUCTION

ACCORDING to the statistical theory of nuclear reactions[1] neutrons or protons produced in nuclear reactions are "boiled off" from an excited compound nucleus produced by the absorption of the bombarding particle by the target nucleus. The energy distribution of the outgoing particles is governed mainly by the distribution of energy levels in the residual nucleus. Since the level density of the residual nucleus increases rapidly with increasing energy, it follows from statistical considerations that the outgoing nucleus will have something like a maxwell distribution centered about some "nuclear temperature" which is much less than the excitation energy; if the excitation energy is in the region of 10 to 20 Mev, the most probable energy of the emitted particle is only a few Mev.

At these energies the emission of protons is severely inhibited, in all but the lightest nuclei, by the coulomb potential barrier which the proton must penetrate. As a result, the emission of protons may be expected to be much less likely than that of neutrons. For reactions in medium weight nuclei ($A\sim100$) produced by 17.6-Mev gamma-rays from $Li^7(p,\gamma)$ the ratio of proton to neutron emission computed on the basis of this theory turns out to be between 10^{-3} and 10^{-5}.

This prediction is not always confirmed experimentally. Hirzel and Wäffler[2] found that in a number of nuclei with A near 100 the (γ,p) to (γ,n) ratios were consistently several percent, 20 to 1000 times higher than expected from the statistical theory. Schiff[3] tries to explain this by modifying the statistical theory, assuming that the effective level density in the residual nucleus increases much less rapidly with energy than Weisskopf[1] assumed. On the other hand, the author[4] and Jensen[5] attempt to explain the result by postulating that the process is not an evaporation process at all but a direct photoelectric emission process in which the photon interacts directly with one of the protons in the nucleus and gives it enough energy to overcome the potential barrier without the formation of an intermediate "compound nucleus" state. The cross section for this direct process has to be only a few percent of the cross section for formation of a compound nucleus in order to account for the observed (γ,p) cross section. In this paper we shall attempt to show that this is the case.

The angular distribution of the emitted protons should furnish clues to the mechanism of the process. For the case of direct photoelectric emission we expect a maximum of the cross section at 90°. On the other hand, in the evaporation model we expect isotropic distributions, although other angular distributions are also possible.[6] Experimentally, Curtis, Hornbostel, Lee, and Salant[7] and Diven and Almy[8] have found high energy photoprotons produced preferentially at 90°, while Price and Kerst[9] found that photoneutrons are produced isotropically. This lends support to the hypothesis that photoneutrons are generally produced by evaporation while at least a substantial portion of the photoprotons are produced by direct interaction.

II. DIRECT ABSORPTION CROSS SECTIONS

We compute the absorption cross section on the basis of the following model: We describe the nucleus

* Most of this work was done at the Brookhaven National Laboratory under the auspices of the AEC. Some preliminary work was done at Cornell University with the support of an ONR contact.

† Now on leave at Princeton University, Princeton, New Jersey.

[1] V. F. Weisskopf, Phys. Rev. **52**, 295 (1937); V. F. Weisskopf and D. H. Ewing, Phys. Rev. **57**, 472 (1940).

[2] O. Hirzel and H. Wäffler, Helv. Phys. Acta **20**, 373 (1947).

[3] L. I. Schiff, Phys. Rev. **73**, 1311 (1948).

[4] E. D. Courant, Phys. Rev. **74**, 1226A (1948).

[5] P. Jensen, Naturwiss. **35**, 190 (1948).

[6] L. Wolfenstein, Phys. Rev. **78**, 322A (1950).

[7] Curtis, Hornbostel, Lee, and Salant, Phys. Rev. **77**, 290 (1950).

[8] B. C. Diven and G. M. Almy, Phys. Rev. **80**, 407 (1950).

[9] G. A. Price and D. W. Kerst, Phys. Rev. **77**, 806 (1950).

as a square well with Z protons filling the Z lowest states. The interaction between nucleons is supposed to be replaced entirely by this square well potential; thus, each nucleon has its own independent wave function. This approximation is justifiable because, owing to the Pauli principle, the mean free path of a nucleon in nuclear matter is large compared to the nuclear radius in spite of the large free nucleon-nucleon cross sections.[10] We compute the photoelectric absorption matrix element between this state and a final state in which one of the protons is raised into the continuum while the others are undisturbed. For ease of computation we first neglect the coulomb barrier and then multiply the resulting cross section by the barrier penetration probability.

This method is predicated on the assumption that the independent particle approximation is valid for the final state as well as the initial state. The argument for this is much weaker than that for the ground state,[10] since the Pauli principle no longer forbids all collisions. However, a quantitative comparison with the theory of Goldberger[11] shows that the mean free path of a proton of energy about 10 Mev (kinetic energy about 30 to 40 Mev inside the nucleus) in nuclear matter is at least of the order of, and probably somewhat larger than the nuclear diameter. This calculation should, therefore, lead to results of the right order of magnitude.

Our model implies that the entire photon absorption cross section is due to a combination of absorption of individual neutrons and protons. The proton emission cross section is a small part of this, because when a proton absorbs a photon it may not only be emitted, but it may instead radiate (especially for low energy photons) or collide with other nucleons, owing to the presence of nucleon-nucleon interaction. The latter process will result in the formation of a compound nucleus with subsequent decay as expected from the statistical model.

It is not expected that the shape of the effective nuclear potential will influence the order of magnitude of the results. The square well is chosen for ease of calculation.

If the nuclear radius is R and the depth of the well W, the initial wave function is

$$\psi_0 = A_l j_l(ar) \Upsilon_l^m(\theta, \phi), \qquad r<R$$
$$= A_l \frac{j_l(aR)}{k_l(bR)} k_l(br) \Upsilon_l^m(\theta, \phi), \quad r>R,$$

where $a^2=(2M/\hbar^2)(W-|E_0|)$; $b^2=2M|E_0|/\hbar^2$; the eigenvalue E_0 is determined by the continuity condition

$$-bk_{l-1}(bR)/k_l(bR) = aj_{l-1}(aR)/j_l(aR);$$

$\Upsilon_l^m(\theta, \phi)$ are the spherical harmonics normalized so as to make $\int |\Upsilon_l^m(\theta, \phi)|^2 d\Omega = 1$; A_l is determined by the normalization condition $\int |\psi|^2 dV = 1$, where the integral is taken over all space, and we employ the "spherical bessel functions"

$$j_l(x) = (\pi/2x)^{\frac{1}{2}} J_{l+\frac{1}{2}}(x), \quad n_l(x) = (-1)^{l+1}(\pi/2x)^{\frac{1}{2}} J_{-l-\frac{1}{2}}(x),$$
$$k_l(x) = (2/\pi x)^{\frac{1}{2}} K_{l+\frac{1}{2}}(x).$$

The final state wave function is of the form

$$\psi_1 = C_{l'} j_{l'}(cr) \Upsilon_{l'}^{m'}(\theta, \phi), \qquad r<R,$$
$$= C_{l'} \frac{j_{l'}(cR)}{z_{l'}(dR)} z_{l'}(dr) \Upsilon_{l'}^{m'}(\theta, \phi), \quad r>R,$$

where $c^2=a^2+2M\hbar\omega/\hbar^2$, $d^2=-b^2+2M\hbar\omega/\hbar^2$, $\hbar\omega$ is the energy of the absorbed quantum, and $z_{l'}(dr)$ is that particular solution of the radial wave equation which satisfies the continuity condition

$$dz_{l'-1}(dR)/z_{l'}(dR) = cj_{l'-1}(cR)/j_{l'}(cR).$$

The normalization constant $C_{l'}$ is chosen such that $r\phi_1$ is a sine wave of unit amplitude at infinity, where ϕ_1 is the radial part of the wave function.

Let us confine ourselves to light incident in the z-direction and circularly polarized in the $(x+iy)$ direction. Cross sections and angular distributions for $(x-iy)$ polarization will be the same. The cross section for the dipole absorption of a photon of energy $\hbar\omega$ is then

$$\sigma = \frac{e'^2}{\hbar c} \frac{4\pi M\omega}{\hbar d} \left| \int \psi_0 \left(\frac{x+iy}{\sqrt{2}} \right) \psi_1 dV \right|^2. \tag{1}$$

The effective charge e' here is eN/A because of the motion of the center of mass of the nucleus.[12] For the same reason dipole absorption by a neutron is possible, with the neutron having the effective charge $-eZ/A$.

Integration over the angles yields the angular momentum selection rules $m'=m-1$, $l'=l\pm1$:

$$(l, m|x+iy|l+1, m-1)$$
$$= \left[\frac{(l-m+1)(l-m+2)}{(2l+1)(2l+3)} \right]^{\frac{1}{2}} (l|r|l+1), \tag{2}$$

$$(l, m|x+iy|l-1, m-1)$$
$$= -\left[\frac{(l+m-1)(l+m)}{(2l-1)(2l+1)} \right]^{\frac{1}{2}} (l|r|l-1). \tag{3}$$

Since all values of m between $-l$ and $+l$ are equally probable, we must average over m, obtaining

$$\sigma_{l\to l+1} = S \left[\int_0^\infty r^3 \phi_0 \phi_1 dr \right]^2 \tfrac{2}{3}(l+1)/(2l+1), \tag{4}$$

$$\sigma_{l\to l-1} = S \left[\int_0^\infty r^3 \phi_0 \phi_1 dr \right]^2 \tfrac{2}{3} l/(2l+1), \tag{5}$$

where $S=(e'^2/hc)(2\pi M\hbar\omega/\hbar^2 d)$.

[10] V. F. Weisskopf, Helv. Phys. Acta **23**, 187 (1950).
[11] M. Goldberger, Phys. Rev. **74**, 1267 (1948).
[12] H. A. Bethe, Revs. Modern Phys. **9**, 221 (1937).

Carrying out the integrations for the matrix elements and normalization constants (see Appendix), with due regard for the continuity conditions at $r=R$, we finally obtain the cross section for one proton of angular momentum l:

$$\sigma_l=\frac{16\pi}{3}\frac{e'^2}{\hbar c}\frac{b^2(a^2+b^2)R}{(c^2-a^2)^2d}\cdot\frac{j_l^2(aR)}{-j_{l-1}(aR)j_{l+1}(aR)}\times\left\{\frac{l}{2l+1}C_{l-1}^2j_{l-1}^2(cR)+\frac{l+1}{2l+1}C_{l+1}^2j_{l-1}^2(cR)^2\right\} \quad (6)$$

with

$$C_l^2=(1/R^2)\{[dRj_{l-1}(dR)j_l(cR)-cRj_l(dR)j_{l-1}(cR)]^2+[dRn_{l-1}(dR)j_l(cR)-cRn_l(dR)j_{l-1}(cR)]^2\}^{-1}.$$

This expression may be further simplified by replacing the bessel functions by their asymptotic approximations. The ratio $[j_l(aR)]^2/[-j_{l+1}(aR)j_{l+1}(aR)]$ then equals a^2/b^2 because of the continuity conditions at $r=R$, and the last factor in (6) becomes

$$\frac{d^2\sin^2(cR+\alpha)}{R^2[c^2-(c^2-d^2)\sin^2(cR+\alpha)]}, \quad (7)$$

where α is a phase angle. This is an oscillating function; since the phase of cR is random, we may average over the phase α, obtaining

$$d/[R^2(c+d)]. \quad (8)$$

It should be noted however, that the phase of $(cR+\alpha)$ in (7) changes rather slowly with energy, so that for a particular transition the value of (7) may differ considerably from (8) over an energy interval of several Mev. This may lead to large variations in the cross section from one element to another and from one energy level to another.

If we nevertheless adopt the average (8), we obtain the following approximate expression for the cross section for one proton:

$$\sigma=\frac{16\pi}{3}\frac{e'^2}{\hbar c}\frac{a^2(a^2+b^2)}{(c^2-a^2)^2(c+d)R}=\frac{16\pi}{3}\frac{e^2}{\hbar c}\left(1-\frac{Z}{A}\right)^2\times\frac{TW}{(\hbar\omega)^2[(\hbar\omega+T)^{\frac{1}{2}}+(\hbar\omega+T-W)^{\frac{1}{2}}]}\left(\frac{\hbar^2}{2MR^2}\right)^{\frac{1}{2}}R^2. \quad (9)$$

Here T is the kinetic energy of the proton in the nucleus and W is the depth of the nuclear well. This expression is evidently valid only if the asymptotic expressions for the bessel functions are valid, i.e., if aR, bR, cR, and dR are all greater than l. This requirement is fairly well satisfied, in medium weight nuclei, for those protons whose energy is above or near the top of the coulomb barrier.

TABLE I. Experimental and theoretical (γ,p) cross sections for 17.6-Mev gamma-rays.

Nucleus	σ_{exp} (millibarns)	σ_{theor}	σ_α part	$\sigma_{statist}$
$_{34}Se^{77}$	4.8	0.35	1.0	0.14
$_{42}Mo^{96}$	3.5	0.26	0.75	0.12
$_{46}Pd^{105}$	7.3	0.25	0.75	0.07
$_{48}Cd^{111}$	4.4	0.24	0.72	0.026
$_{48}Cd^{112}$	5.3	0.24	0.72	0.09
$_{48}Cd^{113}$	6.0	0.24	0.72	0.05
$_{50}Sn^{117}$	2.9	0.23	0.70	0.013
$_{50}Sn^{118}$	1.5	0.23	0.70	0.017

The actual cross section is further reduced by the coulomb barrier. This may be taken into account by using Weisskopf's[13] tables of penetration cross sections; the penetration probability for a proton of given energy is taken to be Weisskopf's penetration cross section divided by πR^2. Assuming a Fermi distribution inside the nucleus, and taking $\hbar\omega=17.6$ Mev, $T_{max}=22$ Mev, $W=30$ Mev (binding energy 8 Mev), $R=1.5A^{\frac{1}{3}}\times10^{-13}$ cm, we obtain for the total cross section

$$\sigma=0.044(Z/A^{\frac{1}{3}})^2\int_0^{x_1}Pdx, \quad (10)$$

where P is the penetration probability, x is the energy of the outgoing protons measured in units of the barrier height, and x_1 is the maximum energy of the outgoing protons.

In Table I we compare the experimental cross sections found by Hirzel and Wäffler to cross sections computed from (10), cross sections from the alpha-particle model (see below), and cross sections from the statistical theory assuming neutron binding energies of 7.5 Mev, as computed by Hirzel and Wäffler. The "experimental" cross sections were obtained from Hirzel and Wäffler's work, together with the absolute value of 100 millibarns for the $Cu^{63}(\gamma,n)$ reaction at 17.6 Mev recently obtained by Diven and Almy.[8]

The experimental cross sections vary considerably from nucleus to nucleus. This may be ascribed partly to the fluctuations in the factor (7), to variations in the proton binding energy, and to variations in the proton energy distribution near the top of the distribution.

In addition, the theoretical cross sections are consistently smaller than the experimental ones, although the agreement is much better than for the statistical theory.

This disagreement with experiment is not surprising, in view of the crudity of the model used. In the first place, the individual particle model is only an approximation, especially for the final state. The actual wave functions will therefore be considerably more com-

[13] V. F. Weisskopf, MDDC-1175, *Lecture Series in Nuclear Physics* (U. S. Government Printing Office, 1947), p. 105.

plicated than those taken here and may well lead to different overlap integrals. Furthermore, even if the single particle model is accepted, the best well may be different from the one taken here, and may in fact be different for the initial and final states. Finally, the method used for estimating the effect of the coulomb barrier—which is the critical factor in reducing proton emission below neutron emission—may lead to errors; it would be better to take exact coulomb wave functions.

The dependence of the cross section on the well depth for a square well can be inferred from (9). The cross section for high energy photons increases with well depth, not only because of the factor TW but also because a deeper well requires a smaller radius in order that the top of the Fermi distribution remain at the binding energy. On the other hand, as the well depth increases, so does the barrier height (owing to the decrease in radius), leading to decreased penetrability; the net result is that for the square well the calculated (γ,p) cross section is roughly independent of well depth. However, if the shape of the well is changed, the cross section will change. Specifically, if the assumed potential inside the nucleus is less smooth than the square well, the wave functions will be less similar to those of free particles and the matrix elements may be expected to be larger. In addition, the energy level distribution will favor large internal kinetic energies more strongly than the $T^{\frac{1}{2}}$ distribution. Thus, if the square well is replaced by the "wine bottle" potential suggested by Feenberg and Hammack,[14] the theoretical cross sections are increased. A detailed calculation (see Appendix) shows that the cross section per proton may be as much as 4 times greater when an infinitely high central elevation is assumed for $0<r<R/4$, which leads to cross sections in better agreement with experiment.

Additional support for the central elevation model comes from the angular distribution of the photoprotons from Rh and Ag.[7,8] As we shall see shortly, the observed angular distributions in these elements indicates that s-protons contribute considerably to the total (γ,p) cross sections, which means that an s shell, presumably the $2s$ shell, lies near the top of the distribution for Z just below 50. This agrees with the predictions of the central elevation model but not with the simple square well which is the basis of Mayer's[15] nuclear shell model.

The agreement between the calculated and observed total cross sections is also improved if an alpha-particle model is assumed for the nucleus. In the alpha-particle model the radius R in the expression for the cross section per proton should be taken to be the radius of the alpha-particle. If we make this assumption and assume at the same time that the energy distribution in the nucleus is as in the Fermi gas model we obtain the cross sections in the fourth column of Table I.

[14] E. Feenberg and K. C. Hammack, Phys. Rev. **75**, 1877 (1949).
[15] M. G. Mayer, Phys. Rev. **78**, 16 (1950).

The alpha-particle model is also supported by the calculations of Levinger and Bethe,[16] who find that something like an alpha-particle model can account for the behavior of the total photodisintegration cross section as a function of energy much better than can the Fermi gas model. Furthermore, Cheston and Goldfarb and Tamor[17] find that the energy spectrum of protons produced by nuclear capture of π-mesons is most satisfactorily explained by means of a mechanism based on the alpha-particle model.

We have also neglected the existence of exchange forces, which tend to increase the cross sections by factors of the order of 1.5 to 2.[16]

The remaining discrepancy, if any, may be removed by assuming a mechanism intermediate between that of direct one-step interaction as assumed here and evaporation from the nucleus as a whole, namely, "local heating" of a portion of the nucleus and evaporation from the heated region before the excitation spreads over the whole nucleus.[18]

III. ANGULAR DISTRIBUTION

Irrespective of the detailed shape of the nuclear potential the angular distribution of the protons will depend only on the angular momentum of the proton before and after the absorption. For a transition $l\rightarrow l+1$ it will be proportional to

$$\sum_{m=-l-1}^{l+1}[l(l+1)+m^2]\,|\,\Theta_{l+1}{}^m(\theta,\phi)\,|^2 = l(l+1)+\tfrac{1}{2}(l+1)(l+2)\sin^2\theta;$$

for $l\rightarrow l-1$, to

$$\sum_{m=-l+1}^{l-1}[l(l+1)+m^2]\,|\,\Theta_{l-1}{}^m(\theta,\phi)\,|^2 = l(l+1)+\tfrac{1}{2}l(l-1)\sin^2\theta.$$

In general, the angular distribution should, therefore, be of the form $A+B\sin^2\theta$. The ratio B/A depends on the particular angular momentum of the protons involved. In particular, if $B/A>1.5$, i.e., if the intensity at 90° is more than 2.5 times that at 0°, the reaction must necessarily involve at least some protons making $l=0\rightarrow l=1$ transitions, since $B/A\leqslant 1.5$ for $l\geqslant 1$. If $B/A<1.5$, it is more difficult to draw any conclusions regarding the angular momenta, since for $l\geqslant 1$ the values of B/A may range anywhere between $\frac{1}{2}(l-1)/(l+1)$ and $\frac{1}{2}(l+2)/l$, which are rather wide limits for all angular momenta ($l\lesssim 5$) likely to exist inside a nucleus.

Both Curtis *et al.*[7] and Diven and Almy[8] find $B/A>1.5$, for the highest energy protons ejected from Rh and Ag, respectively. It follows, as remarked before, that an s-shell is at or near the top in the region $Z\approx 45$.

An angular distribution of the form $A+B\sin^2\theta$ is also

[16] J. S. Levinger and H. A. Bethe, Phys. Rev. **78**, 115 (1950).
[17] S. Tamor, Phys. Rev. **77**, 412 (1950); W. B. Cheston and L. J. B. Goldfarb, Phys. Rev. **78**, 682 (1950).
[18] L. Rosenfeld, *Nuclear Forces* (Interscience Publishers, New York, 1948), p. 198.

consistent with the alpha-particle model. For an alpha-particle at rest a pure $\sin^2\theta$ distribution is to be expected; this will be modified by the internal motion of the alpha-particle inside the nucleus.

We have assumed here that we are dealing with pure dipole transitions. Quadrupole transitions would modify the angular distribution. However, Levinger and Bethe[16] have shown that in the energy range considered dipole absorption must be predominant; quadrupole effects can only account for a small fraction of the total cross section.

IV. DISCUSSION

The values obtained here for $(\gamma-p)$ cross sections agree fairly well with those obtained experimentally by Hirzel and Wäffler[2] at a γ-ray energy of 17.6 Mev. However, the experiments on the energy spectrum of the protons, performed with betatron x-rays, show more low energy protons than expected from our direct interaction mechanism. In particular, Diven and Almy[3] found with 21-Mev x-rays on Ag that the energy distribution and absolute yield (or rather yield relative to the neutron yield) agreed quite well with the statistical theory except near the upper energy limit, where more protons were found than expected statistically. The Rh energy spectrum found by the Brookhaven group[7] is similar, so that the same conclusion applies.

It should be noted, however, that Rh and Ag are odd Z-even N nuclei, leading to stable even-even end products; the proton binding energy is therefore relatively low (about 6 Mev). On the other hand, Hirzel and Wäffler were necessarily restricted by their activation method to nuclei which would lead to radioactive products; the proton binding energies in those cases are considerably higher (8–9 Mev). Therefore, it is not surprising that in the cases of Ag and Rh the statistical cross section is comparable to or even larger than the direct cross section, while in the cases studied by Hirzel and Wäffler the statistical cross section is negligible.

The betatron results are thus explained by postulating that the low energy protons are produced primarily by nuclear evaporation, while the high energy tail is caused by the direct photoelectric effect discussed in this paper. This view is supported by the angular distribution, which is nearly (but not quite, in the case of Rh) isotropic for low energy protons and markedly anisotropic for the high energy protons. It would be desirable to repeat the angular and energy distribution experiments with some of the elements bombarded by Hirzel and Wäffler; if our view is correct, the energy distribution should be markedly shifted towards the high energy end and the angular distribution should be markedly anisotropic at all energies.

It would also be of interest to perform the energy and angular distribution experiments with monochromatic gamma-rays such as those obtained from the $Li^7(p,\gamma)$ or $H^3(p,\gamma)$ reactions. We would expect discrete lines each with its own angular distribution characteristic of the angular momentum of the corresponding nuclear shell.

Our theory applies to neutron emission as well as to proton emission, with the neutron having an effective charge $-eZ/A$. It is, therefore, to be expected that the photoneutron spectrum will contain, in addition to the relatively low energy neutrons from evaporation, a high energy "tail" containing a few percent of all the neutrons emitted, with an anisotropic distribution of the high energy neutrons. This is confirmed by an experiment by Poss,[19] who irradiated Bi, Pb, and W with 20-Mev x-rays and found high energy neutrons (>4 Mev) with an intensity ratio $I(90°)/I(0°)\approx 2$. Similar results have also been obtained at the University of Illinois.[20] On the other hand, Price and Kerst[9] found that if all photoneutrons are detected, the angular distribution is isotropic, which means that the anisotropic high energy tail can only represent a small fraction of all the photoneutrons produced.

Our conclusions may be compared with Schiff's theory.[8] Both theories lead to γ,p cross sections and (γ,p) to (γ,n) ratios of the right order of magnitude. But Schiff predicts a rather different energy distribution; his energy distribution, both for protons and for neutrons, should be much like the statistical one but shifted towards higher energies. Diven and Almy[3] compared their energy distribution with Schiff's theory and found that the low and intermediate energy yields were lower than predicted by Schiff's theory, agreeing much better with Weisskopf's statistical theory, while the high energy tail appeared to be near that predicted by Schiff. The anisotropy of the high energy protons is also most easily explained by the direct interaction theory, although, as Schiff has pointed out,[21] his theory does not necessarily require isotropy.

Another test of these competing theories is afforded by the study of other reactions involving proton emission. Schiff's theory is based on the supposition that photon excitation can lead only to a restricted subset of all the states of the compound nucleus. This feature is supposed to be peculiar to photon excitation and not to apply to particle bombardment. Accordingly, the competition between proton and neutron emission following particle bombardment should be governed by Weisskopf's statistical theory. On the other hand, the direct interaction mechanism should work with particle bombardment as well as with photon bombardment.[22] Thus, an incident neutron or proton could knock a proton out of the nucleus without greatly perturbing the residual nucleus (as is known to happen in the 100-Mev range). There is evidence that this is the case. Wäffler[23] finds that $n-p$ cross sections in elements between Fe and La, with neutrons having maximum energies of about 14

[19] H. L. Poss, Phys. Rev. **79**, 539 (1950).
[20] Private communication from M. Goldhaber.
[21] L. I. Schiff, private communication.
[22] This possibility has also been suggested by Weisskopf (reference 10).
[23] H. Wäffler, Helv. Phys. Acta **23**, 238 (1950).

Mev, are also higher than predicted by the statistical theory, though not by factors as large as for $\gamma-p$ reactions. On the other hand, he finds that $n-2n$ cross sections agree fairly well with statistical theory; thus, a modification of the level density in the statistical theory, such as proposed by Schiff, could lead to agreement with $n-p$ cross sections only at the expense of the agreement with $n-2n$ cross section. The most likely explanation would seem to be a direct interaction between the incident neutron and a proton of the nucleus. It might be desirable to check this hypothesis by investigating the energy distribution of the protons. Gugelot[34] has measured the neutron spectra from reactions induced by 16-Mev protons and obtains good agreement with a statistical theory except at the high energy end of the neutron spectrum, where he finds somewhat more neutrons than expected. This may again be accounted for by the direct interaction hypothesis.

A modified direct interaction mechanism is also called for by the experiments on meson absorption by nuclei as interpreted by Tamor.[17]

In the case of alpha-particle bombardment, on the other hand, direct energy transfer to one nucleon would appear difficult. Therefore, (α,p) to (α,n) ratios should be as predicted by the statistical theory. It would be interesting to check this experimentally.

It would thus seem that, for nuclear excitation energies of the order of 20 Mev or more, reactions can proceed by direct interaction as well as by way of an intermediate compound nucleus. This does not affect the total cross section or the cross sections for the most prevalent modes of disintegration to any large degree, but the probabilities of rarer processes such as proton emission may be greatly enhanced by the direct mechanism.

The author wishes to express his thanks to P. Morrison and H. A. Bethe for discussions which first stimulated his interest in the subject, and to J. Hornbostel, H. Poss, and P. C. Gugelot for informing him of their experimental results in advance of publication.

APPENDIX

(a) Square Well

The normalization constant A_l is determined from the condition

$$A_l^2\left[\int_0^R r^2 j_l^2(ar)dr+\{j_l^2(aR)/k_l^2(bR)\}\int_R^\infty r^2 k_l^2(br)dr\right]=1. \quad \text{(A1)}$$

Carrying out the integrations and making use of the continuity conditions at $r=R$, we obtain

$$A_l^2=\frac{2b^2}{(a^2+b^2)R^2}\frac{1}{[-j_{l-1}(aR)j_{l+1}(aR)]}. \quad \text{(A2)}$$

The constant C_l is determined from the conditions

$$\begin{aligned} C_l j_l(cR)&=d[\alpha j_l(dR)+\beta n_l(dR)],\\ cC_l j_{l-1}(cR)&=d^2[\alpha j_{l-1}(dR)+\beta n_{l-1}(dR)] \end{aligned} \quad \text{(A3)}$$

with $\alpha^2+\beta^2=1$. Solving for α, β, and C_l we obtain

$$\begin{aligned} C_l=R^{-2}|&[dj_l(cR)j_{l-1}(dR)-cj_{l-1}(cR)j_l(dR)]^2\\ &+[dj_l(cR)n_{l-1}(dR)-cj_{l-1}(cR)n_l(dR)]^2|^{-\frac{1}{2}}. \end{aligned} \quad \text{(A4)}$$

The matrix element

$$(0|r|1)=\int_0^\infty r^3\phi_0\phi_1 dr$$

is most easily evaluated by noting that the equation of motion

$$M\ddot{\mathbf{r}}=-\nabla V \quad \text{(A5)}$$

holds as a matrix equation. Thus, we have

$$(0|\mathbf{r}|1)=-(1/\omega^2)(0|\ddot{\mathbf{r}}|1)=(1/M\omega^2)(0|\nabla V|1). \quad \text{(A6)}$$

In our case $\nabla V=(\mathbf{r}/r)W\delta(r-R)$, so that we have, for the radial part of the matrix element,

$$\begin{aligned} (0|r|1)&=(WR^3/M\omega^2)\phi_0(R)\phi_1(R)\\ &=(WR^2/M\omega^2)A_lC_{l'}j_l(aR)j_{l'}(cR), \end{aligned} \quad \text{(A7)}$$

which leads to the expression (6) for the cross section.

(b) Central Elevation

In the case of an infinite central elevation extending to $r=R_0$ the wave functions ϕ_0 and ϕ_1 inside the nucleus take the form

$$\begin{aligned} \phi_0&=A_l[\alpha_0 j_l(ar)+\beta_0 n_l(ar)] \quad R_0<r<R,\\ \phi_1&=C_{l'}[\alpha_1 j_{l'}(cr)+\beta_1 n_{l'}(cr)] \quad R_0<r<R, \end{aligned}$$

where α_0, α_1, β_0, and β_1 must be chosen so as to make $\phi_0=\phi_1=0$ for $r=R_0$. For convenience, let us write $\alpha_0 j_l(ar)+\beta_0 n_l(ar)=y_l(ar)$; $\alpha_1 j_{l'}(cr)+\beta_1 n_{l'}(cr)=y_{l'}(cr)$. Then the normalization condition gives

$$\begin{aligned} \tfrac{1}{2}A_l^2R^3[&-(a^2+b^2)b^{-2}y_{l-1}(ar)y_{l+1}(aR)\\ &+(R_0/R)^2y_{l-1}(aR_0)y_{l+1}(aR_0)]=1. \end{aligned} \quad \text{(A8)}$$

If the asymptotic expressions for the bessel functions are valid, i.e., if $aR_0>l$, we have

$$\begin{aligned} y_{l-1}(aR)y_{l+1}(aR)&=-b^2/[(a^2+b^2)(aR)^2],\\ y_{l-1}(aR_0)y_{l+1}(aR_0)&=-1/(aR_0)^2 \end{aligned}$$

so that

$$A_l^2=2a^2/(R-R_0). \quad \text{(A9)}$$

The expressions for C_l are the same as in the case of the square well, except that $j_l(cR)$, $j_{l-1}(cR)$ must be replaced by $y_l(cR)$, $y_{l-1}(cR)$.

In computing the matrix element the formula (A7) must be modified by the addition of a term arising from the infinite potential jump at $r=R_0$. This is most easily done by first considering a finite jump W_0 and then letting W_0 tend to infinity. We have, then,

$$(0|r|1)=(1/M\omega^2)[WR^3\phi_0(R)\phi_1(R)-W_0R_0^3\phi_0(R_0)\phi_1(R_0)]. \quad \text{(A10)}$$

As W_0 tends to infinity, $\phi_0(R_0)$ and $\phi_1(R_0)$ tend to zero, and we must evaluate the limit of the product. From the continuity conditions at $r=R_0$ we have, for large W_0,

$$\phi_0'(R_0)/\phi_0(R_0)\approx\phi_1'(R_0)/\phi_1(R_0)\approx(2MW_0/\hbar^2)^{\frac{1}{2}}, \quad \text{(A11)}$$

so that

$$\lim_{W_0\to\infty} W_0R_0^3\phi_0(R_0)\phi_1(R_0)=(\hbar^2/2M)R_0^3\phi_0'(R_0)\phi_1'(R_0) \quad \text{(A12)}$$

and

$$\begin{aligned} (0|r|1)=(WR^3A_lC_{l'}/M\omega^2)&[y_l(aR)y_{l'}(cR)\\ &-(\hbar^2/2MR^2W)R^3\alpha c y_l'(aR_0)y_{l'}'(cR_0)]. \end{aligned} \quad \text{(A13)}$$

If asymptotic formulas hold throughout, $y_l(aR)=(a^2+b^2)^{-\frac{1}{2}}R^{-1}$, $y_{l'}(cR)=[\sin(cR+\alpha)]/cR$, $y_l'(aR_0)=1/aR$, $y_{l'}'(cR_0)=1/cR_0$, and

$$(0|r|1)=\frac{WA_lC_{l'}}{M\omega^2}\left[\frac{\sin(cR+\alpha)}{c(a^2+b^2)^{\frac{1}{2}}}-\frac{\hbar^2}{2MW}\right] \quad \text{(A14)}$$

with

$$C_{l'}=cd[c^2-(c^2-d^2)\sin^2(cR+\alpha)]^{-\frac{1}{2}}, \quad \text{(A15)}$$

where α is a phase angle. Squaring and averaging over the phase

[34] P. C. Gugelot, Phys. Rev. 81, 51 (1951).

angle as before we find

$$\langle|(0|r|1)|^2\rangle_{Av}=\frac{W^2A^2}{M^2\omega^4}\frac{c^2d^2R^2}{c^2(a^2+b^2)}\left[\frac{1}{d(c+d)}\frac{\gamma^2}{cd}\right], \quad \text{(A16)}$$

where $\gamma^2=c^2/(a^2+b^2)$.

Thus, the cross section is increased over that for the square well by the factor

$$[R/(R-R_0)][1+c(c+d)/(a^2+b^2)]. \quad \text{(A17)}$$

To compare the modified cross sections with experiment, we must choose a value for R_0. We choose $R_0=R/4$, since then the $2s$ level is pushed up near the top of the distribution for Z near 45, as required by the angular distributions of Rh and Ag photoprotons. For this value of R_0 the depth of the well need not be increased substantially over that of the square well. We then find, for the parameters chosen in the text, an increase in the cross section by a factor of 3.7 as compared with (9). This asymptotic estimate is, however, good only for $l=0$ or 1, since it is predicated on the assumption $aR_0>l$. For higher values of l the change in the cross section will be less pronounced, since the wave functions do not differ as much from those for the square well.

PHYSICAL REVIEW VOLUME 82, NUMBER 5 JUNE 1, 1951

Photoprotons from Magnesium

M. Elaine Toms and William E. Stephens
Department of Physics, University of Pennsylvania, Philadelphia, Pennsylvania

(Received February 9, 1951)

The distributions in energy and in angle of the protons ejected from magnesium by the bremsstrahlung x-rays of a 24-Mev betatron have been observed in nuclear emulsions. Both normal magnesium and enriched Mg^{25} show a uniform angular distribution for all proton energies. The energy distribution of the protons from enriched Mg^{25} is compared to the distributions calculated from an evaporation process using various energy level densities. Good agreement is obtained using the known Na^{24} level densities. The integrated cross section of the $Mg^{25}(\gamma,p)$ reaction is determined as 0.056 ± 0.03 Mev-barn.

I. INTRODUCTION

EARLY measurements[1] of the ratio of (γ,p) to (γ,n) cross sections have indicated larger values than expected from the statistical theory of nuclei.[2] The observation of a broad resonance in the photoexcitation curves was also surprising.[3–5] The explanations[6,7] which were advanced for these phenomena seemed to differ in the angular and energy distributions to be expected of the ejected protons. Consequently, this investigation was initiated to examine such characteristics of the photoprotons in the hope that they would help determine the predominant mechanisms. Magnesium was chosen as the first element to be investigated since its photoproton yield was known to be appreciable.[1,5] Initial results on the angular distribution of photoprotons from normal magnesium indicated no appreciable direct photoelectric effects.[8] Enriched magnesium was secured from the AEC, and further work was undertaken to refine the observations. Meanwhile other experimental data[9,10] and theoretical calculations[11–15] have been published.

II. APPARATUS

The x-ray beam from an Allis-Chalmers betatron is defined, as shown in Fig. 1, by a collimator which has about 16 in. of lead plus 16 in. of steel and lead with a magnetic field to remove the electrons. The x-ray beam which emerges from the collimator is $\frac{1}{4}$ in. in diameter and is diverging at an angle of only eleven minutes. The shielding afforded by the collimator is at least a factor of 10^4 between the beam intensity and the stray radiation. A concrete wall 16 to 24 in. thick surrounds the collimator to reduce the neutron background. Under normal running conditions, the beam intensity at the camera is about 25 roentgens/min as measured by a Victoreen and has passed through 0.7 cm of

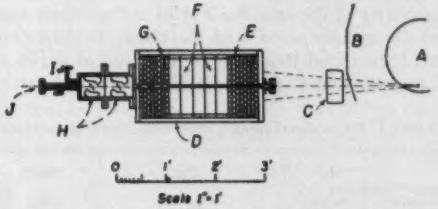

FIG. 1. Experimental arrangement showing *A*—betatron doughnut, *B*—coil box, *C*—monitor, *D*—collimator, *E* and *G*—lead collimating disks, *F*—steel and lead disks holding Alnico magnets, *H*—double camera, *I*—to vacuum pump, and *J*—window.

[1] O. Hirzel and H. Wäffler, Helv. Phys. Acta **20**, 373 (1947).
[2] V. F. Weisskopf and D. H. Ewing, Phys. Rev. **57**, 472, 935 (1940).
[3] G. C. Baldwin and G. S. Klaiber, Phys. Rev. **73**, 1156 (1948).
[4] M. L. Perlman and G. Friedlander, Phys. Rev. **74**, 422 (1948).
[5] McElhinney, Hanson, Becker, Duffield, and Diven, Phys. Rev. **75**, 542 (1949).
[6] L. I. Schiff, Phys. Rev. **73**, 1311 (1948).
[7] M. Goldhaber and E. Teller, Phys. Rev. **74**, 1046 (1948).
[8] Toms, Halpern, and Stephens, Phys. Rev. **77**, 753(A) (1950).
[9] Curtis, Hornbostel, Lee, and Salant, Phys. Rev. **77**, 290 (1950).
[10] B. C. Diven and G. M. Almy, Phys. Rev. **80**, 407 (1950).
[11] E. D. Courant, Phys. Rev. **74**, 1226(A) (1948); and private communications.
[12] P. Jensen, Naturwiss. **35**, 190 (1948).
[13] L. Wolfenstein, Phys. Rev. **78**, 322(A) (1950).
[14] J. S. Levinger and H. A. Bethe, Phys. Rev. **78**, 115 (1950).
[15] K. J. LeCouteur, Proc. Phys. Soc. (London) **63**, 259 (1950).

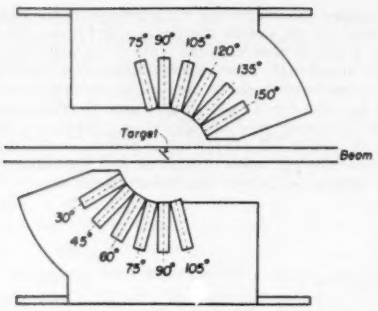

FIG. 2. The nuclear emulsion plate holders showing the positions of the plates.

aluminum and one cm of porcelain. The camera is bolted onto the collimator, and both are evacuated to a pressure of about 100 microns of mercury. The alignment of the beam with the camera and collimator is checked by exposing x-ray film to the beam at the end of the collimator and at the end of the camera. A cylindrical shell slides inside the camera and carries the plate holders and the foil support. Ilford C-2, 100μ-emulsions are cut to $1\times\frac{1}{4}$ in., and the edges are painted with dilute Duco cement to avoid peeling. These plates are cemented to the Lucite supports at $\frac{1}{16}$ in. from the target and $\frac{9}{32}$ in. below the center of the beam, and are set at various angles to the beam as shown in Fig. 2. The camera is shielded from stray radiation by 2 in. of lead piled around it.

The plates are processed by a constant temperature development. After fixing and washing, the plates are soaked in a one percent solution of glycerine to prevent peeling later. After drying, the plates are removed from their supports, remounted in a holder, and examined under a Spencer binocular microscope using 10× oculars and a 97× objective with oil immersion. The green lines from a mercury arc are used for illumination. Similarly situated regions in each plate are scanned and the proton tracks measured only when they enter the top surface of the emulsion and have the correct angle and dip to have come from the target, as determined from their initial 10 μ of path. The allowed angles are 0° to ±12° and 4° to 21° dip. Horizontal and vertical

TABLE I. Magnesium isotopes, thresholds, and cross sections.

	Mg^{24}		Mg^{25}		Mg^{26}	
Isotope abundances						
Normal	0.784		0.102		0.114	
Enriched	0.107		0.868		0.025	
	$-Q$	$\sigma_{17.5}$	$-Q$	$\sigma_{17.5}$	$-Q$	$\sigma_{17.5}$
(γ, n)	16.8 Mev	0.001 barn	6.8 Mev		11.2 Mev	
(γ, p)	12.3		10.6	0.00283 barn	14.2	0.00156 barn
(γ, d)			16			
(γ, np)			18.2			
(γ, α)	10		9		10	
		$\sigma_{RaBe\ n}$				
(n, p)	2	0.1 barn				

lengths are measured on all acceptable tracks and the real lengths calculated using corrections for emulsion shrinkage and microscope calibration. Half the effective foil thickness in emulsion distance is added to each track and the energy determined from the Ilford range-energy curve.[16]

The background was estimated in two ways. In several sample regions, all tracks in the emulsion were counted and all those which entered the surface were observed for angle and dip. The tracks coming in a direction other than from the foil were roughly random in their direction and point of origin. (90 tracks in 1.4 mm².) Those originating in the emulsion were presumably neutron recoils. Those entering the surface most probably were scattered protons but may also have been neutron recoils. Assuming that these tracks contributed to the background by originating, by chance, in the top two microns of the emulsion and having, also by chance, the correct direction to have originated in the foil gives a background of 0.035 tracks in 1.4 mm² compared to an average number of protons from the foil of 26.5 tracks in 1.4 mm² or approximately 0.1 percent. Another check on the background was afforded by a separate run with a gold foil in the beam. A sample scanning of the nuclear emulsions yielded a few random tracks, 24 in 0.4 mm², but none entering the surface with the correct direction.

A correction was necessary for otherwise good tracks which emerged from the emulsion before stopping. These tracks were corrected by increasing the length of each to the average length of all tracks longer than it. In order to check this correction a geometric factor was calculated for the fraction of tracks expected to go through the emulsion at each energy. Applying this to the corrected distribution gave the number expected to go through. The observed number, 138, is somewhat greater than the calculated number, 98, but the difference is not much greater than the statistical fluctuations and uncertainties in the geometry.

Protons from magnesium can be caused by several transmutations. Table I gives the relative abundances of the three magnesium isotopes and the thresholds for the various possible phototransmutations together with cross sections, where known. The photocross sections were determined with 17.5-Mev gamma-rays and the neutron cross section with radium beryllium neutrons.

It might be expected that the Mg^{24} reactions would be predominate with normal magnesium foil. In order to investigate the possibility of protons from $Mg^{24}(n,p)Na^{24}$ reaction produced by neutrons from the betatron, a sample of magnesium was irradiated first in the direct x-ray beam and then just out of the beam. The background neutron intensity would be expected to be approximately the same at each position. Appreciable

[16] Lattes, Fowler, and Cuer, Proc. Phys. Soc. (London) **59**, 883 (1947).

Na^{24} activity was observed when the magnesium was exposed in the x-ray beam (due to the $Mg^{25}(\gamma,p)Na^{24}$) but none (less than one percent of the activation in the beam) when the magnesium was out of the beam. As an additional check the number of neutrons from the betatron with energies (>2 Mev) sufficient to activate Si^{31} by $P^{31}(n,p)Si^{31}$ was determined by observing the Si^{31} activation near the betatron. A RaBe source whose neutron emission could be calculated was also used to produce both $P^{31}(n,p)Si^{31}$ and $Mg^{24}(n,p)Na^{24}$ reactions. From these observations, it was calculated that about 10^9 neutrons/sec came from the betatron and 2×10^5 n/sec/cm^2 would be expected to be in the collimated x-ray beam at the foil. A considerable number of neutrons, of the order of 4×10^7 n/sec, are produced by the stopping of the x-rays in the collimator,[17] but the camera was shielded from most of these neutrons. From the activation in the normal magnesium of $Mg^{24}(n,p)Na^{24}$ by the RaBe neutrons and the $Mg^{25}(\gamma,p)Na^{24}$ from the betatron, it was estimated that 6×10^5 neutrons/sec/cm^2 would produce the same amount of activation (and hence equal numbers of protons) as the betatron x-ray beam. Consequently, the (n,p) reactions are considered negligible.

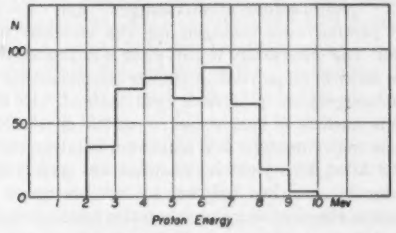

FIG. 3. Energy distribution of the proton tracks observed with normal magnesium foil at a betatron energy of 22.5 Mev.

III. MEASUREMENTS

The first exposure totaled 7000 roentgens on a 2.77-mil thick (12.2-mg/cm^2) magnesium metal foil. The betatron was run at a nominal energy of 22.5 Mev. Equal areas, 2 mm wide by 12 mm long, were scanned on plates situated at 30°, 60°, 120°, and 150°. Half this area was scanned on each of the opposite 90° plates. The agreement between these opposite plates checked the alignment and centering of the beam. The energy distribution of the 423 measured tracks is shown in Fig. 3. The foil half-thickness, which is the uncertainty in the proton range, is equivalent to about $\frac{3}{4}$ Mev for 2-Mev protons and about 0.2 Mev for 10-Mev protons. The angular distribution of these tracks is indicated in Fig. 4. The vertical lines are the statistical uncertainty, while the horizontal lines through each point indicate the angular spread allowed.

[17] J. S. Levinger, Nucleonics **6**, No. 5, 64 (1950).

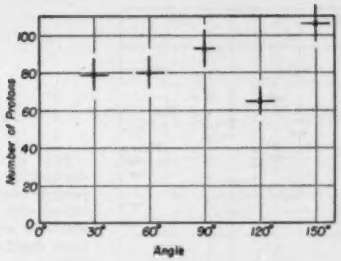

FIG. 4. Angular distribution of the proton tracks observed with a normal magnesium foil at a betatron energy of 22.5 Mev.

In order to improve the statistics and refine the measurements, a foil of enriched magnesium was prepared. Magnesium oxide containing 86.8 percent of Mg^{25} with only 2.5 percent of Mg^{26} and 10.7 percent of Mg^{24} was kindly loaned us by the Isotopes Division of the AEC. Forty milligrams of this magnesium oxide was reduced with aluminum in a vacuum and the resulting lump of magnesium metal rolled into a foil 2.2 mils thick (9.62 mg/cm^2) and about one centimeter square. Spectroscopic tests indicated negligible amounts of aluminum in the magnesium metal. This enriched foil was exposed to 36,900 roentgens of the bremsstrahlung x-rays from 24-Mev electrons hitting the platinum target of the betatron donut. An area 1 mm by 10 mm was scanned on plates at 30°, 60°, 90°, 120°, and 150°. This same area was scanned on the appropriate plates at 75° and 105°. No significant differences in the number of tracks found on opposite plates at 75°, 90°, and 105° again confirmed the beam alignment. The energy and angular distributions are shown in Figs. 5 and 6. The uncertainty in proton

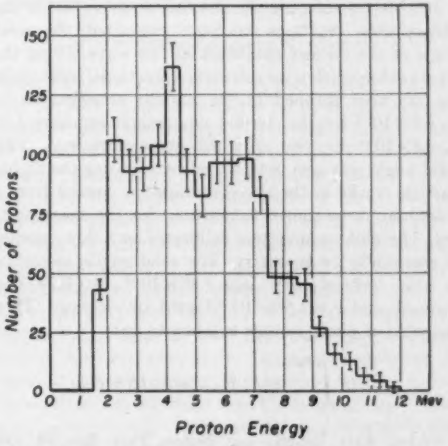

FIG. 5. Energy distribution of the proton tracks observed with enriched Mg^{25} foil at a betatron energy of 24 Mev.

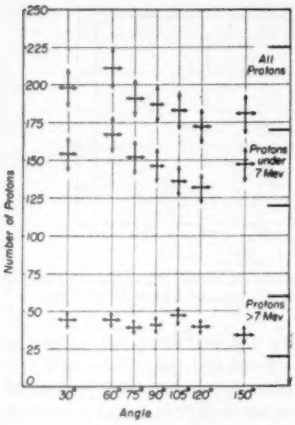

FIG. 6. Angular distribution of the proton tracks observed with enriched Mg^{25} foil at a betatron energy of 24 Mev.

energy (equivalent to half the foil thickness) for the enriched foil varies from ± 0.15 Mev for the 10-Mev protons to ± 0.5 Mev for the 2-Mev protons at the best angles. In Fig. 6 the angular distribution of the protons with energies greater than 7 Mev and less than 7 Mev is shown in addition to the totals.

In order to compute the expected energy distribution of the protons we have measured the yield curve of the $Mg^{25}(\gamma,p)Na^{24}$ reaction in ordinary magnesium by observing the 15-hour half-life of Na^{24} activated at different betatron energies. The activation counting rate per unit x-ray intensity is plotted in Fig. 7 as a function of the nominal betatron energy. This yield curve was reduced to a relative cross-section curve by the use of normalized bremsstrahlung curves.[15] The relative cross-section curve is shown in Fig. 8. Only the statistical errors carried over from the differentiation of the yield curve are indicated.

In order to compute the absolute cross section of the photoproton reactions we have evaluated the solid angle of the nuclear emulsions in two ways. Using the measured geometry we calculate a fractional solid angle for the area scanned in the nuclear emulsion to be $\omega_n = 3\times10^{-4}$ for the normal magnesium exposure and $\omega_e = 2\times10^{-4}$ for the enriched magnesium run. This solid angle was also determined by counting the alpha-particle tracks in the nuclear emulsions coming from a polonium alpha-source substituted for the magnesium foil. The alpha-source was calibrated in a flow counter of essentially 2π-geometry. The solid angles measured in this fashion were $\omega_n = 3.48\times10^{-4}$ for 0.24 cm^2 scanned, and $\omega_e = 1.95\times10^{-4}$ for 0.1 cm^2 scanned. Then the yield of photoprotons is taken to be:

$$ANtR\int_0^{E_{max}} n(E, E_{max})\sigma(E)dE = P/\omega,$$

where P/ω is the number of protons ejected from the foil by R roentgens, A is the area of the x-ray beam, t is the thickness of the foil in the direction of the beam, N is the number of nuclei per cc, n is the number of photons/Mev interval/cm^2/roentgen unit, when the betatron is run at an energy of E_{max}, σ is the photoproton cross section for photons of energy E, and P is the number of protons observed in the nuclear emulsions when an area, a, constituting a fractional solid angle of ω is scanned. The integral is the yield per atom per roentgen unit.

$$y = \int_0^{E_{max}} n(E, E_{max})\sigma(E)dE = P/ANtR\omega.$$

Multiplying by Avogadro's number gives Y, the yield per mole per roentgen unit. We have used n from Katz's[15] curves and calculated the absolute cross sections from the observed yields. The data involved in the calculation of the yield from the enriched foil are: $N = 4.2\times10^{22}$ nuclei of Mg/cc, $t = 7.9\times10^{-3}$ cm, $A = 0.267$ cm^2, $\omega_e = 2\times10^{-4}$ for 0.1 cm^2 scanned, and $P = 190$ protons in 0.1 cm^2 scanned. Thus, $y = 2.92\times10^{-19}$ photoprotons/atom/roentgen, and $Y = 1.75\times10^5$ protons/mole/roentgen for the enriched magnesium. The uncertainty in this yield is estimated to be of the order of 50 percent. A similar calculation for the normal magnesium foil gives a yield of about 3.1×10^{-19} protons/nucleus of magnesium/roentgen or 18.6×10^4 protons/mole/roentgen at a maximum betatron energy of 22.5 Mev. This yield is somewhat less certain than that for the enriched foil due to inaccuracies in the ionization chamber monitor integrator readings and is estimated as ± 75 percent. Taking into account the relative abundances of the magnesium isotopes in the

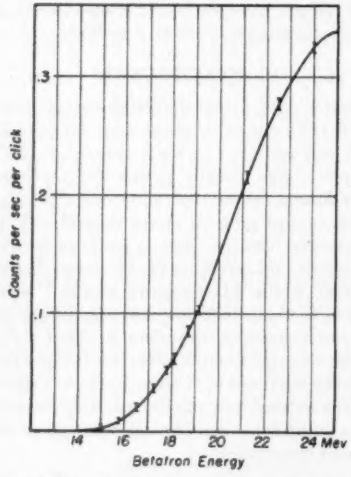

FIG. 7. $Mg^{25}(\gamma,p)Na^{24}$ yield curve based on Na^{24} activity.

[15] Johns, Katz, Douglas, and Haslam, Phys. Rev. **80**, 1062 (1950). We are indebted to Professor Katz for sending us these curves before publication.

normal and enriched foils and the observed proton yields, we calculate the isotopic yields to be $y_{25}=1.74\times10^{5}$ protons/mole/roentgen and $y_{24}=2\times10^{5}$ protons/mole/roentgen. Although Mg^{24} has a higher proton threshold than Mg^{25}, it also has a higher neutron threshold to compensate. The Mg^{25} yield determines the ordinate scale of Fig. 8 to be 0.0896×10^{-26} cm² in absolute units. The peak cross section is then 0.0137 barn at 20.5 Mev, and the integrated cross section is 0.056 Mev-barn. The cross section at 17.5 Mev is 0.004 barn. The uncertainty in these cross sections is also estimated to be of the order of 50 percent.

IV. DISCUSSION

The cross section of 0.004 ± 0.002 barn observed for $Mg^{25}(\gamma,p)Na^{24}$ at 17.5-Mev photon energy can be compared with the measurements of Hirzel and Wäffler[1] on the Na^{24} radioactivity produced by the lithium gamma-rays. They give a ratio of $Mg^{25}(\gamma,p)$ to $Cu^{63}(\gamma,n)$ of 0.0283 ± 0.0030. Using a cross section for $Cu^{63}(\gamma,n)$ at 17.5 Mev of 0.10 barn[18] gives for $Mg^{25}(\gamma,p)$, 0.0028 barn. The yield of protons from the normal magnesium, 18.6×10^{4} protons/mole/roentgen, is about one-third that observed by Mann and Halpern[19] with a scintillation detector at 23.5-Mev betatron energy, but this difference is within the sum of the uncertainties. If we were to use Mann and Halpern's normal magnesium proton yield, the y_{24} would be about three times as great and the y_{25} about two-thirds the value we have calculated. Using our yields, 88 percent of the protons from the enriched foil are from $Mg^{25}(\gamma,p)$; using Mann and Halpern's value, 60 percent from the enriched foil are from Mg^{25}. For the normal magnesium foil, the corresponding values of the protons produced by $Mg^{24}(\gamma,p)$ are 84 and 96 percent.

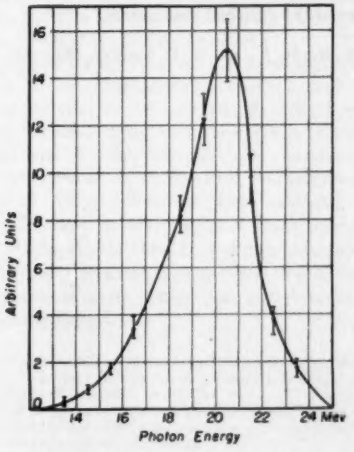

FIG. 8. Calculated relative cross-section curve for $Mg^{25}(\gamma,p)Na^{24}$ as a function of photon energy.

[19] A. K. Mann and J. Halpern, Phys. Rev. 81, 318 (1951).

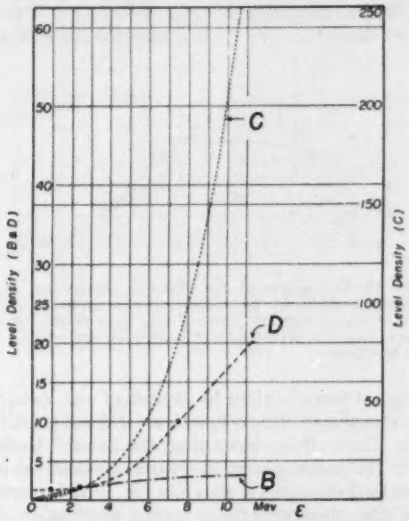

FIG. 9. Assumptions as to the energy level density of the resultant nucleus Na^{24}: curve B—ω_R from Schiff's formula, curve C—ω_R from Weisskopf and Ewing's formula, curve D—ω_R from Na^{24} levels.

Although the statistical model is not usually applicable in detail to such a light nucleus as magnesium, the calculation of the expected proton energy distribution is aided by the heterogeneous energy of the x-rays, which tends to average out the details of the level structure. Weisskopf and Ewing[2] give the distribution in energy ϵ of the protons from a nucleus b which has absorbed a photon of energy E as

$$I(\epsilon)=\text{const}\;\epsilon\,S_b(\epsilon)\xi_b\omega_R(E-E_b-\epsilon),$$

where ω_R is the level density of the resultant nucleus, ξ_b is the sticking factor (assumed to be unity), S_b is the coulomb penetration factor taken from tables,[20] and E_b is the binding energy of the proton. A distribution curve, I, is calculated for each E and normalized to the product of the 24-Mev bremsstrahlung curve and the relative cross-section curve at that E. The curve resulting from the addition of these I curves is normalized to the number of protons observed and compared to the observed proton energy distribution. Such a curve was calculated for each of several level density formulas. The assumed level densities of the resultant nucleus Na^{24} are plotted in Fig. 9 as a function of resultant nucleus excitation energy $\mathcal{E}=E-E_b-\epsilon$. Curve B is plotted from Schiff's formula[6] $\omega_R=(1/a)\times\ln[(\epsilon_0-\epsilon+a)/a]$, where $a=20/A$. Curve C is the

[20] We are indebted to Professor Weisskopf for providing us with the latest tables of these penetration factors.

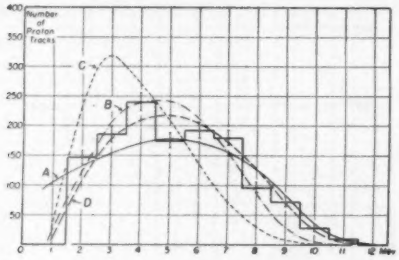

FIG. 10. Comparison of the observed photoproton energy distribution, shown by the histogram, with calculated curves: curve A—ω_E, a constant, curve B—ω_E from Schiff's formula, curve C—ω_E from Weisskopf and Ewing's formula, curve D—ω_E from Na^{24} levels.

statistical formula given by Weisskopf and Ewing[8] as $\omega_E = C \exp[a(E-E_b-\epsilon)]^{\frac{1}{2}}$, with $a=A/5$ and $C=0.2$ per Mev. Curve D is drawn from the known[21] levels of Na^{24}. The proton energy distributions calculated from these level densities are shown in Fig. 10 and compared with the observed proton energy distribution. The good agreement between the experimental curve and the curve D deduced from the known Na^{24} levels supports the concept of absorption of the photon energy into a compound nucleus with the subsequent evaporation of a proton (or a neutron). The uniformity of the angular distribution of the protons confirms this view. The observed integrated cross section of 0.056±Mev-barn can be compared with the values calculated on the dipole interaction. Goldhaber and Teller[7] estimate a total integrated photon absorption cross section of 0.36 Mev-barn for Mg^{25}. Price and Kerst[22] give 1.8×10^5 neutrons/mole/roentgen for normal magnesium photoneutron yield, much of which may be $Mg^{25}(\gamma,n)$ because of the high $Mg^{24}(\gamma,n)$ threshold. The sum of the $Mg^{25}(\gamma,p)$ and $Mg^{25}(\gamma,n)$ integrated cross sections seems smaller than, but may be consistent with, Goldhaber and Teller's value as well as Levinger and Bethe's[14] value of 0.52 Mev-barn for the integrated photon absorption. The resonance which is here observed at 20.5 Mev is predicted near 23.5 Mev on Goldhaber and Teller's picture and at about 29 Mev from Bethe and Levinger's calculations. There seems to be no major disagreement between these experiments, nor those of Diven and Almy on aluminum,[10] and the simple picture of photon absorption by dipole interaction, formation of a compound nucleus, and subsequent evaporation of neutrons and protons. In heavier nuclei, however, there seem to be anomalies[9,10,23] suggesting that occasionally the photoproton is ejected before its photoelectric energy is shared with the compound nucleus.[11] This may be the result of an increased nuclear mean free path at the higher energies available to the proton absorbing the photon because of lower proton binding energies. This can show up more easily in the heavier nuclei also because of the increased coulomb barrier which inhibits proton evaporation at the lower proton energies and consequently enhances the relative number of higher energy protons.

This research was supported in part by the joint program of the ONR and AEC. It was also aided by a grant from the Committee on the Advancement of Research of the University of Pennsylvania. The preparation of the enriched magnesium foil was accomplished by Mr. Victor Verbinski with the advice of Professor Knut Krieger of the Chemistry Department of the University of Pennsylvania. We appreciate the cooperation of the Isotopes Division of the AEC in the loan of the enriched magnesium.

[21] D. E. Alburger and E. M. Hafner, Revs. Modern Phys. **22**, 373 (1950).
[22] G. A. Price and D. W. Kerst, Phys. Rev. **77**, 806 (1950).
[23] P. R. Byerly, Jr., and W. E. Stephens, Phys. Rev. **81**, 473 (1951).

A Phenomenological Derivation of the First- and Second-Order Magnetostriction and Morphic Effects for a Nickel Crystal

W. P. MASON
Bell Telephone Laboratories, Murray Hill, New Jersey
(Received October 23, 1950)

In order to account for experimental results which showed that the saturation elastic constants of a single nickel crystal varied with the direction of magnetization, a phenomenological investigation has been made of the stress, strain, and magnetic relations for single nickel crystals. The variation in elastic constants is shown to be a "morphic" effect caused by the change in the crystal symmetry due to the magnetostriction effect. In the energy equation this effect is represented by additional terms which involve squares and products of both the magnetic intensities and stresses. These terms are as large as the magnetostrictive terms when the stresses are of the order of 10^{10} dynes/cm^2. The energy equation has been used to derive the first- and second-order magnetostrictive effect, and the resulting terms agree with Becker and Döring's empirical constants for saturation conditions. For smaller magnetic intensities the terms divide up into first- and second-order terms which vary differently with magnetic field intensity. It is shown that the morphic effects involve six measurable constants, and some of these are evaluated experimentally.

I. INTRODUCTION

CAREFUL measurements of the change in elastic constants with magnetization in single nickel crystals[1] have shown that the elastic constants for a saturated crystal depend on the direction of saturation. It is the primary purpose of this paper to show that the change in saturation elastic constants with direction of magnetization is due to what Mueller[2] has called a "morphic" effect; namely, that the distortion of the crystal by the magnetostrictive effect produces a crystal of lower symmetry which involves more than the three elastic constants of a cubic crystal. It is shown in this paper that the additional elastic constants and their variation with magnetic orientation can be obtained by adding terms to the energy equation which involve squares and products of both the magnetic intensity and the stresses. Symmetry determines the number of constants, and it is shown that there are six measurable constants which characterize the effect.

The complete energy equation has been applied to a derivation of the magnetostrictive effect, and it is shown that first-and second-order terms are involved. At saturation the terms agree with those given previously by Becker and Döring,[3] but for lower magnetic intensities the terms divide up into first- and second-order terms which vary differently with magnetic field intensity. The experimental results of Masiyama[4] for a single nickel crystal are fitted by the phenomenological formula derived here, and a slightly better fit is obtained. The evaluation of some of the first- and second-order terms is accomplished.

The tensor method is followed, since this results in a considerable economy of effort and readily allows one to change from one coordinate system to another. The tensors are all of the cartesian type, since only rectangular coordinate systems are considered. The method followed is to add terms to the energy equation of a form required to agree with the measured effects and to determine the resulting constants by means of symmetry considerations.

II. ENERGY FUNCTIONS FOR MAGNETOSTRICTIVE CRYSTALS

It is well known that the changes in dimensions, magnetic fields, and temperature for any body subject to magnetostrictive and magnetic effects can be derived from a thermodynamic function. In order to use the measured magnetostrictive constants, it is better to use the stress, intensity of magnetization, and entropy as the independent variables. To do this we introduce the elastic enthalpy H_1, defined by the equation

$$H_1 = U - T_{ij}S_{ij}, \tag{1}$$

where U is the internal energy function and T_{ij} and S_{ij} are respectively the stresses and tensor strains, i.e., $[\frac{1}{2}(\partial u_i/\partial x_j)+\partial u_j/\partial x_i]$, where u is the displacement. The differential form of H_1 is known to be

$$dH_1 = -S_{ij}dT_{ij} + H_m dI_m + \Theta d\sigma, \tag{2}$$

where H_m are the magnetic fields, I_m the intensities of magnetization, Θ the absolute temperature, and σ the entropy. Hence, one obtains

$$S_{ij} = -\partial H_1/\partial T_j; \quad H_m = \partial H_1/\partial I_m; \quad \Theta = \partial H_1/\partial \sigma. \tag{3}$$

Since all of the measurements have been carried out under adiabatic conditions, the entropy change is zero and H_1 can be considered to be a function of the stresses and magnetizations.

The usual method for deriving the energy terms is to add first- and second-order terms and to determine the number and types of constants by the symmetry con-

[1] These measurements were made primarily to determine the "ΔE" effect and the microeddy current effects in single nickel crystals and will be discussed in another paper, "The frequency dependence of elastic constants and losses in nickel," by Bozorth, Mason, and McSkimin. The measurements are reproduced here in order to evaluate the morphic effect.
[2] H. Mueller, Phys. Rev. **58**, 805 (1940).
[3] R. Becker and W. Döring, *Ferromagnetismus* (Verlag. Julius Springer, Berlin, 1934), page 275.
[4] Y. Masiyama, Sci. Rep. Tohoku Imp. Univ. **17**, 945 (1928).

dition. Use can be made of the fact that nickel has a center of symmetry which results in having all the odd rank tensors equal to zero. Furthermore, nickel can be described as being soft magnetically but hard elastically. Hence, we can neglect all energy terms that involve terms higher than products or squares of the stresses. With these limitations, the elastic enthalpy function H_1 can be written in the form

$$\begin{aligned}2H_1=&-[s^I_{ijkl}T_{ij}T_{kl}+R_{ijklmo}I_mI_oT_{ij}T_{kl}\\&+M_{ijmn}I_mI_nT_{ij}+N_{ijmnop}I_mI_nI_oI_pT_{ij}]\\&+K^T_{mn}I_mI_n+K^T_{mnop}I_mI_nI_oI_p\\&+K^T_{mnopqr}I_mI_nI_oI_pI_qI_r.\end{aligned}\tag{4}$$

These equations hold for a crystal with a large number of domains when the directions of the domains are uncorrelated, for then the components of magnetization are independent. For a single domain, the magnetic intensity has a fixed value, the saturation value I_0, and only the direction of magnetism can be changed. If α_1, α_2, α_3 are the direction cosines of the magnetic intensity with respect to the crystal axes, then one has

$$I_1=\alpha_1I_0;\quad I_2=\alpha_2I_0;\quad I_3=\alpha_3I_0;\tag{5}$$

and there is a relation between the three direction cosines, namely,

$$\alpha_1^2+\alpha_2^2+\alpha_3^2=1.\tag{6}$$

The stresses T_{ij} and the strains S_{kl} are symmetrical tensors, and hence we can interchange the order of the subscripts. The same is true for the subscripts of the magnetic intensities, and hence it has become customary to use a single index related to the two indices by the equations

$$\begin{gathered}11=1;\quad 22=2;\quad 33=3;\quad 12=21=6;\\13=31=5;\quad 23=32=4.\end{gathered}\tag{7}$$

Similarly, for the fourth-rank tensors s_{ijkl}, M_{klmn}, K_{mnop} we can interchange i and j, k and l, o and p so that only two indices are necessary for these terms. Furthermore, for the tensor $s_{ab}=s_{ijkl}$ it is proved in elastic theory that a and b can be interchanged so that there are at most 21 independent constants. This is not true for the magnetostrictive tensor $M_{ab}=M_{ijkl}$ and in general there are 36 independent terms. For the anisotropic magnetic energy tensor $K_{ab}=K_{ijkl}$ all four of the terms i, j, k, l can be interchanged, and in general there are only 15 independent terms. The number and type of these independent constants for the symmetry of nickel O_h are well known from crystal theory.[5] Since the number and type of the constants of a sixth-rank tensor do not appear to have been completely worked out, they are considered in Appendix I.

With these components known, the expression for H_1 can be written down. In this equation I_s is replaced by α_1I_0, etc., indicating that it is a component of the saturation intensity of magnetization I_0. The energy for the demagnetized case given by $\alpha_1^2=\alpha_2^2=\alpha_3^2=\frac{1}{3}$ has also been subtracted from the expression so that the energy represents the difference between any state and the demagnetized state. Certain combinations of the α-values have also been made to cut the number of independent terms to a minimum. With these simplifications, we can write $-2H_1$ as

$$\begin{aligned}-2H_1=&s^I_{11}(T_1^2+T_2^2+T_3^2)+2s^I_{12}(T_1T_2+T_1T_3+T_2T_3)+2s^I_{44}[T_4^2+T_5^2+T_6^2]\\&+(\alpha_1^2-\tfrac{1}{3})I_0^2[(R_{111}-R_{112})T_1^2+2(R_{123}-R_{121})T_2T_3+4(R_{441}-R_{551})T_4^2]\\&+(\alpha_2^2-\tfrac{1}{3})I_0^2[(R_{111}-R_{112})T_2^2+2(R_{123}-R_{121})T_1T_3+4(R_{441}-R_{551})T_5^2]\\&+(\alpha_3^2-\tfrac{1}{3})I_0^2[(R_{111}-R_{112})T_3^2+2(R_{123}-R_{121})T_1T_2+4(R_{441}-R_{551})T_6^2]\\&+8\alpha_1\alpha_2I_0^2\{T_6[R_{144}T_3+R_{155}(T_1+T_2)]+R_{456}T_4T_5\}\\&+8\alpha_1\alpha_3I_0^2\{T_5[R_{144}T_2+R_{155}(T_1+T_3)]+R_{456}T_4T_6\}\\&+8\alpha_1\alpha_2I_0^2\{T_4[R_{144}T_1+R_{155}(T_2+T_3)]+R_{456}T_5T_6\}\\&+\{(M_{11}-M_{12})I_0^2+[2(N_{112}-N_{123})+4(N_{551}-N_{441})]I_0^4\}[(\alpha_1^2-\tfrac{1}{3})T_1+(\alpha_2^2-\tfrac{1}{3})T_2+(\alpha_3^2-\tfrac{1}{3})T_3]\\&+\{[N_{111}-3N_{112}+2N_{123}+4(N_{441}-N_{551})]I_0^4[(\alpha_1^4+\tfrac{2}{3}s-\tfrac{1}{3})T_1+(\alpha_2^4+\tfrac{2}{3}s-\tfrac{1}{3})T_2+(\alpha_3^4+\tfrac{2}{3}s-\tfrac{1}{3})T_3]\}\\&+[\tfrac{2}{3}(N_{111}-N_{123}-4N_{551}-2N_{441})]I_0^4(\tfrac{1}{3}-s)(T_1+T_2+T_3)\\&+[2M_{44}I_0^2+4(N_{112}+N_{551})I_0^4][\alpha_2\alpha_3T_4+\alpha_1\alpha_3T_5+\alpha_1\alpha_2T_6]\\&+4[N_{123}+N_{441}+2N_{456}-N_{112}-N_{551}]I_0^4[\alpha_1^2\alpha_2\alpha_3T_4+\alpha_1\alpha_2^2\alpha_3T_5+\alpha_1\alpha_2\alpha_3^2T_6]\\&-K^T_1(\tfrac{1}{3}-s)-K^T_2[(1/27)-\alpha_1^2\alpha_2^2\alpha_3^2],\end{aligned}\tag{8}$$

[5] See, for example, W. G. Cady, *Piezoelectricity* (McGraw-Hill Book Company, Inc., New York, 1946) or W. P. Mason, *Piezoelectric Crystals* (D. Van Nostrand Company, Inc., New York, 1950) for the elastic tensors. The magnetostrictive tensor is the same as the photoelastic tensor of Pockels. For the tensor K_{ijkl} there are only two independent constants.

where

$$s=\alpha_1^2\alpha_2^2+\alpha^2{}_1\alpha_3^2+\alpha_2^2\alpha_3^2,$$

$$K^T{}_1=[(-2K^T{}_{11}+6K^T{}_{12})I_0^4+(-3K^T{}_{111}+15K^T{}_{112})I_0^6],$$

$$K^T{}_2=[66K^T{}_{123}-45K^T{}_{112}+3K^T{}_{111}]I_0^6.$$

The first three terms represent the elastic energy, the next six terms represent the energy stored by morphic effects, i.e., by the change of shape of the body, the next five terms represent the energy stored by the first- and second-order magnetostrictive effects, while the last two terms represent the magnetic anisotropy terms measured at constant stress. If we neglect the morphic energy terms and set the five constants for the magnetostrictive terms equal to B_1 to B_5, the internal energy reduces to the form given by Becker and Döring.[4] From the value of the R constants found experimentally, the morphic energy terms are about equal to the magnetostrictive terms for stresses in the order of 10^{10} dynes/cm^2, but are smaller for smaller stresses. The anisotropy energy constants K_1 and K_2 are those measured for constant stress. As shown by Kittel,[6] these include the anisotropy energy for constant lattice separation plus the magnetostrictive energy caused by the lattice distortion. To obtain the tensor strains from this function one differentiates with respect to the corresponding stress, as shown by Eq. (3). For the engineering strain values which are twice as large as the tensor strain values for the shearing components

$$S_n=-2\partial H_1/\partial T_n; \quad n=4, 5, 6. \tag{9}$$

Hence, the shear elastic constants s'_{44}, and other terms which are multiplied by the stresses T_4, T_5, and T_6 are one-fourth as large as the corresponding terms which express the relationship between engineering strains and stresses.

III. MAGNETOSTRICTIVE EFFECTS IN CUBIC CRYSTALS

When a nickel crystal is magnetized, it contracts along the direction of magnetization and expands at right angles to the direction of magnetization. The measurements of Masiyama[4] are all elongations along crystallographic axes or along directions such as the [110] or [111]. The elongations or contractions for any direction z' can be obtained from the energy expression (8) by differentiation with respect to the longitudinal stress in this direction or

$$S_{33}'=-\partial H_1/\partial T_{33}'; \tag{10}$$

but the strain S_{33}' is related to the strains referred to the crystallographic axes by the tensor transformation equation

$$S_{33}'=\frac{\partial x_3'}{\partial x_i}\frac{\partial x_3'}{\partial x_j}S_{ij}=-\frac{\partial x_3'}{\partial x_i}\frac{\partial x_3'}{\partial x_j}\frac{\partial H_1}{\partial T_{ij}}, \tag{11}$$

[6] C. Kittel, Revs. Modern Phys. 21, 541 (1949).

where the partial derivatives are the direction cosines β_1, β_2, and β_3 between the z' axis and the x, y, and z axes, respectively. In terms of the one index stress and strain terms

$$\begin{aligned}S_3'=&-(\beta_1^2\partial H_1/\partial T_1)-(\beta_2^2\partial H_1/\partial T_2)-(\beta_3^2\partial H_1/\partial T_3)\\&-(2\beta_2\beta_3\partial H_1/\partial T_4)-(2\beta_1\beta_3\partial H_1/\partial T_5)\\&-2\beta_1\beta_2\partial H_1/\partial T_6.\end{aligned} \tag{12}$$

Performing this differentiation, we have for the magnetostrictive terms

$$\begin{aligned}S_3'=&h_1[\alpha_1^2\beta_1^2+\alpha_2^2\beta_2^2+\alpha_3^2\beta_3^2-\tfrac{1}{3}]\\&+h_2[\alpha_1\alpha_2\beta_1\beta_2+\alpha_1\alpha_3\beta_1\beta_3+\alpha_2\alpha_3\beta_2\beta_3]\\&+h_3(\tfrac{1}{3}-s)+h_4[\alpha_1^4\beta_1^2+\alpha_2^4\beta_2^2+\alpha_3^4\beta_3^2+\tfrac{2}{3}s-\tfrac{1}{3}]\\&+h_5[\alpha_1^3\alpha_2\alpha_3\beta_2\beta_3+\alpha_1\alpha_2^3\alpha_3\beta_1\beta_3+\alpha_1\alpha_2\alpha_3^3\beta_1\beta_2],\end{aligned} \tag{13}$$

where

$$\begin{aligned}h_1&=[\tfrac{1}{2}(M_{11}-M_{12})I_0^2+[N_{112}-N_{123}+2N_{551}-2N_{441}]I_0^4],\\h_2&=[2M_{44}I_0^2+4(N_{112}+N_{551})I_0^4],\\h_3&=\tfrac{1}{3}[N_{111}-N_{123}-4N_{551}-2N_{441}]I_0^4,\\h_4&=[\tfrac{1}{3}(N_{111}-3N_{112})+N_{123}+2(N_{441}-N_{551})]I_0^4,\\h_5&=4[N_{123}+N_{441}+2N_{456}-N_{112}-N_{551}]I_0^3.\end{aligned} \tag{14}$$

For nickel the volume magnetostriction is zero. If we add the sum of S_1', S_2', and S_3' and set the resultant equal to zero for any direction of magnetization, $h_3=0$ and there is a relation between four of the constants

$$\begin{aligned}&N_{111}-N_{123}-4N_{551}-2N_{441}=0\\\text{or}\quad&2N_{551}=\tfrac{1}{2}(N_{111}-N_{123})-N_{441}.\end{aligned} \tag{15}$$

This reduces the formulas for the h values to the values given below:

$$\begin{aligned}h_1&=[\tfrac{1}{2}(M_{11}-M_{12})I_0^2+[\tfrac{1}{2}(N_{111}-N_{112})\\&\qquad+\tfrac{3}{2}(N_{112}-N_{123})-3N_{441}]I_0^4],\\h_2&=[2M_{44}I_0^2+(4N_{112}+N_{111}-N_{123}-2N_{441})I_0^4],\\h_3&=0,\\h_4&=[\tfrac{3}{2}(N_{123}-N_{112})+3N_{441}]I_0^4,\\h_5&=[5(N_{123}-N_{112})-(N_{111}-N_{112})+6N_{441}+8N_{456}]I_0^4.\end{aligned} \tag{16}$$

An empirical formula for the magnetostrictive constant in nickel has been given by Becker and Döring[3] which takes the same form as Eq. (13) with $h_3=0$. Equation (13) with the constants of Eq. (14) is more general when it refers to the multidomain crystal with uncorrelated domains, it gives the magnetostriction as a function of magnetization when we replace $\alpha_1 I_0$ by I_1, etc. Hence, when one measures the magneto-

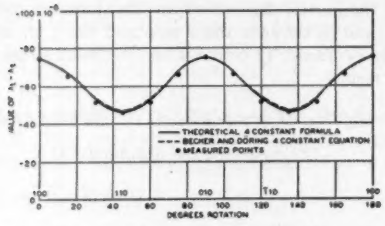

FIG. 1. Difference between longitudinal and transverse magnetostrictive constants for 001 plane.

striction starting from a fully demagnetized crystal, Eq. (13) gives the magnetostriction as a function of the magnetic intensity.

Becker and Döring have compared this formula with the measured curves of Masiyama[4] for the magnetostriction at saturation for nickel. They compare the difference between the longitudinal and transverse magnetostriction with their formula for the 001 plane, the $01\bar{1}$ plane, and the $\bar{1}11$ plane. This difference was chosen because it is independent of the domain structure of the demagnetized state. By choosing the values

$$h_1=-24\times10^{-6},\ h_2=-94\times10^{-6},\ h_4=-51\times10^{-6},$$
$$h_5=+104\times10^{-6},\quad h_3=0, \tag{17}$$

the dotted curves of Figs. 1, 2, and 3 result for these three planes.

Another comparison was made with the experimental data, and it appears that the data are fitted better with slightly different coefficients. For the $00\bar{1}$ plane the equation for $\lambda_l-\lambda_t$, the difference between the longitudinal and transverse magnetostrictive constants becomes

$$\lambda_l-\lambda_t=(h_1+h_4)\cos^2\!2\theta+\tfrac{1}{2}h_2\sin^2\!2\theta. \tag{18}$$

The solid curve of Fig. 1 results when

$$h_1+h_4=-76\times10^{-6},\quad \tfrac{1}{2}h_2=-46\times10^{-6}. \tag{19}$$

For the $01\bar{1}$ plane the equation for $\lambda_l-\lambda_t$ is

$$\lambda_l-\lambda_t=\tfrac{1}{6}(6h_1+5h_4)[\cos^2\!\Psi-\sin^2\!\Psi][\cos^2\!\Psi-\sin^2\!\tfrac{1}{2}\Psi]$$
$$+\tfrac{1}{4}h_2\sin^2\!\Psi[7\cos^2\!\Psi+2\sin^2\!\tfrac{1}{2}\Psi]$$
$$+\tfrac{1}{2}h_5\sin^2\!\Psi\cos^2\!\Psi, \tag{20}$$

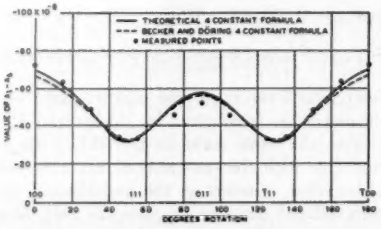

FIG. 2. Difference between longitudinal and transverse magnetostrictive constants for $01\bar{1}$ plane.

where Ψ is the angle measured from the 100 direction The best fit with the measured points is obtained by setting

$$\tfrac{1}{6}(6h_1+5h_4)=-70\times10^{-6},\quad \tfrac{1}{2}h_5=+54\times10^{-6}. \tag{21}$$

The solid line of Fig. 2 results. This still does not fit the measured values completely, which indicates that higher order energy terms are not negligible; but a better agreement is obtained than with the values used by Becker and Döring. If we combine the first value of (19) with the first value of (21), we have the relation

$$h_1=-40\times10^{-6},\quad h_4=-36\times10^{-6}. \tag{22}$$

For the $\bar{1}11$ plane, a calculation of $\lambda_l-\lambda_t$ shows that the difference is independent of orientation and has the value

$$\lambda_l-\lambda_t=h_1/3+2h_4/9+h_2/3+h_5/18. \tag{23}$$

No new constants are involved, but one check is obtained for the values determined previously. These add up to -46×10^{-6}, which agrees well with the measured results as shown by Fig. 3.

These measurements do not allow one to separate out all of the constants, since we cannot resolve the values of the constants of Eq. (13). The two involving both second- and fourth-order constants, h_1 and h_2,

$$h_1=\tfrac{1}{2}(M_{11}-M_{12})I_0^2+[\tfrac{1}{2}(N_{111}-N_{112})$$
$$+\tfrac{3}{2}(N_{112}-N_{123})-3N_{441}]I_0^4, \tag{24}$$
$$h_2=2M_{44}I_0^2+[4N_{112}+(N_{111}-N_{123})-2N_{441}]I_0^4,$$

could be resolved if the magnetostriction constants were measured in terms of the magnetic intensity, since terms in I^3 and I^4 occur. Unfortunately, however, Masiyama's measurements are presented in terms of the field strengths. Two of these measurements for the 001 plane are shown by Fig. 4. In order to obtain the magnetic intensities, one would need to know the permeabilities for the two directions as a function of field strength. The initial slopes of these two curves, however, can be used to determine approximately the ratio of the M_{44} constant to the $M_{11}-M_{12}$ constant. This follows from the fact that the initial permeability is a second-rank tensor and hence has the same value for all directions for a cubic crystal. From the initial slopes it appears that the ratio is

$$2M_{44}/(M_{11}-M_{12})=69/40$$
or
$$M_{44}=0.86(M_{11}-M_{12}). \tag{25}$$

Further constants could be evaluated if shear magnetostriction measurements were available.

IV. CHANGE OF ELECTRIC CONSTANTS WITH THE DIRECTION OF MAGNETIZATION FOR A SATURATED CRYSTAL

When the crystal is magnetically saturated, it is found experimentally that for elastic waves propagated along the [110], [111], and [100] directions the

velocity depends on the direction of magnetic saturation. This can be explained if we include "morphic" effects; i.e., if we take account of the change of shape of the crystal from a cubic form due to the magnetostrictive effects in the crystal. These changes are caused by the R terms of Eq. (8).

For a plane progressive ultrasonic wave it is much more advantageous to express the stresses in terms of the strains, since only one strain occurs in an uncoupled plane progressive wave. This involves expressing the results in terms of the internal energy function U rather than the elastic enthalpy function H_1. The resulting terms can be determined by eliminating the stresses fro H_1 and replacing them by the strains. The details are discussed in Appendix II.

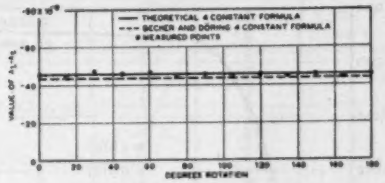

FIG. 3. Difference between longitudinal and transverse magnetostrictive constants for 111 plane.

If we differentiate U with respect to S_n and neglect the constant forces generated by the magnetostrictive effect, the stress-strain relation can be expressed in the matrix form

	S_1	S_2	S_3	S_4	S_5	S_6
T_1	$c^I_{11}+\delta_{11}$	$c^I_{12}+\delta_{12}$	$c^I_{12}+\delta_{13}$	δ_{14}	δ_{15}	δ_{16}
T_2	$c^I_{12}+\delta_{12}$	$c^I_{11}+\delta_{22}$	$c^I_{12}+\delta_{23}$	δ_{24}	δ_{25}	δ_{16}
T_3	$c^I_{12}+\delta_{13}$	$c^I_{12}+\delta_{23}$	$c^I_{11}+\delta_{33}$	δ_{24}	δ_{15}	δ_{36}
T_4	δ_{14}	δ_{24}	δ_{24}	$c^I_{44}+\delta_{44}$	δ_{45}	δ_{46}
T_5	δ_{15}	δ_{25}	δ_{15}	δ_{45}	$c^I_{44}+\delta_{55}$	δ_{56}
T_6	δ_{16}	δ_{16}	δ_{36}	δ_{46}	δ_{56}	$c^I_{44}+\delta_{66}$

where c^I_{11}, c^I_{12}, c^I_{44} are the saturated elastic constants and the δ's are the modifications caused by the morphic effects. These are given in terms of the R values in Appendix II.

All the measurements were made on a (110) section and for transmission in this direction the resulting velocities are determined by solving the determinant[7]

$$\begin{vmatrix} \tfrac{1}{2}(c^I_{11}+c^I_{44}+\delta_{11}+\delta_{66}+2\delta_{16})-\rho v^2; & \tfrac{1}{2}(c^I_{12}+c^I_{44}+\delta_{12}+\delta_{66}+2\delta_{16}); & \tfrac{1}{2}(\delta_{14}+\delta_{15}+\delta_{46}+\delta_{56}) \\ \tfrac{1}{2}(c^I_{12}+c^I_{44}+\delta_{12}+\delta_{66}+2\delta_{16}); & \tfrac{1}{2}(c^I_{11}+c^I_{44}+\delta_{22}+\delta_{66}+2\delta_{16})-\rho v^2; & \tfrac{1}{2}(\delta_{24}+\delta_{25}+\delta_{46}+\delta_{56}) \\ \tfrac{1}{2}(\delta_{14}+\delta_{15}+\delta_{46}+\delta_{56}); & \tfrac{1}{2}(\delta_{24}+\delta_{25}+\delta_{46}+\delta_{56}); & \tfrac{1}{2}(2c^I_{44}+\delta_{44}+\delta_{55}+2\delta_{45})-\rho v^2 \end{vmatrix} = 0. \tag{26}$$

If we neglect squares of the δ-quantities, the three solutions of this equation can be written

$$\begin{aligned} \rho v_1^2 &= \tfrac{1}{2}(c^I_{11}+c^I_{12})+c^I_{44}+\tfrac{1}{4}(\delta_{11}+\delta_{22}+2\delta_{12}) \\ &\quad +\delta_{66}+2\delta_{16} \quad \text{(long)}, \\ \rho v_2^2 &= \tfrac{1}{2}(c^I_{11}-c^I_{12})+\tfrac{1}{4}(\delta_{11}+\delta_{22}-2\delta_{12}) \\ &\quad \text{(shear, particle velocity along } [1\bar{1}0]), \\ \rho v_3^2 &= c^I_{44}+\tfrac{1}{2}(\delta_{44}+\delta_{55}+2\delta_{45}) \\ &\quad \text{(shear, particle velocity along } [001]). \end{aligned} \tag{27}$$

From the last shear velocity v_3, we find that the morphic value of the shear elastic constant is

$$c^M_{44}=c^I_{44}+\tfrac{1}{2}c^I_{44}{}^2I_0{}^2[(\alpha_3{}^2-\tfrac{1}{3})(R_{441}-R_{551}) -2\alpha_1\alpha_2R_{456}]. \tag{28}$$

This allows one to derive one relation between two of the independent constants.

For the other shear velocity v_2, one has an elastic constant

$$c^M_{66}{}'=\tfrac{1}{2}(c^I_{11}-c^I_{12})+\tfrac{1}{2}(c^I_{11}-c^I_{12})^2I_0{}^2 \times[(\alpha_3{}^2-\tfrac{1}{3})(R_{111}-R_{112}+2R_{122}-2R_{121})]. \tag{29}$$

The measurement allows one to determine the sum of two other combinations.

Finally, for the longitudinal velocity v_1, the elastic

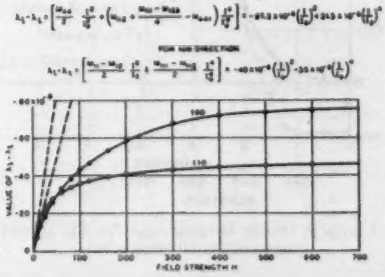

FIG. 4. Longitudinal minus transverse magnetostriction effect plotted as a function of field strength H for 001 plane.

[7] Love, *Theory of Elasticity*, Fourth Edition (Cambridge University Press, London, 1928), p. 298.

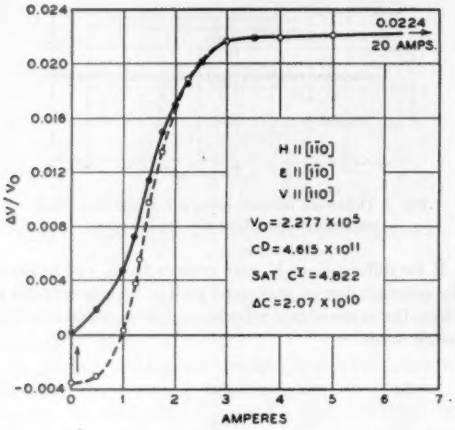

FIG. 5. Change in velocity for shear wave No. 1 as a function of magnetization (10 megacycles).

constant becomes

$$c^{M}{}_{11}{}' = \tfrac{1}{2}[c^{I}{}_{11}+c^{I}{}_{12}]+c^{I}{}_{44}+(\alpha_3{}^2-\tfrac{1}{3})I_0{}^2 \times\{[\tfrac{1}{2}(c^{I}{}_{11}+c^{I}{}_{12})^2-c^{I}{}_{12}{}^2](R_{111}-R_{112}) -\tfrac{1}{2}(c^{I}{}_{11}{}^2-c^{I}{}_{12}{}^2)(R_{123}-R_{121})-c^{I}{}_{44}{}^2(R_{441}-R_{551})\} -2c^{I}{}_{44}\alpha_1\alpha_2 I_0{}^2[c^{I}{}_{12}R_{144}+(c^{I}{}_{11}+c^{I}{}_{12})R_{244}]. \quad (30)$$

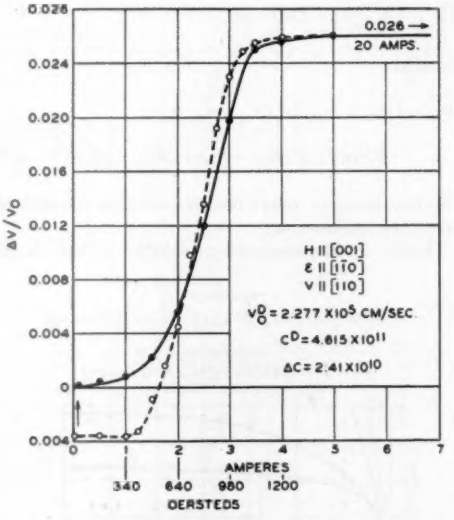

FIG. 6. Change in velocity for shear wave No. 1 as a function of magnetization (10 megacycles).

[8] These measurements were made by H. J. McSkimin by a technique described in J. Acoust. Soc. Am. 24, 413 (1950).

V. EXPERIMENTAL RESULTS

The original measurements[8] which indicated the presence of a "morphic" effect were measurements of the velocity and attenuation of ultrasonic waves in single nickel crystals. These were made primarily to determine the "ΔE" effect in single crystals and will be discussed in detail in a companion paper.[1] The values are reproduced here in order to evaluate the magnitude of the morphic effects. All the measurements were made on a (110) section, since it has been shown that three independent waves, two shear and one longitudinal, can be propagated in such a section. One shear wave (called No. 1) is generated when the particle motion is along the [1$\bar{1}$0] direction, while the other (No. 2) is generated when the particle motion is along

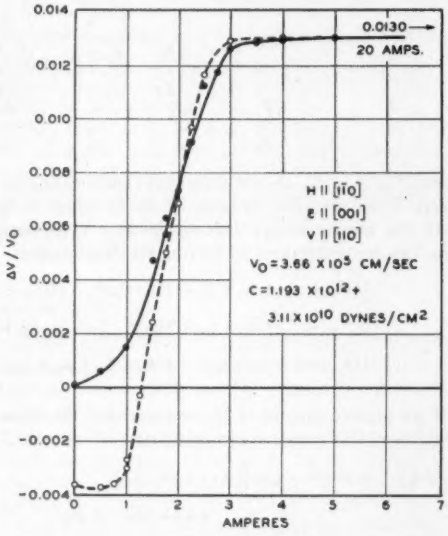

FIG. 7. Change in velocity for shear No. 2 as a function of magnetization (10 megacycles).

the [001] direction. Figure 5 shows the increase in velocity divided by the velocity for the demagnetized condition as a function of current through the magnetizing coil for the No. 1 shear when the field is in the direction of particle motion [1$\bar{1}$0]. At saturation the velocity is increased by a factor of 0.0224. The dotted curve shows the velocity under decreasing conditions. The velocity at zero field is less than that for the demagnetized case, but returns to it when the crystal is again demagnetized. Figure 6 shows a measurement for the same shear with the field parallel to the [001] direction. For this case the increase is 0.026 giving an increase in elastic constant Δc of 2.41×10^{10} dynes/cm, compared with 2.07×10^{10} dynes/cm^2 for the field in the [1$\bar{1}$0] direction. The difference between these of 3.4×10^9 dynes/cm is a morphic effect. Figures 7 and 8

show similar measurements for the No. 2 shear as a function of magnetic orientation. Here the morphic effect is 2.5×10^9 dynes/cm². Figures 9 and 10 show similar measurements for the longitudinal wave, giving a morphic effect of 0.9×10^9 dynes/cm². All these effects are gathered together in Table I, which shows also the combinations of constants involved.

The measurements give three relations between the six measurable combinations. While these are not enough to evaluate all of the constants, they do show the existence of a morphic effect. It is interesting to observe that the changes measured are in the same order of magnitude as the change in the elastic constant occasioned by a temperature expansion which produces a distortion comparable to the magnetostrictive distortion. Since the temperature expansion coefficient of nickel is 12 parts in 10^6 per degree C, an increase in temperature of 4°C will produce an expansion as large as the magnetostrictive effect. This increase in temperature will cause a decrease of the elastic modulus of 0.14 percent[9] or a change of 3×10^9 dynes/cm² in Young's modulus, which is intermediate between the values measured for the longitudinal and shear effects. While no direct comparison can be made between magnetostriction effects and temperature effects, since one causes a change in volume and the other does not, the fact that they produce effects of the same order of magnitude is indicative of the related nature of the effects, i.e., a separation of adjacent molecules.

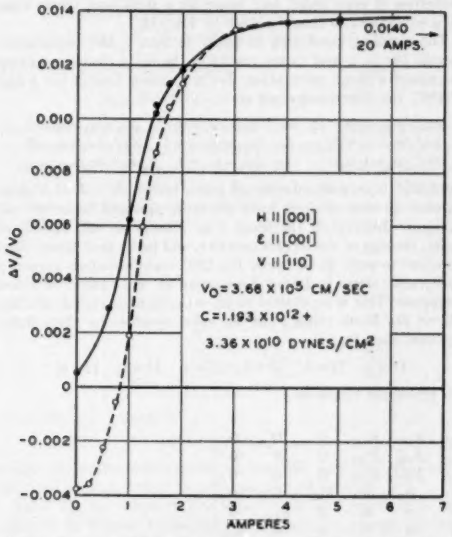

FIG. 8. Change in velocity for shear wave No. 2 as a function of magnetization (10 megacycles).

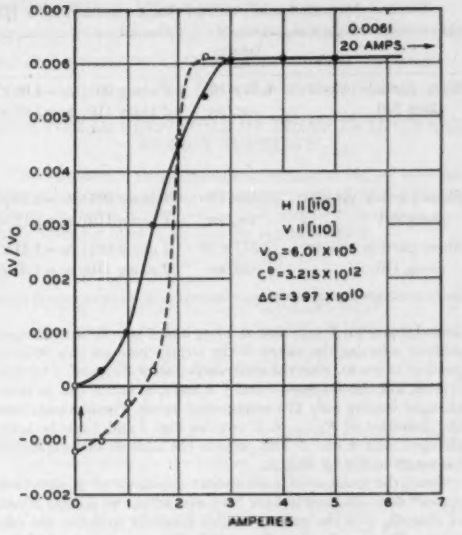

FIG. 9. Change in velocity for longitudinal wave as a function of magnetization (10 megacycles).

APPENDIX I. NUMBER OF INDEPENDENT TERMS OF A SIXTH-RANK TENSOR FOR A CUBIC CRYSTAL OF CLASS $O_h=(4/m)\bar{3}-(2/m)$

When second-order effects are taken account of in magnetostrictive effects, there are 3 sixth-rank tensors to consider, N_{ijmnpq}, R_{ijklmn}, and K_{mnopqr} of Eqs. (4). For the most general case there are 729 terms in a sixth-rank tensor; but since i and j can be

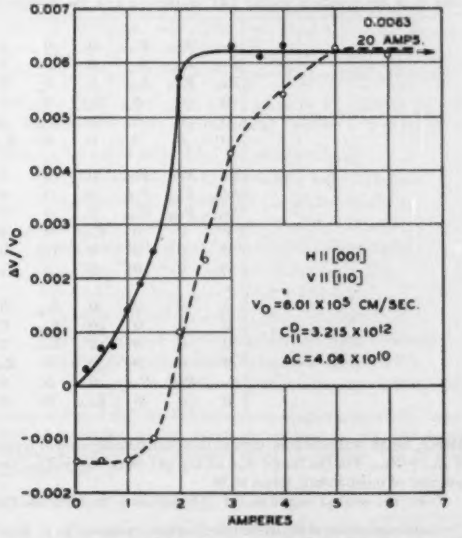

FIG. 10. Change in velocity for longitudinal wave as a function of magnetization (10 megacycles).

[9] See G. W. Pierce, Proc. Am. Acad. Arts Sci. 63, No. 1 (1928).

TABLE I. Measured velocities and elastic constants for a 110 section of a nickel crystal as a function of magnetic orientation.

Crystal No. 1 mode	Velocity demagnetized	Δc	Constants determined
Long. particle velocity along 110	6.01×10^5 cm/sec	I along 001; $\Delta c=4.06\times10^{10}$ dynes/cm^2 I along 1$\bar{1}$0; $\Delta c=3.97\times10^{10}$ dynes/cm^2	$c^M{}_{11}(001)-c^M{}_{11}(1\bar{1}0)=9\times10^{8}$ dynes/cm^2 $=I_0{}^2[[\frac{1}{2}(c^I{}_{11}{}^2-c^I{}_{12}{}^2)-c^I{}_{12}{}^2](R_{111}-R_{112})$ $+\frac{1}{2}(c^I{}_{11}{}^2-c^I{}_{12}{}^2)(R_{121}-R_{122})+c^I{}_{44}{}^2(R_{551}-R_{441})$ $+c^I{}_{44}(c^I{}_{12}R_{144}+(c^I{}_{11}+c^I{}_{12})R_{344})]$
Shear particle velocity along 001	3.66×10^5 cm/sec	I along 001; $\Delta c=3.36\times10^{10}$ dynes/cm^2 I along 1$\bar{1}$0; $\Delta c=3.11\times10^{10}$ dynes/cm^2	$c^M{}_{44}(001)-c^M{}_{44}(1\bar{1}0)=2.5\times10^{9}$ dynes/cm^2 $=c^I{}_{44}{}^2[R_{441}-R_{551}-R_{466}]I_0{}^2$
Shear particle velocity along 1$\bar{1}$0	2.277×10^5 cm/sec	I along 001; $\Delta c=2.41\times10^{10}$ dynes/cm^2 I along 1$\bar{1}$0; $\Delta c=2.07\times10^{10}$ dynes/cm^2	$c^M{}_{66}(001)-c^M{}_{66}(1\bar{1}0)=3.4\times10^{9}$ dynes/cm^2 $=\frac{1}{2}(c^I{}_{11}-c^I{}_{12})^2[R_{111}-R_{112}+2(R_{123}-R_{121})]I_0{}^2$

interchanged in N_{ijmnpq} and m, o, p, and s can be interchanged without affecting the values of the terms, there are only 90 independent terms for even the most unsymmetrical crystal, a triclinic crystal. For the R tensor, i and j, k and l, m, and o, can be interchanged leaving only 216 independent terms. Furthermore, from the definition of R_{ijklmo}, it is obvious that i and j can be interchanged with k and l. This reduces the number of independent constants to 126 for $R_{ijklmno}$.

Since the number of independent constants of a sixth-rank tensor[10] does not seem to have been worked out for a cubic crystal of class O_h, it is the purpose of this appendix to derive the constants. This can be done by applying the symmetry conditions for this crystal in conjunction with the transformation equations for a sixth-rank tensor

$$R_{i'j'k'l'm'o'}=\frac{\partial x_i'}{\partial x_i}\frac{\partial x_j'}{\partial x_j}\frac{\partial x_k'}{\partial x_k}\frac{\partial x_l'}{\partial x_l}\frac{\partial x_m'}{\partial x_m}\frac{\partial x_o'}{\partial x_o}R_{ijklmo}, \tag{31}$$

where $\partial x_i'/\partial x_i$, $\cdots$, $\partial x_o'/\partial x_o$, the partial derivatives, are the direction cosines l_1 to n_3.

For a cubic crystal of class $T_d=\bar{4}3m$, the symmetry conditions are

$$x=-x;\ y=-y;\ z=-z(\bar{4},m) \text{ and } x=y;\ y=z;\ z=x(3); \tag{32}$$

that is, if the x axis is shifted 180° to the $-x$ axis, the constants remain unchanged, etc. The symmetry O_h is similar to this except that a center of symmetry is added. This does not affect polar properties of even order, and hence for a sixth-rank tensor class O_h is equivalent to class T_d given by Eq. (32).

The simplest conditions to apply is that a 180° orientation around the x, y, and z axes results in the same elastic constants as existed without orientation. For a rotation around the z axis of 180°, the direction cosines are

$$\begin{array}{lll}\partial x_1'/\partial x_1=l_1=-1; & \partial x_1'/\partial x_2=m_1=0; & \partial x_1'/\partial x_3=n_1=0\\ \partial x_2'/\partial x_1=l_2=0; & \partial x_2'/\partial x_2=m_2=-1; & \partial x_2'/\partial x_3=n_2=0\\ \partial x_3'/\partial x_1=l_3=0; & \partial x_3'/\partial x_2=m_3=0; & \partial x_3'/\partial x_3=n_3=1.\end{array}$$

Applying this transformation, all terms for which 1, 2, or 3 occur an even number of times have the same sign and hence are not changed. However, if the terms 1 or 2 occur an odd number of times, the sign of the term is negative, and hence such terms must be equal to zero. If we apply the 180° transformation around x and y also, terms 1, 2, and 3 occurring an odd number of times disappear. This is equivalent to an orthorhombic crystal of class 222 or D_2. If we replace the six index symbols by three index symbols, such that

$$11=1,\quad 22=2,\quad 33=3,\quad 23=4,\quad 13=5,\quad 12=6,$$

the remaining terms are

$$\begin{vmatrix} R_{111} & R_{121} & R_{131} & 0 & 0 & 0\\ R_{211} & R_{221} & R_{231} & 0 & 0 & 0\\ R_{311} & R_{321} & R_{331} & 0 & 0 & 0\\ 0 & 0 & 0 & R_{441} & 0 & 0\\ 0 & 0 & 0 & 0 & R_{551} & 0\\ 0 & 0 & 0 & 0 & 0 & R_{661}\end{vmatrix}\quad\begin{vmatrix} R_{112} & R_{122} & R_{132} & 0 & 0 & 0\\ R_{212} & R_{222} & R_{232} & 0 & 0 & 0\\ R_{312} & R_{322} & R_{332} & 0 & 0 & 0\\ 0 & 0 & 0 & R_{442} & 0 & 0\\ 0 & 0 & 0 & 0 & R_{552} & 0\\ 0 & 0 & 0 & 0 & 0 & R_{662}\end{vmatrix}$$

$$\begin{vmatrix} R_{113} & R_{123} & R_{133} & 0 & 0 & 0\\ R_{213} & R_{223} & R_{233} & 0 & 0 & 0\\ R_{313} & R_{323} & R_{333} & 0 & 0 & 0\\ 0 & 0 & 0 & R_{443} & 0 & 0\\ 0 & 0 & 0 & 0 & R_{553} & 0\\ 0 & 0 & 0 & 0 & 0 & R_{663}\end{vmatrix}\quad\begin{vmatrix} 0 & 0 & 0 & R_{144} & 0 & 0\\ 0 & 0 & 0 & R_{244} & 0 & 0\\ 0 & 0 & 0 & R_{344} & 0 & 0\\ R_{414} & R_{424} & R_{434} & 0 & 0 & 0\\ 0 & 0 & 0 & 0 & 0 & R_{564}\\ 0 & 0 & 0 & 0 & R_{654} & 0\end{vmatrix} \tag{33}$$

$$\begin{vmatrix} 0 & 0 & 0 & 0 & R_{155} & 0\\ 0 & 0 & 0 & 0 & R_{255} & 0\\ 0 & 0 & 0 & 0 & R_{355} & 0\\ 0 & 0 & 0 & 0 & 0 & R_{465}\\ R_{515} & R_{525} & R_{535} & 0 & 0 & 0\\ 0 & 0 & 0 & R_{645} & 0 & 0\end{vmatrix}\quad\begin{vmatrix} 0 & 0 & 0 & 0 & 0 & R_{166}\\ 0 & 0 & 0 & 0 & 0 & R_{266}\\ 0 & 0 & 0 & 0 & 0 & R_{366}\\ 0 & 0 & 0 & 0 & R_{456} & 0\\ 0 & 0 & 0 & R_{546} & 0 & 0\\ R_{614} & R_{624} & R_{634} & 0 & 0 & 0\end{vmatrix}$$

Hence, for an orthorhombic crystal there are 60 independent terms if $R_{abc}\neq R_{bac}$. For the tensor R_{abc} of Eq. (4), since $R_{abc}=R_{bac}$, the number of independent terms is 39.

From the second condition of (32) we have in addition the symmetry that a rotation of 90° around x, y or z results in the same elastic constants as in the unrotated crystals. These three rotations are given by the direction cosines:

$$\begin{array}{ccc}x \text{ rotation} & y \text{ rotation} & z \text{ rotation}\\ \begin{pmatrix}1&0&0\\0&0&1\\0&-1&0\end{pmatrix} & \begin{pmatrix}0&0&-1\\0&1&0\\1&0&0\end{pmatrix} & \begin{pmatrix}0&1&0\\-1&0&0\\0&0&1\end{pmatrix}.\end{array} \tag{34}$$

[10] Sixth-rank tensors of the elastic type have been considered by F. Birch, Phys. Rev. 71, 809 (1947); but these are not general enough for the R_{ijklmo} tensor, since only the ij and kl terms can be interchanged rather than all three sets.

Applying these symmetries to the remaining constants, there are number of relations between the constants. These are

$$\begin{aligned}
&R_{111}=R_{222}=R_{333},\\
&R_{112}=R_{113}=R_{221}=R_{223}=R_{331}=R_{332},\\
&R_{121}=R_{131}=R_{212}=R_{232}=R_{311}=R_{313}\\
&\qquad=R_{133}=R_{313}=R_{322}=R_{323}=R_{233}=R_{323},\\
&R_{123}=R_{132}=R_{213}=R_{312}=R_{231}=R_{321},\\
&R_{441}=R_{552}=R_{663},\\
&R_{551}=R_{442}=R_{662}=R_{553}=R_{661}=R_{663},\\
&R_{144}=R_{414}=R_{255}=R_{525}=R_{366}=R_{636},\\
&R_{155}=R_{515}=R_{188}=R_{818}=R_{244}=R_{424}\\
&\qquad=R_{288}=R_{828}=R_{344}=R_{434}=R_{355}=R_{535},\\
&R_{456}=R_{546}=R_{465}=R_{645}=R_{564}=R_{654}.
\end{aligned} \tag{35}$$

Hence, there are nine remaining independent constants for the R tensor. These relations are used in Eqs. (8). For the N tensor, since the last four numbers can be interchanged, there are three relations between the 9 constants and the number reduce to six. The relations are

$$\begin{aligned}
&N_{112}=N_{111122}=N_{111213}=N_{133}=N_{166}=N_{155};\\
&\qquad N_{123}=N_{113223}=N_{144}.
\end{aligned} \tag{36}$$

The remaining constants are then

$$N_{111},\ N_{112},\ N_{123},\ N_{441},\ N_{551},\text{ and }N_{456}. \tag{37}$$

This is the same number and type as in Birch's sixth-rank tensor,[28] but the order of some of the subscripts is different.

Finally, for the tensor K_{mnopqr} of Eq. (4), since all of the six subscripts can be interchanged separately, there are three more relations between the constants and there are only three independent constants. These relations are

$$K_{112}=K_{551};\quad K_{123}=K_{441}=K_{456}; \tag{38}$$

and there are only three independent constants,

$$K_{111},\ K_{112},\text{ and }K_{123}. \tag{39}$$

APPENDIX II. DERIVATION OF TERMS IN INTERNAL ENERGY FUNCTION

The method for transforming the expression for H_1 into the potential function U, the internal energy is one of solving for the stresses in terms of the strains and magnetic intensities and substituting for these in H_1. For the strains we have

$$S_n=-\partial H_1/\partial T_n$$

or

$$\begin{aligned}
S_1&=(s^I_{11}+\Delta_{11})T_1+(s^I_{12}+\Delta_{12})T_2+(s^I_{13}+\Delta_{13})T_3+\Delta_{14}T_4\\
&\quad+\Delta_{15}T_5+\Delta_{16}T_6+h_1(\alpha_1^2-\tfrac{1}{3})+h_4[\alpha_1^4+\tfrac{2}{3}s-\tfrac{1}{3}]+h_5(\tfrac{1}{3}-s) \qquad (40)\\
&\cdots\cdots\cdots\cdots\cdots\cdots\cdots\cdots\cdots\cdots\\
S_6&=\Delta_{16}T_1+\Delta_{16}T_2+\Delta_{36}T_3+\Delta_{46}T_4+\Delta_{56}T_5+(s^I_{44}+\Delta_{66})T_6\\
&\quad+h_2\alpha_1\alpha_2+h_3\alpha_1\alpha_2\alpha_3^2,
\end{aligned}$$

where

$$\Delta_{11}=(\alpha_1^2-\tfrac{1}{3})I_0^2(R_{111}-R_{112});\quad\cdots;\quad\Delta_{66}=(\alpha_3^2-\tfrac{1}{3})I_0^2(R_{441}-R_{551}).$$

If we solve these for the stresses, we find that the stresses T_1 to T_6 can be expressed in terms of the strains S_1' to S_6' given by

$$\begin{aligned}
S_1'&=S_1-[h_1(\alpha_1^2-\tfrac{1}{3})+h_4(\alpha_1^4+\tfrac{2}{3}s-\tfrac{1}{3})+h_5(\tfrac{1}{3}-s)] \qquad (41)\\
&\cdots\cdots\cdots\cdots\cdots\cdots\cdots\cdots\cdots\cdots\\
S_6'&=S_6-[h_2\alpha_1\alpha_2+h_3\alpha_1\alpha_2\alpha_3^2]
\end{aligned}$$

according to the relation

$$\begin{array}{c|cccccc}
 & S_1' & S_2' & S_3' & S_4' & S_5' & S_6' \\
\hline
T_1 & c^I_{11}+\delta_{11} & c^I_{12}+\delta_{12} & c^I_{12}+\delta_{13} & \delta_{14} & \delta_{15} & \delta_{16} \\
T_2 & c^I_{12}+\delta_{12} & c^I_{11}+\delta_{22} & c^I_{12}+\delta_{23} & \delta_{24} & \delta_{25} & \delta_{26} \\
T_3 & c^I_{12}+\delta_{13} & c^I_{12}+\delta_{23} & c^I_{11}+\delta_{33} & \delta_{34} & \delta_{35} & \delta_{36} \\
T_4 & \delta_{14} & \delta_{24} & \delta_{34} & c^I_{44}+\delta_{44} & \delta_{45} & \delta_{46} \\
T_5 & \delta_{15} & \delta_{25} & \delta_{35} & \delta_{45} & c^I_{44}+\delta_{55} & \delta_{56} \\
T_6 & \delta_{16} & \delta_{15} & \delta_{36} & \delta_{46} & \delta_{56} & c^I_{44}+\delta_{66}
\end{array}, \tag{42}$$

where any c^I_{ij} is equal to

$$c^I_{ij}=(-1)^{i+j}\Delta s^{ij}/\Delta s, \tag{43}$$

where Δs is the determinant of Eq. (40) and Δs^{ij} the minor obtained by suppressing the ith row and jth column.

Since the Δ_{ij} terms of Eq. (40) are all very small, it is permissible to neglect terms having products or powers of these small quantities. With that restriction one finds that the δ_{ij} values are

$$\begin{aligned}
\delta_{14}&=-2\alpha_1\alpha_2I_0^2c^I_{44}[c^I_{11}R_{144}+2c^I_{12}R_{244}],\\
\delta_{15}&=\delta_{16}=-2\alpha_1\alpha_2I_0^2c^I_{44}[(c^I_{11}+c^I_{12})R_{244}+c^I_{12}R_{144}],\\
\delta_{18}&=\delta_{26}=-2\alpha_1\alpha_2I_0^2c^I_{44}[(c^I_{11}+c^I_{12})R_{244}+c^I_{12}R_{144}],\\
\delta_{24}&=\delta_{34}=-2\alpha_1\alpha_2I_0^2c^I_{44}[(c^I_{11}+c^I_{12})R_{244}+c^I_{12}R_{144}],\\
\delta_{25}&=-2\alpha_1\alpha_2I_0^2c^I_{44}[c^I_{11}R_{144}+2c^I_{12}R_{244}],\\
\delta_{28}&=-2\alpha_1\alpha_2I_0^2c^I_{44}[c^I_{11}R_{144}+2c^I_{12}R_{244}],\\
\delta_{44}&=-c^I_{44}{}^2(\alpha_1^2-\tfrac{1}{3})I_0^2(R_{441}-R_{551}),\\
\delta_{55}&=-c^I_{44}{}^2(\alpha_2^2-\tfrac{1}{3})I_0^2(R_{441}-R_{551}),\\
\delta_{66}&=-c^I_{44}{}^2(\alpha_3^2-\tfrac{1}{3})I_0^2(R_{441}-R_{551}),\\
\delta_{45}&=-c^I_{44}{}^2\alpha_1\alpha_2I_0^2R_{456},\quad\delta_{46}=-c^I_{44}{}^2\alpha_1\alpha_3I_0^2R_{456},\\
\delta_{56}&=-c^I_{44}{}^2\alpha_2\alpha_3I_0^2R_{456},\\
\delta_{11}&=-(c^I_{11}-c^I_{12})(\alpha_1^2-\tfrac{1}{3})I_0^2[(c^I_{11}+c^I_{12})(R_{111}-R_{112})\\
&\qquad-2c^I_{12}(R_{122}-R_{121})],\\
\delta_{22}&=-(c^I_{11}-c^I_{12})(\alpha_2^2-\tfrac{1}{3})I_0^2[(c^I_{11}+c^I_{12})(R_{111}-R_{112})\\
&\qquad-2c^I_{12}(R_{122}-R_{121})],\\
\delta_{33}&=-(c^I_{11}-c^I_{12})(\alpha_3^2-\tfrac{1}{3})I_0^2[(c^I_{11}+c^I_{12})(R_{111}-R_{112})\\
&\qquad-2c^I_{12}(R_{122}-R_{121})],
\end{aligned} \tag{44}$$

$$\begin{aligned}
\delta_{12}&=-(c^I_{11}-c^I_{12})(\alpha_3^2-\tfrac{1}{3})I_0^2[c^I_{11}(R_{122}-R_{121})-c^I_{12}(R_{111}-R_{112})],\\
\delta_{13}&=-(c^I_{11}-c^I_{12})(\alpha_2^2-\tfrac{1}{3})I_0^2[c^I_{11}(R_{122}-R_{121})-c^I_{12}(R_{111}-R_{112})],\\
\delta_{23}&=-(c^I_{11}-c^I_{12})(\alpha_1^2-\tfrac{1}{3})I_0^2[c^I_{11}(R_{122}-R_{121})-c^I_{12}(R_{111}-R_{112})].
\end{aligned}$$

Inserting the values of T_1 to T_6 given by Eq. (42) in Eq. (8) for H_1, the value of the internal energy function U is given by

$$\begin{aligned}
2U&=c^I_{11}[S_1^2+S_2^2+S_3^2]+2c^I_{12}[S_1S_2+S_1S_3+S_2S_3]\\
&\quad+c^I_{44}[S_4^2+S_5^2+S_6^2]+\delta_{11}S_1^2+\delta_{22}S_2^2+\delta_{33}S_3^2+2\delta_{12}S_1S_2\\
&\quad+2\delta_{13}S_1S_3+2\delta_{23}S_2S_3+2\delta_{14}S_1S_4+2\delta_{15}S_1S_5+2\delta_{16}S_1S_6\\
&\quad+2\delta_{24}S_2S_4+2\delta_{25}S_2S_5+2\delta_{26}S_2S_6+2\delta_{34}S_3S_4+2\delta_{35}S_3S_5\\
&\quad+2\delta_{36}S_3S_6+\delta_{44}S_4^2+\delta_{55}S_5^2+\delta_{66}S_6^2+2\delta_{45}S_4S_5+2\delta_{46}S_4S_6\\
&\quad+2\delta_{56}S_5S_6-2h_1(c^I_{11}-c^I_{12})[(\alpha_1^2-\tfrac{1}{3})S_1+(\alpha_2^2-\tfrac{1}{3})S_2\\
&\quad+(\alpha_3^2-\tfrac{1}{3})S_3]-2h_4(c^I_{11}-c^I_{12})[(\alpha_1^4+\tfrac{2}{3}s-\tfrac{1}{3})S_1\\
&\quad+(\alpha_2^4+\tfrac{2}{3}s-\tfrac{1}{3})S_2+(\alpha_3^4+\tfrac{2}{3}s-\tfrac{1}{3})S_3]-2h_5(c^I_{11}+2c^I_{12})\\
&\quad\times[\tfrac{1}{3}-s][S_1+S_2+S_3]-2h_2c^I_{44}[\alpha_2\alpha_3S_4+\alpha_1\alpha_3S_5+\alpha_1\alpha_2S_6]\\
&\quad-2h_3c^I_{44}[\alpha_1^3\alpha_2\alpha_3S_4+\alpha_1\alpha_2^3\alpha_3S_5+\alpha_1\alpha_2\alpha_3^3S_6]\\
&\quad+2K_1^S(\tfrac{1}{3}-s)+2K_2^S(\alpha_1^2\alpha_2^2\alpha_3^2-1/27),
\end{aligned} \tag{45}$$

where K_1^S and K_2^S are the anisotropy magnetic constants measured at constant strain. These are related to the anisotropy constants measured at constant stress (as used in Eq. (8)) by the equations

$$\begin{aligned}
K_1^S&=K_1^T-(c^I_{11}-c^I_{12})(h_1^2+(7/3)h_1h_4+(4/9)h_4^2)\\
&\quad-(3/2)(c^I_{11}+2c^I_{12})h_5^2(\tfrac{1}{3}-s)+\tfrac{1}{2}c^I_{44}h_2^2, \qquad (46)\\
K_2^S&=K_2^T-(c^I_{11}-c^I_{12})(3h_1h_4+(8/3)h_4^2)+\tfrac{1}{2}c^I_{44}(6h_2h_3+h_3^2).
\end{aligned}$$

Current Fluctuations in the Direct-Current Gas Discharge Plasma*

P. PARZEN AND L. GOLDSTEIN
Federal Telecommunication Laboratories, Inc., Nutley, New Jersey
(Received August 24, 1950)

The noise power from a gas discharge plasma may be ascribed to the electron current fluctuations in the plasma due to collisions of electrons with atoms or ions. The noise power, in general, is derived from both the thermal velocities, which are characterized by the electron temperature, and from the dc power, which is characterized by the average current.

I. INTRODUCTION

RADIOFREQUENCY energy produced in a dc discharge plasma in different gases has been measured by Goldstein.[1] Mumford[2] has recently indicated the use of such tubes as noise sources in the microwave region. This noise power can be accounted for by a study of the electron-current fluctuations in a gas discharge plasma, and, in general, in any electron gas. It will be seen that the electron-current fluctuations can be separated into two parts. One can be ascribed to the electron temperature and the other to the direct current in the gas discharge tube.

II. CALCULATION OF CURRENT FLUCTUATIONS IN A GAS DISCHARGE TUBE

Let us consider the electrons in the gas discharge (Fig. 1) whose thermal speeds lie between v and $v+dv$ with a mean collision frequency Z_v. This means that on the average an electron in this range will suffer Z_vT collisions in a time T. Actually, there will be fluctuations in this number, and the probability $p(K)$ that an electron will experience K collisions in a time T is[3]

$$p(K)=(Z_vT)^K[\exp(-Z_vT)]/K! \tag{1}$$

The probability that the time between consecutive collisions of an electron lies between θ and $\theta+d\theta$ is

$$q(\theta)=Z_v\exp(-Z_v\theta)d\theta. \tag{2}$$

The convection current measured between the electrodes due to an electron that has collided at time t_k with a subsequent free time θ_k is

$$\left.\begin{aligned} i_x(t-t_k;\theta_k)&=(e/d)[v_x+a(t-t_k)]\\ i_y(t-t_k;\theta_k)&=(e/d_y)v_y\\ i_z(t-t_k;\theta_k)&=(e/d_z)v_z\\ &=0\end{aligned}\right\}t_k\le t\le t_k+\theta_k \tag{3}$$

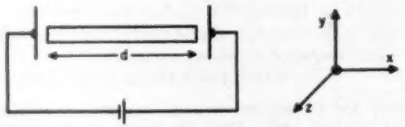

FIG. 1. Direct-current-maintained gas discharge plasma.

everywhere outside this time interval, where d is the length of the tube parallel to the direction of applied electric field E; $a=eE/m$; d_y and d_z are transverse dimensions; v_x, v_y, v_z are components of the thermal velocity; and, similarly, i_x, i_y, i_z are components of the convection current.

We shall now restrict ourselves to the calculation of i_x as the calculations for the others are quite similar. Now let

$$\phi_k=t-t_k. \tag{4}$$

Hence, we have

$$\begin{aligned} i_x(\phi_k;\theta_k)&=(e/d)(v_x+a\phi_k), \quad 0\le\phi_k\le\theta_k\\ &=0 \text{ elsewhere.}\end{aligned} \tag{3a}$$

The current $I(t)$ will be a random function of time, depending on the values of ϕ_k and θ_k, which may be looked on as random values. Thus, the methods described by Rice[3] for the study of shot-effect processes may be used to compute the average value and the spectrum of $I(t)$.

Computation of $\langle I(t)\rangle_{Av}$

Following Rice,[3] the time average of the current $I(t)$ due to a single electron is found by averaging $I(t')$ for a given t' over M intervals of duration T; M being very large. Thus, we have

$$\langle I(t)\rangle_{Av}=\lim 1/M\sum_{i=1}^{M}I_i(t'). \tag{5}$$

$I_i(t')$ is the current at time t' in the i'th interval. In $Mp(K)$ of these intervals, an electron will experience K collisions that occur at times $t_1, t_2\cdots t_K$. The t_i will vary in a random manner over these $Mp(K)$ intervals. For these intervals, the contribution to the time average is

$$p(K)\langle I_K(t-t_i;\theta_i)\rangle_{Av}. \tag{6}$$

The latter average is now over all the random-varying t_i in these $Mp(K)$ intervals. Now let us consider those intervals for which $t_i<t'<t_{i+1}$. The average contribution for such intervals would be

$$\int_0^T\int_0^{\theta_i}i_x(\phi_i)T^{-1}d\phi_iZ_v\exp(-Z_v\theta_i)d\theta_i, \tag{7}$$

$$\theta_i=t_{i+1}-t_i,$$

* This work was sponsored by the Signal Corps Engineering Laboratories of the United States Army.

[1] L. Goldstein and N. Cohen, Phys. Rev. **73**, 83 (1948).
[2] W. W. Mumford, Bell System Tech. J. **28**, 608 (1949).
[3] S. O. Rice, Bell Sys. Tech. J. **23**, 282 (1949).

which equals

$$(Z_v e/Td)(v_x/Z_v^2+a/Z_v^3) \quad \text{as} \quad T\to\infty. \tag{8}$$

Hence, summing over all t_i, we obtain

$$\langle I_x(t)\rangle_{Av}=\sum_{K=0}^{\infty}\frac{Kp(K)}{T}\frac{e}{d}\left(\frac{v_x}{Z_v}+\frac{a}{Z_v^2}\right), \tag{9}$$

$$\langle I_x(t)\rangle_{Av}=\frac{ev_x}{d}+\frac{ea}{d}\frac{1}{Z_v}, \tag{10}$$

since

$$\sum_{K=0}^{\infty}Kp(K)=Z_vT.$$

Similarly, we have

$$\left.\begin{aligned}\langle I_y(t)\rangle_{Av}&=ev_y/d_y\\ \langle I_z(t)\rangle_{Av}&=ev_z/d_z.\end{aligned}\right\} \tag{11}$$

III. CALCULATION OF CORRELATION FUNCTION

Following Rice, the correlation function $\psi_{Av}(\tau)$ is given by

$$\langle\psi(\tau)\rangle_{Av}=\lim_{T\to\infty}1/T\int_0^T\langle I(t)I(t+\tau)\rangle_{Av}dt, \tag{12}$$

where the average is, as previously, over many intervals of duration T. Thus, we have

$$\langle I(t)I(t+\tau)\rangle_{Av}$$

$$=\sum_{K=0}^{\infty}p(K)\langle I_K(t-t_i;\theta_i)I_K(t+\tau-t_j;\theta_j)\rangle_{Av}, \tag{13}$$

where the average is now over the random variables t_i and θ_i. Now for those intervals (t_i, t_{i+1}) for which t and $t+\tau$, $\tau>0$, both lie in this interval or $0<\phi_i<\theta_i-\tau$, the contribution is

$$\langle\psi_1(\tau)\rangle_{Av}=\sum_{K=0}^{\infty}Kp(K)\frac{Z_v}{T}\int_\tau^T\int_0^{\theta_i-\tau}i_x(\phi_i)i_x(\phi_i+\tau)$$

$$\times\exp(-Z_v\theta_i)d\phi_i d\theta_i. \tag{14}$$

For those intervals (t_i, t_{i+1}) and (t_j, t_{j+1}) for which t and $t+\tau$ lie in different intervals, the contribution is

$$\langle\psi_0(\tau)\rangle_{Av}=\sum_{K=0}^{\infty}K(K-1)p(K)T^{-2}Z_v^2$$

$$\times\left[\int_0^T\int_0^{\theta_i}i_x(\phi_i)\exp(-Z_v\theta_i)d\phi_i d\theta_i\right]^2. \tag{15}$$

Substituting for i_x from (3a) and neglecting those terms that are proportional to v_x inasmuch as they will not contribute to the average over-all velocity classes, we obtain

$$\psi_{Av}(\tau)=\langle\psi_1(\tau)\rangle_{Av}+\langle\psi_0(\tau)\rangle_{Av},$$

$$\langle\psi_1(\tau)\rangle_{Av}=\frac{e^2}{d^2}\left[v_x^2+\frac{2a^2}{Z_v^2}+\frac{a^2\tau}{Z_v}\right]\exp(-Z_v\tau_i), \tag{16}$$

$$\langle\psi_0(\tau)\rangle_{Av}=\frac{e^2}{d^2}\left[v_x^2+\frac{a^2}{Z_v^2}\right]. \tag{17}$$

IV. CALCULATION OF THE SPECTRUM $\langle w(f)\rangle_{Av}$ OF CURRENT FLUCTUATIONS

$$\langle w(f)\rangle_{Av}=4\int_0^{\infty}\psi(\tau)\cos 2\pi f\tau d\tau \tag{18}$$

The spectrum resulting from $\psi_0(\tau)$ does not represent a fluctuation as it is due to $\langle I(t)\rangle_{Av}$. Thus, we have

$$\langle[I(t)-\langle I(t)\rangle_{Av}]^2\rangle_{Av}=\int\langle w_1(f)\rangle_{Av}df=\langle\psi_1(0)\rangle_{Av}$$

$$=e^2d^{-2}(v_x^2+2a^2/Z_v^2) \tag{19}$$

and

$$w_1(f)=4\int_0^{\infty}\langle\psi_1(\tau)\rangle_{Av}\cos 2\pi f\tau d\tau$$

$$=\frac{4e^2}{d^2}\left[\left(v_x^2+\frac{2a^2}{Z_v^2}\right)\frac{Z_v}{Z_v^2+4\pi^2f^2}\right.$$

$$\left.+\frac{a^2(Z_v^2-4\pi^2f^2)}{Z_v(Z_v^2+4\pi^2f^2)^2}\right]. \tag{20}$$

A similar derivation for metals with no direct current has been carried through by Bakker and Heller.[4] In their case, the current fluctuations, assuming classical statistics, is given by (20) with $a=0$.

V. SUMMATION OVER ALL ELECTRONS

It now remains to sum over all electrons. It is assumed that all electrons act independently of each other. Naturally, some assumptions will have to be made about the number of electrons per unit velocity range F and the variation of Z_v with v.

We shall assume that F in the gas discharge plasma is maxwellian,[5]

$$\left.\begin{aligned}F(v_x, v_y, v_z)&=A\exp[-\beta^2(v_x^2+v_y^2+v_z^2)],\\ A&=N(m/2\pi kT_e)^{\frac{3}{2}},\\ \beta^2&=m/2kT_e,\end{aligned}\right\} \tag{21}$$

where N is the total number of electrons $=n_0Sd$, n_0 is the number of electrons per cubic centimeter, S is the cross-sectional area of the tube, and T_e is the electron

[4] C. J. Bakker and G. Heller, Physica **6**, 262 (1939).
[5] I. Langmuir and G. Mott-Smith, Phys. Rev. **28**, 727 (1926).

temperature. It is also assumed that Z_v is independent of v and equal to Z. This is true for some gases; e.g., A, Kr, Xe for velocities less than 1 volt and Hg for still higher velocities.[6]

With these assumptions, the total quantities being denoted (sum over all electrons) by a subscript N, the average total current is given by

$$\langle I_N(t)\rangle_{Av}=eaN/dZ. \tag{22}$$

Hence, the dc resistance R_0 is given by

$$R_0=md^2Z/Ne^2. \tag{23}$$

Furthermore, in accordance with the theory of conductivity of electrons in gases,[7] the ac admittance is given by

$$Y_\omega=\frac{Ne^2}{md^2}\left[\frac{Z+j2\pi f}{Z^2+4\pi^2f^2}\right]=G(\omega)+jB(\omega), \tag{24}$$

$$\langle[I_N(t)-\langle I_N(t)\rangle_{Av}]^2\rangle_{Av}=\frac{Ne^2}{md^2}kT_e+2\frac{[\langle I_N(t)\rangle_{Av}]^2}{N}. \tag{25}$$

Except for a numerical factor of 2, this checks with a result obtained by other considerations by Brillouin[8] for electrons in metals

$$\langle w_1(f)_N\rangle_{Av}=4kT_eG(\omega)$$
$$+4\frac{[\langle I_N(t)\rangle_{Av}]^2}{N}\left[\frac{2Z}{Z^2+4\pi^2f^2}+\frac{Z(Z^2-4\pi^2f^2)}{(Z^2+4\pi^2f^2)^2}\right]. \tag{26}$$

For I_y and I_z, the spectrum will be given by just the first term of (26).

VI. CALCULATION OF AVAILABLE NOISE POWER IN WAVE GUIDES

We shall now apply these results to calculate the available noise power from a gas discharge plasma placed in the transverse plane of a rectangular wave guide propagating only in its lowest mode.

The available noise power

$$P_\omega=\tfrac{1}{4}|I_E|^2/G_\omega, \tag{27}$$

where I_E is the current in the direction of the E vector. Hence, in this case we have

$$P_\omega=\left\{kT_e+\frac{P_0}{NZ}\cos^2\theta\left[2+\frac{Z^2-4\pi^2f^2}{Z^2+4\pi^2f^2}\right]\right\}df, \tag{28}$$

θ is the angle between the E vector and axis of tube, P_0 is the dc power dissipated in the tube; and at $\theta=\pi/2$ this reduces to the case of Mumford,[2] for which

$$P_\omega=kT_edf. \tag{29}$$

VII. CONCLUSIONS

The noise power from gas discharge plasma may be ascribed to the electron-current fluctuations in the plasma due to collisions of electrons with atoms or ions. The noise power, in general, is derived both from the thermal velocities, which are characterized by the electron temperature, and from the dc power, which is characterized by the average current. The fluctuations due to the positive-ion current may be neglected, since the ion gas temperature is usually much lower than that of the electron gas, and the ionic current is much less than the electronic current. It has been assumed that the electron velocity-distribution function is maxwellian and that the collision frequency of an electron is independent of speed. This has been verified by experiment in certain cases. However, for those discharges where these assumptions are not experimentally verified, the current fluctuations and noise power may still be computed by a similar method from the experimentally obtained distribution function and variation of collision frequency with speed. The current fluctuations due to the fluctuations in the various electron removal and production processes in the plasma have not been accounted for by this method.

In general, the frequency-sensitive portion of the available noise power is only a few percent of the kT_e term. However, it may become important in low electron temperature gas discharge plasma, such as occur in caesium vapor.

[6] R. B. Brode, Revs. Modern Phys. **5**, 257 (1933).
[7] H. Margenau, Phys. Rev. **69**, 508 (1946).
[8] L. Brillouin, Helv. Phys. Acta **7**, 47 (1934). This discrepancy is due to the fact that in Brillouin's model the average current is not produced by an accelerating dc electric field but is assumed to be given. Brillouin's answer may be obtained by putting $a=0$ and increasing the thermal velocity by a constant drift velocity.

Dielectric Properties of Sodium and Potassium Niobates

B. T. MATTHIAS AND J. P. REMEIKA
Bell Telephone Laboratories, Murray Hill, New Jersey
(Received January 25, 1951)

The following paper deals with evidence of ferroelectricity in $KNbO_3$ and $NaNbO_3$. Temperatures at which both materials undergo crystallographic changes and corresponding changes in dielectric constant and loss tangent are reported. Photographs of dielectric hysteresis loops and values of saturation polarization taken at various points over a temperature range are given for $KNbO_3$.

INTRODUCTION

WE have recently reported[1] finding evidence of ferroelectric behavior in a number of substances not previously known to be ferroelectric. The evidence for ferroelectricity has included one or more of the following: (1) unusually high dielectric constant, (2) crystal structure changes accompanied by optical and dielectric constant changes, (3) spontaneously polarized domains visible with the polarizing microscope and showing dielectric hysteresis loops and saturation of the polarization, and (4) a Curie temperature above which spontaneous polarization disappears and the crystal becomes cubic. Many crystals have been observed to show either or both of the first two phenomena without showing evidence of spontaneous polarization. In some cases this has appeared to be due to impurities and a resulting increase in conductivity sufficient to obscure the dielectric hysteresis.

The substances for which some of the above-listed evidences of ferroelectricity have been obtained are $KNbO_3$, $NaNbO_3$, $LiNbO_3$, $KTaO_3$, $NaTaO_3$, $LiTaO_3$, and WO_3. This paper presents more complete dielectric information on $KNbO_3$ and $NaNbO_3$ crystals and shows that they meet the above criteria for ferroelectricity. A paper by Dr. E. A. Wood[2] presents the results of optical and x-ray examination of these materials.

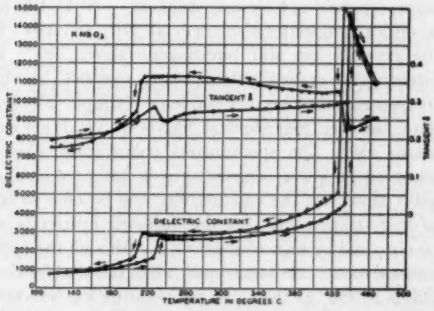

FIG. 1. Dielectric constant and loss tangent curves for single crystals of $KNbO_3$ at 10 kc.

The difficulty of growing large single crystals of these materials with sufficiently low conductivity has been an impediment to further dielectric measurements. There is a strong tendency for some of these materials to be reduced at the high temperatures necessary for their preparation. This usually results in discolored and semiconducting crystals. The preparation of polarizable ceramics of these materials has been a separate and frequently more difficult task. Such materials will not be considered here.

PREPARATION OF CRYSTALS

Growth of $NaNbO_3$ crystals has been reported by Holmquist,[3] who obtained them from a flux of NaF which contained Na_2CO_3 and Nb_2O_5 in the stoichiometric proportions. With minor variations in temperature and composition, we found it possible to obtain crystals of several mm edge length which permitted x-ray identification and were large enough for reliable optical and dielectric measurements.

The growth of $KNbO_3$ crystals had been reported by Joly,[4] who used CaF_2 as a flux at rather high temperatures. Repeating this method several times as described and with variations, we were not able to obtain crystals. Using a low melting K-salt as flux, such as KF or KCl, large and clear crystals were obtained up to 1-cm edge length. They were, unfortunately, of a dark blue color, probably caused by the formation of a small amount of

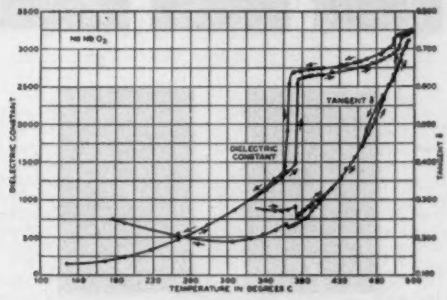

FIG. 2. Dielectric constant and loss tangent curves for single crystal of $NaNbO_3$ at 10 kc.

[1] B. T. Matthias, Phys. Rev. **75**, 117 (1949); **76**, 430 (1949); B. T. Matthias and J. P. Remeika, Phys. Rev. **76**, 1886 (1949).
[2] E. A. Wood, Acta Cryst. (to be published).
[3] Holmquist, Z. Krist. **31**, 306 (1896).
[4] Joly, Ann Sci. de l'ecole Norm. Sup. Paris **6**, 164 (1877).

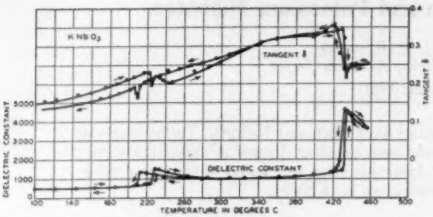

FIG. 3. Dielectric constant and loss tangent curves at 150 kc for same single crystal if $KNbO_3$ as in Fig. 1.

Nb_2O_4. These colored crystals were useful for optical and x-ray investigation, but because of their high conductivity were not suitable for dielectric tests. The final crystals were clear cubes from 1 to 3 mm edge length. Somewhat less perfect crystals have been obtained as large as 1 cm on a side. It has not been possible to obtain single domain crystals of either sodium or potassium niobate. X-ray analyses by Mrs. Wood have checked the identification of both substances and confirmed that they have the pseudocubic perovskite structure.

DIELECTRIC MEASUREMENTS

Figures 1 and 2 show the curves of dielectric constant and tanδ for $KNbO_3$ and $NaNbO_3$ over a range of temperatures and at a frequency of 10 kc. These measurements are for small signal voltages and on crystals not subjected to polarizing voltage. Large changes in dielectric constant and loss tangent are observed at about 224° and 434° for $KNbO_3$ and at about −80°, 370°, and 480° for $NaNbO_3$. These measurements were made on small single crystals of a few mm² electrode area and about 0.5 mm thick. They were repeated on several samples, all of which showed the same discontinuities and approximately the same value of dielectric constant. The dielectric loss varied somewhat from sample to sample being highest in crystals which were discolored. The values given are for the clearest crystals. The dielectric constant for $KNbO_3$ remained at essentially the same value as shown for 100° even down to −190°, where the conductivity was much lower. Figure 3 for $KNbO_3$ at 150 kc shows the same discontinuities as observed at 10 kc. Here, however, the level of dielectric constant is lower, although the loss tangent has about the same value. Measurement at the high temperatures made necessary the use of gold electrodes evaporated on the crystals and a crystal holder which when empty showed little change of dielectric properties with temperature.

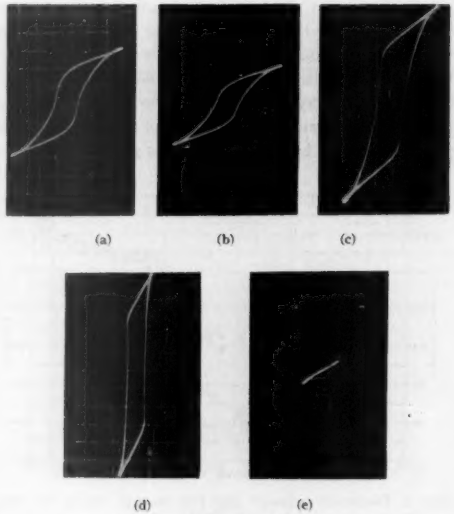

FIG. 4. Dielectric hysteresis loops for $KNbO_3$ crystals. (a) 220°C $P_s=1.33\times10^{-6}$ coulombs/cm²; (b) 237°C $P_s=0.92\times10^{-6}$ coulombs/cm²; (c) 329°C $P_s=3.03\times10^{-6}$ coulombs/cm²; (d) 410°C $P_s=3.78\times10^{-6}$ coulombs/cm²; (e) 472°C crystal is cubic.

The Curie temperature for $KNbO_3$ is found to be at 434°C. Above this temperature, optical and x-ray studies show that the crystals become cubic. Here, also, the hysteresis and saturation of polarization disappear. Below 434° the $KNbO_3$ crystals are tetragonal. The change in dielectric constant at 220° corresponds to a change in crystal structure from tetragonal to orthorhombic. No further changes of structure have been observed in $KNbO_3$, unlike $BaTiO_3$, which shows an additional low temperature change to rhombohedral symmetry. All of these changes in crystal structure and dielectric properties show a temperature hysteresis which is, however, smaller at high than at low temperatures.

In $NaNbO_3$ two breaks are shown in the dielectric constant curve, the lower at about 370° and the upper at 480°C. In contrast to $KNbO_3$, the larger dielectric constant change occurs at the lower temperature discontinuity. A third and smaller change in dielectric constant, which is not shown, occurs at −80°C. Changes in optical properties also occur at 370° and 480°, but the crystals are still birefringent above 480°. The birefringence gradually decreases up to 640°C, at which temperature they become suddenly isotropic. The x-ray data, however, indicate that $NaNbO_3$ crystals are cubic above 480°. The spontaneous polarization which is observed at lower temperatures is not present above 480°. However, the conductivity has become so large at that temperature that the dielectric hysteresis may be obscured by high conductivity. Although the optical measurements cast some doubt, all of the other evidence points to 480° as the Curie temperature for $NaNbO_3$.

Field polarization hysteresis loops have been obtained for $KNbO_3$ crystals which tend to saturate and resemble those obtained for $BaTiO_3$ crystals. The photographs, Fig. 4, show these hysteresis curves at several temperatures. Figure 4(a) was obtained just below the 224°

transition and Fig. 4(b) just above it. A decrease in the value of the polarization is observed with little change in coercive force. Midway between the two transitions, the polarization has increased and the coercive force decreased, as shown in Fig. 4(c). Just below the Curie temperature, Fig. 4(d), the polarization is nearly double its low temperature value. At 472°, Fig. 4(e), the trace is an ellipse and when compensated for dielectric loss becomes a single line. Values of the saturation polarization have been estimated from these photographs and the calibrating data to be 0.9×10^{-6} coulombs/cm^2 at room temperature and 3.8 just below the curie temperature.

It is clear from the work reported here that sodium and potassium niobates are ferroelectric and are comparable with the more thoroughly investigated $BaTiO_3$.

PHYSICAL REVIEW VOLUME 82, NUMBER 5 JUNE 1, 1951

Theory of Antiferroelectric Crystals

C. KITTEL
Department of Physics, University of California, Berkeley, California
(Received January 10, 1951)

An antiferroelectric state is defined as one in which lines of ions in the crystal are spontaneously polarized, but with neighboring lines polarized in antiparallel directions. In simple cubic lattices the antiferroelectric state is likely to be more stable than the ferroelectric state. The dielectric constant above and below the antiferroelectric curie point is investigated for both first- and second-order transitions. In either case the dielectric constant need not be very high; but if the transition is second order, ϵ is continuous across the Curie point. The antiferroelectric state will not be piezoelectric. The thermal anomaly near the Curie point will be of the same nature and magnitude as in ferroelectrics. A susceptibility variation of the form $C/(T+\theta)$ as found in strontium titanate is not indicative of antiferroelectricity, unlike the corresponding situation in antiferromagnetism.

I. INTRODUCTION

IN the ferroelectric state a crystal exhibits a spontaneous electric polarization. We define the antiferroelectric state as one in which lines of ions in the crystal are spontaneously polarized, but with neighboring lines polarized in antiparallel directions, so that the spontaneous macroscopic polarization of the crystal as a whole is zero. We exclude molecular crystals from the present discussion, and we do not explicitly consider antiferroelectric arrays in which more than two sublattices are involved. It is not yet certain that realizations of antiferroelectrics have been observed,[1] as it has not previously been known how to recognize them correctly.

In ferroelectrics the occurrence of spontaneous polarization is believed at present to be the result of a Lorentz catastrophe in which the constant of proportionality connecting the applied electric field with the polarization exhibits a singularity. Illuminating contributions to the theory of the effect have been made, in particular by Wul,[2] Devonshire,[3] and Slater.[4] It would appear to be quite possible for an antiferroelectric arrangement of dipole moments to be produced by a somewhat generalized form of the Lorentz catastrophe. We shall speak throughout of crystals (such as perovskites) in which specifically quantum-mechanical effects are not of major importance.

We need only consider an arrangement of highly polarizable ions located at the lattice points of a simple tetragonal lattice with an axial ratio[5] $c/a\ll1$, so that the structure may be thought of as constructed of lines of atoms parallel to the c-axis. Because of the geometry of dipolar fields, ions in the same line will tend to be polarized parallel to each other, but the sense of adjacent lines will be opposite.[6]

In looking for realizations of antiferroelectricity in

[1] Private communication from Professor B. T. Matthias; I am also indebted to Professor P. Scherrer for a discussion of possible realizations. *Note in proof:* Kehl, Hay, and Wahl have recently observed by x-ray methods the occurrence of an antiferroelectric arrangement in tungsten trioxide crystals above 750°C (private communication from G. Jeffrey).

[2] B. Wul, J. Phys. U.S.S.R. **10**, 95 (1946), V. Ginsburg, J. Phys. U.S.S.R. **10**, 107 (1946).

[3] A. F. Devonshire, Phil. Mag. **40**, 1040 (1949).

[4] J. C. Slater, Phys. Rev. **78**, 748 (1950).

[5] Actually, as we know from the work of J. A. Sauer and A. N. V. Temperley [Proc. Roy. Soc. (London) **A176**, 203 (1940)] and J. M. Luttinger and L. Tisza [Phys. Rev. **70**, 954 (1946)], even in a simple cubic crystal ($c=a$) the alternating polarized line arrangement of dipoles is the lowest state. This is just our antiferroelectric arrangement. Calculations for barium titanate currently being made by Mr. M. H. Cohen suggest that almost exactly the same polarizabilities as lead to a ferroelectric catastrophe in $BaTiO_3$ would also lead to an antiferroelectric catastrophe. The observed ferroelectricity may be the consequence of short-range interactions.

[6] We may of course discuss by methods similar to those employed in the present paper the case of "quasi-ferroelectricity," in which different types of ions are spontaneously polarized in different directions, but still give a net macroscopic polarization. The ferromagnetic analog of this condition actually occurs in the ferrites and perhaps in other compounds, as suggested by Guillaud and Néel. Jonkers and van Santen [Science **109**, 632 (1949)] have suggested that this situation may obtain in barium titanate.

nature we must inquire first into the signs by which it may be recognized. The present examination of the problem was stimulated by the observation made by Hulm[7] that the dielectric susceptibility of polycrystalline strontium titanate $SrTiO_3$ may be expressed with fair accuracy in the region from 50°K to room temperature in the form

$$\chi = C/(T+\theta) \tag{1}$$

with $\theta = 35$°K and $C = 6.6\times 10^3$ per °K. Now it is known that above the curie point the ferroelectric crystal barium titanate has a dielectric susceptibility of the form

$$\chi = \text{const.}/(T-\theta) \tag{2}$$

with $\theta = 393$°K. This is, of course, also the form of the Curie-Weiss law

$$\chi = \text{const.}/(T-\theta) \tag{3}$$

for the magnetic susceptibility of ferromagnetic substances above the curie point. It is further known that antiferromagnetic crystals exhibit above the Curie point a magnetic susceptibility of the form[8]

$$\chi = \text{const.}/(T+\theta). \tag{4}$$

It is tempting to grasp at the conclusion that the similarity of Eqs. (1) and (4) implies that in the dielectric case a denominator of the form $T+\theta$ is a sign of antiferroelectricity and in particular that strontium titanate is antiferroelectric. It will be seen below that such a conclusion would be wrong.

II. ANTIFERROELECTRIC LORENTZ CATASTROPHE

We describe first the manner in which the antiferroelectric state may arise. We suppose for simplicity that we have to deal with a lattice of similar atoms or similar unit cells, which may be decomposed into two identical interpenetrating lattices labelled a and b, with polarizations (dipole moment per unit volume) P_a and P_b. The local fields acting on the lattices are

$$F_a = E+\beta_1 P_a - \beta_2 P_b; \quad F_b = E+\beta_1 P_b - \beta_2 P_a. \tag{5}$$

Here E is the applied external electric field; β_1 and β_2 are Lorentz constants which may be calculated from the geometry of the lattice, and in the antiferroelectric case both will be positive.

If we take the polarization as proportional to the local field,

$$\gamma_1 P_a = F_a; \quad \gamma_1 P_b = F_b; \tag{6}$$

where $\gamma_1 = (\Sigma n_i \alpha_i)^{-1}$ in the usual notation, the α_i being the atomic polarizabilities, we have

$$\gamma_1 P_a = E+\beta_1 P_a - \beta_2 P_b; \quad \gamma_1 P_b = E+\beta_1 P_b - \beta_2 P_a. \tag{7}$$

These equations have a non-zero solution for the P's when $E=0$ only if the determinant of the coefficients of the P's is zero:

$$\begin{vmatrix} \gamma_1-\beta_1 & \beta_2 \\ \beta_2 & \gamma_1-\beta_1 \end{vmatrix} = 0, \tag{8}$$

so that

$$\gamma_1 = \beta_1 \pm \beta_2. \tag{9}$$

The root corresponding to the solution $P_a/P_b = -1$ is

$$\gamma_1 = \beta_1+\beta_2. \tag{10}$$

However, the catastrophe in the dielectric susceptibility is determined by the other root. Adding the two Eqs. (7) together, we have

$$(P_a+P_b)(\gamma_1-\beta_1+\beta_2) = 2E; \tag{11}$$

so that the dielectric susceptibility per unit volume is

$$\chi = (P_a+P_b)/E = 2/(\gamma_1-\beta_1+\beta_2), \tag{12}$$

which has its crisis when

$$\gamma_1 = \beta_1-\beta_2, \tag{13}$$

at which point $P_a/P_b = 1$, corresponding to ferroelectricity.

We see on substituting Eq. (10) into Eq. (12) that the susceptibility at the antiferroelectric curie point, but on the "high temperature" or unpolarized side, is given by

$$\chi = 1/\beta_2. \tag{14}$$

III. SUSCEPTIBILITY IN THE ANTIFERROELECTRIC STATE WHEN THE TRANSITION IS SECOND ORDER

At this point our interest in the effects of varying temperature makes it expedient to alter our approach to the problem and introduce a phenomenological expansion for the Helmholtz free energy per unit volume:

$$A(P_a, P_b, T) = A_0 + f(P_a^2+P_b^2) + gP_aP_b + h(P_a^4+P_b^4). \tag{15}$$

In this approximation the transition will be second order, as is known from the ferroelectric case. The term in P_a^4 and P_b^4 is introduced to restrict the catastrophe to a finite polarization. The quantities f, g, h are functions of the temperature and are, if we were to neglect entropy changes, simply related to the polarizability and local field constants.

We have

$$\partial A/\partial P_a = E = 2fP_a + gP_b + 4hP_a^3, \tag{16}$$

so that the spontaneous polarization ($E=0$) in the

[7] J. K. Hulm, Proc. Phys. Soc. (London) **63A**, 1185 (1950). Below 50°K the dielectric constant leveled off, and there was no evidence of a peak down to the lowest temperature reached in the measurements, which was 1.3°K, where the dielectric constant was 1300.

[8] In the antiferromagnetic case θ is not in general equal to the transition temperature T_c, although θ is always positive. For an excellent summary of antiferromagnetism the reader may refer to a forthcoming review article by J. H. Van Vleck to appear in the *Journal de Physique*.

antiferroelectric state ($P_{sa}=-P_{sb}$) is given by

$$P_{sa}^2=(g-2f)/4h. \tag{17}$$

If in the antiferroelectric state we apply a small electric field ΔE the macroscopic polarization $\Delta P=P_a+P_b$ is given by, taking $P_a\cong -P_b$,

$$2\Delta E=2f\Delta P+g\Delta P+12hP_{sa}^2\Delta P,$$

or,

$$\chi=\Delta P/\Delta E=1/2(g-f); \tag{18}$$

at the Curie point $g=2f$, so that

$$\chi(T=T_c)=1/g \tag{19}$$

on the antiferroelectric side. In the unpolarized state we neglect the fourth-power terms in Eq. (15) and find

$$\chi=2/(2f+g), \tag{20}$$

which reduces at the Curie point to

$$\chi(T=T_c)=1/g \tag{21}$$

on the unpolarized side. A comparison of Eqs. (19) and (21) shows that the dielectric constant is continuous across the Curie point, and it does not necessarily have a high value.

We suppose that f, which is related to the atomic polarizabilities, varies with temperature near the curie point as

$$f=\tfrac{1}{2}g+\lambda(T-T_c), \tag{22}$$

where λ is a constant and in $BaTiO_3$ is positive, with a value of the order of 10^{-4} per °K. This expression has as consequences

$$(T<T_c)\quad P_{sa}^2=P_{sb}^2=\lambda(T_c-T)/2h; \tag{23}$$

$$(T<T_c)\quad \chi=1/[g-2\lambda(T-T_c)]; \tag{24}$$

$$(T>T_c)\quad \chi=1/[g+\lambda(T-T_c)]. \tag{25}$$

If λ is positive, the antiferroelectric region lies on the low temperature side of the curie point, and the dielectric constant changes slope slightly and goes through a maximum (which may not always be discernible) at the transition point. If λ is negative the antiferroelectric state lies on the high temperature side of the curie point and the dielectric constant will be a minimum there.

For a simple cubic lattice we find by manipulating the results of Luttinger and Tisza (reference 5) that

$$\beta_1=4.770;\quad \beta_2=0.581; \tag{26}$$

so that an antiferroelectric arrangement is favored, while for body-centered and face-centered cubic lattices, β_2 is negative (when the crystal surfaces are grounded or if domains are formed), favoring ferroelectricity.

Anomalous Heat Capacity

The entropy is given from the Helmholtz free energy by $(\partial A/\partial T)_{P_a}=-S$, so that, supposing that g and h are independent of temperature,

$$\Delta S=-(P_{sa}^2+P_{sb}^2)(\partial f/\partial T)_{P_a} \tag{27}$$

per unit volume. The anomaly in the heat capacity per unit volume at constant pressure p at the curie point is

$$\Delta C_p=T_c\left(\frac{\partial S}{\partial T}\right)_p=\frac{T_c}{h}\left(\frac{\partial f}{\partial T}\right)_p\left(\frac{\partial f}{\partial T}\right)_p, \tag{28}$$

where the derivatives are taken at $T=T_c$. This is essentially the same expression as found in the Wul theory of barium titanate; we may perhaps expect on this account an anomaly in the heat capacity of antiferroelectrics of the same order of magnitude as that found in ferroelectrics, of the order of 5 percent of the normal heat capacity above the Debye temperature.

The spontaneous polarization of each sublattice below the Curie point is related to the excess heat capacity by essentially the same relation as that derived for ferroelectrics.

IV. THEORY FOR FIRST-ORDER TRANSITIONS

Devonshire[3] has suggested that it is possible to give a better account of the transition in ferroelectrics from the polarized to the unpolarized state by treating the transition as first order rather than as second order as we have above. This introduces greater flexibility into the treatment of the dielectric constant near the Curie point, and accounts quite naturally for the rapid drop in saturation polarization near the Curie point, the drop being more rapid than can be accounted for by a second order transition. It is well known that in solids particularly it is rather difficult to decide whether a transition exhibits a latent heat or a discontinuity in the heat capacity. The x-ray evidence of Kaenzig[8] gives strong support to a first-order transition in $BaTiO_3$.

It may be appropriate to comment here on several consequences of the first-order transition theory for ferroelectrics which have escaped common notice. One is that the dielectric susceptibility measured in the direction of the spontaneous polarization may be expected to be about four times as great above the transition in the unpolarized state as below the transition in the polarized state. Writing (reference 3)

$$A=A_0+\alpha P^2+\beta P^4+\gamma P^6, \tag{29}$$

we have at the critical point $A=A_0$ the relations

$$P_c^2=-2\alpha/\beta;\quad P_c^4=\alpha/\gamma;\quad 4\alpha\gamma=\beta^2. \tag{30}$$

The susceptibility just below the transition temperature is found by the usual method to be

$$\chi^{(-)}=1/8\alpha_c, \tag{31}$$

while just above

$$\chi^{(+)}=1/2\alpha_c, \tag{32}$$

[8] W. Kaenzig, Phys. Rev. 80, 94 (1950).

so that

$$\chi^{(+)}/\chi^{(-)}=4 \tag{33}$$

in fairly good agreement with the results $\chi^{(+)}=1400$, $\chi^{(-)}\approx 300-500$ of Shirane *et al.*[10] on polycrystalline lead zirconate, although the discrepancy is much greater on the measurements by Roberts.[11]

The second result, as shown by Devonshire, is that it is natural to expect that the principal part of the temperature dependence of the susceptibility above the transition is given by

$$\chi^{(+)}=\frac{1}{2\alpha_c}\frac{T_c-T_0}{T-T_0}, \tag{34}$$

where T_c is the transition temperature, but T_0 is a parameter to be determined. Roberts finds $T_c=234°C$; $T_0=193°C$; $\alpha_c\approx 1.2\times 10^{-4}$ for lead zirconate.

We develop now a first-order transition theory for antiferroelectrics, and write

$$A=A_0+f(P_a^2+P_b^2)+gP_aP_b \\ +h(P_a^4+P_b^4)+j(P_a^6+P_b^6). \tag{35}$$

We have

$$\partial A/\partial P_a=E=2fP_a+gP_b+4hP_a^3+6jP_a^5,$$

so that the spontaneous polarization in the antiferroelectric state ($P_{sa}=-P_{sb}$) is given by

$$6jP_{sa}^4+4hP_{sa}^2+(2f-g)=0. \tag{36}$$

At the Curie point the free energy for this solution is equal to that for the unpolarized solution $P_a=P_b=0$ when

$$(2f-g)+2hP_{sa}^2+2jP_{sa}^4=0. \tag{37}$$

The solution of the two Eqs. (36) and (37) gives us

$$(T=T_c)\quad P_{sa}^2=(g-2f)/h, \tag{38}$$

$$(T=T_c)\quad P_{sa}^4=(2f-g)/2j. \tag{39}$$

We find that in the antiferroelectric state just below the transition we have

$$\chi^{(-)}=1/(4f-g), \tag{40}$$

while just above the transition in the unpolarized state we have

$$\chi^{(+)}=2/(2f+g). \tag{41}$$

Thus, if the antiferroelectric transition is first order, there will be a discontinuity in the dielectric constant at the Curie point. The condition for the Curie point is found from Eqs. (38) and (39):

$$2j(2f-g)=h^2. \tag{42}$$

If the transition is second order, a ferroelectric crystal will have a very high dielectric constant at the Curie point, whereas if the transition is first order, the dielectric constant need not necessarily be very high. An antiferroelectric crystal need not necessarily have a high dielectric constant for either first, or second-order transitions. The character of the transition is determined largely by the sign of h in Eq. (35), a negative sign tending to make the transition first order.

[10] Shirane, Sawaguchi, and Takeda, Phys. Rev. **80**, 485 (1950).
[11] S. Roberts, J. Am. Cer. Soc. **33**, 63 (1950).

V. CONCLUSIONS

From the considerations given above we may suggest, within the limits of the approximations made, the following conclusions:

(1) Antiferroelectric crystals may be expected to occur in nature although a lack of knowledge of what to look for may have handicapped their identification.

(2) The dielectric constant at the antiferroelectric Curie point will not in general be particularly large; if the transition is second order, the dielectric constant will be continuous and nearly constant with temperature at the Curie point, with a small discontinuity in the temperature coefficient. In a first-order transition there will be a discontinuity in the dielectric constant. In ferroelectrics the dielectric constant is very large at the curie point if the transition is second order. The antiferroelectric dielectric constant need not be isotropic.

(3) The antiferroelectric state will not be piezoelectric, as a center of symmetry will exist. In the ferroelectric state one generally finds a large piezoelectric effect. This feature may be the most convenient way to distinguish the two states.

(4) The anomaly in heat capacity at the Curie point should be quite similar in antiferroelectrics to that found in ferroelectrics. The spontaneous polarization should be detectable by x-ray structure determinations above and below the Curie point.

(5) A susceptibility variation of the form $\chi=C/(T+\theta)$ with no apparent transition as found in strontium titanate is *not* indicative of antiferroelectricity. It is suggestive of a crystal which would be ferroelectric "below" 0°K. That is, we have to deal here with the "high temperature" or unpolarized phase of a ferroelectric[12] with a negative Curie temperature.

I wish to thank Mr. Morrel H. Cohen for several valuable discussions and for his kindness in checking the manuscript. Dr. P. W. Anderson has offered helpful suggestions on the manuscript. I am grateful to Prof. G. Jeffrey of the University of Pittsburgh for calling to my attention the x-ray work on WO_3, which has an antiferroelectric structure at high temperatures. I wish here to record also my gratitude to Professor R. T. Birge and the staff of the Department of Physics at Berkeley for their kind hospitality during my stay there on a visiting appointment.

[12] A susceptibility variation of the above form could also, in principle, result from a case in which the polarized ferroelectric state occurs at all temperatures, which could occur if the temperature coefficient of $d\gamma_1/dT$ (see Eq. (6)) had the opposite sign of that observed in $BaTiO_3$ and if the Curie point corresponded to a negative temperature. The two cases could be easily distinguished experimentally by the usual signs of a polarized ferroelectric state —hysteresis, piezoelectricity, and x-ray superstructure.

Yields of Photoprotons from Twenty Elements*

A. K. MANN AND J. HALPERN
University of Pennsylvania, Philadelphia, Pennsylvania
(Received February 5, 1951)

Scintillation counters have been applied to the study of the yields of photoprotons from twenty elements. The relative yields increase by a factor of approximately one hundred as Z increases from 4 to 28, and then decrease to a value, at $Z=50$, of about one-tenth that of the maximum at $Z=28$. An upper limit is placed on the yields from several heavy elements. The absolute values are compared with the neutron data of Price and Kerst, and the sum of the two yields is compared with theory.

INTRODUCTION

ONE of the general features of photonuclear reactions which is of interest is the dependence of the yields of these reactions on atomic number. The yields of γ-n reactions have been investigated most extensively,[1] because experimental difficulties generally involved in the study of photonuclear disintegrations can be surmounted in many of the γ-n processes. The high background attending the intense x-ray beams required to produce these reactions has limited the use of counters for observing directly and rapidly the emitted particles. Many of the γ-n reactions, however, lead to products which are beta-active and whose half-lives are such that these products can be examined conveniently some time after their formation. There are also available slow neutron detectors such as indium and rhodium foils which are insensitive to the γ-ray background and which have been used in the investigation of γ-n processes. Recently, boron trifluoride counters in conjunction with a moderator have been applied successfully to the detection of γ-n processes.[2] Further, since target absorption is not a factor with neutrons, large samples can be irradiated with consequent large yields. In the main, the products of reactions in which charged particles are emitted are not radioactive; and these reactions have been observed primarily with cloud chambers and nuclear emulsions, which necessarily prohibit a comprehensive survey. However, Wäffler and Hirzel,[3] using the Li 17.6-Mev γ-ray, measured the γ-p cross sections of fourteen isotopes (all of which have an observable beta-decay after proton emission) relative to the γ-n cross section in Cu^{63}. The relatively large γ-p cross sections found by them indicated that these reactions were considerably more probable, especially in the lighter elements, than had previously been assumed and suggested the need for a more complete study.

The present paper describes a method, employing scintillation counters, for the direct detection of protons from γ-p reactions and its application to an investigation of the absolute yields of γ-p processes in 20 elements bombarded by bremsstrahlung from the University of Pennsylvania 25-Mev betatron.

METHOD AND PROCEDURE

Two scintillation counters, to be described in detail below, were contained in a scattering chamber completely shielded by four inches of lead, through which passed the collimated x-ray beam from the betatron. The complete experimental arrangement is shown in Fig. 1. The concrete wall provides shielding against neutrons produced in the betatron target. The lead wall and collimator shield the counters from the direct and scattered x-ray beam. The collimator sharply defines an x-ray beam with an angular divergence of 0.22 degree and a circular cross section at the target position $\frac{9}{32}$ in. in diameter. The thickness of the

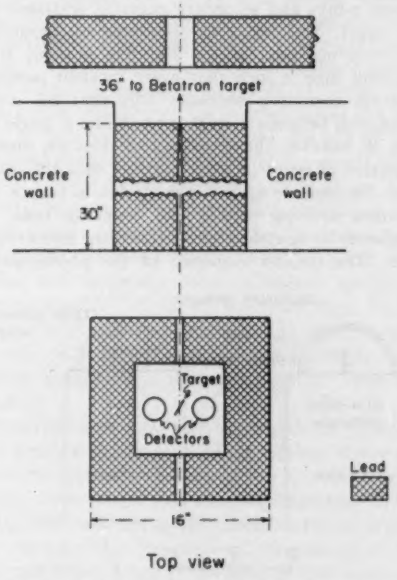

FIG. 1. Diagram of experimental arrangement.

* Assisted in part by the joint program of the ONR and AEC.
[1] G. C. Baldwin and G. S. Klaiber, Phys. Rev. **73**, 1156 (1948); G. Friedlander and M. L. Perlman, Phys. Rev. **74**, 442 (1948); G. Friedlander and M. L. Perlman, Phys. Rev. **75**, 988 (1949); G. A. Price and D. W. Kerst, Phys. Rev. **77**, 806 (1950); Johns, Katz, Douglas, and Halsam, Phys. Rev. **80**, 1062 (1950).
[2] McDaniel, Walker, and Stearns, Phys. Rev. **80**, 807 (1950); Sher, Halpern, and Stephens, Phys. Rev. **81**, 154 (1951).
[3] H. Wäffler and O. Hirzel, Helv. Phys. Acta **21**, 200 (1948).

scattering chamber shield was determined from lead absorption measurements of the scattered radiation attending the x-ray beam. The counters and target were mounted on a rotatable table to permit angular

FIG. 2. Schematic diagram of a complete counting channel.

distribution measurements. It was possible to align the scattering chamber and the target with the beam by irradiating x-ray film in the target position.

The output pulses from the two counters, operated independently, were fed into identical, separate channels. A complete channel for a single tube is shown schematically in Fig. 2. The cathode followers were mounted on the underside of the table supporting the counters and exhibited a linear response over the range of pulse sizes which were observed. The data of these experiments are integral bias curves. The four scalers allowed four points on a bias curve to be obtained simultaneously. The 5819 photomultiplier tube was operated at approximately 900 volts, divided such that 193 volts appeared between the photocathode and the first dynode, 129 volts between the first and second dynodes, and 65 volts between each remaining pair of dynodes.

In order to count protons from reactions induced in a target in the scattering chamber, it is necessary that the detector be capable of sufficient discrimination against x-rays and secondary electrons scattered from the target. The degree of discrimination depends on the resolving time of the counting system. If the resolving time is such that every incident particle is resolved, then it is necessary only that the counter distinguish between a single proton and a single electron. If, however, the resolving time does not allow the resolution of every incident particle, then the counter must discriminate against pile-up due to two or more electrons arriving within the resolving time. The counter to be described here satisfied the latter requirement. The counter consisted of the photomultiplier

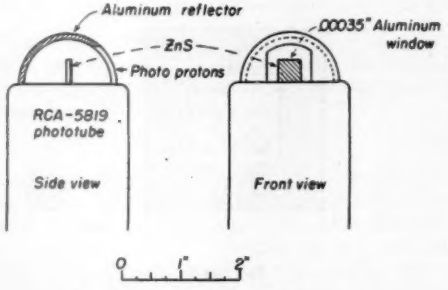

FIG. 3. Diagram of scintillation counter.

tube, a silver-activated ZnS scintillator screen, and an aluminum reflector, arranged as shown in Fig. 3. The scintillator screen was made by depositing powdered crystals on a 0.1 cm thick glass plate, which allowed the screen to be mounted vertically. This orientation of phototube and scintillator was possible because the reflector and the large photocathode surface of the 5819 provided satisfactory light collecting conditions.

The performance of the counter is determined principally by the properties of the scintillator screen. The resolving time is indirectly limited by the decay time of the light pulses from ZnS, and no resolution is attempted within the half-width of the betatron pulses ($\sim$0.5 μsec). However, powdered ZnS is opaque to its own radiation in a thickness corresponding roughly to the range of million-volt protons. For protons with energies from about 1 to 10 Mev, the light yield from the ZnS screen is approximately independent of energy. This saturation effect also occurs for electrons, but the region of approximately constant light yield begins at a much lower energy. It is known that the energy required for the emission of a light quantum from ZnS is about equal for both protons and electrons.[4] Consequently, except for very low energies, the light yield from the ZnS screen is considerably greater for protons than for electrons, independent of their respective energies. This strong discrimination against electrons is not completely realized because of the pile-up effect mentioned previously. However, if the magnitude of the pile-up is restricted to values below a certain maximum by limiting the intensity of the x-ray beam from the betatron, almost complete discrimination is obtained, as is illustrated by the bias curves in Fig. 4. The steeply rising portion of these curves is due to electron pile-up which increases rapidly with decreasing bias voltage until the betatron pulse recurrence rate (180 sec^{-1}) is reached. This may or may not occur outside the region of phototube noise, depending on the incident x-ray beam intensity and the atomic number of the target. The relatively flat portion of the integral curve is due to protons from a γ-p reaction in the target. The long tail extending to low bias voltages in the differential bias curve results from protons with energies below the flat response region of the counter.

The counter was not sensitive to neutrons. This is indicated by the curves in Fig. 5, which were taken under the following conditions: with the counters in the positions shown in Fig. 1, i.e., at right angles to the direction of the incident x-ray beam, a deuterated paraffin target was irradiated and bias curves were obtained for each of the counters. One of the counters was then shielded by 0.027 in. of aluminum and the target irradiated again. The proton counts from the unshielded counter were the same in both runs. The bias curves obtained from the other counter are those in Fig. 5. In order to insure that the heavy particles

[4] H. Kallman, Phys. Rev. 75, 623 (1949).

were not α-particles from the carbon, an experiment similar to that above was performed using a total absorption equivalent to 0.0035-in. aluminum shielding-which is sufficient to absorb almost all α's from a γ-α reaction in C^{12}. The heavy particle counting rate remained the same within statistics in both the shielded and unshielded runs.

The low yields from γ-p reactions required the use of thick ($\sim$5 Mev) targets, which minimized the information to be gained from complete aluminum absorption studies. Nevertheless, several such studies were made on different targets to determine the rough absorption characteristics of the emitted particles. The general features of these absorption curves strongly support the identification of the heavy particles as protons from γ-p reactions. This identification is further substantiated by the excitation functions obtained with the method described here.[5]

In the measurement of γ-p yields, the counters were

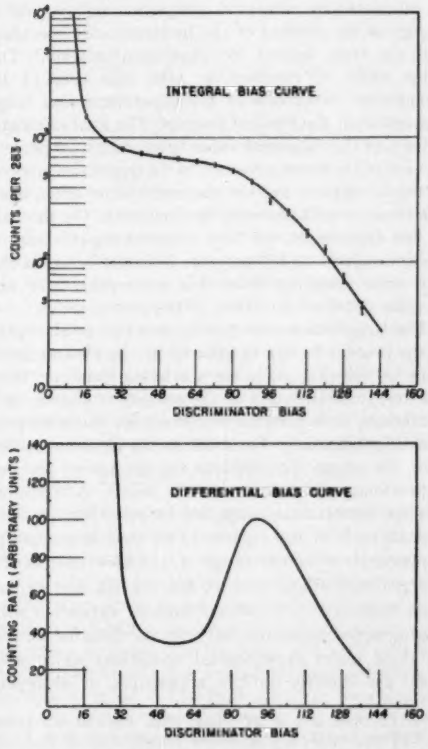

FIG. 4. Bias curves illustrating discrimination against pile-up. The target was nickel.

[5] A. K. Mann and J. Halpern, Phys. Rev. **80**, 470 (1950). Excitation functions of several other elements have since been obtained.

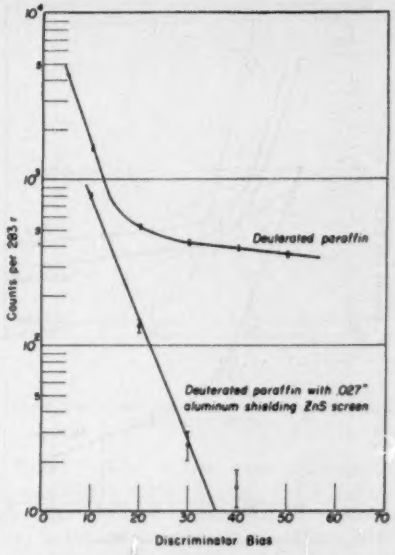

FIG. 5. Bias curves demonstrating the counter insensitivity to neutrons.

fixed at 90 degrees with respect to the direction of the x-ray beam. A target holder was installed which allowed targets to be changed conveniently and with a negligible change in the geometry. The targets were in the form of foils of commercial purity and natural isotopic composition. Target thicknesses were determined from weight and area measurements. Each target was irradiated with a bremsstrahlung spectrum having approximately the same maximum energy of 23.5 Mev. The instantaneous intensity of the incident beam was adjusted so that discrimination against the pile-up was maintained essentially independent of the atomic number of the target during the entire course of any run. The total intensity of x-rays striking the target was determined for each run by integrating the current from an ionization chamber in the path of the beam. The chamber and integrator were calibrated against a Victoreen thimble "r" meter imbedded in a Lucite cylinder of 8-cm outside diameter. Several of the targets were used as standards, and all measurements were made by alternating a standard with an unknown element.

Integral bias curves for several elements are shown in Fig. 6, which also includes a curve obtained without a target in the scattering chamber. These curves represent the data from one of the counting channels. In all cases, the two counters agreed within statistical errors. It will be seen that the slope of the pile-up in the background curve is nearly the same as that observed with low Z elements such as deuterium and aluminum.

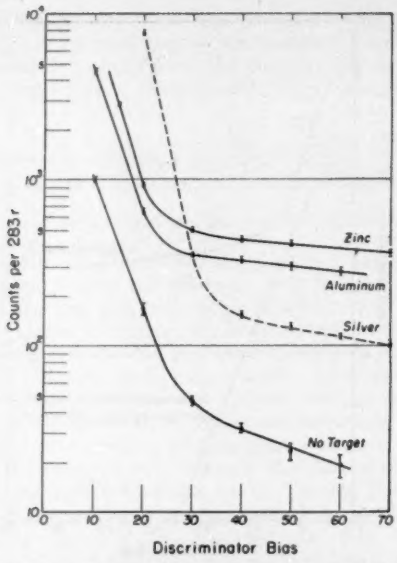

FIG. 6. Typical bias curves for three elements compared with the curve for no target.

That portion of the background curve which extends to higher bias voltages is due to heavy particles, as is shown by comparison with the shielded counter curve in Fig. 5, which exhibits only slight evidence of a heavy particle tail. Because of imperfect control of the incident beam intensity, the magnitude and slope of the pile-up show some increase with increasing atomic number of the target. This in turn results in a steeper slope of the proton regions of curves corresponding to relatively high Z targets, because discrimination against pile-up is lessened. For a given target, the slope of the heavy particle region depends on the relative magnitudes of the pile-up and the heavy particle yield. The low yield accounts for the extreme slope of the heavy particle region of the background curve, while a combination of relatively low yield and high pile-up is responsible for the increased slope of the high Z target curves. In order to facilitate direct comparison of the data for elements of widely different Z, the heavy particle and pile-up components of each of the curves are separated under the assumption that the shape of the pile-up is exponential and independent of its magnitude and, consequently, is the same for all targets.

There are several sources of error which must be considered before the yields can be determined from the reduced data. Since measurements were made only at one angle, it is necessary to make an assumption concerning the angular distributions of protons from those elements for which no information is available. The angular distributions from Al, Mg, Cu, Rh, and Ag have been measured[6] by the photographic emulsion method. We have verified the results for Ag and also made a rough determination of the distribution from Ni with the method of this paper. All of the distributions, except those for Rh and Ag, are spherically symmetric within the accuracy of the experiments. The data for Rh and Ag indicate that, although there is a high energy proton component exhibiting marked assymmetry, the entire energy spectrum shows only small departure from an isotropic distribution. Consequently, we have computed the total yields for all elements from the known geometry of our apparatus, assuming spherical symmetry.

Another source of error arises from uncertainty in the value of the counter efficiency, which was determined from the following experiment. The proton yield from deuterium in a given solid angle at 90 degrees was obtained from the bias curves for normal and deuterated paraffin targets after background corrections were made. The total yield from deuterium can be calculated by numerical integration with respect to energy of the product of the incident x-ray spectrum[7] and the cross section for photodisintegration.[8] This value must be modified to take into account the geometrical conditions of the experiment and target absorption of the emitted protons. The final calculated value and the measured value agree within 20 percent. In view of the errors attached to the quantities involved in the calculation and the measured yield value, closer agreement would probably be fortuitous. On the basis of this experiment, we have assumed the efficiency of our counters to be 100 percent. It should be noted that any error resulting from this assumption will only increase the absolute values of the proton yields.

The largest source of error is that due to absorption of the protons by the target and by the air and aluminum foil (see Fig. 3) in the scattering chamber. When the energy distribution of the protons is known, as in deuterium, it is possible to correct for the absorption with high accuracy. For most of the elements studied here, the energy distributions are not known and only approximate corrections can be made. A first-order relative correction was applied by selecting the thickness of each of the targets to be that corresponding approximately to the range of a 5-Mev proton. The energy distributions from Al, Mg, Cu, Rh, and Ag have been measured[6] with bremsstrahlung excitation using photographic emulsions; but only the data for Cu were obtained under experimental conditions which allow their use directly in the application of absorption

[6] B. C. Diven and G. M. Almy, Phys. Rev. **80**, 407 (1950); M. E. Toms and W. E. Stephens (to be published); P. R. Byerly, doctoral dissertation (University of Pennsylvania, 1950); Curtis, Hornbostel, Lee, and Salant, Phys. Rev. **77**, 290 (1950).

[7] Johns, Katz, Douglas, and Halsam, Phys. Rev. **80**, 1062 (1950).

[8] Collie, Halban, and Wilson, Proc. Phys. Soc. (London) **63**, 994 (1950). This article contains a table of most recent measurements.

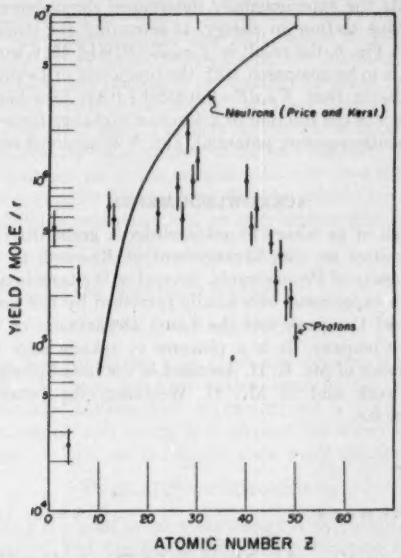

FIG. 7. Plot of the absolute yield values of γ-p reactions in twenty elements as a function of Z.

corrections to the yield data of this paper. However, the experiments with emulsions indicate that the shapes of the distributions do not depend strongly on the atomic number of the target and are closely described by the proton energy distribution predicted by the theory of the compound nucleus.[9] Consequently, for the purpose of absolute absorption corrections, we have used an energy distribution similar in shape to that observed for Cu and of width determined by the γ-p threshold for the element investigated. The calculated corrections increased the observed yield values for all elements except deuterium by about a factor of 2.5.†

RESULTS AND DISCUSSION

The corrected absolute yield values plotted against atomic number are shown in Fig. 7. The estimated errors are indicated by the vertical lines through the points. The errors attached to the relative values of neighboring elements are about one-half as large as those in the figure. In addition to these data, upper limits to the yields of $_{73}$Ta, $_{74}$W, $_{78}$Pt, and $_{79}$Au have also been obtained. The yields from these elements are less than or equal to that from $_{50}$Sn. For the purpose of comparison, there is also shown in Fig. 7 a portion of the curve which fits the absolute γ-n yield data of Price and Kerst.[10] These values were determined with bremsstrahlung of maximum energy of 22 Mev.

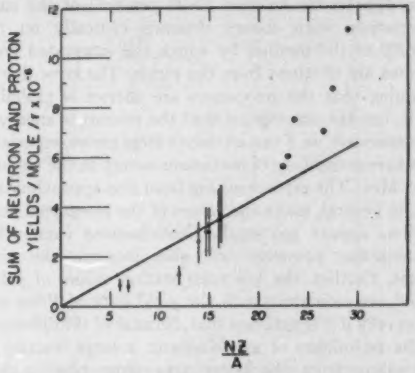

FIG. 8. Plot of the sum of the γ-n and γ-p yields as a function of NZ/A.

The cross section for excitation of a nucleus by photons is known to possess a resonance character.[11] The energy dependence of the resonance and the magnitude of the integrated cross section have been estimated by Goldhaber and Teller[12] and by Levinger and Bethe.[13] Both theories predict that the integrated cross section, $\int \sigma_a dE$, should be proportional to NZ/A. (σ_a is the cross section for photon absorption.) If the spectrum from the betatron contained equal numbers of photons in every energy interval up to the maximum, the neutron yields of Price and Kerst and our proton yields would be exactly proportional to the integrated cross sections of γ-n and γ-p processes, providing also that the maximum photon energy extended beyond the resonance in every element. The yields measured with a betatron are proportional to $\int P\sigma_a dE$, where PdE is the number of photons per cm^2 in the energy interval dE and, to a good approximation, varies as $1/E$. If, however, it is assumed that the half-widths of the cross section resonances are small compared with the energy at resonance and that the variation of the resonance energy with Z is also small, then $\int P\sigma_a dE \approx \text{const} \int \sigma_a dE$. To this approximation, the yields given in Fig. 7 can be taken as proportional to the integrated cross sections. Since $\sigma_a = \sigma_{\gamma-p} + \sigma_{\gamma-n} + \cdots$, it is necessary to add the integrated cross sections for the partial reactions to compare the experimental results with theory. The sum of the neutron and proton yields is plotted as a function of NZ/A in Fig. 8. The neutron yield values were taken directly from the data of Price and Kerst and not from the smooth curve in Fig. 7. Errors have been attached only to those points for which the proton yield

[9] V. F. Weisskopf and D. T. Ewing, Phys. Rev. **57**, 472 (1940).

† *Note added in proof:* Since this paper was written, we have determined the effect of absorption with increased accuracy by measuring the yields from several target thicknesses of the same element. The correction factors obtained in this way are less than those used in the present paper by 30 percent, which is just outside the estimated errors given in Fig. 7.

[10] G. A. Price and D. W. Kerst, Phys. Rev. **77**, 806 (1950).

[11] G. C. Baldwin and G. S. Klaiber, Phys. Rev. **73**, 1156 (1948); Johns, Katz, Douglas, and Halsam, Phys. Rev. **80**, 1062 (1950).

[12] M. Goldhaber and E. Teller, Phys. Rev. **74**, 1046 (1948).

[13] J. S. Levinger and H. A. Bethe, Phys. Rev. **78**, 115 (1950).

is an appreciable fraction (>25 percent) of the sum. Comparison with theory depends critically on the validity of the method by which the integrated cross sections are obtained from the yields. The error due to assuming that the resonances are narrow is probably small; but the assumption that the resonance energy is not dependent on Z can introduce large errors, especially with bremsstrahlung of maximum energy in the vicinity of 25 Mev. The error resulting from this approximation will, in general, make the values of the integrated cross sections appear too small. Contributions from other photonuclear processes will also increase the yield values. Further, the γ-n cross section values of Johns *et al.*[11] are consistent with the yield data of Price and Kerst only if it is assumed that, because of the difference in the techniques of measurement, a large fraction of the values from the latter arise from photonuclear reactions other than γ-n.

If we use the data of Johns *et al.* for copper, which include the experimentally determined dependence of the cross section on energy, to normalize the straight line in Fig. 8, the result is $\int \sigma_\gamma dE = 0.044Z$ Mev-barns. This is to be compared with the prediction of Levinger and Bethe that $\int \sigma_\gamma dE = 0.030Z(1+0.8x)$ Mev-barns, where x is the fraction of attractive exchange force for the neutron-proton potential, and N is assumed equal to Z.

ACKNOWLEDGMENTS

Each of us wishes to acknowledge a grant from the Committee on the Advancement of Research of the University of Pennsylvania. Several of the targets used in this experiment were kindly furnished by the Foote Mineral Company and the Lamp Department of the G.E. Company. It is a pleasure to acknowledge the assistance of Mr. R. H. Asendorf in the initial phase of this work and of Mr. G. Werthner, the betatron technician.

PHYSICAL REVIEW VOLUME 82, NUMBER 5 JUNE 1, 1951

On the γ-Ray Spectrum Resulting from the Absorption of π-Mesons in Deuterium*†

KENNETH M. WATSON AND RICHARD N. STUART
Radiation Laboratory, Physics Department, University of California, Berkeley, California
(Received January 22, 1951)

The γ-ray spectrum resulting from the reaction $\pi^-+D\rightarrow 2n+\gamma$ has been shown to depend strongly on the nature of the n-n interaction and has been calculated for several values of the n-n scattering length. A comparison of the theoretical cross section with preliminary experiments by Aamodt, Panofsky, and Phillips indicates: (1) an upper limit of approximately 200 kev can be put on the binding energy of the di-neutron; (2) photomeson production involves an interaction with the nucleon spin.

I. INTRODUCTION

EXPERIMENTAL studies of thec apture of π^- mesons in deuterium[1] indicate that approximately 30 percent of the capture events lead to a high energy γ-ray. This has been interpreted, for instance, as implying that the π-meson is not scalar.[2,3] However, quite apart from its implications as to the nature of the π-meson and as to meson-nucleon interactions, this experiment, as has been noted previously,[2,3] is of interest in that it offers a means of deducing something about the interaction between two neutrons.

This possibility arises through a measurement of the γ-ray spectrum resulting from the radiative decay and may be seen qualitatively as follows. Since the final state contains three particles—a γ-ray and two neutrons—the γ-ray spectrum is not monochromatic; on the other hand, if there were only the γ-ray and one particle (say a bound di-neutron) in the final state, the γ-ray spectrum would be monochromatic. If the two neutrons in the final state are not actually bound, but interact through an attractive potential, we can expect a tendency for them to recoil in the same direction with about equal velocities and thus cause the γ-ray spectrum to be more nearly monochromatic than if there were no n-n (neutron-neutron) force. That is, the effect of an attractive n-n potential should be such as to make the γ-ray spectrum show a pronounced peak near its high energy limit.

We can obtain in a simple manner the shape of the spectrum near this peak. Let us denote the transition matrix for the radiative capture to a singlet spin state for the two neutrons by M^s, and suppose that the singlet n-n wave function is $\psi^s(r)$. Then M^s will have the form (we use as units $\hbar=c=1$)

$$M^s=\int d^3r\psi^{s*}(r)\times[\text{other factors}]. \qquad (1)$$

Let $\mathbf{p}$ be the relative momentum of the two outgoing

* The work described in this report was performed under the auspices of the AEC.
† This work was reported at the New York Meeting of the American Physical Society in February, 1951.
[1] Panofsky, Aamodt, and Hadley, Phys. Rev. **81**, 565 (1951).
[2] Brueckner, Serber, and Watson, Phys. Rev. **81**, 575 (1951).
[3] S. Tamor and R. E. Marshak, Phys. Rev. **80**, 766 (1950).

neutrons, which is small near the high energy limit of the γ-ray spectrum. We may thus neglect all but the S-wave contribution to the integral (1). Furthermore, the absorption process is presumably an event which involves primarily just the proton, so we should expect the integral in Eq. (1) to show no singular behavior for close distances of approach of the two nucleons. Then the contribution to the integral will come from regions of space much larger than that for which the n–n potential is important, and we may replace $\psi^s(r)$ by

$$\psi_0^s(r)=\sin(pr+\delta)/pr, \tag{2}$$

and Eq. (1) can be put into the form

$$M^s=[I_1\sin\delta+I_2\cos\delta]/p. \tag{3}$$

From Eq. (2) we see that $I_2\to 0$ and $I_1\to$constant as $p\to 0$, i.e., near the high energy limit of the γ-ray spectrum. Near this limit, we can neglect I_2 in Eq. (3). Squaring M^s and taking into account the phase space factor, we have for the singlet state γ-ray spectrum

$$dT^s/dK=(p^{-1}\sin^2\delta)\times\text{constant}, \tag{4}$$

where p is related to the γ-ray energy K by energy conservation, and the phase shift δ is a function of p, depending on the assumed n–n potential. The characteristic shape of the spectrum expected from Eq. (4) is a rapid rise from zero at the high energy limit depending on the behavior of $\sin^2\delta$. Near $p=0$, $1/p$ is a rapidly decreasing function, so we expect the spectrum to fall off rapidly with farther decreasing γ-ray energy. The final triplet state contribution will be small near the high energy limit.

A correction for the finite range of the n–n force can be obtained as follows. The exact correction to Eq. (2) assuming M^s [Eq. (1)] is, of course,

$$\delta\psi^s=(\psi^s-\psi_0^s).$$

We can write this as

$$\delta\psi^s=-(\sin\delta)f(p,r)/pr, \tag{5}$$

where $f(p,r)=(\psi_0^s-\psi^s)pr/\sin\delta$. But $f(p,r)$ is to a very good approximation independent of p,[4] so we can write $f(p,r)\simeq f(r)$. Then the correction to M^s is

$$\delta M^s=-I_1'(\sin\delta)/p, \tag{3'}$$

where I_1' is very nearly a constant near the high energy limit of the spectrum. The correction (3′) is of the same form as Eq. (3) with $I_2=0$, so the shape of the spectrum, as given by Eq. (4), is unchanged to a good approximation.

With sufficiently good energy resolution in the experimental measurement of the γ-ray spectrum, our problem would be essentially complete. The right-hand side of Eq. (4) is proportional to $p\sigma_{n-n}$ times a constant, where σ_{n-n} is the low energy n–n scattering cross section. This simple expression for the shape of the γ-spectrum permits, in principle, a direct comparison of the σ_{n-n} with the low energy p–p and n–p scattering. There is evidence from the binding energies of mirror nuclei, for instance, for believing that σ_{n-n} and σ_{p-p} should be quite similar, except for the coulomb contribution to the latter.

Because of the limitation on present experimental accuracy and energy resolution in the measurement of the γ-ray spectrum, it is necessary to improve Eq. (4), by extending it to lower energies. This will be done in Sec. IV. The nature of this correction can be seen in Fig. 1, where dT^s/dK as given by Eq. (4) and the S-wave component of the cross section as given by the more nearly complete theory are compared.

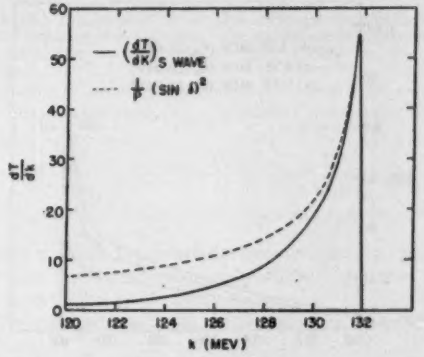

FIG. 1. A comparison of the approximate γ-ray spectrum $p^{-1}\sin^2\delta$ and the corrected S-wave contribution to the spectrum for $a=-8$ Mev.

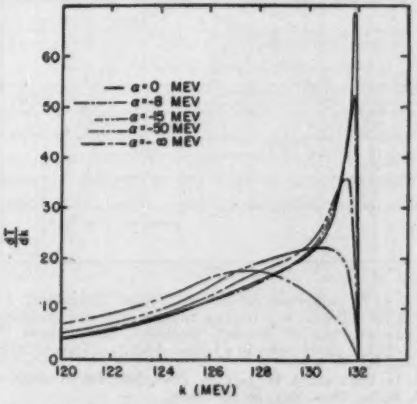

FIG. 2. A plot of the γ-ray spectrum for several negative values of a.

[4] The quantity $f(p,r)$ enters into the definition of the *effective range* in the analysis of low energy scattering [see, for example, H. A. Bethe, Phys Rev. **76**, 38 (1949)] and in this connection has been shown to be very nearly independent of p, for small p. The numerical magnitude of this correction can be approximately given in terms of the effective range.

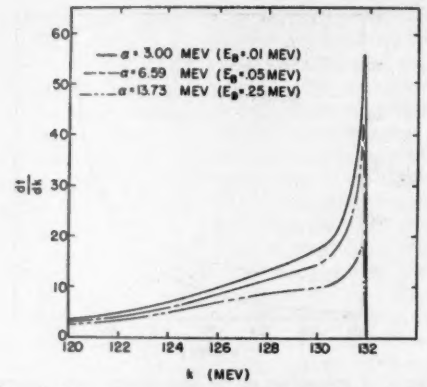

FIG. 3. The γ-ray spectrum for various positive values of α (positive binding energy). The total cross sections including the contribution of the monochromatic component have been normalized to a constant.

II. NUMERICAL RESULTS

The theory outlined in the Introduction and further developed in Secs. IV, V, and VI permits a determination of the ^1S phase shift, δ, for low energy n–n scattering from the shape of the γ-ray spectrum resulting from the reaction $\pi^-+D\rightarrow 2n+\gamma$. For this purpose it is convenient to relate δ to the familiar parameters[5] characteristic of low energy nucleon-nucleon scattering. The relationship is

$$p\cot\delta=-\alpha+\tfrac{1}{2}r_0p^2, \tag{6}$$

where $1/\alpha$ is the "scattering length" and r_0 the "effective range." The spectrum is not very sensitive to the exact value of r_0, so we have given it the value obtained from p–p scattering:[6]

$$r_0=2.65(10)^{-13}\text{ cm}. \tag{7}$$

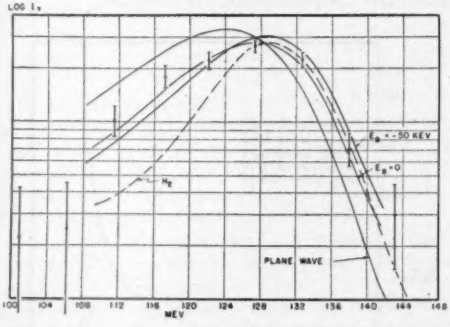

FIG. 4. A comparison of several "folded" theoretical γ-ray spectra for different n–n binding energies with the preliminary experimental data of Aamodt, Panofsky, and Phillips. The $E_B=-50$-kev curve refers to a bound di-neutron state of 50 kev.

[5] J. M. Blatt and J. D. Jackson, Phys. Rev. **76**, 18 (1949) and H. A. Bethe, Phys. Rev. **76**, 38 (1949).

[6] J. D. Jackson and J. M. Blatt, Revs. Modern Phys. **22**, 77 (1950).

The resulting γ-ray spectrum for various assumed values of α was calculated on the basis of the theory to be developed in the following sections. The results are given in Fig. 2 for several negative values of α (i.e., for a potential that has no bound state). Positive values of α correspond to a potential that has a bound di-neutron state. Thus, if α is positive, we have the possibility of forming a bound di-neutron, with a corresponding monochromatic component in the γ-ray spectrum. In Fig. 3 are given the continuous spectra corresponding to several positive values of α. In Table I are given the intensities of the corresponding monochromatic spectra pertaining to formation of a di-neutron. The actual spectrum for a positive value of α is then the sum of the continuous spectrum, as given in Fig. 3, and the monochromatic spectrum, as given in Table I.

III. COMPARISON WITH EXPERIMENT

Aamodt, Panofsky, and Phillips[7] have recently improved earlier measurements[1] of the γ-ray spectrum resulting from π^- absorption in deuterium. In Fig. 4 is given the experimental result along with some of the theoretical curves,[8] as determined in Secs. IV and V. Although these preliminary data have rather poor statistics, it seems clear that positive evidence for the n–n interaction is indicated.

An important qualitative conclusion to be drawn from this point is that a triplet-singlet spin transition does indeed occur, and thus that photomeson production involves an interaction with the nucleon spin. If there were no singlet component present in the spectrum, the resulting triplet spectrum would show even worse agreement with the experimental results than that shown by the plane wave case in Fig. 3.

The results are also quite compatible with an equality of the n–n and p–p singlet forces, although present statistical uncertainties do not permit a quantitative conclusion to be drawn concerning this point. An upper limit, however, of approximately 0.200 Mev can probably be put on the binding energy of the di-neutron.

IV. FORMULATION OF THE PROBLEM

The deuteron is a fairly loosely bound system, the neutron and proton spending a considerable part of the time outside the range of their mutual force. We may thus expect hypothetical nonlinear effects from the overlapping of their meson fields to be small. This conclusion is strengthened when we recall that the absorption of a π-meson by a proton is a high energy process, which should be little affected by the presence of a weakly bound neutron. This suggests that the absorp-

[7] Aamodt, Panofsky, and Phillips, private communication.

[8] The theoretical curves have been "folded" into the experimental energy resolution (see reference 1). If this energy resolution is $S(\epsilon_0-K)$, then the "fold" is

$$\int S(\epsilon_0-K)[dI(K)/dK]dK,$$

where dI/dK is the spectrum as given in Figs. 2 and 3 and Table I.

tion with radiation in deuterium is essentially the same as in hydrogen[1] and is modified primarily by the momentum distribution of the proton in the deuteron and by the n–n interaction. We thus introduce the transition matrix, defined in the center-of-mass system,

$$R \equiv (\mathbf{K}|R|\mathbf{q}) \qquad (8)$$

for the absorption in hydrogen. Here $\mathbf{q}$ is the relative momentum of the meson and proton in the initial state, and $\mathbf{K}$ is that of the photon and neutron in the final state. Because the meson is absorbed essentially from rest under the experimental conditions for which this has been observed, the transition in hydrogen depends only on

$$R^0 = (\mathbf{K}|R|0). \qquad (8')$$

However, the complex conjugate of Eq. (8) is the transition matrix for photomeson production, which has been observed under more general conditions.

The absorption in deuterium takes place from an initial triplet spin state of the n–p system, and it is important to know the relative admixture of singlet and triplet states for the final n–n system. This depends, of course, on the symmetry properties of R [Eq. (8)]. Since, however, for the absorption in deuterium, q is nonvanishing only because of the small effect of the internal motion of the proton in the deuteron (this is discussed in more detail in Sec. VI), we can investigate the simpler symmetry properties of R^0 [Eq. (8′)]. R can be assumed linear in the electromagnetic field strengths, so it must involve linearly either (or both) the electric field $\mathbf{E}$ or the magnetic field $\mathbf{H}$. The only remaining vectors available in R^0 are $\mathbf{K}$ and $\boldsymbol{\sigma}'$, the proton spin. If we make the most likely assumption[2] that the meson is pseudoscalar, R must change sign under coordinate reflection, and we have the unique form for R^0:

$$R^0 = \boldsymbol{\sigma}' \cdot \mathbf{E} R'(K). \qquad (9)$$

This determines the relative admixture of singlet and triplet states as $\frac{1}{3}$ and $\frac{2}{3}$, respectively.

Equation (9) implies that, near threshold at least, photomeson production takes place through an interaction with the nucleon spin. Direct evidence for this would permit us to drop the restrictive assumption that the meson is pseudoscalar. On the other hand, if there were no spin interaction, there would be no final singlet state (since the initial state is triplet), and thus no evidence for the n–n interaction would be found. Happily, we have available the experimental results of Aamodt, Panofsky, and Phillips (see Sec. III), which seem clearly to indicate a ^1S admixture in the final state and thus a spin interaction. If there are not two different competing mechanisms for photomeson production near threshold, we can reasonably except R^0 to have the simple form, $R^0 = \boldsymbol{\sigma}' \cdot \mathbf{A} R'(K)$, where $\mathbf{A}$ is some vector. This is all that we need to determine the above mixture of singlet and triplet states.

Equation (8) is easily generalized to the coordinate system in which the meson-deuteron system is at rest, since the transformation is nonrelativistic and thus R can change by a phase factor only.

TABLE I. Intensities of the monochromatic spectra corresponding to formation of a di-neutron. The monochromatic spikes are separated from the continuum by approximately the binding energy.

Neutron binding energy E_B in Mev	Intensity of monochromatic spike in units of Fig. 3
0.01	34.0
0.05	62.6
0.25	100.6

The transition matrix for the absorption in deuterium is then

$$M^s = (2\pi)^{-6}(\exp[i\mathbf{P}\cdot\mathbf{x} + i\mathbf{K}\cdot\boldsymbol{\rho}]\psi^s, R\omega\phi) \qquad (10)$$

for a final singlet state. Changing "s" to "t" defines it for a final triplet state. Here ω is the coulomb wave function for the meson in the lowest Bohr orbit, and ϕ is the deuteron wave function. The factors $\exp(i\mathbf{P}\cdot\mathbf{x})$ and $\exp(i\mathbf{K}\cdot\boldsymbol{\rho})$ represent the plane wave motion of the center of mass of the two neutrons and the propagation of the photon, respectively. Because the coulomb wave function is very nearly constant over the radius of the deuteron, we can remove ω from the integrals in Eq. (10) and consider it to be a multiplicative factor, ω_0, evaluated at the position of the deuteron. Then a straightforward manipulation of Eq. (8) leads to[3]

$$M^s = \sqrt{2}\omega_0(2\pi)^{-\frac{1}{2}} \int d^3g \int d^3r \psi^{s*}(r) \exp(-\tfrac{1}{2}i\mathbf{K}\cdot\mathbf{r}) \times (\mathbf{K} - (\mu/M+\mu)\mathbf{g}|R|-(\mu/M+\mu)\mathbf{g}) \times \exp(i\mathbf{g}\cdot\mathbf{r})\phi(\mathbf{g}), \qquad (11)$$

where $\phi(\mathbf{g})$ is the momentum representation of ϕ, and R is given by Eq. (8). Here μ is the meson mass, and M is the nucleon mass.

The dependence of R on $\mathbf{g}$ is weakened because of the factor $\mu/(M+\mu)$, which is about $\frac{1}{9}$. The values of g are also limited by the weak binding of the deuteron, whereas R supposedly varies only for changes of its variables of the order of μ, the characteristic energy for meson production. We thus set $g=0$ in R and remove it from the integral in Eq. (11) (a more quantitative estimate of the error hereby incurred is made in Sec. VI).

[3] The occurrence of $\mathbf{g}$ in r [Eq. (11)] is due to the internal motion of the proton in the deuteron. This can be seen as follows: The velocity of the center of mass of the meson and proton is $\mathbf{v} = \mathbf{g}/(M+\mu)$, where $\mathbf{g}$ is the proton momentum. The momenta of the meson and proton in their mutual center-of-mass coordinate system are, respectively, $\mathbf{q}' = -\mu\mathbf{v}$ and $\mathbf{g}' = \mathbf{g} - M\mathbf{v}$. Their relative momentum is thus

$$\tfrac{1}{2}(\mathbf{q}' - \mathbf{g}') = -\mu\mathbf{g}/(M+\mu).$$

But this is the coordinate system in which R is defined [see Eq. (8)].

We then obtain for M^s [see Eq. (9)]

$$M^s=\sqrt{2}\omega_0 R'(K)\int d^3r\psi^{*s}(r)\exp(-\tfrac{1}{2}i\mathbf{K}\cdot\mathbf{r})\boldsymbol{\sigma}'\cdot\hat{e}\phi(r), \quad (12)$$

where we now use the polarization vector $\hat{e}$ of the photon, rather than $\mathbf{E}$ as in Eq. (9), absorbing a numerical factor in $R'(K)$. Here $\phi(r)$ is the coordinate representation of ϕ. We replace the superscript "s" by "t" to define the transition matrix for final triplet states of the n–n system.

If we neglect the n–n interaction for all but the ^1S state (this will be justified in Sec. VI), we have the following wave functions:[10]

$$\begin{aligned}\phi(r)&=[\chi_t{}^m\phi_0(r)+2^{-\frac{1}{2}}\{[3(\boldsymbol{\sigma}^1\cdot\mathbf{r})(\boldsymbol{\sigma}^2\cdot\mathbf{r})/r^2]-1\}\chi_t{}^m\phi_2(r)],\\ \psi^t(r)&=(1/\sqrt{2})[e^{i\mathbf{p}\cdot\mathbf{r}}-e^{-i\mathbf{p}\cdot\mathbf{r}}]\chi_t{}^{m'},\\ \psi^s(r)&=(1/\sqrt{2})[e^{i\mathbf{p}\cdot\mathbf{r}}+e^{-i\mathbf{p}\cdot\mathbf{r}}-(2/pr)\sin pr+2\psi_0]\chi_s,\end{aligned} \quad (13)$$

where ψ_0 is the S-wave part of ψ^s, with due account taken for the n–n interaction. $\chi_t{}^m$ and χ_s are triplet and singlet spin wave functions, respectively. ϕ_0 and ϕ_2 are the radial parts of the S- and D-wave components, respectively, of the deuteron wave function. We shall neglect the contribution of ϕ_2 to all but the integral involving the S-wave part of ψ^s, for which its effects will be the largest.

We introduce the following definitions:

$$\begin{aligned}I^t&=\int d^3r[e^{-i\mathbf{p}\cdot\mathbf{r}}-e^{i\mathbf{p}\cdot\mathbf{r}}]e^{-\frac{1}{2}i\mathbf{K}\cdot\mathbf{r}}\phi_0(r),\\ I_1&=\int d^3r[e^{-i\mathbf{p}\cdot\mathbf{r}}+e^{i\mathbf{p}\cdot\mathbf{r}}-(2/pr)\sin pr]e^{-\frac{1}{2}i\mathbf{K}\cdot\mathbf{r}}\phi_0(r),\\ I_2&=2\int d^3r\psi_0{}^*(r)e^{-\frac{1}{2}i\mathbf{K}\cdot\mathbf{r}}\phi_0(r),\\ I_3&=2\int d^3r\psi_0{}^*(r)(\pi/Kr)^{\frac{1}{2}}J_{\frac{1}{2}}(\tfrac{1}{2}Kr)\phi_2(r).\end{aligned} \quad (14)$$

Then

$$M^s=\omega_0R'(K)\Big\{(\chi_s,\boldsymbol{\sigma}'\cdot\hat{e}\chi_t{}^m)[I_1+I_2]-2^{-\frac{1}{2}}\Big(\chi_s,\boldsymbol{\sigma}'\cdot\hat{e}\Big[\frac{3(\boldsymbol{\sigma}'\cdot\mathbf{K})(\boldsymbol{\sigma}^2\cdot\mathbf{K})}{K^2}-1\Big]\chi_t{}^m\Big)I_3\Big\}, \quad (15)$$

and

$$M^t=\omega_0R'(K)(\chi_t{}^m,\boldsymbol{\sigma}'\cdot\hat{e}\chi_t{}^m)I^t. \quad (16)$$

The volume in phase space per unit photon energy accessible to the particles in the final state is

$$dJ=2K^2d\Omega_K(Mp/2)d\Omega_p, \quad (17)$$

where the $d\Omega$ are elements of solid angle. Defining

$$\begin{aligned}G^t&\equiv(1/4\pi)\int d\Omega_p|I^t|^2,\\ G^s&\equiv(1/4\pi)\int d\Omega_p|I_1+I_2|^2,\end{aligned} \quad (18)$$

we have for the transition rates per unit photon energy

$$\begin{aligned}dT^t/dK&=\tfrac{3}{4}2(2\pi)^3\omega_0{}^2|R'(K)|^2K^2MpG^t,\\ dT^s/dK&=\tfrac{1}{4}2(2\pi)^3\omega_0{}^2|R'(K)|^2K^2Mp\{G^s-\sqrt{2}I_2I_3\},\end{aligned} \quad (19)$$

where in the latter expressions we have kept only the largest term involving I_3—the D-state part of the deuteron wave function.

There is also the possibility that there exists a bound di-neutron ^1S state. Denoting this wave function by $\psi^B\chi_s$, we obtain the transition matrix to form a bound di-neutron by replacing $\sqrt{2}\psi_0{}^*$ in I_2 [Eq. (14)] by $(2\pi)^{\frac{1}{2}}\psi^{*B}$ to give a new integral, say, $I_2{}^B$. The resulting spectrum is monochromatic, and its intensity is given to a sufficient approximation by

$$T^B=\tfrac{1}{4}4(2\pi)^2K^2\omega_0{}^2|R'(K)|^2|I_2{}^B|^2. \quad (20)$$

V. EVALUATION OF THE INTEGRALS

For the S-wave part of the deuteron wave function, that is, $\phi_0(r)$, we use the Chew-Goldberger[11] expression

$$\phi_0(r)=N(e^{-\alpha r}-e^{-\beta r})/r, \quad (21)$$

where $\alpha=(Me_D)^{\frac{1}{2}}$, and $\beta=7\alpha\cdot e_D$ is the deuteron binding energy. As the recoil neutron energies in which we are interested are small, the integrals involving $\phi_0(r)$ do not depend critically on its form at close distances. Indeed, most of the contribution comes from values outside the range of the n–p potential, where the term $e^{-\alpha r}/r$ is rigorous. The correction arising from the term $e^{-\beta r}/r$ is small and fairly reliable. (The value of β is determined by the low energy n–p triplet scattering.[11])

The D-state part of the deuteron wave function, ϕ_2, occurs in our approximation only in I_3. Because of the smallness of $J_{\frac{1}{2}}$ near the origin, contributions to I_3 from distances within the nuclear potential are quite negligible, and we can use the asymptotic form for ϕ_2, the functional form of which is, of course, independent of the exact nature of the tensor force. The ratio ϕ_2/ϕ_0 in the asymptotic range is only approximately known,[12] but seems sufficiently reliable for our purposes, since the D-state correction is small anyway. Evaluation of I_3 in the vicinity of the high energy limit of the γ-spectrum indicates that the term $\sqrt{2}I_2I_3$ in Eq. (19) amounts to about a three percent correction to G^s. The actual importance of this correction is considerably less, how-

[10] W. Rarita and J. Schwinger, Phys. Rev. **59**, 436 (1941).

[11] G. F. Chew and M. L. Goldberger, Phys. Rev. **77**, 470 (1950). For our application the contribution from the term $e^{-\beta r}/r$ is nearly independent of this specific functional form, being expressible in terms of the n–p triplet effective range. See H. A. Bethe and C. Longmire, Phys. Rev. **77**, 647 (1950).

[12] R. S. Christian and E. Hart, Phys. Rev. **77**, 441 (1950).

ever, since according to the arguments given in the Introduction, the functional form of I_2I_3 is approximately the same as that of G^*. Thus, the correction amounts primarily to about a three percent decrease in the magnitude of the transition rate rather than a change in the shape of the spectrum. In any case it is negligible as far as present requirements as to accuracy are concerned. It should be noted that the smallness of this correction is due more to the smallness of the overlap of J_1 and ϕ_2 than to the actual smallness of ϕ_2.

Using the form (21) for ϕ_0, the evaluation of I' and I_1 [Eq. (14)] is straightforward.

For the evaluation of I_2, we proceed as outlined in the Introduction. Set

$$I_2=I_2'+I_2'',$$

where

$$I_2'=2\int d^3r[\sin(pr+\delta)/pr]e^{-\frac{1}{2}i\mathbf{K}\cdot\mathbf{r}}\phi_0(r),$$
$$I_2''=2\int d^3r[\psi_0^*(r)-\sin(pr+\delta)/pr]e^{-\frac{1}{2}i\mathbf{K}\cdot\mathbf{r}}\phi_0(r). \tag{22}$$

Again the evaluation of I_2' is elementary. For I_2'', the method described in the Introduction can be carried out in a fairly reliable manner, but for the additional correction of the order of 3 percent we have used the exact wave functions for a square well, whose depth and range were chosen to give the assumed phase shift, δ.

The bound di-neutron wave function has the form

$$\psi^B=N_Be^{-\alpha r}/r \tag{23}$$

outside the range of the n–n force. Corrections can be obtained as described in connection with Eq. (22). $\gamma=(ME_B)^{\frac{1}{2}}$, where E_B is the assumed binding energy of the di-neutron.

VI. ESTIMATES AS TO THE VALIDITY OF THE THEORY

We now inquire further into the justification for removing R from under the integral in Eq. (11) and into the expected behavior of $R'(k)$ in Eq. (12). For instance, both the absorption in hydrogen and photomeson production depend upon R only on the energy shell, whereas in Eq. (11) we need more general values —although, indeed, these are not far from the energy shell, as argued above. In particular, the threshold for photomeson production in the center-of-mass system (and the energy of the γ-ray for the absorption in hydrogen) is at a γ-ray energy of about 131 Mev. The peak of the γ-ray spectrum for the absorption in deuterium, on the other hand, occurs at about 132 Mev. Thus, in the vicinity of the peak of the spectrum, which is the region of most interest to us, the γ-ray energy lies very close to its value defined by the energy shell for photomeson production.

In the hope of obtaining further information about the matrix R, we have analyzed the excitation function of Steinberger and Bishop[13] for photomeson production. Transforming this to the center-of-mass system and removing the phase space factor, we have essentially

$$\Gamma\equiv|(\mathbf{K}|R|\mathbf{q})|^2 \tag{24}$$

[see Eq. (8)] on the energy shell. The experiments measure this down only to within 20 Mev of threshold and are not very accurate in this region. Nevertheless, they were consistent with a constant Γ near threshold. This did not agree very well with the Γ as deduced from pseudoscalar meson theory, since this has a factor $1/K$ [$1/\sqrt{K}$ in $R'(K)$ of Eq. (12)]. Again, a Γ, as deduced on the basis of an interaction with the nucleon magnetic moments, behaves as q^2 near threshold and is in violent disagreement with the experimental results.

In view of these considerations, we have taken $R'(K)$ as a constant in Eq. (18) for the numerical results given in Sec. II. A correction for any other assumed functional dependence on K can be easily obtained merely by multiplying each point on the spectra given by the corresponding value of $|R'(K)|^2$. The errors incurred are, in any case, small near the interesting part of the spectrum, and are very unlikely to be of much importance since there are few γ-rays emitted at much lower energies. This uncertainty does, however, make it desirable to employ as sharp an energy resolution as possible in measuring the spectrum, so that the low energy tail of the spectrum will not enter into the determination of the n–n force. More complete measurements of the excitation function for photomeson production may also be of help in resolving this difficulty, which at present constitutes, perhaps, the greatest uncertainty in the theoretical analysis.

We have mentioned that the absorption in hydrogen does prove that $(\mathbf{K}|R|\mathbf{q})$ [Eq. (8)] approaches a constant limit as q approaches zero. In order to remove R from the integral in Eq. (11), we must also assume that R does not have a singular behavior near $q=0$. Aside from the somewhat inconclusive evidence from the excitation function for photomeson production, the arguments that this is not the case are twofold: (1) There is a rather weak argument from pseudoscalar meson theory, which fits quite well the angular distribution for photomeson production,[14] that $(\mathbf{K}|R|\mathbf{q})$ varies smoothly with q as q approaches zero. (2) The relative amounts of observed absorption with and without radiation[1] as analyzed[2] on the basis of detailed balancing arguments from photomeson production and meson production in nucleon-nucleon collisions are quite consistent with a smooth, slow variation of $(\mathbf{K}|R|\mathbf{q})$ to its value at threshold. On the other hand, even a linear dependence of $(\mathbf{K}|R|\mathbf{q})$ on $\mathbf{q}$ near threshold would decrease the rate of radiative absorption to about one percent of its previously calculated value[2] and make it difficult to account for the observed ratio.

[13] J. Steinberger and A. S. Bishop, Phys. Rev. **78**, 493 (1950); A. S. Bishop, Thesis, University of California (unpublished). The corrections for absorption were included.

[14] K. A. Bruckner, Phys. Rev. **79**, 641 (1950).

The meson rest mass, μ, is the natural parameter to describe the structure of R. That is $K/\mu \simeq 1$ and $\mathbf{q}/\mu$ would seem to be the proper dimensionless parameters to describe its functional behavior. This was, indeed, seemingly borne out from the analysis of the experimental excitation function. Γ [Eq. (24)] was roughly constant for $q<\mu$ and showed a marked change in slope (decreasing rapidly) for $q>\mu$. On this basis, we can now estimate the error incurred by removing R from the integral in Eq. (11). For purposes of the argument, we define a "modified deuteron wave function" as

$$\phi'(\mathbf{g})=R[\mu\mathbf{g}/(M+\mu)]\phi(\mathbf{g}), \tag{25}$$

where R is the matrix element of Eq. (11). Since we have argued that R is approximately constant for small q, we can expect the coordinate representation of ϕ' to differ from that of ϕ only in the vicinity of the origin. This is fortunate, as we have seen that our results do not depend much on the form of the deuteron wave function near the origin. Using the Chew-Goldberger wave function, we can write Eq. (25) as

$$\phi'(\mathbf{g})=R[\mu\mathbf{g}/(M+\mu)]/(\alpha^2+g^2)(\beta^2+g^2). \tag{25'}$$

As we have noted that the functional dependence of R on q is apparently such that it becomes important when $\mu g/(M+\mu)\simeq\mu$, we can define the following parameters to describe the values of g for which the three factors in Eq. (25') become important:

$$\alpha=45.5 \text{ Mev}, \quad \beta=318 \text{ Mev},$$
$$[(M+\mu)/\mu]\mu=1080 \text{ Mev}.$$

We have stated that the factor $(\beta^2+g^2)^{-1}$ gives only a small correction to the results, so it follows that any correction due to the variation of R with g is likely to be much less. Indeed, this uncertainty may very well be of the same order as the uncertainty in the deuteron wave function.

As to uncertainty in the deuteron wave function, we note that the factor $(\beta^2+g^2)^{-1}$ in Eq. (25'), or $e^{-\beta s}/r$ in Eq. (21), gives a correction of less than 10 percent to the leading term in Eqs. (14). Since this correction is quite reliable,[11] it would seem that the error resulting from the uncertainty in the deuteron wave function is, indeed, small.

The p-wave phase shifts for the final n–n state have been verified to be negligibly small over the energy range for which there are an appreciable number of γ-rays. Thus, the use of plane waves for ψ' in Eq. (13) is well justified.

To summarize our arguments, we note that the gross features of the spectrum seem to be well determined independently of the details in the calculations. The general shape of the tail of the spectrum at lower energies is determined by the deuteron wave function. According to the arguments given in the Introduction, the shape of the spectrum near the high energy limit is given quite accurately by Eq. (4). At lower energies we must rely for the detailed shape of the spectra on the arguments for removing R in Eq. (11) from under the integral sign. But here the exact identification of R with the matrix element for photomeson production is not necessary.[15] We need only the argument that R approaches a constant value smoothly as q approaches zero. If R is only to a fair approximation related to the matrix element for photomeson production, we can still expect the detailed balancing arguments[2] quoted above to apply.

VII. CONCLUSION

It appears that the γ-ray spectrum resulting from the absorption of π^- mesons in deuterium offers considerable promise for a quantitative determination of the parameters characteristic of low energy n–n scattering. A better experimental determination of the excitation function for photomeson production near threshold should make it possible to resolve the greatest of the present uncertainties in the theory. In any case, the calculated spectrum would seem to be quite accurate near its high energy limit (and is probably quite accurate over the entire energy range for which an appreciable number of γ-rays are emitted).

The authors are indebted to Professor R. Serber and to Dr. K. A. Brueckner, with whom the initial phases of the present work were done in connection with the considerations reported in reference 2. To Dr. L. Aamodt, Professor W. K. H. Panofsky, and Mr. Robert Phillips, we are indebted for encouragement concerning the feasibility of measuring the γ-ray spectrum and for permission to quote the experimental results in advance of their publication.

[15] Deviation of the R in Eq. (11) from the transition matrix for photo-meson production can be expected to be of importance only when the neutron and proton are very close together in the deuteron. However, we have seen that our results are insensitive to the nature of the interactions at close distances.

Letters to the Editor

PUBLICATION of brief reports of important discoveries in physics may be secured by addressing them to this department. The closing date for this department is five weeks prior to the date of issue. No proof will be sent to the authors. The Board of Editors does not hold itself responsible for the opinions expressed by the correspondents. Communications should not exceed 600 words in length.

Interaction of Pi-Mesons with Carbon and Aluminum Nuclei

M. CAMAC, D. R. CORSON, R. M. LITTAUER, A. M. SHAPIRO, A. SILVERMAN, R. R. WILSON, AND W. M. WOODWARD
*Cornell University, Ithaca, New York**
(Received April 9, 1951)

THE experimental arrangemeut used for the production and observation of pi-mesons is shown in Fig. 1. The target T is exposed to 310-Mev bremsstrahlung radiation. Mesons produced

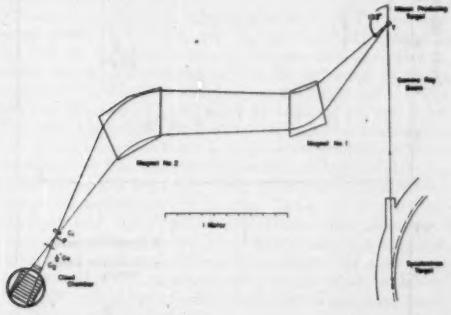

FIG. 1. Experimental arrangement of magnets and detectors.

in the target enter the double-focusing magnetic analyzer,[1] after which they are detected by a coincidence between Geiger counters C_1 and C_2 which triggers a 12-in. cloud chamber. The focusing properties of the magnets were investigated with a current carrying wire, and the magnetic fields were adjusted so that 60-Mev mesons were focused at point P.

The cloud chamber has provision for mounting nine absorber plates. To investigate the nature of the particles entering the cloud chamber, preliminary experiments were done with ¼-in. copper plates placed in the chamber. The range distribution of 91 particles is shown in Fig. 2. It is seen that approximately 80 percent of the particles have ranges between 15 g/cm² and 23 g/cm² corresponding to pi-meson energies between 55–70 Mev. The two tracks with ranges about 30 g/cm² are assumed to be mu-mesons. The tracks with ranges between 6 and 12 g/cm² are mesons which have undergone nuclear interactions. From the mean scattering angle of the particles in the copper and the absence of shower production, it is clear that the electron contamination is small. Of the 91 tracks observed, one was probably an electron.

The interaction of pi-mesons with carbon and aluminum was studied by mounting either carbon or aluminum plates in the cloud chamber. Light elements were chosen to minimize coulomb scattering and to increase the angular width of the diffraction scattering. The types of events observed were large angle scatterings, stars with 0, 1, and 2 prongs, and small angle scatterings. A large angle scattering is defined as being at an angle greater than

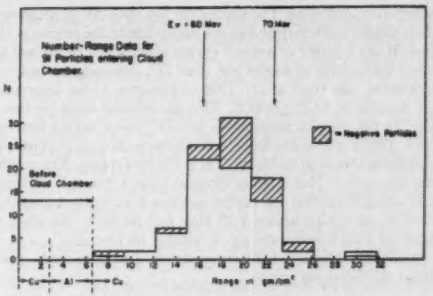

FIG. 2. Range distribution among 90 particles entering the cloud chamber containing ¼-in. Cu plates.

the first zero of the diffraction scattering distribution (75° in the case of carbon and 50° for aluminum). Figure 3 shows a picture of a large angle scattering and a star. There is some ambiguity in differentiating between large angle scatterings and one prong stars. However, these events are lumped together in the analysis of the data. Events which appeared to be scatterings of about 15° in the gas were also observed. These were almost certainly pi-mu decays.

Carbon Results:—In 4187 traversals of ¼-in. carbon plates, by approximately equal numbers of positive and negative mesons, the following events were observed:

	Scatterings		
Stars	(>75°)	(20°–75°)	(10°–20°)
17	3	7	21

The stars and large angle scatterings are assumed to be specific nuclear events. The scatterings from 20°–75° are assumed to be due

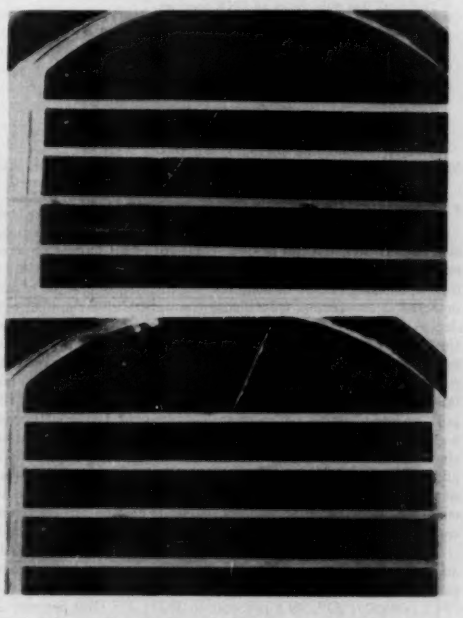

FIG. 3. A large angle scattering and a nuclear star produced by π^+ mesons in flight through ¼-in. Al plates.

to diffraction scattering. The scatterings less than 20° were ignored, since coulomb scattering and pi-mu decay falsify the results in this region. If the number of nuclear events is corrected to include the nuclear scatterings at angles less than 75°, assuming an isotropic distribution, the total is 21. This corresponds to an interaction cross section of (0.22±0.05)b. The geometrical cross section is 0.37b. In the angular range from 20°–75°, seven events were observed. This is reduced to five if one subtracts the expected number of nuclear scatterings and pi-mu decays in this region. The number to be expected in this angular interval from a "black" nucleus is 26. It seems clear that the carbon nucleus is partially transparent to mesons of energy between 20 Mev and 60 Mev. The data are consistent with a transparency of roughly 60 percent.

Aluminum Results:—1323 traversals of ¼-in. aluminum plates yielded the following results:

	Scatterings		
Stars	(>50°)	(20°–50°)	(10°–20°)
6	5	4	10

Correcting the large angle scatterings as above, we obtain 12 nuclear events, corresponding to a cross section of (0.48±0.14)b. The geometrical cross section is 0.60b. The expected number of diffraction scatterings in the 20°–50° region for a "black" aluminum nucleus is 8, while the corrected observed number is 3. The data are consistent with a nuclear transparency of about 80 percent but do not exclude a "black" nucleus.

An additional result of the experiment, obtained by reversing the magnetic field of the analyzer, is the ratio of negative to positive mesons produced in several targets. For meson energies between 55 Mev and 70 Mev, this ratio is 1.12±0.07 for carbon and 2.40±0.20 for beryllium. The carbon result is in good agreement with the results of Peterson, Gilbert, and White.[2] It seems likely that the high ratio in beryllium is due to the extra neutron. The result depends on the decay time for π^+ and π^- mesons being the same.

* This work was done under an ONR contract.
[1] M. Camac, Rev. Sci. Instr. **22**, 197 (1951).
[2] Peterson, Gilbert, and White, Phys. Rev. **81**, 1003 (1951).

Production of Photomesons*

RAPHAEL M. LITTAUER AND DARCY WALKER
Newman Laboratory of Nuclear Studies, Cornell University, Ithaca, New York
(Received April 9, 1951)

THE beam of bremsstrahlung from the 300-Mev electron synchrotron was allowed to strike targets containing various elements in their natural isotopic compositions. Charged mesons[1] emitted at 135°, and of energies about 50 Mev, were selected by a double-focusing system of magnets (see the preceding letter),[2] and detected in an array of coincidence counters. Cloud-chamber evidence[3] as well as rough absorption measurements indicated that the contamination of the meson beam by electrons, if any, was extremely small. A small percentage of μ-mesons was observed, but since these represent decay products of the π-mesons they do not falsify the present results, unless the decay characteristics of the positive and negative π-mesons are not identical. In the latter case a systematic error could be present in the measured π^-/π^+ ratios, since the time of flight of the mesons through the apparatus is about ½ the mean life. The densities of the targets (except Be) were so adjusted that they had equal stopping powers for mesons. All counting rates were normalized to unit gamma-ray flux and corrected for gamma-ray absorption in the thickness of the target.

The elements so far examined are: $_1H^1$ (99.98 percent) in H_2O and in hydrocarbon mixtures of suitable density and known composition; $_1D^2$ (>99.8 percent) in D_2O; $_4Be^9$ (100 percent); $_6C^{12}$ (98.9 percent); $_8O^{16}$ (99.8 percent) in H_2O; $_9F^{19}$ (100 percent) in $(CF_2)_n$; $_{13}Al^{27}$ (100 percent); $_{16}S^{32}$ (96 percent); $_{20}Ca^{40}$ (96.8 percent) in CaF_2; and $_{83}Bi^{209}$ (100 percent).

Assuming that the photoproduction of mesons takes place according to the reactions

$$p+\gamma \rightarrow n+\pi^+$$

and

$$n+\gamma \rightarrow p+\pi^-,$$

we have calculated the production cross sections *per relevant nucleon* for each of the above elements. The results are displayed in Fig. 1, where the cross sections have been normalized arbitrarily

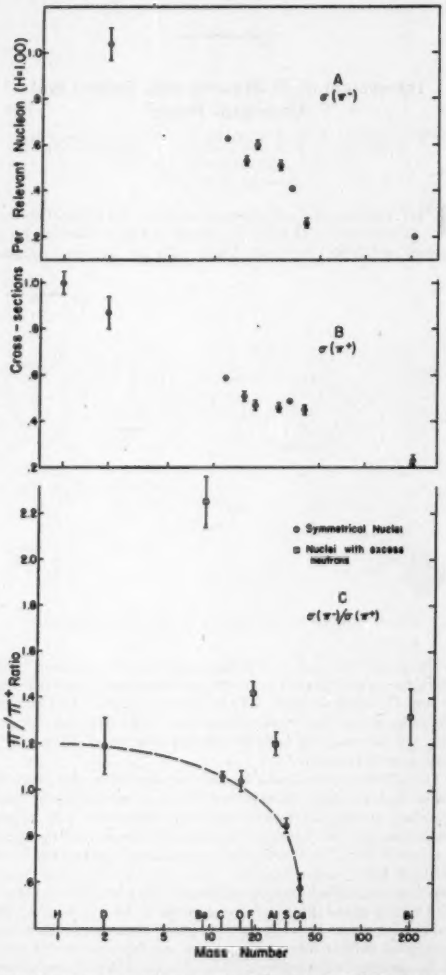

FIG. 1. A: π^- cross section per neutron; B: π^+ cross section per proton; C: π^-/π^+ ratio for the whole nucleus. Meson energy ~50 Mev, angle of emission (lab. system) =135°. Errors are statistical standard deviations.

to $\sigma_{\pi^+}(H)=1.00$. On this scale, the π^- cross section for H is 0.04±0.05. The π^- and π^+ cross sections of D do not differ very significantly from the π^+ cross section of H. Figure 1(c) shows the π^-/π^+ ratio for each *nucleus*. The sum of the π^- and π^+ cross sections *per nucleus* has been plotted logarithmically against mass number in Fig. 2; the points from D to Bi follow an $A^{\frac{1}{3}}$ law fairly

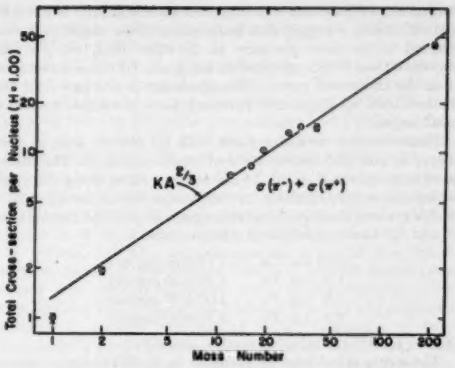

FIG. 2. Sum of π^- and π^+ cross sections per nucleus.

closely, i.e., $\sigma_{total} \sim$ surface area of the nucleus. This would be the expected law if mesons created below the surface had a small escape probability.[3]

The results exhibit some interesting features. (1) For the symmetrical nuclei D, C, O, S, and Ca, the π^-/π^+ ratio, which is 1.19 ± 0.12 for D, shows a steady decrease with increasing A, reaching the value 0.58 ± 0.06 for Ca. Unfortunately no stable symmetrical nuclei exist in nature above the magic Ca^{40}. (2) The nuclei Be^9, F^{19}, and Al^{27}, each with an unpaired neutron, have π^-/π^+ ratios lying considerably above the curve for symmetrical nuclei. If we assume that this enhanced ratio is due entirely to the production of π^- from the unpaired neutron, we can calculate the cross section for this neutron in terms of the cross section for one of the paired neutrons in the nucleus. The ratios obtained are 4.6 ± 0.5, 3.8 ± 0.5, and 3.9 ± 0.7 for Be^9, F^{19}, and Al^{27}, respectively. Clearly, under this quite arbitrary assumption, the unpaired neutrons in all three nuclei would make roughly the same large contribution. However, it is interesting to note that the heavy nucleus Bi^{209}, which contains 50 percent excess neutrons, has a π^-/π^+ ratio of only 1.32 ± 0.12.

One of us (Darcy Walker) is indebted to the Commonwealth Fund for support.

* This work performed under contract with the ONR.

[1] McMillan, Peterson, and White, Science 110, 579 (1949); J. Steinberger and A. S. Bishop, Phys. Rev. 78, 494 (1950); Peterson, Gilbert, and White, Phys. Rev. 81, 1003 (1951).
[2] Camac, Corson, Littauer, Shapiro, Silverman, Wilson, and Woodward, Phys. Rev. 82, 745 (1951).
[3] R. F. Mozley, Phys. Rev. 80, 493 (1950).

Ratio of Negative to Positive π-Mesons in the Stratosphere*

W. F. FRY
Department of Physics, Iowa State College, Ames, Iowa
(Received April 10, 1951)

SINGLE stacks of 12 electron sensitive NTB-3 plates were exposed in the stratosphere by means of meteorological balloons at altitudes near 60,000 feet. On the average a total of 500 grams of material, consisting mainly of Al, glass, and paper was in the immediate vicinity of the plates. The plates weighed an additional 100 grams. They were searched for meson tracks which stopped in the emulsion. Incidental to a study of low energy electrons from μ-mesons,[1] the number of meson induced stars and the number of π-μ-decays were noted. A total of 118 meson stars and 41 π-μ-decays were found in the same plates, along with 500 mesons which stopped in the emulsion without associated particles other than electrons. It has been shown that essentially all of the negative π-mesons which stop in photographic emulsions are captured and do not decay,[2] while essentially all of the positive π-mesons which stop in photographic emulsions decay into μ-mesons.[3] It is known that 27 percent of the negative π-mesons which stop in photographic emulsions do not produce stars.[4] Recent studies[5] indicate that 8.7 ± 1.7 percent of the negative μ-mesons cause stars in photographic emulsions. Nearly all of these stars are one prong stars. This conclusion is further substantiated by a comparison of the prong distribution of the 118 meson stars with the known prong distribution of stars produced by negative π-mesons.[4] Correcting for the number of negative π-mesons which did not produce stars, 37 ± 6 percent of the mesons produced one prong stars. Assuming that 8.7 percent of the negative μ-mesons produced one prong stars, then 26 ± 6 percent of the negative π-mesons produced one prong stars which is in agreement with the results of Adelman and Jones[4] who found that 23.6 percent of the negative π-mesons which stopped in photographic emulsions produced one prong stars.

Of the 118 stars due to mesons, about $(500)(0.087)/2=22$ are caused by negative μ-mesons. The remaining 96 stars are presumably due to negative π-mesons. Correcting for the number of negative π-mesons which did not produce stars in the emulsion, the ratio of negative to positive low energy π-mesons would seem to be $(96)/(0.73)(41)=3.2\pm0.7$. This ratio is in agreement with similar measurements at lower altitudes. Bonetti[6] found 89 σ-stars and 45 π-μ-decays in plates exposed at 2800 meters. Barton, George, and Jason[7] found the ratio of negative to positive π-mesons to be 3.1 ± 0.25 in plates exposed under carbon absorbers at 3457 meters. However, Barbour[8] found 87 σ-stars and 147 π-μ-decays in plates exposed in a magnetic field at altitudes of 70,000 and 90,000 feet.

Since the π-mesons traversed the glass backing of the outer plates, they must have been created with a kinetic energy greater than 6 Mev. Similarly, an estimate can be made of the maximum initial kinetic energy of the π-mesons which stopped in the emulsion, by assuming that they traversed the entire stack of plates. Since the lifetime of the π-mesons is very short, the energy lost in the air is small. Therefore nearly all of the π-mesons which stopped in the emulsions must have been generated with a kinetic energy in the interval from 6 to 50 Mev. It is to be expected that the probabilities of escaping from a nucleus would be about the same for negative or positive π-mesons if their energy were greater than the potential energy of the barrier. Assuming that p-p and p-n interactions are about equal, the relative numbers of negative and positive π-mesons should be determined essentially by the number of ways that mesons of either sign can be formed.[9] The excess of negative π-mesons indicates that a large portion of the low energy mesons ($6\ \text{Mev}<E<50$ Mev) are produced at these altitudes by neutrons.

* Supported in part by grants from the Research Corporation and the Iowa State College Research Foundation.

[1] W. F. Fry, Phys. Rev. 79, 893 (1950).
[2] H. Bradner, Univ. Calif. Rad. Report No. 486, 1949 (unpublished).
[3] F. M. Smith, Phys. Rev. 81, 897 (1951).
[4] F. L. Adelman and S. B. Jones, Phys. Rev. 75, 1468A (1949).
[5] E. P. George and J. Evans, Proc. Phys. Soc. (London) 64, 193 (1951).
[6] A. Bonetti, private communication (1950).
[7] Barton, George, and Jason, Proc. Phys. Soc. (London) 64, 175 (1951).
[8] I. Barbour, Phys. Rev. 78, 518 (1950).

Angular Distribution of Photons in Showers in Lead*

JACK W. ROSE
Radiation Laboratory, Department of Physics, University of California, Berkeley, California
(Received April 16, 1951)

A STUDY of the angular distribution of photons in showers in lead has been carried out using the 322-Mev x-ray beam of the Berkeley synchrotron.[1] The experimental arrangement is shown in Fig. 1. The x-ray beam, collimated to $\frac{1}{4}$ inch, produced

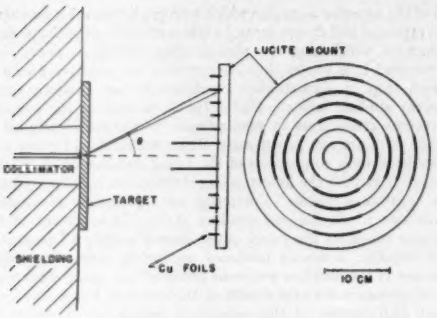

FIG. 1. Experimental arrangement.

showers in a target which usually was a slab of lead. The shower photons emerging from the target at various angles with the incident beam were detected by the radioactivity induced in copper foils. The 16-mil thick foils were 3-inch squares used whole or cut into halves or fourths and mounted as cylindrical segments with the beam as their axis. The mount was 21 cm from the target for angles $<31°$. For data at angles $>31°$ the mount was 11 cm from the target and only the outer four foil positions were used.

The reaction employed was $Cu^{63}(\gamma, n)Cu^{62}$, the Cu^{62} undergoing decay with a ten-minute half-life. The excitation curve of this reaction has a peak at 17.5 Mev and a full width at half-maximum of about 5½ Mev;[2] hence the photons detected are those of energy near 17.5 Mev. After a 20-minute bombardment the fractional foils at a given angle were Scotch-taped together to form "standard" 3-inch square foils and were counted along with the monitor foil for 15 minutes using Victoreen 1B85 aluminum walled Geiger tubes.

Primarily this work was carried out with a target of 2.8 shower units of lead (taking 1 s.u. = 0.52 cm of Pb). 2.8 shower units is roughly the depth in lead at which there are a maximum number of gammas which can produce the reaction $Cu^{63}(\gamma, n)Cu^{62}$, and also it is about the depth at which maximum ionization occurs. Distributions at the shower maximum are easiest to calculate theoretically. The experimental results for 2.8 shower units are shown in curve 1, Fig. 2. The background, which is the relative activity observed when the target was absent, ranged between 15 percent at small angles to 10 percent at large angles. There was no straightforward way of subtracting off this background, but the relative error introduced is probably less than 10 percent. Points on the theoretical curve as calculated by Eyges and Fernbach[3] are indicated by the X's. The two curves are arbitrarily set equal at 9°. The agreement in shape seems good. To further compare the

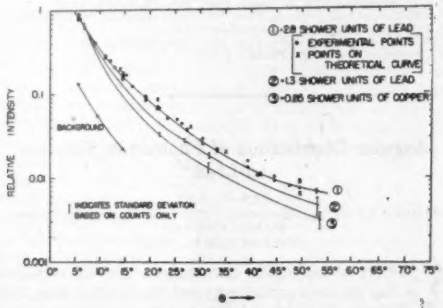

FIG. 2. Angular distribution of photons in showers in lead and copper.

two curves the total flux was integrated experimentally between 0° and 5½°, using a copper disk intercepting these angles and normalized to the same geometry as the other detectors. For the curves equal at 9° the experimental integral is 1.3 times the integral from the theoretical curve. This agreement is not bad since the method used by Eyges and Fernbach gives unreliable results at small angles.

Measurements were also made with 1.3 shower units of lead (curve 2) and 0.85 shower units of copper (curve 3). The curves have been set equal to the 2.8 shower unit curve at 7½. No theoretical curves were available for comparison. For curves normalized in this manner the experimental integrals of the total flux between 0° and 5½° have the following relative values:

0.85 s.u. Cu	1.75±10 percent
1.3 s.u. Pb	1.59±10 percent
2.8 s.u. Pb	1.00±10 percent
5.9 s.u. Pb	0.70±10 percent.

(Curve for 5.9 s.u. taken at small angles only.)

The writer is indebted to Professor A. C. Helmholz for helpful discussions of this work.

* This work was sponsored by the AEC.
[1] J. W. Rose, Phys. Rev. **81**, 649A (1951).
[2] B. C. Diven and G. M. Almy, Phys. Rev. **80**, 407 (1950).
[3] L. Eyges and S. Fernbach, Phys. Rev. **82**, 307A (1951).

Nuclear Magnetic Resonance Fine Structure in Liquids

H. S. GUTOWSKY AND D. W. MCCALL
Noyes Chemical Laboratory, University of Illinois, Urbana, Illinois*
(Received April 16, 1951)

MULTIPLE nuclear magnetic resonance lines with separations of about 0.3 and 0.7 gauss, respectively, have been observed for F^{19} and P^{31} in several liquid phosphorus halides. The ratio of the P^{31} line splitting to that for F^{19}, in the same compound, equals $\mu(F^{19})/\mu(P^{31})$, indicating that the effect is associated with the local nuclear magnetic-dipole fields in the molecule. In the simpler, rigid-lattice solids, these local fields may split the resonance line into several components separated by as much as 5 to 10 gauss.[1] In liquids, molecular rotation ordinarily produces a zero time average for the local fields and single, narrow lines result.[2] The appearance of multiple nuclear magnetic resonance lines in particular liquids suggests an appreciable restriction of molecular rotation[3] in the liquid state.

Observations were made on $POCl_3$, $POCl_2F$, $POClF_2$, and CH_3OPF_2, at room temperature in an applied field of 6365 gauss, using the equipment and general procedures described previously.[4] The F^{19} magnetic resonances in all of the fluorine containing compounds are doublets with components of equal intensity. The P^{31} magnetic resonance is a singlet in $POCl_3$ and a doublet in $POCl_2F$ with components of equal intensity. In $POClF_2$ and CH_3OPF_2 the P^{31} resonance is a triplet in which the central line is double the intensity of the two equal, symmetrically placed satellites. The separations in gauss between adjacent components are summarized in Table I. The widths of the individual components

TABLE I. Multiple F^{19} and P^{31} nuclear magnetic resonance lines in liquids at room temperature.

	F^{19}		P^{31}		P^{31} splitting[c]
	Structure[a]	Splitting[b]	Structure[a]	Splitting[b]	F^{19} splitting
$POCl_3$	—	—	singlet	0.000 gauss	—
$POCl_2F$	doublet(1–1)	0.294 gauss	doublet(1–1)	0.684	2.328
$POClF_2$	doublet(1–1)	0.270	triplet(1–2–1)	0.658	2.356
CH_3OPF_2	doublet(1–1)	0.320	triplet(1–2–1)	0.739	2.308

[a] The numbers refer to the relative intensities of the component lines.
[b] Probable errors are ±0.003 gauss for the P^{31} resonance and ±0.001 gauss for F^{19}.
[c] $\mu(F^{19})/\mu(P^{31}) = 2.334$.

were determined in all cases by the magnetic field inhomogeneities and modulation effects, which gave apparent half-maximum widths of about 0.05 gauss.

The single P^{31} line in $POCl_3$ reflects the absence of other important magnetic nuclei in the molecule. The P^{31} doublet in $POCl_3F$ corresponds to an m_I for F^{19} of $\pm\frac{1}{2}$. In $POClF_2$ and CH_3OPF_2, the two F^{19} nuclei form a singlet and a triplet nuclear state. For the singlet, the total nuclear spin component from the two F^{19} nuclei is $M_I(F^{19})=0$; in the triplet, $M_I(F^{19})=0, \pm 1$. The central component of the P^{31} resonance line corresponds to P^{31} transitions in which $M_I(F^{19})=0$. The satellites correspond to $M_I(F^{19})=\pm 1$. The double intensity of the central line is a result presumably of the existence of two $M_I(F^{19})=0$ states.

In general, for AX_n with structurally identical X's, the A magnetic resonance should have $(2nI_x+1)$ equally spaced components with relative intensities given by the binomial coefficients. Proctor and Yu have reported[5] a five-component antimony resonance in aqueous solutions of SbF_6^-. Inspection of their experimental curve,[5] however, suggests that two additional weak satellites may be present; moreover, the relative intensities follow the proper sequence for seven components.

The splitting of the F^{19} resonance appears to arise solely from the P^{31} $m_I=\pm\frac{1}{2}$ states. The absence of any observable splitting by other F^{19} nuclei in molecules such as $POClF_2$, CH_3OPF_2, and PF_3 contrasts with the fine structure observed in rigid-lattice solids as a consequence of magnetic dipole interactions between like nuclei.[1] The difference may arise from the coupling of the nuclear and rotational angular momenta and the nature of the selection rules. Additional experiments and a more detailed analysis are in progress.

We are indebted to Drs. C. P. Slichter and L. M. Slifkin for several interesting conversations and suggestions regarding the interpretation of the results. Also, we wish to thank Dr. D. R. Martin for furnishing some of the compounds. Equipment was provided mainly by a Grant-in-Aid from Research Corporation.

* Supported in part by ONR.

[1] Gutowsky, Kistiakowsky, Pake, and Purcell, J. Chem. Phys. **17**, 972 (1949).
[2] Bloembergen, Purcell, and Pound, Phys. Rev. **73**, 679 (1948).
[3] H. S. Gutowsky and G. E. Pake, J. Chem. Phys. **18**, 162 (1950).
[4] H. S. Gutowsky and C. J. Hoffman, Phys. Rev. **80**, 110 (1950); H. S. Gutowsky and R. E. McClure, Phys. Rev. **81**, 276 (1951).
[5] W. G. Proctor and F. C. Yu, Phys. Rev. **81**, 20 (1951).

Detection of Slow Neutrons*

R. Hofstadter, J. A. McIntyre, H. Roderick, and H. I. West, Jr.
Department of Physics, Stanford University, Stanford, California
(Received April 2, 1951)

In the original publication on alkali halide scintillation counters[1] it was suggested by one of the present authors that a neutron counter could be made with a thalliated lithium halide as a scintillator. Subsequently, with the help of F. B. Harrison at Princeton, single crystals of LiI with a 1 percent TlI impurity were grown,[2] and it was found that they responded to ionizing radiation (gamma-rays and electrons). Since thermal neutrons are captured by Li^6 (7.4 percent relative abundance) with a very large cross section (~900 barns), it may be expected that the alpha-particle and triton, which are released with a combined energy of 4.785 Mev,[3] will produce a large light pulse when slow neutrons are stopped in the Li^6 of the LiI(Tl) crystal. Because the heavy particle pulse ($_2He^4$, $_1H^3$) will correspond uniquely to 4.79 Mev, while gamma-rays in a small crystal may be expected to lose a considerably smaller and variable energy, the proposed method of detecting slow neutrons would appear to be natural and simple: energy discrimination will distinguish slow neutrons from γ-rays, electrons, etc. This method was actually tried by one of the authors[4] without success because suitable crystals of LiI(Tl) had not been grown at the time.

Recently, we have examined single crystals of LiI(Tl) as neutron detectors[5] using the Stanford cyclotron as a source of slow neutrons. Figure 1(a) shows the pulses obtained when slow neutrons are

FIG. 1. Time exposures of LiI(Tl) scintillation pulses as observed on an oscilloscope screen. (a) crystal in beam of thermal neutrons, no absorber; (b) same as (a) except for boron absorber; (c) same as (a) except for cadmium absorber; (d) Co^{60} calibration pulses with double gain in amplifier.

allowed to impinge on the LiI(Tl) crystal which had been set atop a 5819 photomultiplier tube. Figures 1(b) and 1(c) show, respectively, the pulses obtained for a similar exposure, when the crystal was surrounded by thin boron and cadmium shields. The absence in 1(b) and 1(c) of the group of uniform pulses in 1(a) shows that slow neutrons formerly detected by the crystal are now being absorbed by the boron and cadmium and hence do not activate the crystal. The uniformity of the neutron pulses and their relatively large size indicate that most other radiations can be screened out by energy discrimination methods where desirable. The crystal of LiI(Tl) is thus selective to slow neutrons.

Figure 1(d) shows the pulses due to Co^{60} gamma-rays when the amplifier gain is doubled. By measuring relative pulse heights, and assuming that the light pulse size is proportional to energy, whatever the particle responsible for the energy loss may be, one obtains a value of 4.1 Mev for the neutron pulse heights. Since distortion by the amplifier occurs at larger pulse sizes, and since the crystal was yellow and not uniform, the agreement with the expected energy release must be considered good. In all parts of Fig. 1 the small pulses at the bottom appear to be due to photomultiplier noise and slow-neutron induced radioactivity in the iodine component of LiI(Tl).

A natural crystal of LiI(Tl), of thickness one centimeter, will capture about 0.6 of all the thermal neutrons passing through it. Hence the efficiency of this counter is very high. With enriched Li^6 the efficiency can be made even higher. In these experiments the crystals used were $4\times4\times6$ mm³ and $2\times4\times5$ mm³ in size. The crystals were somewhat yellow, indicating the possible presence of an unwanted impurity. Clear colorless LiI(Tl) crystals should give even better results. The decay constant of LiI(Tl) is close to 1.2 microseconds; thus the speed is high enough to permit coincidence experiments with scintillation detectors for neutrons. The emitted light is blue-green and the density of LiI(Tl) is 4.06 g/cc. Since LiI(Tl) is extremely deliquescent, it must be placed in an air-tight container. This imposes no hardships with respect to detecting slow neutrons. The pulse heights for ionizing particles are of the order of $\frac{1}{10}$ the size of NaI(Tl) pulses for equal energies.

The authors wish to thank Dr. W. E. Meyerhof for putting the cyclotron at their disposal.

* This work was aided by the joint program of the ONR and AEC, and at an earlier time by a Signal Corps contract.

[1] R. Hofstadter, Phys. Rev. **74**, 100 (1948).
[2] R. Hofstadter, Research Reviews (ONR) **1**, 4 (September, 1949); Nucleonics **6**, No. 5, 70 (1950).
[3] Hornyak, Lauritsen, Morrison, and Fowler, Revs. Modern Phys. **22**, 291 (1950).
[4] R. Hofstadter, Brookhaven National Laboratory Internal Report, BNL-1-7 (November 1, 1949), unpublished.

The Energy of the Gamma-Ray from Se^{77m}

ROBERT CANADA, W. H. CUFFEY, A. E. LESSOR, AND ALLAN C. G. MITCHELL
*Indiana University, Bloomington, Indiana**
(Received April 12, 1951)

A METASTABLE state of Se^{77} of 17.5-sec half-life has been produced by neutron excitation of Se by Arnold and Sugarman,[1] and by Goldhaber and Muehlhause.[2] This isomer has also been produced by x-ray excitation by Gideon, Miller, and Waldman[3]. The isomer, Se^{77m}, decays to the ground state of Se^{77} with the emission of a highly internally converted gamma-ray. The absorption in aluminum of the internal conversion electrons has been measured by Gideon, Miller, and Waldman, who give the energy of the gamma-ray as approximately 150 kev. Flammersfeld and Ythier[4] have made similar measurements and give the value 165 kev for the energy of the gamma-ray. Der Mateosian and Goldhaber[5] have measured the energy of the gamma-ray using a scintillation counter and find an energy of 150 kev.

The present experiments stem from an investigation of Br^{77} (57 hr) which is in progress in this laboratory. Br^{77} was made by the reaction $As^{75}(\alpha, 2n)Br^{77}$ in the Indiana cyclotron. The spectrum of the photoelectrons ejected from a lead radiator and also the particle spectrum (internal conversion electrons and positrons) were measured in a magnetic lens spectrometer. Among other things a very weak gamma-ray of 160 kev was found in the photoelectric spectrum, and a very strong internal conversion line corresponding to the same gamma-ray was found in the particle spectrum.

Experiments were performed to see whether a Se activity was growing from the Br^{77}. To a solution containing activated Br^{77} ion there was added a small amount of $SeO_3^{=}$. The $SeO_3^{=}$ was reduced to Se metal by the addition of stannous chloride. The solution was filtered, washed, and transferred to a counter for measurement. The whole procedure took about one minute. The decay curve of the resulting Se^{77m} yields a half-life of 17.5 sec, with a probable error of about 10 percent. The energy of the gamma-ray associated with this transition is 159.9 ± 1.0 kev.

* Supported by the joint program of the ONR and AEC.
[1] J. R. Arnold and N. Sugarman, J. Chem. Phys. **15**, 703 (1947).
[2] M. Goldhaber and C. O. Muehlhause, Phys. Rev. **74**, 1248 (1948).
[3] Gideon, Miller, and Waldman, Phys. Rev. **75**, 329 (1949).
[4] A. Flammersfeld and C. Ythier, Z. Naturforsch. **5a**, 401 (1950).
[5] E. der Mateosian and M. Goldhaber, private communication.

Nuclear Magnetic Moment of Rb^{85}, Rb^{87}, and I^{127}

E. YASAITIS AND B. SMALLER
Argonne National Laboratory, Chicago, Illinois
(Received April 16, 1951)

WE have recently completed a series of measurements of the nuclear magnetic moment of Rb^{85}, Rb^{87}, and I^{127} using the nuclear resonance absorption method of Purcell *et al.*[1] The apparatus described elsewhere[2] had been modified to permit the precise determination of the deuteron[3] by a side band modulation technique, and it was considered profitable to exploit the technique used in the latter measurement for the more accurate determinations of other isotopes. The side band modulation technique requires use of a master oscillator of frequency f_0, a harmonic amplifier and mixer, and a modulation oscillator of frequency f to generate the required side band. The ratio of proton to unknown Larmor precession frequency is given by

$$f_H/f_x = (af_0 \pm f)/bf_0,$$

where a and b are integers chosen to have the lowest value consistent with a low value for f. The imprecision in the frequency ratio is reduced by the factor f/f_H from that obtained with direct techniques. The samples and the coils were arranged[3] so that simultaneous measurement of proton and unknown resonance was possible.

Because of the theoretical interest in the nuclear moments of isotopic pairs,[4] the rubidium isotopes were investigated in the form of saturated solutions of RbCl. The operating conditions for the Rb^{85} were roughly $f_0 = 3.0 \times 10^6$ cycles/sec, $f = (+)1.071 \times 10^6$ cycles/sec, $a = 10$, $b = 1$, and a line width of 0.32 gauss. In all cases the field inhomogeneity limited the proton line width to about 0.02 gauss. The ratio of resonant frequencies (uncorrected for diamagnetic effects) was

$$f_H/f_{Rb^{85}} = 10.357105 \pm 0.000030,$$

where, as in all cases, the indicated error is three times the probable error. This value is to be compared with the previous value of Chambers and Williams[5] of 10.351 ± 0.004.

For the Rb^{87} isotope, the conditions were $f_0 = 1.0 \times 10^7$ cycles/sec, $f = (+)5.61 \times 10^5$ cycles/sec, $a = 3$, $b = 1$, and a line width of 0.20 gauss. The resultant frequency ratio

$$f_H/f_{Rb^{87}} = 3.0561097 \pm 0.0000055$$

is in good agreement with the value of Zimmerman and Williams[6] of 3.0564 ± 0.0015.

Using the assigned spin values of 5/2 and 3/2 for the Rb^{85} and Rb^{87} isotopes, respectively, we find the ratio of the moments to be

$$\mu_{Rb^{87}}/\mu_{Rb^{85}} = 2.0333905 \pm 0.0000075,$$

in good agreement with the value of Adams *et al.*[7] of 2.033380 ± 0.000028.

The I^{127} isotope in a saturated solution of KI was investigated under conditions of $f_0 = 6.17 \times 10^6$ cycles/sec, $f = (-)1.3 \times 10^6$ cycles/sec, $a = 5$, $b = 1$, and where the line width was broadened, presumably by the large quadrupole moment, to 2.5 gauss. The precision was severely limited by this width and yielded

$$f_H/f_I = 4.99763 \pm 0.00015,$$

in good agreement with the value of Zimmerman and Williams[6] of 4.9993 ± 0.0020.

[1] Bloembergen, Purcell, and Pound, Phys. Rev. **73**, 679 (1948).
[2] H. L. Anderson, Phys. Rev. **76**, 1460 (1949).
[3] Smaller, Yasaitis, and Anderson, Phys. Rev. **80**, 137A (1950); **81**, 896 (1951).
[4] A. Bohr, Phys. Rev. **81**, 331 (1951).
[5] W. H. Chambers and D. Williams, Phys. Rev. **76**, 638 (1949).
[6] J. R. Zimmerman and D. Williams, Phys. Rev. **76**, 350 (1949).
[7] Adams, Wimett, and Bitter, Phys. Rev. **82**, A343 (1951).

On the Low States of He^5 and Li^5

ROBERT K. ADAIR
University of Wisconsin, Madison, Wisconsin
(Received February 9, 1951)

AN examination of the experimental material available on the low states of He^5 and Li^5 might be expected to provide information on the charge independence of nuclear forces and the strength of spin orbit forces in nuclei. The available material consists of measurements of the $p-\alpha$ differential scattering cross section[1] and the $n-\alpha$ total cross section[2] as well as more qualitative measurements of the $n-\alpha$ angular distribution[3] and back scattering.[4]

Though a $P_{1/2}-P_{1/2}$ doublet may be involved, their associated scattering phase shifts will be independent of one another, since states with different values of spin, j, or parity will not interact. These phase shifts, $\delta(l, j)$, may then be approximated by the single level formula of nuclear dispersion theory and written as:[5]

$$\delta(l,j) = \tan^{-1}\frac{k\gamma^2[F_l^2(a)+G_l^2(a)]^{-1}}{E_\lambda+\Delta-E} - \tan^{-1}\left\{\frac{F_l(a)}{G_l(a)}\right\}, \quad (1)$$

where F and G are the regular and irregular free particle wave functions,[6] a is the reaction radius, and γ^2 is the energy independent reduced width. E_λ is a characteristic energy of the state, the energy at which the logarithmic derivative of the wave function becomes

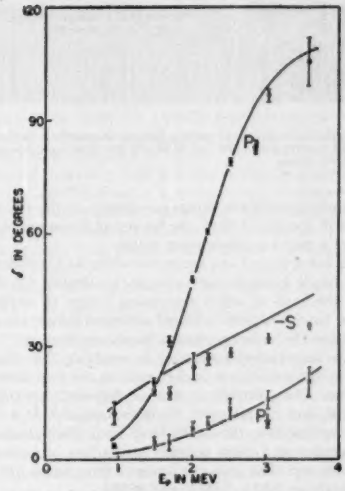

FIG. 1. Phase shifts for $p-\alpha$ scattering as a function of proton bombardment energy.

equal to $-l$ at the nuclear surface. The level shift, Δ, is equal[7] to

$$-\frac{\gamma^2}{a}\left(a\frac{\ln(F_l^2(a)+G_l^2(a))^{\frac{1}{2}}}{d\ln ka}+l\right).$$

Critchfield and Dodder[8] have shown that the $p-\alpha$ differential cross section is consistent with either of two sets of phase shifts, one representing an inverted doublet with an undetermined large splitting, the other corresponding to a regular doublet with a splitting of about one Mev. The points on Fig. 1 represent their values for the phase shifts in the former case, together with their estimate of the probable error. The curves represent the best fit, obtained by trial and error, of Eq. (1) to the points. Corresponding values of the parameters were $a=2.9\times10^{-13}$ cm, $\gamma^2(P_{3/2})=\gamma^2(P_{1/2})=17.6\times10^{-13}$ Mev cm, $E_\lambda(P_{3/2})=3.65$ Mev, and the doublet splitting $E_\lambda(P_{1/2})-E_\lambda(P_{3/2})=5$ Mev. The S-wave curve was calculated using only the potential scattering part of the resonance formula, $\delta_0=-\tan^{-1}[F_0(a)/G_0(a)]$. Effects of high lying levels would be expected to reduce this phase shift in agreement with the experimental results.

The total $n-\alpha$ cross section will equal

$$\sigma_t=2\pi k^{-2}\sum_{l,j}(2j+1)\sin^2\delta(l,j), \qquad (2)$$

where $\delta(P_{3/2})$ and $\delta(P_{1/2})$ are calculated from Eq. (1). The points on Fig. 2 are the experimental values of reference 2, while the curve represents the fit of Eq. (2) to the data, using the same values of the parameters, a, γ^2, and the splitting $E_\lambda(P_{1/2})-E_\lambda(P_{3/2})$, as for the $p-\alpha$ analysis. The discrepancy between the data and the curve at 1.2 Mev can be accounted for by an experimental effect discussed in reference 2. The $n-\alpha$ levels are 1.25 Mev lower than the $p-\alpha$ levels, a shift attributable to the difference in coulomb energy. The $n-\alpha$ S-wave phase shifts were calculated by requiring the wave function to have the same logarithmic derivative at the nuclear surface as the $p-\alpha$ S-wave. This leads to a value of about 0.8 barn for the low energy cross section, consistent with reference 2, but in disagreement with the value of 1.45 barns reported by Harris.[9] The sign of the S-wave phase shift is negative,[10] as is the proton phase shift. It seems reasonable to assume that the higher angular momenta phase shifts are negligible. Goldstein[11] has pointed out that this assignment of levels is consistent with the $n-\alpha$ angular distribution and back scattering experiments. For both Li[6] and He[6] the parameters for the $P_{1/2}$ level are somewhat arbitrary.

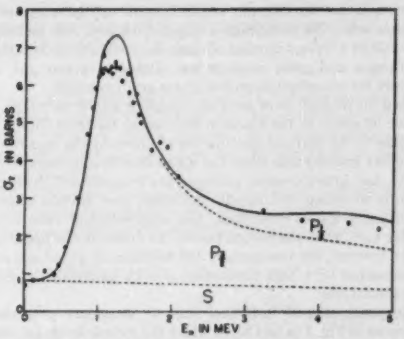

FIG. 2. $n-\alpha$ total cross section as a function of neutron bombardment energy. The dashed lines separate the contributions of the various partial waves.

The value obtained for the reduced width, γ^2, is about equal to $\hbar^2/ma$, where m is the reduced mass of the system. With this value of γ^2 and $|E_\lambda-E|\lesssim\gamma^2/a$, Eq. (1) takes the same form as the result for scattering by a square well of depth E', where $(E'+E_\lambda)^{\frac{1}{2}}(2ma/\hbar^2)^{\frac{1}{2}}=\pi(l+1)$, indicating that the interaction may be represented adequately as a one-body interaction. E' should provide an estimate of the average interaction energy. $E'+E_\lambda$ is equal to 38 Mev for a radius a of 2.9×10^{-13} cm.

In summary, it appears that the data are consistent with the thesis of charge independent forces and the formation of a widely spaced inverted $P_{3/2}-P_{1/2}$ doublet. The doublet splitting of the order of five Mev is much larger than Dancoff's[12] estimate of the effect of tensor forces and may be evidence for the importance of velocity dependent forces,[13] or some other large spin orbit coupling as is postulated for one of the nuclear shell models.[14]

[1] Freier, Lampi, Sleator, and Williams, Phys. Rev. **75**, 1345 (1949).
[2] Bashkin, Petree, and Mooring, Phys. Rev. **82**, 378 (1951).
[3] H. H. Barschall and M. H. Kanner, Phys. Rev. **58**, 590 (1940); T. A. Hall and P. G. Koontz, Phys. Rev. **72**, 196 (1947).
[4] H. Staub and H. Tatel, Phys. Rev. **58**, 820 (1940).
[5] Feshbach, Peaslee, and Weisskopf, Phys. Rev. **71**, 145 (1947); E. P. Wigner and L. Eisenbud, Phys. Rev. **72**, 29 (1947).
[6] These functions were computed with the aid of tables of coulomb wave functions prepared by Bloch, Hull, Broyles, Bouricius, Freeman, and Breit (private communication).
[7] R. G. Thomas, Phys. Rev. **81**, 148 (1951).
[8] C. L. Critchfield and D. C. Dodder, Phys. Rev. **76**, 602 (1949).
[9] S. Harris, Phys. Rev. **79**, 219 (1950).
[10] A. W. McReynolds and R. J. Weiss (private communication).
[11] Herbert Goldstein, Phys. Rev. **79**, 740 (1950).
[12] S. Dancoff, Phys. Rev. **58**, 326 (1940).
[13] C. H. Blanchard and R. Avery, Phys. Rev. **81**, 35 (1951); J. Hughes and K. J. LeCouteur, Proc. Phys. Soc. (London) **63**, 1219 (1950).
[14] M. G. Mayer, Phys. Rev. **75**, 1969 (1949); Haxel, Jensen, and Suess, Phys. Rev. **75**, 1766 (1949).

Emission of the Forbidden Oxygen Lines by Molecular Dissociation

RENÉE HERMAN
Observatoire de Meudon
CHARLES WENIGER
Laboratoire du Grand Electroaimant de Bellevue
AND
LOUIS HERMAN[*]
Laboratoire de Recherches Physiques, Université de Paris, Paris, France
(Received February 23, 1951)

THE process which occurs in a gas when it is excited by an electrical discharge is often quite complicated. It is not easy to distinguish in the emission spectrum the parts coming from the direct electronic excitation, from the recombination of ions and electrons, and from secondary reactions such as atomic recombination or molecular decomposition.

The radiative ion-electron recombination can be observed in afterglow when the excitation is stopped. In fact, this method is applicable in a limited number of cases, for instance, for rare gases, for nitrogen and gases more or less diluted in a rare gas, and generally for non-electronegative atoms and molecules.

When the production of an atom in a given level is very high, the relative intensity of the emission line can be far from that corresponding to the thermal distribution of atoms in the upper state. This effect is noticeable when the upper level is a metastable one. In this case, intermolecular collisions are frequent and the deactivation is so strong that usually forbidden lines are not observed except under special conditions. The observation of these lines is possible only when the destruction of the atoms in the upper level can be lowered, for instance, by the addition of a rare gas or by compensation by a high production of such metastable atoms in some special way.

The production of forbidden lines by secondary processes is illustrated in Fig. 1 (a and b), in which the atomic levels are shown

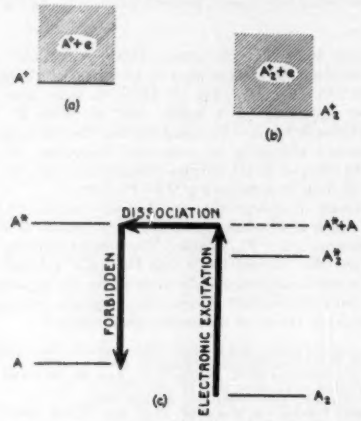

FIG. 1. Illustration of the process of excitation of the forbidden lines 6300 ($^3P_2-{}^1D_2$) and 6364 ($^3P_1-{}^1D_2$) of O*I* by dissociation into atoms of the O_2 molecule in the $B^3\Sigma_u^-$ state.

on the left, and the molecular levels on the right. Atomic lines and molecular bands can be excited by electron collisions or can be emitted by ion recombination. Since atoms can associate and molecules can dissociate, an interaction between the two main processes can take place. Two such examples occur in connection with emission of forbidden oxygen lines in the upper part of the atmosphere. The first concerns the red auroral lines 6300A ($^3P_2-{}^1D_2$) and 6364A ($^3P_1-{}^1D_2$) of high strength in the light of the high altitude aurora. The second concerns the common green auroral line 5577A ($^1D_2-{}^1S_0$) which is the main part of the emission of the night sky and aurora.

The process of electronic excitation, we believe, may be illustrated by the pattern indicated in heavy lines in Fig. 1(c).

In the case of the red aurora lines the upper excited molecular state is $B^3\Sigma_u^-$. This state is stable and the corresponding transition gives the Schumann-Runge bands $B^3\Sigma_u^-\rightarrow X^3\Sigma_g^-$ in absorption and in emission. To reach the dissociation of the upper state into two atoms $O(^3P)+O(^1D_2)$, a considerable development of this band system must be obtained. In fact, this is observed together with an important relative enhancement of the 6300 and 6364 lines in pure oxygen at atmospheric pressure (Fig. 2).

The second example concerns the emission of a mixture of a rare gas like xenon or argon and a small amount of oxygen. The green emission observed in the direct discharge and in afterglow is composed of two parts, the auroral line 5577A ($^1D_2-{}^1S_0$), and a

FIG. 2. Emission spectrum of pure oxygen at atmospheric pressure. The forbidden red auroral lines 6300 and 6364 and the Schumann-Runge bands are particularly strong.

quasi-continuous molecular spectrum mainly on the short wavelength side of the line.[1,2] Here, the lower and the upper molecular states have a very low dissociation energy.

In a mixture of oxygen and xenon, one observes a well-developed system of bands which is relatively easy to identify. On the contrary, in the case of argon containing traces of oxygen, the vibrational bands are most confused and upon examination under low dispersion the emission appears purely continuous.[3–5]

We have nevertheless succeeded in resolving the vibrational structure in the continuous background on the two sides of the auroral line. The complete system is degraded towards short wavelengths, and the intensity diminishes rapidly. At a distance from the auroral line, the bands have been photographed with lower dispersion and show definite fluctuations of intensity degraded to the red. The apparent heads of these bands are located approximately at 5487A, 5529A, and 5555A.

On the other hand, a somewhat complex structure appears near the green line. We attribute this to vibrational bands of the electronic transition $AO(^1S_0;{}^1S_0)\rightarrow AO(^1S_0;{}^1D_2)$. A tentative vibrational classification of the most intense bands[6] is shown in Table I.

For the XO molecule the vibrational frequency ω' is nearly 10 times and ω'' 20 times greater than for the AO molecule; the

TABLE I. Wave numbers of the green band system observed near the forbidden oxygen line 5577 ($^1D_2-{}^1S_0$) of O *I* in a mixture of argon and oxygen. v' and v'' are the vibrational quantum numbers of the upper and the lower states.

v' \ v''	0	1	2	3	4	5	6	7
0	17939	17915						
1	17956	17933						
2		17948						
3		17962	17937					
4			17953					
5				17945	17920			
6					17936			
7				17976		17928	17910	
8					17967	17945	17926	17905
9					17981			
10							17958	

latter is thus much less stable since $\omega''>\omega'$, and the individual bands will be degraded to the red. On the microphotometer traces we recognized no degradation as the bands strongly overlap.

It is probable that the bands 5487A, 5529A, and 5555A are likewise capable of resolution. To resolve them, it will be necessary to employ a spectrograph which is (at the same time) of higher speed and of greater dispersion than the one at our disposal.

The spectral composition of this green emission is the same in afterglow and in the direct discharge. Thus, the green auroral line seems closely connected with the quasi-continuous part. On the other hand, the remaining permitted and forbidden O*I* lines are very faint if not absent, and it is hardly to be supposed that there exists a low electronic excitation of the diluted atomic oxygen.

* Temporarily at the Geophysical Institute, College, Alaska.

[1] Kenty, Aicher, Noel, Poritsky, and Paolino, Phys. Rev. **69**, 36 (1946).
[2] R. Herman, Compt. rend. **222**, 492 (1946).
[3] L. Herman and R. Herman, Ann. Geophys. **I**, 165 (1944).
[4] Vegard, and Kvifte, Nature **162**, 967 (1948).
[5] Jenkins, Bowtell, and Strong, Nature **163**, 401 (1949).
[6] K. G. Emeleus and N. D. Sayers, University of Belfast, found a partially similar structure in their independent work on the same band system (private communication).

Polarization Effects in $(n-\gamma)$ Reactions

OTTO HALPERN
University of Southern California, Los Angeles, California
(Received April 11, 1951)

THE use of polarized neutron beams permits one to induce reactions in which the reaction products may show certain characteristic polarization properties. Perhaps the simplest case of interest can be described as follows:

A polarized neutron $\sigma_s=\frac{1}{2}\hbar$ of long wavelength is captured by a nucleus A of spin 0 leading to a nucleus $A+1$ of spin $i=\frac{1}{2}\hbar$ and a single γ-ray. We denote the total angular momentum of radiation and nucleus by $f\hbar$; then for reasons of conservation $|f|=f_s=\frac{1}{2}\hbar$. It is clear that the γ-ray must be due to dipole emission; all higher poles are forbidden.

Now the only spin eigenfunction for $f=f_s=\frac{1}{2}\hbar$ is given by

$$(1/\sqrt{3})[\sqrt{2}\varphi_i(-\tfrac{1}{2})\chi_i(1)-\varphi_i(\tfrac{1}{2})\chi_i(0)].$$

Here φ_i's denote the two spin eigenfunctions of the resultant nucleus $A+1$, and χ_i's the three symbolic angular momentum eigenfunctions of the right quantum created by dipole radiation. The resulting spin eigenfunction contains the following results: The γ-ray intensity is radiated isotropically. The resultant nucleus is partially polarized with $i_s=-\frac{1}{3}\cdot\frac{1}{2}\hbar$. The γ-rays radiated perpendicularly to the direction of the neutron spin are unpolarized, while those emitted along the z-direction are circularly polarized.

The discussion of a proper analyzer for a circularly polarized γ-ray and its connection with electron polarization will be left to a later paper, in which also other cases of interest will be treated.

A Variational Method for Inelastic Collision Problems

B. L. MOISEIWITSCH
University College, London, England
(Received April 13, 1951)

A GENERALIZATION of Hulthèn's variational method[1] to the inelastic scattering of electrons by atoms has been derived using the integral

$$L=\int \Psi^*(H-E)\Psi d\tau, \tag{1}$$

where H is the hamiltonian of the system.

In the case of the scattering of electrons by hydrogen atoms

$$H=-\nabla_1^2-\nabla_2^2-2/r_1-2/r_2+2/r_{12}, \tag{2}$$

where r_1, r_2, r_{12} are the distances of the electrons from the nucleus and from each other, respectively, in atomic units.

For slow incident electrons exciting the ground $1s$ state of the hydrogen atom to the $2s$ state, the total wave function of the system may be written in the form

$$\Psi(r_1,r_2)=r_2^{-1}\{f_0(r_2)\psi_0(r_1)+f_1(r_2)\psi_1(r_1)\} \pm r_2^{-1}\{f_0(r_1)\psi_0(r_2)+f_1(r_1)\psi_1(r_2)\}, \tag{3}$$

where

$$f_0(r)\sim\sin kr+a\cos kr,$$
$$f_1(r)\sim d\exp(ik_1r),$$

as $r\to\infty$, corresponding to the zero order partial wave only; and ψ_0 and ψ_1 are the $1s$ and $2s$ hydrogen atom wave functions, respectively. The initial energy of the incident electron is k^2, while the energy of the scattered electron after the $2s$ state has been excited is k_1^2. It is important to notice that a and d are complex quantities. With the above asymptotic forms it follows by Green's theorem that

$$\delta L=4\pi k\delta a-8\pi ik_1d^*\delta d, \tag{4}$$

if $(H-E)\Psi=0$. Hence

$$\mathcal{I}(\delta L)=4\pi k\delta(y-|d|^2k_1/k), \tag{5}$$

where $\mathcal{I}(\delta L)$ is the imaginary part of δL, and $a=x+iy$. It can be shown that application of the principle of conservation of charge[2] results in the relation

$$y=|d|^2k_1/k. \tag{6}$$

Therefore, if the condition $L=0$ is imposed for all small variations of the wave function Ψ so that $\delta L=0$, then $\delta a=2i(k_1/k)d^*\delta d$ and the conservation of charge equation (6) remains satisfied. This suggests the following procedure for the approximate determination of a and d.

Form a trial wave function Ψ_t containing n parameters c_i in addition to the parameters a and d, and satisfying the required boundary conditions at the origin and at infinity, then

$$\delta L_t=\left(\frac{\partial L_t}{\partial d}+2i\frac{k_1}{k}d^*\frac{\partial L_t}{\partial a}\right)\delta d+\frac{\partial L_t}{\partial c_i}\delta c_i +\left(\frac{\partial L_t}{\partial d^*}-2i\frac{k_1}{k}d\frac{\partial L_t}{\partial a^*}\right)\delta d^*+\frac{\partial L_t}{\partial c_i^*}\delta c_i^*, \tag{7}$$

if $\delta a=2i(k_1/k)d^*\delta d$. Therefore $\delta L_t=0$ if

$$\frac{\partial L_t}{\partial d}+2i\frac{k_1}{k}d^*\frac{\partial L_t}{\partial a}=0 \quad\text{and}\quad \frac{\partial L_t}{\partial c_i}=0,$$

since

$$\frac{\partial L_t}{\partial d^*}-2i\frac{k_1}{k}d\frac{\partial L_t}{\partial a^*}=0 \quad\text{and}\quad \frac{\partial L_t}{\partial c_i^*}=0$$

are their respective complex conjugate equations. Hence the $2n+4$ equations

$$L_t=0,\quad \frac{\partial L_t}{\partial d}+2i\frac{k_1}{k}d^*\frac{\partial L_t}{\partial a}=0,\quad \frac{\partial L_t}{\partial c_i^*}=0 \tag{8}$$

may be used to determine the complex parameters $a, d, c_1, \cdots, c_n$.

But, in contrast to Hulthèn's variational method applied to the *elastic* scattering of electrons, the condition $L=0$ does not imply that $\delta a=0$. A correction to the parameter may be obtained by considering the integral

$$L'=\int \Psi(H-E)\Psi d\tau. \tag{9}$$

For it can be shown that

$$\delta L'=4\pi k\delta a. \tag{10}$$

Therefore the corrected value λ of the parameter a is given by

$$\lambda=a-L'/4\pi k. \tag{11}$$

The variational method outlined above can be extended to include any order partial wave, and excitation to any state of the atom.

Calculations are now in progress on the $1s-2s$ excitation of hydrogen. The preliminary results obtained seem promising.

In conclusion I wish to thank Professor H. S. W. Massey for his assistance and interest in this work, and I am also indebted to Dr. R. B. Makinson and Mr. H. H. Robertson for a helpful discussion of the problem.

[1] L. Hulthèn, K. Fys. Sallsk, Lund Forhandl 14, No. 21 (1944); H. S. W. Massey and B. L. Moiseiwitsch, Proc. Roy. Soc. (London) 205, 483 (1951).
[2] N. F. Mott and H. S. W. Massey, *Theory of Atomic Collisions* (Clarendon Press, Oxford, 1949), second edition. Chapter VIII.

Erratum: Q-Values for (α,p) Reactions on Aluminum and Boron by Means of Photographic Emulsions

[Phys. Rev. 81, 641 (1951)]

HILDING SLÄTIS, ELIS HJALMAR, AND RUNE CARLSSON
Nobel Institute of Physics, Stockholm, Sweden
(Received April 9, 1951)

THE following correction should be made: line 10 of column 1, p. 642, should read ". . . There is, however, a difference of about 0.21 Mev . . ." .

On the Production of π^+ Mesons in Carbon*

E. M. Henley and R. H. Huddlestone
Radiation Laboratory, University of California, Berkeley, California
(Received April 12, 1951)

THE cross section for production of π^+ mesons by 345-Mev protons on carbon has been measured by Richman and Wilcox.[1] The experimental points of the meson energy spectrum are shown in Fig. 1. We have treated this process on the basis of the phenomenological analysis of meson production in free nucleon-nucleon collisions carried out by Watson and Brueckner.[2]

In terms of the free nucleon cross section, $d\sigma_f/dTd\Omega$, using a closure approximation over the unstruck nucleons, it is possible to

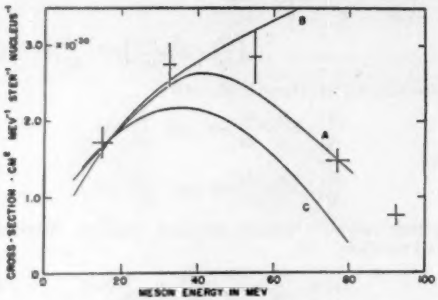

FIG. 1. The π^+ meson production spectra from C^{12} at 90°.

reduce the meson production spectrum from a complex nucleus, $d\sigma/dTd\Omega$, to the form

$$\frac{d\sigma}{dTd\Omega}=\int \frac{d\sigma_f}{dTd\Omega}(\mathbf{k})\rho(\mathbf{k})d\mathbf{k},$$

where T and Ω are the kinetic energy and solid angle of the meson, respectively; $\rho(\mathbf{k})$ is the momentum distribution of a nucleon in the nucleus.

From the experiments on meson production from free nucleons by Cartwright, Richman, Whitehead, and Wilcox,[3] the treatment of Watson and Brueckner[2] indicates that the mesons are produced predominantly into p-states. It has been assumed that this type of coupling is still the most important for a bound nucleon. Therefore, the same free nucleon cross section has been used, omitting contributions arising from deuteron formation.

The meson spectra at 90°, corresponding to various momentum distributions assumed for C^{12}, are shown in Fig. 1. The normalization of these curves has been determined from the normalization of the free nucleon cross section to the experimental data. Curve A was obtained using a gaussian momentum distribution corresponding to an average kinetic energy of 19.3 Mev for a nucleon in C^{12}. This distribution is shown as curve A in Fig. 2 and has been chosen to fit the low momentum points obtained by Chew and Goldberger[4] from the deuteron pick-up data of York.[5] Curve B, Fig. 1, is the spectrum corresponding to the Chew-Goldberger momentum distribution, curve B, Fig. 2. The difference in these two spectra is chiefly due to the large number of high momentum components present in the latter distribution. However, as pointed out by Chew and Goldberger,[4] their momentum distribution is in doubt at the high end. Curve C, Fig. 1, is the cross section obtained with a Fermi degenerate gas (maximum momentum = 200 Mev/c).

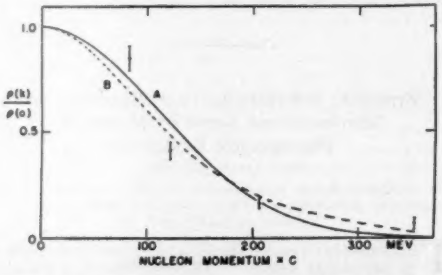

FIG. 2. Assumed momentum distributions for a nucleon in C^{12}.

For the Fermi model, the Pauli exclusion principle was found to modify the meson spectrum only below 25 Mev. In addition, a nuclear model, with a ground state corresponding to momentum distribution A, was examined. The exclusion effect was of the order of 10 percent. Due to the uncertainties in the free nucleon cross section, these corrections have not been included in these preliminary results.

The differences between the spectra at high meson energies indicate a fairly sensitive dependence on the assumed momentum distribution.

The effects of meson absorption and other aspects of meson production in complex nuclei are being studied. These results will appear in a forthcoming paper.

It is with pleasure that we acknowledge the continual guidance of Dr. K. Watson and the stimulating discussions with Professor R. Serber.

* This work was performed under the auspices of the AEC.
[1] C. Richman and H. A. Wilcox, Phys. Rev. **78**, 496 (1950).
[2] K. Watson and K. Brueckner, Phys. Rev. **83**, to be published.
[3] Cartwright, Richman, Whitehead, and Wilcox, Phys. Rev. **78**, 823 (1950).
[4] G. F. Chew and M. L. Goldberger, Phys. Rev. **77**, 470 (1950).
[5] H. York, Phys. Rev. **75**, 1467A (1949).

On Measuring Very Short Half-Lives*

Z. Bay, R. R. Meijer, and G. Papp†
George Washington University, Washington, D. C.
(Received April 9, 1951)

IN a paper given at the April, 1951, meeting of the American Physical Society[1] the principle of a differential coincidence counting method was presented. One possible use of the counting rate *versus* delay curve of the differential-output (we call it the differential delay curve here) was given there, namely narrowing delay curves.

It is interesting to note that the differential delay curve can also be used directly to obtain information about short time relationships. The theorems which have been previously given[2] regarding the moments of the delay curve also hold for the differential delay curve. In addition it is easy to show that, within limits, the change in the counting rate in the linear part of a delay curve (when going from the source producing simultaneous events to the source producing delayed events) is the product of the slope of the curve and the first moment of the decay curve.

To show the limitations, we may write the genuine coincidence counting rate, $N_g(T)$, (where T is the experimentally introduced time delay) as follows:

$$N_g(T)=\int_{-\infty}^{\infty} \nu_g(T-t)p(t)dt, \qquad (1)$$

where $\nu_g(T)$ is the delay curve in the case of the source producing simultaneous events, and $p(t)dt$ is the probability of the time delay between events of the decaying source. Expanding $\nu(T-t)$ in a series about T and integrating, we obtain

$$N_g(T)=\nu(T)M^{(0)}[p(t)]-\frac{d\nu}{dT}M^{(1)}[p(t)]+\frac{1}{2}\frac{d^2\nu}{dT^2}M^{(2)}[p(t)], \qquad (2)$$

where $M^{(n)}[p(t)]$ is the nth moment of the $p(t)$ curve. If the

* This work was performed under the auspices of the AEC.
† Now at Physics Department, Rice Institute, Houston, Texas.
[1] Bay, Meijer, and Papp, Phys. Rev. **83**, 204 (1951).
[2] Bay, Meijer, and Papp, Phys. Rev. **82**, 956 (1951).

short decay process falls within the linear portion of the $\nu(T)$ curve, then

$$N_\phi(T)\cong\nu(T)-(d\nu/dT)M^{(1)}[\phi(t)], \quad (3)$$

if the disintegration rates of the two sources are reduced to the same value, which means that the area under the $\phi(t)$ curve is unity. In the case of a simple decay process with a mean life θ, the difference Δ in the counting rates for the two sources is

$$\Delta\cong(d\nu/dT)\theta. \quad (4)$$

It should be noted that this result provides a means for measuring very short half-lives without changing the artificial time delays in the equipment during the measurements. It is necessary only to exchange the two sources and measure counting rates at one proper value of the artificial time delay.

This also holds for the differential delay curve. Using this curve has several advantages: (1) It has a greater slope; (2) It is linear over an interval whose width can be experimentally controlled; (3) It is linear even in the region where the counting rate is near zero, and so the statistical error of Δ is less.

Experiments using these ideas are in progress and preliminary results indicate that half-lives as short as 10^{-10} sec or less can be measured.

* Supported by the ONR and AEC.
[1] Z. Bay, Bull. Am. Phys. Soc. 26, No. 3, 51 (1951).
[2] Z. Bay, Phys. Rev. 77, 419 (1950).

Scattering of Secondary Electrons Produced by γ-Rays in Materials of Various Atomic Numbers*

GERALD J. HINE†
Department of Physics, Massachusetts Institute of Technology, Cambridge, Massachusetts
(Received April 16, 1951)

THE secondary electrons, such as those emitted from the walls of a G-M counter or from the material which covers a photographic emulsion, determine the sensitivity of any γ-ray detector.[1] For a γ-ray of given energy, the number of Compton electrons produced per gram of various materials decreases only slightly with increasing atomic number Z of the absorber. However, the relative number of secondary electrons emitted from a converter in the forward and backward direction varies strongly with Z. This has been demonstrated previously only for the radium γ-rays by Bragg and Madsen[2] and later by other authors. In the present experiment, the scattering of secondary electrons produced by monochromatic γ-rays in materials of various Z has been studied as a function of the γ-ray energy.

A collimated beam of γ-rays from the various radio-isotopes passes through two adjacent ionization chambers; each chamber being a cube about 5 inches on a side. With the exception of a Lucite bottom plate, the chamber walls are made of very thin aluminum foils (0.00025 in.) supported by four rods at the corners of each chamber. Absorbers can be placed vertically into the 1-cm wide opening between the two chambers, as indicated in Fig. 1. A magnetic field placed between the γ-ray collimator and chamber (A) deflects the secondary electrons emitted from the collimator. For a given γ-ray source, the ion current in each chamber, with no absorber between them, is regarded as chamber background. It is caused by γ-ray absorption in the chamber walls and the air volume. With an absorber in place any additional ion current observed in chamber (A) must be due to backscattered secondary electrons produced by the γ-rays in the absorber, while the emergent electrons increase the ion current in chamber (B). A lead absorber always yielded an ion current in each chamber of about twice the background reading. For each γ-ray energy the absorber thickness was chosen approximately equivalent to the range of the secondary electrons.

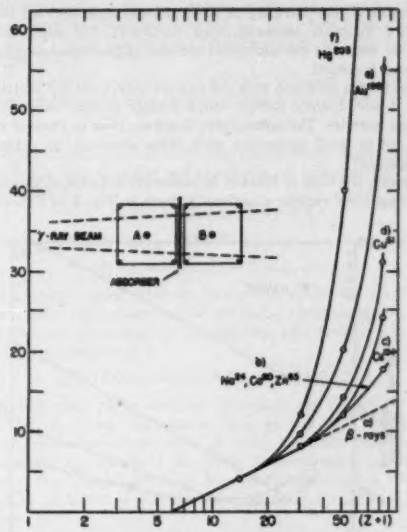

FIG. 1. Relative intensity of backscattered secondary electron emission produced by γ-rays from various nuclides as a function of $\log(Z+1)$ of the absorber.

The results obtained with seven nuclides are shown in Figs. 1–3. For the various sources, their strengths have been adjusted to equal intensity backscattered from aluminum absorbers. The chamber background was always subtracted from the actual reading. Curve (a) in Fig. 1 is the saturation backscattering factor for β-ray sources, which appears to be independent of the maximum energy of the β-ray emitter.[3] This backscattering factor has been found[4] to be a linear function of $\log(Z+1)$. Curve (b) in Fig. 1 shows that for the high energy γ-rays of Na^{24}, Co^{60}, and Zn^{65} the backscattered secondary electrons follow curve (a) up to copper, while the values obtained with tin and lead are somewhat higher. The production of photoelectrons, in addition to the Compton electrons, becomes more pronounced for the lower energy γ-rays, curves (c–f) in Fig. 1.

The emission of secondary electrons in the forward direction is shown in Fig. 2. Because of the increased backscattering with

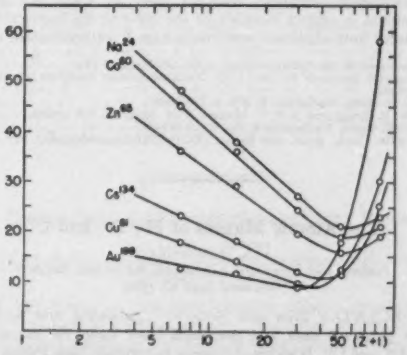

FIG. 2. Relative intensity of secondary electron emission in the forward direction produced by γ-rays from various nuclides as a function of $\log(Z+1)$ of the absorber.

increasing Z, the intensity of Compton electrons emitted in the forward direction decreases with $\log(Z+1)$. For high atomic number materials the additional emission of photoelectrons again becomes apparent.

The results obtained with the radium γ-rays are not plotted in Figs. 1 and 2, since radium emits a large number of γ-rays of various energies. The radium curves appear close to those of Zn^{65}, and are in good agreement with those obtained by other investigators.[3]

Finally, the ratio of forward to backward emission of secondary electrons from various absorbers is given in Fig. 3 as a function

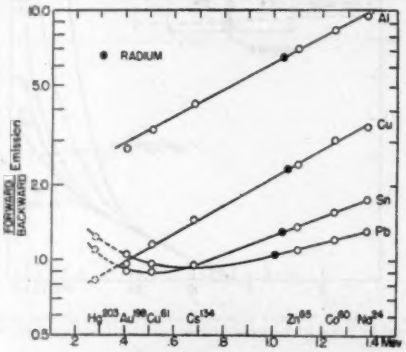

FIG. 3. Ratio of forward to backward emission of secondary electrons from various absorbers as a function of the γ-ray energies.

of the γ-ray energies. Since the Na^{24} values are not much different from those obtained with Co^{60}, they have been plotted arbitrarily at 1.38 Mev neglecting the 2.76-Mev Na^{24} γ-rays. The radium values fit on these curves which have been determined with monochromatic γ-rays, at an energy of about 1 Mev. For aluminum and copper absorbers, the ratio of forward to backward emission increases rapidly with increasing γ-ray energy. Lead, however, emits about equal amounts of secondary electrons in both directions rather independent of the γ-ray energy.

The results indicated here have to be taken into account for the construction of efficient γ-ray detectors. For high energy γ-rays, the front wall should be made of low Z, the back wall of high Z material. Furthermore, two methods become apparent which allow a quick and reasonably accurate determination of the "effective" γ-ray energy, of any source. Either the ratio of emergent to backscattered secondary electrons from an about 0.4 g/cm² aluminum or copper absorber or the ratio of the backscattered intensity from aluminum and from a high Z material can be used.

* Assisted by the joint program of the ONR and AEC.
† Special Research Fellow of the National Cancer Institute, Bethesda, Maryland.
[1] G. J. Hine, Nucleonics **7**, No. 4, 18 (1950).
[2] W. H. Bragg and J. P. V. Madsen, Phil. Mag. **16**, 918 (1908).
[3] B. P. Burtt, Nucleonics **5**, No. 2, 28 (1949).
[4] Failla, Clark, Rossi, and Baily, AECD-2142 (unpublished).

The Atomic Masses of H^1, D^2, and C^{12}

A. H. WAPSTRA
*Instituut voor Kernphysisch Onderzoek, Amsterdam, Holland**
(Received April 17, 1951)

RECENTLY Nier and Roberts[1-3] published new spectrographical data and computed from them the masses of H^1, D^2, and C^{12}. It seems of interest to compare their values with nuclear reaction data, especially as their values for C^{12} do not agree very well (see Table III, columns N^1 and R^2). Therefore, we

TABLE I. Reaction energies (Mev).

1	$D(\gamma, n)H$	2.226 ±0.003	a
2	$Be^9 \rightarrow 2He^4$	0.091 ±0.005	b,c
3	$Be^9(p, d)Be^8$	0.560 ±0.003	c
4	$B^{11}(p, \alpha)Be^8$	8.567 ±0.011	c
5	$B^{11}(d, \alpha)Be^9$	8.018 ±0.007	c
6	$C^{13}(d, \alpha)B^{11}$	5.160 ±0.010	d
7	$C^{13}(d, n)N^{14}$	−0.281 ±0.003	c
8	$C^{13}(p, n)N^{13}$	−3.003 ±0.003	c
9	$C^{13}(d, p)C^{14}$	5.948 ±0.008	e
10	$C^{14}(\beta^-)N^{14}$	0.156 ±0.001	c
11	$O^{18}(d, \alpha)N^{14}$	3.112 ±0.006	d

[a] R. C. Mobley and R. A. Laubenstein, Phys. Rev. **80**, 309 (1950).
[b] J. Crussard, Nature **166**, 825 (1950).
[c] Reference 11.
[d] Reference 12.
[e] Sperduto, Holland, Van Patter, and Buechner, Phys. Rev. **80**, 769 (1950).

computed from the reactions mentioned in Table I the mass doublets of Table II (column Q); column NR in the same table gives the values of Nier and Roberts and column M those of Mattauch,[4] except for the doublet D_2-He^4 which has been measured by Ewald.[5] For the difference in mass of neutron and H atom we assume the value[6] 782±2 kev and for the energy-mass conversion factor 1 MU = 931.15±0.05 Mev (from a value 299,790±2 km/sec for the velocity of light[7,8] and 96,520±3 coulomb[8,10] for the faraday). The reaction energy value for the D_2-He^4 doublet was computed from reaction cycles as mentioned in a former paper,[9] using however new values for various reaction energies.[11,12] The results from different cycles agree very well: the values from 16 cycles scattered only between 25.608 and 25.572 mMU. In the computation of the last two doublets in Table II the mean value

TABLE II. Mass doublets (mMU).

	Q	M	NR
H_2-D	1.551 ±0.004	1.539 ±0.002	1.5519 ±0.0017
D_2-He^4	25.596 ±0.009	25.604 ±0.008	25.612 ±0.009
CH_2-N^{14}	12.579 ±0.012	12.578 ±0.021	12.586 ±0.013
CH_4-O^{16}	36.388 ±0.016	36.381 ±0.028	36.478 ±0.022
$D_2-\frac{1}{2}C^{12}$	42.316 ±0.015	42.239 ±0.021	

of the three results for the D_2-He^4 doublet was used, yielding a difference in binding energies $E(He^4)-2E(D)=23.838\pm0.006$ Mev. Using the result of reaction 1 of Table I for the binding energy of the deuteron, which agrees with the results of various reaction cycles,[9] the binding energy of the α-particle becomes 28.290±0.009 Mev.

The results for the mass doublets D_2-He^4 and CH_2-N^{14} agree very well. The disagreement for the H_2-D doublet is not serious, as the reaction energy value seems to be entirely reliable;[6] therefore, it looks as though there must be an error in Mattauch's value. However, the doublets CH_4-O^{16} and $D_2-\frac{1}{2}C^{12}$ cause difficulties. The reactions (Table I) used in their computation can all be checked by cycles of other precisely measured reactions, except reactions 6 and 11. It is however not likely that there is a serious error in these two (d, α) reactions, as various other (d, α) reactions measured by the same group[12] agree very well with other nuclear reaction data. Moreover, the Q-value of the $N^{14}(d, \alpha)C^{12}$ reaction agrees with the two measurements of the $C^{13}H_2-N^{14}$ doublet in Table II.

In view of these facts we believe the nuclear reaction values for the $C^{13}H_2-O^{16}$ and $D_2-\frac{1}{2}C^{12}$ doublets to be the most reliable.

TABLE III. Nuclear masses: $M-A$ in 10^{-4} MU.

	N	R	N_7	R_7	Q
H^1	8154 ±6	8168 ± 5	8135 ±5	8152 ± 5	8146 ± 3
D^2		14785 ±10		14751 ± 9	14740 ± 4
C^{12}	3850 ±6	3803 ±13	3850 ±6	3781 ±13	3807 ±19

Therefore, we computed the masses of H, D, and C^{12} from these doublets combined with a value 1.552 ± 0.002 mMU for H_2-D; the results are collected in column Q, Table III. For comparison we also included values computed from Nier's and Roberts' energy cycles, using however the reaction energy value for $C^{12}H_2-O^{16}$ (columns Nr and Rr). It is seen, that the values of Roberts' cycle are in agreement with the nuclear reaction data, but in Nier's cycles there remains an unsolved discrepancy.

We thank Professor C. J. Bakker for his interest in this work.

* Financially supported by the foundation F.O.M.

[1] A. O. Nier, Phys. Rev. **81**, 624 (1951).
[2] T. R. Roberts, Phys. Rev. **81**, 624 (1951).
[3] A. O. Nier and T. R. Roberts, Phys. Rev. **81**, 507 (1951).
[4] J. Mattauch and A. Flammersfeld, Isotopenbericht (1949).
[5] H. Ewald, Z. Naturforsch. **5a**, 1 (1950).
[6] A. H. Wapstra, Physica **16**, 611 (1950).
[7] K. Bol, Phys. Rev. **80**, 298 (1950).
[8] E. Bergstrand, Arkiv. Fys. **2**, 119 (1950).
[9] Sommer, Thomas, and Hipple, Phys. Rev. **80**, 487 (1950).
[10] D. Norman Craig and J. J. Hoffman, Phys. Rev. **80**, 487 (1950).
[11] Hornyak, Lauritsen, Morrison, and Fowler, Revs. Modern Phys. **22**, 291 (1950).
[12] M.I.T. group; private communications of P. M. Endt and D. M. Van Patter.

Note on the General Theory of Scattering

M. L. GOLDBERGER
Institute for Nuclear Studies, University of Chicago, Chicago, Illinois
(Received April 9, 1951)

THE usual presentation of scattering theory proceeds from a discussion of the integral equations[1]

$$\Psi_a^{(\pm)}=\Phi_a+\frac{1}{E_a\pm i\epsilon-H_0}H_1\Psi_a^{(\pm)}. \tag{1}$$

The transition probability per unit time from a state characterized by Φ_a to an initially unoccupied state Φ_b may be expressed as

$$w_{ba}=(2\pi/\hbar)\,|\mathbf{R}_{ba}|^2\delta(E_b-E_a)$$
$$\mathbf{R}_{ba}=-(\Phi_b,\,H_1\Psi_a^{(+)})=-(\Psi_b^{(-)},\,H_1\Phi_a). \tag{2}$$

The matrix $\mathbf{R}_{ba}$ is defined only on the energy shell $E_a=E_b=E$. (Bold-face quantities hereafter always refer to the energy shell, E.) The integral equation (1) may be replaced by a pair of integral equations: Introduce a "standing wave" state vector $\Psi_a^{(1)}$ which, except for a normalizing factor, is $(\Psi_a^{(+)}+\Psi_a^{(-)})/2$ by the equation

$$\Psi_a^{(1)}=\Phi_a+P\left(\frac{1}{E_a-H_0}\right)H_1\Psi_a^{(1)}. \tag{3}$$

It is then easy to show that (1) is satisfied if

$$\Psi_a^{(+)}=\Psi_a^{(1)}+i\pi\,\Sigma_c\,\Psi_c^{(1)}\delta(E_a-E_c)\mathbf{R}_{ca} \tag{4}$$

from which, using (2), we find the Heitler integral equation[2]

$$\mathbf{R}_{ba}=\mathbf{G}_{ba}+i\pi\,\Sigma_c\,\mathbf{G}_{bc}\delta(E-E_c)\mathbf{R}_{ca}, \tag{5}$$

with

$$\mathbf{G}_{ba}=-(\Phi_b,\,H_1\Psi_a^{(1)})=-(\Psi_b^{(1)},\,H_1\Phi_a)=\mathbf{G}_{ab}{}^*. \tag{6}$$

From (3) we obtain an integral equation for G (*not* on the energy shell):[3]

$$G_{ba}=B_{ba}-P\,\Sigma_c\frac{B_{bc}G_{ca}}{E_a-E_c},$$
$$B_{ba}=-(\Phi_b,\,H_1\Phi_a). \tag{7}$$

B_{ba} is the Born approximation matrix element of the elementary scattering act. It should be carefully noted that G in contrast to $\mathbf{G}$ is *not* hermitian. This may in fact be utilized to derive an expression for the energy dependence of G near the energy shell.

A formulation of scattering theory in which (5) and (7) are regarded as fundamental rather than (1) is attractive for several reasons: (1) Only the existence of the wave functions Φ_a of the separated system, needed for finding B_{ba}, is presumed. (2) Approximation procedures based on approximate solution of (7) and exact solution of (5) have proved very useful in specific applications mentioned below and in all cases have the property of preserving the unitarity of the collision matrix. (3) The whole formalism may be derived from variational principles which are very useful in applications.

A variational basis for (5) and (7) will now be presented. Recalling that for a large class of problems the collision matrix

$$S_{ba}=\delta_{ba}+2\pi i\delta(E_b-E_a)\mathbf{R}_{ba} \tag{8}$$

is both symmetric and unitary, that consequently $\mathbf{R}$ is symmetric, and finally that $\mathbf{G}$ is real and symmetric,[4] it is easy to show[5] that the matrix I,

$$I=\mathbf{RG}+\mathbf{GR}+i\pi\mathbf{RGR}-\mathbf{RR}, \tag{9}$$

with matrix multiplication defined by

$$(\mathbf{RG})_{ba}=\Sigma_c\,\mathbf{R}_{bc}\delta(E-E_c)\mathbf{G}_{ca},\ \text{etc.},$$

is stationary under arbitrary variations about the correct $\mathbf{R}$. Conversely, the requirement of vanishing variation leads to (5). An alternate normalization independent expression of the same stationary principle is

$$I_{ba}{}'=(\mathbf{RG})_{ba}(\mathbf{GR})_{aa}[(\mathbf{RR})_{aa}-i\pi(\mathbf{RGR})_{aa}]^{-1}. \tag{10}$$

The stationary value obtained (the same for (9) and (10)) is $(\mathbf{R}-\mathbf{G})/i\pi$. These expressions have proved very useful for approximate determinations of $\mathbf{R}$. They have also been used to investigate the nature of the errors involved using the Heitler prescription of replacing $\mathbf{G}$ by $\mathbf{B}$.[6] An analogous pair of relations may be given for $\mathbf{G}$. Consider the matrix J_{ba} with $E_a=E_b=E$ defined by

$$J_{ba}=P\,\Sigma_c\frac{G_{bc}{}^\dagger G_{ca}}{E-E_c}+P\,\Sigma_{c,d}\frac{G_{bc}{}^\dagger B_{cd}G_{da}}{(E-E_c)(E-E_d)}$$
$$-P\,\Sigma_c\frac{G_{bc}{}^\dagger B_{ca}+B_{bc}G_{ca}}{E-E_c}. \tag{11}$$

J_{ba} is stationary under arbitrary variations about the correct G and $G^\dagger$, the demand of vanishing variation yields (7) and its adjoint. A normalization independent form of (11) is

$$J_{ba}{}'=-(G^\dagger B)_{ba}(BG)_{ba}[(G^\dagger G)_{ba}+(G^\dagger BG)_{ba}]^{-1}, \tag{12}$$

where matrix multiplication is defined by

$$(G^\dagger G)_{ba}=P\,\Sigma_c\,G_{bc}{}^\dagger G_{ca}/(E-E_c),\ \text{etc.}$$

The stationary value of J and J' is $\mathbf{G}-\mathbf{B}$.

A detailed discussion of the above material together with the results of applications to nucleon-nucleon and meson-nucleon scattering problems, and to the nonrelativistic Compton effect will be presented shortly.

[1] B. Lippmann and J. Schwinger, Phys. Rev. **79**, 469 (1950). We follow the notation of these authors except $\mathbf{T}\to-\mathbf{R}$, $\mathbf{K}\to-\mathbf{G}$.
[2] See, for example, W. Pauli, *Meson Theory of Nuclear Forces* (Interscience Publishers, Inc., New York).
[3] Equation (7) is usually given only in iterated form, reference 2; this is neither desirable nor necessary.
[4] J. A. Wheeler, Phys. Rev. **52**, 1107 (1937); W. Heisenberg, Z. Physik **120**, 513, 673 (1943); E. P. Wigner and L. Eisenbud, Phys. Rev. **72**, 29 (1947). In cases for which S is not symmetric in the elementary sense, a somewhat more complicated formulation can be made. This will be discussed in a later publication.
[5] See also, S. T. Ma and C. F. Hsueh, Phys. Rev. **67**, 303 (1945). I am indebted to Dr. Ma for a discussion of this work and the work of the present paper.
[6] W. Heitler, *Quantum Theory of Radiation* (Oxford University Press, London, 1944), second edition.

A Comparison of Theories of Secondary Emission

JAMES J. BROPHY
Physics Department Illinois Institute of Technology, Chicago, Illinois
(Received April 13, 1951)

THE theory of secondary emission using a quantum-mechanical attack has achieved reasonable success in predicting the variation of the secondary emission ratio with primary energy for several materials.[1] Recently an admittedly approximate theory using the free-electron approximation has appeared.[2] It is

interesting to observe that by means of a simple manipulation of Wooldridge's result a remarkable similarity between the two theories is evident.

The result of the free-electron approximation attack can be written

$$\delta/\delta_{max}=1.85F[0.92E_p/E_{p\,max}], \quad (1)$$

where

$$F(x)=\exp(-x^2)\int_0^x \exp(t^2)dt,$$

where δ is the secondary ratio, E_p is the primary energy, and $E_{p\,max}$ is the primary energy for the maximum secondary ratio, δ_{max}. The numerics in Eq. (1) result from the behavior of $F(x)$.

The result of the quantum-mechanical method given by Wooldridge is

$$\delta/\delta_{max}=1-\exp[-K(E_p/E_0-1)]+M\int_0^{K(E_p/E_0-1)}[E_p/E_0-v/K]^{\frac{1}{2}}e^{-v}dv,$$

where

$$K=\frac{1}{2\delta_{max}}\left[1-\left(\frac{W_a}{E_0+E_F}\right)^2\right]$$

$$M=\frac{1}{2}\left[1+\left(\frac{W_a}{E_0+E_F}\right)^2\right],$$

where E_0 is the average energy given a secondary by a primary, W_a is the height of the energy barrier at the surface, and E_F is the mean Fermi energy of the electrons in the lattice. Introducing the substitutions

$$E_p/E_0-v/K=t^2/K$$

and

$$KE_p/E_0=x^2,$$

the relation becomes after some manipulation,

$$\delta/\delta_{max}=1-A\exp(-x^2)+BF(x), \quad (2)$$

where $F(x)$ is the same function as in Eq. (1) and the constants are

$$A=e^K+2MK^{\frac{1}{2}}\int_0^K \exp(t^2)dt\cong e^K+2MK(1+K/3)$$

$$B=2MK^{\frac{1}{2}}.$$

It is seen that the same function appears in both theories, although the method of attack varies widely. For materials like gold, silver, and platinum, for which the Wooldridge theory is most accurate, the constants A and B are roughly 1.5 and 0.6, respectively, which means that neither term can be neglected. Figure 1

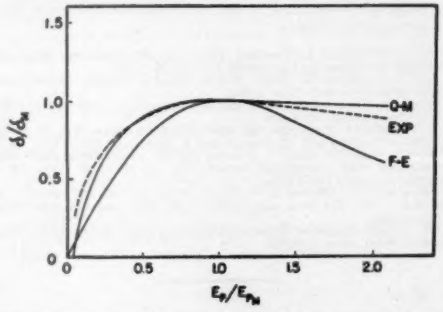

FIG. 1. Comparison of the quantum-mechanical and free-electron results with the universal secondary efficiency curve suggested by Baroody. The experimental curve is taken from reference 2.

compares the results of the two theories with the universal secondary emission curve suggested by Baroody. For this plot the above values of A and B have been used.

In addition to the appearance of the new exponential term in Eq. (2), there is a difference in the dependence on E_p. In Eq. (1) the argument is a linear function of the primary energy while in Eq. (2) the argument is proportional to the square root of this energy. With Wooldridge's relation in the form given by Eq. (2), the application to experimental results is considerably simplified since the graphical integration need be done only once to evaluate $F(x)$.

I am indebted to Dr. P. L. Copeland for his kindness in discussing this work with me.

[1] D. E. Wooldridge, Phys. Rev. 56, 562 (1939).
[2] E. M. Baroody, Phys. Rev. 78, 780 (1950).

Decay of Np^{236}

D. A. ORTH AND G. D. O'KELLEY
Radiation Laboratory and Department of Chemistry, University of California, Berkeley, California*

(Received April 9, 1951)

RECENT work at this laboratory on the nuclear energy surface[1] in the heavy region has demonstrated the value of precise determinations of the transition energies in radioactive decay in these elements. As part of a program of such measurements, the beta-decay energy of 22-hour Np^{236} came under consideration. The decay cycles involving this isotope of neptunium (Fig. 1)[2] showed that the experiment might be complicated by

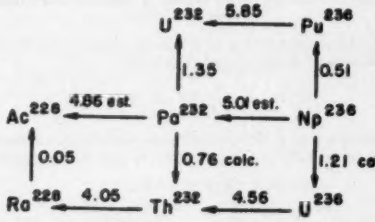

FIG. 1. Closed cycles involving the decay energies of Np^{236}.

orbital electron capture decay to U^{236}, so an attempt has been made to establish the decay scheme of Np^{236}.

Samples of neptunium were prepared by bombardment of U^{235} with the deuteron beam from the 60-inch cyclotron at Crocker Radiation Laboratory. The electron spectrum of purified neptunium fractions was observed on a beta-ray spectrometer employing the double-focusing principle proposed by Svartholm and Siegbahn,[3] and Shull and Dennison.[4] The detector is a Geiger counter filled with 8.8 cm of 90 percent argon, 10 percent ethylene mixture, and has a 30-μg/cm^2 Formvar window supported on a mesh grid. Window absorption corrections are necessary only below about 30 kev and can be made with fair accuracy.

Samples of chemically separated Np^{236} were evaporated from concentrated hydrochloric acid solution on conducting Tygon films about 30 μg/cm^2 thick. Auger electrons, internal conversion electrons, and beta-particles were seen. The beta-spectrum is complex, and resolution of Fermi-Kurie plots of the data indicate beta-energies of 0.51 Mev (59 percent) and 0.36 Mev (41 percent). A pair of internal conversion lines corresponding to the K and L conversion of a 150-kev gamma-ray was also observed. This gamma-ray is approximately 100 percent converted if it is assumed to follow the 0.36-Mev transition. The measured intensities of the electrons from Auger conversion of the K and L x-rays were far in excess of the Auger electrons expected from K and L electron vacancies due to the observed internal conversion of the 150-kev gamma-ray.

The radiations were resolved by beryllium and silver absorption into electrons, L x-rays, and K x-rays; and the relative abundance of each was determined. These were corrected for the counting efficiencies under the experimental conditions, and the L Auger conversion factor was assumed to be[5] 0.5. An estimate of the

amount of K electron capture may be made if the K x-rays observed in the absorption experiments are corrected for the contribution from internal conversion of the gamma-ray. If the L electron vacancies resulting from the K vacancies are subtracted from the total calculated from the absorption experiments, a further estimate of the amount of L electron capture is obtained. When these are related to the number of beta-particles, a decay scheme may be postulated in which the relative abundances of beta-decay and electron captures should be correct to ± 20 percent (Fig. 2).

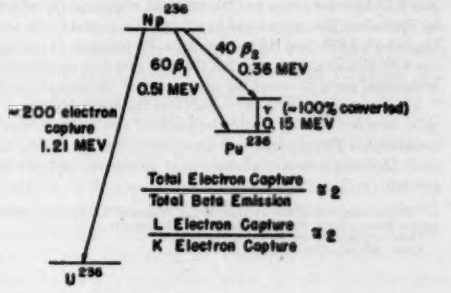

FIG. 2. Decay scheme of Np^{236}.

Apparently there is a considerable amount of L electron capture, even at this large disintegration energy of about 1.2 Mev. However, other heavy nuclides such as Am^{242m}, U^{231}, and Np^{235} have demonstrated predominant capture of L electrons[6-8] at lower transition energies.

We wish to thank Professor G. T. Seaborg for his continued interest and advice.

* This work was performed under the auspices of the AEC.
[1] Perlman, Ghiorso, and Seaborg, Phys. Rev. **77**, 26 (1950).
[2] The alpha-disintegration energy of U^{236} is from Ghiorso, Brittain, Manning, and Seaborg, Phys. Rev. **82**, 558 (1951); and Jaffey, Diamond, Hirsch, and Mech, to be published. The alpha-disintegration energies of Np^{236} and Pa^{232} were estimated as discussed by I. Perlman, *et al.* (reference 1). The other energies are based on the data reviewed by G. T. Seaborg and I. Perlman, Revs. Modern Phys. **20**, 585 (1948).
[3] N. Svartholm and K. Siegbahn, Arkiv. Mat. Astron. Fysik. **33A**, No. 21 (1946); Hedgran, Siegbahn, and Svartholm, Proc. Phys. Soc. (London) **63A**, 960 (1950).
[4] F. Shull and D. Dennison, Phys. Rev. **71**, 681 (1947); **72**, 256 (1947).
[5] B. B. Kinsey, Can. J. Research **A**, 404 (1948).
[6] O'Kelley, Barton, Jr., Crane, and Perlman, Phys. Rev. **80**, 293 (1950).
[7] Crane, Ghiorso, and Perlman, to be published.
[8] R. A. James and A. Ghiorso, to be published.

The Splitting of l-Shells in Heavy Nuclei by the Tensor Interaction

JULIAN KEILSON*
Cruft Laboratory, Harvard University, Cambridge, Massachusetts
(Received February 19, 1951)

TO explain the nuclear "magic numbers,"[1] a strong spin-orbit interaction favoring single-particle states of total angular momentum $j=l+\frac{1}{2}$ is needed. A study has been made of the contribution to this splitting of a tensor interaction

$$V=\Sigma_j J(r_{oj})T_{oj}=\Sigma_j J(r_{oj})[3(\boldsymbol{\sigma}_o\cdot\mathbf{r}_{oj}/r_{oj})(\boldsymbol{\sigma}_j\cdot\mathbf{r}_{oj}/r_{oj})-\boldsymbol{\sigma}_o\cdot\boldsymbol{\sigma}_j]$$

between the outer particle Q_o, and the particles Q_j of a spherically symmetrical spin-saturated core, regarded as moving independently in the states ψ_i of a spherical potential well.

The first-order perturbation energy is zero for all outer particle states and so can contribute nothing to the splitting. The second-order perturbation energy is $\Sigma_i(o|V|i)(i|V|o)/(E_o-E_i)$. A Fermi-Thomas approximation and other crude approximations to the part of this energy dependent on the spin of the outer particle give zero, and a direct evaluation of the above expression incorporating complete antisymmetry is required. The isotopic spin plays no essential role. The only feasible way of treating the denominators in the above summation is to expand them about a mean excitation energy, $\bar{\epsilon}$, and to deal with the first two terms of the expansion,

$$\frac{1}{E_o-E_i}=-\frac{1}{\bar{\epsilon}}+\frac{E_i-\bar{E}_i}{\bar{\epsilon}^2}\cdots.$$

For the spin-dependent part of the perturbation, the first term of the expansion gives

$$(\Delta\epsilon)_1=\frac{-18i}{\bar{\epsilon}}\Sigma_\sigma\int\psi_o^*(\mathbf{r}_1)\chi_o(\sigma)\Big\{\boldsymbol{\sigma}\cdot\Big(\frac{\mathbf{r}_{12}}{r_{12}}\times\frac{\mathbf{r}_{12}'}{r_{12}'}\Big)\Big(\frac{\mathbf{r}_{12}}{r_{12}}\cdot\frac{\mathbf{r}_{12}'}{r_{12}'}\Big)$$
$$\times J(r_{12})J(r_{12}')[\delta(\mathbf{r}_1-\mathbf{r}_1')-\rho_c(\mathbf{r}_1,\mathbf{r}_1')][\delta(\mathbf{r}_2-\mathbf{r}_2')-\rho_c(\mathbf{r}_2,\mathbf{r}_2')]$$
$$\times[\rho_c(\mathbf{r}_2,\mathbf{r}_2')\psi_o(\mathbf{r}_1')\chi_o(\sigma)-\rho_c(\mathbf{r}_2,\mathbf{r}_1')\psi_o(\mathbf{r}_2')\chi_o(\sigma)]\Big\}$$
$$\times d\mathbf{r}_1d\mathbf{r}_2d\mathbf{r}_1'd\mathbf{r}_2'.$$

The second term is similar in character.

The integrals are evaluated by expanding the wave functions ψ_o and the core matrix densities ρ_c about $\mathbf{r}_1$, say, chosen as the local coordinate and carrying out the local integrations. We then find that

$$\Delta\epsilon\rightarrow K(\chi_o'\psi_o|\boldsymbol{\sigma}\cdot\mathbf{L}V(r)|\chi_o\psi_o),$$

where

$$V(r)=-(1/r)\rho_c(r)d\rho_c(r)/dr.$$

Contributions to the splitting of the correct sign can come only from a region of radially-increasing core density. If the outer particle spends most of its time in such a region and if the above approximations have validity, splitting of the needed sign and the magnitude could be available. The positive quantity K varies as $J_o^2/\bar{\epsilon}$, where J_o is the strength of the tensor interaction and $\bar{\epsilon}$ is the mean excitation energy of the nucleus. K also depends in a complicated way upon the range and form of the tensor interaction and the structure of the core density $\rho_c(\mathbf{r},\mathbf{r}')$. A rough approximation to the energy difference of the $j=l+\frac{1}{2}$ and $j=l-\frac{1}{2}$ levels of a particle moving about a moderately heavy core is given by

$$\epsilon_{l-\frac{1}{2}}-\epsilon_{l+\frac{1}{2}}\simeq(2l+1)J_o^2/(250\bar{\epsilon}).$$

Several particles outside the core will polarize it independently, and show a consequent individual preference for the appropriate j states. The particles will also be acted on by a change in potential due to the core polarization of the other exterior particles. These cross effects may be expected to be small and to tend to cancel as a new shell forms.

The details of this analysis are available in the author's Doctoral thesis, Department of Physics, Harvard University, June 1950.

I would like to thank Professor Julian Schwinger, who sponsored and encouraged this investigation.

* This work was carried out under an AEC Predoctoral fellowship.
[1] M. G. Mayer, Phys. Rev. **78**, 16 (1950). S. M. Dancoff, Phys. Rev. **58**, 326 (1940).

Radiations of Ag^{110}

MAX GOODRICH*
Oak Ridge National Laboratory, Oak Ridge, Tennessee
and
Louisiana State University, Baton Rouge, Louisiana
(Received April 12, 1951)

FROM studies of the radiations of the 225-day silver activity, Siegbahn[1] has proposed a decay scheme in which the activity originates in a metastable level 116 kev above the ground state. A small complex fraction of the beta-radiation, with end points of 2.86 and 2.12 Mev, is placed with its origin in the ground state and is presumed to be the beta-radiation of the well-known 24-sec activity. Siegbahn's data suggested that still other low intensity beta-rays may connect the Ag^{110} ground state with excited levels

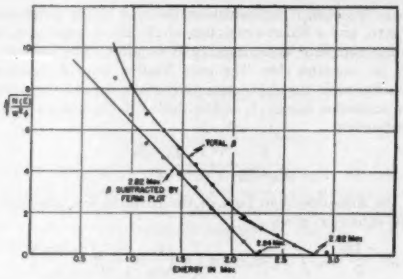

FIG. 1. Fermi plot of β-spectrum of 24-sec Ag^{110}.

of the Cd^{110} nucleus. Confirmation of the assignment to the ground state, of the 24-sec period, has been found.[2] Further confirmation is provided in the present work by the measurement of the energies of the beta- and gamma-rays in the 24-sec activity.

Using a scintillation spectrometer, direct measurement of the spectrum of the short-lived radiations has been made with the fast pneumatic tube installed at the Oak Ridge graphite reactor. The apparatus, details of which will be published later, uses a 5819 photomultiplier tube with either an anthracene or a NaI(Tl) crystal. Electromagnetically separated silver (91 percent Ag^{109}) in samples of AgCl about 10 mg/cm^2 in thickness was examined with the spectrometer after being irradiated for a few seconds in the reactor. The beta-spectrum is indeed complex and has been found by Fermi analysis (Fig. 1) to contain components having end points of 2.82±0.1 Mev and 2.24±0.1 Mev. The gamma-spectrum shows a relatively strong line at 0.66±0.02 Mev, a very much weaker line at about 0.9 Mev and a suggestion of other extremely weak lines. Within the limits of error, the two beta-rays and the strong gamma-ray can be identified, respectively, with the 2.86- and 2.12-Mev beta-rays and the 0.656-Mev gamma-ray observed by Siegbahn. The gamma-ray at about 0.9 is probably the sum of Siegbahn's 0.885- and 0.935-Mev lines. Its presence (5 percent of the 0.66-Mev line) indicates that the spectrum does contain a weak component going to one of the upper levels of the product nucleus.

The lower energy beta-ray constitutes the larger fraction of the total beta-ray activity. Estimates made of this fraction from the extrapolated Fermi plots, and also from the ratio N_β/N_γ along with Siegbahn's decay scheme, gave values of from 60 to 70 percent.

* This study was made at Oak Ridge National Laboratory while the author was on leave from Louisiana State University.

[1] Kai Siegbahn, Phys. Rev. **77**, 233 (1950).

[2] John Miskel, Phys. Rev. **79**, 403 (1950).

Proceedings of the American Physical Society

Minutes of the Meeting at Pittsburgh, March 8–10, 1951

THE 304th meeting of the American Physical Society was held at Pittsburgh, Pennsylvania, on Thursday, Friday, and Saturday, March 8, 9, and 10, 1951. This was the largest March meeting in the history of the Society, with an attendance of six hundred. It remains an open question how the credit for this expansion is to be shared between the location of the meeting, the activity of the Division of Solid-State Physics, and the inauguration of our new Division of Chemical Physics. Both Divisions provided exhaustive programmes of symposia, the first of which was a joint symposium of the two Divisions preceded by words of welcome from the Vice-President of the Society and the Chairman of the Division of Solid-State Physics and by a response from the Chairman of the Division of Chemical Physics. Five other half-day symposia were given by the new Division and four others by the older one. Sixty ten-minute papers, mostly but not altogether in the field of solid-state physics, were fitted into sessions which perforce were simultaneous with the symposia. E. C. Creutz described the new cyclotron of the Carnegie Institute of Technology. Our meetings were held in the Mellon Institute and the Bureau of Mines, and the efficient Chairman of the Local Committee was J. E. Goldman. The weather was flawless, the halls comfortably full but not overcrowded; everyone will have pleasant memories of this agreeable meeting.

The dinner of the Society was held on Thursday evening in the Webster Hall Hotel, with an attendance of nearly 300. The after-dinner speakers were President Warner of the Carnegie Institute of Technology, who spoke on problems of scientific manpower, and R. Smoluchowski of the same Institute, who spoke under the title "Why Didn't you Find It First?"

The Council met on Saturday afternoon, and elected to Fellowship two candidates and to Membership 102 candidates; their names are appended.

According to reports reaching the office of the Society, we have lost through death J. S. Gooden (Birmingham, England), J. W. Hornbeck (Kalamazoo College), and A. T. Jones (Smith College).

Elected to Fellowship: J. E. Goldman and R. H. Kent.

Elected to Membership: Richard M. Adams, Berni J. Alder, John J. Antal, Val J. Ashby, James W. Ballard, Roy A. Berg, Alex Berman, Sukumar Biswas, Robert L. Brock, Laird C. Brodie, Maarten Bogaardt, Bert E. Brown, Harry A. Brown, Charles B. Bryant, Earl Callen, Eugene H. Canfield, Rodney D. Chamberlain, Sheo-Chu Chen, Arthur B. Chilton, Henry L. Cox, Sumner P. Davis, Vernon L. Dawson, James W. Deer, Donald E. DeGraaf, Robert F. Doolittle, II, Kenneth L. Dunning, Robert F. Dvorak, Pieter M. Endt, Olive G. Engel, Charles C. Fiorino, Hugie L. Foote, Jr., William H. Fonger, Lloyd D. Fosdick, James R. Freeman, James B. Gerhart, James M. Goldey, Newton Grant, Donald Hagerman, William G. Hammerle, Jack Haugsnes, Wilmot N. Hess, Myron E. Heusinkveld, Edwin R. Hill, Lawrence J. E. Hofer, Lewis E. Hollander, Jr., Lee Edgar Hollingaworth, Martin H. Jachter, Israel S. Jacobs, Raymond Kaplan, John D. Keating, Clarence F. Kooi, Harry W. Knop, Jr., Jay W. Lathrop, Omer Lefort, Lawrence B. Leipuner, Aaron Lemonick, Solomon L. Linder, Ralph H. Lovberg, John B. Lyon, John L. Magee, Edward F. Mayer, Harden M. McConnell, Charles E. McFarland, Clare L. Mengel, Jack R. Mentzer, Robert L. Mills, Gordon E. Moore, Kenneth C. Morgan, Jose E. Moyal, J. Barry Oakes, Samuel Olanoff, Harry N. Olsen, Elbert C. Palmer, Anton Peterlin, John B. Phelps, Harvey Picker, Francis M. Pipkin, Alan M. Portis, Otto Redlich, Edward J. Ryder, Abdus Salam, Paul N. Schatz, David C. Schubert, Allan Shepp, Ivan Simon, Raymond W. Sloan, Charles V. Stephenson, II, Frederick E. Steigert, Lee P. Stephenson, Sister M. M. Stimson, Robert M. Talley, Robert K. Tasaka, David R. Teeters, Robert D. Tripp, Mario P. Vano, Thomas L. Weatherly, John M. Westhead, Charles W. Wilson, III, Gordon G. Wiseman, Edythe P. Woodruff, Robert A. Young, and Ariel C. Zemach.

KARL K. DARROW, *Secretary*
American Physical Society
Columbia University
New York 27, N.Y.

Errata Pertaining to Papers D3, D11, F3, G13, J8, L5, M4, and P7

D3, by E. E. Klontz and K. Lark-Horovitz. In the fourth line from the bottom, "for 10 incident electrons" should read "for 10^8 incident electrons (at the energy of 0.68 Mev)."

D11, by Egon E. Loebner. In line seven from the bottom, "examination" should read "explanation."

F3, by W. Gordy. In the by-line, "University of North Carolina" should read "Duke University."

G13, by C. H. Blanchard and U. Fano. In the title, "Multiple" should read "Multiply." In line 10, "numbers" should read "number." An equality sign should be added at the end of line 10. In line 11, "$2Z^2e^4$" should read "$2\pi Z^2e^4$."

J8, by E. J. Huibregtse, D. B. Baker, and G. C. Danielson. The values for the magnetic susceptibility should be multiplied by 10^{-6}.

L5, by Elliot Montroll and T. Berlin. The by-line should read "New York University and The Johns Hopkins University."

M4, by James P. Palmer. In line 14, the number 1.5 should read 0.66.

P7, by R. K. Willardson and G. C. Danielson. In line 12, the number 5 should be omitted.

PROGRAMME

THURSDAY MORNING AT 10:00

Mellon Institute Auditorium

(F. SEITZ presiding)

Inaugural Remarks. J. H. VAN VLECK, *Harvard University.*
Welcome to the new Division of Chemical Physics. A. VON HIPPEL, *M.I.T.*
Response by the Chairman of the Division of Chemical Physics. R. S. MULLIKEN, *University of Chicago.*

Joint Symposium (DSSP and DCP) on Electronic States of Molecules and Solids

A1. Some Aspects of the Electronic Structure Theory of Molecules. R. S. MULLIKEN, *University of Chicago.* (40 min.)
A2. Electronic Theory of Molecules and Crystals. J. C. SLATER, *M.I.T.* (40 min.)
A3. Overlap Integrals and Many-Orbital Effects in the Theory of Molecules and Crystals. P. O. LOEWDIN, *University of Uppsala.* (40 min.)

THURSDAY AFTERNOON AT 2:15

Mellon Institute Auditorium

(J. C. SLATER presiding)

Symposium (DSSP) on Vibration and Relaxation Spectra of Solids

B1. Vibrational Spectra of Solids. E. W. MONTROLL, *New York University.* (40 min.)
B2. Dielectric Relaxation Phenomena in Liquids and Solids. A. VON HIPPEL, *M.I.T.* (40 min.)
B3. Elastic Spectra of Liquids and Solids. K. HERZFELD, *Catholic University of America.* (40 min.)

THURSDAY AFTERNOON AT 2:15

Bureau of Mines

(J. O. HIRSCHFELDER presiding)

Beginning of the Symposium (DCP) on Molecular Structure and Valence Theory

C1. The Self-Consistent-Field Molecular-Orbital Theory. C. C. J. ROOTHAAN, *University of Chicago.* (40 min.)
C2. Theory of Normal and Excited States and Ultraviolet Spectra of Unsaturated Hydrocarbons. R. G. PARR, *Carnegie Institute of Technology.* (40 min.)
C3. Nuclear Magnetic Resonance in Studies of Molecular Structure and Internal Motions. G. E. PAKE, *Washington University.* (40 min.)

First Annual Business Meeting of the Division of Chemical Physics

---

THURSDAY AFTERNOON AT 2:15

Mellon Institute Social Room

(J. BARDEEN presiding)

Semi-Conductors Mostly

D1. Germanium Films. J. W. THORNHILL AND K. LARK-HOROVITZ, *Purdue University.*—Deposition of germanium films in a high vacuum onto quartz and glass was studied as a function of rate of evaporation and temperature of substrate The thickness (0.5μ–7μ) of these films was measured interferometrically. (K. W. Meissner) x-ray diffraction indicated

the normal diamond lattice without any preferential orientation and particle size of 100–400A, depending on the temperature of the substrate. Measurements of resistivity and Hall effect show that all films, regardless of the starting material used, are P-type with apparent room temperature mobilities between 1–50 cm²/sec volt indicating resistivity contributions due to scattering by defects, grain boundaries, and possibly trapping. High frequency measurements between 2 kilocycles and 2 megocycles show no variations of film resistance or capacity (Odell).

D2. Capacity Effects in $P-N$ Boundaries in Germanium.* N. H. ODELL AND H. Y. FAN, *Purdue University.*—The capacity of a $P-N$ junction produced by deuteron bombardment[1] has been measured as a function of temperature and of frequency. The frequency range was 50 kilocycles per second to 4 megacycles per second. The temperature range was room temperature to −155°C. A signal voltage, small compared with kT/e, was applied across the barrier in all cases. The barrier capacity exhibited a decided dependence on temperature, decreasing by several orders of magnitude from room temperature to −55°C at the lower frequencies and by a factor of approximately 3 for the same temperature range at the higher frequencies. Between −55°C and −155°C, the decrease was approximately by a factor of 2. At room temperature, the capacity of the sample exhibits a frequency dependence of approximately $1/f$, whereas at the two lower temperatures, the dependence is small. These results are consistent with the hypothesis that at room temperature part of the current is carried by holes in the N region at the barrier and by electrons in the P region.

* Work assisted by Signal Corps contract.
[1] Davis, Johnson, Lark-Horovitz, and Siegel, Phys. Rev. 74, 1255 (1948).

D3. Electron Bombardment of Ge. E. E. KLONTZ AND K. LARK-HOROVITZ, *Purdue University.**—Theory (M. M. Mills)[1] predicts lattice displacements produced in Ge by electrons of energies greater than 0.56 Mev. By using electron currents of 1–5 microamps (energies between 0.7 and 2.0 Mev.) from a Van de Graaff generator,[2] the following displacements were observed: N-type Ge is converted to P-type, thus allowing detection of the effect by observing the rectification characteristic. A threshold for the effect was found between 0.5 and 0.7 Mev. As is observed in heavy particle irradiation,[3] the resistance of an N-type sample increases on bombardment, reaches a maximum, and then on conversion decreases again. The resistance of a P-type sample decreases. From the conductivity *vs* irradiation curve on one N-type sample, it was found that about one defect occurs for 10 incident electrons. After irradiation, a decrease in the resistance of N-type samples indicates healing. In some cases, barriers produced by irradiation are highly photosensitive at low temperature.

* Partially supported by the U. S. Signal Corps and the AEC.
[1] Personal Communication.
[2] We are indebted to the Van de Graaff group at the University of Notre Dame and to the Argonne National Laboratories in Chicago for the irradiations.
[3] Lark-Horovitz, Bleuler, Davis, and Tendam, Phys. Rev. 73, 1256 (1948).

D4. Conversion of a Classical Semiconductor in Thermal Equilibrium from N- to P-Type.* V. A. JOHNSON AND K. LARK-HOROVITZ, *Purdue University.*—The behavior of germanium under the effects of bombardment-induced transmutations is similar to that of lead sulfide under the action of oxygen or sulfur. Irradiation converts N-type germanium into P-type. If lattice defects are healed out, the observed changes in electrical properties are due to transmutations.[1] These changes agree with theoretical predictions[2] assuming a classical semiconductor in thermal equilibrium. At constant temperature, the electron concentration times holes concentration is constant ($n_e n_h = K$). As acceptor impurities, n_A, are produced, electrons leave the conduction band until only intrinsic electrons remain; then holes are produced in the full band. Taking the mobility ratio as 1.5, one calculates that a germanium sample with an initial impurity electron concentration N shows, as bombardment progresses, increase in magnitude of the negative Hall coefficient R until $N-n_A=1.24K^{\frac{1}{2}}=2.4\times10^{13}$ cm^{-3} at 300°K. R then decreases in magnitude while the conductivity continuously decreases to a minimum when $n_A-N=0.41K^{\frac{1}{2}}=0.78\times10^{13}$ cm^{-3} at 300°K. The conductivity then increases, whereas R becomes zero when $n_A-N=0.83K^{\frac{1}{2}}=1.6\times10^{13}$ cm^{-3} at 300°K and passes through a positive maximum at $n_A-N=3.01K^{\frac{1}{2}}=5.7\times10^{13}$ cm^{-3} at 300°K.

* Assisted by Signal Corps Contract.
[1] Cleland, Lark-Horovitz, and Pigg, Phys. Rev. 78, 814 (1950).
[2] V. A. Johnson and K. Lark-Horovitz, Report on Reading Semiconductor Conference (in press).

D5. The Effect of Fast Neutron Bombardment on the Conductivity of P-Type Ge. J. W. CLELAND, J. H. CRAWFORD, K. LARK-HOROVITZ, AND J. C. PIGG, *Oak Ridge National Laboratory.*—The number of positive carriers introduced per incident neutron into P-type Ge depends to some extent on the past history of the sample and the temperature of the exposure. The former factor exists since it has been shown that the P-type conductivity slope is dependent on the initial carrier concentration at low temperature and when the material is originally N-type and has been converted by bombardment. The latter factor is expected, since only those carriers which are thermally ionized are effective in increasing the conductivity. Data is presented concerning the dependence of rate of P-type conductivity change with bombardment on the initial properties of the material for different temperatures. The effect of temperature on carrier concentration and mean free path is also discussed.

D6. Pile Irradiation of Semiconducting Cu_2O. J. C. PIGG, J. W. CLELAND, J. H. CRAWFORD, AND K. LARK-HOROVITZ, *Oak Ridge National Laboratory.*—A number of Cu_2O polycrystalline plates[1] were exposed in the Oak Ridge nuclear reactor and the conductivity was measured during the bombardment. Several Cu_2O rectifiers, both commercial units and specially prepared disks,[1] were also exposed and the resistance, forward and back, was followed during the bombardment at a reference voltage. In addition, on several of the rectifiers, forward and back I–V characteristic curves were measured, periodically, throughout the bombardment. The conductivity of Cu_2O plates decreases, initially quite rapidly, with bombardment approaching a limiting value. Cu_2O rectifiers show large increases of forward resistance on bombardment with only a small increase in the reverse direction. After sufficient bombardment, the units approach ohmic behavior. The commercial units behave qualitatively the same as the specially prepared disks.

[1] We are greatly indebted to Dr. S. J. Angello of Westinghouse Research Laboratories for making available to us the Cu_2O plates and rectifying disks.

D7. Electron Bombardment Induced Conductivity in Germanium Point Contact Rectifiers. A. R. MOORE AND F. HERMAN, *RCA.*—Bombardment of semiconductors with Mev electrons results in transient changes in conductivity, as well as semi-permanent changes due to lattice defects. By operating with electron beams in the kev range, which is below the threshold for introduction of defects, we have studied the transient effects of bombarding electrons on germanium point contact rectifiers. The experimental method employs television-type scanning of the crystal by the electron beam in the neighborhood of the probe. The results are presented on a kinescope as a map of induced conductivity over the surface

of the germanium. The maximum diode current flows when the beam is within 2×10^{-3} cm of the probe. Recombination of electrons and holes reduces the current as the beam moves away from the probe. The ratio of change in diode current to beam current is unusually large; values up to 5×10^{4} have been measured for a 10 kev beam. Some of this current multiplication is attributed to a secondary effect at the barrier. By measuring the delay of the signal at different scanning lines, the mobility of holes in *N*-type germanium was obtained. The result was 1590 cm²/volt-sec, in agreement with other methods.

D8. On the Direct Current Voltage Characteristic of Metal-Semiconductor Contacts. K. LEHOVEC, *Signal Corps Engineering Laboratory.*—The influence of surface states on the current voltage characteristic of a metal-semiconductor contact is calculated under the following assumptions: (1) there is a continuous energy spectrum of surface states; (2) the occupation of the surface states with electrons is determined (a) by the electron distribution in the metal, if the carriers of current flow from metal to semiconductor (blocking direction), and (b) by the electron distribution in the bulk semiconductor, if the carriers flow from semiconductor to metal (forward direction). For sufficiently large voltages, E, the current increases as

$$I\approx I_F\cdot\exp(aE);\quad a\lesssim e/kT\quad\text{(forward direction)}$$

and

$$I\approx I_B\cdot\exp[b(e)^{\frac{1}{2}}]\qquad\text{(blocking direction).}$$

Measurements on Ge-, Si-, and SiC-detectors, and on Cu_2O- and Se-rectifiers are compared with these results.

D9. Germanium-Indium Alloys as Low Temperature Resistance Thermometers.* SIMEON A. FRIEDBERG, *Carnegie Institute of Technology.*—A previous survey of semiconducting samples** indicates that materials with about 2×10^{17} impurity centers/cm³ and room temperature resistivities of about 0.05 ohm cm should have large enough temperature coefficients of resistivity at liquid helium temperatures to make good secondary thermometers. Experiments on *p*-type samples cut from a melt of germanium and 0.001 atomic percent indium are described. The influence of the original location of a sample in the melt on the magnitude and reproducibility of its change of resistivity with temperature is discussed. Satisfactory thermometers have been obtained from such a melt by surveying the resistivities between 4.2°K and 1.6°K of samples from slices taken perpendicular to the vertical axis. Strips from the uppermost layer of the melt are found to have about 1.5×10^{17} impurity centers/cm³ and resistivities at 300°K of about 0.08 ohm cm. From this group, a thermometer has been selected having a temperature coefficient of resistivity of -1 (deg. K)$^{-1}$ at 4°K and -370 (deg K)$^{-1}$ at 2°K. Its use in temperature measurement, reproducible to better than 0.01°K throughout the helium range, is discussed.

* This work has been assisted by the ONR and the Research Corporation.
** I. Estermann, Phys. Rev. 78, 83 (1950).

D10. The Optical Properties of Donor and Acceptor Impurities in Silicon. E. BURSTEIN, J. J. OBERLY, J. W. DAVISSON, AND B. W. HENVIS, *Naval Research Laboratory.*—Data on the optical absorption of neutral donor and acceptor impurities have been obtained from low-temperature infrared transmission measurements for impurity concentrations ranging from 10^{16} to 10^{18} atoms per cm³. The impurities are found to exhibit absorption bands characteristic of the photoelectric absorption by *K* shell electrons. Data obtained near the ionization limit in *N*-type silicon containing 10^{16} donor atoms per cm³ ($E_I\sim0.05$ ev) indicate an optical cross section of 3×10^{-18} cm² per impurity atom, which is in fairly good agreement with the theoretical value (1.7×10^{-18} cm²) for the hydrogen-like model.[1] The observed absorption at frequencies beyond the ionization limit ($h\nu\gtrsim3E_I$) in *P*-type silicon containing 10^{18} acceptor atoms per cm³ is likewise in rough agreement with the theoretical values. These results are a further confirmation of the validity of hydrogen-like models for neutral donor and acceptor impurity atoms in homopolar semiconductors with high dielectric constants.

[1] H. Hall, Revs. Modern Phys. 8, 358 (1936); H. Bethe, *Handbuch der Physik*, 2nd Edition XXIV/1, p. 477.

D11. Thermoelectric Power in Carbons and Graphite. EGON E. LOEBNER, *University of Buffalo* (*Introduced by* S. MROZOWSKI).—Raw cokes and baked carbon rods prepared by different processes were treated to different temperatures, and their thermoelectric powers were determined *versus* platinum at room temperature. All emf's found are negative; their absolute values show an interesting variation with temperature of treatment. Starting from cokes treated to 700°C, for which the resistivity is low enough to enable a measurement, the thermal emf decreases from a value of several tens of microvolts per °C to a minimum of approximately 8 microvolts/°C around 1400°C. A maximum of about 35 microvolts/°C occurs around 2200°C. This is followed by a sudden drop to about 10 microvolts/°C at 2550°C, and then a slow decrease with increasing graphitizing temperature toward a limiting value of a few microvolts/°C for Ceylon graphite. This general trend is in best agreement with the proposed examination of the electronic conductivity of graphite and carbons.[1] The treatment dependence in the lower region is caused by an increase of the number of excess electrons (removal of hydrogens) followed by a decrease due to crystallite growth. The drop above 2200°C occurs when the decreasing band separation becomes comparable to kT, thus allowing additional electrons to be activated.

S. Mrozowski, Phys. Rev. 77, 838 (1950).

THURSDAY EVENING AT 7:00

Webster Hall Hotel

(C. C. LAURITSEN or J. H. VAN VLECK presiding)

Banquet of the American Physical Society

FRIDAY MORNING AT 9:30

Mellon Institute Auditorium

(A. VON HIPPEL presiding)

Symposium (DSSP) on Divers Topics

E1. The Frequency Dependence of the Permeability of Ferromagnetics. R. BECKER, *University of Goettingen.* (40 min.)

E2. The Properties of Silver-Halide Crystals. F. SEITZ, *University of Illinois.* (40 min.)

E3. The Behavior of Holes and Electrons in Germanium. W. SHOCKLEY, *Bell Telephone Laboratories.* (40 min.)

Annual Business Meeting of the Division of Solid-State Physics

---

FRIDAY MORNING AT 9:30

Bureau of Mines

(E. BRIGHT WILSON presiding)

Conclusion of the Symposium (DCP) on Molecular Structure and Valence Theory

F1. Bridge Bonds and Valence Theory. R. E. RUNDLE, *Iowa State College.* (30 min.)

F2. Evidence on Bond Characters from Nuclear Quadrupole Effects. C. H. TOWNES, *Columbia University.* (40 min.)

F3. Molecular Structures from Microwave Spectra. W. GORDY, *University of North Carolina.* (30 min.)

F4. Predissociation of the Nitrogen Molecule. G. HERZBERG, *National Research Council of Canada.* (20 min.)

FRIDAY MORNING AT 9:30

Mellon Institute Social Room

(DAVID HALLIDAY presiding)

Optical, Chemical, and General Physics

G1. Atmospheric Transmission of Solar Radiation in the 35 to 75 Micron Region.* GLENN L. MUSSER AND RICHARD C. RAYMOND, *Pennsylvania State College.*—Radiation from the sun in the 35 to 75 micron region has been isolated by means of differential filters. The radiation was focused by a sixty-inch parabolic mirror onto a thermocouple. The mirror surface was blackened, and a combination of quartz and deposited filters removed most of the short wave radiation. The 35 to 75 micron components reaching the thermocouple were identified by use of a sodium chloride plate, which removes these components of radiation. The system was calibrated by use of a black-body source placed approximately ten meters from the receiver. Solar signals could be obtained only when the sky was perfectly clear. The total power in the 35- to 75-micron region was of the order of 0.1 microwatt per square centimeter. Assuming the sun is a black body at 6000 degrees and using Randall's[1] water spectrum, there should be about 0.3 microwatt per square centimeter. This agreement indicates that the water data may be used to compute the windows in this region to a fair degree of accuracy.

* This paper is based on a thesis submitted in partial fulfillment of the degree of Doctor of Philosophy to the Pennsylvania State College. It was supported in part by the United States Air Force.

[1] Randall, Dennison, Ginsburg, and Weber, Phys. Rev. 52, 160 (1937).

G2. Transition Probabilities II. Semi-Theoretical *f*-Numbers for Hydrogen Using the Dipole Velocity Operator.* HARRISON SHULL, *Iowa State College.*—The computations of transition probabilities for hydrogen by Mulliken and Rieke[1] using the LCAO MO and the AO methods have been repeated using the alternative velocity form of the transition moment operator. Calculations were carried through for both the Lyman bands ($^1\Sigma_g^+ \rightarrow {}^1\Sigma_u^+$) and the Werner bands ($^1\Sigma_g^+ \rightarrow {}^1\Pi_u$). In general the agreement is moderately good between the dipole length and dipole velocity methods. The dipole velocity method gives somewhat higher results for the Werner bands (0.49 instead of 0.38) but correspondingly lower results for the Lyman bands (0.18 instead of 0.24). As with the dipole length method, it is found necessary to use an effective Z value of 1.2 (the variation value) for the bonding orbital and a Rydberg form for the antibonding orbital in order to obtain reasonable results.

* Supported in part by the Ames Laboratory of the AEC.

[1] R. S. Mulliken and C. A. Rieke, Repts. Prog. Phys. 8, 231 (1941).

G3. Absorption and Emission Spectra of OH in Methane-Air Flames. HERBERT P. BROIDA, *National Bureau of Standards.*—In flames of premixed methane and air burning above

a one-half inch nozzle at atmospheric pressure, the rotational distributions of the $^2\Sigma \leftrightarrow {}^2\Pi$ transition (O↔O band) of OH in absorption and emission were measured and corresponding temperatures calculated. In addition, three separate line-reversal temperatures were determined by comparing the emission from added sodium, from added mercury, and from the $Q_1(5)$ rotational line of OH with a calibrated tungsten lamp. The rotational absorption and sodium reversal temperatures agree with calculated equilibrium temperatures to within the experimental errors of 50°C. The "rotational emission temperature" of the inner cone is approximately 3250°K at fuel to air ratios from 5.6 to 10.8 percent by volume; this is approximately 1100°C greater than the maximum equilibrium temperature. The abnormal distribution is interpreted to mean that excited OH radicals are formed in a chemical reaction with excess rotational energy, which is independent of the over-all energy release. The absorption (20 percent) of the $Q_1(5)$ line gives a concentration of 10^{14} OH radicals/cm³. A high resolution grating spectrometer with an attainable resolution of 0.55 cm^{-1} was used, but because of the weak intensities, the ultimate resolution was not obtained.

G4. Vibrational Constants of $Cl^{35}O_2$. J. B. Coon and E. Ortiz, *A. and M. College of Texas.*—A rough vibrational analysis of the violet absorption spectrum of ClO_2 vapor has been reported,[1] giving approximate values for the three fundamentals ν_i of both electronic states. The band system is described theoretically by $\nu = \nu_e + G'(v_1', v_2', v_3') - G''(v_1'', v_2'', v_3'')$. Fairly accurate values for the six zero-order frequencies ω_i' and ω_i'' and for all but three of the twelve anharmonic constants x_{ij}' and x_{ij}'' have now been obtained using all published data including infrared measurements as well as a few new data at the red end of the violet absorption region. The results in cm^{-1} are $\nu_e = 21369.5$, $\omega_1' = 722.0$, $\omega_2' = 296.1$, $\omega_3' = 804.4$, $x_{11}' = -3.45$, $x_{22}' = -1.3$, $x_{33}' = -3.6$, $x_{13}' = -4.6$, $x_{12}' = -9.4$, $x_{23}' = -3.1$; $\omega_1'' = 964.8$, $\omega_2'' = 451.8$, $\omega_3'' = 1127.3$, $x_{11}'' = -4.0$, $x_{22}'' = -0.8$, $x_{33}'' = -4.6$, $x_{13}'' = -2.2$, $x_{12}'' = -21.0$, $x_{23}'' = -3.1$. The values of x_{33}', x_{23}'', and x_{33}'' are not determined by the known data. It was, therefore, necessary to estimate them in order to determine the best values for the ω_i. For the most part, bands involving upper state quantum numbers v_1' greater than 5 were not used in evaluating the above constants, since a slight discontinuity is observed at this point. Predissociation has been reported to start at $v_1' = 6$.

[1] J. B. Coon, Phys. Rev. **58**, 926 (1940).

G5. Binding Energy and Dipole Moment of Alkali Halide Molecules. E. S. Rittner, *Philips Laboratories, Inc.*—A simple theory of alkali halide gas molecules in the spirit of Born-Mayer Lattice Theory is presented. The molecule is considered to be constituted of ions, each of which is polarized by the electrostatic field of the other. This deformation polarization has two important consequences: (1) the net dipole moment of the molecule becomes appreciably lower than that given by the product of the electric charge, e, and the internuclear separation, a; (2) the repulsion constants (determined from empirical data) become different from the corresponding constants for the crystal. The theory yields satisfactory results for the binding energy, vibration frequency, and dipole moment, μ, in all instances where necessary data are available. In cases where the internuclear distances are not known experimentally, they are calculated from the theory using experimental binding energies. It is possible to assign to the ions Goldschmidt-like radii, the sums of which reproduce reasonably well both the calculated and the observed internuclear distances. Finally, item (1) above explains why Pauling's criterion for the fraction of ionic character, $f = \mu/ea$, is not a very good measure of ionicity[1] for these completely ionic substances.

[1] G. Herzberg, I. "Spectra of diatomic molecules." *Molecular Spectra and Molecular Structure* (D. Van Nostrand Company, Inc., New York, 1950), second edition, p. 377.

G6. A Variation-Iteration Method for Calculating Energy Levels in Periodic Potentials. W. A. Bowers, *University of North Carolina.*—A variation-iteration method of attacking nuclear problems using eigenfunctions in momentum space has been developed by Svartholm.[1] The same method can be applied to the problem of a periodic potential; instead of an integral equation, one has then, in view of the periodicity, an infinite set of simultaneous equations. These can be made the basis of a variational calculation of the energy; in addition, an iterative procedure for improving the original functions can be formulated. To test the method, it has been applied to the one-dimensional model of Kronig and Penney.[2] In this case, starting with a constant wave function, the first iteration yields a function for which the various infinite series occurring in the expression for the energy can be summed exactly, and the energy, thus, found for the lowest state agrees with the exact value within less than 1 percent over a wide range of values of two parameters (depth of "valleys"; ratio of "valley" width to "hill" width). The method can be extended to higher states and also to three-dimensional problems.

[1] N. Svartholm, Thesis, University of Lund (1945).
[2] Kronig and Penney, Proc. Roy. Soc. (London) **130A**, 499 (1931).

G7. Infrared Absorption Study of Hydrogen Bonding Equilibria. Norman D. Coggeshall and Eleanor L. Saier, *Gulf Research and Development Company.*—A study has been made of hydrogen bonding equilibria using the infrared absorption due to the unassociated hydroxyl group. Sterically unhindered molecules associate in polymeric complexes. Agreement between theory and experiment obtained by the use of two equilibria constants, one for the dissociation of dimeric complexes and one for the dissociation of higher order complexes, is better than that obtained by the single equilibrium constant scheme of Kempter and Mecke.[1] These constants have been evaluated for a series of simple alcohols and phenols. If a phenol has one ortho position occupied by a large substituent, such as a *t*-butyl group, it will be sterically hindered and will associate almost entirely in dimeric complexes. The equilibrium constants for several such partially hindered phenols have been evaluated. Hydrogen bonding occurs between hydroxylated materials and proton acceptor compounds. Equilibrium constants have been evaluated for the systems of benzyl alcohol and methyl ethyl ketone and of benzyl alcohol and 1,4-dioxane. At higher concentrations of the proton acceptor materials, an anomalous effect which results in an apparent strengthening of the inter-molecular bonding between unlike molecules is observed.

[1] H. Kempter and R. Mecke, Z. physik. Chem. **46**, 229 (1941).

G8. A Collision Theory of Chemical Kinetics. F. A. Matsen, *The University of Texas.*—The Schroedinger equation for the reacting system is expressed in nuclear coordinates only. Its solutions are expanded as products of internal wave functions and initially undetermined functions of the relative displacements of the reaction products. With a simplifying assumption about the rotational functions and with the familiar techniques using Green's function, there is obtained, to the first Born approximation, an expression for the probability of transition from a given reactant state to a given product state for a unit incident flux. On summing over the product states, averaging over the reactant states, and adjusting for the actual flux and number of scattering centers, there is obtained an expression for the average rate of the chemical reaction similar to that obtained by Golden[1] from first-order time-

dependent perturbation theory. The effect of higher approximations to the collision theory will be briefly discussed.

[1] S. Golden, J. Chem. Phys. 17, 620 (1949).

G9. On the Formalism of Thermodynamic Fluctuations. R. F. GREENE,* *University of Pennsylvania.*—The Einstein expression for the probability of fluctuations δx^1, δx^2, $\cdots$, in the extensive parameters of a thermodynamic system, i.e.,

$$p = \exp[(\Sigma_{i,k} S_{ik}\delta x^i \delta x^k + \text{higher terms})/2k],$$

where

$$S_{ik} = \partial^2 S/\partial\langle x^i\rangle_{\text{av}}\partial\langle x^k\rangle_{\text{av}},$$

has been used almost exclusively. For ease in calculation, it has been the practise to drop the higher terms, apparently thereby introducing an error usually considered to be small. This apparent error has been of interest in several connections, notably in critical fluctuations. All the extensive parameter fluctuation moments, however, may be calculated by an exact method based upon the canonical formalism of statistical mechanics. It can then be shown that the Einstein expression, with the higher terms formally omitted, yields the second moments with no error.

* Sponsored, in part, by the ONR.

G10. Ionization by Electron Impact in CO, N_2, NO, and O_2. H. D. HAGSTRUM, *Bell Telephone Laboratories.*—All the ionization processes which occur on electron impact in CO, N_2, NO, and O_2 have been restudied with a special mass spectrometer in which mass, appearance potential, and initial kinetic energy (by retarding potentials after mass analysis[1]) can be determined simultaneously. Results agree well with kinetic energy determinations based on velocity dispersion in the analyzer,[2] transverse deflection in the analyzer and discrimination at the exit slit,[3] and retarding potential measurements without mass analysis.[4,5] Appearance potential measurements generally agree very well with previous measurements.[2,4,5] In oxygen the present work reveals structure in the appearance potential data missed before[5] and brings agreement with the accepted values of $D(O_2)$ and $EA(O)$. The new measurements in CO, N_2, and NO appear to strengthen the "electron impact position" regarding controversial energetic quantities related to these molecules,[6] indicating again that $D(CO) = 9.61$ ev, $L(C) = 136$ kcal, $D(N_2) = 7.38$ ev, $D(NO) = 5.30$ ev, $EA(O) = 2.2$ ev, and that the O^- ion has an excited state very near the positive energy continuum.

[1] R. E. Fox and J. A. Hipple, Rev. Sci. Instr. 19, 462 (1948).
[2] H. D. Hagstrum and J. T. Tate, Phys. Rev. 59, 354 (1941).
[3] C. E. Berry, Phys. Rev. 78, 597 (1950).
[4] W. W. Lozier, Phys. Rev. 44, 575 (1933); ibid. 45, 850 (1934); ibid. 46, 268 (1934).
[5] E. E. Hanson, Phys. Rev. 51, 86 (1937).
[6] H. D. Hagstrum, Phys. Rev. 72, 947 (1947); J. Chem. Phys. 16, 848 (1948).

G11. A Model of an Imperfect Gas. T. H. BERLIN AND L. WITTEN, *The Johns Hopkins University.*—A volume V containing N particles is divided into cells of volume $v = V/N$. The partition function can be expressed as $\Sigma' I(\{n_i\})$, where $\{n_i\}$ represents the number of particles in the ith cell. $I(\{n_i\})$ is the integral of the Boltzmann factor over all spatial configurations of the particles consistent with a given $\{n_i\}$ weighted by the probability of the set $\{n_i\}$. The partition function is evaluated in the limit $N \to \infty$, $V \to \infty$, and v finite assuming that: (1) particles in a given cell are at the cell center; (2) the sum over the lattice points $\{n_i\}$ can be replaced by a special multiple integral; (3) fluctuations are small; and (4) surface effects are negligible. It is found that the limiting free energy is a nonanalytic function of v. For temperatures lower than a critical temperature, T_c, the $p-v$ curve consists of *three* pieces. The two discontinuities are in d^2p/dv^2, not in dp/dv. For $T > T_c$, the $p-v$ curve is regular. The existence of critical phenomena requires that $U(r)$, the potential energy of a pair of particles, have the *shape* of the usual molecular potential.

G12. Effect of a Non-linear Impedance on Narrow Band Noise.* J. L. MCLUCAS AND R. C. RAYMOND, *The Pennsylvania State College.*—An experimental program was undertaken to check the ability of the theory of Middleton[1] to predict the power spectrum of the current flowing in a nonlinear impedance excited by a noise voltage and to compare this power spectrum with the power spectrum of the current in the same nonlinear element excited by a continuous wave voltage of the same power level as the noise excitation. It was found that the Middleton theory predicts the general features of the output for the noise case. No appreciable differences in power level between the harmonic components of the output current for noise excitation and those for continuous wave excitation were found. A c-w signal at 1.6 mc/s or a narrow band of noise centered at the same frequency were used to drive a type 1N34 crystal diode. The crystal output was passed through attenuators (for isolation purposes) to a radio receiver which was used to analyze the radiofrequency components of the output. The low frequency components were studied with an audiofrequency wave analyzer.

* This paper is taken from a thesis submitted to the Physics Department, The Pennsylvania State College.
[1] D. Middleton, Quart. Appl. Math. 5, 445 (1948).

G13. A Formula for Multiple Scattered Electrons.* C. H. BLANCHARD AND U. FANO, *National Bureau of Standards.*—The theory of multiple scattering[1] leads to a formula which relates the progressive loss of memory of the original direction to the accompanying energy dissipation by inelastic collisions. Calling θ the angle between the direction of an electron of kinetic energy T and its direction at the initial energy T_0 and taking an average over all electrons with energy T, we have:

$$\langle\cos\theta\rangle_{\text{av}} = [(T/T_0)(T_0+2mc^2)/(T+2mc^2)]^{(Z/2)(C/B)};$$

Z = atomic numbers of scatterer, $B = -(dT/dx)/(2\pi NZe^4/mv^2)$ stopping number, $C = (p^2v^2/2Z^2e^4)\int_{4\pi}\sigma_{el}(T,\ \Theta)(1-\cos\Theta)d\Omega = \int_{-1}^{1}[\sigma_{el}(T,\ \Theta)/\sigma_{\text{Ruth}}(T,\ \Theta)]d\cos\Theta/(1-\cos\Theta) =$ "scattering number." The equation for $\langle\cos\theta\rangle_{\text{av}}$ results from an integration which assumes C/B independent of T. Both C and B vary logarithmically with T, but their ratio remains remarkably constant and a little greater than $\frac{1}{2}$, all of which follows from their representation as angular integrals. Using $\sigma_{el} = (Z^2e^4/p^2v^2)[1-\cos\Theta+(Z^1/2\ 137^2)(mc/p)^2]^{-2}$, we find for carbon at 50 and 1000 kev, $C/B = 0.52$ and 0.55, and for lead, respectively, 0.64 and 0.63; use of the Mott σ_{el} would give a less constant C/B.

* Supported by the ONR.
[1] See e.g. H. W. Lewis, Phys. Rev. 78, 526 (1950).

G14. Integro-Causality and Interaction with a Memory in a Divergence-Free Field Theory. FREDERIK J. BELINFANTE, *Purdue University.*—The Schrödinger functional Ψ describing a physical situation at time t depends not only on t and occupation numbers N but also on variables labeling experimental evidence determining the initial value of Ψ, say on time t_0 of last experiment. A new experiment by observer A at t_1 changes for A the prediction $\Psi(t_1, t_0)$ into a new initial value $\Psi(t_1, t_1)$. If a long-range causal connexion $\Psi(t, t_0) = U(t, t_1)\Psi(t_0, t_1)$ is given with unitary matrix U, then there is no longer a reason why $U(t_2, t_1)U(t_1, t_0)$ should equal $U(t_2, t_0)$. Thus, the Schrödinger equation is generalized to $i\hbar\partial\Psi(t, t_0)/\partial t = B(t, t_0)\Psi(t, t_0)$ with hermitian operator B depending also on t_0, thus generalizing "immediate causality" to "integro-causality." $B(t, t_0)$ has a "memory back to t_0, which enables us to postulate that B has vanishing matrix elements $\langle N'(t')|B(t, t_0)|N''(t')\rangle$ to and from Feynman diagrams "unallowable" between t_0 and t. "Unallowable" are all

self-energy parts, vertex parts, high order scattering parts or other possible causes of divergencies. Lamb-shift effects etc. are incorporated as part of interaction and of commutation relations directly in matrix element factors corresponding to diagram vertices and lines.

G15. Sampling Methods for Fourier Transform; Computations on *X-RAC*.* RAY PEPINSKY, *The Pennsylvania State College.*—In x-ray analysis, the relationships between the scattering function and the distribution of scattering material are those of Fourier mates. Thus, any device which can transform from scattering to density space can operate equally well in the converse direction. In computing density functions, *X-RAC* utilizes values of the scattering function—obtained at nodes of the reciprocal lattice by x-ray scattering measurements on a crystal—as Fourier coefficients and computes the transform of this as a periodically repeated contour map of the density function. But the machine can equally well sample an assumed density function, on a periodic sublattice of the unit cell, and compute the transform of this as a (periodically repeated, continuous) structure factor map. Sampling of this continuous structure factor on the nodes of the reciprocal lattice then gives discrete structure-factor values, which can be compared in amplitude with those observed by x-ray scattering from the crystal. Fineness of sampling is essential to reduction of overlapping of the resulting periodically reproduced continuous Fourier transforms, because the transform will be set down at points reciprocal to the sampling sublattice. If the sublattice is sufficiently fine, furthermore, the density function can be approximated by spherical atoms positioned on nearest sampling nodes. A method is described for extension of the number of sampled values—i.e., Fourier coefficients—any synthesizer can accommodate.

* Development supported by ONR.

FRIDAY AFTERNOON AT 2:15

Mellon Institute Auditorium

(W. SHOCKLEY presiding)

Symposium (DSSP) on Luminescence, Photo-Effect, Electron, and Exciton Migration

H1. Photo-luminescence of Inorganic Solids. J. H. SCHULMAN, *Naval Research Laboratory.* (40 min.)

H2. Basic Physical Processes in Crystal Counters. H. KALLMANN, *New York University.* (40 min.)

H3. Exciton-Induced Photoelectric Effects in Alkali Halides. L. APKER AND E. TAFT, *General Electric Company.* (40 min.)

FRIDAY AFTERNOON AT 2:00

Bureau of Mines

(F. G. BRICKWEDDE presiding)

Symposium (DCP) on Barriers to Internal Rotation of Molecules and Related Stereo-Isomerism

I1. Introduction; Review of the Theoretical Calculation of Barriers to Internal Rotation of Molecules. G. E. KIMBALL, *Columbia University.* (30 min.)

I2. The Contributions of Thermodynamics and Statistical Mechanics as to the Problem of Barriers Hindering Internal Rotation. J. G. ASTON, *Pennsylvania State College.* (30 min.)

I3. Rotational Isomerism by the Spectroscopic Method. H. J. BERNSTEIN, *National Research Council of Canada.* (40 min.)

I4. Strain and Steric Effects in Tautomeric Structures of Several Normal and Cyclic Hydrocarbon Molecules and Their Simple Derivatives. C. W. BECKETT, *National Bureau of Standards.* (30 min.)

I5. Some Microwave Aspects of Hindered Rotation in Methyl Alcohol. D. G. BURKHARDT, *University of Colorado.* (30 min.)

FRIDAY AFTERNOON AT 2:15

Mellon Institute Social Room

(J. E. GOLDMAN presiding)

Metals

J1. The Analysis of Solids with the Mass Spectrometer. J. G. GORMAN,* E. A. JONES, AND J. A. HIPPLE, *National Bureau of Standards.*—Quantitative analyses of solid samples have been successfully performed with a mass spectrometer using a high frequency spark in vacuum. The ions from the source pass through an energy filter and enter a magnetic

analyzer, where the various masses are sorted out by varying the magnetic field and scanning the ions across an exit slit. The current to this ion collector fluctuates through a wide range because of the instability of the spark source. To compensate for these fluctuations, a monitoring electrode is placed at the entrance to the magnetic field; and, as the various ions are scanned across the exit slit, the ratio of the current passing through the exit slit to that received by the monitor is recorded. Since these two collectors receive currents from the same source, the fluctuations of this source are effectively nullified in comparing the ion currents corresponding to different masses. The effectiveness of the method will be demonstrated with some results on the chemical composition of six stainless steel samples. These samples vary in chromium and nickel concentration from a fraction of 1 percent to 25 percent, and the calibration of the instrument was found to be linear over this range.

* Present address: Carnegie Institute of Technology, Pittsburgh, Pennsylvania.

J2. Atomic Displacements and Crystallite Orientations in the Deformation of Single Crystals. B. L. AVERBACH AND B. E. WARREN, *M.I.T.*—Single crystals of a Cu−2 percent Si alloy have been deformed by cold rolling in the (110) [112] direction. Rocking curves, obtained by means of a double-crystal spectrometer, indicated that the annealed crystals had a half-maximum width of approximately 8 minutes (intensity *vs* crystal setting). After a cold reduction of 50 percent, the mean orientation of the crystal remained unchanged; but the half-maximum width of the rocking curve was increased to 168 minutes. Average atomic displacements introduced by cold rolling were evaluated by means of a Fourier analysis[1] of intensity curves (intensity *vs* chamber setting, 2θ) obtained with monochromatic radiation and a single-crystal spectrometer. The intensity peaks were considerably broadened by the plastic deformation, with a large part of the broadening appearing in the form of elongated tails. The plastically deformed crystals showed considerable recovery on annealing at 300°C. The intensity peaks (intensity *vs* 2θ) sharpened, but the double crystal rocking curves did not decrease in width. This indicates that the spread in crystallite orientation introduced by the plastic deformation is not removed during recovery, although considerable strain relief may occur in each of the individual crystallites. No macroscopic polygonization was observed under these recovery conditions.

[1] B. E. Warren and B. L. Averbach, J. Appl. Phys. 21, 595 (1950).

J3. The Effect of Pile Irradiation on the Stress-Strain Curve of Copper. T. H. BLEWITT AND R. R. COLTMAN, *Oak Ridge National Laboratory.*—Two single crystals of the same orientation were grown by the Bridgman method in a high vacuum. These specimens were grown to conform with A.S.T.M. specifications of standard $\frac{1}{4}''$ tensile specimens. One of the specimens was then sealed in an evacuated quartz tube and exposed in the Oak Ridge pile to a fast neutron flux of 1.8×10^{19} nvt. Stress strain curves on both crystals were subsequently measured. The critical shear stress was found to be 0.241 Kg/mm^2 for the unirradiated and 1.938 Kg/mm^2 for the irradiated sample.

J4. The Change in Resistivity of Copper by Low Temperature Annealing. T. H. BLEWITT, W. TAYLOR, AND R. R. COLTMAN, *Oak Ridge National Laboratory.*—Frederick Seitz[1] has suggested that atomic vacancies and interstial atoms can be generated by solids and that dislocations act as sources and sinks for lattice vacancies and interstial atoms. Measurements of the ionic conductivity by Gyulai and Hartly[2] show that imperfections created by plastic deformation are annihilated in one hour at 38°C in NaCl. Samples of polycrystalline copper cold-worked at liquid nitrogen temperatures show a decrease in resistivity upon annealing at 20°C of approximately one-third of the total increase in resistivity induced by the plastic deformation. It was found that a similar effect was also observed by a short anneal ($\frac{1}{4}$ hour) at dry ice temperatures. Apparently, if this effect is due to the annihilation of vacancies and interstials, the relaxation time for the annihilation of these imperfections is comparatively short in metals compared to that of ionic crystals. The results for the room temperature annealing were obtained independently of the research of Molenar and Aarts[3] are in agreement with their results.

[1] Conference on Plastic Properties of Solids, Carnegie Institute of Technology, Pittsburgh, Pennsylvania.
[2] Gyulai and Hartly, Z. Physik 51, 378 (1928).
[3] Molenar and Aarts, Nature (October, 1950).

J5. Recovery of Internal Friction in Alpha-Brass. HERBERT I. FUSFELD, *Frankford Arsenal.*—Fine-grained annealed specimens of 70-30 cartridge brass were given various amounts of cold-working, then annealed at temperatures below the recrystallization temperature. Internal friction measurements were conducted continuously during the anneals. Among the general features of the curves are the following. (a) Extensive recovery occurs within a matter of minutes. (b) The recovery curves at a given temperature intersect, so that the order of the curves depends on the time of measurement. (c) The data indicates an equivalent activation energy for the process considerably lower than in atomic interchange processes as diffusion. (d) A plot of recoverable internal friction (instantaneous minus final value) *versus* time is a straight line on a log-log scale, so that the internal friction falls off inversely as a simple power of time. The exponent has a range of about 0.2 to 0.8.

J6. Heat Conduction in Alloys at Low Temperatures. J. ZIMMERMAN,* *Carnegie Institute of Technology.*—Thermal and electrical conductivity measurements have been made on a number of copper-nickel and stainless-steel alloys in the temperature region between 2.6 and 80°K. Cryostat used was a Simon-type helium liquefier which functioned also as a cryostat for the liquid-hydrogen and liquid-nitrogen temperature regions. Heat was supplied electrically to one end of each specimen, and the difference of temperature between two points was measured by means of two gas thermometers connected to a differential pressure indicator. It was found that the Wiedemann-Franz ratio for these alloys generally exceeds the theoretical value of 2.45×10^{-8} watt-ohm/deg.^{2}, except in the liquid-helium region, where it approaches the theoretical value quite closely for three of the specimens (hard-drawn monel and two stainless steels). Also, it was found that annealed specimens have about the same electrical conductivity but greater thermal conductivity than hard-drawn specimens of the same material. These results suggest an appreciable lattice contribution to the thermal conductivity, at least in the case of the annealed specimens.

* The author started this work as a Gerard Swope fellow and continued it with assistance by the ONR and the Research Corporation.

J7. Alternating Hall Voltage Measurement.* D. B. BARKER, E. J. HUIBREGTSE, AND W. C. CALDWELL, *Iowa State College.*—With a constant magnetic field and an alternating primary current,[1] an alternating Hall voltage is obtained which may be amplified conveniently and which eliminates thermal emf if the frequency is sufficiently high for a given thermal conductivity of the sample. As a compromise between noise and heat flow considerations, a frequency of 10 cycles per second was chosen. The sign of the Hall coefficient may be determined by displaying the primary current and the Hall voltage on an oscilloscope by means of an electronic switch. The problems of noise and of induction between the primary circuit and the detection circuit will be discussed.

* This work was performed in the Ames Laboratory of the AEC.
[1] W. F. Leverton and A. J. Dekker, Phys. Rev. 80, 732 (1950).

J8. Electrical Properties of Sodium Wolfram Bronze.* E. J. HUIBREGTSE, D. B. BARKER, AND G. C. DANIELSON, *Iowa State College.*—With the addition of sodium atoms the ferroelectric insulator WO_3 acquires metallic properties. We have grown single crystals of Na_xWO_3 using a method developed at Linde Air Products. These crystals have been chemically analyzed yielding $x=0.68$. The electrical conductivity at 0°C is $(5.3\pm0.7)10^3$ ohm^{-1} cm^{-1} and decreases linearly with increasing temperature in the range -180°C to 40°C. The Hall coefficient[1] is $(-5.3\pm0.8)10^{-4}$ cm^3/coulomb and decreases slowly with decreasing temperature. This value indicates one electron carrier for each sodium atom added to the crystal. On Pauli's theory of paramagnetism the calculated magnetic susceptibility is 0.51. The value observed by Stubbin and Mellor[2] is 0.45 ± 0.003. The mobility of the electrons is low compared with the mobility in most metals.

* This work was performed in the Ames Laboratory of the AEC.
[1] See preceding paper by Barker, Huibregtse, and Caldwell.
[2] P. M. Stubbin, and D. P. Mellor, Proc. Roy. Soc. N. S. Wales **82**, 225 (1948).

J9. Experimental Evidence of Relaxation during Diffusionless Phase Changes of Single Crystal Beta-Au-Cd Alloys Containing 47.5 Atomic Percent Cd. L. C. CHANG AND T. A. READ, *Columbia University.**—The β-Au-Cd alloy containing 47.5 atomic percent Cd (CsCl structure, 2 atoms per unit cell, $a_0=3.317k\mathring{X}$ units) transforms by a diffusionless mechanism to β' (orthorhombic structure, 4 atoms per unit cell, $a=3.148$, $b=4.755$, $c=4.855$ $k\mathring{X}$ units) on cooling to about 60°C and the reverse diffusionless transformation from β' to β takes place when the β'-alloy is heated to about 70–80°C. The transformation takes place typically in well-annealed crystals by the slow movement of an interface between the two phases from one end of the specimen to the other until transformation is complete. It was found that by holding the interface at a given position of the specimen (on cooling) for a certain length of time t at a given temperature T, the same interface (on reheating at a constant heating rate) stops at exactly the same position for a time interval t' and then proceeds with a jerky motion. Preliminary results show that t' varies both with t and T, suggesting that the relaxation phenomenon is diffusion controlled, for example, by the diffusion of foreign atoms to the interface. More detailed studies of this phenomenon are still in progress.

* This work was supported by the AEC.

J10. Relaxation Processes in the β'-Phase of the Alloy Au Cd. D. S. LIEBERMAN, T. A. READ, AND L. C. CHANG, *Columbia University.**—Single crystals of the Au Cd alloy containing 47.5 atomic percent Cd were grown by the Bridgman method from 99.95 percent purity gold and 99.99 percent purity cadmium and were found to have a body centered cubic structure in the high temperature phase.[1] A diffusionless phase change results in an orthorhombic phase below the transformation temperature. For certain orientations of the orthorhombic domains in the low temperatures phase, the specimen exhibits a rubber-like behavior.[2,3] Immediately after transformation, however, the specimen is soft; and it has been found that the rate of appearance of rubber-like behavior is dependent on the temperatures, the time, and the strains imposed on the specimen. The velocity of sound in the low temperature phase was also found to exhibit a time-temperature dependence characteristic of diffusion phenomena.

* This work was supported by AEC.
[1] L. C. Chang and T. A. Read, J. Metals (January, 1951).
[2] A. Olander, Z. Krist. **83A**, 145 (1932).
[3] C. Benedicks, Arkiv Mat. Astron. Fysik **27A**, No. 18 (1940–1941).

J11. Short Range Order in CuAu. B. W. ROBERTS, JR., *M.I.T.** (*Introduced by* B. E. WARREN).—Diffuse x-ray scattering from the 100 face of a CuAu single crystal has been measured throughout a volume in reciprocal space sufficient to give the short range order parameters. Bent-quartz monochromated copper radiation was used with a Ni-Al balanced filter and detected with a G-M counter. Temperature diffuse scattering was subtracted out by extrapolation from three temperatures below T_c. The short range order diffuse peaks are roughly spherical in shape when considered in reciprocal space. The 100 and 300 peaks are found to be displaced away from the origin, suggesting a tendency to a layer type ordering above T_c. An assymmetry around the 200 and 400 fundamental reflections has been observed and shown to result from the randomness of position of the Cu and Au atoms with their different radii and scattering factors. Short range order parameters are given for crystals quenched from 500°C, and held at temperatures of 425°C and 525°C. The values of the short range order coefficients are similar to those found for Cu_3Au.

* Research sponsored by the ONR.

J12. A Refinement of the Ineffectiveness Concept in the Theory of the Anomalous Skin Effect in Metals.* PAUL M. MARCUS, *University of Illinois.*—The electromagnetic behavior of a metal at low temperatures and high frequencies may be roughly described by the ineffectiveness concept,[1] which introduces the effective conductivity $\sigma_e=(\delta_e/l)\sigma$ (δ_e=effective skin depth of field, l=mean free path of electrons, σ=dc conductivity). This formula yields dimensionally correct, order-of-magnitude values of surface resistance, R, and surface reactance, X, but fails to reveal important physical detail and is based on physical arguments which do not emphasize the dominant contribution to the electric current. The modified formula $\sigma_e=(\sigma/2ikl)(1+p)$ (k=complex propagation constant of field, p=electron reflection coefficient at metal surface) is derivable by simple argument which considers electrons to contribute effectively to the current in proportion to the drift velocity acquired in the skin layer. The correct relation $X=R\sqrt{3}$ and the effect of the reflection coefficient now follow. More precise considerations of the kinetics of electron motions in an exponential field give formulas agreeing more closely with rigorous results.[2] Although the rigorous field is not exponential, these calculations justify an exponential as a reasonable approximation.

* This work has been assisted by the ONR.
[1] A. B. Pippard, Proc. Roy. Soc. (London) **A191**, 385 (1947).
[2] G. E. H. Reuter and E. H. Sondheimer, Proc. Roy. Soc. (London) **A195**, 336 (1948).

FRIDAY EVENING AT 8:15

Syria Mosque

Concert of the Pittsburgh Symphony Orchestra

SATURDAY MORNING AT 9:30

Mellon Institute Auditorium

(J. H. VAN VLECK presiding)

Symposium (DSSP) on Ferromagnetism and Antiferromagnetism

K1. Some Aspects of Gyromagnetic Resonance in Ferrites. H. B. G. CASIMIR, *Philips Research Laboratories, Eindhoven.* (40 min.)

K2. Antiferromagnetism and the Néel Theory of the Ferrites. CHARLES KITTEL, *Bell Telephone Laboratories.* (40 min.)

K3. Magnetic Resonance Absorption in Antiferromagnetic Materials. L. R. MAXWELL, *National Bureau of Standards.* (40 min.) *Naval Ordnance Laboratory.* (40 min.)

K4. Magnetic Structure Studies by Neutron Diffraction. C. G. SHULL, *Oak Ridge National Laboratory.* (40 min.)

SATURDAY MORNING AT 9:30

Bureau of Mines

Beginning of the Symposium (DCP) on Statistical-Mechanical Aspects of Chemical Physics

L1. Introduction to the Symposium. J. O. HIRSCHFELDER, *University of Wisconsin.* (10 min.)

L2. Methods of Calculating the Equation of State. J. E. MAYER, *University of Chicago.* (30 min.)

L3. Some Problems in the Kinetic Theory of Gases. J. O. HIRSCHFELDER AND C. F. CURTISS, *University of Wisconsin and Naval Research Laboratory.* (30 min.)

L4. Solution of Some Rarefied-Gas Flows Using the Boltzmann Equation. HAROLD GRAD, *New York University.* (30 min.)

L5. Delta-Function Methods in Statistical Mechanics. ELLIOT MONTROLL AND T. BERLIN, *New York University.* (30 min.)

SATURDAY MORNING AT 9:30

Cathedral of Learning, Room 324

(E. C. CREUTZ presiding)

Nuclear Physics

M1. Electron Mobilities and Delay Times in Geiger-Mueller Counters.* ALDEN STEVENSON,† *Bartol Research Foundation (Introduced by* C. E. MANDEVILLE*).*—Using a coincidence counting arrangement to measure transit times of electrons in G-M counter gases, electron mobilities in argon-butane and argon-ether mixtures have been obtained. At field strengths corresponding to distances up to as little as three millimeters from the wire, the mobility in the argon-ether mixture is more than twice as great as that in the argon-butane mixture, suggesting more rapid transit times for argon-ether G-M tubes. The measurement of time intervals between coincident discharges in two argon-ether counters of diameter 1.5 cm shows that the *maximum* delay time is $<10^{-7}$ sec.

* Assisted by the joint program of the ONR and AEC.
† At present at the University of Virginia.

M2. Delay Times and Coincidence Resolving Times for G-M Counters.* C. E. MANDEVILLE, *Bartol Research Foundation.*—The results of the preceding abstract will be discussed, and their bearing upon data already published[1] will be considered. The mobility measurements agree with earlier observations[2] of genuine coincidence loss that the argon-butane mixture is unsatisfactory for a double coincidence resolving time of less than about 0.2 microsecond, whereas the argon-ether mixture can be used without loss at 0.08 microsecond in G-M counters of diameter 1.5 cm. The delayed coincidence measurements of the preceding abstract were made with glass-Aquadag counters chosen at random from a supply of counters used by this writer during the last four years for beta-gamma, gamma-gamma, and beta-beta coincidence measurements.

* Assisted by the joint program of the ONR and AEC.
[1] C. E. Mandeville and M. V. Scherb, Phys. Rev. 73, 90 (1948).
[2] C. E. Mandeville and M. V. Scherb, unpublished data (1947).

M3. On the Measurement of Times of 10^{-10} Second between Ionizing Events.* S. DE BENEDETTI AND H. J. RICHINGS, *Carnegie Institute of Technology.*—By means of scintillation counters in coincidence we were able to detect the time of flight of gamma-rays over a distance of 3 cm. A source of annihilation radiation was located half-way between two scintillation counters (either stilbene or terphenyl in xylene, with 5819 photo-multipliers), the pulses of which, without amplification and after shaping with a shorted line, were fed through cables of various length to a coincidence circuit of 10^{-9}-sec resolving time. In a typical experiment the source was displaced 3 cm along the line joining the counters

and an easily detectable shift in the coincidence curve (counts *versus* cable length) was observed. The delay of 2×10^{-10} sec introduced by displacing the source produced a variation of ≈50 percent in the counting rate along the slope of the coincidence curve. Under the same conditions a delay of 5×10^{-11} sec would produce a variation of 10 percent.

* This work was done under the auspices of the AEC.

M4. Beta-Ray Spectroscopy with Anthracene.* JAMES P. PALMER.†—A scintillation coincidence spectrometer in block form is described. This device was constructed so that it could be used as a scintillation counter without coincidence. A theoretical analysis of the response of the instrument to monokinetic beta-particles is reported. Formulas for correcting the experimental data for the poor resolution of the instrument are discussed. By beta-gamma-coincidence spectrometry, the lower beta-spectrum of Rb^{86} has been found to have an end point of 0.67 kev within about 15 percent. At a maximum x-ray energy of nominally 70 Mev, using the Iowa State College synchrotron to produce Ag^{112} and Ag^{113} from Cd^{113} and Cd^{114}, respectively, by a gamma-proton reaction, the ratio of the cross section of Ag^{112} to Ag^{113} is found to be 1.5. Beta-end-point determinations for Ag^{112} and Ag^{113} have been found to be 4.2 Mev and 2 Mev, respectively, within 8 percent.

* Work performed in the Ames Laboratory of the AEC.
† Now at Oak Ridge National Laboratory.

M5. The Pairing Effect in Nuclei and the Beta-Labile Elements. TRUMAN P. KOHMAN, *Carnegie Institute of Technology.*—Glueckauf[1] has shown that in the region of the heaviest elements the pairing energy of protons exceeds that of neutrons by 0.2 Mev on the average. Statistical examination of the beta-stable odd-A nuclides according to parity of Z shows that this situation is probably general except for light elements. A small part of the effect can be accounted for by differences in the spacing of individual-particle levels of protons and neutrons in the same potential well[2] when their numbers are different. The major part is probably due to the greater magnetic moments of protons, resulting from the orbital charge motion, causing stronger magnetic dipole interaction[3] in pairing. The beta-lability of $_{43}$Tc and $_{61}$Pm is attributable to the combined action of this effect, suggested *ad hoc* by Kowarski[4] and the increased slope of the beta-stability curve in regions near closed neutron shells, as described by Aten.[5]

[1] E. Glueckauf, Proc. Phys. Soc. (London) **61**, 25 (1948).
[2] L. Feenberg, Revs. Modern Phys. **19**, 239 (1947).
[3] L. Feenberg, Phys. Rev. **76**, 1275 (1949).
[4] L. Kowarski, Phys. Rev. **78**, 477 (1950).
[5] Aten, Science **110**, 260 (1949).

M6. A New Rare Earth Alpha-Emitter.* K.-H. SUN, F. A. PECJAK AND B. JENNINGS, *Westinghouse Research Laboratories,* AND A. J. ALLEN AND J. F. NECHAJ, *University of Pittsburgh.*—The only natural existing alpha-emitter in the lanthanide rare earth region has been recently identified[1,2] as $_{62}Sm^{147}$. Thompson *et al.*[3] have produced three alpha-emitting nuclides with half-lives of 7-min, 20-min, and 4-hr by bombarding Gd_2O_3 and Dy_2O_3 with 200-Mev protons. The 4-hr nuclide has since been identified[2] as $_{65}Tb^{149}$. We have observed a new alpha-emitter with 7.0-hr half-life by bombarding a thin film of Sm_2O_3 with 30-Mev alphas. Since the same activity was not produced by proton (8 Mev) and deuteron (15 Mev) bombardments on Sm_2O_3, the new nuclide is apparently not $_{63}$Eu. From the general considerations of reaction products of alpha-bombardment and also of shell model and alpha-systematics,[4] the new nuclide is probably $_{64}Gd^{149}$ or $_{64}Gd^{148}$.

* Assisted by the joint program of the ONR and AEC.
[1] B. Weaver, Phys. Rev. **80**, 301 (1950).
[2] Rasmussen, Reynolds, Thompson, and Ghiorso, Phys. Rev. **80**, 475 (1950).
[3] Thompson, Ghiorso, Rasmussen, and Seaborg, Phys. Rev. **76**, 1406 1949).
[4] Perlman, Ghiorso, and Seaborg, Phys. Rev. **77**, 26 (1950).

M7. Relative Cross Sections and Excitation Characteristics of 6.5-Mev Triton Reactions on Cu and Ag. D. N. KUNDU AND M. L. POOL, *Ohio State University.*—A triton beam (6.5 Mev) in the cyclotron bombarded stacks of foils (0.0006″ Ag and 0.001″ Cu). The reactions (t, d), (t, p), (t, n), and (t, He^3) were produced and showed quite varied energy dependence. The thresholds in terms of the number of the foil up to which appropriate activities were traced are: $Ag^{109}(t, d)$ foil 4; $Ag^{109}(t, p)$, $Ag^{109}(t, He^3)$, $Cu^{63}(t, p)$, $Cu^{63}(t, d)$, and $Cu^{63}(t, n)$ foil 2; $Cu^{63}(t, He^3)$ foil 1. Relative cross sections at 6.5 Mev for Cu $\sigma^{63}(t, p):\sigma^{65}(t, He^3):\sigma^{63}(t, d):\sigma^{63}(t, n) = 10:6:11:64$, and for Ag $\sigma^{109}(t, p):\sigma^{109}(t, He^3):\sigma^{109}(t, d) = 10:1:17$. The $Ag^{109}(t, d)$ excitation curve rises steeply at the low energy beginning and then very slowly up to 6.5 Mev. The shape is different from that expected for compound nucleus processes and also from usual (d, p) excitation curves. This indicates a pronounced O−P process with the compound nucleus formation gradually taking over. A comparison of (t, p) reactions in Ag, Cu, Al, and C shows that in general this cross section increases very rapidly as Z diminishes. The marked polarization of the triton makes it plausible that the two neutrons in (t, p) reactions are mostly captured simultaneously as a dineutron. The comparatively higher thresholds for (t, He^3) reactions in both cases are consistent with their endothermic nature.

M8. Neutrons from Deuterons on Silicon 28.* C. P. SWANN AND C. E. MANDEVILLE, *Bartol Research Foundation.*—A thick target of isotopic $Si^{28}O_2$ was irradiated by deuterons of energy 1.4 Mev, supplied by the Bartol Van de Graaff statitron. A single group of neutrons at $Q = 0.36\pm0.05$ Mev was observed by the recoil proton-photographic plate technique. Using the mass values given by Bethe in 1947, the mass of P^{29} is calculated to be $28.9928\pm6\times10^{-4}$ mu. The data of Peck[1] would now indicate a level in P^{29}, at 1.16 ± 0.11 Mev. Measurements relating to $Si^{29}(D, n)P^{30}$ and $Si^{30}(D, n)P^{31}$ are in progress.

* Assisted by the joint program of the ONR and AEC.
[1] R. A. Peck, Jr., Phys. Rev. **73**, 947 (1948).

M9. Apparatus for Precision Scattering Measurements.* RALPH ELY, JR., A. J. ALLEN, J. ARTHUR, R. S. BENDER, H. J. HAUSMAN, L. A. PAGE, AND E. M. REILLEY, *University of Pittsburgh.*—A schematic layout of the equipment constructed for precision scattering studies at the Radiation Laboratory of the University of Pittsburgh is presented. Two 6-ton magnets are used to direct the cyclotron beam through 35 feet of evacuated duct to the scattering chamber in a shielded room, providing a rather monoenergetic beam of relatively high intensity. The beam energy can be varied by use of absorbing foils. A third magnet analyzes the scattered particles. The University of Pittsburgh cyclotron provides 8-Mev protons, 16-Mev deuterons, and 32-Mev alpha-particles. Available proton beam and energy resolutions will be given.

* Assisted by the joint program of the ONR and AEC.

M10. Performance of Analyzer Magnets.* LORNE A. PAGE, A. J. ALLEN, J. ARTHUR, R. S. BENDER, R. ELY, H. HAUSMAN, AND E. REILLEY, *University of Pittsburgh.*—In the precision scattering project for medium energies, electromagnets have been constructed to define the energy of a beam of charged particles from the University of Pittsburgh cyclotron and to analyze the energy of charged particles emerging from the target. The magnets are designed for H_ρ values up to 10^8 gauss-cm. After fabrication according to preliminary design, the pole pieces are trimmed empirically using polonium alpha-particles. With a source width and detector slit width of $\frac{1}{16}$ inch, at a solid angle of 0.001 steradian, the resolution in momentum has a width at half-maximum less than 1 part

in 500. For 8-Mev protons, the dispersion figure is 13 kev per mm.

* Assisted by the joint program of the ONR and AEC.

M11. Magnet Current Control Unit.* E. M. REILLEY, III, AND R. S. BENDER, *University of Pittsburgh.*—An electronic control unit capable of regulating the current from a large generator has been devised and used with magnets of size from 1 ton to 100 tons. An amplidyne generator is used to drive the large generator. The circuit is essentially a dc potentiometer whose dc error signal is chopped by a vibrating reed switch, the resultant ac voltage being amplified by a large factor and demodulated. Negative feedback is provided both from the amplidyne output and the main generator output in order to stabilize systems. Currents up to 100 amperes have been stabilized to better than one part in 100,000 for a period of one hour.

* Assisted by the joint program of the ONR and AEC.

M12. Automic Operation of a Beta-Ray Spectrometer.* W. C. KELLY AND K. J. METZGAR, *University of Pittsburgh.*—Apparatus has been developed which permits the collection of data with a magnetic lens beta-ray spectrometer without requiring the attendance of the operator. The apparatus does electronically, in a repetitive fashion, what the operator would otherwise do in adjusting the focusing current and finding the time to accumulate a given number of counts. Cyclically, the following events occur. (1) A pre-set change is produced in the current by means of a helipot driven by a synchronous motor. (2) The time is stamped on a paper tape. (3) The scalar accumulates 2000 counts from the Geiger counter on the spectrometer. (4) The final time is stamped. The magnitude of the change produced in the current is determined by the time required for the scaler to accumulate 2000 counts at a standard pulse rate furnished by a blocking oscillator. An electronic switch then disconnects the blocking oscillator from the scaler and connects the Geiger counter. Results obtained with the apparatus will be described.

* Assisted by the joint program of the ONR and AEC.

M13. A 300-Volt and an rf Power Supply.* H. J. HAUSMAN, R. S. BENDER, AND E. M. REILLEY, *University of Pittsburgh.*—A general purpose rf power supply has been developed for use with photo-multiplier tubes, proportional counters, etc., capable of an adjustable output voltage of from 500 to 3000 volts, and having a short time regulation of 0.01 percent and a long time regulation of 0.03 percent at a maximum current of 1 ma. A general purpose laboratory 300-volt power supply has also been designed having a maximum output current of 250 ma regulated to 0.03 percent, hum level of 1 mv. Detailed performance figures will be given.

* Assisted by the joint program of the ONR and AEC.

SATURDAY AFTERNOON AT 2:15

Mellon Institute Auditorium

(G. E. UHLENBECK presiding)

Conclusion of the Symposium (DCP) on Statistical-Mechanical Aspects of Chemical Physics

N1. The Statistical-Mechanical Theory of Spherical and Plane Interfaces. F. P. BUFF, *University of Rochester.* (30 min.)

N2. Relations between Plasticity, Electrical Resistances, and Rates of Magnetization. HENRY EYRING AND PETER GIBBS, *University of Utah.* (30 min.)

N3. The Stability of Chemical Reactions in Extended Media. BRUCE HICKS, *Aberdeen Ballistics Research Laboratory.* (30 min.)

N4. Radial Distribution Functions in Solutions Composed of Large Ions. JACOB MAZUR, *University of Chicago,* and J. G. KIRKWOOD, *California Institute of Technology.* (30 min.)

SATURDAY AFTERNOON AT 2:15

Cathedral of Learning, Room 324

(R. SMOLUCHOWSKI presiding)

Invited Paper

P1. The New Cyclotron of the Carnegie Institute of Technology. E. C. CREUTZ, *Carnegie Institute of Technology.* (25 min.)

Magnetism; Non-Metallic Crystals

P2. Observation of Magnetic Domains by the Kerr Effect. H. J. WILLIAMS, F. G. FOSTER, AND E. A. WOOD, *Bell Telephone Laboratories.*—Magnetic domains have been observed by means of the Kerr magneto-optic effect. Plane polarized light incident normal to a surface with normal magnetization is rotated upon reflection, the sense of rotation depending upon the polarity of the surface. By using a Bausch and Lomb Research Metallographic microscope equipped with a Foster prism and a polarized light compensator[1] magnetic domains have been observed on surfaces of cobalt cutting the *C* axis

which is the direction of easy magnetization.[2] The change in domain pattern as a function of the angle between the surface and the C axis has been observed on a cylindrical surface of a single crystal.

[1] Turner, Benford, and McLean, Econ. Geol. 40, No. 1 (1945).
[2] Williams, Foster, and Wood (to be published).

P3. The Magnetic Susceptibility of Chromium. T. R. McGuire and Charles J. Kriessman, Jr., *U. S. Naval Ordnance Laboratory.*—The magnetic susceptibility of metallic chromium[1] has been determined as a function of temperature from 20°C to 1460°C. A body-force method of measurement was used in conjunction with a balance previously described.[2] Several sets of measurements have been made on chromium samples which were subjected to various heat treatments. For a specimen which was annealed at 1400°C in vacuum, the magnetic susceptibility was found to increase regularly with temperature from 3.70×10^{-6} emu per gram at 20°C to 4.25×10^{-6} emu per gram at 1460°C. Field dependence measurements showed a decrease in susceptibility with increasing H which is attributed to a slight ferromagnetic impurity. The measurements will be discussed with regard to the probability of metallic chromium being antiferromagnetic.

[1] The chromium used, having high purity, was kindly furnished by I. D. Armstrong who had previously used it for specific heat measurements. See L. D. Armstrong and H. Grayson-Smith, Can. J. Research. A28, 51 (1950).
[2] T. R. McGuire and C. T. Lane, Rev. Sci. Instr. 20, 489 (1949).

P4. On the Quantum Theory of Antiferromagnetism.* Ralph J. Harrison,† *M.I.T.*—In neutron diffraction experiments on antiferromagnetic crystals, attention must be paid to quantum effects when interpreting results for short and long range magnetic order. The uncertainty principle for angular momentum shows the Ising model is inadequate to describe magnetic ordering of an antiferromagnet. For antiferromagnetism, concepts drawn from molecular theory are more useful. Thus, the "bond order"[1] is a measure of the short range correlation in direction of spin magnetic moment. For the linear antiferromagnet we have obtained an expansion of the lowest spin eigenfunction in terms of an infinite set of valence bond spin functions, grouped according to "degree of excitation."[2] This eigenstate description supplements previous treatments of this linear case by Bethe,[3] Slater,[4] and Hulthén.[5]

* This work has been supported in part by the Signal Corps, the Air Materiel Command, and ONR.
† Now at Battelle Memorial Institute.
[1] W. G. Penney, Proc. Roy. Soc. (London) A158, 306 (1937).
[2] L. Pauling and G. W. Wheland, J. Chem. Phys. 1, 362 (1933).
[3] H. Bethe, Physik 71, 205 (1931).
[4] J. C. Slater, Phys. Rev. 38, 1109 (1931).
[5] L. Hulthén, Arkiv Mat. Astron. Fysik 26A, No. 11 (1938).

P5. High Temperature Phases of WO_3. W. L. Kehl, R. G. Hay, and D. Wahl, *Gulf Research and Development Company.*—Tungsten trioxide (WO_3) has been examined at temperatures up to 980°C by means of differential thermal analysis and x-ray diffraction. The differential thermal analysis curve exhibited strong reversible endothermic peaks centered at 750°C and 915°C. Debye-Scherrer x-ray diffraction patterns were obtained at room temperature and in the temperature interval from 600°C to 980°C. A new tetragonal form appeared in the pattern taken at 740°C. No further structural changes were observed up to 980°C which might explain the peak in the differential thermal analysis curve at 915°C.

P6. Low Temperature Luminescence of Inorganic Solids. Clifford C. Klick, *Naval Research Laboratory.*—The emission spectra of a representative group of inorganic solid phosphors have been measured at temperatures down to 4°K. Only phosphors having "edge" emission show a tendency to become a line spectrum at low temperatures; the ordinary impurity activated materials show little or no change in emission below 100°K. Emission of single crystal phosphors does not differ from that of the same material after grinding; nor does an increase in concentration of impurity from one part per million to one part per thousand have an appreciable effect. It is therefore improbable that the breadth of emission is due to the interaction of the luminescent center with other impurities or lattice defects. Possible explanations of the broad band low temperature emission are the existence of a zero-point vibrational energy of a non-photo-conducting luminescent center in its excited state; and, in the case of photo-conducting phosphors, the distortion of exciton and conduction levels near the luminescent center.

P7. Optical Properties of Counting Diamonds.* R. K. Willardson and G. C. Danielson, *Iowa State College.*—The relation of ultraviolet transmission, infrared absorption, luminescence, and birefringence to the gamma-counting properties of thirty diamonds will be described. The classification of diamonds into two types (I and II) on the basis of their ultraviolet transmission is not useful in selecting diamonds which will count gamma-rays, because most counting diamonds are in an intermediate class or are a mixture of the two types. An infrared absorption peak at 21 microns has been observed. The absence of strong infrared absorption peaks in the 5, 8, and 21 micron regions is a necessary but not a sufficient condition for gamma-counting diamonds. In specifying the initial counting condition of a diamond, it is not always sufficient to specify absence of polarization due to trapped carriers, because many diamonds appear to retain a positive charge for long periods of time. This positive charge induces a negative charge on the electrodes and thus influences the pulse height. This condition cannot always be eliminated by removal or reversal of the electric field. The value for the product of the mobility and mean lifetime is usually much larger for crystals of greater thickness.

* This work was performed in the Ames Laboratory of the AEC.

P8. Dielectric Loss and Ionic Conductivity in Alkali Halides. B. W. Henvis, J. W. Davisson, and E. Burstein, *Naval Research Laboratory.*—The dielectric loss of a series of alkali halides with and without added impurities has been measured as a function of temperature and frequency. The anomalous loss peaks which Breckenridge[1] reported in the dielectric loss curves of alkali and heavy metal halides were not observed in these measurements although special effort was made to find them. Any irregularities in the loss curves which were noted could be traced either to improper electroding or to erratic temperature control. One of the important results of the investigation is the development of an ac method for determining the ionic conductivity of alkali and heavy metal halides by dielectric loss measurements. This method has the advantage of eliminating polarization effects which complicate dc measurements. Results obtained with it are in good agreement with those obtained by dc pulse methods.[2]

[1] R. G. Breckenridge, J. Chem. Phys. 16, 959 (1948).
[2] H. W. Etzel and R. J. Maurer, J. Chem. Phys. 18, 1003 (1950).

P9. Piezoelectric Coefficients of Polycrystalline Barium Titanate in the Tetragonal and Orthorhombic States. G. N. Cotton and Hans Jaffe, *The Brush Development Company.*—The piezoelectric coefficient g_{31}, giving voltage output per applied stress, was measured on polycrystalline barium titanate over a temperature interval including the second transition point near 15°C. A sample polarized above this point shows only minor variation of g_{31} in this range. A sample polarized and measured below the transition point shows a coefficient about 40 percent higher than the sample polarized at room temperature. Upon warming through the transition point, g_{31} drops sharply to its room temperature value and maintains this lower value on renewed cooling. An elementary theory of the piezoelectric effect in polarized polycrystalline barium titanate states that g_{31} should be proportional to

retained polarization. Single crystal studies[1,2] have shown that barium titanate passes from tetragonal to orthorhombic quasi-cubic symmetry at the second transition point, the amount of spontaneous polarization remaining nearly constant. Higher values of polarization and g_{11} in the polycrystalline material below the transition point can be explained at least in part by the presence of twelve directions of spontaneous polarization in the orthorhombic state, compared with only six such directions in the tetragonal state.

[1] P. W. Forsbergh, Jr., Phys. Rev. 76, 1187 (1949).
[2] H. F. Kay and P. Vousden, Phil. Mag. 40, 1040 (1949).

P10. The Infrared Spectra of Crystalline Tetranitromethane.* P. H. LINDENMEYER AND P. M. HARRIS.—X-ray investigations have indicated the existence of two crystalline forms of $C(NO_3)_4$. Just below its freezing point the crystal is body-centered cubic, whereas powder photographs at the temperature of liquid air could not be indexed in either the cubic or tetragonal systems. Cooling curve investigations show that the transition between these two crystalline forms occur at −98.8°C and the transition is a "lambda-type" typical of order-disorder transitions. The infrared spectra of tetranitromethane were obtained at 25°C (vapor), 18°C (liquid), −40°C (solid I), −88°C (solid I), −104°C (solid II), and −126°C (solid II). A normal coordinate analysis was carried out to the point of completely assigning the fundamental modes. The spectra of the vapor can best be interpreted by a molecule with S_4 symmetry. The reported Raman spectra,[1] however, strongly indicate D_{2d} symmetry. Satisfactory agreement between these and the x-ray data is obtained by assuming molecules of both symmetries exist. The appearance of frequencies attributed to torsion about the C−N bond precludes internal rotation of the nitro groups. We observed a complete lack of selection rules in both crystalline forms, as has been predicted for the spectra of disordered crystals.

* This work was supported in part by a contract between the ONR and The Ohio State University Research Foundation.
[1] Mathieu and Massignon, Compt. rend. 211, 323 (1940).

P11. An Investigation of Plastically Deformed Crystals. D. WAHL,* *M.I.T.*—The plastic deformation by bending and the subsequent annealing of lithium fluoride single crystals have been studied. Most measurements were made on crystals bent to ½-inch radius on a special machine. With the microscope, traces (which disappeared after annealing) of the 110 slip planes were visible with spacings of 0.01 mm along the curve and 0.05 mm along the height of the crystal. Crossed polarizers made the strains "visible" with spacings along the curve of 0.01 mm. These strains disappeared slowly on annealing. An x-ray technique showed strains remaining in a minute section of a sample and the disorientations of the crystallites. Crystallographically, these small blocks varied by about 45 minutes of arc from a mean direction. On annealing, the deformed crystal underwent recrystallization and grain growth at temperatures above 600°C. The new grains had the same deviations from the mean but grew to 0.06 mm along the curve of the crystal. This indicates a mosaic block structure with strain in the deformed crystal that recrystallizes on annealing to a larger block structure without strain. The 45-minute deviation is relatable to the rotation of slip lamellae under tension. The work was done in the laboratory of Professor D. C. Stockbarger.

* Formerly, Harshaw Research Fellow; present address: Gulf Research and Development Company, Pittsburgh, Pennsylvania.

Post-deadline Papers, if any

Author Index to Papers Presented at the Pittsburgh Meeting

Apker, L. and E. Taft—H3
Aston, J. G.—I2
Averbach, B. L. and B. E. Warren—J2
Barker, D. B., E. J. Huibregtse, and W. C. Caldwell—J7
Becker, R.—E1
Beckett, C. W.—I4
Belinfante, Frederik J.—G14
Berlin, T. H. and L. Witten—G11
Bernstein, H. J.—I3
Blanchard, C. H. and U. Fano—G13
Blewitt, T. H. and R. R. Coltman—J3
Blewitt, T. H., W. Taylor, and R. R. Coltman—J4
Bowers, W. A.—G6
Broida, Herbert P.—G3
F. P. Buff—N1
Burkhardt, D. G.—I5
Burstein, E., J. J. Oberly, J. W. Davisson, and B. W. Henvis—D10
Casimir, H. B. G.—K1
Chang, L. C. and T. A. Read—J9
Cleland, J. W., J. H. Crawford, K. Lark-Horovitz, and J. C. Pigg—D5
Coggeshall, Norman D. and Eleanor L. Saier—G7
Coon, J. B. and E. Ortiz—G4
Cotton, G. N. and Hans Jaffe—P9
Creutz, E. C.—P1
De Benedetti, S. and H. J. Richings—M3
Ely, Ralph, Jr., A. J. Allen, J. Arthur, R. S. Bender, H. J. Hausman, L. A. Page, and E. M. Reilley—M9
Eyring, Henry and Peter Gibbs—N2
Friedberg, Simeon A.—D9
Fusfeld, Herbert I.—J5
Gordy, W.—F3
Gorman, J. G., E. A. Jones, and J. A. Hippie—J1
Grad, Harold—L4
Greene, R. F.—G9
Hagstrum, H. D.—G10
Harrison, Ralph J.—P4
Hausman, H. J., R. S. Bender, and E. M. Reilley—M13
Henvis, B. W., J. W. Davisson, and E. Burstein—P8
Herzberg, G.—F4
Herzfeld, K.—B3
Hicks, Bruce—N3
Hirschfelder, J. O.—L1
Hirschfelder, J. O. and C. F. Curtiss—L3
Huibregtse, E. J., D. B. Barker, and G. C. Danielson—J8
Johnson, V. A. and K. Lark-Horovitz—D4
Kallmann, H.—M2
Kohl, W. L., R. G. Hay, and D. Wahl—P5
Kelley, W. C. and K. J. Metzgar—M12
Kimball, G. E.—I1
Kittel, Charles—K2
Klick, Clifford C.—P6
Klontz, E. E. and K. Lark-Horovitz—D3
Kohman, Truman P.—M5
Kundu, D. N. and M. L. Pool—M7
Lehovec, K.—D8
Lieberman, D. S., T. A. Read, and L. C. Chang—J10
Lindenmeyer, P. H. and P. M. Harris—P10
Loebner, Egon E.—D11
Loewdin, P. O.—A3
Mandeville, C. E.—M2
Marcus, Paul M.—J12
Matsen, F. A.—G8
Maxwell, L. R.—K3
Mayer, J. E.—L2
Mazur, Jacob—N4
McGuire, T. R. and Charles J. Kriessman, Jr.—P3
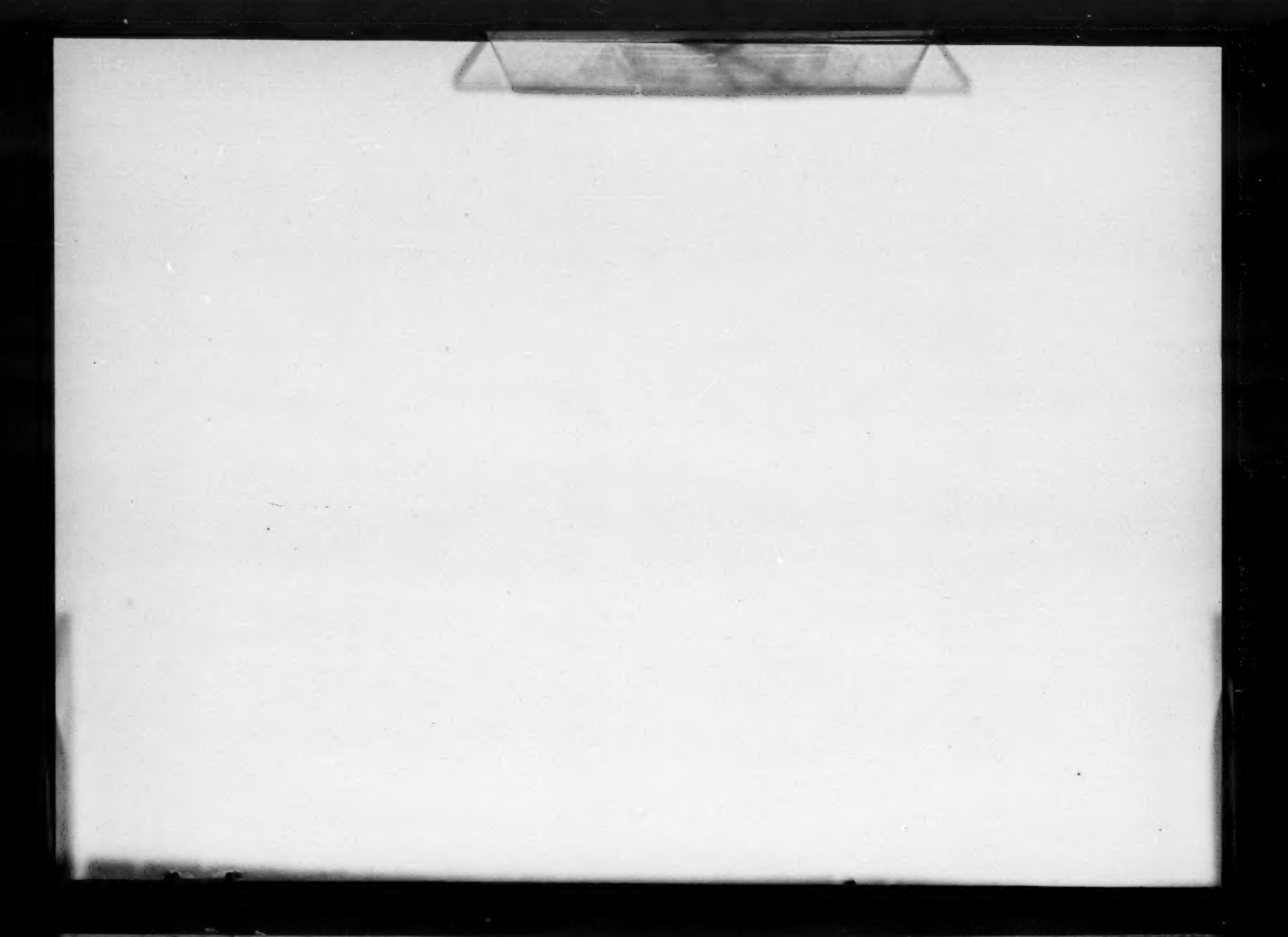
McLucas, J. L. and R. C. Raymond—G12
Montroll, E. W.—B1
Montroll, Elliot and T. Berlin—L5
Moore, A. R. and F. Herman—D7
Mulliken, R. S.—A1
Musser, Glenn L. and Richard C. Raymond—G1
Odell, N. H. and H. Y. Fan—D2
Page, Lorne A., A. J. Allen, J. Arthur, R. S. Bender, R. Ely, H. Hausman, and E. Reilley—M10
Pake, G. E.—C3
Palmer, James P.—M4
Parr, R. G.—C2
Pepinsky, Ray—G15
Pigg, J. C., J. W. Cleland, J. H. Crawford, and K. Lark-Horovitz—D6
Reilley, E. M., III, and R. S. Bender—M11
Rittner, E. S.—G5
Roberts, B. W., Jr.—J11
Roothaan, C. C. J.—C1
Rundle, R. E.—F1
Schulman, J. H.—H1
Seitz, F.—E2
Shockley, W.—E3
Shull, C. G.—K4
Shull, Harrison—G2
Slater, J. C.—A2
Stevenson, Alden—M1
Sun, K.-H., F. A. Pecjak, B. Jennings, A. J. Allen, and J. F. Nechaj—M6
Swann, C. P. and C. E. Mandeville—M8
Thornhill, J. W. and K. Lark-Horovitz—D1
Townes, C. H.—F2
Von Hippel, A.—B2
Wahl, D.—P11
Willardson, R. K. and G. C. Danielson—P7
Williams, H. J., F. G. Foster, and E. A. Wood—P2
Zimmerman, J.—J6